Methods in Molecular Biology™

VOLUME 114

Calcium Signaling Protocols

Edited by

David G. Lambert

HUMANA PRESS

1

Fluorescent Measurement of $[Ca^{2+}]_c$

Basic Practical Considerations

Alec W. M. Simpson

1. Introduction

It is extremely difficult to write a prescriptive account of how to measure cytosolic-free Ca^{2+} ($[Ca^{2+}]_c$) that will suit all potential investigators, given the wide diversity of fluorescent Ca^{2+} indicators that are now available, the variety of cells to be investigated, and an increasing range of detection equipment that can be used. Therefore, this chapter is designed to provide the user with sufficient background in the technology so that he or she can move toward developing a protocol that will suit the cells, the experimental objectives, and the equipment available to the investigator.

The main approaches to measuring $[Ca^{2+}]_c$ before the synthesis of fluorescent Ca^{2+} indicators involved using the Ca^{2+}-activated photoprotein aequorin, Ca^{2+}-selective microelectrodes, or absorbance indicators ***(1)***. The use of aequorin and microelectrodes was generally restricted to large cells (usually from invertebrates) that were easy to handle and manipulate with micropipets. With a few notable exceptions (e.g., injection of hepatocytes and myocytes with aequorin by Cobbold and colleagues ***[2,3]***), these approaches were not applied to the wide diversity of cells present in mammalian tissues. The use of absorbance dyes did not become widespread since they are not very sensitive to the typical $[Ca^{2+}]_c$ found in cells, and did not offer any real potential for investigating $[Ca^{2+}]_c$ in monolayers or single cells.

The synthesis of quin2 by Tsien ***(4,5)*** in the early 1980s heralded a new era in the measurement of Ca^{2+}, by making available fluorescent probes that could be readily introduced into living cells. The most commonly used fluorescent Ca^{2+} indicator at present is fura-2, which, along with indo-1,

From: *Methods in Molecular Biology, Vol. 114: Calcium Signaling Protocols*
Edited by: D. G. Lambert

formed a new generation of ratiometric indicators also designed by Tsien and colleagues ***(6)***.

The Ca^{2+}-binding properties of these indicators is formed by the presence of a tetracarboxylic acid core as found in the Ca^{2+}-chelator EGTA. Whereas the Ca^{2+} binding of EGTA is highly pH dependent, the original Ca^{2+} indicator quin2 and its successors were designed around an EGTA derivative, BAPTA, also synthesized by Tsien ***(7)***. For a compound to act as an intracellular Ca^{2+} indicator, selectivity of the indicator for Ca^{2+} over other physiologically important ions is essential. EGTA already showed a much greater selectivity for Ca^{2+} over Mg^{2+}, Na^+ and K^+, but unfortunately, its Ca^{2+} binding is very pH sensitive. Cells undergo physiological changes in pH ***(8)***, which in the case of an EGTA-like chelator would affect the reported $[Ca^{2+}]$. Calibrating a pH-sensitive Ca^{2+} indicator would be quite difficult, since small changes in pH of the calibration solutions would affect the measured fluorescence and the K_d for Ca^{2+}. The synthesis of BAPTA, a largely pH-insensitive Ca^{2+} chelator, was therefore an important step in the development of fluorescent probes for measuring $[Ca^{2+}]_c$ ***(7)***.

Since the introduction of quin2, fura-2, and indo-1, numerous other fluorescent Ca^{2+} indicators have been synthesized, each with varying fluorescence characteristics and K_ds for Ca^{2+} *see* **ref. *9***; **Tables 1–3**). The fundamental properties of these indicators are similar, in that the binding of Ca^{2+} produces a wavelength shift in either the excitation or emission fluorescence spectra ***(6,9)***. When there is little or no shift in the excitation spectra, a Ca^{2+}-dependent change in the emission intensity is used to report changes in Ca^{2+} ***(5,9)***. This can arise from Ca^{2+}-dependent changes in the intensity of absorbance or quantum efficiency.

In terms of fluorescence properties, the indicators can be divided into two main groups, those that are excited by near ultraviolet (UV) wavelengths 340–380 nm (e.g., quin2, fura-2, and indo-1) and those that are excited with visible light at or above 450 nm (e.g., fluo-3, Calcium Green, rhod-2; *see* **refs. *9*** and ***10***) The fluorophores for the visible indicators tend to be fluoroscein and rhodamine derivatives. This is advantageous since a great deal of fluorescence instrumentation has been designed for use with fluoroscein- and rhodamine-based dyes.

2. Overview

2.1. Single Excitation Indicators

The first of this family is quin2, Tsien's ***(5)*** original fluorescent Ca^{2+} indicator. When excited at 340 nm, an increase in emission intensity peaking at 505 nm is observed on binding Ca^{2+}. Under physiological conditions, quin2 has a K_d of

115 n*M*, making it useful for measuring $[Ca^{2+}]_c$ changes at or close to those found in unstimulated (resting) cells; however, the dye is of little use in monitoring changes in $[Ca^{2+}]_c$ in excess of 1 μ*M*. Poor quantum efficiency has limited the use of this indicator, especially after the introduction of the more fluorescent ratiometric probes. However, quin2 does have some useful properties; like BAPTA, it is a very good buffer of $[Ca^{2+}]_c$, and its use has allowed Ca^{2+}-independent phenomena to be observed ***(11,12)***. Subsequently improved single excitation indicators have been developed that are more fluorescent and have K_ds for Ca^{2+} between ~200 n*M* and 20 μ*M* ***(9,10,13)*** (*see* **Table 1**). These indicators include fluo-3 ***(10)***, and the Calcium Green and Calcium Orange series of indicators. With these indicators there is little or no shift in either the excitation or emission spectra; however, a marked increase in fluorescence intensity can be observed on Ca^{2+} binding. Calcium Green-2™ has a K_d of 550 n*M* (**Table 1**) and produces approx 100-fold increase in fluorescence between being Ca^{2+}-free and Ca^{2+}-saturated. For fluo-3 this increase is reported to be approx 200-fold. The fluo and Calcium Green indicators all have peak excitation spectra at or close to 490 nm (*see* **Table 1**), allowing them to be readily used with argon-ion lasers (488 nm excitation). Peak emission lies close to 530 nm. There are Ca^{2+} indicators that can be excited even at longer wavelengths, e.g., rhod-2, the Calcium Crimson and Calcium Orange series, and KJM-1 (**Table 1**). Rhod-2 is excited at 520 nm, with a peak emission at 580 nm ***(10)***, and has been used to measure mitochondrial Ca^{2+} rather than $[Ca^{2+}]_c$ ***(14)***. Fura-Red (strictly a ratiometric indicator) when excited at wavelengths close to 480 nm can be used in combination with fluo-3 to obtain a ratio derived from their respective 530- and 650-nm emission signals. Thus, combinations of visible excitation indicators can be used to obtain ratio measures of $[Ca^{2+}]_c$ ***(15,16)***.

2.1.1. Visible Excitation Indicators

Visible wavelength indicators are attractive because they can avoid problems such as light absorbance by optical elements and cellular autofluorescence. The lower excitation energies of the longer wavelengths also means that photobleaching is reduced. The visibly excited dyes are more suited to the laser-based illumination systems used in confocal microscopy and flow cytometry. The advantage of having a range of indicators that can be excited at different wavelengths is that combinations of ion-indicators can be used together. Thus, Ca^{2+} can be monitored simultaneously with other physiologically important ions such as Na^+ or H^+ ***(17–19)***. Moreover, Ca^{2+} can be monitored using indicators in separate domains as with simultaneous measurements of intracellular and extracellular Ca^{2+} ***(20)***.

Table 1
Single Excitation Wavelength Indicators

Indicator	Source[a]	UV/V	K_d	AM loading	Absorbance		Emission		Comments
					$-Ca^{2+}$	$+Ca^{2+}$	$-Ca^{2+}$	$+Ca^{2+}$	
Quin2	MP/TL	UV	60[b](115)[d]	✔	352	332	492	498	High intracellular buffering
Methoxyquin2MF	MP	UV	65[b]	✔	352	332	492	498	MethoxyquinMF[19] for nuclear magnetic resonance
Oregon Green 488 BAPTA-1	MP	V	170[b]	✔	494	494	523	523	Designed for argon-ion lasers
Calcium Orange™	MP	V	185[b](380)[e]	✔	549	549	575	576	*See* **ref. *13***
Calcium Crimson™	MP	V	185[b](221)[c]	✔	590	589	615	615	*See* **ref. *13***
Calcium Green-1™	MP	V	190[b](221)[e]	✔	503	506	534	533	*See* **ref. *13***; fluorescence lifetime measurements
Calcium Green C_{18}	MP	V	280[b](62)[f]	✘	509	509	530	530	Near membrane Ca^{2+} indicator; K_d affected by lipids; **ref. *53***
Fluo-3	MP/TL	V	390[b]	✔	506	506	526	526	AM ester and Ca^{2+}-free forms only weakly fluorescent; large increase in fluorescence on Ca^{2+} binding
KJM-1	TL	V	500[c]	✔	560	560	Em640		
Calcium Green-2™	MP	V	550	✔	503	503	536	536	
Fluo LR	TL	V	550[c]	✔	506	506	525	525	Leakage-resistant indicator
Rhod-2	MP/TL	V	570[b]	✔	549	552	571	571	Can be loaded as dihydro derivative; will locate in mitochondria and peroxisomes
Oregon Green 488 BAPTA-2	MP	V	580[b]	✔	494	494	523	523	Designed for argon-ion lasers

Fluo-535	TL	V	800	✔	535	535	560	560	Lower-affinity derivative (Fluo-535FF) also available
Magnesium Green™	MP	V	6 μ*M*[b]	✔	506	506	531	531	K_d in 0-Mg^{2+}; indicator will be Mg^{2+} sensitive
Calcium Green-5N™	MP	V	14 μ*M*[b]	✔	506	506	532	532	
Calcium Orange-5N™	MP	V	20 μ*M*[b]	✔	549	549	582	582	Exhibits very fast kinetics suitable for millisecond time resolution; **ref. *77***
Oregon Green 488 BAPTA-5N™	MP	V	20 μ*M*[b]	✔	494	494	521	521	Designed for argon-ion lasers
Fluo-3FF	TL	V	41 μ*M*[b]	✔	Ex 515		526	526	

[a]MP, Molecular Probes; TL, Teflabs; MP/TL, Molecular Probes, Teflabs, and other suppliers.
[b]K_d determined in 100 m*M* KCl, pH 7.2, at 22°C.
[c]K_d determined at pH 7.2 and 22°C.
[d]K_d determined in 100 m*M* KCl, pH 7.05, at 37°C.
[e]Values taken from **ref. *13***.
[f]K_d reported to be 230 n*M* at 0.1*M* ionic strength, pH 7.2, at 22°C and 62 n*M* in the presence of phospholipid vesicles. *See* **ref. *50***.

Table 2
Dual Excitation Ratiometric Indicators

Indicator	Source[a]	UV/V	K_d	AM loading	Absorbance		Emission		Comments
					$-Ca^{2+}$	$+Ca^{2+}$	$-Ca^{2+}$	$+Ca^{2+}$	
Fura Red™	MP	V	140[b]	✔	472	436	657	637	Low quantum yield; used in combination with single ex indicators to obtain ratios
Fura-2	MP/TL	UV	145[b](224)[c]	✔	363	335	512	505	
Fura C_{18}	MP	UV	150[b]	✘	365	338	501	494	Lipophilic near-membrane Ca^{2+} indicator
Fura PE3	TL	UV	250[d]	✔	364	335	508	500	Leakage-resistant indicator
FFP18	TL	UV	400	✔	364	335	502	495	Lipophilic near-membrane Ca^{2+} indicator
Bis-fura-2	MP	UV	370[b](525)[e]	✘	366	338	511	505	Brighter and has lower affinity than fura-2; not available as an ester
BTC	MP	V	7 μ*M*[b]	✔	464	401	533	529	Visible-excitation ratiometric indicator
Mag-fura-2 (Furaptra)	MP	UV	25 μM[b]	✔	369	329	511	508	K_d in 0-Mg^{2+}; indicator will be Mg^{2+} sensitive
Mag-fura-5	MP	UV	28 μ*M*[b]	✔	369	330	505	500	K_d in 0-Mg^{2+}; indicator will be Mg^{2+} sensitive
Fura-2FF	TL	UV	35 μM[d]	✔	335	364	512	505	

[a]MP, Molecular Probes; TL, Teflabs; MP/TL, Molecular Probes, Teflabs, and other suppliers.
[b]K_d determined in 100 m*M* KCl, pH 7.2, at 22°C.
[c]K_d determined in 100 m*M* KCl, pH 7.05, at 37°C.
[d]Conditions for K_d determined not defined.
[e]Conditions same as in footnote *b*, but with 1 m*M* Mg^{2+} present.

Table 3
Dual Emission Ratiometric Indicators

Indicator	Source[a]	UV/V	K_d	AM loading	Absorbance		Emission		Comments
					$-Ca^{2+}$	$+Ca^{2+}$	$-Ca^{2+}$	$+Ca^{2+}$	
Indo-1	MP/TL	UV	230[b](250)[c]	✔	346	330	475	401	
Indo PE3	TL	UV	260[d]	✔	346	330	475	408	Leakage-resistant indicator
FIP18	TL	UV	450[d]	✔	346	330	475	408	Lipophilic near-membrane Ca^{2+} indicator
Indo-1FF	TL	UV	33 μ*M*[d]	✔	Ex 348		475	408	
Mag-indo-1	MP	UV	35 μ*M*[e]	✔	349	328	480	390	K_d in 0-Mg^{2+}; indicator will be Mg^{2+} sensitive

[a]MP, Molecular Probes; TL, Teflabs; MP/TL, Molecular Probes, Teflabs, and other suppliers.
[b]K_d determined in 100 m*M* KCl, pH 7.2, at 22°C.
[c]K_d determined in 115 m*M* KCl, 20 m*M* NaCl, 10 m*M* K-MOPS, pH 7.05, 1 m*M* Mg^{2+} at 37°C.
[d]Conditions for K_d determination not defined.
[e]K_d determined in 100 m*M* KCl, 40 m*M* HEPES, pH 7.0, at 22°C.

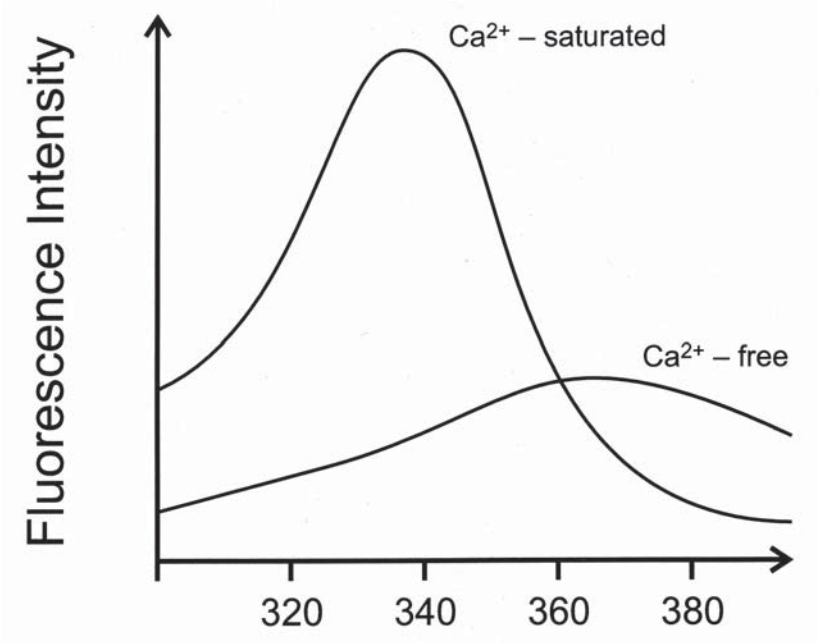

Fig. 1. Ca^{2+}-free and Ca^{2+}-saturated excitation spectra of fura-2. The two spectra coincide at 360 nm, the isobestic (or isoemissive) point. It can be seen that when Ca^{2+} binds, the fluorescence signal will increase when the indicator is excited at 340 nm, remain the same when it is excited at 360 nm, and decrease when it is excited at 380 nm.

2.1.2. Caged Compounds

Bioactive molecules can be incorporated into physiologically inert (caged) molecules and subsequently released in a controlled manner by photolysis of the chemical "cage." Introduction of the visible excitation indicators has allowed $[Ca^{2+}]_c$ to be measured during UV-induced flash photolysis of caged compounds such as caged Ins(1,4,5)P_3 and Nitr-5 (caged Ca^{2+}) ***(21)***. This advance has enabled second messengers to be manipulated in a controlled manner while simultaneously monitoring $[Ca^{2+}]_c$.

2.2. Dual Excitation Indicators

Fura-2 is the archetypal dual excitation Ca^{2+} indicator ***(6)***. In low Ca^{2+}, fura-2 shows a broad excitation spectrum between 300 and 400 nm, with a peak at approx 370 nm. On Ca^{2+} binding, the excitation peak increases in intensity and also shifts further into the UV (**Fig. 1**). Consequently, if the dye is excited at 340 nm (emission monitored at 510 nm), Ca^{2+} binding will produce an increase in fluorescence, whereas a decrease in the fluorescent signal is observed when the dye is excited at 380 nm (**Figs. 1** and **2**). When the dye is excited in quick

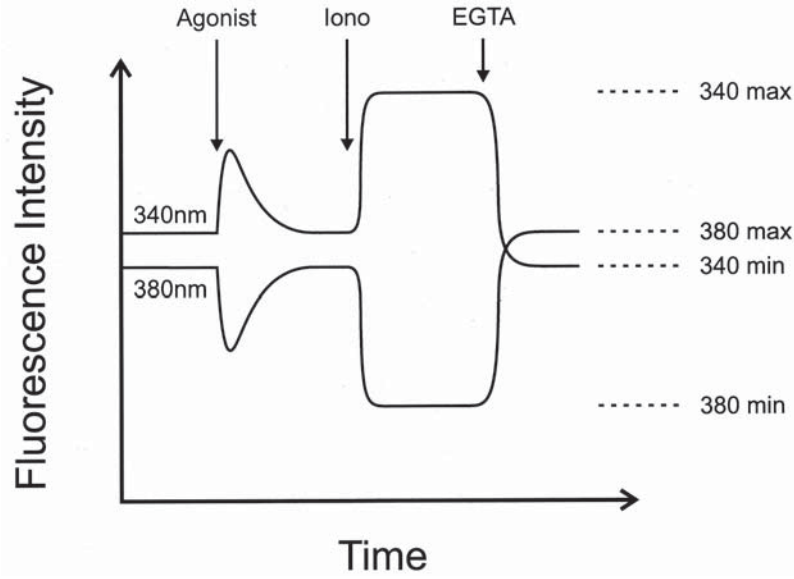

Fig. 2. The typical signals obtained from a fura-2–loaded cell when it is excited alternately at 340 and 380 nm. Agonist stimulation will cause an increase in the 340-nm signal and a decrease in the 380-nm signal. Addition of a Ca^{2+} ionophore (Iono), in the presence of Ca^{2+}, will give F_{340max} and F_{380min}, whereas subsequent addition of EGTA will give F_{380max} and F_{340min}. The time taken to reach F_{340max} and F_{380min} after addition of ionophore and EGTA can vary and be in excess of 30 min. Curve-fitting the decay toward R_{min} has been suggested as a strategy to speed up the calibration process ***(34)***. The long time period required to obtain R_{min} (340min/380max) is not ideal for imaging experiments since the dimensions of the cell may change during the calibration.

succession at 340 and 380 nm, a ratio of the respective emission signals can be used to monitor $[Ca^{2+}]$. Ratiometric measurements have a number of advantages over single wavelength probes. The ratio signal is not dependent on dye concentration, illumination intensity, or optical path length. Therefore, spatial variations in these parameters will not affect the estimations of $[Ca^{2+}]_c$. Such factors are especially important if the dyes are to be used for imaging of $[Ca^{2+}]_c$, which illumination intensity and optical properties vary across the field of view ***(6,22)***. Dye leakage and photobleaching frequently lead to a loss of indicator during an experiment; thus, the active indicator concentration cannot be assumed to be constant ***(23,24)***. Under such conditions, a ratiometric indicator gives a more stable measure of $[Ca^{2+}]_c$ than could be obtained from a single excitation indicator. Ratiometric measurements also produce an additional increase in sensitivity.

A further useful property of ratiometric indicators is the presence of an isobestic or isoemissive point. For example, when fura-2 is excited at 360 nm,

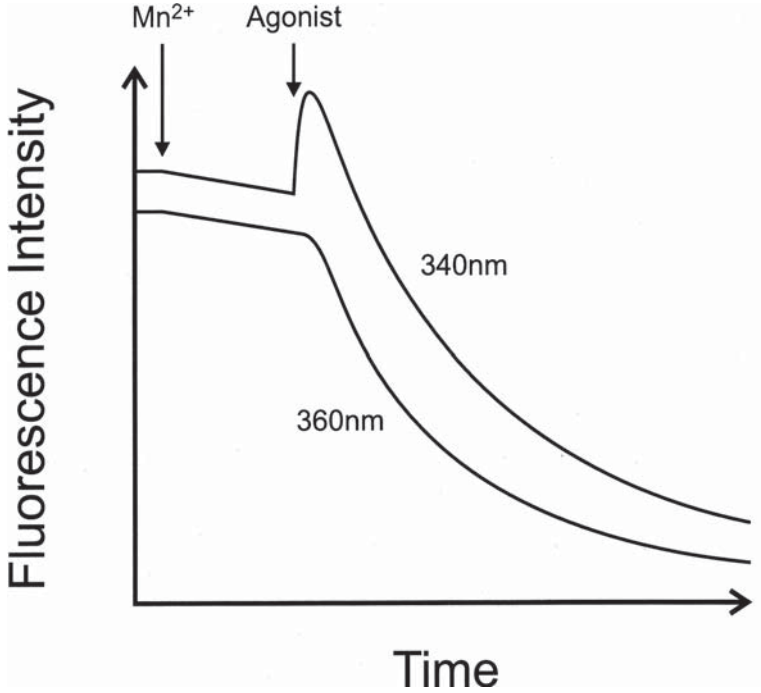
Mn2+
Agonist
Fluorescence Intensity
340nm
360nm
Time

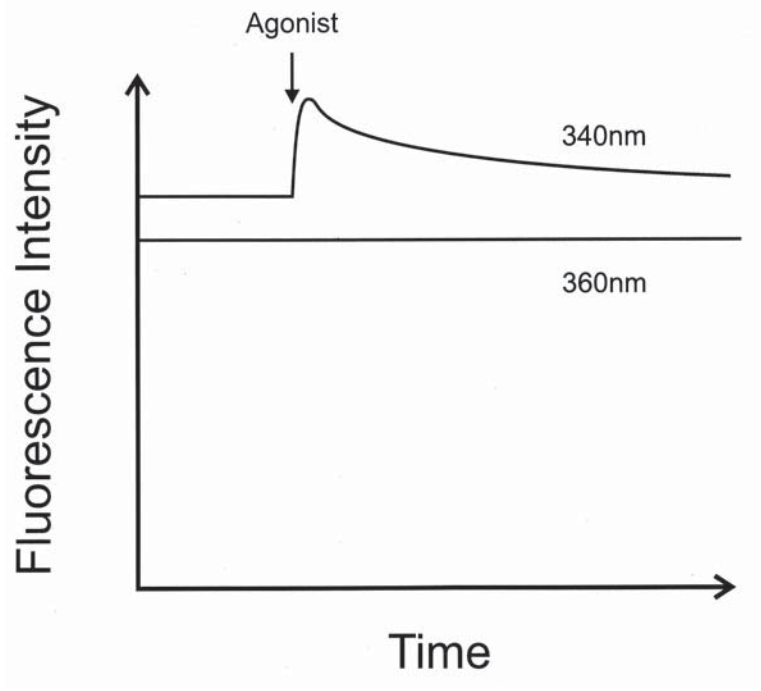
Agonist
Fluorescence Intensity
340nm
360nm
Time

no Ca^{2+}-dependent change in fluorescence occurs, since at this wavelength the Ca^{2+}-saturated and Ca^{2+}-free excitation spectra coincide (*see* **ref. *6***; **Fig. 1**). If Mn^{2+} is used to quench fura-2 fluorescence, excitation at 360 nm can be used to measure its influx (*see* **ref. *25***; **Fig. 3**). Thus, Mn^{2+} can act as a surrogate for Ca^{2+} in influx studies. Excitation at 360 nm will also reveal the intracellular distribution of fura-2 (***[24]***; see below). If the cytosolic indicator is lost by permeabilizing the plasma membrane (or quenched using Mn^{2+}), the localization of compartmentalized dye will be unveiled ***(23)***.

2.3. Dual Emission Indicators

The Ca^{2+} indicator indo-1 shows a shift and an increase in the peak of its emission spectra when Ca^{2+} binds, whereas the excitation spectra remains unaltered ***(6)***. Thus, the dye is excited at a single wavelength between 338 and 350 nm and emission is monitored at 400 and 450 nm, the respective peaks of the Ca^{2+}-bound and Ca^{2+}-free spectra. Indo-1 has a K_d for Ca^{2+} of 250 n*M* under physiological conditions (**Table 3**). Another indicator in this class is mag-indo-1. It was originally designed for monitoring Mg^{2+}; however, because Mg^{2+} generally changes very little, these indicators have been used as low-affinity Ca^{2+} indicators (**Table 3**). The dual emission indicators are ideal for simple photometric measurements of Ca^{2+} from cells. They need only a monochromatic light source (which could be via an interference filter) and a beam-splitting dichroic mirror on the emission side to separate the emission signals (400 and 450 nm for indo-1). Two photomultiplier tubes (PMTs) running simultaneously can be used to monitor the emission signals. This arrangement gives the apparatus a very rapid time resolution that is limited by the kinetic properties of the indicators. However, these dyes are not ideal for conventional fluorescence imaging experiments, because either two cameras are required or some method of rapidly changing an emission filter is needed. Aligning the image frames is not easy, and introducing additional optical elements on the emission pathway is not desirable since the amount of light per pixel on

---

Fig. 3. *(opposite page)* **(A)** The effect of Mn^{2+} on fura-2 fluorescence when the dye is excited at 340 and 360 nm. Addition of Mn^{2+} will often initiate a slow quench of fura-2 that is markedly enhanced when the cell(s) is stimulated with an agonist. The 360-nm signal represents the Mn^{2+} quench, whereas the 340-nm trace is influenced initially by the increase in $[Ca^{2+}]_c$, as well as by subsequent Mn^{2+} entry. **(B)** The control experiment that should be carried out when using Mn^{2+} quench to follow influx. Whereas the 340-nm signal will reflect changes in $[Ca^{2+}]_c$, the 360-nm signal should not change when the cells are stimulated with an agonist. The exact isobestic point should be determined for each cell type and each fluorescence system.

the camera is much less than that hitting the photocathode of a PMT tube. Indo-1 is, however, suited for the emerging technology of two-photon confocal imaging (*see* **Subheading 2.10.**).

2.4. Loading of Ca^{2+} Dyes

2.4.1. Loading Using Acetoxymethyl (AM) Esters

The Ca^{2+} indicators, by their very nature, are charged molecules that cannot cross lipid membranes. However, they can be readily introduced into cells by esterifying the carboxylic acid groups, making them lipophilic and therefore membrane permeant ***(4)***. Fortuitously cells contain many esterases that remove the ester groups, leaving the charged Ca^{2+} indicator trapped inside. Suppliers of the indicators usually sell them as the AM esters as well as in free acid or salt form. Introducing the dyes into cells involves incubating them with 1–10 μ*M* of the esterified indicator, and incubation times vary, usually between 15 min and 2 h. Loading is best achieved in a physiological buffer, but it can also be carried out in serum and in culture media, although there will be a certain degree of extracellular esterase activity ***(26)***. Some cells may show poor esterase activity; in others, the esterified indicator accumulates in intracellular compartments, where hydrolysis may be incomplete ***(23,24,26–28)***. As a result, signals from cells may not be entirely derived from the cytoplasm. Recently this "problem" with loading has been used to good effect to actually monitor Ca^{2+} inside organelles ***(15,29)***. The multidrug-resistance transporters (widely expressed in some tumor cells) will remove the esterified indicator directly from the plasma membrane ***(30)***, thereby reducing the loading efficiency. Optimizing the loading protocol is discussed in **Subheading 2.6.**

2.4.2. Microinjection and the Patch Pipet

The introduction of the patch-clamp technique for recording whole-cell and single ion channel currents has provided a great deal of information on the properties of the many selective and nonselective ion channels that are present in the plasma membrane. Some of these channels are Ca^{2+} permeable whereas many others can be regulated by Ca^{2+}. It was therefore extremely useful to combine $[Ca^{2+}]_c$ measurements with simultaneous recordings of ion channel activity ***(27,31)***. When recordings are made in the whole-cell configuration, the contents of the patch pipet are continuous with the cytoplasm of the cell. This allows the contents of the patch pipet to diffuse out and equilibrate within the cell. Hence, the patch pipet becomes a convenient way of introducing Ca^{2+} indicators and buffers into the cytoplasm of cells, avoiding the hazards of ester loading. Typically the indicator is introduced at concentrations in excess of 50 μ*M* in the patch pipet. Because the internal volume of the pipet is much larger than

that of the cell, the concentration of the dye in the patch pipet will eventually be reflected within the cell.

Microinjection can be used to introduce Ca^{2+} indicators into the cell nucleus as well as into the cytoplasm. Typically the indicators are introduced at concentrations in the order of 1 m*M* to allow for the small nanoliter volumes that are microinjected. Introduction by patch pipet or microinjection is necessary if either the dextran conjugates of the indicators or other impermeable indicators such as bis fura-2 are to be used. This fura-2 derivative has a lower affinity for Ca^{2+} (370 n*M*) and is more fluorescent than fura-2 but, unfortunately, is not available as a cell-permeant ester (**Table 2**).

2.4.3. Reversible Permeabilization

There are a number of ways in which the plasma membrane can be made temporally permeable to Ca^{2+} indicators. Streptolysin O, electroporation, and ATP^{4-} have all been used successfully ***(26,32–34)***. The advantage of these techniques is that cytoplasmic loading of poorly or impermeant indicators can be carried out on cell populations. However, the amount of loading may be small and damage to the cells is an inherent risk. Usually millimolar concentrations of the acidic indicator are needed, which is expensive and therefore will tend to limit the loading volume and hence the number of cells that can be loaded in this way.

2.5. Subcellular Localization of the Ca^{2+} Indicators

A number of reports have revealed that the Ca^{2+} indicators can become localized within intracellular compartments ***(23,24,26–29)***. In some cases these compartments appear to be mitochondria, or even the endoplasmic reticulum (ER). If signals from the cytosolic indicator can be eliminated, then selective monitoring of organelle Ca^{2+} is possible. However, when one wants to measure $[Ca^{2+}]_c$, obtaining Ca^{2+}-dependent fluorescence from other compartments is clearly a problem. Incomplete hydrolysis can be an additional complication with compartmentalized indicators ***(23)***, although in many respects a constant background fluorescence signal is easier to subtract than one that may change with time and with $[Ca^{2+}]$. Experimental approaches that can be used to optimize the cytosolic loading of the indicator are discussed next.

2.6. Optimization of Loading

There are a number of procedures that can increase the loading of the ester into cells, increase the likelihood of the dye being cytoplasmic, and finally, improve the retention of the indicator by the cells. One problem with the esterified indicators is their relatively poor solubility in physiological media. This can be improved by using Pluronic F-127, a nonionic detergent, and by includ-

ing bovine serum albumin in the loading buffer ***(34)***. Pluronic F-127 (25% w/v in dimethyl sulfoxide) is most effective when it is mixed directly with the indicator, before they are added together to the loading buffer. Loading is impaired when the esterified indicator is removed from the plasma membrane by the P-glycoprotein multidrug transporter ***(30)***. If this transporter is saturated with another substrate, such as verapamil (10 μ*M*), then introduction of the ester into cells is enhanced.

Compartmentalization of the indicator within cells can be reduced if the loading temperature is decreased from 37°C to room temperature ***(23,24)***. This is most likely mediated through a reduction in endocytosis, a process that will cause the indicators to accumulate in endosomes and topologically related organelles. When reducing the loading temperature, the loading period usually has to be increased. Thus, a balance of optimal temperature and loading period should be found for each cell type.

Once inside a cell, the hydrolyzed indicator should not escape easily; however, rapid decreases in signal intensities during experiments often occur. The cause can be twofold: photobleaching, and transport of the indicators out of the cell. Retention of the indicators can be enhanced by the presence of anion exchange inhibitors such as sulphinpyrazone and probenecid ***(35,36)***. (These agents should be present during both the loading period with the ester and afterward during the actual experiment.) Fura PE3, Indo PE3, and fluo LR are derivatives of fura-2, indo-1, and fluo-3 that are resistant to leakage. These indicators form a zwitterion from a piperazine nitrogen and an adjacent carboxylic acid that apparently enhances their retention ***(37)***. Fortuitously they too are available as cell-permeant AM esters.

2.7. Organelle Targeting

Although loading procedures may be designed to optimize the presence of the indicators in the cytosol, selective localization of the indicators may provide useful information about Ca^{2+} regulation in specific organelles or cellular domains ***(14,29,38)***. Indo-1 has been used to monitor mitochondrial $[Ca^{2+}]_m$ after the cytosolic dye was quenched using Mn^{2+} ***(38)***. The indicator rhod-2 was found to load preferentially into the mitochondria of some cells ***(14)***. This probably resulted from the fact that it is highly charged and is readily retained by the polarized mitochondria. The dihydro derivative of rhod-2 also locates preferentially into mitochondria and lysosomes since it can be oxidized within these organelles ***(9,10,14)***. Fluo-3 has been reported to co-load into the cytosol and mitochondria of endothelial cells such that simultaneous recordings could be made from separate mitochondrial and cytosolic domains identified by confocal microscopy ***(39)***.

Low-affinity Ca^{2+} indicators are needed to measure Ca^{2+} in the ER since even the most conservative estimates suggest that the concentration is likely to be in excess of 5 μ*M* ***(29,40–42)***. At these concentrations, indo-1 and fura-2 will be saturated with Ca^{2+}. Mag-fura-2 (Furaptra) has been used to monitor ER Ca^{2+} ***(43)***. Although it was designed as an Mg^{2+} indicator ***(44)***, it is in effect a low-affinity Ca^{2+} indicator ***(45,46)***, given that Mg^{2+} is unlikely to change dramatically. Other low-affinity indicators include fura-2FF, indo-1FF fluo-3FF ***(29,37)*** and the "5N" indicator derivatives produced by Molecular Probes (**Tables 1–3**). The problem of loading such indicators selectively into the ER is not easily solved, although "normal" loading with esterified indicator at 36°C is reportedly sufficient to locate fura-2 into the mitochondria ***(39)***, and Furaptra and fura-2FF into the sarco/ER ***(29)***. Another approach is to load permeabilized cells with indicators, thus allowing the ester greater access to the organelle membranes and the cytosolic dye to diffuse out of the cell ***(43)***. Unfortunately, cell permeabilization quite dramatically changes the ultrastructure of the ER ***(47)***, which is not at all desirable. Information on endoplasmic reticulum $[Ca^{2+}]_{ER}$ has also been obtained by isolating the cell nuclei along with the nuclear envelope that is continuous with the ER. These isolated nuclei are subsequently loaded with esterified indicators ***(48)*** to give measurement of $[Ca^{2+}]$ in the perinuclear ER, while incubation of the nuclei with indicator-dextran conjugates allows the $[Ca^{2+}]$ to be monitored in the nucleoplasm.

Injection of dextran-conjugated indicators into the nucleus itself would allow selective measurements of nuclear $[Ca^{2+}]_{N.}$ This could be combined with another indicator-dextran conjugate that could be injected into the cytoplasm, allowing selective monitoring of Ca^{2+} from the two subcellular regions in an intact cell. For the nucleus and cytoplasm, confocal microscopy offers an alternative approach to monitoring $[Ca^{2+}]$, in that the spatial resolution is such that the cytoplasm and nucleus are separated in single confocal planes. Hence, as long as one can identify the region from which the signal originated, nuclear and cytosolic Ca^{2+} can be monitored by a single, freely diffusable Ca^{2+} indicator ***(49)***.

There is increasing evidence for microdomains of $[Ca^{2+}]_c$ within cells ***(50–52)***. The Ca^{2+} indicators are, by their nature, Ca^{2+} buffers that can diffuse freely within cells. As such they can act to buffer microdomains, making them harder to resolve. If the Ca^{2+} buffers are made immobile or their diffusion is restricted, more dramatic localized changes in Ca^{2+} should be observed. One approach along these lines has been to add a lipophilic tail allowing the indicator to be attached to membranes ***(53–55)***. Such indicators include fura C_{18}, Calcium Green C_{18} (Molecular Probes) and FFP18, FIP18, and Fluo-FP-18 (Teflabs). When injected into the cell, they locate to the cytoplasmic faces of lipid membranes. Thus peri-ER and subplasmalemmal Ca^{2+} can be monitored. It has been reported that when added extracellularly, they can be used to monitor Ca^{2+}

efflux ***(55)***, although I have found it difficult to get sensible data with Calcium Green C_{18}. An elegant refinement of this approach has been to conjugate fura-2 with the specific oligopeptides allowing the indicator to be geranyl geranylated ***(56)***. A lipid tail added by prenylation (common to Ras proteins) would allow such indicators to monitor subplasmalemmal Ca^{2+} selectively.

2.8. Indicator Mobility and Buffering of Ca^{2+}

As indicated in **Subheading 2.7.**, restricting the mobility of the Ca^{2+} buffer will also restrict the mobility of Ca^{2+} and potentially aid its detection. In intact cells, Ca^{2+} is not believed to diffuse freely owing to the presence of endogenous Ca^{2+} buffers and stores capable of rapidly sequestering Ca^{2+} ***(57)***. Thus, freely mobile indicators such as fura-2 can act to dissipate naturally occurring Ca^{2+} gradients and microdomains of elevated $[Ca^{2+}]_c$. This is, of course, disadvantageous when the aim is to investigate local changes in $[Ca^{2+}]_c$. When fura-2 is introduced at high concentrations so that it is the dominant Ca^{2+} buffer, changes in fluorescence actually report the Ca^{2+} flux. At low concentrations at which the buffering is minimal, fura-2 will reflect more faithfully the actual changes in $[Ca^{2+}]_c$ ***(58)***. Fura-2 is a relatively high-affinity indicator that will tend to buffer $[Ca^{2+}]_c$. **Tables 1–3** list some of the common indicators ranked in order of their K_d values. The lower-affinity buffers will of course be better suited to monitoring $[Ca^{2+}]_c$ without increasing intracellular buffering. A potential problem with using immobile indicators is that if they saturate with Ca^{2+} or photobleach, the ability to monitor $[Ca^{2+}]$ at a specific location is lost since nonsaturated or unbleached indicator cannot easily replace the impaired dye. As such, this could negate any beneficial effects that localized indicators may confer in the reporting of local changes in $[Ca^{2+}]_c$. Lower-affinity probes may avoid this problem since they would not readily saturate with microdomains of high $[Ca^{2+}]_c$, although the dramatic images of elementary Ca^{2+} events appear to be resolved quite adequately with freely mobile buffers ***(50)***.

2.9. Calibration

There are a number of factors that can influence calibration of which users of the fluorescent Ca^{2+} indicators need to be aware. The K_d for Ca^{2+} will vary with temperature, pH, and ionic strength, and for some indicators, the presence of Mg^{2+} will affect the K_d for Ca^{2+} ***(6,7,9,18,19,23,59)***, Viscosity also affects the signals ***(23,60)***. It is therefore advisable to calculate the K_d under conditions that mimic, as far as possible, the expected environment in which the dye is to be used. Not all of the published K_d values will relate to the ionic conditions or temperature that may be chosen for one's experiments; many values have been determined at 22°C and in the absence of Mg^{2+} (*see* **Tables 1–3**). Apparently, the K_ds of the dextran-conjugated indicators vary from batch to

batch ***(9)***, so their values would have to be checked. It is, of course, hard to predict precisely what effect the internal cellular environment will have on the Ca^{2+} indicators; however, it is unlikely that the K_d will vary significantly as long as the key parameters outlined above remain constant.

If the K_d is known, all that is required to calibrate a single excitation wavelength indicator is to determine the maximum and minimum fluorescence values of the indicator (F_{max} and F_{min}) when it is Ca^{2+} saturated and Ca^{2+} free, along with any background fluorescence ***(5)***. After subtracting the background fluorescence from the signals, $[Ca^{2+}]_c$ can be calculated as follows:

$$[Ca^{2+}]_c = K_d \cdot (F - F_{min})/(F_{max} - F)$$

When the cells are in suspension, leaked dye will contribute to the background signal particularly if extracellular Ca^{2+} is present, since the extracellular indicator will be saturated with Ca^{2+}. The contribution of the extracellular dye to the signal can be determined either by centrifuging the cells and measuring the fluorescence arising from the supernatant or by adding Mn^{2+} and measuring the instantaneous drop in the signal. This latter approach will only work when using those indicators that are quenched by Mn^{2+}. When adjusting for extracellular dye in this way, the Ca^{2+}-saturated signal from extracellular dye should be subtracted from F_{max} and from the fluorescence values *(F)* obtained during the experiment. A fluorescence value equivalent to that from Ca^{2+}-free extracellular dye should be subtracted from F_{min}. Usually this latter component is small and can be ignored unless the indicator gives a relatively large Ca^{2+}-free signal. A major source of background signals is cellular autofluorescence which is more pronounced when the cells are excited in the UV. The signal from unloaded cells can be used to estimate the background fluorescence, as can certain Mn^{2+} quench protocols as indicated in **Fig. 4**.

For single excitation indicators, optical path length and dye concentration are critical and must remain constant. Consequently in cell suspensions, lysing the cells and determining F_{max} and F_{min} works well because the overall dye concentration in the sample chamber does not change, nor does the optical path length. If the measurements are being made on cover slips, then on lysis the dye will diffuse out of the cells and, therefore, out of the focal plane. For such adherent cells, a Ca^{2+} ionophore can be used to estimate F_{max}. Obtaining F_{min}, however, is more difficult, since even in the presence of extracellular EGTA, sufficient Ca^{2+} may remain within the cell to affect the estimation of R_{min}. When calibrating with a suspension, sufficient EGTA must be added to chelate all the 1 m*M* initial Ca^{2+} that is present in many experiments (with adherent cells the bathing buffer can simply be replaced). This means that there has to be at least a 10-fold excess of EGTA to Ca^{2+} in the cuvet ***(6,59)***. When adding EGTA to Ca^{2+} (or vice versa), it should be remembered that 1 m*M* Ca^{2+} bound

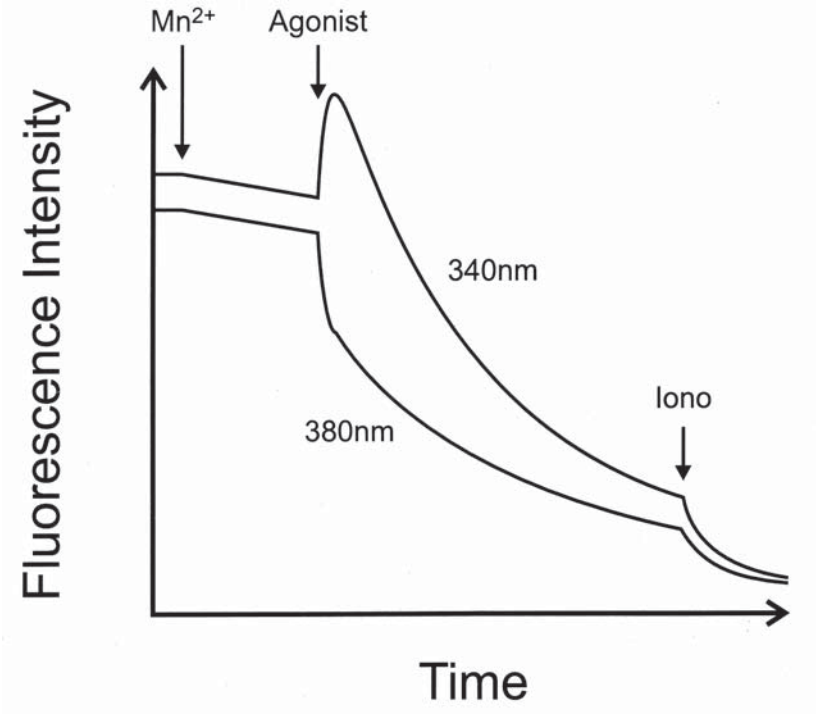

Fig. 4. The effect of adding Mn^{2+} to a cell, excited at 340 and 380 nm, that is subsequently stimulated by an agonist. The Mn^{2+} quenches both the 340- and 380-nm signals. Usually a steady state is reached when the cytosolic indicator has been quenched. The remaining fluorescence is derived from compartmentalized indicator plus autofluorescence. The intensity values of the 340- and 380-nm signals at this stage represent the background fluorescence. Subsequent addition of an ionophore allows Mn^{2+} to quench the compartmentalized indicator, revealing the autofluorescence at 340 and 380 nm.

to EGTA will liberate 2 m*M* H^+. These protons can be removed by adding Tris base or by adding the EGTA as an alkali solution (pH 8.0–9.0). Fluo-3 can be calibrated using the Mn^{2+}-quenched signal to estimate both F_{min} and F_{max} ***(10,61)***. In other instances, it may be simpler to normalize the fluorescence signal to F_{max}. For imaging with a single wavelength indicator, the normalization has the added benefit that it can be carried out *in situ* on a pixel-to-pixel basis. During calibration of adherent cells, a potential problem is that increased dye leakage may lead to an underestimate of F_{max} and F_{min} in relation to the F values obtained prior to the calibration. When using a ratiometric indicator, this would not be such a problem because R_{max} and R_{min} values are not affected so dramatically by dye leakage.

With the ratiometric dyes, such as fura-2, the calibration is similar to that for the single wavelength indicators ***(6)***. Hence the R_{max} and R_{min} values are needed;

instead of F_{max} and F_{min}, the maximum and minimum ratio values, R_{max} and R_{min}, are required. Because the ratio is not made with reference to the isobestic point (360 nm) but usually with the 380-nm signal (to improve the SNR ratio) a scaling factor, the F_{380max}/F_{380min} ratio is also required. At 360 nm this factor would be equal to 1. Therefore

$$[Ca^{2+}]_c = K_d\,(R - R_{min})/(R_{max} - R)(F_{380max}/F_{380min})$$

where $R = F_{340}/F_{380}$.

With adherent cells, R_{max} and R_{min} are best determined *in situ*. R_{max} is relatively easy to obtain using Ca^{2+} ionophores such as ionomycin and Br-A23187 (*see* **refs. *34*** and **59**). The same problems in obtaining a reliable R_{min} apply to the ratiometric probes as well as to obtaining F_{min} with the single wavelength indicators. Consequently, the calibration protocol is essentially the same as that described above. With fura-2, the Ca^{2+}-saturated signal, determined by addition of ionophore in the presence of 1–10 m*M* extracellular Ca^{2+}, will give the F_{340max} and F_{380min} (R_{max}). However, problems can arise if the F_{380min} signal is close to autofluorescence, since dividing by zero or small numbers can play havoc with the software and generate very large erroneous R_{max} values. This is a particular problem when using an 8-bit camera, since autofluorescence values are likely to be close to zero. R_{min}, which is F_{340min}/F_{380max}, is obtained by incubating the cells with ionophore in the presence of relatively large amounts of EGTA as outlined above. Note, however, that Br-A23187 is reported to be more effective at transporting Ca^{2+} at acid pH values than ionomycin ***(34,59)***.

Figure 2 is a schematic diagram of the 340- and 380-nm signals of fura-2 during agonist stimulation and calibration.

With fura-2, Mn^{2+} quench of the 340- and 380-nm excitation signals can be used to determine the background fluorescence at each wavelength (**Fig. 4**). Some groups use ionomycin and Mn^{2+} to determine background fluorescence; however, this approach would also quench signals coming from dye trapped inside organelles. To quench the cytosolic signal, it is better to use a maximal concentration of an agonist (or thapsigargin) so that Mn^{2+} rapidly enters the cytosol. Thus, any remaining signal will represent compartmentalized dye and autofluorescence. Ionomycin can be added subsequently to reveal autofluorescence alone, if desired.

When imaging, the calibration should ideally be carried out on a pixel-to-pixel basis (including background subtraction) ***(62,63)***. However, the dimensions of a cell may change between the beginning and the end of an experiment, making the perfect calibration virtually impossible. Frequently, the R_{max} and R_{min} values are averages determined for the entire field of view rather than on a pixel-to-pixel basis, although there are analysis packages that allow pixel-to-

pixel generation of R_{max} and R_{min} values. I generally use photometric data gained by summing the signal arising from each cell. In this case, it is sufficient to subtract the total background fluorescence originating from each cell.

When calibrating R_{max} and R_{min} on an imaging system, one problem is that 8-bit cameras only just manage to cover the dynamic range of the indicator. Thus, when the gain and black level are optimized, F_{340min} may be on scale, but F_{340max} may saturate the camera and vice versa with the 380-nm signals. It is more than likely that while gain settings may suit some cells in the field of view, for others the setting will mean that they are either too bright or too dim. The wider availability of 12- and 16-bit cameras should alleviate this problem in the future. Where possible, cameras should show a linear response to light ***(22,63)***. Confocal microscopes using PMTs should have a very large dynamic range (typically from 10^1 to 10^6 counts per second for PMTs), but this will depend on the analogue-to-digital converter within the system.

2.10. Detection of Fluorescence Signals

In its simplest form, measurement of $[Ca^{2+}]_c$ using fluorescent indicators requires only an appropriate light source and a PMT detector. A xenon lamp used in combination with interference filters or monochromators can be used to excite the UV, and most of the visible indicators. More sophisticated light sources involving beam-splitting optics are needed for dual excitation indicators and multiple excitation of indicators used in combination. Photomultipliers are commonly attached to microscopes for photometric detection of $[Ca^{2+}]_c$ in single cells or from the field of view. Conventional imaging using a low-light intensified charged-coupled device (ICCD) camera attached to the fluorescence microscope is now common. This technique provides very good photometric data from individual cells within the field of view; however, improved spatial resolution of $[Ca^{2+}]_c$ is provided by confocal microscopy.

A major limitation of conventional imaging has been that even the high numerical aperture objectives that are used to gain sufficient light for detection also collect light from out-of-focus planes. This has a blurring effect on the resulting image. Confocal microscopy avoids this problem by exciting the indicator and collecting the emission via a pinhole or sometimes a narrow slit ***(64)***. The geometry is such that light originating from an out-of-focus plane cannot pass through the pinhole. To construct an image, the "confocal spot" has to be scanned over the object in view. This is achieved by generating a series of line scans over the image.

The use of confocal microscopy (usually confocal laser-scanning microscopy [CLSM]) to view fluorescent Ca^{2+} indicators is now becoming widespread. (For a review of confocal microscopy and Ca^{2+} imaging *see* **ref. *64***). The increased spatial resolution and rapid response time in the line-scan mode

has revealed elementary Ca^{2+} release events in excitable and nonexcitable cells ***(15,16,65)***. The increased resolution provided by these microscopes is particularly advantageous when the indicator has been targeted to a particular domain of the cell ***(29,42,53,56)***. In addition to CLSM, there are a number of approaches that can give similar spatial resolution and, in some cases, potentially faster whole-frame data acquisition. Mathematical deconvolution using a series of image planes in the *z* axis to calculate the blurring effect of the out-of-focus planes is one method ***(66,67)***. Using a calculated point spread function for the objective is another variation on this approach. Other optical methods include the Nipkow disc and a recent variation described by Wilson ***(68)*** that has a greater light throughput. These systems have the potential to give confocal-like images without the need to use lasers. The advantage would be that a monochromator-based excitation source could be used, allowing excitation at any desired wavelength or combination of wavelengths. Although expensive, however, lasers are now available that can be tuned to almost any excitation wavelength. These "optical parametric oscillators" generate coherent light that can be tuned over infrared and visible wavelengths. No doubt they will find applications in two-photon confocal microscopy and CLSM.

Two- and three-photon confocal microscopy can also be applied to fluorescence Ca^{2+} indicators ***(64,69,70)***. Here the indicator is excited at a longer wavelength and either two or three coincident photons (depending on the dye and excitation wavelength) are able to excite the indicator. Indo-1, e.g., is normally excited at approx 350 nm, but can also be excited by light close to 700 nm. The resolution over conventional imaging is enhanced, since, statistically, the arrival of coincident photons only occurs in a very narrow focal plane. Excitation by longer wavelengths reduces autofluorescence and photobleaching, and therefore the technique has some advantages over other methods. The longer wavelengths allows deeper penetration of the sample in the *z* axis owing to reduced scatter and absorbance by the tissue and chromophore. The principal handicap at present is the cost of the lasers that are normally required, although commercial two-photon systems are now available.

2.11. Calcium Flux Measurements

In addition to providing information on $[Ca^{2+}]_c$, the fluorescent indicators can be used to provide data on Ca^{2+} fluxes. Where influx and efflux are abolished (e.g., by La^{3+}), or where the cells have been permeabilized, the indicators can give kinetic information on the release of Ca^{2+} from intracellular stores ***(71,72)***. When information is required on Ca^{2+} influx, an easy approach is to use the Mn^{2+} quench of fura-2 signals (**Fig. 3**). If Mn^{2+} is used as a surrogate for extracellular Ca^{2+}, its influx into cells can be followed using fura-2 excited at 360 nm ***(25)***. Monochromator-based light sources are best for these experi-

ments since they allow accurate excitation at the isobestic point. If excitation occurs slightly to the right of the isobestic point (i.e., >360 nm), a Ca^{2+}-dependent decrease in fluorescence can be confused with Mn^{2+} entry.

The relative permeability of Ca^{2+} influx pathways to Mn^{2+} may be of interest alone. This quench technique can be used to look at the rapid kinetics of cation entry by stopped flow fluorescence ***(73)***. In experiments investigating capacitative or store-operated Ca^{2+} entry, Ba^{2+} and Sr^{2+} have also been used as surrogates for Ca^{2+}. These ions actually behave like Ca^{2+} when they bind to fura-2, and do not quench the signal ***(74)***. Barium is also poorly removed from the cell, making it a good indicator of unidirectional fluxes. Interestingly, Sr^{2+} does not appear to enter via store-operated channels but will enter in response to vasopressin, indicating that selective use of permeant cations can be used to distinguish between different influx pathways ***(75)***.

The indicators can be used to monitor Ca^{2+} efflux whether it is a release from vesicles, Ca^{2+} stores in permeabilized cells, or extrusion from an intact cell. Efflux can be measured from individual cells by either restricting the extracellular volume ***(76)*** or using indicator-dextran conjugates to generate a gel around the cells ***(20)***. This restricts the diffusion of Ca^{2+} away, thereby aiding its detection. With the wide variety of Ca^{2+} indicators now available, it is, of course, possible to combine Ca^{2+} efflux studies using one indicator with measurements of $[Ca^{2+}]_c$ at the same time, using another indicator ***(20)***.

2.12. Dextran-Conjugated Indicators

Many of the Ca^{2+} indicators are now available as dextran-conjugates ***(9)***. They are supplied as 3000, 10,000, and 70,000 MW dextrans containing poly-(α-D-1,6-glucose) linkages making them resistant to cellular glucosidases. The dextran indicators have a number of useful properties because they

1. Have a restricted mobility
2. Are not transported out of cells
3. Remain cytosolic
4. Are less likely to bind proteins
5. Can be linked to peptides to allow specific targeting by peptide signal motifs.

2.13. Fluorescent Protein Indicator for Ca^{2+}

The usefulness of aequorin as a modern indicator for Ca^{2+} was greatly enhanced when it was shown that cells could be transfected with aequorin cDNA, allowing specific expression of the photoprotein within cells ***(41,51)***. Selective targeting of aequorin to specific organelles such as the mitochondria and ER meant that this luminescent probe was well suited for measuring organelle $[Ca^{2+}]$. Fluorescent protein indicators for Ca^{2+} have now been pro-

duced ***(42)***. They are based on the observation that fluorescence resonance energy transfer (FRET) can take place between the blue- or cyan-emitting mutants of the green fluorescent protein (GFP) and the green- or yellow-emitting GFP mutants. The fusion protein consists of two GFP mutants separated by calmodulin attached to a calmodulin-binding peptide. When Ca^{2+} binds to the calmodulin, the complex binds to the Ca^{2+}-calmodulin–binding peptide, bringing the GFP mutants sufficiently close for FRET to take place. Thus, when the camelion-1 is excited at 380 nm, there is an increase in the 510/445 emission ratio on Ca^{2+} binding. By using calmodulin mutants, this family of indicators should be able to monitor $[Ca^{2+}]$ in the range of 10^{-8}–$10^{-2}M$. With appropriate targeting strategies, these indicators have the potential to be targeted to almost any intracellular or extracellular domain.

3. Summary

Over the last decade the range of fluorescent indicators for Ca^{2+} has increased dramatically so that there are now a host of probes available. Each may offer particular advantages depending on the design of the experiment and the fluorometric equipment available. Careful choice of the indicator is therefore central to achieve a successful outcome. The probe that is chosen will, of course, depend on the aims of the experiment, on how the indicator will be introduced into the cell(s), and on the excitation source and detection equipment that are available. I hope that this chapter will not only help investigators choose the most appropriate indicator but, in addition, give an insight into what can be achieved using fluorescent Ca^{2+} indicators.

Acknowledgments

I would like to express my thanks to Dr. Alexi Tepikin, Dr. Alan Conant, and Dr. Stephen Pennington for reading this manuscript. I would also like thank the Wellcome Trust, The British Heart Foundation, and The Medical Research Council for their support in recent years.

References

1. Ashley, C. C. and Campbell, A. K. (eds.) (1979) *Detection and Measurement of Free Calcium in Living Cells*," Elsevier, Amsterdam.
2. Woods, N. M., Cutherbertson, K. S. R., and Cobbold, P. H. (1986) Repetitive transient rises in cytoplasmic free calcium in hormone-stimulated hepatocytes. *Nature* **319,** 600–602.
3. Cobbold, P. H. and Bourne, P. K. (1984) Aequorin measurements of free calcium in single heart cells. *Nature* **312,** 444–446.
4. Tsien, R. Y. (1981) A non-disruptive technique for loading calcium buffers and indicators into cells. *Nature* **290,** 527–528.

5. Tsien, R. Y., Pozzan, T., and Rink, T. J. (1982) Calcium homeostasis in intact lymphocytes: Cytoplasmic free calcium monitored with a new intracellularly trapped fluorescent indicator. *J. Cell Biol.* **94,** 325–334.
6. Grynkiewicz, G., Poenie, M., and Tsien, R. Y. (1985) A new generation of Ca^{2+} indicators with greatly improved fluorescence properties. *J. Biol. Chem.* **260,** 3440–3450.
7. Tsien, R. Y. (1980) New calcium indicators and buffers with high selectivity against magnesium and protons: Design, synthesis, and properties of prototype structures. *Biochemistry* **19**, 2396–2404.
8. Nuccitelli, R. and Deamer, D. W. (1982) *Intracellular pH: Its Measurement, Regulation and Utilization in Cellular Functions*, Alan R Liss, New York.
9. Haughland, R. P. (1996) *Handbook of Fluorescent Probes and Research Chemicals* (6th ed.), Molecular Probes Inc., Eugene, OR.
10. Minta, A., Kao, J. P. Y., and Tsien, R. Y. (1989) Fluorescent indicators for cytosolic calcium based on rhodamine and fluorescein chromophores. *J. Biol. Chem.* **264,** 8171–8178
11. Hallam, T. J., Sanchez, A., and Rink, T. J. (1984) Stimulus-response coupling in human platelets. *Biochem. J.* **218,** 819–827.
12. Simpson, A. W. M., Hallam, T. J., and Rink, T. J. (1986) Low concentrations of the stable prostaglandin endoperoxide U44069 stimulate platelet shape change in quin2-loaded platelets without a measurable increase in $[Ca^{2+}]_i$. *FEBS Lett.* **210,** 301–305.
13. Eberhard, M. and Erne, P. (1991) Calcium binding to fluorescent calcium indicators: Calcium green, calcium orange and calcium crimson. *Biochem. Biophys. Res. Commun.* **180,** 209–215.
14. Hajnoczky, G., Robb-Gaspers, L. D., Seitz, M. B., and Thomas, A. P. (1995) Decoding of cytosolic calcium oscillations in the mitochondria. *Cell* **82,** 415–424.
15. Lipp, P. and Niggli, E. (1993) Ratiometric confocal Ca^{2+} measurements with visible wavelength indicators in isolated cardiac myocytes. *Cell Calcium* **14,** 359–372.
16. Lipp, P. and Niggli, E. (1993) Microscopic spiral waves reveal positive feedback in subcellular calcium signalling. *Biophys. J.* **65,** 772–780.
17. Simpson, A. W. M. and Rink, T. J. (1987) Elevation of pH_i is not an essential step in calcium mobilisation in fura-2-loaded human platelets. *FEBS Lett.* **222,** 144–148.
18. Morris, S. J., Weigmann, T. B., Welling, L. W., et al. (1994) Rapid simultaneous estimation of intracellular calcium and pH. *Methods Cell Biol.* **40,** 183–220.
19. Martinez-Zaguilan, R., Parnami, G., and Lynch, R. M. (1996) Selection of fluorescent ion indicators for simultaneous measurements of pH and Ca^{2+}. *Cell Calcium.* **19,** 337–349.
20. Belan, P. V., Garasimenko, O. V., Berry, D., Saftenku, E., Petersen, O. H., and Tepekin, A. V. (1996) A new technique for assessing the microscopic distribution of cellular calcium exit sites. *Pflügers Arch.* **433,** 200–208.
21. Kao, J. P. Y., Harootunian, A. T., and Tsien, R. Y. (1989) Photochemically generated cytosolic calcium pulses and their detection by Fluo-3. *J. Biol. Chem.* **264,** 8179–8184.
22. Ryan, T. A., Milard, P. J., and Webb, W. W. (1990) Imaging $[Ca^{2+}]_i$ dynamics during signal transduction. *Cell Calcium* **11,** 145–155.

23. Roe, M. W., Lemasters, J. J., and Herman, B. (1990) Assessment of fura-2 for measurements of cytosolic free calcium. *Cell Calcium* **11,** 63–73.
24. Malgoroli, A., Milani, D., Meldolesi, J., and Pozzan, T. (1987) Fura-2 measurements of cytosolic free Ca^{2+} in monolayers and suspensions of various types of animal cells. *J. Cell Biol.* **105,** 2719–2727.
25. Merritt, J. E., Jacob, R., and Hallam, T. J. (1988) Use of manganese to discriminate between calcium influx and mobilization from internal stores in stimulated human neutrophils. *J. Biol. Chem.* **264,** 1522–1527.
26. Rink, T. J. and Cobbold, P. H. (1987) Fluorescence and bioluminescence measurement of cytoplasmic free calcium. *Biochem. J.* **248,** 313–328.
27. Almers, W. and Neher, E. (1985) The Ca^{2+} signal from fura-2-loaded mast cells depends strongly upon the method of loading. *FEBS Lett.* **192,** 13–18.
28. Steinberg, S. F., Belizikian, J. P., and Al-Awqati, Q. (1987) Fura-2 fluorescence is localised to mitochondria in endothelial cells. *Am. J. Physiol.* **253,** C744–C754.
29. Golovina, V. A. and Blaustein, M. P. (1997) Spatially and functionally distinct Ca^{2+} stores in sarcoplasmic and endoplasmic reticulum. *Science* **275,** 1643–1648.
30. Homolya, L., Hollo, Z., Germann, U. A., Pastan, I., Gottesmann, M. M., and Sarkadi, B. (1993) Fluorescent cellular indicators are extruded by the multidrug resistance protein. *J. Biol. Chem.* **268,** 21,493–21,496.
31. Neher, E. (1989) Combined fura-2 and patch clamp measurements in rat peritoneal mast cells, in *Neuromuscular Junction* (Sellin, L. C., Libelius, R., and Thesleff, S., eds.) Elsevier, Amsterdam, pp. 65–76.
32. Steinberg, T. H., Newman, A. S., Swanson, J. A., and Silverstein, S. C. (1987) ATP^{4-} permeabilizes the plasma membrane of mouse macrophages to fluorescent dyes. *J. Biol. Chem.* **262,** 8884–8888.
33. Di Virgilio, F., Fasolato, C., and Steinberg, T. H. (1988) Inhibitors of membrane transport system for organic anions block fura-2 excretion from PC12 and N2A cells. *Biochem. J.* **256,** 959–963.
34. Kao, J. P. Y. (1994) Practical aspects of measuring $[Ca^{2+}]$ with fluorescent indicators. *Methods Cell Biol.* **40,** 155–181.
35. Di Virgilio, F., Steinberg T. H., and Silverstein, S. C. (1990) Inhibition of fura-2 sequestration and secretion with organic anion transport blockers. *Cell Calcium* **11,** 57–62.
36. Di Virgilio, F., Steinberg, T. H., Swanson, J. A., and Silverstein, S. C. (1988) Fura-2 secretion and sequestration in macrophages. *J. Immunol.* **140,** 915–920.
37. Teflabs Catalogue (1998). Texas Fluorescence Labs Inc., 9503 Capitol View Drive, Austin, TX 78747.
38. Miyata, H., Silvermann, H. S., Sollott, S. J., Lakatta, E. G., Stern, M. D., and Hansford, R. G. (1991). Measurement of mitochondrial free Ca^{2+} concentration in living single rat cardiac myocytes. *Am. J. Physiol.* **261,** H1123–H1134.
39. Donnadieu, E. and Bourguinon, L. Y. W. (1996) Ca^{2+} signalling in endothelial cells stimulated by bradykinin: Ca^{2+} measurement in the mitochondria and the cytosol by confocal microscopy. *Cell Calcium* **20,** 53–61.
40. Kendall, J. M., Dormer, R. L., and Campbell, A. K. (1992) Targeting aequorin to the endoplasmic reticulum of living cells. *Biochem. Biophys. Res. Commun.* **189,** 1008–1016.

41. Montero, M., Brini, M., Marsault, R., Alverez, J., Sitia, R., Pozzan, T., and Rizzuto, R. (1995) Monitoring dynamic changes in free Ca^{2+} concentration in the endoplasmic reticulum of intact cells. *EMBO J.* **14,** 5467–5475.
42. Miyawaki, A., Llopis, J., Heim, R., McCaffrey, J. M., Adams, J. A., Ikura, M., and Tsien, R. Y. (1997) Fluorescent indicators for Ca^{2+} based on green fluorescent proteins and calmodulin. *Nature* **388,** 882–887.
43. Hofer, A. M. and Machen, T. E. (1993) Technique for *in situ* measurement of calcium in intracellular inositol 1,4,5-trisphosphate-sensitive stores using the fluorescent indicator mag-fura-2. *Proc. Natl. Acad. Sci. USA* **90,** 2598–2602.
44. Raju, B., Murphy, E., Levy, L. A., Hall, R. D., and London, R. E. (1989) A fluorescent indicator for measuring cytosolic free magnesium. *Am. J. Physiol.* **256,** C540–C548.
45. Konishi, M., Hollingworth, S., Harkins, A. B., and Baylor, S. M. (1991) Myoplasmic Ca^{2+} transients in intact frog skeletal muscle fibres monitored with the fluorescent indicator furaptra. *J. Gen. Physiol.* **97,** 271–302.
46. Ogden, D., Khodakhah, K., Carter, T., Thomas, M., and Capoid, T. (1995) Analogue computation of transient changes of intracellular free Ca^{2+} concentration with the low affinity Ca^{2+} indicator furaptra during whole-cell patch clamp recording. *Pflügers Arch.* **429,** 587–591.
47. van de Put, F. M. M. and Elliott, A. C. (1996) Imaging of intracellular calcium stores in individual permeabilized pancreatic acinar cells. *J. Biol. Chem.* **271,** 4999–5006.
48. Gerasimenko, O. V., Gerasimenko, J. V., Tepekin, A. V., and Petersen, O. H. (1995). ATP-dependent accumulation and inositol trisphosphate- or cyclic ADP-ribose mediated release of Ca^{2+} from the nuclear envelope. *Cell* **80,** 439–444.
49. Minamikawa, T., Takahashi, A., and Fujita, S. (1995) Differences in features of calcium transients between the nucleus and the cytosol in cultured heart muscle cells: Analyzed by confocal microscopy. *Cell Calcium* **17,** 165–176.
50. Cheng, H., Lederer, W. J., and Cannell, M. B. (1993) Calcium sparks—elementary events underlying excitation-contraction coupling in heart muscle. *Science* **262,** 740–744
51. Rizzuto, R., Brini, M., Murgia, M., and Pozzan, T. (1993) Microdomains with high Ca^{2+} close to IP_3-sensitive channels that are sensed by neighbouring mitochondria. *Science* **262,** 744–747.
52. Berridge, M. J. (1997) The AM and FM of calcium signalling. *Nature* **386,** 759–760.
53. Etter, E. F., Kuhn, M. A., and Fay, F. S. (1994) Detection of changes in near-membrane Ca^{2+} concentration using a novel membrane-associated Ca^{2+} indicator. *J. Biol. Chem.* **269,** 10141–10149.
54. Etter, E., Minta, A., Poenie, M., and Fay, F. S. (1996) Near membrane Ca^{2+} transients resolved using the Ca^{2+} indicator FFP18. *Proc. Natl. Acad. Sci. USA* **93,** 5368–5373.
55. Lloyd, Q. P., Kuhn, M. A., and Gay, C. V. (1995) Characterization of calcium translocation across the plasma-membrane of primary osteoblasts using a lipophilic calcium-sensitive fluorescent dye, calcium green-C-18. *J. Biol. Chem.* **270,** 22445–22451.

56. Horne, J. H. and Meyer, T. (1997) Elementary calcium release units induced by inositol trisphosphate. *Science* **276,** 1690–1692.
57. Clapham, D. E. (1995) Calcium signalling. *Cell* **80,** 259–268.
58. Neher, E. and Augustine, G. J. (1992) Calcium gradients and buffers in bovine chromaffin cells. *J. Physiol.* **450,** 273–301.
59. Williams, D. A. and Fay, F. S. (1990) Intracellular calibration of the fluorescent calcium indicator fura-2. *Cell Calcium* **11,** 75–83.
60. Poenie, M. (1990) Alteration of intracellular fura-2 fluorescence by viscosity: A simple correction. *Cell Calcium* **11,** 85–91.
61. Merrit, J. E., McCarthy, S. A., Davies, M. P. A., and Moores, K. E. (1990) Use of fluo-3 to measure Ca^{2+} in platelets and neutrophils. *Biochem. J.* **269,** 513–519.
62. Tsien, R. Y. and Harootunian, A. T. (1990) Practical design criteria for a dynamic ratio imaging system. *Cell Calcium* **11,** 93–109.
63. Moore, E. D. W., Becker, P. L., Fogarty, K. E., Williams, D. A., and Fay, F. S. (1990) Ca^{2+} imaging in single living cells: Theoretical and practical issues. *Cell Calcium* **11,** 157–179.
64. Schild, D. (1996) Laser scanning microscopy and calcium imaging. *Cell Calcium* **19,** 281–296.
65. Berridge M. J. (1997) Elementary and global aspects of calcium signalling. *J. Physiol.* **499,** 291–306.
66. Agard, A. D. (1984) Optical sectioning microscopy: Cellular architecture in three dimensions. *Annu. Rev. Biophys. Bioeng.* **13,** 191–219.
67. Monck, J. R., Oberhauser, A. F., Keating, T. J., and Fernandez, J. M. (1992) Thin-section ratiometric Ca^{2+} images obtained by optical sectioning of fura-2-loaded mast cells. *J. Cell Biol.* **116,** 745–759.
68. Juskaitis, R., Wilson T., Neil, M. A. A., and Kozubek, M. (1996) Efficient real-time confocal microscopy with white-light sources. *Nature* **383,** 804–806.
69. Zhang, Z. X., Sonek, G. J., Wei, X. B., Berns, M. W., and Tromberg, B. J. (1997) Continuous wave diode laser induced two-photon fluorescence excitation of three calcium indicators. *Jpn. J. Applied Phys.* **36,** L1598–L1600.
70. Konig, K., Simon, U., and Halbhuber, K. J. (1996) 3D resolved two photon fluorescence microscopy of living cells using a modified confocal laser scanning microscope. *Cell. Mol. Biol.* **42,** 1181–1194.
71. Toescu, E. C. and Petersen, O. H. (1994) The thapsigargin-evoked increase in $[Ca^{2+}]_i$ involves an $InsP_3$-dependent Ca^{2+} release process in pancreatic acinar cells. *Pflügers Arch.–Eur. J. Physiol.* **427,** 325–331.
72. Wilcox, R. A., Strupish, J., and Nahorski, S. R. (1995) Measurement of Ca^{2+} fluxes in permeabilised cells using $^{45}Ca^{2+}$ and fluo-3. *Methods Mol. Biol.* **41,** 215–227.
73. Sage, S. O., Reast, R., and Rink, T. J. (1990) ADP evokes biphasic Ca^{2+} influx in fura-2-loaded human platelets. *Biochem. J.* **265,** 675–680.
74. Hatae, J., Fujishiro, N., and Kawata, H. (1996) Spectroscopic properties of fluorescence dye fura-2 with various divalent cations. *Jpn. J. Physiol.* **46,** 423–429.

75. Byron, K. L. and Taylor, C. W. (1995) Vasopressin stimulation of Ca^{2+} mobilization, two bivalent cation entry pathways and Ca^{2+} efflux in A7r5 rat smooth muscle cells. *J. Physiol.* **485,** 455–468.
76. Tepikin, A. V., Voronina, S. G., Gallagher, D. V., and Petersen, O. H. (1992) Acetylcholine-evoked increase in the cytoplasmic Ca^{2+} concentration and Ca^{2+} extrusion measured simultaneously in single mouse pancreatic acinar cells. *J. Biol. Chem.* **267,** 14,073–14,076.
77. Escobar, A. L., Velez, P., Kim, A. M., Cifuentes, F., Fil, M., and Vergara, J. L. (1997) Kinetic properties of DM-nitrophen and calcium indicators: Rapid transient response to flash photolysis. *Pflügers. Arch.–Eur. J. Physiol.* **434,** 615–631.

2

Measurement of $[Ca^{2+}]_i$ in Whole Cell Suspensions Using Fura-2

Robert A. Hirst, Charlotte Harrison, Kazuyoshi Hirota, and David G. Lambert

1. Introduction

An elevation in intracellular calcium concentration ($[Ca^{2+}]_i$) acts to trigger a range of cellular events including neurotransmitter release, muscle contraction, and oocyte fertilization ***(1,2)***. The pattern of elevation in $[Ca^{2+}]_i$ and response to that elevation is dependent on the agonist and the cell type.

The introduction of the calcium-sensitive dye fura-2 ***(3)*** revolutionized the measurement of $[Ca^{2+}]_i$ in whole cell suspensions, populations of adherent cells, single cells, and in subcellular regions (*see* **ref. *4***). Fura-2 is a ratiometric dye in that when Ca^{2+} binds, the excitation spectrum shifts rightward. In the presence of Ca^{2+}, maximum fura-2 fluorescence (at 510 nm emission) is observed at a wavelength of 340 nm and in Ca^{2+}-free conditions at 380 nm. Therefore, it follows that the concentration of free intracellular Ca^{2+} is proportional to the ratio of fluorescence at 340/380. The Grynkiewicz equation describes this relationship ***(3)***.

$$[Ca^{2+}]_i \text{ (n}M) = K_d \times [(R - R_{min})/R_{max} - R)] \times \text{Sfb}$$

where K_d (for Ca^{2+} binding to fura-2 at 37°C) = 225 nM, R = 340/380 ratio, R_{max} = 340/380 ratio under Ca^{2+}-saturating conditions, R_{min} = 340/380 ratio under Ca^{2+}-free conditions, and Sfb = ratio of baseline fluorescence (380 nm) under Ca^{2+}-free and -bound conditions. The K_d for Ca^{2+} binding to fura-2 decreases with decreasing temperature.

As noted in Chapter 1, fura-2–free acid is Ca^{2+} sensitive but membrane impermeant. To effect cell loading, cells are incubated with fura-2 pentaacetoxymethyl

From: *Methods in Molecular Biology, Vol. 114: Calcium Signaling Protocols*
Edited by: D. G. Lambert

(AM) ester; this form of the dye is Ca^{2+} insensitive. Once inside the cell, esterase enzymes sequentially cleave the AM groups to leave fura-2–free acid trapped inside the cell, where it is able to bind Ca^{2+}.

In this chapter the authors will describe the use of fura-2 to measure $[Ca^{2+}]_i$ in suspension of several different cell types (*see* **ref. *4***). The technique is quite straightforward and involves incubating cells with fura-2/AM, a postincubation period to allow full de-esterification and extensive washing.

In cell suspensions, an estimate of global changes in $[Ca^{2+}]_i$ can only be made. This is useful in combination with the currently available pharmacological agents to study sources of Ca^{2+} (intracellular vs extracellular) in a given response and to screen for Ca^{2+} mobilizing drugs and receptors. However, detailed information regarding subcellular localization requires more sophisticated measurements using standard subcellular imaging (*see* Chapter 6) or confocal microscopy (*see* Chapters 4 and 5).

2. Materials

2.1. Cell Culture

1. Undifferentiated SH-SY5Y human neuroblastoma cells (gift from Dr. J. L. Beidler, Sloane Kettering Institute, Rye, NJ).
2. Culture medium for SH-SY5Y cells: minimum essential medium supplemented with 10% fetal calf serum (FCS), 2 m*M* glutamine, 100 IU/mL penicillin, 100 IU/mL streptomycin, and 2.5 µg/mL fungizone (*see* **Note 1**).
3. NG108-15 neuroblastoma X glioma hybrid cells (*see* **Note 2**).
4. Culture medium for NG108-15 cells: Dulbecco's minimum essential medium supplemented with 10% FCS, 2 m*M* glutamine, 100 IU/mL penicillin, 100 IU/mL streptomycin, 2.5 µg/mL fungizone, and HAT (hypoxanthine [0.1 m*M*], aminopterin [0.4 µ*M*], thymidine [16 µ*M*]) (*see* **Note 1**).
5. Chinese hamster ovary (CHO) cells expressing the recombinant δ opioid receptor (gift from Dr. L. A. Devi, Department of Pharmacology, New York University, NY).
6. Culture medium for CHO cells: HAMS F12 medium supplemented with 10% FCS, 100 IU/mL penicillin, 100 IU/mL streptomycin, 2.5 µg/mL fungizone, and 100 µg/mL geneticin (*see* **Notes 1** and **3**).

2.2. Buffers

1. Krebs HEPES buffer (for loading and washing): 143.3 m*M* Na^+, 4.7 m*M* K^+, 2.5 m*M* Ca^{2+}, 1.3 m*M* Mg^{2+}, 125.6 m*M* Cl^-, 25 m*M* HCO_3^-, 1.2 m*M* $H_2PO_4^-$, 1.2 m*M* SO_4^{2-}, 11.7 m*M* glucose, and 10 m*M* HEPES, pH 7.4 titrated with 10*M* NaOH.
2. Nominally Ca^{2+}-free Krebs HEPES buffer, pH 7.4, as in **item 1** omitting Ca^{2+} and adding 0.1 m*M* EGTA. This should be made in plastic beakers as glass leaches significant amounts of Ca^{2+}.
3. Low Na^+ Krebs HEPES buffer, pH 7.4, for depolarization: 43.3 m*M* Na^+, 2.5 m*M* Ca^{2+}, 1.3 m*M* Mg^{2+}, 125.6 m*M* Cl^-, 25 m*M* HCO_3^-, 1.2 m*M* $H_2PO_4^-$, 1.2 m*M*

SO_4^{2-}, 11.7 m*M* glucose, and 10 m*M* HEPES. With this buffer, 100 m*M* K^+ is added (*see* **Note 4**).

4. Cell harvest buffer: 10 m*M* HEPES-buffered 0.9% saline plus 0.05% EDTA, pH 7.4 (with 10 *M* NaOH).

2.3. General Reagents

1. Fura-2/AM (Sigma, Dorset, UK). Make up as a stock (1 m*M*) solution by dissolving in dimethylsulfoxide and storing aliquots (10 µL) at –20°C until required.
2. Triton X-100 (Sigma). Make a stock (4%) solution in warmed water.
3. EGTA (Sigma). Make a stock (90 m*M*) solution in 1 *M* NaOH.
4. Probenecid (Sigma). Dissolve at 50 mg/mL (175 m*M*) stock in 1 *M* NaOH. Use at 2.5 m*M* in buffer (*see* **Note 5**).

3. Methods

3.1. Tissue Culture and Monolayer Harvesting

1. Maintain confluent monolayers (75 cm^2) of cells in the appropriate media.
2. Split one flask of confluent cells using trypsin (0.5g/L)-EDTA (2g/L, 5 mL) solution as supplied (*see* **Note 1**) into nine other flasks each containing 20 mL of supplemented media. After 2 d of incubation (37°C, 5% CO_2 incubator), remove the media and replace with 25 mL of fresh supplemented media.
3. Culture cells (feed 24 h before use with fresh medium) until confluent (use cells up to 3 d post confluency).
4. On the day of the experiment, remove medium and add 5 mL of harvest buffer to cell monolayer.
5. Remove 5 mL of harvest buffer immediately, and add a further 5 mL of fresh harvest buffer and incubate at 37°C for ~5 min.
6. Gently tap the side of the flask to dislodge the adherent cell monolayer.
7. When all the cells are in suspension, transfer it to a centrifuge tube. Rinse the cells out of the flask by adding approx 15 mL of experimental buffer. Transfer this to the centrifuge tube.
8. Sediment at 1000*g* in a low-speed centrifuge for 3 min.
9. Remove supernatant and resuspend the pellet into 30 mL of fresh experimental buffer. Invert the tube three times and resediment at 500*g* for 3 min.
10. Repeat **step 9** once more, and finally resuspend the pellet in 3 mL of experimental buffer.

3.2. Fura-2 Loading and Measurement of Intracellular Calcium

Optimal fura-2 loading time and de-esterification time may vary depending on the cell type used, and hence it is recommended that these times should be adjusted accordingly. The protocol used by the authors in a range of cell types is as follows:

1. Incubate cell suspensions with 3 µ*M* of fura-2/AM in 3 mL (10 µL of 1 m*M* fura-2/AM) for 30 min at 37°C in the dark.

2. Sediment the cells (500*g* for 2 min) and resuspend in 30 mL of Krebs/HEPES buffer.
3. Incubate a further 15 min at room temperature in the dark to allow for de-esterification of the fura-2/AM.
4. Sediment the cells (500*g* for 2 min) and resuspend in 30 mL of Krebs/HEPES buffer twice more.
5. Sediment (500*g* for 2 min) and resuspend in buffer allowing 2 mL per determination (*see* **Note 6**).
6. Place cell suspensions (2 mL) in a quartz cuvet containing a magnetic stirrer and place in the cuvet holder, which is maintained at 37°C with a water jacket.
7. Simultaneously monitor and, if possible, display 340 and 380 excitation intensity (at 510 emission). Signal sampling should be set according to the kinetics of the changes in $[Ca^{2+}]_i$; the authors routinely make one ratio measurement per second (*see* **Note 7**).
8. Following establishment of stable 340 and 380 recordings, add compounds to be tested (*see* **Note 8**).
9. Maintain stock of loaded cells on ice (*see* **Note 9**).
10. Calibrate the fluorescence signal as follows (*see* **Note 10**):
    a. Add 0.1% Triton X-100 to the cuvet to produce cell lysis and liberate fura-2 into a Ca^{2+}-containing buffer. Under these conditions, fura-2 saturates with Ca^{2+} and maximum fluorescence ratio (R_{max}) is determined (*see* **Note 11**).
    b. 4.5 m*M* EGTA, pH >8.0, to chelate Ca^{2+} and determine minimum fluorescence ratio (R_{min}) (*see* **Note 12**).
    c. Substitute R_{max}, R_{min}, and the derived Sfb along with measured *R* values from cell suspensions into the Grynkiewicz equation ***(3)*** and estimate $[Ca^{2+}]_i$. This can be accomplished using a spreadsheet type program, although the authors use FLDM software associated with the fluorimeter (*see* **Note 7**).

3.3. Examples of $[Ca^{2+}]_i$ Measurements Made in Cell Suspensions

3.3.1. Carbachol Stimulation in SH-SY5Y Cells

SH-SY5Y cells express a homogenous population of M_3 muscarinic receptors that are coupled to phospholipase C and increased $[Ca^{2+}]_i$. The authors have shown that this $[Ca^{2+}]_i$ is biphasic, with a peak phase mediated by release from intracellular stores and a plateau phase resulting from Ca^{2+} entry across the plasma membrane ***(4,5)***. A typical experiment is described below:

1. Cells are harvested (*see* **Subheading 3.1., steps 4–10**).
2. Suspensions are loaded with fura-2 as described in **Subheading 3.2.**
3. Following de-esterification and washing, cells are placed into a cuvet and 340/380 nm fluorescence monitored.
4. Stocks of loaded cells are kept on ice.
5. As can be seen in **Fig. 1**, the response to 10 μ*M* carbachol was biphasic (**Fig. 1A**). Also shown for comparison is a typical 340/380 nm recording (**Fig. 1B**) and the derived 340/380 ratio (**Fig. 1C**).

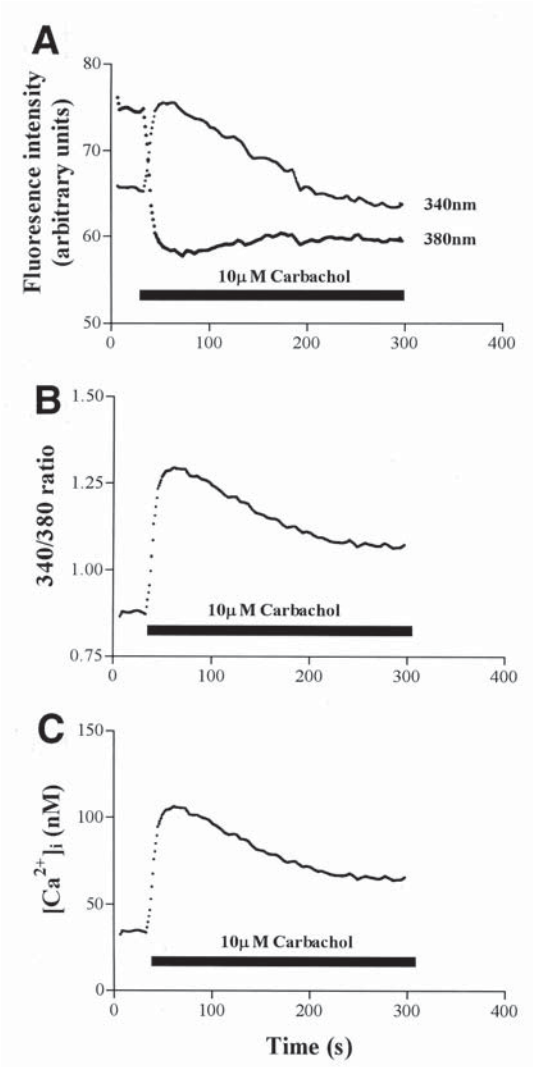

Fig. 1. Carbachol increases $[Ca^{2+}]_i$ in suspensions of SH-SY5Y cells. **(A)** Emission at 340 and 380 nm excitation. Note the antiparallel movement of both traces. **(B)** Derived 340/380 ratio and **(C)** $[Ca^{2+}]_i$ after calibration. In these studies R_{max}, R_{min}, and Sfb were 4.61, 0.64, and 2.39, respectively. Autofluorescence at 340 and 380 were 1.67 and 3.18 arbitrary units $\lesssim$2% of cell signal.

3.3.2. K^+ Stimulation in NG108-15 Cells

The authors have previously reported a nifedipine sensitive increase in $[Ca^{2+}]_i$ in NG108-15 cells in response to depolarization with high K^+ ***(6)***. A typical experiment is described next:

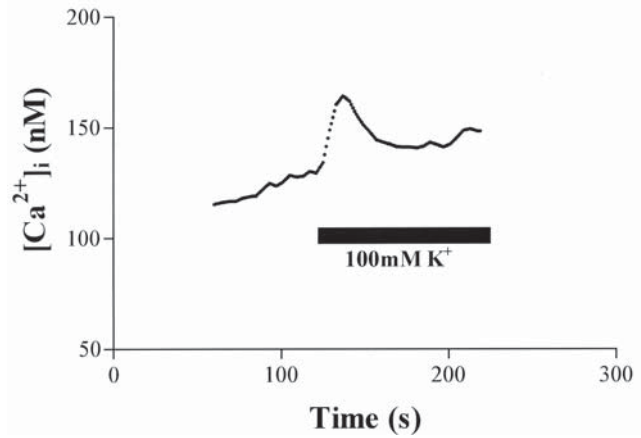

Fig. 2. K^+ depolarization (100 m*M*, bar) of NG108-15 cells results in a monophasic increase in $[Ca^{2+}]_i$. Representative trace modified from **ref. *6***.

1. Cells are harvested (*see* **Subheading 3.1.**, **steps 4–10**).
2. Suspensions are loaded with fura-2 as described in **Subheading 3.2.**
3. Following de-esterification and washing in low Na^+ buffer (**Subheading 2.2.**, **item 3**), cells are placed into a cuvet and 340/380 nm fluorescence monitored.
4. Cells are challenged with 100 m*M* K^+.
5. Stocks of loaded cells are kept on ice
6. As can be seen in **Fig. 2**, depolarization with K^+ produces a monophasic increase in $[Ca^{2+}]_i$. This response is mediated by L-type, voltage-sensitive Ca^{2+} channels ***(6)***.

3.3.3. D-[Pen^{2,5}]enkephalin and Adenosine Triphosphate (ATP) Stimulation in CHO Cells

CHO cells have been shown to express low levels of the multidrug-resistance efflux pump, P-glycoprotein ***(7)***. It is possible that this pump is responsible for extrusion of fura-2 from the cell and, hence, increasing baseline measurements. Probenecid is an organic anion transport inhibitor, originally developed to prevent excretion of penicillin from the kidney, that has been shown to block efflux of fura-2 ***(7,8)***. The authors have noted that with the use of CHO cells expressing recombinant opioid receptors (and endogenous purinergic receptors ***[9]***), high rates of fura-2 leakage that can be reduced by inclusion of probenecid (**Fig. 3A**). A typical experiment is described below.

1. Cells are harvested (*see* **Subheading 3.1.**, **steps 4–10**).
2. CHO cell suspensions are loaded, washed, and then de-esterified in the presence of 2.5 m*M* probenecid as noted in **Subheading 3.2.**
3. Cells are challenged with either 1 μ*M* DPDPE or 100 μ*M* ATP.
4. Between determinations, the stock of loaded cells is kept on ice.

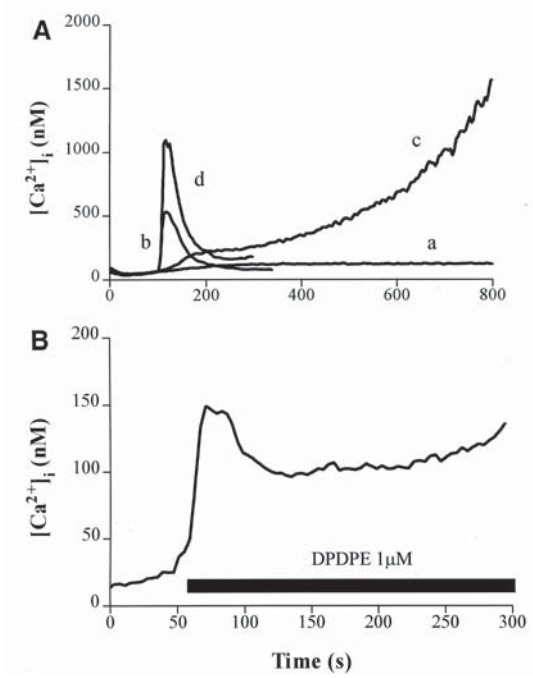

Fig. 3. **(A)** Representative time course showing effects of 2.5 m*M* probenecid in CHO cells expressing the recombinant δ opioid receptor. Probenecid reduced fura-2 leakage in unstimulated cells (A) when compared to unstimulated control (C) and reduced the peak and plateau phases of 100 μ*M* ATP-stimulated (B) when compared to stimulated control (D). **(B)** 1 μ*M* DPDPE increased $[Ca^{2+}]_i$ in CHO cells expressing the recombinant δ opioid receptor. Probenecid was not included in this experiment.

5. As can be clearly seen in **Fig. 3A**, fura-2 leakage was significantly reduced in the presence of probenecid. However, the peak phase response to ATP was also reduced. Careful characterization of the effects of probenecid on the signaling process under study should always be made (*see* **Note 5**).

4. Notes

1. All tissue culture media and reagents are supplied by Life Technologies, Paisley, Scotland.
2. From European Collection of Animal Cell Cultures (web site http://www.biotech.ist.unige.it/cldb/cname-dh.html).
3. Where geneticin (G418) or similar is included in cells expressing recombinant receptors and so on as a selection agent, only the stock cultures should be treated. Experimental cultures should be free of selection medium as G418 may inhibit phospholipase C–mediated responses.

4. For varying levels of K^+, adjust Na^+ accordingly.
5. Probenecid is insoluble at millimolar concentrations in Krebs HEPES buffer. Therefore, a stock solution was made at 50 mg/mL (175 m*M*) in 1 *M* NaOH. This was then diluted in Krebs HEPES buffer prior to addition of $CaCl_2$ (2.5 m*M*). The Krebs HEPES buffer containing probenecid (NaOH) was set at pH 7.4 by the addition of HCl (10 *M*, ~100 µL). Caution should be used when using probenecid to reduce fura-2 leakage as the authors have shown that agonist-induced increases in $[Ca^{2+}]_i$ could be inhibited by this agent (*see* **Fig. 2**).
6. One confluent 75-cm^2 flask of SH-SY5Y cells is sufficient to give five determinations (i.e., resuspend in 10 mL of buffer). For larger numbers of determinations, load more flasks. However, remember that as the loaded cells stand they leak fura-2, leading to a time-dependent increase in basal. This can be overcome to some extent by sedimenting and resuspending aliquots of the loaded suspension periodically. Some cells leak fura-2 more than others, notably CHO cells *(see below)*.
7. The authors routinely use a Perkin-Elmer LS50B fluorimeter (Beaconsfield, UK) equipped with the software FLDM. Files are saved to disk and 340/380 ratios can be converted to $[Ca^{2+}]_i$ following calibration. It is always advisable to be familiar with the software that controls the configuration and experimental settings of the fluorimeter. Different software packages are available, and for information and troubleshooting the reader is advised to consult the software supplier.
8. For drugs make up 100 times more concentrated so that when 20 µL is added to 2 mL of buffer + cells, the desired concentration is achieved. Additions are made as swiftly as possible to avoid light entering the fluorimeter. All agents used should be tested for fluorescence properties. This can be accomplished by adding to a cuvet containing nominally Ca^{2+}-free buffer (containing several micromolar Ca^{2+}) and fura-2–free acid (0.5 µ*M*).
9. The authors have noted that de-esterified cells that extrude fura-2 should be maintained on ice between experiments as this reduces the loss of fura-2. In addition, care should be taken to ensure that fura-2–loaded cells are used for experiments immediately after de-esterification.
10. For cells loaded from a single batch of cells, the authors make a single calibration (i.e., they do not calibrate each cuvet of cells), normally the last cuvet used. This needs to be checked for all cell lines and they recommend a comparison of individually calibrated data with all data calibrated from the first and last run of the batch.
11. Addition of Triton X-100 causes complete cell lysis and an increase in 340 and a decrease in 380 nm fluorescence. A globular residue remains in the cuvet, and, therefore, the reusable quartz cuvet should be thoroughly rinsed between experiments using deionized water.
12. Autofluorescence is an important issue for many cell types. This is the fluorescence produced from unloaded cells and can be determined in two ways. First, place an aliquot of unloaded cells into the fluorimeter and measure the fluorescence at 340 and 380 nm (FLDM software has this capability). The main drawback with this method is that the density of unloaded cells should be identical to

the density of cells used for Ca^{2+} measurements. The second method is to add 0.1 m*M* Mn^{2+} to the lysed cell suspension after determination of R_{min}. In this protocol, the quenching properties of Mn^{2+} are utilized. In the authors' studies using SH-SY5Y, NG108-15, and CHO cells, they have found the autofluorescence to be negligible when compared to the signal from loaded cells and, therefore, do not routinely subtract autofluorescence (e.g., *see* **Fig. 1**). However, they recommend that whenever using a new cell line, autofluorescence should be assessed.

References

1. Clapham, D. (1995) Calcium signalling. *Cell* **80,** 259–268.
2. Berridge, M. J. (1993) Inositol trisphosphate and Ca^{2+} signalling. *Nature* **361,** 315–325.
3. Grynkiewicz, G., Poenie, M., and Tsien, R. Y. (1985) A new generation of Ca^{2+} indicators with greatly improved fluorescence properties. *J. Biol. Chem.* **260,** 3440–3449.
4. Lambert, D. G., Wojcikiewicz, R. J. H., Safrany, S. T., Whitham, E. M., and Nahorski, S. R. (1992) Muscarinic receptors, phosphoinositide metabolism and intracellular calcium in neuronal cells. *Prog. Neuro-Psychopharmacol. Biol. Psychiat.* **16,** 253–270.
5. Cobbold, P. H. and Rink, R. J. (1987) Fluorescence and bioluminescence measurement of cytoplasmic free calcium. *Biochem. J.* **248,** 313–328.
6. Hirota, K. and Lambert, D. G. (1997) A comparative study of L-type voltage sensitive Ca^{2+} channels in rat brain regions and cultured neuronal cells. *Neurosci. Lett.* **223,** 169–172.
7. Brezden, C. B., Hedley, D. W., and Rauth, A. M. (1994) Constitutive expression of P-glycoprotein as a determinant of loading with fluorescent calcium probes. *Cytometry* **17,** 343–348.
8. Edelman, J. L., Kajimura, M., Woldemussie, E., and Sachs, G. (1994) Differential effects of carbachol on calcium entry and release in CHO cells expressing the m3 muscarinic receptor. *Cell Calcium* **16,** 181–193.
9. Iredale, P. A. and Hill, S. J. (1993) Increases in intracellular calcium via activation of an endogenous P(2)-purinoceptor in cultured CHO-k1 cells. *Brit. J. Pharmacol.* **110,** 1305–1310.

3

Measurement of $[Ca^{2+}]_i$ in Cell Suspensions Using Indo-1

Adriaan Nelemans

1. Introduction

Intracellular calcium, in particular the cytosolic free ionized calcium concentration $[Ca^{2+}]_i$, is tightly regulated under physiological conditions. Stimulation of receptors, belonging to almost all the classes so far described, will result in changes in $[Ca^{2+}]_i$. These changes might be directly induced by either Ca^{2+}-influx or Ca^{2+}-mobilization from intracellular stores, or indirectly by a number of other mechanisms ***(1–4)***. The development of fluorescent indicators of free $[Ca^{2+}]$ that could be loaded into intact cells has contributed enormously to the understanding of cellular Ca^{2+} homeostasis, especially dyes that respond to Ca^{2+} with shifts of excitation or emission spectra ***(5–7)***. By measuring at two selected wavelengths (either dual emission or dual excitation), it is possible to calculate the proportion of dye in the Ca^{2+}-bound and Ca^{2+}-free forms.

This ion-dependent spectral shift of Ca^{2+} indicators allows them to be used ratiometrically, making Ca^{2+} measurement essentially independent of dye loading, cellular distribution, and photobleaching. Indo-1 shows a shift in its emission maximum on Ca^{2+} binding. It is less suitable for imaging $[Ca^{2+}]_i$ by fluorescence microscopy, and is more often used for single-cell photometer measurements, flow cytometry, and studies in a fluorometer using cells in monolayer or in suspension ***(7,8)***. Further information on the technical and practical aspects of ion measurements using fluorescent indicators can be obtained in Chapter 1 and in **refs. *7–11***.

The method described in this chapter is generally applicable to measurements of intracellular $[Ca^{2+}]$ in cell suspensions, e.g., for a variety of blood cells, but it is based on the author's experience with the smooth muscle cell line DDT_1 MF-2. A number of cellular mechanisms have been investigated

From: *Methods in Molecular Biology, Vol. 114: Calcium Signaling Protocols*
Edited by: D. G. Lambert

using fluorometric indo-1 detection with this method at various levels in the signal transduction cascade. These include (1) induction of intracellular [Ca^{2+}] changes after stimulation of different types of receptors such as α-adrenergic, purinergic, and histaminergic ***(12–15)***; and (2) the effects of arachidonic acid and inhibition of protein kinase C on Ca^{2+} influx ***(16,17)***. The relative contributions of Ca^{2+} influx and Ca^{2+} mobilization to the intracellular changes are determined using La^{3+}- or Ca^{2+}-free extracellular solution ***(16-19)***. H_1 histaminergic and P_2 purinergic receptors mobilize Ca^{2+} from separate specific intracellular stores ***(19)*** and use this Ca^{2+} together with inositol tetrakisphosphate to initiate K^+ efflux ***(18)***. The alterations in receptor-induced changes in $[Ca^{2+}]_i$ were established on the production of other second messengers ***(14,17,20)***.

2. Materials

1. The acetoxymethyl (AM) ester of the fluorescent indicator indo-1 can be obtained from a number of suppliers in varying packaging sizes. In the author's studies on DDT_1 MF-2 cells, indo-1/AM from Molecular Probes (Eugene, OR) was used (*see* **Notes 1** and **2**).
2. Cell incubation medium DMEM/FCS: Dulbecco's modified essential medium (DMEM) supplemented with 7 m*M* $NaHCO_3$, 10 m*M* HEPES, pH 7.2, 10% fetal calf serum.
3. Buffered salt solution (BSS): 145 m*M* NaCl, 5 m*M* KCl, 0.5 m*M* $MgSO_4$, 1 m*M* $CaCl_2$, 10 m*M* glucose, 10 m*M* HEPES, pH 7.4.
4. Solutions used for calibration: Triton® X-100 1% aqueous solution (vol/vol); 500 m*M* EGTA, pH 8.0; 1*M* $MnCl_2$.

3. Methods

1. Prepare stock solution of 1 m*M* indo-1/AM in dry dimethylsulfoxide (DMSO), mix well to dissolve, distribute into tubes in aliquots sufficient for a single experiment, and freeze at –20°C (*see* **Notes 3–7**).
2. Prepare a stock cell suspension of 2×10^5 cells/mL in DMEM containing 10% FCS (*see* **Notes 8** and **9**).
3. Prepare fresh indicator solution in DMEM/FCS at a final concentration of 2 μ*M* indo-1/AM just before addition and mix well. Avoid exposure to light as much as possible by wrapping the tube or flask with aluminium foil (*see* **Notes 10** and **11**).
4. Preincubate the cells in DMEM/FCS for 15 min at 37°C (*see* **Note 12**).
5. Take 10 mL of this solution and centrifuge for 5–10 min at 1000*g* (*see* **Note 13**).
6. Resuspend the cell pellet in 2 mL of DMEM/FCS, containing 2 μ*M* indo-1/AM (*see* **Note 14**).
7. Incubate the cells for 45 min at 37°C, preferably in an orbital shaker (100 rpm) (*see* **Notes 15–17**).
8. Wash the cells twice, by centrifugation and resuspension in 2 mL of BSS (*see* **Notes 18–21**).
9. Check for homogeneous cytosolic indo-1 labeling (*see* **Notes 22** and **23**).

10. The cell suspension can now be transferred to a cuvet for fluorometric measurements (*see* **Note 24**).
11. The cell suspension in the cuvet should be continuously stirred, and if applicable the temperature of the solution in the cuvet should be controlled (*see* **Notes 25** and **26**).
12. Most of the commercially available spectrofluorometers have preset parameters for Ca^{2+} measurements with indo-1. However, the following standard settings can be used: excitation wavelength, 325; emission wavelength 1, 405 (Ca^{2+}-bound dye); emission wavelength 2, 485 (Ca^{2+}-free dye); bandwidth filters 2–10 nm (*see* **Note 27**).
13. The appropriate experiments can now be performed. The fluorescence ratio R = Ca^{2+}-bound/Ca^{2+}-free should be measured (*see* **Note 28**).
14. Calibrate the fluorescence signal at the end of the experiment as follows. Permeabilize the cells by addition of 30 µL of a 1% Triton X-100 aqueous solution (vol/vol) to cell suspension in the cuvet. Cell lysis may take several minutes. When a stable maximal fluorescence level is obtained, the ratio value under saturating conditions R_{max} is determined. The value under Ca^{2+}-free conditions R_{min} is obtained after addition of 200 µL of EGTA solution (500 m*M*, pH 8). After a stable minimal response (within 1 min), background levels are obtained by addition of 30 µL of $MnCl_2$ (1*M*) (*see* **Notes 29–31**).
15. Calculate the intracellular $[Ca^{2+}]$ according to the following equation:

$$[Ca^{2+}] = K_d \times [(R - R_{min})/(R_{max} - R)] \times (S_{f2}/S_{b2})$$

The term (S_{f2}/S_{b2}) is the signal ratio of fluorescence measured at emission wavelength 2 in the absence of Ca^{2+} and at Ca^{2+} saturation. The dissociation constant of indo-1 is K_d = 250 n*M* as determined in vitro at 37°C ***(5)*** (*see* **Notes 32** and **33**).

4. Notes

1. The use of small pack sizes is recommended to minimize the chance of decomposition.
2. Some companies offer stock solutions of fluorescent dyes in aqueous-free DMSO.
3. AM ester derivatives of Ca^{2+} indicators are not soluble in aqueous solutions.
4. It is advisable to prepare concentrated stock solutions so that minimal amounts of DMSO are present in the loading solution.
5. Stock solutions should be extensively mixed, because remaining undissolved particles will facilitate intracellular compartmentalization of the dye.
6. To avoid indo-1/AM hydrolysis, the stock solution must be kept anhydrous, and aliquots sufficient for a single experiment should be stored desiccated at –20°C.
7. Exposure of indicator containing solutions to light should be avoided.
8. If cells are not grown in suspension, a cell suspension can be obtained by either scraping off the cells from cell monolayers with a rubber policeman (as is the case for DDT_1 MF-2 cells), or by detachment from the monolayer using Trypsin/EDTA treatment. Cells growing in monolayer are washed with a Ca^{2+}-free physiological salt solution and subsequently treated with a solution of Trypsin 1:250,

0.05% (w/v) and EDTA, 0.02% (w/v) in physiological salt solution. Immediately aspirate this mixture and incubate the cells in monolayer at 37°C for 1–5 min depending on the cell type. Cells are resuspended with at least 5 mL of DMEM containing 10% FCS.

9. The number of cells/mL can vary depending on the type of cells used. For lymphocytes and blood platelets, most often minimal concentrations of 10^7 cells/mL are used.
10. As an alternative to DMEM/FCS as a loading solution, most other appropriate physiological buffer solutions can be used, although the presence of 2% bovine serum albumin (w/w) is mandatory.
11. For each cell type, optimal parameters should be assessed for Ca^{2+} indicator dye loading, regarding dye concentration, incubation temperature, and time of incubation (*see* **Notes 14–17**).
12. This pre-incubation allows the cells to stabilize and to equilibrate their ion gradients.
13. This is the correct centrifugation procedure for DDT_1 MF-2 cells. It can also probably be used for other types of cells. Integrity of the cells should be tested after centrifugation, e.g., by trypan blue dye exclusion assay.
14. Usually loading solutions are used with dye concentrations in the range from 1 to 10 μ*M* indo-1/AM. This concentration should be kept as low as possible to avoid artifacts from overloading, such as incomplete hydrolysis, fluorophore quenching, extreme intracellular Ca^{2+} buffering capacity, or toxicity of formaldehyde produced on AM ester hydrolysis.
15. The time of loading must be kept as short as possible. Optimal incubation time is variable between 15 and 120 min for different cell types and incubation conditions. For experiments with DDT_1 MF-2 cells, 45 min is convenient.
16. Accumulation of the dye proceeds rapidly at 37°C, but longer incubation at lower temperature (20–30°C) can reduce redistribution of the dye from the cytosol to various intracellular organelles.
17. Loading is often facilitated by dissolving the AM ester in a solution of the nonionic detergent Pluronic® F-127 in DMSO (20% [w/v]) (*see* **ref. *7***).
18. The procedure to wash away remaining extracellular indo-1/AM after the incubation period will take 20–30 min, which is also necessary to obtain complete hydrolysis of the intracellular esterified dye.
19. Fluorescence spectra before and after esterification are informative not only to follow the process of ester hydrolysis, but also regarding the purity of the dye preparation. The unesterified indo-1/AM has maxima for excitation and emission at 361 and 479 nm, respectively ***(7,8)***.
20. Emission spectra (350–650 nm) can be obtained (at a fixed excitation wavelength, e.g., 325 or 355 nm) with increasing levels of Ca^{2+} or with a saturating concentration of Ca^{2+} obtainable with 1 m*M* excess $CaCl_2$.
21. Assessment of the completeness of AM ester hydrolysis can be achieved by release of indo-1 from the cell by digitonin in Mn^{2+}-containing buffer, which will quench almost all the fluorescence of the indicator. Although any BSS can be used, BSS containing 145 m*M* NaCl, 5 m*M* KCl, 0.5 m*M* $MgSO_4$, 1 m*M* $CaCl_2$,

10 m*M* glucose, 10 m*M* HEPES, pH 7.0, is preferred ***(21)***. Autofluorescence is reduced under these conditions in DDT_1 MF-2 cells.

22. After establishment of the optimal parameters, a uniformly labeled cytosol should be observed by fluorescence microscopy. Compartmentalization of indo-1 is less likely to occur than for other fluorescent Ca^{2+} indicators ***(8)***.
23. Where compartmentalized dye remains, the experimental data can still be used, by choosing the appropriate calibration procedures. Interaction of digitonin with cholesterol releases only cytosolic Ca^{2+}, since most of the cellular cholesterol is present in the plasma membrane (*see* **Note 30**).
24. A cell suspension of 2 mL is sufficient to obtain an undisturbed errorless signal in a standard fluorometric quartz cuvet.
25. Thermostatic control of the cuvet holder enables control of temperatures at which intracellular responses occur. Depending on the study, working at 37°C as the physiological temperature is not always ideal (compared with, e.g., 22°C). Lower temperatures will minimize indo-1 leakage from the cells. With respect to the physiological increases in internal Ca^{2+} concentration induced by receptor stimulation, these develop slower at 22°C in DDT_1 MF-2 cells, but responses are of similar magnitude at both temperatures ***(15)***.
26. If despite a uniformly indo-1–labeled cytosol the cells consistently respond to external stimuli with a small increases in internal Ca^{2+} concentration or do not respond at all, it is likely that too much indicator has accumulated in the cell. This will result in a lower signal owing to quenching of the fluorescence signal and/or buffering inappropriate amounts of intracellular Ca^{2+}. Re-establish the optimal indo-1/AM loading procedure.
27. Optimal parameters vary slightly between different setups and experimental conditions. Optimal parameters can be obtained from excitation and emission spectra. For measuring intracellular Ca^{2+} changes in DDT_1 MF-2 cells with the equipment as described ***(18)***, these parameters were, e.g., 325 nm for excitation and 400 and 480 nm for emission wavelengths, with a bandwidth filter of 10 nm.
28. Many receptor ligands or other drugs have fluorescent properties, and can therefore interfere with fluorimetric measurements. Fluorescence spectra should be determined.
29. A final concentration of 0.015% Triton X-100 is sufficient to lyse DDT_1 MF-2 cell suspensions. For other cell types, other optimum concentrations may be necessary. The optimum concentrations should be determined e.g., by Trypan blue exclusion.
30. Alternatively, detergents other than Triton X-100 with minimum light scattering properties can be used. Digitonin (10–100 µg/mL), which primarily affects the plasma membrane, is often used to exclude compartmentalization errors (*see* **Note 23**).
31. R_{max} must be determined when the dye is saturated with calcium ($[Ca^{2+}] > 1$ m*M*). If the experiment is performed in a buffered solution with less Ca^{2+}, $CaCl_2$ must be added at this stage.
32. The background or autofluorescence values obtained after addition of Mn^{2+} must be subtracted from the fluorescence intensities before calculation of the ratio.
33. The K_d value at 22°C for indo-1 is 230 n*M* ***(7)***.

References

1. Himpens, B., Missiaen, L., and Casteels, R. (1995) Ca^{2+} homeostasis in vascular smooth muscle. *J. Vascular Res.* **32,** 207–219.
2. Thomas, A. P., Bird, G. S., Hajnoczky, G., Robb-Gaspers, L. D., and Putney, J. W., Jr. (1996) Spatial and temporal aspects of cellular calcium signalling. *FASEB J.* **10,** 1505–1517.
3. Carl, A., Lee, H. K., and Sanders, K. M. (1996) Regulation of ion channels in smooth muscles by calcium. *Am. J. Physiol.* **271,** C9–34.
4. Cheng, H., Lederer, M. R., Xiao, R. P., Gomez, A. M., Zhou, Y. Y., Ziman, B., Spurgeon, H., Lakatta, E. G., and Lederer, W. J. (1996) Excitation-contraction coupling in heart: New insights from Ca^{2+} sparks. *Cell Calcium* **20,** 129–140.
5. Grynkiewicz, G., Poenie, M., and Tsien R. W. (1985) A new generation of Ca^{2+} indicators with greatly improved fluorescence properties. *J. Biol. Chem.* **260,** 3440–3450.
6. Lipscombe, D., Madison, D. V., Poenie, M., Reuter, H., Tsien, R. W., and Tsien, R. Y. (1988) Imaging of cytosolic Ca^{2+} transients arising from Ca^{2+} stores and Ca^{2+} channels in sympathetic neurons. *Neuron* **1,** 355–365.
7. Haugland, R. P. (1996) *Handbook of fluorescent probes and research chemicals.* 6th ed. Molecular Probes Inc., Eugene, OR.
8. Thomas, A. P. and Delaville, F. (1991) The use of fluorescent indicators for measurements of cytosolic-free calcium concentration in cell populations and single cells, in *Cellular Calcium: A Practical Approach* (McCormack, J. G. and Cobbold, P. H., eds.), IRL, Oxford, UK, pp. 1–54.
9. Rawlings, S. R., Theler, J. M., and Schlegel, W. (1994) Monitoring of receptor-mediated changes in intracellular calcium at the cellular and subcellular level by microfluorimetry and imaging, in *Methods in Enzymology*, vol. 238 (Iyengar, R., ed.), Academic, San Diego, pp. 295–308.
10. Demaurex, N., Rawlings, S. R., Krause, K. H., Jaconi, M. E. E., Lew, P. D., and Schlegel, W. (1994) Combination of microfluorimetric monitoring of cytosolic calcium and pH with patch clamp electrophysiological recordings in neutrophil granulocytes, in *Methods in Enzymology*, vol. 238 (Iyengar, R., ed.), Academic, San Diego, pp. 308–320.
11. Silver, R. A., Whitaker, M., and Bolsover, S. R. (1992) Intracellular ion imaging using fluorescent dyes: Artefacts and limits to resolution. *Pflugers Arch. Eur. J. Physiol.* **420,** 595–602.
12. Nelemans, A., Hoiting, B., Molleman, A., Duin, M., and den Hertog, A. (1990) alpha-Adrenoceptor regulation of inositol phosphates, internal calcium and membrane current in DDT_1 MF-2 smooth muscle cells. *Eur. J. Pharmacol.* **189,** 41–49.
13. Hoiting, B., Molleman, A., Duin, M., den Hertog, A., and Nelemans, A. (1990) P_2 purinoceptor-mediated inositol phosphate formation in relation to cytoplasmic calcium in DDT_1 MF-2 smooth muscle cells. *Eur. J. Pharmacol.* **189,** 31–39.
14. Sipma, H., Duin, M., Hoiting, B., den Hertog, A., and Nelemans, A. (1995) Regulation of histamine- and UTP-induced increases in $Ins(1,4,5)P_3$, $Ins(1,3,4,5)P_4$ and Ca^{2+} by cyclic AMP in DDT_1 MF-2 cells. *Br. J. Pharmacol.* **114,** 383–390.

15. Sipma, H., Fredholm, B. B., den Hertog, A., and Nelemans, A. (1996) Plasma membrane Ca^{2+} pumping plays a prominent role in adenosine A_1 receptor mediated changes in $[Ca^{2+}]_i$ in DDT_1 MF-2 cells. *Eur. J. Pharmacol.* **306,** 187–194.
16. van der Zee, L., Nelemans, A., and den Hertog, A. (1995) Arachidonic acid is functioning as second messenger in activating the Ca^{2+} entry process on H_1-histaminoceptor stimulation in DDT_1 MF-2 cells. *Biochem. J.* **305,** 859–864.
17. Sipma, H., van der Zee, L., van den Akker, J., den Hertog, A., and Nelemans, A. (1996) The PKC inhibitor GF109203X releases Ca^{2+} from internal stores and provokes Ca^{2+} entry in DDT_1 MF-2 cells. *Br. J. Pharmacol.* **119,** 730–736.
18. Molleman, A., Hoiting, B., Duin, M., van den Akker, J., Nelemans, A., and den Hertog, A. (1991) Potassium channels regulated by Ins(1,3,4,5)-tetrakisphosphate and internal calcium in DDT_1 MF-2 smooth muscle cells. *J. Biol. Chem.* **266,** 5658–5663.
19. den Hertog, A., Hoiting, B., Molleman, A., van den Akker, J., Duin, M., and Nelemans, A. (1992) Calcium release from separate receptor-specific intracellular stores induced by histamine and ATP in a hamster cell line. *J. Physiol. (Lond.)* **454,** 591–607.
20. Sipma, H., den Hertog, A., and Nelemans, A. (1995) Ca^{2+} Dependent and independent mechanisms of cyclic-AMP reduction mediated by bradykinin B_2 receptors. *Br. J. Pharmacol.* **115,** 937–944.
21. Hesketh, T. R., Smith, G. A., Moore, J. P., Taylor, M. V., and Metcalfe, J. C. (1983) Free cytoplasmic calcium concentration and mitogenic stimulation of lymphocytes. *J. Biol. Chem.* **258,** 4876–4882.

4

Confocal Microscopy

Theory and Applications

Laura C. Mongan, Joanne Gormally, Andrew R. D. Hubbard, Christopher d'Lacey, and Colin D. Ockleford

1. Introduction

This chapter will attempt to provide an overview of the theory and details of some basic applications of the technique of confocal microscopy. Since this is intended to be a general introduction to the possibilities available, it is not appropriate to include detailed descriptions of the specialized techniques used in physiological studies leading to the imaging and measurement of Ca^{2+}-containing samples. Instead, the reader is referred to Chapter 5 in this volume that deals specifically with these imaging techniques. In this chapter our aim is to define the properties of the instrumentation and to give a few examples of basic preparation techniques for defining structure and localizing target molecules in cells. As one example, however, we will refer to our simple imaging technique for studying the three-dimensional (3D) microscopic distribution of calcium during skeletogenesis in the mammalian fetus.

1.1. Theory

Confocal microscopy is well described by its complete title: confocal laser-scanning microscopy (CLSM). This describes the component elements of the technique, which, when combined, result in the generation of images with resolution approaching the theoretical diffraction-limited maximum. To describe the theory of modern confocal microscopy, it is necessary to discuss each of these technologies independently. Then accessory equipment required will be briefly discussed, along with the latest developments in this field.

From: *Methods in Molecular Biology, Vol. 114: Calcium Signaling Protocols*
Edited by: D. G. Lambert

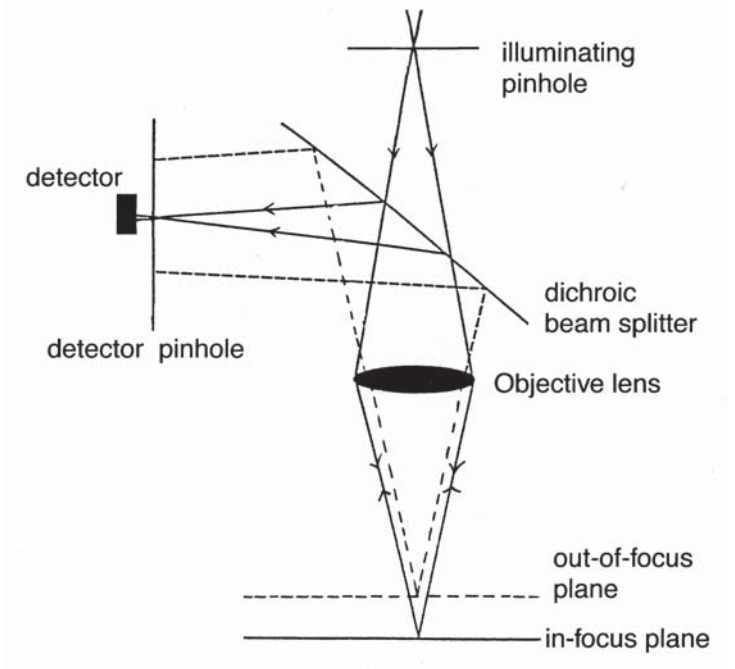

Fig. 1. Schematic representation of the fundamental principles of confocal optics. For simplicity, only extraneous light reflected from above the focal plane (dotted line) is shown in this diagram. The principle of exclusion of such extraneous light is identical for light originating from below the focal plane.

1.1.1. Confocal Optics

The limitations to the clarity of the image achievable by the best standard light microscopes stem from at least two fundamental problems: those of light scatter, and extraneous light being detected from above and below the focal plane. The phenomenon known as scatter occurs when randomly deflected light deviates many times before it finally impinges on the detector. When these problems are combined, a loss of sharpness, or blurring, of the image results. The confocal principle ***(1)***, however, neatly addresses both these flaws.

The principle of confocal optics depends on the presence of two pinhole apertures in the light path. One pinhole aperture produces a sharp, intense point of illumination, the intensity of which falls off either side of a chosen depth within the specimen. The second pinhole serves to process the transmitted/fluorescent/reflected light, the type dependent on the system in use, and allows only light information from that illuminated point to reach the detectors (**Fig. 1**).

This principle can be used in standard transilluminated format, or in the case of examination of fluorescently labeled specimens, epi-illumination format *(vide infra)*. One obvious drawback is that this method produces a beautifully crisp image of only a tiny portion of the specimen. This problem is circumvented by scanning the specimen, producing a series of images of discrete points within the specimen.

The restricted depth of field intrinsic to the confocal principle effectively produces "optical sections" of the specimen, thus making it the technique of choice for the study of thick biological specimens The nondestructive nature of the technique allows its use for the examination of living material.

Fluorescence microscopy is arguably one of the most important techniques available to modern cell biologists, with a wide range of technologies allowing for the labeling of material with fluorescent tags. However, fluorescent biological specimens when examined using conventional optics produce images that suffer from extreme blurring. Ironically, it is the high sensitivity that makes the technique so valuable that contributes to its downfall in the form of out-of-focus interference.

Epifluorescence microscopy is the most popular form of fluorescence microscopy. The key design feature of the type of microscope used in epifluorescence microscopy is that a single lens acts as both the objective and condenser. Hence, illumination and imaging light paths are necessarily perfectly aligned. Thus, it becomes simpler to satisfy the conditions required for CLSM. Light, usually from a mercury vapor source, is reflected downward by a dichroic mirror, through the objective lens that focuses the light onto the specimen. Fluorescent light emitted by the specimen on excitation is collected by the same lens, and the dichroic mirror then functions to separate the longer wavelength fluorescent light from any unabsorbed exciting light.

Not surprisingly, since epifluorescence microscopy seems preadapted to the confocal principle ***(2)***, confocal microscopy is most commonly used to examine fluorescent or fluorescently labeled specimens ***(3,4)***. However, CLSM can also be used in reflectance mode and contribute the same, if not improved, sharpening of images. For example, *z*-axis approximate resolution can extend to 0.4 µm, compared to 0.7 µm achievable with epifluorescence ***(5)***. In addition, it is also possible to detect colloidal gold-labeled molecules using CLSM ***(6)***. Detecting the gold label using the back-scattered light mode, it is possible to *triple-label* samples by combining a gold label with two fluorescent labels ***(7,8)***.

Terasaki and Dailey ***(9)*** give a comprehensive review of confocal microscopy of living cells that includes extensive information on the use of various dyes to serve specific purposes. Another useful source of reference material is a catalogue by Molecular Probes (Molecular Probes Europe BV, PoortGebouw, Rijnsburgerweg 10, 2333 AA Leiden, The Netherlands; Website: http://

www.probes.com), which also provides extensive information on the physical and chemical characteristics of the dyes available, as well as a large bibliography. This handbook highlights the wide-ranging possibilities for the study of biological systems, whether they be living cells in culture or tissues specimens.

1.1.2. Laser Illumination

In the original confocal microscope designed by Minsky ***(1)***, the specimen was moved in a raster pattern in order to achieve a crisp image of the entire object. The light collected through the exit pinhole struck a photomultiplier tube (PMT) that in turn generated a flow of electrical signals that were then collected and collated to form an image of the specimen. However, in Minsky's original design this image collection process was slow. To increase the speed of image acquisition, many modern microscopes now use pivoting mirrors. A narrow beam of light is reflected from these mirrors and sequentially illuminates the specimen in a raster pattern. Such a design requires an intense illumination source, which was not available to Minsky. Laser instruments that have subsequently become available are ideally suited as illumination sources for confocal microscopes. Lasers offer a source of intense monochromatic light with low divergence, a property that optimizes the effectiveness of the confocal light path. Monochromaticity of the light source eliminates chromatic aberration, and the high-intensity illumination increases the speed of image acquisition. Three major types of continuous-wave gas lasers are available ***(10)***. Argon, helium, neon, and krypton-argon are most commonly used for illumination in CLSM. These lasers each have emission lines in different parts of the spectrum, making it possible to choose a laser best suited to the purpose for which it is required. However, some disquiet has been expressed recently about the short operating lifetime of the mixed gas krypton-argon lasers used in this setting.

1.1.3. Scanning Microscopy

The importance of advances in the field of video technology might not be immediately evident. However, the relevance of the work of Nipkow ***(11)*** to scanning light microscopy is worth noting. Using a spinning disc perforated with a series of holes in a spiral array (Nipkow disc), Nipkow was able to dissect a two-dimensional image using a raster scanning pattern, converting it into a one-dimensional electrical signal (Noran-Tracor Tandem Scanning Microscope, Noran Instruments, Milton Keynes, UK). The brightness of each dissected portion of the image could then be collected by a photodetector.

Petráñ and colleagues ***(12,13)*** developed a variation of Nipkow's spinning disc to use in their tandem scanning confocal microscope. In such a microscope the image can be viewed directly.

The early work of Nipkow also led to the subsequent development of modern cathode ray tube (CRT) technology and modern television. In CLSM, a CRT re-creates the image rather than it being viewed directly ***(14)***. The images collected by each scan of the laser across the specimen are commonly collected and stored by a computer as digital images.

The ability to scan the specimen improves resolution and allows for the construction of 3D images. So-called x,y resolution (point resolution in the plane orthogonal to the optical axis) can approach the diffraction-limited theoretical maximum calculated by Abbe ***(15)*** in modern instruments by restricting the area of the specimen under illumination at any one time. A "z-series" of images through the depth of a specimen can be produced by scanning at successively deeper planes in the specimen. This is achieved through the use of a stepwise, motor-driven focus control ***(16)***.

1.1.4. Multiple Photon Excitation

CLSM as described above does indeed give an enormous improvement in image quality over that obtained by the standard microscopical techniques of epifluorescence light microscopy. However, there are some limitations that are now being overcome.

A significant problem in the examination of living cells and/or tissues by CLSM is "phototoxicity" *(vide infra)*, whereby the fluorescent markers used in labeling of sites of interest release toxic by-products on excitation by the illuminating source. The two-photon excitation method ***(17)*** minimizes the problems of phototoxicity. Without discussing the physics of two-photon excitation in any great depth, suffice it to say that a fluorochrome can simultaneously absorb two photons of longer wavelength and lower energy than that of any single photon required to excite the fluorochrome. The combination of energies of the two photons equals the energy required for excitation ***(18)***.

The probability of simultaneous two-photon absorption is dependent on the square of the intensity of the illuminating light. Intensity of the laser beam is at its highest at the focal point, and, therefore, fluorochrome excitation takes place only within the *focal volume*. Thus, photodamage and photobleaching are reduced in areas of the cell or tissue outside the focal volume, which, by definition, in confocal microscopy is the majority of the tissue.

1.1.5. Image Processing

A wide range of image processing techniques are available ***(19)***, including the following:

1.1.5.1. Enhancement

Examples of possible image enhancement include background subtractions, enhancement of contrast, improvement of signal-to-noise ratio by averaging

the results of many scans of a specimen, and application of filters to eliminate noise generated in the amplification systems.

1.1.5.2. Image Analysis

Image analysis possibilities range from simple scaling of images to calculate their final magnifications to advanced automation of a wide range of complex measurements and calculations. For example, it is possible to segment the image to isolate areas containing pixels within a particular gray scale (i.e., fluorescence intensity). That area, as a proportion of the area of the tissue as a whole, can then be computed. Of course, images can also be segmented according to other criteria such as size and shape of the structures imaged. Image feature quantitation allows estimation of circularity, roughness, orientation, Feret diameters, and center of area. Images can be added to and subtracted from each other and manipulated according to a variety of mathematical transformation procedures. The digital format of images derived using CLSM makes semiquantitative microscopy relatively simple. Our work in which subtle differences in the localization patterns of two human immunoglobulin G subclasses, IgG_1 and IgG_2, were identified using the software package SOM line scans is an example of the use of fluorescence comparative quantitation. In this simple type of image analysis, a graphical readout of pixel intensity along a transect through the important parts of the specimen is generated. This led to the postulation of a possible mechanism whereby one of these subclasses, namely IgG_2, appears to be discriminated against in transport across the human placenta ***(20)***.

1.1.5.3. Rendering

Because images generated by modern confocal microscope instruments are necessarily in digital form, it becomes possible to render these images easily into more useful forms. Typical digital images are composed of variations along a "gray scale" comprised of 256 steps. The human eye can interpret subtle contrast variations more easily if an image is in color. Therefore, images can be rendered in pseudo-color display using predetermined look-up tables (LUTs).

A single line scanned in the same position repetitively but at successively greater depths into the specimen can generate a side view (an x,z scan) when these horizontal rows are displayed in sequence to fill the screen from top to bottom.

An "extended focus series" can be generated from a series of images taken along stepwise optical sections of a specimen, and formed digitally into a single image. Similarly, a series of optical sections of a thick specimen can be used to generate a "z series." When in digital form, the numerical information can be said to describe a 3D structure when the structure is sampled as a series of small volumes that are defined by the pixel dimension multiplied by the spac-

ing between adjacent sections ***(21)***. This volume is known as a *voxel*, and calculations of projections through voxel arrays allows for powerful image manipulations. Specialized applications such as ThruView™ (BioRad, Hemel Hempstead, UK) can produce images that appear to rock or roll or rotate along a given axis, giving valuable 3D information.

Increased resolving power of CLSM allows for specific subcellular localization of components (e.g., *see* **ref. *22***). The greater sensitivity of the method allows the *detection* of objects with dimensions less than the resolution limits of the microscope provided that they are spaced a greater distance apart than the resolution limit.

Thus, we see that CLSM is a technique that offers many advantages over conventional microscopy, including reduction in the blurring of images from light scattering and increased resolution. It is now possible to view a specimen in many different planes using specialized computer applications, and to obtain valuable 3D information about a particular specimen. The possibilities for the study of biological processes are tremendous owing to the rapid recent rate of production of new fluorescent labels and probes, coupled with the capacity of CLSM to delve beneath the surface of thick biological specimens to draw out hitherto concealed information. A properly set up confocal microscope operated with expertise will frequently give an image superior to any gained by conventional methods. In this chapter, the Bio-Rad MRC600 equipped with COMOS or SOM software (BioRad, Hemel Hempstead, UK) is described.

2. Materials

1. Phosphate buffered saline (PBS): 80.0 g NaCl, 11.5 g Na_2HPO_4, 2.0 g KH_2PO_4, 2.0 g KCl, made up to 1000 mL using distilled water. Mix on a magnetic stirrer, slightly warmed, to aid the dissolving of the solids. *Do not* stopper the bottle while on the stirrer. Make PBS solution on demand.
2. 3% formaldehyde: 38 mL of 40% formaldehyde in 500 mL of PBS. Wear surgical gloves and a mask; mix within a fume hood. Store solution at 4°C; avoid prolonged storage, i.e., longer than 1 mo.
3. 0.05% Triton X-100: 250 µL in 500 mL of PBS. Mix on a magnetic stirrer, slightly warmed to ensure the viscous detergent mixes properly with the PBS. *Do not* stopper the bottle while on the stirrer. Store solution at 4°C, avoid storage for longer than 1 mo.
4. 0.25*M* lysine: 3.655 g poly-L-lysine in 100 mL of PBS. Dissolve the lysine in the PBS with gentle agitation. Make on demand.
5. Propidium iodide: This fluorescent intercalating nucleic acid stain will label nuclei strongly and regions of cytoplasm containing RNA less intensely, so it has, since its introduction, established a useful niche as a fluorescent nuclear counterstain ***(23)***. It is carcinogenic and should be handled using gloves and disposed of as a hazardous liquid. A stock solution of 2500 µg/mL should be diluted

for final use in PBS to give a concentration of <10 µg/mL. The optimum dilution must be determined empirically for each new specimen. The tissue may be stained by immersion for short time periods (<30 min) at any stage in the preparation. The most convenient application is by addition during the second-stage antibody incubation or as part of one of the early PBS unbound-antibody elimination washes just after this incubation. Store the stock solution in a light-proof container at 4°C.

6. Antibodies: On receipt of an antibody, ensure that the supplied data sheet is read thoroughly. If the antibody is to be stored at 4°C, then place it in a refrigerator immediately. If the antibody requires storage at –20°C, then aliquot the antibody into Eppendorf tubes in 20-µL amounts, label the Eppendorfs, and freeze them immediately. In this way one can avoid damage by repeated freeze/thawing of antibodies. Use an aliquot on demand at the predetermined dilution. Store a diluted aliquot at 4°C for no more than 7 d. If the antibody has a fluorochrome attached, store it in a light-proof container at 4°C.
7. Antibody solutions: Dilute stock antibodies in PBS; add 20% normal serum of the host animal of the second-stage antibody if using an indirect immunofluorescence technique. If a direct technique is being undertaken, add 20% bovine serum albumen to the solution. The serum serves as a block for nonspecific antibody binding. Ensure that no serum of the host of the primary antibody is used. Prior to use, clarify all diluted antibody solutions by centrifuging at 15,000*g* for 10 min.
8. Proprietary mountants: Mounting media such as Fluoromount (BDH, UK), Vector Shield (Vector Labs, Peterborough, UK), and Citifluor (Agar Scientific, Essex, UK) are all useful. Antiphotobleaching properties of additives such as *n*-propyl gallate and paraphenylene diamine significantly prolong the lifetime of observation of many common fluorophores under the conditions of laser light excitation used. These compounds should be handled with great care.
9. Octadecyl indo-carbocyanine (DiI) (Molecular Probes, Leiden, The Netherlands): The lipophilic tracer DiI is extensively used as a vital fluorescent tracer in cell biology ***(24)***. The stock solution is prepared at 0.5 mg/mL using sunflower oil as the diluent. It is stored at –20°C. The working dilution used is 0.005 mg/mL.
10. Alizarin Red S (Sigma, Poole, UK): This Ca^{2+} dye is commonly used to stain ossified bone for the purpose of skeletal examination. The original method according to Dawson ***(25)*** recommends 1 mg of alizarin dissolved in 10 mL of 1% KOH. For our purposes this is excessive. Experimental fetuses are therefore prepared with a more dilute solution of the dye. Instead, 1 mg of alizarin is dissolved in 20 mL of 0.7% KOH.
11. 20% polyacrylamide gel: Mix 250 µL Tris buffer, pH 8.8, 500 µL 40% acrylamide; 225 µL water; 25 µL glycerol, 1.2 µL TEMED, and 4 µL 10% ammonium persulphate. (Add ammonium persulphate last, because it acts as a polymerization catalyst.) For volumes larger than 1 mL, it may be preferable to reduce the ratio of ammonium persulphate to allow a longer working period before the gel sets.

3. Methods

3.1. Indirect Immunofluorescence Microscopy of an Adherent Cell Culture

3.1.1. Preparation of Cover Slips

1. Cover slips should be 170 µm in thickness for optimal confocal resolution. They may be coated using poly-D-lysine, laminin, or fibronectin to aid cell adhesion.
2. Poly-D-lysine is made up to 5 µg/mL in distilled water and sterile filtered. Cover each cover slip with 100 µL of the solution and leave for 30 min at room temperature. Remove any excess and allow to dry.
3. Laminin is made up at 5 µg/mL in PBS. Coat cover slips as in poly-D-lysine (**item 2**), then further coat with the laminin solution. Allow to stand for 30 min at room temperature. Remove any excess and allow to dry.
4. Fibronectin is made up at 2 µg/mL in PBS. Coat cover slips with the fibronectin solution. Allow to stand for 30 min at room temperature. Remove any excess and allow to dry.

3.1.2. Immunofluorescence Labeling

1. Seed tissue culture plates (100 mm) containing four or five prepared coverslips using an inoculum of 6×10^5 cells. Leave for 3 d.
2. Place seeded cover slips into 9-cm diameter or larger Petri dishes with filter paper soaked in PBS (to maintain a humid environment and reduce evaporation of the small volumes of antibody solution applied). Wash in PBS twice, 2 min each wash. Remove excess PBS using a vacuum-driven filter pump.
3. Fix in 3% formaldehyde for 10 min at room temperature. Ensure that no air gets trapped under the cover slips because this may cause problems when manipulating them.
4. Permeabilize cells in 0.05% Triton X-100 for 10 min at 20°C. If an exposed cell surface membrane protein is under investigation, the permeabilization stage should be omitted.
5. Wash in PBS several times until the hydrophobic properties return to the cover slip (surface tension of the liquid returns).
6. If a problem with cellular autofluorescence (generally a yellow to brown color when viewed using ultraviolet (UV) or blue light excitation) is suspected or known, then the cover slips may be immersed in 0.25*M* poly-L-lysine for 30 min at 4°C to quench the autofluorescence.
7. Thoroughly remove excess liquid from the cells using a vacuum-driven filter pump.
8. Add 60 µL of the primary antibody solution to each cover slip and 60 µL of PBS to the control cover slip. Place the Petri dishes containing the cover slips in an incubator at 37°C and leave for 1 h. Antibody incubations may also be carried out at room temperature overnight, or at 4°C for 24 h. Generally longer incubations at low temperatures improve the ratio of specific-to-background labeling.
9. Remove excess antibody from cover slips by briefly washing with PBS, followed by two additional washes in PBS, each for 2 min.

10. Wash in PBS for 30 min at 4°C.
11. Thoroughly remove excess antibody from the cover slips using a vacuum-driven filter pump.
12. Add 60 µL of the secondary antibody to each cover slip including the control cells. Incubate for 1 hour at 37°C, overnight at room temperature, or 24 h at 4°C. Be aware that a fluorophore is now included, so ensure that the preparation is stored in the dark.
13. Remove excess antibody from cover slips by briefly washing with PBS, followed by two additional washes in PBS, each for 2 min.
14. Counterstain the nuclei by adding 2% propidium iodide (PI) solution to the cover slips for 5 min at 4°C. This counterstain is suitable only if a fluorophore such as fluorescein isothiocyanate (FITC) is used. Do not add PI to a preparation if tetramethyl rhodamine isothiocyanate (TRITC) or Texas Red has been used. Other counterstains such as Hoechst or DAPI may be considered if a UV laser is available (all fluorochromes are available from Sigma, UK, Molecular Probes, Inc., Leiden, The Netherlands).
15. Remove excess counterstain from cover slips by rinsing in PBS, followed by two additional washes in PBS, each for 2 min.
16. Wash for 30 min in PBS, with changes every 10 min.
17. Mount cover slips on slides using an antiphotobleaching mountant.

3.2. Indirect Immunofluorescence Microscopy of Frozen Sections

3.2.1. Preparation of Slides for Sections (Slide Subbing)

1. Rack up slides and soak in 5% "Decon 90" (Merck, Lutterworth, UK) overnight.
2. Wash slides in hot running water for 30 min with occasional agitation.
3. Wash slides three times in distilled water.
4. Dry in a glass drying oven.
5. Make up the subbing solution: 2% 3-(triethoxysilyl)-propylamine (Sigma) in acetone (8 mL 3-[triethoxysilyl]-propylamine in 400 mL acetone).
6. Subbing procedure (1 min in each staining dish with gentle agitation):
   a. Staining dish 1: 3-(triethoxysilyl)-propylamine/acetone.
   b. Staining dish 2: acetone.
   c. Staining dish 3: acetone.
   d. Staining dish 4: distilled water.
   e. Staining dish 5: distilled water.
7. Dry in a glass drying oven.
8. Store in a dry box for later use.

3.2.2. Indirect Immunofluorescence of Frozen Tissue Sections

1. To a suitably sized and oriented sample in a disposable plastic mold, add sufficient OCT embedding medium (Tissue-Tek, Bayer UK Ltd, Basingstoke, UK) to cover the tissue. Freeze the filled mold on a hexane/dry-ice slush in the bottom of a Dewar flask.

2. Store the frozen samples at between –20° and –80°C in a sealed bag/box containing a small amount of hexane (BDH, UK) to prevent them from drying out.
3. Take sections using a cryostat, with the cabinet temperature set at –25°C, the blade temperature at –22°C, and the block temperature at –15°C. Mount sections on subbed slides.
4. Wash in PBS twice, 2 min for each wash.
5. Fix in 3% formaldehyde for 10 min at room temperature.
6. Wash in PBS twice, 2 minutes for each wash.
7. Permeabilize in 0.05% Triton X-100 for 10 min at room temperature.
8. Wash in PBS several times until surface tension returns to the surface of the slide.
9. If problems with autofluorescence are suspected or known, the sections may be immersed in poly-L-lysine for 1 h at 4°C to quench the autofluorescence.
10. Thoroughly remove excess liquid from the slides using a vacuum-driven filter pump.
11. Add a sufficient amount of first-stage antibody to each experimental section to ensure that the sections are covered. Add the same volume of fluid to a control section. Add the same amount of preimmune antibody, nonimmune or simply PBS to a control sample. Ideally the control solution should be as close as possible barring its antigen-binding specificity to the experimental one. A monoclonal antibody of the same isotype raised in the same species but against a different antigen is often used as a control. Incubate the sections either at 4°C overnight, at room temperature for 12 h, or at 37°C for 1 h.
12. Remove excess antibody from the sections and wash in PBS twice, 2 min for each wash.
13. Wash in PBS overnight at 4°C.
14. Thoroughly remove excess PBS from the slides using a vacuum-driven filter pump.
15. Add sufficient second-stage antibody to cover all the sections completely. Incubate the sections either at 4°C overnight, at room temperature for 12 h, or at 37°C for 1 h.
16. Remove excess antibody from the sections and wash in PBS for 30 min. Change the PBS every 10 min.
17. Thoroughly remove excess PBS from the slides using a vacuum-driven filter pump.
18. Mount in antiphotobleaching mountant, and seal with nail varnish if necessary.

3.2.3. Dual-Label Immunofluorescence Protocol

The dual-label immunofluorescence protocol is an extension of the previous two. It can successfully be applied to cells and sections. The key considerations concern the antibodies to be used. Careful thought should be applied to their choice. Of primary importance is to ensure that the two fluorophores attached to the secondary antibodies excite/emit in different parts of the spectrum. Useful combinations include FITC/TRITC or Oregon Green/Texas Red (Molecular Probes, Inc, Leiden, The Netherlands). These absorb maximally at blue and green wavelengths, respectively, whereas they emit green and red fluorescent light, respectively. Once again, be careful to choose an appropriate

nuclear counterstain. PI also emits red light, which may be confused with TRITC fluorescence. Also it must be ensured that the two primary antibodies are raised in different species of animal; otherwise the secondary antibodies will bind to both primary antibodies. Always check the supplier's antibody data sheets for any cross-reactions with experimental tissue.

1. Obtain cell preparations or tissue sections.
2. Wash in PBS twice, 2 min for each wash.
3. Fix in 3% formaldehyde for 10 min at room temperature.
4. Wash in PBS twice, 2 min for each wash.
5. Permeabilize in 0.05% Triton X-100 for 10 min at room temperature. This step should be omitted if cell surface proteins are targeted because cellular membranes are disrupted.
6. Wash in PBS several times until surface tension returns to the surface of the slide.
7. If problems with autofluorescence are suspected or known, the sample may be immersed in poly-L-lysine for 1 h at 4°C to quench the autofluorescence.
8. Thoroughly remove excess liquid from the slides using a vacuum-driven filter pump.
9. Add a sufficient amount of the first primary stage antibody to each experimental slide to ensure that the samples are covered. Add the same amount of preimmune serum, nonimmune serum or simply PBS to a control sample. Ideally the control antibody solution should be as close as possible barring its antigen-binding specificity to the experimental one. A monoclonal antibody raised in the same species but against a different antigen of the same isotype is often used as a control. Incubate the sections either at 4°C overnight, at room temperature for 12 h, or at 37°C for 1 h.
10. Remove excess antibody from the slides and wash in PBS twice, 2 min for each wash.
11. Wash in PBS for 30 min at 4°C.
12. Thoroughly remove excess PBS from the slides using a vacuum-driven filter pump.
13. Add a sufficient amount of the second primary stage antibody to each experimental slide to ensure that the samples are covered. Add the same amount of PBS to a control section. Incubate the sections either at 4°C overnight, at room temperature for 12 h, or at 37°C for 1 h.
14. Remove excess antibody from the slides and wash in PBS twice, 2 min for each wash.
15. Wash in PBS overnight at 4°C.
16. Add a sufficient amount of the first secondary stage antibody to all slides, ensuring that the samples are fully covered. Incubate the sections either at 4°C overnight, at room temperature for 12 h, or at 37°C for 1 h.
17. Remove excess antibody from the slides and wash in PBS twice, 2 min for each wash.
18. Wash in PBS for 30 min, with changes of PBS every 10 min.
19. Add a sufficient amount of the second secondary stage antibody to all slides. Ensure that the samples are completely covered. Incubate the sections either at 4°C overnight, at room temperature for 12 h, or at 37°C for 1 h.

20. Remove excess antibody from the slides and wash in PBS twice, 2 min for each wash.
21. Wash in PBS for 30 min, with changes of PBS every 10 min.
22. Thoroughly remove excess PBS from the slides using a vacuum-driven filter pump.
23. Mount in antiphotobleaching mountant, and seal with nail varnish if necessary.

3.3. Whole Tissue Examination and Examination of Living Cells

It is possible, using specially constructed microscope CLSM stages, to maintain whole tissue alive in culture for sufficient time to study aspects of the structure and *function* of that tissue. For example, it has been possible to maintain small pieces of placental tissue in a temperature-controlled environment ***(16)***. This technique has been used to follow the fate of a fluorescent lipid soluble marker, DiI, over time to gain information about the structure of the unusually extensive (10–14 m^2) syncytial epithelial layer that forms the fetally derived surface of the human placental chorionic villus tree.

1. A glass micropipet loaded with DiI (0.005 mg/mL dissolved in sunflower oil) is mounted in a micromanipulator and brought close to the tissue.
2. The chorionic villus tissue is obtained immediately after term delivery, by natural means, of a healthy baby. The tissue is maintained in precooled Dulbecco's modified Eagle's medium without pyruvate and without $NaHCO_3$, and supplemented with 4.5 mg/mL of glucose and 10% human pregnant women's serum.
3. The medium is kept at 4°C following transfer to a Peltier temperature-controlled stage chamber equipped with a flat base formed from a standard cover slip. The stage is attached to the body of an inverted microscope (Axiovert, Zeiss) that permits observation from below. The GHS (Bio-Rad) dichroic filter set, usually used for the detection of TRITC and Texas Red, is fitted.
4. A droplet of oil/DiI is partly expressed from the mouth of a glass micropipet using pressure from an N_2 gas cylinder controlled by a PV800 Picopump (WPI, Stevenage, UK). The droplet at the tip of the pipet is brought into brief contact with the distal part of a chorionic villus and is then carefully withdrawn.
5. The fluorescent phospholipid analog is allowed to diffuse following an increase in temperature of the Peltier-controlled stage to 37°C. The stage chamber is covered to prevent evaporation of culture medium.
6. The progress of the diffusion of the probe is monitored by scanning the specimen at standard time intervals. Digital images are made at each time point as a permanent record.

3.4. Calcium Imaging Protocol for Fetal and Neonatal Skeletogenesis Studies

1. Pregnant animals are sacrificed by exposure to carbon dioxide, 2 L/min for 3 min. Fetuses are removed from the uterus and individually identified by dam number and uterine position. Live fetuses and neonates are given lethal ip injections of sodium pentobarbitone.

2. Fetuses and neonates are preserved in 99% industrial methylated spirits before staining. A modified method ***(25)*** is used to stain specimens with Alizarin red S as follows:
   a. Clear with 1 to 2% potassium hydroxide.
   b. Stain with a 1% potassium hydroxide/0.005% Alizarin red S solution.
   c. Remove excess dye using 1% potassium hydroxide in 25% glycerol.
   d. Place in glycerol using a 50% glycerol solution.
   e. Replace with a 70% glycerol solution.
   f. Store in 100% glycerol. Samples stored in this way are still usable at least 5 yr after preparation.
3. The period of time for each step is varied according to specimen size, with older specimens requiring more time for complete preparation.
4. After gross examination, limbs from fetuses and neonates are removed using ophthalmological scissors and a stereomicroscope (×10 magnification) with a fitted eyepiece graticule, accurate to one-tenth of a millimeter, for any necessary bone measurement.
5. The best CLSM images are achieved when the specimen is close to the microscope lens; removal of surrounding soft tissues mechanically facilitates this. An alternative chemical method is also available (*see* **Notes 1** and **2**).
6. Microdissection under a stereomicroscope (×6.5 magnification) is accomplished using fine forceps and tungsten wire drawn to a sharp point. The cartilage model is nipped off with forceps so that the bone lies as flat as possible in the observation chamber. Care is taken not to scratch or puncture the bone.
7. Glass slides (75 mm × 26 mm) containing 10-mm diameter holes drilled in their center are prepared.
8. A no. 0 glass cover slip is attached to one side of the bored slide using dental wax. This creates a 1-mm deep well into which specimens are placed. Where a specimen is over 1 mm in depth, a double-deck slide is made by aligning two bored slides on top of one another and fixing them together with dental wax.
9. A solution of 20% polyacrylamide gel is pipeted into the well containing the developing bone flattened against the cover slip (*see* **Notes 3–5**). A second cover slip is sealed to the slide with nail polish to close the well.
10. Slides are labeled and maintained in a humidified atmosphere. The edges of the cover slips may be recoated with nail polish to prevent gel dehydration.
11. An argon ion laser line at a wavelength of 488 nm is used to excite the dye. The 1% transmission neutral density filter is selected at the output port of the laser (*see* **Note 7**).
12. A standard dichroic filter set, as used for observing specimens labeled with FITC, is inserted into the microscope light path.
13. Specimens are observed using the CLSM microscope equipped with objective lenses of ×10 and ×20 magnification (*see* **Note 8**). Data are processed using COMOS or SOM software (Bio-Rad) and stored on rewriteable optical discs (Panasonic).
14. Images captured by a second detector may be recorded as a separate image plane and the two merged by image processing to provide collateral information

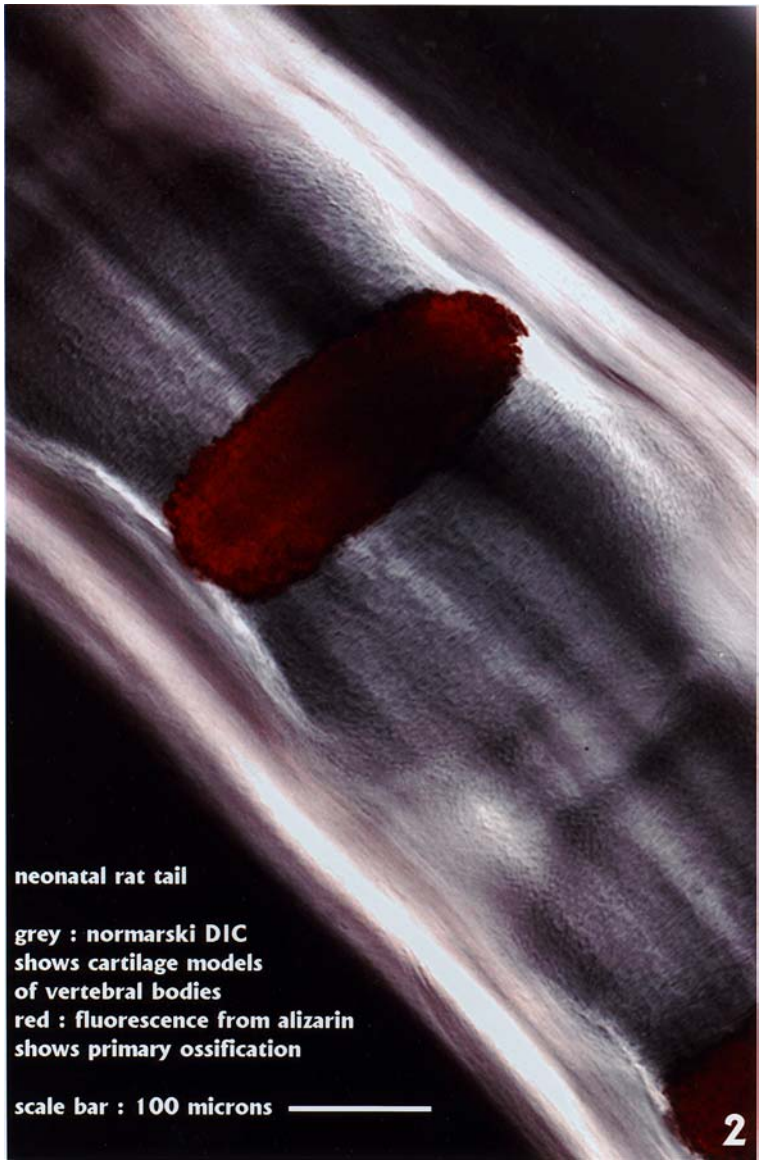

Fig. 2.

regarding the specimen. In certain cases (e.g., **Fig. 2**) a non-confocal image such as a Nomarski DIC image is merged with an epifluorescence confocal image. For Nomarski DIC microscopy, a reverse optical path is adopted with the laser light transmitted by the objective lens and collected by the condenser being light-piped by fiberoptic cable to the second red-sensitive photomultiplier detector. When

rendered following use of the merge file routine in the COMOS software, the images will be assigned a single but separate color from the RGB selection to distinguish the two planes. Select the image plane to view the Nomarski image and activate all three color guns (R, G, and B) to give the familiar gray image. It is conventional to assign the appropriate color (i.e., green for fluorescein and red for TRITC) when viewing the epifluorescence channel.

3.4.1. Rendering an Image Using a False Color LUT

Gray scale optical section images may be rendered in pseudo-color in which the intensity is defined by an LUT. The assigned color is related to the fluorescence intensity and, hence, Ca^{2+} concentration at that site in the specimen (**Fig. 3**). This rendering constitutes a real advantage because the color contrast discrimination of the human eye exceeds that of its gray-scale contrast discrimination, and is unable to make use of all 256 contrast steps used for digitally encoding brightness in each pixel of a gray-scale image.

It is relatively hard to produce a good new LUT. However, the library of existing LUTs is an excellent starting point. The Bio-Rad LUTs GEOG and AUTUMN are the ones that we use most frequently. To produce a new LUT use the following procedure:

1. Display a gray-scale image on the viewing monitor. If necessary process it by, e.g., contrast stretching or median filtering. Then continue with **steps 2–7**.
2. From the **DISPLAY** menu first select **HOLD LUTs**.
3. From the **DISPLAY** menu now select **OUTPUT LUTs**. A graphic display will appear.
4. Click on the circle **Pseudo Color**. Note that the circle labeled **Red LUT** is selected. Point the mouse anywhere on the graph. Click the left button and drag it, then let go. Note what happens to the graph and the display.
5. Now click and move with the right mouse button and note what happens.
6. Click on the circles labeled **Green & Blue LUT** and repeat **steps 3** and **4**.
7. When you are happy with your finished look-up table, click on **SAVE** and assign it a file name.

3.5. Collecting a Z-Series to Produce an Extended Focus Projection or to Make a 3D Reconstruction

The following schedule was devised for use with a Zeiss Axiovert Microscope equipped with a Bio-Rad MRC 600 Confocal Microscope attachment (*see* also **Notes 9** and **10**).

1. Find a suitable area of the specimen and center it in the field.
2. Reset the Zeiss Axiovert to use the confocal light path, by allowing the laser illumination access through the port to the intermediate tube of the microscope.
3. On the COMOS menu, select the option **PMT1** and check that the objective lens magnification setting is correct.

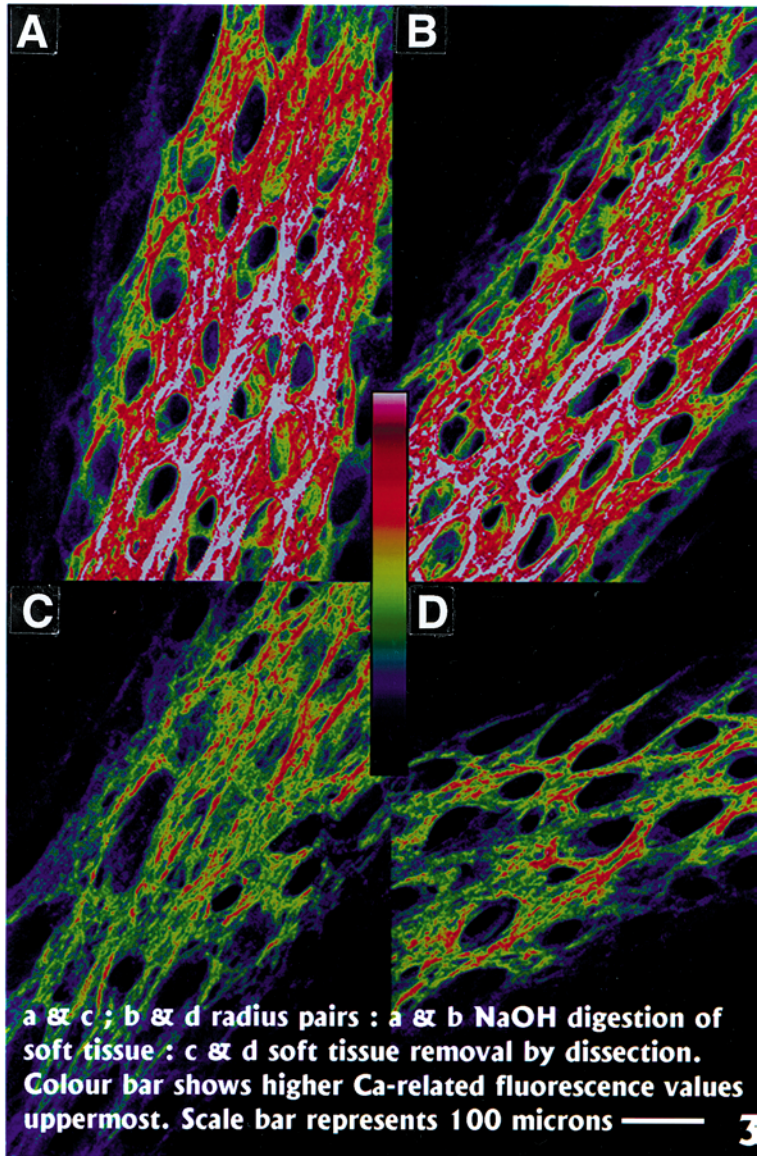

Fig. 3.

4. Press the space bar to initiate scanning.
5. When an image appears on screen, gently adjust the fine focus control to maximize image brightness. (Note: tissues are often not uniformly stained.) If there is still no image, or the image is very dim, then proceed as follows: either fully open the confocal aperture or increase the gain control (signal amplification), or both.

Then try the fine focus again. Bearing in mind that a wide confocal aperture means optical sections are at their thickest, optimize these settings to obtain the best image you can.

6. Click the **FOCUS MOTOR** on or perform manual equivalent function. Now use the remote control focus clockwise until the region of interest just disappears. This represents the bottom end of the tissue, in the inverted microscope, the point nearest to the slide.
7. Record this point in the **FOCUS MOTOR** box by clicking on **Z-START**. Now click the *right* arrow (>) in the box labeled **POSITION**. The motor will move away from the slide by a default setting of 0.72 µm. Step through the tissue (toward the cover slip) until the far side of the region you want is reached. Click on the box labeled **Z-STOP**. You will now have set the start and stop positions for the z-series. *Important:* From the **FILE/IMAGE PARAMETERS BOX**, make a note of Pixel size.
8. Select **KALMAN** filtering and an appropriate number of *n* scans.
9. From the drop-down menu **COLLECT**, select **Z-SERIES/TIME SERIES**. An options menu will appear telling how many images will be collected. This is dependent on the z-increment of the stepper motor. This "step size" is adjustable, up or down. *Important:* Make a note of the step size you choose.
10. Click OK. Type in a file name for your series (tip: start it with a *z*).
11. When the z-series is complete, click on the drop-down menu **ENHANCE** and select **PROJECT Z-SERIES**. A new options box will appear. By default, a *maximum brightness projection* is selected. Click on OK. When the projection is complete, click on **FILE** and **SAVE** the image to disk (start the file name with a *p*).

3.5.1. Projections of 3D Data Sets

1. From the **PROGRAM** menu, select **SOM**. SOM is a keyboard-operated software that predates COMOS. When SOM is loaded, press **ALT** and **T** together to bring up the **ThruView** box.
2. Press **3** and then **C** and type in the name of the file of *optical sections* the reconstruction will be built from. Press Enter.
3. Press **P** and enter a name of your choosing for the file of *projections* that are to be built.
4. Press B to enter the BUILD menu.
5. Decide on the number of views to be made of the section stack and an appropriate increment in degrees, then enter these values under the **N** and **I** options. To make a full 360° reconstruction, 36 views at 10° would often be a reasonable first option, which avoids giving too jerky an appearance. The more views used, the smoother the apparent rotation achieved, but the greater the time is required for processing. Enter a suitable z-stretch factor into the **SCALING/LAYERS** menu (*see* **Note 9**).
6. Press **O** to enter the **BUILD OPTIONS** menu.
7. Choose either a *Maximum brightness projection* or an *Average brightness projection.*
8. Press **B** to go back to the **BUILD** menu.

9. Press **Enter**. A message will appear at the bottom of the screen giving an estimate of how much disk space will be used. Press Enter again to begin the reconstruction.
10. As the reconstruction progresses, *orthogonal* sections in the XZ plane are displayed on the screen, beginning at the top of the sample and moving steadily down.
11. When the reconstruction is complete, the computer will write the contents of its calculations to the file name given for one's projections in **step 3**). Press **Enter**, and your animation will be displayed on the screen.
12. When the rotation has finished displaying, press **M** to enter the **MODE** menu. Select **K** for keypad display.
13. Press **D** to return to the **DISPLAY** menu. Press **Enter**. The rotation is now under one's (keyboard) control via the left and right arrow keys. Pressing **Enter** again will terminate the display.
14. Press **ALT** and **E** together to return to the COMOS menu.
15. The series of images shown in **Fig. 4** are extended focus projections made from a z-series of optical sections of the posterior aspect of mid-diaphysis humerus bone of rat at 19–25 d of pre- and postnatal development (DD). Sections are taken at successively greater depth (5-µm focal step) from the bone surface to approx 50 µm from the surface. They show the formation and thickening of trabeculae during a period when ossification of the cartilage skeleton has only just begun and ossification is rapid. There is potential for this method to be used in analysis of drug effects on the skeleton in embryo-fetal development studies. Adverse effects on calcification and subtle changes in bone texture may be seen at this histological level. Differences between age groups are readily detected. At DD 19 the trabeculae are disorganized and irregular in structure. Specimens from the DD 20 group show more regularity, and the orientation of the trabeculae are becoming apparent. Adjacent trabeculae become contiguous, and form intertrabecular spaces. At DD 21 the structure of the bone remains similar to that at DD 20. The longitudinal orientation of the trabeculae, with respect to the long axis, becomes obvious by DD 22, and the intertrabecular spaces are more elongated. The trabecular matrix appears thicker at DD 23, and the intertrabecular spacing decreases. This change becomes more obvious on DD 24 when scalloped surface markings can be detected on the trabecular matrix. By GD 25 intertrabecular spaces have diminished in size and are circular in shape, rather than elongated. The trabecular matrix has finally become a continuous sheet of dense bone.

4. Notes

4.1. Removal of Soft Tissue with NaOH

1. Removal of soft tissue with NaOH can be achieved with any concentration >3*M*. Limbs are placed into NaOH (1*M*, 2*M*, 3*M*, and 4*M*). They are left for set periods of time in tubes on an automatic roller. After removal of soft tissue, the bones are returned to 100% glycerol. However, the intensity of the staining increases on immediate contact with any of the concentrations of NaOH used. Specimens placed in 4*M* NaOH lose all soft tissues, including the cartilage model, leaving only the ossified bones. The majority of the soft tissue surrounding the bones is

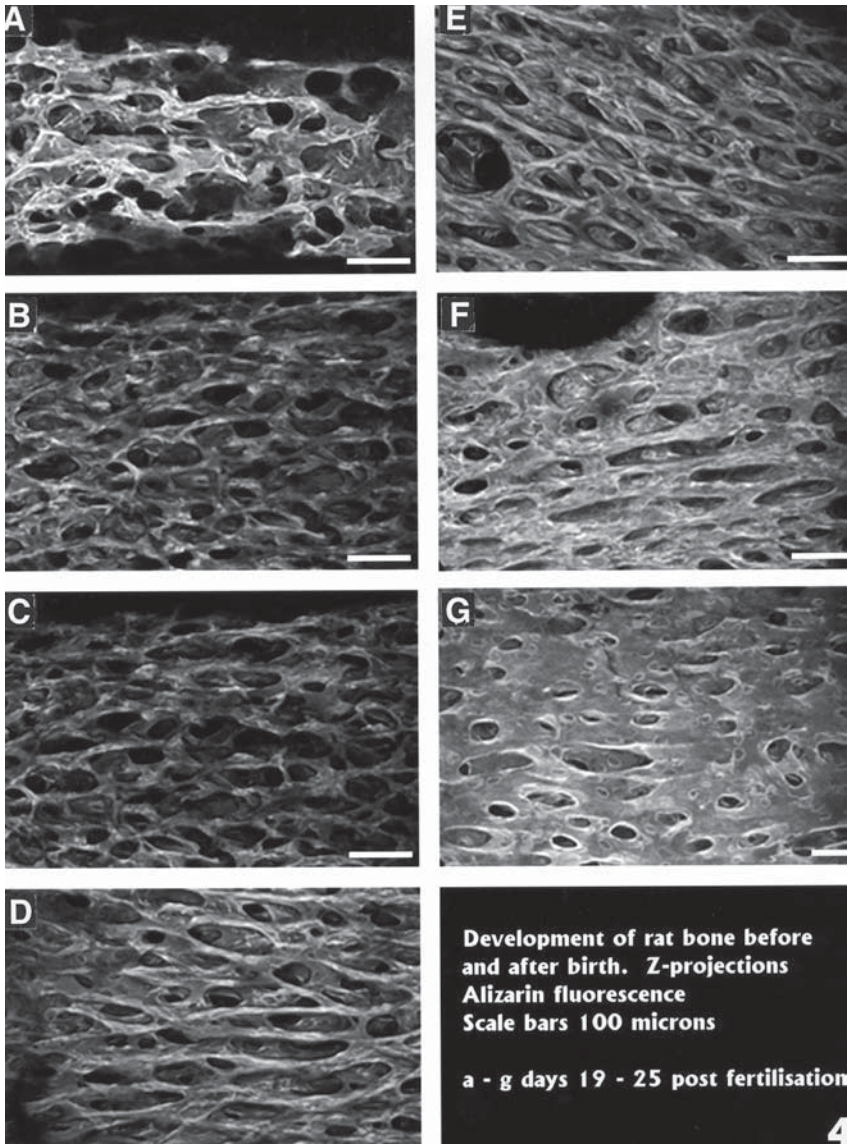

Fig. 4.

routinely removed satisfactorily using microdissection, and provides satisfactory images for this type of study.

2. Many specimens that have soft tissue removed with NaOH are unsuitable for viewing with the CLSM. Even using a neutral density filter allowing only 1% of the laser power to excite alizarin fluorescence resulted in extensive oversampling and lack of contrast in the images. A chemical change, associated with a color

change, induced by the NaOH caused a dramatic increase in quantum efficiency. With crystalline calcium salts and, therefore, alizarin highly concentrated in these specimens, excessive fluorescence was a problem. This was true for all the concentrations of NaOH used. Perhaps this technique would be more effective in localizing low levels of calcification in which high sensitivity would be an advantage. Examples of such situations might include very early calcification changes and pathological examples of ectopic calcification ***(26)***.

4.2. Mounting

3. In the mounting of relatively large objects in polyacrylamide gel, it was possible to immobilize the specimen completely as a prerequisite for z-series recording. In doing so, using bored slides, pockets of trapped air had to be carefully avoided because they caused image distortion. Storing slides in a moist environment reduced the rate of dehydration of polyacrylamide gel and prolonged the lifetime of these preparations for several days. Once embedded in polyacrylamide, remounting bones was impractical because residual gel degraded image quality. It is possible that samples could be retrieved from glycerol/PBS slides and processed further for histological sectioning and examination. More permanent mounting may be possible in proprietary mountants such as fluoromount, if necessary.

4.2.1. Aperture, Laser, and PMT Settings

4. The size of the pinhole aperture determines the thickness of the optical section viewed. This is often not fixed—many systems have adjustable pinhole apertures, which allows for the selection of the optimal setting for each specimen examined. For example, in the case of particularly light-sensitive specimens, the aperture size can be set large, increasing the amount of light signal collected by one scan of the laser. Thus, the deleterious effects of the exposure to the laser are minimized.
5. As a general rule, PMTs should be set at the largest possible gain, whereas the laser intensity should be kept as low as possible. Scanning specimens to determine where critical microscopy should be carried out should be undertaken at fast scan speeds at which the dwell time of the laser is minimized and the image is refreshed more frequently.

4.3. Photobleaching and Phototoxicity

6. Damage to the fluorochrome (photobleaching) and tissue or cells (phototoxicity) is often dependent on the presence of molecular oxygen ***(27)***. On excitation the dye enters a triplet excited state, and in the case of many dyes, this state can react with molecular oxygen to produce singlet oxygen, a highly reactive species. Addition of antioxidants to the mountant medium ***(28)*** has been used to attenuate this problem. When imaging live cells or tissues, for ablation of phototoxicity, use of a biological oxidant scavenging system would be preferable. For example, the glucose oxidase plus glucose system has been used ***(29)***.

4.4. Limits of Depth

7. Bone preparations were observed using ×10 and ×20 magnification objective lenses. At ×10 objective lens magnification, signals were detected 100 µm deep to the bone surface. At ×20 objective lens magnification, an approximate depth of 50–60 µm could be reached before the signal was completely lost. Depth attained was highly dependent on the porosity and density of the bone. The depth into a given specimen at which useful images can be obtained is clearly dependent on the transparency of the specimen. Therefore it must be determined empirically. The working distance of the objective is an important factor that frequently limits the degree of penetration. The relationship between numerical aperture (NA) and working distance limits the highest resolution observations made with high NA lenses to regions closer to the specimen surface.

4.5. Two-Channel Merged Images

8. Recording a second image simultaneously using Nomarski DIC to reveal the distribution of tissue components on the basis of their refractive index/dry mass can be helpful because it reveals the specificity of localizations based on immunofluorescence microscopy. The latter is a dark field technique that excludes all information from the image except the distribution of the fluorophore being applied as the label.

4.6. Z-Stretch

9. Press **S** to enter the **SCALING/LAYERS** box. You now need to press **Z** and enter a *z-stretch factor*. (z-stretch = distance moved in 1 motor-driven focus step/XY pixel edge length.) The z-stretch factor is a compensatory measurement to aid the accurate reconstruction of pixels in the z-plane. The ideal situation would be a 1:1:1 ratio X:Y:Z in which 1 is the maximum instrument resolution. When ThruView™ recalculates views, it has to interpolate any missing information in the z-plane between the optical section data sets. In X and Y, resolution on the CLSM is relatively good and it is as little as 0.2 µm. In XZ, the minimum distance between optical sections is the smallest increment on the stepper motor (0.18 µm) turning the fine focus, but the maximum resolution is less than this at approx 0.4 µm in reflectance mode or worse, at 0.7 µm in epifluorescence mode with high N.A. lenses. Hence it makes no sense to sample at less than these step distances. The z-stretch factor in the case of a 0.18-µm step size would be almost unity because 0.2/0.18 ~ 1, meaning that ThruView™ is dealing with nearly *cubic* entities or *voxels* as they are known in 3D terms (voxel = a volume element). The specimen, however, would be extensively oversampled. In a more practical example with efficient sampling exploiting the maximum available resolution, the XZ spacing is larger than the XY pixel edge length. Here ThruView™ would be dealing with voxels like house bricks in shape standing on end. Clearly one must enter a z-stretch figure to ensure that the step size one uses to sample is reflected accurately in the reconstruction.

4.7. Extended-Focus Image

10. The advantage of an extended-focus image over a conventional light microscope image is that the former is a projection of several in-focus images and the latter a projection of one in-focus image and several out-of focus images.

References

1. Minsky, M. (1957) Microscopy apparatus. U. S. Patent No 3013467.
2. Ockleford, C. D. (1995) The confocal laser scanning microscope (CLSM). *J. Pathol.* **176,** 1–2.
3. Ockleford, C. D. (1990) *An Atlas of Antigens.* Macmillan, London, and Stockton, New York, pp. 1–323.
4. White, J. G., Amos, W. B., and Fordham, M. (1987) An evaluation of confocal versus conventional imaging of biological structures by fluorescence light microscopy. *J. Cell Biol.* **105,** 41–48.
5. Sarafis, V. (1990) Biological perspectives of confocal microscopy, in *Confocal Microscopy* (Wilson, T., ed.), Academic, London, pp. 325–337.
6. Bacallao, R., Bomsel, M., Steltzer, E. H. K., and De Mey, J. (1995) Guiding principles of specimen preservation for confocal fluorescence microscopy, in *Handbook of Biological Confocal Microscopy*, 2nd ed. (Pawley, J. B., ed.), Plenum, pp. 311–325.
7. Pawley, J. B., Amos, W. B., Dixon, A., and Brejle, T. C. (1993). Simultaneous non-interfering collection of optimal fluorescent and back-scattered light signals on the MRC500/600, in Proc 51st Annual Meeting of the Microscopical Society of America (Bailey, G. W. and Reider, C. L., eds.), San Francisco Press, pp. 156–157.
8. Linares-Cruz, G., Rigaut, J. P., Vassey, J., De Oliviera, T. C., De Cremoux, P., Olofsson, B., and Calvo, F. (1994) Reflectance in situ hybridisation (RISH): Detection by confocal reflectance laser microscopy of gold-labeled riboprobes in breast cancer cell lines and histological specimens. *J. Microsc.* **173,** 27–38.
9. Terasaki, M. and Dailey, M. E. (1995) Confocal microscopy of living cells, in *Handbook of Biological Confocal Microscopy*, 2nd ed. (Pawley, J. B., ed.), Plenum, pp. 327–346.
10. Bloom, A. L. (1968) *Gas Lasers.* Wiley, New York.
11. Nipkow, P. (1884) German Patent No. 30,105.
12. Egger, M. D. and Petráñ, M. (1967) New reflected-light microscope for viewing unstained brain and ganglion cells. *Science* **157,** 305–307.
13. Petráñ, M., Hadravsky, M., Egger, D., and Galambos, R. (1968) Tandem-scanning reflected light microscopy. *J. Opt. Soc. Am.* **58,** 661–664.
14. LeMasters, J. J., Chacon, E., Zaherbelski, G., Reece, J. M., and Nieminen, A. L. (1993) Laser scanning confocal microscopy of living cells, in *Optical Microscopy: Emerging Methods and Applications* (Herman, B. and LeMasters, J. J., eds.), Academic, New York, pp. 339–354.
15. Abbe, E. (1884) A note on the proper definition of the amplifying power of a lens system. *J. Royal Microscopical Soc.* **4,** 348–351.

16. Ockleford., C. D., Mongan, L. C., and Hubbard, A. R. D. (1997) Techniques of advanced light microscopy and their applications to morphological analysis of human extra-embryonic membranes. *Microsc. Res. Technique* **38,** 153–164.
17. Denk, W., Strickler, J. H., and Webb, W. W. (1990) Two-photon laser scanning fluorescence microscopy. *Science* **248,** 73.
18. Denk, W., Piston, D. W., and Webb., W. W. (1995) Two-photon molecular excitation in laser scanning microscopy, in *Handbook of Biological Confocal Microscopy*, 2nd ed. (Pawley, J. B., ed.), Plenum, New York, pp. 445–458.
19. Niblack, W. (1986) *An Introduction to Digital Image Processing.* Prentice Hall, Englewood Cliffs, NJ, pp. 1–255.
20. Mongan, L. C. and Ockleford C. D. (1996) Behaviour of two IgG subclasses in transport of immunoglobulin across the human placenta. *J. Anat.* **188,** 43–51.
21. Carlsson, K., Danielsson, P., Lenz., R., Liljeborg., A., Majlöf., L., and Åslund., N. (1985) Three-dimensional microscopy using a confocal laser scanning microscope. *Op. Lett.* **10,** 53–55.
22. Ockleford, C., Bright, N., Hubbard, A., D'Lacey, C., Smith, J., Gardiner, L., Sheikh, T., Albentosa, M., and Turtle, K. (1993) Micro-trabeculae, macro-plaques, or mini-basement membranes in human term fetal membranes. *Philos. Trans. Royal Soc. London B* **342,** 121–136.
23. Ockleford, C. D., Hsi, B., Wakely, J., Badley, A., Whyte, A., and Page Faulk, W. (1981) Propidium iodide as a nuclear marker in immunofluorescence 1. Use with tissue and cytoskeleton studies. *J. Immunol. Methods* **43,** 261–267.
24. Honig, M. G. and Hume, R. I. (1989) DiI and DiO: Versatile fluorescent dyes for neuronal labelling and pathway tracing. *Trends Neurosci.* **12,** 333–341.
25. Dawson, A. B. (1926) A note on the staining of cleared specimens with Alizarin Red. *Stain Technol.* **1,** 123–124.
26. Bernacca, G. M.,Gibson, S. A., Wilkinson, R., and Wheatley, D. J. (1994) Confocal laser scanning microscopy of calcified bioprosthetic heart valves. *J. Heart Valve Dis.* **3(2),** 205–211.
27. Tsien, R. Y. and Waggoner, A. (1995) Fluorophores for confocal microscopy, in *Handbook of Biological Confocal Microscopy*, 2nd ed. (Pawley, J. B., ed.), Plenum, pp. 267–279.
28. Gilot, H. and Sedat, J. W. (1982) Fluorescence microscopy: Reduced photobleaching of rhodamine and fluorescent protein conjugates by n-propyl gallate. *Science* **217,** 1252–1255.
29. Bloom, J. A. and Webb, W. W. (1984) Photodamage to intact erythrocyte membranes at high laser intensities: Methods of assay and suppression. *J. Histochem. Cytochem.* **19,** 608–616.

5

Measurement of Intracellular Calcium Concentration Using Confocal Microscopy

Carmen Perez-Terzic, Marisa Jaconi, and Lisa Stehno-Bittel

1. Introduction

Many cellular functions are tightly regulated by intracellular calcium concentrations ($[Ca^{2+}]_i$), and, therefore, the measurement of $[Ca^{2+}]_i$ is of critical importance. To determine Ca^{2+}-related cellular dynamics accurately, it is necessary to measure three-dimensionally resolved $[Ca^{2+}]_i$ with sufficient temporal resolution to follow fast cellular responses that generate signal pulses and wave propagation. Several techniques have been developed to assay $[Ca^{2+}]_i$, but a revolution in the study of intracellular $[Ca^{2+}]_i$ occurred when fluorescent dyes for Ca^{2+} were developed ***(1)***. Since then, fluorescent dyes and fluorescent microscopy have been used to observe resting and nonresting $[Ca^{2+}]$ in intact cells as well as in subcellular fractions.

1.1. Confocal Microscopy

Confocal fluorescence microscopy produces images in which the out-of-focus fluorescence is virtually eliminated ***(2)***. The term "confocal" refers to the fact that the objective and the condenser lenses are focused on the same spot. To produce an image using confocal microscopy, only a small volume in the specimen is illuminated at any time, and this volume is imaged into a pinhole placed in front of a detector so that only the light from a single plane is detected, and out-of-focus fluorescence is rejected. In essence, confocal microscopy allows optical sectioning of living tissues, in slices as thin as 500 nm, and three-dimensional (3D) reconstruction can be made without deconvolution of images. With this high-resolution method, dynamic events, such as spatial changes of Ca^{2+} concentration as a function of time, can be studied.

From: *Methods in Molecular Biology, Vol. 114: Calcium Signaling Protocols*
Edited by: D. G. Lambert

1.2. Confocal Calcium Imaging Combined with Two-Photon Uncaging Techniques

An alternative technique to measure intracellular $[Ca^{2+}]_i$ using confocal microscopy is two-photon excitation microscopy ***(3)***. Two-photon excitation microscopy provides a temporal and a spatial resolution comparable to that of conventional confocal microscopy, but with several advantages. Conventionally, a fluorochrome is excited by the absorption of a single photon of sufficient energy to raise the molecule to the excited state (from which it subsequently decays with the emission of a longer wavelength photon). However, the intense ultraviolet (UV) excitation radiation that is often used to excite the chromophores results in cell damage and photobleaching all along the excitation light cone. Using femtosecond lasers in the near-infrared wavelength region and high numerical aperture (NA) objective lenses, it is possible to provide a photon flux that allows one to excite the chromophores via the nonlinear two-photon absorption (TPA) process. This new nonlinear laser microscopy is based on the fact that the transition to the excited state of the chromophore is reached by the simultaneous absorption of two low energy photons, namely, in the near-infrared wavelength region. A high-power, near-infrared pulsed laser produces peak photon densities high enough that when focused into an appropriate medium, excitation by photon energy combinations can occur. For example, two red photons at 720 nm can interact simultaneously with a fluorescent molecule to produce a 360-nm UV electronic transition corresponding to twice the energy of each single photon.

The main advantage of two-photon fluorescence excitation is that the light is absorbed only at the focal spot. As the TPA process requires two excitation photons, the fluorescence photon flux depends on the square of the incident photon flux. Thus, when only in the sub-μm^3 focal region of the microscope objective lenses, the excitation photon flux is sufficient to give rise to efficient two-photon excitation. The majority of the cell excitation is confined to a volume <1 fL (1 μm^3) around the focal point; thus, photobleaching and photodamage take place only within the in-focus volume. Moreover, owing to the long excitation wavelength, this technique results in reduced scattering and high penetration depth (>100 μm below the surface of the preparation ***[4]***), compared to conventional confocal microscopy. This highly localized excitation process is therefore intrinsically confocal and confers a 3D resolution and produces an optical section without the use of a pinhole in front of the detector. This is in contrast to confocal techniques in which light is absorbed throughout the sample, and the depth discrimination is achieved using emission pinholes.

Some biological applications have been described, specifically, imaging of vital DNA stains in developing cells and embryos, imaging of cellular metabolic activity from NADH optically induced autofluorescence, spatially

resolved measurements of cytoplasmic Ca^{2+} ion activity, and optically induced micropharmacology using caged bioeffector molecules (such as caged Ca^{2+}, H^+, nucleotides, and neurotransmitters) ***(5–7)***.

1.3. Ca^{2+} Measurements and Confocal Microscopy: Technical Problems and Solutions

In this chapter, the authors will discuss some of the common difficulties encountered when viewing Ca^{2+}-sensitive fluorophores using confocal microscopy. When possible, they will attempt to provide solutions to the problems they present.

1.3.1. Compartmentalization of Ca^{2+}-Sensitive Fluorophores

The characterization of Ca^{2+} transients and gradients has been made possible by the many fluorescent probes developed over the past two decades. The Ca^{2+}-sensitive indicators have many advantageous qualities including the ability to respond to changes in Ca^{2+} within milliseconds. Researchers have used this fact to their advantage by designing detection methods with a temporal resolution as fast as one millisecond per line with submicrometer spatial resolution ***(8)***. The probes can be introduced into cells without compromising the plasma membrane, and these probes can be used at all levels of organization from whole organs to tissue fragments to dissociated single cells, and even single organelles. The majority of these probes measure the free $[Ca^{2+}]_i$ as opposed to the total $[Ca^{2+}]_i$. Many excellent review articles have dealt with the strengths and limitations of these molecules ***(9)***.

The suggestion that many of the Ca^{2+}-sensitive probes may be bound within cells has been prevalent for many years ***(10)***. However, quantifying the compartmentalization is difficult. The authors' studies focus of the compartmentalization of fluorophore molecules within the nucleus of *Xenopus laevis* oocytes. When they attempted to calculate the $[Ca^{2+}]$ in the nucleus, they observed that the nucleus from *X. laevis* oocytes consistently present with higher emission fluorescence than the cytoplasm ***(11)***. Further studies revealed similar patterns in other cell types.

1.3.2. Fluorescence Properties are Sensitive to the Environment

It is intuitive that the fluorescent properties of the Ca^{2+} indicators are sensitive to other elements in the environment. Both the extinction coefficient at the excitation wavelength and the quantum yield are sensitive to the local environment. This is best illustrated by experiments described by Tsien and Waggoner ***(12)*** showing that fluorescein had a high quantum yield in an aqueous solution (0.7), but that that yield decreased to 0.3 when the fluorophores were bound to an antibody molecule. Still, many researchers choose to ignore the effects of

the local environment (e.g., pH and solvent polarity), and readily make comparisons in the emission values of dyes between subcellular regions with extremely different environments. This was not a problem prior to the use of the confocal microscope, but the confocal microscope now provides researchers the ability to compare fluorescence emission between small regions.

1.3.3. Photobleaching During 3D Reconstructions Using Confocal Microscopy

Although photobleaching occurs in conventional and confocal microscopy, it is of greater concern when using confocal microscopy. This is owing to two unique features of the confocal microscope. First, the confocal microscope limits the amount of light, rejecting out-of-focus light. Thus, the researcher is typically working with relatively low emission light levels, and a further reduction owing to photobleaching is more noticeable and more bothersome. Second, a tremendous advantage of confocal microscopy is the ability to produce 3D reconstructions of an object of interest. The 3D reconstruction is created by sequentially capturing images within a series of *z* planes. The more *z* planes captured the sharper the 3D reconstruction. However, the excitation light pierces the entire sample with each image collected, and thus photobleaching intensifies with each scan. By the time the latter *z* planes are captured, the fluorophore emission may be significantly less than the initial images captured, making quantitative comparisons between the *z* planes difficult, if not impossible. An additional complicating factor when producing 3D reconstructions with confocal microscopy is that the emitted light is prone to "self-shadowing" effects, in which fluorescence is attenuated by reflection, refraction, scattering, and absorption by the other structures in the way of the light path ***(13)***. This effect is greater when the *z* plane is adjusted further into the sample (or away from the cover slip).

One theory concerning photobleaching suggests that its effects may be minimal with confocal microscopy, because as dye molecules are bleached, other "fresh" molecules will diffuse into the area of illumination and replenish the supply of dye within the focal plane ***(10)***. However, this is not the case because the excitation beam responsible for photobleaching illuminates more than the focal spot including cone-shaped regions above and below the focal plane, thereby photobleaching a large quantity of the fluorophore.

2. Materials

2.1. Ca^{2+} Measurements and Confocal Microscopy

1. Stage V *X. laevis* oocytes from *X. laevis* (adult females frogs were purchased from Xenopus I, Ann Arbor, MI).
2. NG108-15 neuroblastoma cells were cultured as described ***(14)***.

3. Barth's solution: 82 m*M* NaCl, 2 m*M* KCl, 20 m*M* $MgCl_2$, 5 m*M* HEPES, pH 7.6, with NaOH.
4. ND 96 buffer: 95 m*M* NaCl, 2 m*M* KCl, 5 m*M* $MgCl_2$, 5 m*M* HEPES, 1.8 m*M* $CaCl_2$, pH 7.5.
5. Mock intracellular solution: 140 m*M* KCl, 10 m*M* HEPES, 3 m*M* $MgCl_2$, pH 7.2.
6. Fluo-3 (dissolved in mock intracellular solution to obtain a stock solution of 1 m*M*) (Molecular Probes, Eugene, OR).
7. Fluo-3/AM (stock solution of 5 m*M* in dimethylsufoxide/Pluronic acid) (Molecular Probes).
8. Zeiss LSM-410 Laser Confocal Microscopes were used to image fluo-3 (510 nm dichroic mirror, 515 nm Long Pass [LP] emission filter; Chroma Technology, Brattleboro, VT) (*see* **Note 1**).
9. Caged inositol(1,4,5)trisphosphate [Ins(1,4,5)P_3] dissolved in Mock intracellular solution to obtain a stock solution of 1 m*M*).
10. The light source for two-photon uncaging was a pulsed Ti:sapphire laser (Mira 900, Coherent Laser, Palo Alto, CA).
11. Collagenase type I (Worthington Biochemical Corp, Lakewood, NJ).
12. Priming media: 5 m*M* Tris-HCl, pH 7.8, 10 m*M* $MgCl_2$, 1 mg/mL Pronase B (Calbiochem, San Diego, CA).
13. Buffer A: 5 m*M* Tris-HCl, pH 7.8, 10 m*M* $MgCl_2$, 20 mg/mL bovine serum albumin (BSA).
14. Buffer B: 70 m*M* NH_4Cl, 7 m*M* $MgCl_2$, 0.1 m*M* EDTA, 2.5 m*M* dithiothreitol, 10 m*M* HEPES, pH 7.4, 20 mg/mL BSA.
15. Buffer C: 70 m*M* NH_4Cl, 7 m*M* $MgCl_2$, 0.1 m*M* EDTA, 2.5 m*M* DTT, 10 m*M* HEPES, pH 7.4, 5% glycerol.
16. Buffer J: 70 m*M* NH_4Cl, 7 m*M* $MgCl_2$, 0.1 m*M* EDTA, 2.5 m*M* DTT, 10 m*M* HEPES, pH 7.4, 10% glycerol.
17. Lysis medium: 70 m*M* NH_4Cl, 7 m*M* $MgCl_2$, 0.1 m*M* EDTA, 2.5 m*M* DTT, 10 m*M* HEPES, pH 7.4, 0.3% Nonidet-P40.

3. Methods

3.1. Ca^{2+} Measurements and Confocal Microscopy

3.1.1. Obtention of Oocytes and NG108-15 Neuroblastoma Cells

1. Under sterile conditions, make a 1-cm paramedian incision in the inferior abdominal wall with a no. 10 carbon steel surgical blade to remove two ovaries from an adult *X. laevis* female frog anesthetized by hypothermia. With the ovaries in Barth's solution. Close the abdominal wall, together with the peritoneum, using 6-0 ethilon monofilament nylon, and close the skin with three sutures.
2. Defolliculate oocytes by incubation for 30 min at room temperature in 150 mL of Barth's with 2 mg/mL of collagenase type I under gentle shaking.
3. At the end of each 30-min incubation, check the cells and add fresh collagenase solution. Typically, cells are free of most follicle cells within 1.5–2 h of collagenase exposure.
4. Then wash single oocytes five times in Barth's solution to remove the collagenase. During the washes, discard the stage I–II oocytes.

3.1.2. Obtention of Isolated Nuclei

1. Bisect stage V and VI oocytes with a fine needle inserted through the oocyte along its equator (the line that divides the oocyte in a vegetal pole and animal pole) in Mock intracellular solution.
2. Remove nuclei using a glass pipet, and place it in a dish filled with Mock intracellular solution.

3.1.3. Confocal Imaging of Nuclei and Neuroblastoma Cells

1. Wash isolated nuclei out of cytoplasm in Mock intracellular solution.
2. Incubate nuclei in Mock intracellular solution containing ~10 μ*M* fluo-3/AM for 15–30 min at 37°C to accomplish loading of the nuclear cisterna with membrane-permeant fluorescent dyes (*see* **Note 1**).
3. Incubate neuroblastoma cells with Barth's solution containing ~10 μ*M* fluo-3/AM for 30 min at 37°C.
4. Induce Ca^{2+} transients by adding bradykinin to the bath (final concentration in the bath 100 μ*M*).
5. Image cells and nuclei using the Zeiss LSM-410 (*see* **Note 1**).

3.2. Confocal Calcium Imaging Combined with Two-Photon Uncaging Techniques

1. Surgically remove stage V–VI albino *X. laevis* oocytes from female adult frogs as described in **Subheading 3.1.**
2. To load the nucleoplasm with a nonpermeant form of a Ca^{2+} indicator dye, inject intact *Xenopus* oocytes with 50 nL of 1 m*M* fluo-3. The estimated concentration of fluo-3 inside oocytes is ~50 μ*M*.
3. To induce Ca^{2+} release from the intracellular stores, inject *Xenopus* oocytes with 50 nL of 1 m*M* caged Ins(1,4,5)P_3 (estimated concentration 1 μ*M*).
4. Perform the oocyte stratification by layering the cells in a discontinuous gradient prepared by adding to an Eppendorf tube 500 μL of Ficoll 400 followed by 500 μL of ND 96 buffer. Centrifuge this preparation for 1 h at 4000*g* as described ***(15,16)***.
5. Set the Ti:sapphire laser for uncaging of Ins(1,4,5,)P_3 to a pulse width ~160 fs; repetition rate 76 MHz; average power at laser output ~1 W; at specimen ~50 mW and wavelength 720 nm.
6. Image the oocytes using confocal microscopy (*see* **Note 2**).

3.3. Ca^{2+} Measurements and Confocal Microscopy: Technical Problems and Solutions

3.3.1. Nucleoplasm Extracts

The protocol for large preparations of isolated nuclei is based on methods described by Ruberti et al. ***(17)***. Briefly:

1. Resuspend 2 mL of packed oocytes in 0.7 mL of priming medium. Continue incubation for 10–15 min at room temperature until the oocytes become flattened and are soft.

2. Remove Pronase completely from the bathing solution by washing the oocytes 5–10 times in Buffer A.
3. Then wash the oocytes once in cold Buffer B and once, very briefly, in lysis medium.
4. Subsequently, incubate the treated oocytes for 10 min at 0°C under mild shaking in 2 mL of lysis medium. The nuclei float to the surface of the medium where they can be collected with a Pasteur pipet and stored in Buffer J (1 µL of buffer/nucleus).
5. Isolate crude nucleoplasm by manually disrupting nuclei that were stored in Buffer J by pipetting them with 1-mL pipet tips. Centrifuge the lysate for 10 min at 500*g* at 4°C, remove the supernatant, and add 10 m*M* HEPES to buffer pH. Store the crude nucleoplasm at –70°C.

3.3.2. Cytoplasm Extracts

1. Owing to similar sedimentation of oocyte nuclear and cytoplasmic components in Percoll layers ***(18)***, manually enucleate oocytes prior to the isolation of crude nucleoplasm ***(19)***.
2. Place enucleated cells in 1 mL of 0.1% Triton X-100, 0.1 *M* Tris, pH 7.4, 0.15% phenylmethylsulfonylfluoride, pipet through a 1-mL pipet tip, and isolate the cytoplasm by centrifugation at 1500*g* for 10 min.

3.3.3. Ca^{2+}-Clamped Extracts

1. When adequate crude nucleoplasmic and cytoplasmic samples are obtained, store the extracts into 50 µL samples.
2. Clamp free Ca^{2+} using methods described by Neher ***(20)***. To achieve the desired Ca^{2+} concentration within each sample, add appropriate ratios of H_2K_2EGTA and CaK_2EGTA. The recipe for the Ca^{2+}-clamped solutions can be found in Neher ***(20)***. Typically, the authors prepare samples with free Ca^{2+} concentrations of 10, 100, 250, 500, and 750 n*M*, and 1 and 10 m*M*. The range of Ca^{2+} concentrations should match the K_d properties of the Ca^{2+}-sensitive fluorophore being tested.
3. Place 50 µL of each sample (nucleoplasmic vs cytoplasmic at each Ca^{2+} concentration) on a cover slip on the confocal microscope.
4. Add fluo/3 or indo-1 to the aliquots to a final concentration of 10 µ*M*.
5. Measure fluorescence emission using confocal microscopy (*see* **Notes 3** and **4**).
6. Carry out the experiments at 20°C.

4. Notes

1. Calcium measurements using confocal microscopy
   a. The author's laboratory has imaged Ca^{2+} using an LSM-410 laser scanning microscope (Carl Zeiss, Thornwood, NY) setup combined with an Axiovert 135 invert microscope. The *x*, *y* resolution is ~200 nm and is obtained using ×16 or ×400 high numerical aperture objectives. The maximal resolution obtained in the *z*-axis is ~500 nm. Maximal temporal resolution of full image

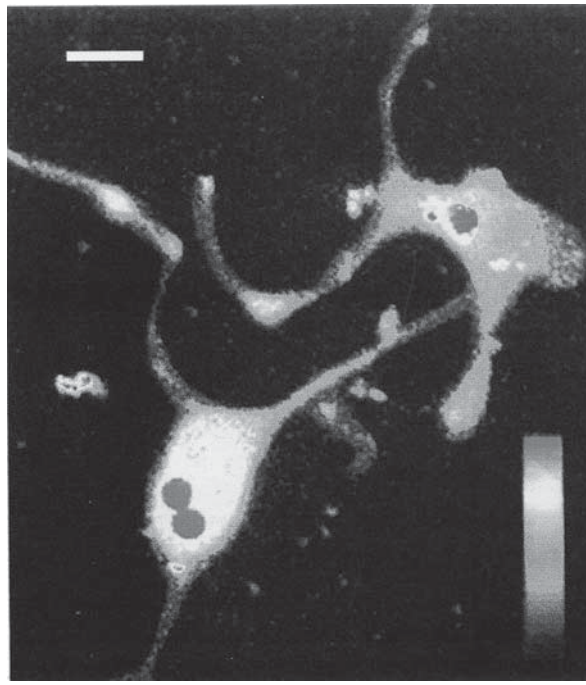

Fig. 1. Nuclei from cultured neuroblastoma cells (NG108-15) have higher fluo-3 emission than the cytoplasm region. Quiescent neuroblastoma cells loaded with the permeant form of the Ca^{2+} indicator fluo-3 have a higher fluorescent emission in the nucleus than in the cytoplasm. These images are representative of over 100 cells loaded with fluo-3 AM. Bar = 10 μm.

acquisition can be obtained in 0.5 s. The line scan is obtained at 1.5 ms resolution. The light sources employed by this microscope are an Argon/Krypton laser (Omnichrone, Chino, CA) for 488-nm light and an Innova 300 laser (Coherent, Palo Alto, CA) for 361-nm light. The scanner is controlled with the LSM 3.91 software provided by Zeiss. Images obtained are stored and studied off-line with ANALYZE (Mayo Foundation, Rochester, MN) using a Silicon Graphics Personal Iris Computer (Mountain View, CA).

b. **Figure 1** depicts typical cultured neuroblastoma cells (NG108-15) that were loaded with the membrane-permeant form of fluo-3 and imaged using the Zeiss LSM-410, with a ×40 oil immersion objective (NA 1.3). The fluorescence from the cell was filtered by a 515-nm long-pass filter. These unstimulated cells displayed such a high level of fluorescence from the nucleus that it saturated the confocal detection device (photomultiplier tube). By contrast, the cytoplasmic fluorescence values indicate a free Ca^{2+} concentration in the range of 75–150 n*M*. Based on observations like these, many published articles have concluded that Ca^{2+} in the nucleus was higher than Ca^{2+} in the cytoplasm ***(21,22)***. Such findings were surprising to the authors, given their

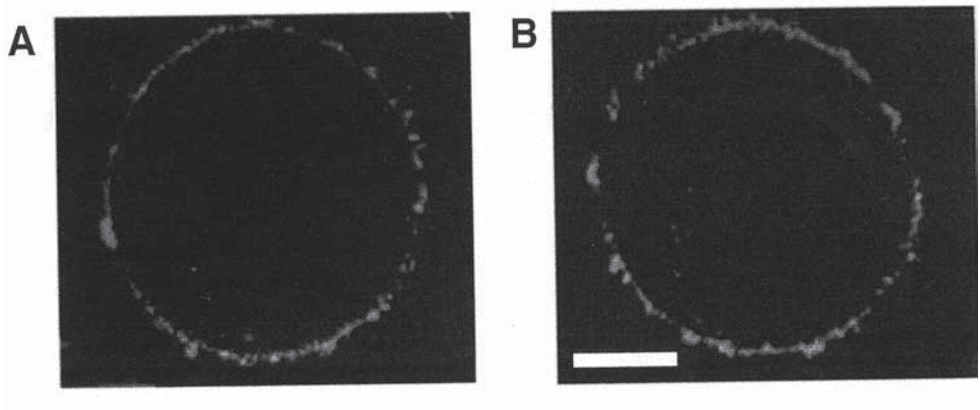

Fig. 2. Isolated nuclei exclude divalent influx into the nuclear cisterna. **(A)** An isolated nuclei loaded with the Ca^{2+} indicator indo-1 illustrates high levels of the dye trapped within the nuclear cisterna. **(B)** The same nucleus was exposed to 1 m*M* $MnCl_2$, which quenches the fluorescence of indo-1 when measured at the Ca^{2+} insensitive wavelength. Five minutes after exposure to $MnCl_2$, no significant decrease in the fluorescence emission was noted. Thus, the indo-1 within the cisterna was not exposed to the bath $MnCl_2$. Bar = 200 µm.

earlier work on isolated nuclei that demonstrated the free flow of ions across the nuclear envelope ***(23)***.

c. The fact that some dyes compartmentalize in intracellular organelles can be useful in studying subcellular Ca^{2+} activity with confocal microscopy. The nuclear cisterna can be loaded with membrane-permeant forms of the Ca^{2+}-sensitive fluorophores, which indicate relative changes in the cisternal Ca^{2+} concentration. However, this compartment of fluorescence can only be viewed using confocal microscopy that allows for the capturing of thin *z* sections. **Figure 2A** is an isolated nucleus incubated in the membrane-permeant form of indo-1. The fluorescent ring indicates the free Ca^{2+} levels in the nuclear cisternal region. Verification of a cisternal loading was obtained by exposing the nucleus to 1 m*M* $MnCl_2$, which binds to indo-1 and quenches the emission fluorescence. **Figure 2B** is a confocal image of the same nucleus 5 min after the addition of 1 m*M* $MnCl_2$. Clearly, the fluorescent ring in the cisterna remained intense in the presence of $MnCl_2$. Thus, the indo-1 present in the nuclear ring was not exposed to the $MnCl_2$, it was in a separate compartment: the nuclear cisterna. The authors have repeatedly used this technique with confocal microscopy to measure ionic flux across the nuclear envelope ***(23)*** and the plasma membrane.

d. Since indo-1 is a ratiometric dye providing the capability of determining Ca^{2+} concentrations, the authors attempted to calculate the Ca^{2+} concentration within this compartment. They found that the average Ca^{2+} concentration calculated depended solely on the manner in which the investigator distinguished the region of interest. Indo-1 ratio values varied widely, and they

concluded that the calculation of absolute Ca^{2+} concentrations within such a small and irregularly shaped region was not wise. Rather, the percentage of change in the emission fluorescence should be reported, given that the investigators have completed the control experiments that the authors described earlier. In other applications, the use of ratiometric dyes to monitor Ca^{2+} with confocal may be appropriate. Using a line scan mode, Helm et al. ***(24)*** illustrated a temporal resolution of 20 ms per line scan that resulted in localized measurements of Ca^{2+} with less than 1% error in control solutions.

e. Preferentially loading an organelle with the membrane-permeant form of a Ca^{2+}-sensitive dye requires that the organelle contain the esterase necessary to activate the fluorescent molecule. It has been the authors experience that the loading of the nuclear cisternal region occurs best at 37°C. Whereas mammalian cells are normally incubated in the AM form of the dye at 37°C for loading, oocytes are normally maintained at 18°C. Exposing isolated nuclei to fluo-3, Ca^{2+} Orange, or Ca^{2+} Green dyes, at 18°C, resulted in no loading of the nuclei with dye even when the incubation was extended overnight. Similarly, the nuclei failed to load with the fluorophores at room temperature. However, when nuclei were incubated for only 15 min at 37°C, they loaded sufficiently with the fluorophore ***(25–26)***. The authors completed control experiments to determine that the transport mechanisms within the nuclear envelope were unaffected by the short 37°C incubation.

2. Confocal calcium imaging combined with two-photon uncaging techniques

a. The authors describe here an application of laser-scanning confocal microscopy implemented with the two-photon technique as a tool for highly localized uncaging (~1 μm^3) of the second messenger $Ins(1,4,5)P_3$. $[Ca^{2+}]_i$ was monitored on a modified Zeiss LSM-410 laser-scanning confocal microscope with a ×16 objective (numerical aperture 0.5) at a wavelength of 488 nm. Two-dimensional images were acquired from each oocyte, by scanning 256 × 256 pixels per image. Confocal images were acquired at 1.4-s intervals. The thickness of the confocal section was controlled by varying the pinhole aperture in the detection pathway. The effective thickness of the confocal optical section was 30 μm.

b. To obtain two-photon uncaging while simultaneously imaging Ca^{2+}, the confocal microscope (Zeiss Axiovert 135) was adapted so that the pulsed beam arrived at the objective via the camera port. This path was designed to minimize the pulse broadening and the subsequent power loss incurred from the LSM optics.

c. Coincidence of the visible and two-photon focal planes was verified using thin confocal sections (~5 μm). An external shutter system controlled exposure times (0.01–1.0 s).

d. The two-photon beam was steered from the Mira 900 laser to the camera port using custom infrared gold reflective mirrors (CVI Laser, Albuquerque, NM). To compensate for the focusing optics within the microscope, a 40-mm achromate was placed in the beam path before entry into the port. The beam was aligned to the back aperture of the objective by comparing the beam diameter

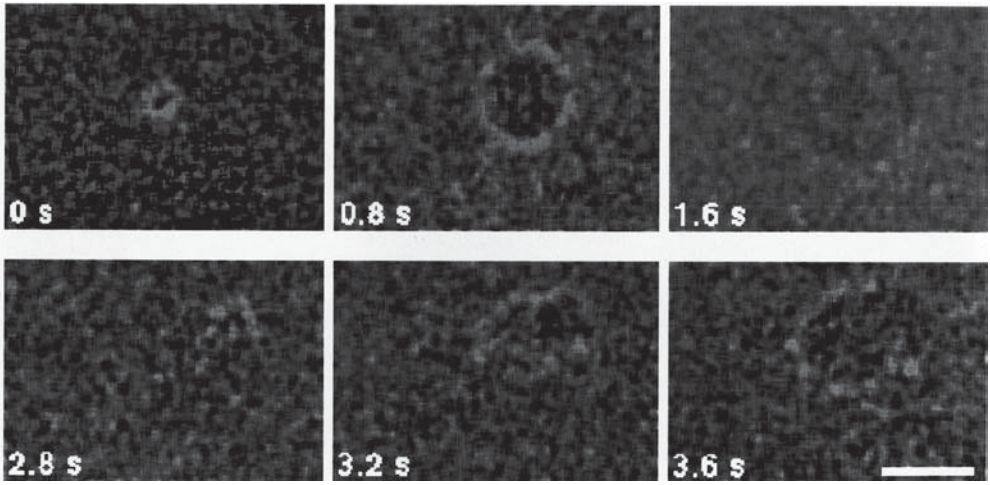

Fig. 3. Two-photon uncaging of Ins(1,4,5)P_3 within a normal Xenopus oocyte. The released Ins(1,4,5)P_3 (~1 μm^3) elicited planar circular waves (**panels 1–3** 0–1.6 s). Following this propagation, a secondary Ca^{2+} wave spontaneously regenerates (**panels 4–6** 2.8–3.6 s). Bar = 50μm.

in both the near and far fields. Adjustments in focusing lenses were made to present a parallel beam to the back aperture of the objective.

e. To allow simultaneous 488-nm imaging and two-photon uncaging on the Axiovert, an extra 610-nm LP dichroic mirror was inserted in the excitation path to reflect the 488 nm and pass the 720-nm two-photon beam to the objective. Emission spectra were passed back through the same 488-nm excitation path to the internal photomultiplier tube of the LSM 410. In this way, the authors were able to induce 3D release of Ins(1,4,5)P_3 while simultaneously recording the changes in intracellular Ca^{2+} concentration. The combination of these two techniques allowed them to functionally characterize the ability of the intracellular stores (i.e., endoplasmic reticulum [ER]) to generate a signal in response to a focal release of this second messenger.

f. As illustrated in **Fig. 3**, planar circular Ca^{2+} waves can be selectively elicited inside *Xenopus* oocytes, similar to those described previously ***(27,28)***. Such circular Ca^{2+} waves can be regenerative (**panels 4–6**), the regeneration center being slightly eccentric and the wave front shape irregular.

g. Ca^{2+} release in response to Ins(1,4,5)P_3 was correlated with the position of the Ca^{2+} stores. Repositioning of the ER into a discrete layer allowed the authors to examine altered pattern of Ins(1,4,5)P_3-induced Ca^{2+} release. This was achieved by stratifying organelles and other cellular components inside an intact *Xenopus* egg by centrifugation ***(29,30)***. The stratification resulted in four predominant layers: lipid-, ER-, mitochondria-, and yolk-enriched layers that partitioned within the cytoplasm based on their density. The structural morphology of the ER and mitochondria are preserved as shown by transmission electron micrographs ***(31)***.

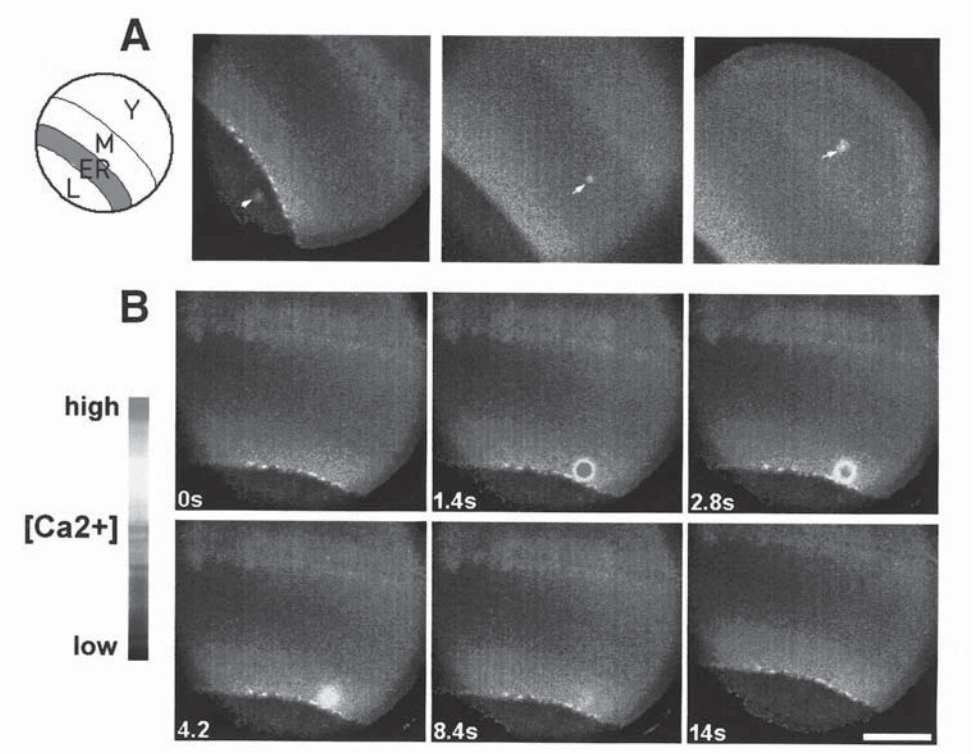

Fig. 4. Localization of Ca^{2+} release in the different layers of the stratified oocyte. **(A)** Two-photon uncaging of Ins(1,4,5)P_3 within the lipid (L), the mitochondria (M), and the yolk (Y) layers. **(B)** Kinetics of the Ca^{2+} release by the uncaged Ins(1,4,5)P_3 within the ER layer. Bar = 100 μm. (Modified from **ref. *31***.)

h. **Figure 4** illustrates the selective uncaging of Ins(1,4,5)P_3 within the different layers of the stratified oocyte. Although minimal or no Ca^{2+} responses were detected in the lipid, mitochondria, and yolk layers (**Fig. 4A**), the Ca^{2+} increase measured within the ER layer confirmed the latter as a major intracellular Ca^{2+} store sensitive to Ins(1,4,5)P_3 (**Fig. 4B**).

i. The ability of fluo-3 to monitor [Ca^{2+}] changes in the different layers (which is especially difficult in the lipid layer in which the dye is confined between the lipid droplets) was confirmed by producing a hole in the plasma membrane of each layer by directing the laser beam to the region at high power (75 mW at sample, 2-s duration). **Figure 5** illustrates that the Ca^{2+} leak through the resulting hole produced a saturating level of fluorescence in the ER- and mitochondria-layers.

j. Images were compiled with ANALYZE software (Mayo Foundation) on a Silicon Graphics Iris Indigo computer.

3. Ca^{2+} measurements and confocal microscopy: technical problems and solutions

   a. The authors' experience lies in the calibration of cytoplasmic or nucleoplasmic fluorescence of *X. laevis* oocytes. However, in vitro fluorophore calibra-

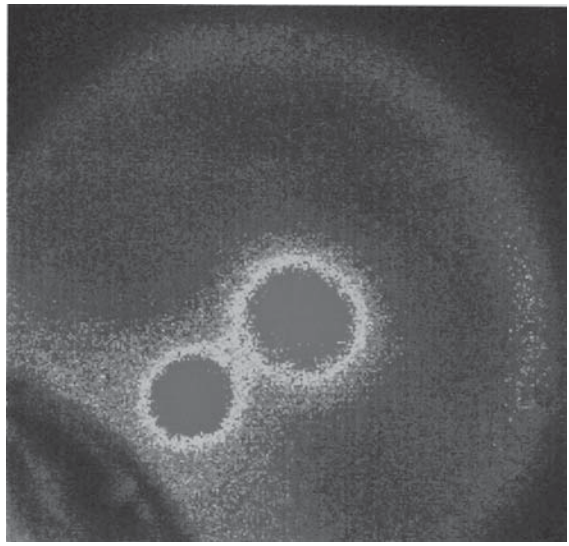

Fig. 5. Test of the Ca^{2+} saturability of the cytoplasmic fluo-3 within the different layers of the stratified oocyte. Comparable massive Ca^{2+} leaks were obtained in the ER and mitochondria layers through the resulting hole produced in the plasma membrane by directing the laser beam to the region at high power (75 mW at sample, 2-s duration).

tion of other subcellular environments could be completed in the same manner, beginning with the instructions in **Subheading 3.3.3.**

b. Stage I–VI oocytes are distinguished by size and appearance *(32)*.
c. Practically, the authors have found photobleaching to be a serious problem that requires extensive controls and precautions. To reduce the effects of photobleaching, the intensity of the excitation light used to irradiate the sample should be as weak as possible, but still allow sufficient emission light. Additionally, rhodamine-based fluorophores are more stable than the fluorescein-based dyes, and thus exhibit less photobleaching *(33)*. However, the lower quantum yield of rhodamine-based dyes makes them darker than their fluorescein counterparts.
d. When capturing images for 3D construction of cells, control experiments should include the collection of images from several different cells with each series beginning in a different *z* plane. The authors collect images of a cell beginning at the point where the cell meets the cover slip. Subsequently, they collect a series of images from another cell beginning at the highest *z* plane. They may also begin capturing images in the center of the cell and work toward the cover slip, then complete the upper region of the cell. The average pixel values are then plotted according to the sequence in which they were collected. In this manner, the decline in emission owing to photobleaching can be calculated. Prior to 3D reconstruction, each *z* plane image is digitally corrected for the percentage of photobleaching measured. The result is a more uniform image even when a hundred *z* plane scans are collected (**Fig. 6**).

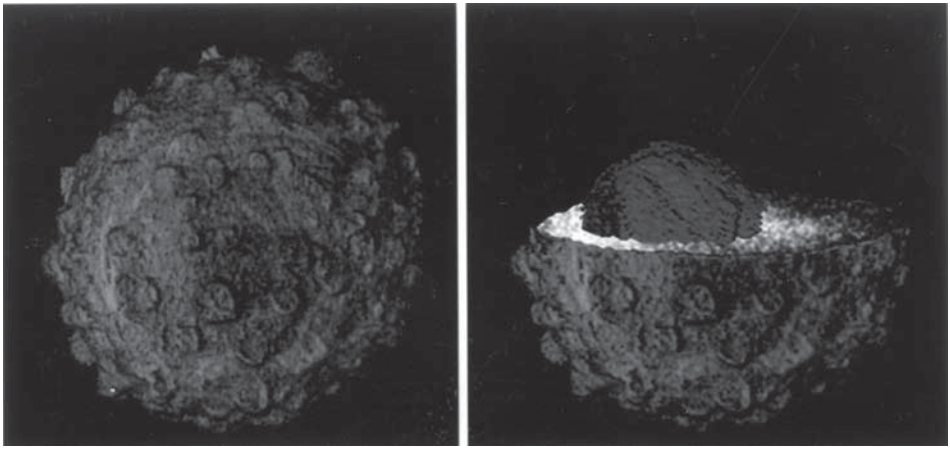

Fig. 6. 3D reconstruction of a triple-stained nucleus. An isolated nucleus was incubated in a membrane-bound fluorophore, rhodamine B. A full set of *z* sections was captured for a later 3D reconstruction (green). The same nucleus was loaded with the Ca^{2+} indicator Calcium Green (Molecular Probes), and another set of *z* sections was collected. Within these images, contaminating fluorescence from the rhodamine B was present. Using the software package ANALYZE, each *z* section image captured with rhodamine B alone was digitally subtracted from each corresponding *z* section taken with rhodamine and Calcium Green present, resulting in images with pure Calcium Green emission. Subsequently, the same nucleus was loaded with the nucleotide-specific fluorophore Hoechst, and the nucleolus was resolved. Nonnucleolar Hoechst fluorescence was removed using the software package ANALYZE. There was no contamination from the other fluorophores during the acquisition of the Hoechst images, because the excitation and emission wavelengths had little overlap. Finally, each set of *z* sections was 3D rendered separately, and was superimposed using the software package Adobe Photoshop.

e. Likewise, if the experiments require monitoring cells over a long period of time, photobleaching can complicate the interpretation of the results. Control experiments that should be completed include the collection of images of quiescent cells over the same time frame. Again, the inherent photobleaching of the sample should be calculated and used to correct the loss of emission owing to photobleaching in experimental groups.

4. Ca^{2+}-clamped extracts
   a. As with any confocal microscope experiment in which quantitative results are obtained, the gain, brightness, contrast, pinhole size, scan speed, or other software and hardware settings on the microscope must not be changed between samples, such as between control and experimental groups. The units for the emission values will vary according to the detection system, but, practically speaking, are arbitrary. The emission values are plotted vs the free Ca^{2+} concentration of the sample ***(11)***.

b. Effective means of controlling for environmental differences exist, but they usually require the ability to isolate the two environments. The authors have used crude cytoplasmic and nucleoplasmic preparations to compare the absorption and emission spectra of fluo-3 ***(11)***, and they have included a full description of that protocol in the **Subheadings 3.3.1.** and **3.3.2.** They demonstrated that fluo-3 within the nucleus contains a different emission and excitation spectra that resulted in an increase in the detected fluorescence ***(11)***. To illustrate this point, fluo-3 diluted in crude nucleoplasm or cytoplasm was placed in drops on the confocal microscope. Subsequently, gain and contrast settings on the confocal microscope were adjusted in a manner that resulted in a linear relationship between the Ca^{2+} concentration and the fluorescence emission of the cytoplasmic samples. However, the same Ca^{2+}-clamped buffers diluted in nucleoplasm saturated the detection device of the confocal microscope at 100 n*M* free Ca^{2+} ***(11)***. These control experiments illustrate the magnitude of the problem that can arise from the shifts in the absorption and emission spectra of the fluorophore within the nucleus. The findings are particularly important for researchers using confocal microscopy when comparing free Ca^{2+} concentrations between the nucleus and cytoplasm in intact cells.

c. This protocol (*see* **Subheading 3.3.3.**) can be modified to determine the extent to which a fluorophore is compartmentalized within the cell. In this case, cells would be loaded with the fluorophore prior to preparation of the extracts. A limitation is placed on the fluorophore, in that it must have a Ca^{2+}-independent wavelength, such as indo-1. After the cells are loaded, the extracts would be prepared as described above. The emission light would be monitored at the Ca^{2+}-insensitive wavelength; thus, clamping of the Ca^{2+} concentration is not necessary. Fifty µL of each extract is placed on the confocal microscope and the emission at the Ca^{2+}-independent wavelength is obtained. Any differences in the emission values would suggest either compartmentalization of the dye, or a difference in the emission or excitation properties of the dye owing to the environmental differences of the extracts.

d. The authors determined that the majority of the nuclear fluo-3 was bound within the nucleus. They loaded intact *X. laevis* oocyte nuclei by incubation in the membrane-permeant form of fluo-3 (10 µ*M*) for 20 min. (The dye molecules enter the nucleoplasm supposedly by diffusing through the nuclear pore complex.) Subsequently, they removed the nuclear envelope using a technique that they have described previously ***(23)***. The bare nucleoplasm, bathed in a mock intracellular solution (*see* **Subheading 2.**, **item 5**), continued to fluoresce for over 30 min ***(25)***. The results indicated that the dye within the nucleus was not free to diffuse into the bath solution but, rather, was bound to the nucleoplasm. A bound form of the fluorophore will lead to a continued concentration gradient of the unbound form of the molecule between the cytoplasm and nucleoplasm. The end result will be a higher concentration of fluo-3 in the nucleus of oocytes. Although the authors have not tested all

Ca^{2+}-sensitive fluorophores for possible concentration gradients across the nuclear membranes, they have obtained similar results with Ca^{2+} Green, and Texas Red (Molecular Probes).

References

1. Tsien, R. Y. (1980) New calcium indicators and buffers with high selectivity against magnesium and protons: design, synthesis and properties of prototype structures. *Biochem.* **19,** 2396–2404.
2. Minsky, M. L. (1988) Memoir on inventing the confocal scanning microscope. *Scanning* **10,** 128–138.
3. Denk, W., Strickler, J., and Webb, W. W. (1990) Two-photon laser scanning fluorescence microscopy. *Science* **248,** 73–76.
4. Denk, W., Delaney, K. R., Gelperin, A., Kleinfeld, D., Strowbridge, B. W., Tank D. W., and Yuste, R. (1994) Anatomical and functional imaging of neurons using 2-photon laser scanning microscopy. *J. Neurosci. Methods* **54,** 152–162.
5. Piston, D. W., Masters, B. R., and Webb, W. W. (1995) Three-dimensionally resolved NAD(P)H cellular metabolic redox imaging of the in situ cornea with two-photon excitation laser scanning microscopy. *J. Microsc.* **178,** 20–27.
6. Piston, D. W., Kirby, M. S., Cheng, J., Lederer, W. J., and Webb, W. W. (1994) Two-photon-excitation fluorescence imaging of three-dimensional calcium-ion activity. *Appl. Opt.* **33,** 662–669.
7. Denk, W. (1994) Two-photon scanning photochemical microscopy: Mapping ligand-gated ion channel distributions. *Proc. Natl. Acad. Sci. USA* **91,** 6629–6633.
8. Parker, I., Callamaras, N., and Wier, W. G. (1997) A high-resolution, confocal laser-scanning microscope and flash photolysis system for physiological studies. *Cell Calcium* **21,** 441–452.
9. Tsien, R. Y. (1989) Fluorescent indicators of ion concentrations, in *Methods Cell Biology* (Taylor, D. and Wang, Y. L., eds.), Academic, San Diego, pp. 127–156.
10. Parker, I. and Ivorra, I. (1993) Confocal microfluorimetry of Ca^{2+} signals evoked in Xenopus oocytes by photoreleased inositol trisphosphate. *J. Physiol.* **461,** 133–165.
11. Perez-Terzic, C., Stehno-Bittel, L., and Clapham, D. E. (1997) Nucleoplasmic and cytoplasmic differences in the fluorescence properties of the calcium indicator Fluo-3. *Cell Calcium* **21,** 275–282.
12. Tsien, R. Y. and Waggoner, A. (1990) *Handbook of Biological Confocal Microscopy*, 2nd ed. (Pawley, J., ed.), Plenum, New York, pp. 169–178.
13. Laurent, M., Johannin, G., Gilbert, N., Lucas L., Cassio, D., Petit, P., and Gleury, A. (1994) Power and limits of laser scanning confocal microscopy. *Biol. Cell* **80,** 229–240.
14. Huang, X. Y., Morielli, A. D., and Peralta, E. G. (1993) Tyrosine kinase-dependent suppression of a potassium channel by the G protein-coupled m1 muscarinic acetylcholine receptor. *Cell* **75,** 1145–1156.
15. Cran, D. G. (1987) The distribution of organelles in mammalian oocytes following centrifugation prior to injection of foreign DNA. *Gamete Res.* **18,** 67–76.

16. Han J. K. and Nuccitelli R. (1990) Inositol 1,4,5-trisphosphate-induced calcium release in the organelle layers of the stratified, intact egg of Xenopus laevis. *J. Cell Biol.* **110,** 1103–1110.
17. Ruberti, I., Beccari, E., and Carnevalli, F. (1989) Large scale isolation of nuclei from oocytes of *Xenopus laevis*. *Analytical Biochem.* **180,** 177–180.
18. Dreyer, C., Singer, H., and Hausen, P. (1981) Tissue specific antigens in the germinal vesicle of *Xenopus laevis* oocytes. *Wilhelm Roux Arch.* **190,** 197–207.
19. Gard, D. L., (1991) Organization, nucleation, and acetylation of microtubules in *Xenopus laevis* oocytes: A study by confocal immunofluorescence microscopy. *Dev. Biol.* **143,** 346–362.
20. Neher, E. (1988) The influence of intracellular calcium concentration on degranulation of dialyzed mast cells from rat peritoneum. *J. Physiol.* **395,** 193–214.
21. Hernandez-Cruz, A., Sala, F., and Adams, P. R. (1990) Subcellular calcium transients visualized by confocal microscopy in a voltage-clamped vertebrate neuron. *Science* **247,** 858–862.
22. Himpens, B., De Smedt, H., Droogmans, G., and Casteels, R. (1992) Differences in regulation between nuclear and cytoplasmic calcium in cultured smooth muscle cells. *Am. J. Physiol.* **263,** C95–C105.
23. Stehno-Bittel, L., Perez-Terzic, C., and Clapham, D. E. (1995) Diffusion across the nuclear envelope inhibited by depletion of the nuclear Ca^{2+} store. *Science* **270,** 1835–1838.
24. Helm, P. J., Franksson, O., and Carlsson, K. (1995) A confocal scanning laser microscope for quantitative ratiometric 3D measurements of $[Ca^{2+}]$ and Ca^{2+} diffusions in living cells stained with Fura-2. *Plugers Arch.* **429,** 672–681.
25. Lee, M. A., Dunn, R., Clapham, D. E., and Stehno-Bittel, L. (1997) Regulation of the nuclear pore complex by nuclear Ca^{2+}. *Cell Calcium*, in press.
26. Stehno-Bittel, L., Luckhoff, A., and Clapham, D. E. (1995) Calcium release from the nucleus by $InsP_3$ receptor channels. *Neuron* **14,** 163–167.
27. Lechleiter, J. D., Girard, S., Peralta, E., and Clapham, D. E. (1991) Spiral calcium wave propagation and annihilation in *Xenopus* oocytes. *Science* **252,** 123–126.
28. Lechleiter, J. D. and Clapham, D. E. (1992) Molecular mechanisms of intracellular calcium excitability in *X. laevis* oocytes. *Cell* **69,** 283–294.
29. Cran, D. G (1987) The distribution of organelles in mammalian oocytes following centrifugation prior to injection of foreign DNA. *Gamete Res.* **18,** 67–76.
30. Han, J. K. and Nuccitelli, R. (1990) Inositol 1,4,5-trisphosphate-induced calcium release in the organelle layers of the stratified, intact egg of *Xenopus laevis*. *J. Cell Biol.* **110,** 1103–1110.
31. Jaconi, M. E. E., Pyle, J., Bortolon, R., Ou, J. and Clapham, D. E. (1997) Calcium release and influx colocalizes with endoplasmic reticulum. *Curr. Biol.* **7,** 599–602.
32. Dumont, J. N. (1972) Oogenesis in *Xenopus laevis*. *J. Morphol.* **136,** 153–180.
33. McKay, I. C., Forman, D., and White, R. G. (1981) A comparison of fluorescein isothiocyanate and lissamine rhodamine as labels for antibody in the fluorescent-antibody technique. *Immunol.* **43,** 591–602.

6

Single Cell and Subcellular Measurement of Intracellular Ca^{2+} Concentration ($[Ca^{2+}]_i$)

Anthony J. Morgan and Andrew P. Thomas

1. Introduction

1.1. Why Measure Ca^{2+} at the Single Cell Level?

Measurement of the intracellular Ca^{2+} concentration ($[Ca^{2+}]_i$) in populations of cells is an excellent tool to complement population measurements of other cell parameters, but the usefulness of this approach is limited by several problems, not the least of which is temporal averaging. In population studies, agonists often evoke a characteristic peak and plateau type of response irrespective of the stimulus intensity. However, equivalent experiments using single cells can often reveal exceedingly complex patterns, such as oscillations of the cytosolic Ca^{2+} concentration ($[Ca^{2+}]_c$) ***(1)***. By and large these patterns cannot be observed in population studies since cells oscillate out of phase and at different frequencies, resulting in a smooth population average. It is only when cells are electrically well coupled that synchronized, population oscillations can be recorded, but this case is more the exception than the rule.

Temporal averaging will also distort the initial kinetics and peak responses to a given stimulus. In populations, the initial response to submaximal concentrations of agonist is influenced by several factors, such as the latency prior to the initial $[Ca^{2+}]_c$ response (which may vary considerably from cell-to-cell), the percentage of responding cells and cell to cell differences in sensitivity (which in turn may affect the degree of synchronization and magnitude). Furthermore, with population recording it is difficult to eliminate signals emanating from contaminating cell types or unhealthy cells.

There are also some technical advantages in measuring Ca^{2+} at the single-cell level. For instance, such measurement facilitates microinjection, simulta-

From: *Methods in Molecular Biology, Vol. 114: Calcium Signaling Protocols*
Edited by: D. G. Lambert

neous electrophysiological recording, and flash photolysis of caged compounds. Moreover, for those studying $[Ca^{2+}]_c$ in very large cells such as oocytes, single-cell recording has to be the method of choice because of optical limitations imposed by cell thickness.

1.2. Why Measure Subcellular Ca^{2+} Responses?

Just as a population $[Ca^{2+}]_c$ recording reflects the average of heterogeneous single-cell responses, so the single-cell response reflects the averaging of heterogeneous subcellular events; it is merely the next level of organization. Such heterogeneity is presumably a consequence of a nonuniform distribution of channel and/or pump activity ***(2,3)*** giving rise to such complex spatial phenomena as the discrete $[Ca^{2+}]_c$ blips and puffs (quarks and sparks) ***(4)***, localized $[Ca^{2+}]_c$ oscillations ***(5)***, right through to full-blown propagating $[Ca^{2+}]_c$ waves (the spatial counterpart of an oscillatory spike) ***(1,4)***. Such rises in heterogeneous $[Ca^{2+}]_c$ have been proposed to afford the cell a means of locally regulating cellular events ranging from polarized fluid secretion, as in pancreatic acini ***(6)***, to the regulation of fertilization in oocytes ***(7)***.

In addition to specialized regions of the cytoplasm forming discrete units, it is now becoming increasingly clear that Ca^{2+} levels fluctuate in a highly controlled manner in subcellular organelles. From the large nucleus ***(8)***, to the smaller mitochondria ***(9,10)*** and secretory vesicles ***(11)***, these membrane-delimited regions of the cell often respond to and in turn influence $[Ca^{2+}]_c$ in a dynamic manner in keeping with their physiological role. It is quite clear then that the $[Ca^{2+}]_i$ response of a cell is far from homogeneous, for which reason one has to examine the subcellular level in order to fully understand Ca^{2+} homeostasis.

1.3. Ca^{2+}-Sensitive Fluorescence Imaging

The method of choice for monitoring single-cell $[Ca^{2+}]_i$ signals is that using Ca^{2+}-sensitive fluorescent probes that have been the subject of previous reviews ***(12,13)***. We shall, nevertheless, briefly discuss their essential features, drawbacks, and practical applications.

Simply stated, this technique relies on the introduction into the cell of a dye whose fluorescent properties change when it binds Ca^{2+}. Consequently, by monitoring the emitted light, one thereby monitors the free intracellular Ca^{2+} concentration ($[Ca^{2+}]_i$). The recording of $[Ca^{2+}]_i$ is no different from any other biological assay with a stringent requirement for specificity, sensitivity over an appropriate concentration range (with a near linear output), and, preferably, a large signal-to-noise ratio (SNR). Usually, the modern Ca^{2+}-sensitive fluorescent dyes satisfy all of these criteria with the additional advantages of being readily available and easy to use (*see* **Note 1** and **Table 1**).

Table 1
Properties of Commonly Used Low- and High-Affinity Ca^{2+} Indicators

	Excitation λ (nm)	Emission λ (nm)	K_d for Ca^{2+} (μM)
Single λ (intensometric) dyes			
Fluo-3	490	525	0.4
Fluo-3FF	490	525	42
Calcium Green-1	490	525	0.19
Calcium Green-2	490	525	0.55
Calcium Green-5N	490	525	14
Rhod-2	550	575	0.57–1.0[a]
Dual λ (ratiometric) dyes			
Dual excitation			
Fura-2	340/380	510	0.22
Fura-2FF	340/380	510	35
Mag-fura-2 (furaptra)	340/380	510	53
BTC	480/400	540	7
Dual emission			
Indo-1	355	405/485	0.25
Mag-indo-1	355	405/485	35

[a]The affinity of rhod-2 for Ca^{2+} is controversial with recent improvements in its purification suggesting a higher affinity than first thought.

1.4. Principles of Loading Cells with Fluorescent Dyes

1.4.1. Esterified Dyes

1.4.1.1. Cytosolic Loading

The most common application of the Ca^{2+}-sensitive dyes is to measure $[Ca^{2+}]_c$ in cells loaded with esterified dyes. The whole process of loading the cell cytosol with BAPTA-based dyes is, in principle, extremely simple because of their availability as acetoxymethyl (AM) esters. By masking the four negatively charged carboxyl groups, the ester moieties render the compound cell permeant, and the modified dye readily enters the cell. Once inside, endogenous esterases remove the ester groups, restoring the hydrophilic nature of the dye and thereby trapping the functional dye inside the cell. Consequently, loading is achieved by the simple process of incubating the cells with AM esters for a defined period. This process can concentrate the dye to such an extent that the final intracellular concentration can exceed 100 times the initial extracellular concentration of AM esters. However, bear in mind that deesterification proceeds as a stepwise process and, as such, intermediate, partially hydrolyzed fluorescent species can be generated. Although these species contribute to the fluorescence emission from the cell, they generally do not respond to Ca^{2+},

meaning that they reduce the Ca^{2+}-dependent dynamic range and result in errors in the calibration (*see* **Subheading 1.5.**). Sufficient time must, therefore, be set aside after loading to allow for complete deesterification.

In addition, the hydrophobic AM ester tends to form micelles in solution that indiscriminately permeate cellular membranes, and hence pass readily into organelles in which they can be hydrolyzed and report $[Ca^{2+}]$. Thus, the relative activity of the esterases found in cytosolic or other compartments will ultimately determine the distribution of reporting dye. This compartmentalization of dye presents problems when the investigator only wishes to monitor $[Ca^{2+}]_c$ since the signal arises from multiple compartments that may not respond in the same manner.

1.4.1.2. Organellar Loading

Although dye compartmentalization presents a serious problem when monitoring $[Ca^{2+}]_c$ changes, this "drawback" can be turned to advantage since it provides a method of measuring intraorganellar Ca^{2+} changes as long as appropriate conditions and dyes are used. Note, however, that "targeting" the AM ester form of Ca^{2+} indicators to specific intracellular organelles is currently more an art than a science because we do not fully understand why some organelles accumulate more dye than others in a given cell type. Whereas some cellular systems prove to be excellent models for measuring Ca^{2+} concentrations in particular organelles, others display a frustrating resistance to load with dye into the compartment of choice. Consequently, one should always empirically test in which compartment the dye resides. The following merely provides a few basic guidelines.

1.4.1.2.1. Endoplasmic Reticulum (Ca^{2+} Stores). Since the free Ca^{2+} concentration of the store lumen ($[Ca^{2+}]_L$) is high (estimates range from 12 μ*M* to several millimolar ***[14]***), the most commonly used high-affinity dyes such as fura-2 ($K_d \approx 0.2$ μ*M*) will be insensitive to lumenal fluctuations. In light of this, many investigators have exploited low-affinity Ca^{2+} dyes such as mag-fura-2, mag-indo-1, and fura-2FF for $[Ca^{2+}]_L$ measurements (K_ds range from 35 to 50 μ*M*), with the latter having the added advantage of being more Ca^{2+} selective. High concentrations of indicator AM esters together with loading at 37°C can promote compartmentalization into stores, whether exclusively ***(15)*** or, as is more common, into both stores and cytosol (necessitating elimination of the contaminating cytosolic signal ***[16,17]***).

1.4.1.2.2. Mitochondria. In contrast to the ER Ca^{2+} dynamics, changes in the mitochondrial Ca^{2+} concentration ($[Ca^{2+}]_{mito}$) have been estimated to be in the low micromolar range ***(9)***, which means that high-affinity indicators are more suitable. Rhod-2 (K_d 0.5–1 μ*M*), unlike the other fluorescent Ca^{2+} indicators, has a net positive charge in the AM ester form and thereby accumulates

into mitochondria as a function of the mitochondrial membrane potential. With some cell preparations, loading is, fortuitously, exclusively mitochondrial, whereas others give a mixed compartment loading. When the latter occurs, one approach is to allow cytosolic rhod-2 to be actively extruded from the cell after AM ester loading, leaving behind the rhod-2 trapped in the mitochondria ***(10)***. Another approach designed to increase the specificity of mitochondrial targeting is to load cells with the AM ester form of Ca^{2+}-insensitive dihydro-rhod-2, the rationale being that its conversion to Ca^{2+}-sensitive rhod-2 occurs primarily in the oxidizing environment of the mitochondrion ***(18)***. Rhod-2 is not, however, the only dye to load into mitochondria, as evidenced by $[Ca^{2+}]_{mito}$ recording using fura-2 ***(19)***. Again it depends on the relative ester activities and/or protocols for circumventing cytosolic contamination.

1.4.2. Free-Acid Form of Dyes

There are times when it may be more appropriate to introduce the free-acid form of the dye directly into the cell (using microinjection, via a patch pipet or reversible electroporation). This need may arise either because of problems with compartmentalization or because of the chemical nature of the dye (large mass, or extreme hydrophobicity). Many of the Ca^{2+} indicators are now available conjugated to large inert dextrans (from 5000 to 500,000 M_r), which lowers their diffusional mobility and reduces movement between different cellular compartments (e.g., nucleus and cytosol), as well as eliminates loss from the cell over prolonged incubation periods.

In addition to attachment to dextrans, peptide conjugation provides an elegant way of targeting free-acid indicators to specific subcellular locales. Examples of the latter approach are "Nuclear Calcium Green Dextran" targeted to the nucleoplasm by a nuclear localization signal peptide ***(20)*** and "CAAX Green" targeted to internal membranes by virtue of endogenous isoprenylation of a consensus sequence peptide ***(21)***. Another class of so-called near-membrane dyes have been designed that have extended carbon chain tails, anchoring them to lipid bilayers, albeit indiscriminately (e.g., fura-C_{18}, Calcium Green-C_{18}, FFP-18) ***(22–25)***. Their hydrophobicity is such that they preferentially bind to the extracellular surface rather than permeate the plasma membrane ***(25)***, and therefore their loading into the cell interior has to be effected by a patch pipet.

1.5. Calibration of Fluorescence Signals

Quantitation of fluorescence changes in terms of absolute $[Ca^{2+}]_i$ is both the joy and the burden of Ca^{2+} imaging. In theory it is relatively straightforward to make such a conversion based on a prior knowledge of the dye's characteristics, but therein lies the problem: one has to make the assumption that the prop-

erty of the dye in free solution mirrors that of the dye in the cellular environment, which is not necessarily the case. Nevertheless, careful calibration can provide a reasonable estimate of the $[Ca^{2+}]_i$ changes, even if the absolute values should be treated with some degree of latitude.

1.5.1. Principles Underlying Calibration of $[Ca^{2+}]_i$ Signals

Calibration is the process of converting the fluorescence signal into an absolute $[Ca^{2+}]$. Since Ca^{2+} binds to the BAPTA-based indicators with a 1:1 stoichiometry (according to the law of mass action, a normal single-site binding isotherm equation can be used to describe the relationship between free $[Ca^{2+}]$ and the fluorescence signal, be it raw fluorescence intensity for single λ [intensometric] dyes, or ratio for dual λ [ratiometric] dyes). Clearly then, the relationship between $[Ca^{2+}]$ and fluorescence is not linear, which necessitates calibration.

1.5.2. Single Wavelength Dyes

$$[Ca^{2+}] = [(F - F_{min})/(F_{max} - F)] \cdot K_d$$

In **Equation 1**, $[Ca^{2+}]$ represents the Ca^{2+} concentration calculated for the fluorescence F at any time; F_{min} and F_{max} are the minimum and maximum fluorescence, respectively; and K_d is the dissociation constant of the indicator.

For a single λ indicator, the simple relationship in **Equation 1** applies. The minimum and maximum fluorescence values represent the limits imposed by the dynamic range of the dye as determined in the absence of Ca^{2+} and in the presence of saturating levels of Ca^{2+}, respectively. When calculating $[Ca^{2+}]$, a K_d should be chosen that was determined under the conditions of temperature and ionic composition that most closely mimic the experiment. Calibration simply involves determining these minimum and maximum fluorescence values since the K_d is a known constant.

To calibrate single-cell fluorescence $[Ca^{2+}]_i$ values, an *in situ* calibration has to be effected with the dye trapped inside the cell. (Because fluorescence is also proportional to the dye concentration it is impossible to mimic this in a cell-free system, and the lysis technique is inappropriate since dye will be lost from the recording area.) This is advantageous since it means that the calibration of the dye is carried out in precisely the same environment as in the experimental run. For fluo-3 (with a K_d approx 0.4 μ*M*), the Ca^{2+} ionophore, ionomycin, is usually used to equilibrate extracellular Ca^{2+} concentration across the plasma membrane with the cytosol: for F_{min} this is carried out in the absence of Ca^{2+} and the presence of EGTA, whereas for F_{max} the extracellular medium contains high Ca^{2+} concentration.

This approach works reasonably well with fluo-3 since its Ca^{2+}-free fluorescence is very low and its affinity means that it is relatively easy to attain the 5–10 μ*M* $[Ca^{2+}]_i$ needed to saturate the dye. However, for other dyes (especially those with a higher K_d), this approach may overestimate the $[Ca^{2+}]_i$ values because there is now good evidence that ionomycin does not efficiently equilibrate $[Ca^{2+}]$ across membranes either *in situ* or in vitro ***(26,27)***, leading to spurious F_{min} and F_{max} values.

1.5.3. Dual Wavelength Dyes

$$[Ca^{2+}] = [(R - R_{min})/(R_{max} - R)] \cdot K_d \cdot (S_{f2}/S_{b2})$$

In **Equation 2**, R represents the ratio of the two wavelengths at any time; R_{min} and R_{max} are the minimum and maximum ratio values, respectively (determined in the absence of Ca^{2+} and in the presence of a saturating concentration of Ca^{2+}); and K_d is the dissociation constant of the dye. The expression s_{f2}/s_{b2} (also known as β) refers to the denominator wavelength (i.e., at 380 nm for fura-2 using a 340/380 excitation ratio) as the ratio of the fluorescence in the Ca^{2+}-free and Ca^{2+} bound forms. Note that the final units of $[Ca^{2+}]$ will be identical to those used for the K_d since the other two fractions are unitless.

With dual λ indicators, the ratio of two wavelengths is related to $[Ca^{2+}]$ by a similar equation (**Equation 2**) ***(28)***. The great advantage of the ratio technique is that factors such as path length, dye concentration, and instrument sensitivity all cancel out in the final calculation, which makes it possible to avoid tedious *in situ* calibrations. Instead, one calibrates the *hardware* using the free-acid form of the indicator in an in vitro buffer system; similar to **Equation 2**, R_{min} and R_{max} are measured in the absence of Ca^{2+} and in the presence of saturating levels of Ca^{2+}. Under these conditions, s_{f2}, and s_{b2}, respectively, are automatically determined, which makes for a rapid and straightforward process. Normally, this calibration is performed on a day-to-day basis and is particularly crucial when there has been a change in the optical components of the system.

Note, however, that in spite of the fact that the *in vitro* calibration is common practice, it does not take into account subtle effects of the intracellular environment on the dye properties (e.g., viscosity, binding of dye to proteins ***[29]***). To compensate for these effects, in vitro buffers can be modified (e.g.. 10% glycerol increases viscosity ***[29]***), or, alternately, R_{min} and R_{max} and β can be determined *in situ* using the ionophore approach described above for single λ dyes.

1.5.4. Ca^{2+}-Insensitive Fluorescence: Autofluorescence and Compartmentalized Dye

It should not be assumed that fluorescence emanating from the cell is only derived from a Ca^{2+}-sensitive indicator. Owing to the presence of endogenous

molecules that fluoresce, the detected signal will be contaminated to some degree by "autofluorescence" and needs to be accounted for if calibration is to be accurate. How much the autofluorescence contributes to the overall signal depends upon the wavelengths recorded and the cell type. For instance, at the wavelengths commonly used for fura-2 measurements (λ_{ex} 340–380 nm; λ_{em}, 420–600 nm), pyridine nucleotides (NAD(P)H) contaminate fluorescence, whereas flavoproteins are excited at longer wavelengths (λ_{ex} 430–500 nm; λ_{em}, 500–650 nm) and will affect measurements using visible dyes such as fluo-3. Indeed, in hepatocytes, pancreatic β-cells, and adrenal glomerulosa cells, the concentration of these nucleotides is substantial enough to allow the fluctuations in their levels to be fluorescently monitored during $[Ca^{2+}]_i$ spiking ***(10,30)***. However, for most cell types, the weak autofluorescence remains a relatively constant and minor (but significant) percentage of the total signal.

When using in vitro calibration values, the cell-derived autofluorescence is subtracted at the end of the experimental run before converting the ratio to $[Ca^{2+}]_i$. To reveal the autofluorescence value in cells already loaded with a ratiometric indicator, the signal from the dye has to be eliminated; this is most readily achieved by incubating the cells in the presence of Mn^{2+} and ionomycin (to facilitate Mn^{2+} entry). When Mn^{2+} binds to some BAPTA-based dyes (particularly the UV dyes fura-2 and indo-1, but not visible dyes such as fluo-3), it results in a complete quenching (elimination) of the fluorescence at all wavelengths, thereby allowing the residual autofluorescence to be determined.

As stated already, for accurate calibration, one must subtract all Ca^{2+}-insensitive fluorescent signals. Therefore, in addition to the autofluorescence, the signal from any Ca^{2+}-insensitive dye component should also be subtracted. One such circumstance is when high-affinity Ca^{2+} indicator is compartmentalized into the high-$[Ca^{2+}]$ environment of the Ca^{2+} store in which it will remain saturated and effectively Ca^{2+}-insensitive under most physiological conditions. Since ionomycin should allow Mn^{2+} access to dye in all compartments including the stores, it should not be used to determine the Ca^{2+}-insensitive fluorescence when there is substantial compartmentalization. Instead, permeabilization of the plasma membrane with digitonin gives a better estimate since it will release cytosolic dye, leaving the mitochondrially derived autofluorescence and compartmentalized dye behind. (It should be ensured that stores be full of Ca^{2+}; otherwise this background fluorescence will not be the same as in the intact cell.) However, this is not as gentle as the ionomycin approach and changes in cell shape on permeabilization can lead to problems.

2. Materials

1. Fluorescent indicators. These compounds are normally stored desiccated at –20°C for many months. The free-acid forms of the dyes are soluble in water and are

prepared as 1–10 m*M* stocks, whereas the AM esters are normally dissolved in dry dimethysulfoxide (DMSO) at 1 m*M*. Dextran-conjugated dyes are water soluble, but their solubility is inversely proportional to their M_r so it is advisable to follow the manufacturer's guidelines. All stock solutions are stored frozen. To minimise excessive cycles of freeze-thawing, which results in indicator deterioration, stocks should be aliquoted into smaller volumes or purchased in a "special packaging" form in which multiple vials contain small amounts of indicator (e.g., 20 × 50 μg). As with the powder form, stocks prepared in hygroscopic DMSO should be desiccated because of their susceptibility to hydrolysis with time. On the day of use, aliquots are thawed and stored on ice and protected from light. DMSO stocks are stable for several weeks with proper storage. (Sources: Molecular Probes, Sigma, Texas Fluorescence Labs (Teflabs) and Calbiochem/Novabiochem.)

2. The nonionic surfactant Pluronic F-127 (free of charge with orders from Molecular Probes) is prepared as a 10% (w/v) solution in DMSO. The solution may be gently warmed to facilitate solubility, and can be stored at room temperature for several weeks.
3. Digitonin is prepared as a 10 mg/mL stock in water. Like Pluronic F-127, the solution should be gently heated to facilitate solubility, and can be stored at room temperature for several weeks.
4. The protease inhibitors leupeptin, antipain, and pepstatin are all prepared as 5 mg/mL stock solutions. Pepstatin is soluble in DMSO whereas the others are prepared in water. These solutions are aliquoted, frozen, and can be stored for a few weeks.
5. MgATP is prepared as a 200 m*M* stock in water and stored frozen for several months. Note that addition to intracellular-like medium (ICM) in this form does not cause pH changes, but stocks should be adjusted to pH 7.2 (with Tris base) when ATP-free acid is favored.
6. Ins(1,4,5)P_3 is made as an aqueous solution up to 5 m*M* concentration and aliquots are stored frozen for months at a time.
7. Endothelial balanced salt solution (EBSS): 145 m*M* NaCl, 5 m*M* KCl, 1 m*M* $MgCl_2$, 1 m*M* $CaCl_2$, 10 m*M* HEPES, 10 m*M* glucose, 1% (v/v) bovine serum albumin (BSA), pH 7.4.
8. Hepatocyte balanced salt solution: 121 m*M* NaCl, 4.7 m*M* KCl , 1.2 m*M* $MgSO_4$, 2 m*M* $CaCl_2$, 25 m*M* HEPES, 1.2 m*M* KH_2PO_4, 5 m*M* $NaHCO_3$, 10 m*M* glucose, 1–2% (w/v) BSA, pH 7.4.
9. Intracellular medium (ICM): 10 m*M* NaCl, 120 m*M* KCl , 20 m*M* HEPES, 1 m*M* KH_2PO_4, pH 7.2 (*see* **Notes 2–4**).
10. Calibration buffer: 10 m*M* NaCl, 120 m*M* KCl , 1 m*M* $MgCl_2$, 20 m*M* HEPES, 200 m*M* EGTA, pH 7.2.

3. Methods

3.1. Instrumentation

A single-cell imaging setup can be thought of as an elaborate fluorimeter in which the sample sits on a microscope instead of in a cuvet, but which other-

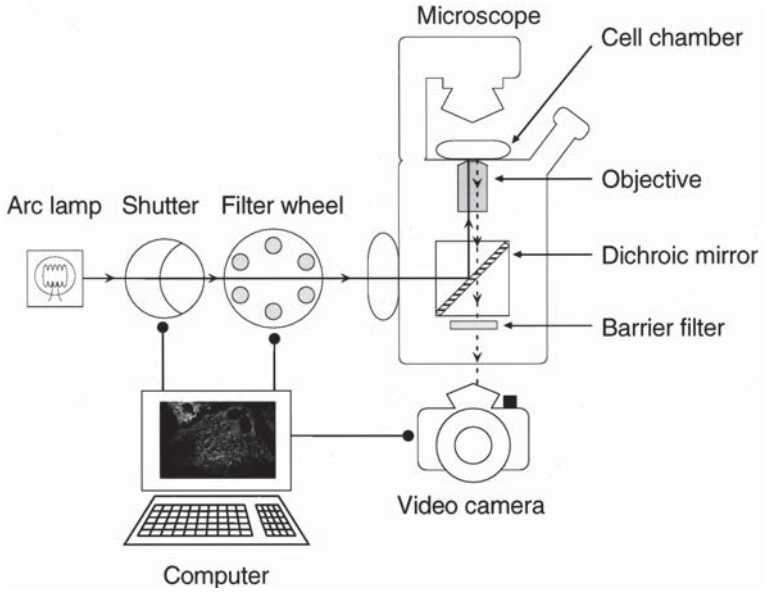

Fig. 1. Schematic representation of a typical Ca^{2+}-imaging setup as detailed in **Table 2**.

wise retains the essential components such as excitation light source, wavelength selection devices, and a photosensitive detector for the emitted light. However, the sophistication and cost of a single-cell setup generally exceeds the requirements for crude population measurements, necessitating additional components such as an epifluorescent microscope, dichroic mirrors, and high-sensitivity detectors. A schematic representation of an epifluorescent microfluorimeter is depicted in **Fig. 1**.

3.1.1. Microscope

An epifluorescent microscope differs from other conventional microscopes in several features: an epifluorescent port at the rear that allows introduction of exciting light, and a housing for dichroic mirrors opposite the port and below the objective to reflect light onto the sample. Both upright and inverted microscopes can be used, but in practice the inverted configuration displays many advantages: e.g., cells can be superfused while allowing a short working distance objective to be used, which offers superior optical properties, and the simultaneous use of micropipets is not hindered by the objective, as is the case with the upright microscope. Nevertheless, a long working distance condensor is required to achieve good access to the cells in the inverted microscope configuration.

3.1.2. Optics

The most crucial elements that determine signal quality are the optical properties of the microscope components (especially of the objective) and the nature of the detector. The very fact that many fluorescent indicators are excited in the near UV means that the objective should ideally transmit light down as low as 340–350 nm, e.g., to facilitate ratiometric recording using fura-2. Since quartz objectives are very costly, most workers utilize the less expensive "fluor" nonquartz counterparts, which generally prove more than adequate. Given that the transmitting properties of the objective decreases with the square of the magnification factor, it is advisable to use as low a magnification objective as possible that still gives sufficient resolution. Another important consideration is the numerical aperture (NA) of an objective, which is an index of its light-transmitting properties (the higher the number the more efficient the light transmission). Use of immersion objectives also increases the effective NA, in which an immersion fluid of higher refractive index than air is placed between the objective and the cover slip. Consequently, an objective of high NA will tend to overcome the loss of signal associated with high magnification.

3.1.3. Incubation Chamber

Once cells are loaded with dye, they are mounted in a suitable incubation chamber that sits on the microscope stage. For an inverted configuration, the base of the chamber is usually formed by the glass cover slip itself (no. 1 thickness) to which the cells have previously adhered. Many chamber designs are commercially available, depending on the requirement for access. Open chambers allow microelectrode access and/or manual addition of agents. On the other hand, closed chambers are more conducive to cell superfusion with a laminar flow. Incidentally, superfusion is best effected with a gravity-fed system that circumvents the pulsatile shearing of peristaltic pumps. In addition to housing the cover slip, the chamber serves as the temperature regulator, in which a specialized, regulated heating element in the chamber precisely controls the bath temperature; feedback temperature control is utilized to avoid the undesirable heating and cooling cycles associated with normal thermostats. The temperature of the sample is also affected by the objective itself, which acts as a heat sink. To minimize this problem, the lens can be jacketed with coils of copper or plastic tubing through which water circulates at the specimen temperature.

3.1.4. Excitation

As mentioned above, each fluorescent indicator is excited by and emits light at characteristic wavelengths. The excitation light is provided by a broad spec-

trum source (typically a 75 W xenon lamp) whose output is then narrowed to the wavelengths of choice by one of two methods. One approach is to use a monochromator, which, although costly, is extremely flexible since it can precisely (±1 nm) select any wavelength across the spectrum, using a series of diffraction gratings. Normally this process is relatively slow unless direct motor-driven gratings are used, which allows rapid alternation between wavelengths (within a few milliseconds). Alternatively, a series of appropriate interference filters placed in the light path will serve the same purpose, although without the precision (a bandwidth of ±5 nm is common) or flexibility (each wavelength requires a different filter). However, for most applications the filter system is sufficient and, since it is the more commonly used, will be elaborated on here.

When using intensometric (single λ) dyes (e.g., fluo-3), or dual-emission dyes (e.g., indo-1), a single interference filter placed in the excitation light path makes for the simplest system. However, when dual-excitation dyes (e.g., fura-2) or when simultaneously recording multiple dyes (e.g., fura-2 and rhod-2) are used, one has to alternate rapidly between different excitation wavelengths. To achieve this, a filter wheel system is used with several interchangeable filters that can be rotated to bring the appropriate filter into the light path in a synchronized fashion. In a photomultiplier tube–based system, a rapidly and continuously rotating wheel can allow multiple excitations up to a 50–200 Hz rate. On the other hand, imaging systems utilize a discontinuous rotating wheel system that simply flips between filter positions as required. To prevent burning out filters and/or photobleaching of cells between exposures, a computer-controlled shutter is placed between the filter wheel and the light source. In addition to the interference filter wheel, a second wheel containing a range of neutral density filters can be used to individually regulate the excitation intensity of each wavelength.

As more components are introduced into the system, the potential maximum rate of acquisition will decrease. Therefore, the collection rate for a single-wavelength excitation photometric system will only be limited by the SNR. With indo-1, rates up to 500 Hz are possible since there is no requirement for moving parts to select wavelengths, which otherwise slows down acquisition times. By contrast, a photometric system using a spinning filter wheel has an upper limit of 50–200 Hz governed by the rotation rate of the wheel. On the other hand, imaging-based systems will be slowed down by the movements between filter positions and the additional shutter open/close time. Together with the readout time of the camera, full video rate (25–30 Hz) currently represents the typical maximum rate for single-wavelength recording.

3.1.5. Emission

Having selected the excitation wavelength(s), one has to define the emission wavelength(s). Unlike a simple cuvet, the excitation and emission light paths are partially shared in the inverted epifluorescent microscope; i.e., they both pass through the objective. In essence, the excitation light entering the rear of the microscope via the epifluorescence port is reflected into the objective (and then to the sample) via a dichroic mirror, also known as a dichroic beam splitter. Part of the emitted light (which is given out in all directions) passes back into the objective, through the dichroic mirror and eventually passes into the port housing the detector. Therefore, one crucial component determining the emission wavelength will be the dichroic mirror itself.

In its simplest form, a single dichroic mirror reflects the (excitation) light shorter than a predetermined wavelength, whereas the (emitted) light above this threshold wavelength passes through. This means that the cutoff of the dichroic mirror clearly has to be higher than the excitation wavelengths to prevent exciting light passing directly to and swamping the detector. Although the emission wavelength is primarily dictated by the dichroic mirror cutoff, another filter is often placed below the dichroic mirror to provide a more precise and additional safety margin. This filter may be either a long-pass (LP) filter (allowing all light above a certain wavelength to pass) or a narrow bandpass filter allowing light to pass within a certain range of wavelengths (i.e., it is an LP filter with an upper limit). Clearly, since emitted light is at a premium, it is preferable to collect across as broad a spectrum as possible. Therefore, for imaging with fura-2, one might use 340 and 380 nm excitation filters with a 400-nm dichroic mirror fitted with a 420-LP filter.

To measure multiple dyes whose spectra are sufficiently separated so that there is little cross over, a double dichroic mirror is often required. Unlike simple dichroic mirrors, which have one single threshold above which light is transmitted, double dichroic mirrors allow light to pass within two discrete bands, so there are effectively two thresholds at different parts of the spectrum. The nontransmitting, reflecting bandwidth between these regions permits use of another excitation filter. Again, a band-pass filter is placed after the dichroic mirror for better control, as for single dichroics, although in this instance it would be a double bandpass, defining two spectral regions. For example, for simultaneous fura-2 and rhod-2 measurements; fura-2 is excited at 340/380 nm and emission is measured approx 510 nm, and rhod-2 is excited at 548 nm with emission centered on 590 nm.

For dual-emission dyes such as indo-1, the emission wavelength selection is more complex. Although the geometry of the microscope requires a dichroic mirror irrespective of the dye's characteristics, this time the dichroic mirror is not the main emission wavelength determinant. Rather, the filters placed after

the dichroic mirror are the more important factor. A setup with a beam splitter and two detectors would have separate band-pass filters dedicated to each one (e.g., 405 and 495 nm for indo-1). Given the expense of using two cameras for imaging indo-1, it is more realistic to have one camera with a filter wheel selecting the *emission* filters positioned immediately next to it.

3.1.6. Detectors

The choice of the type of detector for conventional epifluorescence measurements is essentially between photomultiplier tube (PMT) or high-sensitivity camera.

3.1.6.1. Photometric Recording

The advantages of a photometric or PMT-based system are as follows:

1. It is relatively cheap.
2. Its potential for very rapid data acquisition rates.
3. It places little demand on computer memory and data storage.
4. The dynamic range and sensitivity are greater than most camera-based systems.

On the other hand, the primary disadvantages are that only one single cell can be monitored per run and that spatial information is lost in the global cell signal. The geometry of a standard epifluorescent microscope is such that the emitted light from a large fraction of the field of view is sent to the detector port, which means that the signal would be derived from many cells (when using a 20× or 40× objective). To record exclusively from one cell (or even part of a cell), an adjustable aperture or diaphragm is placed immediately before the PMT; thus, with the aid of a side ocular, the investigator can choose to record from a small region of the field of view while the remainder of the field is masked and does not contribute to the fluorescence signal.

3.1.6.2. Imaging

As prices lower and sensitivity increases, epifluorescent camera-based setups are becoming more routinely used for single-cell analysis. The most commonly used camera is a solid-state cooled charge-coupled device (CCD), which provides a reasonable compromise between speed of acquisition and signal sensitivity. At either extreme, "intensifier" cameras are capable of rapid imaging (but with more noisy images), whereas "slow scan" cameras offer superior quality at the expense of speed. Available with microprocessors capable of digitizing images from 8-bit resolution per pixel through to the superior 12-, 14-, or even 16-bit resolution, CCD cameras have been successfully used to monitor subcellular events such as waves, localized oscillations and even more elemental release units.

The pros and cons of using an imaging system are precisely the reverse of those for the photometric system; i.e., its advantages lie in being able to monitor

Table 2
Example of Components Used in a High-Resolution Imaging System That Does Not Employ a Supplementary Frame Grabber

Microscope	Nikon diaphot epifluorescent
Cell chamber/thermostat	PDMI-2 open perfusion microincubator/TC-202 bipolar temperature controller (Medical Systems, Greenvale NY)
Dichroic beam splitter	400 DM, plus 420 LP filter (Nikon)
Camera	Photometrics PXL slow scan cooled CCD, 14 bit (Tucson, AZ)
Filter wheel control	Ludl Electronic Products (Hawthorne, NY)
Shutter	Uniblitz (Rochester, NY)
Computer	Power PC Macintosh (32 MB RAM)
Software	Custom written (Paul Anderson, Thomas Jefferson University)

more than one single cell simultaneously (desirable when there is considerable cell-to-cell heterogeneity) together with little loss of subcellular spatial information when conditions are optimized (*see* **Subheading 3.5.2.**). However, this does require considerable financial outlay, not only for the camera but also for an adequate computer to cope with acquiring and analyzing large imaging files. This accrual of large amounts of data is another practical reason that routine collection rates tend to be slower than the equivalent photometric recordings.

The *spatial* resolution of the CCD camera is directly proportional to the number of pixels per image as defined by the camera's microprocessor. Under conditions in which the signal is weak, and/or spatial resolution is less critical, some cameras offer a "binning"facility, which allows adjacent pixels to be combined into a brighter "super" pixel. This also has the advantage of enhancing the readout time of the chip. The *temporal* resolution of the camera, on the other hand, is primarily determined by the processor readout time and digitization process; i.e., times of 40–2000 ms are typical.

The primary sources of noise for CCD cameras derive from photon-dependent and -independent sources. The former is statistical noise related to the square root of the light intensity, whereas the latter encompasses such phenomena as thermal noise (the dark current) and the readout noise. Since these parameters are light independent, they are relatively constant and will contribute proportionately less to the signal emanating from bright samples; clearly, low-intensity signals will be more heavily contaminated. Lowering the camera temperature reduces the dark current to a very low level and this may be achieved with thermoelectric cooling or even liquid nitrogen.

A typical setup we have in our laboratory to ratiometrically record using fura-2 is illustrated in **Table 2**.

3.2. Intracellular Loading of Fluorescent Indicators (see Note 5)

3.2.1. Cytosolic Ca^{2+} ($[Ca^{2+}]_c$) Measurement: Loading Cells with Fura-2/AM

3.2.1.1 Human Umbilical Vein Endothelial Cells

1. Cell monolayers attached to 24-mm diameter circular no. 1 glass cover slips for 2–5 d are maintained in 30-mm diameter tissue culture grade plastic Petri dishes in 2 mL of culture medium.
2. Loading solution: 80% (v/v) HEPES-buffered Dulbecco's modified Eagle's medium plus 20% (v/v) fetal calf serum containing 1 μ*M* fura-2/AM.
3. Simultaneously load 3–5 dishes, by removing the culture medium and replacing with 1 mL of loading solution per dish, covering to protect from light and incubating for 30–45 min at room temperature.
4. After the loading period, loading solution is removed and cells are gently washed twice with and then maintained in 2 mL of EBSS at room temperature until use.
5. Cells are left for at least 20 min after loading to facilitate complete deesterification and used within 2 to 3 h after loading.

3.2.1.2. Primary Rat Hepatocytes

1. Cells are seeded overnight onto round polylysine-coated glass cover slips in 2 mL of culture medium.
2. Loading solution: hepatocyte balanced salt solution plus fresh 5 μ*M* fura-2/AM and 0.03% Pluronic F-127.
3. Culture medium is replaced with 2 mL of loading solution, and cells are incubated in a water bath at 37°C for 15–20 min.
4. After loading, cells are washed twice with 1to 2 mL of loading solution *without* dye and detergent and left for 15–20 min to allow deesterification.

3.3. Luminal (Stored) Ca^{2+} ($[Ca^{2+}]_L$) Measurement: Loading Cells with Low-Affinity Indicators (see Notes 6–9, 14–18)

3.3.1. Primary Hepatocytes

1. Hepatocytes are plated overnight onto polylysine-coated glass cover slips in 2 mL of culture medium.
2. Loading solution: hepatocyte balanced salt solution plus fresh 5 μ*M* fura-2FF/AM (or 5 μ*M* mag-fura-2/AM) and 0.03% Pluronic F-127.
3. Culture medium is replaced with 2 mL of loading solution, and cells are incubated in a water bath at 37°C for 60 min.
4. After loading, cells are washed twice with 1 to 2 mL of loading solution *without* dye or Pluronic F-127 and used immediately.

3.4. Mitochondrial Ca^{2+} ($[Ca^{2+}]_{mito}$) Measurement: Loading Endothelial Cells with rhod-2/AM (see Notes 10–18)

1. Calf pulmonary artery endothelial cells are seeded onto glass cover slips for ≥2 d prior to use in 30-mm diameter Petri dishes in culture medium.

Table 3
Typical Collection Parameters for Routine Ca^{2+} Imaging on the Setup Used in Table 2

	Protocol 1 (ratio)
Objective	×20
Excitation λ	340/380
Neutral density	1.6
Image size (pixels)	128 × 96
Binning	3
Time of excitation exposure (ms)	300
Delay between image pairs (ms)	3000

2. Monolayers are loaded with EBSS containing 5 μ*M* rhod-2/AM (plus 0.03% Pluronic F-127) for 10 min at 37°C.
3. After loading, cells are immediately washed gently several times with only EBSS and are ready for use after a 15-min deesterification period.

3.5. Experimental Recording (see Notes 19–33)

3.5.1. Single-Cell Recording

The simplest mode of operation involves recording the *total* fluorescent signal from a single cell without any regard for spatial heterogeneity. With a simple PMT-based photometric system, there is little limitation by acquisition speed, RAM, and data storage as mentioned above, and spinning filter wheel systems mean that multiple wavelengths (at least four) can be simultaneously measured at high temporal resolution (50–200 Hz), depending upon the system configuration. Only one region can be recorded at a time and this can be a cell cluster, single cell, or even part of the cell (depending on the signal strength).

Alternatively, many individual cells can be recorded simultaneously at the expense of temporal resolution by using a video-imaging system. Again, multiple wavelengths can be collected, but in this case there is a restricted amount of data that can be collected. In such cases, acquisition rates of 0.3–1 Hz are typical as given in **Table 3**.

3.5.2. Subcellular Recording

3.5.2.1. Imaging $[Ca^{2+}]_i$ Waves

The spatial equivalent of a $[Ca^{2+}]_i$ spike is a wave in which $[Ca^{2+}]_i$ rises first in one localized region of the cell and then actively propagates across the rest of the cell, usually (but not always) at a constant velocity at all points along the

Table 4
Data Acquisition Parameters to Visualize $[Ca^{2+}]_i$ Waves in Primary Cultures of Rat Hepatocytes

	Protocol 1 (ratio)	Protocol 2 (single λ)
Objective	×20	×40
Excitation λ (nm)	340/380	380
Neutral density	1.6	1.0
Image size (pixels)	128 × 96	92 × 72
Binning	3	3
Time of excitation exposure (ms)	100	40
Delay between image sets (ms)	1000	300

[a]Cells are loaded with fura-2 according to **Subheading 3.3.** and are mounted in an incubation chamber at 37°C. Repetitive waves can be stimulated with 1–3 μ*M* phenylephrine ***(38)***.

wave front. For details of wave types and properties, the reader is referred to several reviews ***(1,4,31,32)***. The speed of the wave is such that rapid data acquisition is required, which often involves making compromises with the data collection parameters (*see* **Notes 19–33**). As an illustration, we have given in **Table 4** the parameters that are suitable for visualizing $[Ca^{2+}]_i$ waves in fura-2–loaded hepatocytes at modest collection rates for ratiometric recording (Protocol 1), and for single λ recording for more rapid measurements (Protocol 2).

3.5.2.2. Measuring Oscillations of $[Ca^{2+}]_L$ in Permeabilized Hepatocytes

A 340/380 ratio pair collected every 2 to 3 s is adequate to resolve spiking. However since the 380-nm changes are small during spiking (~5%, whereas 340 nm is close to the isoemissive λ), these changes will be more readily detected using a PMT or a superior camera-based system (14-bit).

1. Hepatocytes are loaded as above with fura-2FF/AM (**Subheading 3.3.1.**) and used as quickly as possible after loading.
2. On the microscope stage, cells are washed three times with 2 mL of nominally Ca^{2+}-free medium containing 100 μ*M* EGTA.
3. Wash cells twice with 2 mL of chelex-treated ICM containing a cocktail of protease inhibitors (1 μg/mL each of leupeptin, pepstatin, and antipain) (*see* **Notes 2–4**).
4. To permeabilize, the above medium is replaced with 3 mL of ICM supplemented with 10 μg/mL of digitonin. Normally, gentle permeabilization is carried out until a new steady-state fluorescence (~30–50% of initial) is attained in the majority of cells (~4 to 5 min). Overpermeabilization results in damage to internal membranes. (Permeabilization is carried out in the absence of ATP since hepatocytes express purinoceptors coupled to phospholipase C.)

5. Digitonin is washed out with two washes of ICM followed by addition of 3 mL of ICM containing 2 m*M* MgATP. Continue incubation for a few minutes to allow complete store refilling.
6. Oscillations can be stimulated by addition of 100–200 n*M* Ins(1,4,5)P_3.
7. Total stored Ca^{2+} can be determined with 2 µ*M* ionomycin.

3.6. Calibrating $[Ca^{2+}]_C$ Signals

3.6.1. In Situ *Calibration of a Single λ Dye Using Ionophore in Intact Cells*

1. At the end of the run, 5 µ*M* ionomycin is added in nominally Ca^{2+}-free EBSS containing 500 µ*M* EGTA; this determines F_{min}.
2. In the continued presence of ionomycin, extracellular Ca^{2+} is increased to 10 m*M*. Stable signal gives F_{max}.
3. Autofluorescence does not need to be subtracted since it is automatically accounted for in **Equation 1** for single λ dyes when performing an *in situ* calibration.
4. Fluorescence is converted to $[Ca^{2+}]_i$ using **Equation 1** substituting an appropriate K_d.

3.6.2. In Vitro Calibration of a Dual λ Dye

1. Obtain the background fluorescence of the system at both wavelengths using calibration buffer only (**Subheading 2., item 10**). This value should be subtracted from all subsequent measurements.
2. Add 0.5–1 µ*M* free-acid form of the indicator. The ratio will give R_{min}, and the fluorescence at the denominator λ is equivalent to s_{f2}.
3. Add 1 m*M* $CaCl_2$ to obtain R_{max} and s_{b2} in a similar manner.
4. $[Ca^{2+}]$ is calculated using **Equation 2** substituting the experimentally determined parameters and using the most pertinent K_d value from the literature.

3.6.3. Autofluorescence in Cells with Dye Compartmentalized into Ca^{2+} stores

1. Cells are permeabilized in ICM containing 500 µ*M* EGTA, 250 µ*M* $CaCl_2$, and 5–30 µg/mL of digitonin (free $[Ca^{2+}]$ ~100 n*M*).
2. After permeabilization (~5 min), 2 m*M* MgATP is added for several minutes to refill stores fully.
3. Residual fluorescence is comprised of autofluorescence plus compartmentalized dye.

4. Notes

4.1. Choosing a Dye

1. The following represent some of the factors that have to be considered when choosing a Ca^{2+} indicator. As always, there is a compromise between several parameters and the "perfect" dye is not always available.
   a. If possible use a ratiometric rather than an intensometric indicator.
   b. Ensure the K_d is appropriate to the anticipated magnitude of the $[Ca^{2+}]_i$ response in order to prevent dye saturation and to optimize signal changes by working in the most sensitive range of the dye.

c. To avoid excessive buffering by exogenous indicator, use a dye that gives as large a signal change as possible in order to minimize the intracellular concentration of dye.
d. Buffering is less of an issue with lower affinity dyes. In addition, the lower-affinity is usually attributable to a faster dissociation of the Ca^{2+}:indicator complex, which means that the rapid kinetics of Ca^{2+} spikes may be less distorted compared to a high-affinity dye.
e. Conjugated dyes with lower mobility reduce artifacts owing to dye diffusion, often crucial for interpreting kinetic and spatial measurements.
f. Visible wavelength dyes circumvent problems associated with poor UV transmission optics and with complicating autofluorescence changes in the UV range and are also used with non-UV confocal scanning microscopes.
g. The AM ester form of the indicator must load predominantly into the compartment of choice; since different dyes do not necessarily distribute between compartments in the same way, the optimal dye and loading conditions are empirically determined on a trial-and-error basis. Alternatively, the free-acid form can be introduced into the cell, although this is technically more demanding.
h. Use a dye that photobleaches (or is extruded from the cell) at an acceptable rate that can only be determined on a trial-and-error basis.
i. Intensometic dyes that are bright at low $[Ca^{2+}]$ permit more accurate determination of basal $[Ca^{2+}]_i$ levels and visualization of cells (e.g., Calcium Green-1), whereas dyes that are less bright at low Ca^{2+} levels (e.g., fluo-3) make quantitation more uncertain. However, the fold change in fluorescence on Ca^{2+} binding (and hence the dynamic range) is potentially greater for the latter dye and can provide more "contrasty" images to visualize small, intense events, such as Ca^{2+} sparks and puffs.
j. For multiparameter recording using more than one dye simultaneously, ensure that there is minimal spectral interaction between the indicators.
k. In attempting to overcome the lack of a ratiometric visible dye, cells can be simultaneously loaded with two spectrally distinct probes whose fluorescence is expressed as a ratio: to complement the Ca^{2+} indicator, it is possible to include either a Ca^{2+}-insensitive dye, or a Ca^{2+}-sensitive one that gives a reciprocal fluorescence change upon Ca^{2+} binding. (It is crucial that the two probes photobleach/leak at a similar rate and reside in the same compartment.) As an example of the former, a mixed dextran conjugated to the indicator Calcium Green-1 and the Ca^{2+}-independent Texas Red is available from Molecular Probes. In the second case, coloading cells with the two Ca^{2+} indicators fluo-3 and fura-red gives reciprocal changes reminiscent of fura-2 excited at 340 and 380 nm. However, the latter approach can suffer from problems with cell-to-cell differences in relative AM ester loading and nonlinear behavior of the ratio attributable to the different K_ds of the two dyes ***(37)***.

4.2. Intracellular Medium

2. A permeabilized cell system is extremely useful since it allows precise control of the composition of the "cytosolic" environment with the additional advantage of facilitating the use of otherwise cell-impermeant agents. For example, investigation of the regulation of the Ins(1,4,5)P_3 receptor is ideally suited to this approach (providing permeabilization is carefully carried out ***[34]***) since it allows ready manipulation of both the Ins(1,4,5)P_3 and "cytosolic" Ca^{2+} concentration. To mimic the low free [Ca^{2+}] of the cytosol, the ICM is normally supplemented with known quantities of a Ca^{2+} buffer (usually EGTA or BAPTA) and Ca^{2+}. The precise concentrations of each needed to yield the required free [Ca^{2+}] can be calculated with software such as Maxchelator (Dr. Chris Patton, Stanford, CA). However, until recently, Ca^{2+} oscillations had never been reported in permeabilized single cells. The breakthrough came when stored Ca^{2+} was measured in an ICM without exogenous Ca^{2+} buffers, which consequently allows the local Ca^{2+} feedback processes at the Ins(1,4,5)P_3 receptor to occur unhindered ***(35,36)***. This provides an elegant model system for analyzing Ca^{2+} oscillations but, in the absence of Ca^{2+} buffers, necessitates special preparation of the medium.
3. Since unbuffered nominally Ca^{2+}-free ICM is contaminated with at least 5–10 μ*M* [Ca^{2+}], it is necessary to lower this to levels more closely resembling the intracellular concentration. This is achieved by using an exchange resin, Chelex 100 (200–400 mesh, sodium form, Bio-Rad), which can be subsequently separated from the treated medium. Calcium Sponge (Molecular Probes) can also be used, but proves rather expensive for large-scale preparations. The final [Ca^{2+}] can be as low as 50–80 n*M* with careful preparation (as determined fluorimetrically with fura-2 free-acid; *see* **Subheading 1.5.**)
   a. To minimize Ca^{2+} contamination of solutions, all stages are carried out in plasticware and not glassware.
   b. A large (1 L) volume is prepared at a time, for convenience and to reduce the effect of Ca^{2+} contamination at any stage.
   c. The pH of the ICM is adjusted with KOH or Tris base *before* Chelex treatment (note: some batches of Chelex 100 can slightly alter the final pH, which can be accounted for at this stage).
   d. Chelex 100 resin is added directly to the ICM at 50 g/L and the solution is stirred constantly with a magnetic stir bar.
   e. Minimum exchange time is 3 to 4 h at room temperature. Alternatively, overnight at 4°C may be more convenient and seems to be more efficient.
   f. To separate the resin from the ICM, gravity or centrifugal separation is favored over filtration, which can result in Ca^{2+} contamination (but this can be checked for each filtration system).
4. The final free [Ca^{2+}] in the experiment will depend on the extent of Ca^{2+} contamination from the cells and other agents added after treatment (e.g., MgATP, protease inhibitors, Ins(1,4,5)P_3). In our hands, a concentration of 200–400 n*M* is typical. Since fura-2 provides significant Ca^{2+} buffering in the absence of any other chelator, this needs to be accounted for in determining the free [Ca^{2+}], by

using low fura-2 concentrations (e.g., 0.1 μ*M*) and/or back-calculation, deriving the amount bound to fura-2.

4.3. Cytosolic Dye Loading

5. Minimize AM ester overloading, which results in significant intracellular Ca^{2+} buffering and/or toxicity. Use the lowest intracellular concentration of dye that gives a reliable signal by loading with the lowest possible concentration of AM ester feasible (usually 0.5–10 μ*M* range) for the shortest time (15–60 min is typical). This must be empirically determined for each new cell type tested by comparing the kinetics and magnitude of responses following different loading regimens: buffering manifests itself as more sluggish and/or diminutive responses.
   a. When measuring cytosolic Ca^{2+} responses, dye compartmentalization is best reduced by loading cells at room temperature.
   b. Including a micelle dispersant such as serum (10–20% v/v), BSA (1–2% w/v), or the nonionic surfactant Pluronic F-127 (~0.03% w/v) also can reduce compartmentalization and improve loading.
   c. Serum contains esterases that can hydrolyze the AM ester form of the dye before it enters the cell (especially at 37°C). Since the cell-impermeant free acid is generated, this will reduce the efficiency of loading.
   d. Not all cell types possess efficient intracellular esterase activity, and thus, it may be more practical to load cells at 37°C. But this may in turn give loading problems through active extrusion of the dye from the cell, which occurs more efficiently at higher temperatures (*see* **Subheading 1.5.**). The anion transporters can be inhibited with either 1 m*M* probenicid, 200 μ*M* sulphinpyrazone, or 100 μ*M* bromosulphophthalein, although these are not clean reagents and may have other effects. Another approach is to use fura-PE3 instead of fura-2: this Zwitterionic analogue reportedly leaks from some cells at a slower rate than its congener, since it is less efficiently pumped by the anion transporter ***(23)***.
   e. After incubation in the presence of AM esters, allow sufficient time (≥20 min) for complete deesterification.

4.4. Organellar Dye Loading

4.4.1. Store Loading

6. Use high concentrations of indicator (e.g., 3–10 μ*M* AM ester) for longer incubation periods (e.g., 1 h).
7. Loading is best carried out at 37°C. Pluronic F-127 can improve the degree (though probably not the selectivity) of loading.
8. To remove any contaminating cytosolic component, dialyze the cytosol with a patch pipet ***(16)***, and quench cytosolic dye with Mn^{2+} that passively enters the cytosol via plasmalemmal Ca^{2+} channels (e.g., incubate cells in Ca^{2+}-free medium containing 100-300 μ*M* $MnCl_2$). Permeabilization of the plasma membrane releases cytosolic dye for $[Ca^{2+}]_L$ measurements ***(15,35,36)***.

9. Dye redistribution between cellular compartments can sometimes occur with time. This may manifest itself as a decrease in the agonist (or Ins[1,4,5]P_3)-sensitive component as the reporting dye moves out of the Ca^{2+} store to another apparently nonresponding compartment. Under these circumstances, it is more advisable to load and use cells immediately rather than batch-load many cover slips simultaneously.

4.4.2. Mitochondrial Loading

10. Rhod-2 currently displays the highest selectivity for mitochondria, and short incubation times (≤10 min) with concentrations of AM ester ranging from 2 to 10 μ*M* seem to work well in many cell types. For example, in calf pulmonary artery endothelial cells, >95% of the Ca^{2+} signal is derived from mitochondria.
11. If a significant amount of rhod-2 is cytosolic, it can essentially be eliminated after a short loading protocol by overnight culture of cells in fresh medium without indicator, allowing active extrusion mechanisms to remove cytosolic dye, leaving organellar-trapped dye behind.
12. Dihydro-rhod-2 may load more selectively into mitochondria in some cells (*see* **Subheading 1.4.1.2.**). Dihydro-rhod-2/AM preparation: rhod-2/AM is dissolved as a 1 m*M* stock in DMSO as normal. The smallest amount of $NaBH_4$ solid is added that will make the magenta solution colorless (no more than a few grains). This dihydro-rhod-2/AM solution is always prepared on the day of use since it does not store well.
13. Since mitochondrial conversion is required, loading takes longer with dihydro-rhod-2/AM. For example, hepatocytes are loaded with 1 to 2 μ*M* dihydro-rhod-2/AM for 60 min at 37°C in the presence of 2 m*M* acetoacetate (to shift the mitochondria to a more oxidized redox state via the liver-specific β-hydroxybutyrate dehydrogenase, which favors oxidation of dihydro-rhod-2 ***[10]***). After loading, cells are left for 12–16 h in primary culture to facilitate extrusion of residual cytosolic dye.

4.5. How can Dye Compartmentalization be Recognized?

14. Cellular fluorescence is punctate. When a dye is located exclusively in the cytosol, it gives a uniform, diffuse pattern of staining. By contrast, when dye is concentrated in cell organelles, it can appear as punctate, spotty, reticulate, or filamentous fluorescence staining depending on the cell architecture and the organelle in which it is concentrated (e.g., mitochondria, ER). For fura-2, high levels of dye in intracellular stores (in which Ca^{2+} is high) are best viewed at 340 nm, at which fluorescence intensity is proportional to Ca^{2+} concentration. This is always best checked through the microscope binocular since the resolution of many cameras is inferior to the human eye.
15. Low fluorescence of the nuclear matrix*:* In most cells, the nucleus is freely permeable to small molecules such as the Ca^{2+} indicator dyes, thus, as a result, the dye concentration in the nucleus is similar to that in the cytosol (with conventional imaging and no compartmentalization, the nucleus may even appear

brighter if it is the thickest part of the cell). By contrast, dye compartmentalized into organelles (e.g., ER, mitochondria) cannot exchange with the nucleus, which consequently appears relatively dim (especially at 340 nm with fura-2).

16. $[Ca^{2+}]_i$ responses are small or apparently negative when cells are stimulated. This occurs when a substantial fraction of dye is contained within the intracellular store itself and reports the fall in the luminal Ca^{2+} levels as the store empties. Clearly this will be less obvious when high-affinity dyes such as fura-2 are used during low-intensity stimulation since they will normally remain saturated in the high $[Ca^{2+}]$ environment of the store lumen (*see* **Subheading 1.4.1.2.1.**). However, more extensive depletion of stores (e.g., with thapsigargin or cyclopiazonic acid, inhibitors of the store Ca^{2+}-ATPase) may cause $[Ca^{2+}]_L$ to fall to micromolar or below, which is within the working range for the dye. For low-affinity dyes, the problem is more pronounced because their working range may report $[Ca^{2+}]_L$ changes during physiological stimulation. That aside, caution should always be exercised since even apparently "normal" increases in $[Ca^{2+}]_c$ may be tempered by dye reporting decreases in $[Ca^{2+}]_L$.
17. Empirical determination of compartmentalization: Low concentrations of agents that selectively permeabilize the plasma membrane and release only the cytosolic dye reveal the fraction trapped in intracellular organelles. For example, 5–30 µg/mL of digitonin gently releases cytosolic fluorescence into the medium over 3–5 min. Ideally, this should be monitored at a Ca^{2+}-insensitive wavelength (e.g., 360 nm with fura-2); thus the signal is only proportional to dye concentration and not Ca^{2+} concentration. In hepatocytes, up to 50% of ester-loaded dye can be trapped in the ER under appropriate loading conditions.
18. To determine precisely where the dye is located, several structural and functional criteria should be tested. For example, for $[Ca^{2+}]_{mito}$ measurements the pattern of rhod-2 distribution should be compared at as high a resolution as possible with bona fide mitochondrial stains such as JC-1, rhodamine tetramethyl ester, or any of the MitoTracker family (Molecular Probes). Functionally, the resolution afforded by the confocal scanning microscope at high magnification (60×) is able to verify whether Ca^{2+} increases derive solely from a mitochondrial source. In the absence of access to a confocal microscope, a 35-mm single lens reflex camera attached to the appropriate microscope port can offer a finely resolved photographic record. Alternately, $[Ca^{2+}]_{mito}$ changes should be rapidly blocked by mitochondrial inhibitors such as 0.2 µg/mL of antimycin A, 5 µ*M* FCCP/5 µg/ml oligomycin or 1 to 2 µ*M* ruthenium red (which may require microinjection since it does not readily cross the plasma membrane).

4.6. Practical Considerations Regarding Experimental Recording

*4.6.1. General Considerations (*see *also* ***Table 5****)*

19. Single-cell $[Ca^{2+}]_i$ recording can be frustrated by the most fundamental of problems, namely the loss of fluorescent signal and/or cell viability with time. The reduction in the signal strength as a consequence of indicator elimination can be so rapid as to make experimentation impossible, or at least be enough to limit its

Table 5
Troubleshooting Fluorescence Imaging

Problem	Notes
Calibration	
Incomplete dye hydrolysis	Extend postloading incubation period
Binding of dye to cell constituents	Perform an *in situ* calibration
Dye compartmentalisation	Lower loading temperature; lower loading time; use a dispersant; permeabilization-based calibration
Spectral shift *in situ* vs in vitro	Precludes an in vitro calibration, or modify in vitro conditions (e.g., increase viscosity with glycerol)
Constant autofluorescence contribution	Determine at end of run by quenching dye with ionomycin plus Mn^{2+} and subtracting residual fluorescence
Autofluorescence changes during run	Increase dye loading to swamp endogenous fluorescence (beware of buffering)
Saturation of dye when $[Ca^{2+}]_i$ is high	Use a dye of lower affinity
Sluggish $[Ca^{2+}]_i$ responses	Reduce dye loading (if buffering); use lower affinity dye; also see compartmentalization
Photobleaching	Reduce light exposure (decrease exposure time; increase ND filter); free-radical scavengers such as Trolox; use a different dye
Dye leakage	Lower temperature of experimental run; use a less leaky dye; inhibit extrusion pathways
Experimental recording	
Blooming and streaking of image	Reduce exciting light intensity; adjust camera/filter change synchronization
High-frequency extraneous noise at all wavelengths	Change bulb to eliminate lamp flicker
Dim image	Increase loading; reduce ND filters; increase exposure time; check lamp alignment

duration. The first step then is to assess whether photobleaching or leakage (or both) is responsible for the loss of responsive indicator.

20. To resolve this issue, first record the emitted signal for a short time to estimate the rate of change of fluorescence (Intensity 1). The incubation is then continued

for a reasonable period (5–10 min) *without* exposing the cells to exciting light. Subsequently, fluorescence is recorded again, using the same acquisition parameters (Intensity 2). If photobleaching was exclusively responsible for the decline, then intensity 1 = intensity 2. By contrast, if extrusion was exclusively responsible, this would have been unaffected by the light-free period and thus intensity 1 >> intensity 2. Clearly, if both processes contribute to signal loss, some intermediate rate of decline occurs during the light-free period.

21. Irradiation with high-energy light not only degrades the fluorescent indicator but also lowers cell viability and therefore should be reduced to a minimum. As already noted, photobleaching can be reduced to a manageable level in the following ways:
    a. Reduce the intensity and/or duration of the exposure to the exciting light.
    b. Use free-radical scavengers to minimize photodegradation (note, however, the possible biological consequences).
    c. Use a different dye that photobleaches at a slower rate.
22. Leakage, on the other hand, can be countered in different ways:
    a. Inhibit extrusion pathways with agents such as probenicid, sulphinpyrazone and bromosulphophthalein (*see* **Note 5**).
    b. The rate of extrusion is proportional to temperature and is consequently greatest at 37°C. A significant improvement in dye retention can be seen even at 30°C, whereas at room temperature loss of signal can be negligible.
    c. Use a different indicator since they vary in their susceptibility to extrusion (e.g., Calcium Green-1 is less leaky than fluo-3).

4.6.2. Nonspatial Recording Mode

4.6.2.1. Temporal Resolution

23. The highest temporal resolution (up to several hundred hertz acquisition rate) is afforded with a PMT-based system. Camera-based systems run at much slower rates with dual λ indicators (typically 0.3–1 Hz). This means that even non-optimized recording with the photometric system will offer superior temporal resolution than routine measurement with an imaging system. In this way the rise times of Ca^{2+} spikes measured ratiometrically with fura-2 (of the order of a few seconds or less) can be accurately determined with a PMT-based, but not a camera-based system. (Faster kinetics can be measured with an imaging system if only a single wavelength is recorded, but this compromises the advantages of ratiometric measurements.) However, if initial kinetics are not an issue, the slower collection rate of the imaging system is sufficient.

4.6.2.2. Dynamic Range

24. Again, the detector determines the maximum dynamic range of the system. A PMT has an excellent SNR to allow the resolution of small (~5%) changes in fluorescence intensity. By contrast, 8-bit cameras (especially the intensifier cameras) exhibit an inferior SNR and poor dynamic range (pixel intensity graded

from 0 to 255), which makes small changes difficult to detect. However, the more expensive 14-bit slow-scan cameras, for example, offer excellent image quality, high SNR, and large dynamic range.

4.6.2.3. Heterogeneous Responses

25. When there is considerable cell-to-cell heterogeneity in the response, photometric recording usually proves too time-consuming. This is when imaging comes into its own with the ability to simultaneously record from many tens of cells (depending on magnification and cell diameter).

4.6.3. Spatial Recording Mode

26. There are two complementary approaches to gaining information about how Ca^{2+} is regulated in different subcellular regions: either target the dye to the region of interest and photometrically record the specific signal, or record a homogeneously distributed dye but focus on one cell region (either by optically isolating the region with the masking aperture during recording on a PMT-based system, or by using a camera and performing off-line regional analysis after recording). In other words, *both* systems can provide useful spatial information. These two approaches need not be mutually exclusive.

4.6.3.1. Spatial Resolution Limits

27. The maximal theoretical spatial resolution of light microscopy is governed by **Equation 3**:

$$r = (1.22 \times \lambda_o)/(2 \times \mathrm{NA})$$

In **Equation 3** where (r) is the minimum distance by which two points can still be resolved as two points, λ_O is the wavelength of light in air, and NA is the numerical aperture of the lens. Therefore, for an objective of NA = 1.4 and light emitted at 510 nm, the maximum resolution will be 0.22 μm (a reasonable rule of thumb is half the wavelength of the emitted light). Although this limit is well below the size of typical somatic cells (10–100 μm), it should still be considered when carrying out high-resolution imaging of small discrete units such as mitochondria or Ca^{2+} elementary release events (blips, spread 1–2 μm) ***(4)***.

4.6.3.2. Optimization of Resolution

28. As detailed in **Subheading 3.**, the maximum resolving power of the imaging system will be determined primarily by the camera (number of pixels per image) and the objective (magnification and NA). Clearly, the highest resolution will be achieved when there is *no* pixel averaging (binning) together with the highest suitable magnification and NA. However, under these conditions the image may be dimmer, which may necessitate increasing the excitation light intensity (by prolonging the exposure time and/or decreasing the number of the neutral density filter), which may cause photodamage or photobleaching.

4.6.3.3. Image Deconvolution

29. Image quality is adversely affected by out-of-focus fluorescence, which reduces contrast and increases the depth of field, resulting in distortion and blurring of the final image. This is particularly problematic as far as cell clusters and intact tissues are concerned. To improve image quality, optical sectioning can be achieved with a confocal microscope which only detects in-focus information. Alternately, application of deblurring algorithms to conventional images can render sectioning mathematically in one of two ways: either a "nearest neighbor" approach ***(33,38)*** or through "no neighbors" processing ***(39)***. The former necessitates multiple image collection at different focal planes to create a 3D stack from which an optical section can be reconstructed. By contrast, the "no neighbors" algorithm mathematically extracts optical sections without the need to acquire multiple sections, which facilitates faster image acquisition since it obviates slow z plane stepping.
30. Such "image deconvolution" is advantageous in so far as that ratiometric UV dyes such as fura-2 and indo-1 can be used, otherwise untenable with a single-photon, visible confocal scanning microscope. Even so, there is a downside: with most algorithms discarding a substantial amount of the fluorescent signal, bright specimens and cameras of the highest resolution are a prerequisite. However, this problem has been offset to a degree by the development of a mathematical model that allows restoration of extremely high-quality images with minimal light exposure and sectioning from fewer image planes ***(38)***.

4.6.4. Tips on Measuring Ca^{2+} Waves

31. $[Ca^{2+}]_i$ waves generally propagate at a velocity of between 5 and 200 $\mu m \cdot s^{-1}$ ***(1,4,31,32)***. For most somatic cells, this will mean the wave takes ~1–5 s to cross the entire cell. Simply to observe heterogeneous $[Ca^{2+}]_i$ increases and crudely identify wave initiation loci, it is probably sufficient to collect a ratio image every second or so during repetitive waves, such as those in hepatocytes ***(31)***. There is also little need for extremely high-resolution images, so one can increase pixel averaging (binning) and decrease image size to reduce the demand on image storage memory.
32. However, to accurately quantitate the wave velocity, an image will have to be acquired at least every 300 ms, which places demands on the imaging configuration. For rapid visualization of $[Ca^{2+}]_i$ waves (at or approaching video rate, 25–30 Hz), most imaging systems are unable to support ratiometric recording with fura-2, since the time taken to alternate between filter positions introduces a significant delay. For this reason, most rapid analyses of wave fronts are conducted in single λ mode to eliminate slow excitation λ changes (either at 380 nm with fura-2, which gives a relatively large fluorescence decrease, or with intensometric indicators such as fluo-3 or Calcium Green-1). This method is not ideal and represents yet another example of compromise.
33. Because the time taken to write images to the hard disk of the computer is rate limiting (up to a second depending on the computer and image size), rapid data

collection times can only be achieved when images are stored temporarily in RAM, and written to hard disk after the experimental run has been completed. The only limitation here is that RAM tends to be much smaller than the capacity of the hard disk, so fewer images can be collected. Nonetheless, with computers of 30MB or more of RAM, this imitation should not be too restrictive.

References

1. Thomas, A. P., St. J. Bird, G., Hajnóczky, G., Robb-Gaspers, L. D., and Putney, J. W. Jr. (1996) Spatial and temporal aspects of cellular calcium signalling. *FASEB. J.* **10,** 1505–1517.
2. Lee, M. G., Xu, X., Zeng, W., Diaz, J., Wojcikiewicz, R. J. H., Kuo, T. H., Wuytack, F., Racymaekers, L., and Muallem, S. (1997) Polarized expression of Ca^{2+} channels in pancreatic and salivary gland cells. *J. Biol. Chem.* **272,** 15,765–15,770.
3. Lee, M. G., Xu, X., Zeng, W., Diaz, J., Kuo, T. H., Wuytack, F., Racymaekers, L., and Muallem, S. (1997) Polarized expression of Ca^{2+} pumps in pancreatic and salivary gland cells. *J. Biol. Chem.* **272,** 15,771–15,776.
4. Berridge, M. B. (1997) Elementary and global aspects of calcium signalling. *J. Physiol.* **499,** 291–306.
5. Thorn, P., Moreton, R., and Berridge, M. B. (1996) Multiple, coordinated Ca^{2+}-release events underlie the inositol trisphosphate-induced local Ca^{2+} spikes in mouse pancreatic acinar cells. *EMBO J.* **15,** 999–1003.
6. Ito, K., Miyashita, Y., and Kasai, H. (1997) Micromolar and submicromolar Ca^{2+} spikes regulating distinct cellular functions in pancreatic acinar cells. *EMBO J.* **16,** 242–251.
7. Busa, W. B. and Nuccitelli, R. (1985) An elevated free cytosolic Ca^{2+} wave follows fertilization in eggs of the frog *Xenopus laevis. J. Cell. Biol.* **100,** 1325–1329.
8. Gerasimenko, O. V., Gerasimenko, J. V., Tepikin, A. V., and Petersen, O. H. (1996) Calcium transport in the nucleus. *Pflügers Archiv - Eur. J. Physiol.* **432,** 1–6.
9. Rizzuto, R., Brini, M., Murgia, M.. and Pozzan, T. (1993) Microdomains with high Ca^{2+} close to IP_3-sensitive channels that are sensed by neighbouring mitochondria. *Science* **262,** 744–747.
10. Hajnóczky, G., Robb-Gaspers, L. D., Seitz, M. B., and Thomas, A. P. (1995) Decoding cytosolic calcium oscillations in the mitochondria. *Cell* **82,** 415–424.
11. Petersen, O. H. (1996) Can Ca^{2+} be released from secretory granules or vesicles? *Trends Neurosci.* **19,** 411–413.
12. Cobbold, P. H. and Rink, T. J. (1988) Fluorescence and bioluminescence measurement of cytoplasmic free calcium. *Biochem. J.* **248,** 313–328.
13. Tsien, R. Y. (1989) Fluorescent probes of cell signalling. *Ann. Rev. Neurosci.* **12,** 227–253.
14. Bygrave, F. L. and Benedetti, A. (1996) What is the concentration of calcium ions in the endoplasmic reticulum? *Cell Calcium* **19,** 547–551.
15. Golovina, V. A. and Blaustein, M. P. (1997) Spatially and functionally distinct Ca^{2+} stores in sarcoplasmic and endoplasmic reticulum. *Science* **275,** 1643–1648.

16. Tse, F. W., Tse, A., and Hille, B. (1994) Cyclic changes in intracellular stores of gonadotropes during gonadotropin-releasing hormone-stimulated Ca^{2+} oscillations. *Proc. Natl. Acad. Sci. USA* **91,** 9750–9754.
17. Hofer, A. M. and Machen, T. E. (1993) Technique for *in situ* measurement of calcium in intracellular inositol 1,4,5-trisphosphate-sensitive stores using the fluorescent indicator mag-fura-2. *Proc. Natl. Acad. Sci. USA* **90,** 2598–2602.
18. Mix, T. C. H., Drummond, R. M., Tuft, R. A., and Fay, F. S. (1994) Mitochondria in smooth muscle sequester Ca^{2+} following stimulation of cell contraction. *Biophys. J.* **66,** A97.
19. Glennon, M. C., Bird, G. S., Takemura, H., Thastrup, O., Leslie, B. A., and Putney, J. W. Jr (1992) In situ imaging of agonist-sensitive calcium pools in AR4-2J pancreatoma cells. Evidence for an agonist- and inositol 1,4,5-trisphosphate-sensitive calcium pool in or closely associated with the nuclear envelope. *J. Biol. Chem.* **267,** 25,568–25,575.
20. Allbritton, N. L., Oancea, E., Kuhn, M. A., and Meyer, T. (1994) Source of nuclear calcium signals. *Proc. Natl. Acad. Sci. USA* **91,** 12,458–12,462.
21. Horne, J. H. and Meyer, T. (1997) Elementary calcium-release units induced by inositol trisphosphate. *Science* **276,** 1690–1693.
22. Etter, E. F., Kuhn, M. A., and Fay, F. S. (1994) Detection of changes in near-membrane Ca^{2+} concentration using a novel membrane-associated Ca^{2+} indicator. *J. Biol. Chem.* **269,** 10,141–10,149.
23. Vorndran, C., Minta, A., and Poenie, M. (1995) New fluorescent calcium indicators designed for cytosolic retention or measuring calcium near membranes. *Biophys. J.* **69,** 2112–2124.
24. Etter, E. F., Minta, A., Poenie, M., and Fay, F. S. (1996) Near membrane $[Ca^{2+}]_i$ transients resolved using the Ca^{2+} indicator FFP-18. *Proc. Natl. Acad. Sci. USA* **93,** 5368–5373.
25. Lloyd, Q. P., Kuhn, M. A,. and Gay, C. V. (1995) Characterisation of calcium translocation across the plasma membrane of primary osteoblasts using a lipophilic calcium-sensitive fluorescent dye, calcium green-C_{18}. *J. Biol. Chem.* **270,** 22,445–22,451.
26. Morgan, A. J. and Jacob, R. (1994) Ionomycin enhances Ca^{2+} influx by stimulating store-regulated cation entry and not by a direct action at the plasma membrane. *Biochem. J.* **300,** 665–672.
27. Erdahl, W. L., Chapman, C. J., Taylor, R. W., and Pfeiffer, D. R. (1995) Effects of pH conditions on Ca^{2+} transport catalyzed by ionophores A23187, 4-Br-A23187 and ionomycin suggest problems with common applications of these compounds in biological systems. *Biophys. J.* **69,** 2350–2363.
28. Grynkiewicz, G., Poenie, M., and Tsien, R. Y. (1985) A new generation of Ca^{2+} indicators with greatly improved fluorescence properties. *J. Biol. Chem.* **260,** 3440–3450.
29. Roe, M. W., Lemasters, J. J., and Herman, B. (1990) Assessment of fura-2 for measurements of cytosolic free calcium. *Cell Calcium* **11,** 63–73.
30. Pralong, W. F., Spät, A., and Wollheim, C. B. (1994) Dynamic pacing of cell metabolism by intracellular Ca^{2+} transients. *J. Biol. Chem.* **269,** 27,310–27,314.

31. Thomas, A. P., Renard, D. C., and Rooney, T. A. (1992) Spatial organization of Ca^{2+} signalling and Ins(1,4,5)P_3 action. *Adv. Second Messenger Phosphoprotein Res.* **26,** 225–263.
32. Clapham, D. E. and Sneyd, J. (1995) Intracellular Ca^{2+} waves. *Adv. Second Messenger Phosphoprotein Res.* **30,** 1–24.
33. Carrington, W. A., Lynch, R. M., Moore, E. D. W., Isenberg, G., Fogarty, K. E., and Fay, F. S. (1995) Superresolution three-dimensional images of fluorescence in cells with minimal light exposure. *Science* **268,** 1483–1487.
34. Renard-Rooney, D. C., Hajnóczky, G., Seitz, M. B., Schneider, T. G., and Thomas, A. P. (1993) Imaging of inositol 1,4,5-trisphosphate-induced Ca^{2+} fluxes in single permeabilized hepatocytes. *J. Biol. Chem.* **268,** 23,601–23,610.
35. Tanimura, A. and Turner, R. J. (1996) Inositol 1,4,5-trisphosphate-dependent oscillations of luminal [Ca^{2+}] in permeabilized HSY cells. *J. Biol. Chem.* **271,** 30,904–30,908.
36. Hajnóczky, G. and Thomas, A. P. (1997) Minimal requirements for calcium oscillations driven by the IP_3 receptor. *EMBO J.* **16,** 3533–3543.
37. Floto, R. A., Mahaut-Smith, M. P., Somasundarum, B., and Allen, J. M. (1995) IgG-induced Ca^{2+} oscillations in differentiated U937 cells: a study using laser scanning confocal microscopy and co-loaded fluo-3 and fura-red fluorescent probes. *Cell Calcium* **18,** 377–389.
38. Agard, D. (1984) Optical sectioning microscopy: cellular architecture in three dimensions. A*nn. Rev. Biophys. Bioeng.* **13,** 191–219.
39. Monck, J. R., Oberhauser, A. F., Keating, T. J., and Fernandez, J. M. (1992) Thin-section ratiometric Ca^{2+} images obtained by optical sectioning of fura-2 loaded mast cells. *J. Cell. Biol.* **116,** 745–759.

7

Measurement of [Ca^{2+}] Using the Fluorometric Imaging Plate Reader (FLIPR)

Elaine Sullivan, Emily M. Tucker, and Ian L. Dale

1. Introduction

Ionized calcium plays a major role in the regulation of cellular processes in both eukaryotic and prokaryotic cells ***(1)***. A wide variety of cell surface receptors and ion channels utilize a calcium signal to initiate events such as cell motility, contraction, and secretion. To a large extent, the advent of fluorescent indicators of free calcium ion concentration that could be loaded into cells in a nondisruptive manner has been responsible for our current knowledge of cellular calcium homeostasis ***(2)***. Typically, the fluorescent signal has been monitored using cuvet-based fluorometers or by confocal fluorescent microscopy. Although acceptable for a number of applications, these methods are relatively labor intensive and are not suitable for screening large numbers of compounds.

To address the need for an instrument capable of high throughput, the Fluorometric Imaging Plate Reader (FLIPR) (Molecular Devices Corporation, Sunnyvale, CA) was developed as a screening tool for cell-based fluorescent assays (**Fig. 1**). The FLIPR allows the simultaneous stimulation and measurement of 96 separate cell populations. Therefore, it is possible to quantify transient signals, such as the release of intracellular calcium, from cell populations in parallel and in real time.

An overview of the FLIPR system is shown in **Fig. 2**. The FLIPR has a test chamber that, if required, can be maintained at 37°C. The test chamber holds up to three microtiter plates: one microtiter plate contains the cells (test plate) whereas the other two 96-well plates can be used as reservoirs for agonists, antagonists, or test compounds. A further position outside the test chamber allows additions to be made from a reagent reservoir, which is useful if multiple repetitive additions of one reagent are required.

From: *Methods in Molecular Biology, Vol. 114: Calcium Signaling Protocols*
Edited by: D. G. Lambert

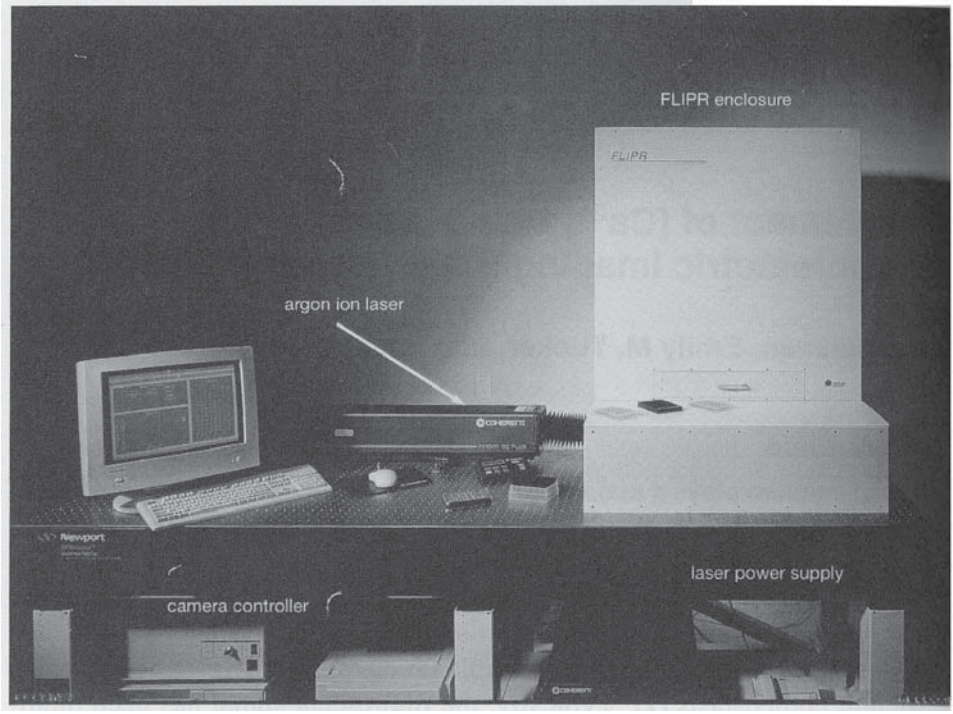

Fig. 1. FLIPR system.

Within the instrument is an integrated computer-controlled 96-well pipettor that uses disposable tips to eliminate carryover between data runs. The pipettor can dispense volumes in a range from 5 to 250 µL and is used to aspirate, dispense, and mix fluid from the reservoir plates into the test plate. The height of the pipettor, timing, order, and speed with which the fluids are dispensed throughout the experiment are operator controlled.

The FLIPR features an argon ion laser that provides discrete spectral lines spaced from approx 350 to 530 nm. For use with fluorescent Ca^{2+} dyes such as fluo-3 and Calcium Green-1, the 488-nm line of the laser is employed. This laser simultaneously illuminates all the wells in a test plate. The image of each well in the plate is captured by a cooled charge coupled device (CCD) camera, which updates images once per second, if required, for the measurement of rapid calcium responses. As both excitation and emission are read via the bottom of the plate, black-walled, transparent bottomed 96-well plates are used. The camera is an "integrating" type detector, such that the accumulated light signal can be varied using different exposure times. The depth of field of the CCD camera is limited to ~200 µm on the base of each well via a unique optical detection technique. This feature is particularly important for assays in which extracellular

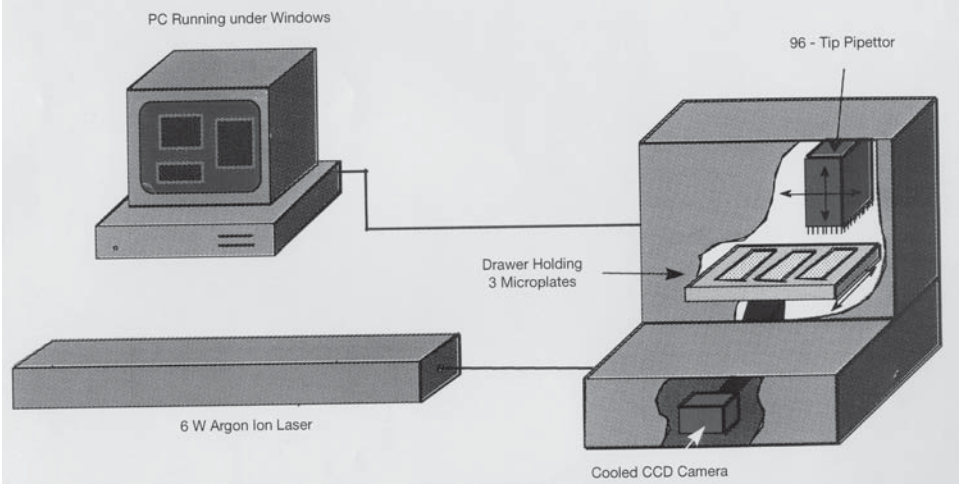

Fig. 2. A diagrammatic representation of the FLIPR system. The FLIPR has a temperature-controlled test chamber that holds up to three microtiter plates and contains a 96-well pipettor. The image is recorded using a cooled CCD camera located in the base of the instrument. The excitation source used by FLIPR is a 6-W argon ion laser.

dye is present, e.g., measurement of membrane potential using the *bis*-oxonol dye $DiBAC(4)_3$ ***(3)***, although it is not so critical for measurement of intracellular calcium.

Data captured by the CCD camera is converted to digital data and then transferred to the PC. As one has the option to add two reagents in rapid succession, it is possible to determine the effect of an antagonist on an agonist response. Therefore, it is feasible to screen thousands of compounds in 1 d to ascertain their effect on an induced calcium change—this rate of screening has hitherto been impossible using conventional cuvet-based fluorometers. In addition to its ability to measure cellular calcium responses, the FLIPR has been used for the measurement of membrane potential and intracellular pH, utilizing $DiBAC(4)_3$ and BCECF, respectively ***(3,4)***.

2. Materials

1. Fluo-3/acetoxymethyl (AM), Molecular Probes, (Leiden, Netherlands). 2 m*M* stocks are prepared by dissolving in anhydrous dimethyl sulfoxide (DMSO). This stock should be aliquoted as appropriate and stored at –20°C until required.
2. Calcium Green-1/AM (Molecular Probes). 2 m*M* stocks are prepared by dissolving in anhydrous DMSO. This stock should be aliquoted as appropriate and stored at –20°C until required.
3. Phosphate-buffered saline (PBS) wash buffer supplemented with 10 m*M* D-glucose, 20 m*M* HEPES, pH 7.3.

4. Hank's balanced salt solution (HBSS) buffer supplemented with 20 m*M* HEPES, pH 7.3.
5. Pluronic F-127 (Molecular Probes Leiden, Netherlands), 20% (w/v) in DMSO.
6. Probenecid (Sigma, Poole, UK).
7. Jurkat E6 human T-cell leukemia cell line (*see* **Note 1**).
8. Culture medium for Jurkat cells: RPMI-1640 medium supplemented with 10% fetal bovine serum and 2 m*M* L-glutamine (*see* **Note 1**).
9. ECV304 human cell line (*see* **Note 1**).
10. Culture medium for ECV304 cells: Medium 199 containing 10% fetal calf serum and 2 m*M* L-glutamine (*see* **Note 1**).
11. Black plates with a transparent base for FLIPR system (Whatman Polyfiltronics, UK; or Costar, High Wycombe, UK).
12. Black disposable pipet tips (Robbins Scientific, Solihull, UK).
13. Denley Cellwash and Multidrop Pipettor (Life Sciences International, Basingstoke, UK).

3. Methods

3.1. Loading Cells with Fluo-3/AM and Calcium Green-1/AM

In general it has been found that the optimum dyes for experiments using the FLIPR system are the calcium indicators Calcium Green-1/AM and fluo-3/AM. Fluo-3 and Calcium Green-1 exhibit an increase in fluorescence emission intensity on binding to Ca^{2+} and hence are used to detect increases in the level of intracellular calcium (*see* **Note 2**). The best dye to use with a given cell line should be determined experimentally, although the authors have found that fluo-3 generates a larger fluorescent signal than Calcium Green-1 with most cell types tested. Both dyes excite with the 488-nm excitation line of the argon laser and emit in the 500–560 nm range. Cell loading can be enhanced in some cases by premixing the hydrophobic dye AM esters with low levels of Pluronic F-127, a nonionic surfactant, prior to dispersion into the aqueous loading buffer. With certain cell lines, such as Chinese hamster ovary cells, the anion transporter inhibitor probenecid is required to inhibit the efflux of dye from cells during and following loading.

3.1.1. Adherent Cells

1. Plate cells at an appropriate density in black-walled, transparent bottomed 96-well plates and culture (overnight is usually sufficient) until they form a confluent monolayer.
2. For most cell lines, the authors have found that a final concentration of 4 μ*M* dye in the loading medium (tissue culture medium) is adequate for good dye loading. If Pluronic F-127 is required to enhance loading, mix 20 μL of 2 m*M* fluo-3/AM stock solution with 20 μL of Pluronic F-127 solution prior to addition to 10 mL of

loading medium (*see* **Note 3**). Final concentrations in the loading medium are 4 μ*M* fluo-3/AM, 0.04% Pluronic F-127.

3. If cell loading is poor, include 2.5 m*M* probenecid in the loading medium and wash buffer (*see* **Note 4**).
4. Aspirate medium from 96-well plate containing cells. Add 100 μL of loading medium per well and incubate the cells at either 37°C or room temperature for between 60 and 180 min, depending on the cell type.
5. Aspirate loading medium and wash between two and four times with 200 μL of wash buffer. Wash buffer is typically PBS or HBSS supplemented with HEPES, pH 7.3, although buffer composition is dependent on requirements of the cell line and/or assay. Aspiration may be performed manually or using the Denley Cellwash (the authors have identified this washer as particularly suitable for the gentle washing of cells in microtiter plates (*see* **Note 5**)]. A final volume of 100–150 μL of buffer should be left in the wells before analysis on the FLIPR. In some cases, it may be advantageous to incubate at 37°C for 15 min before the final wash.
6. Transfer plate to the FLIPR for assay. To establish that cells are loaded with dye, the test plate is transferred to the test chamber and a "signal test" initiated, in which the CCD camera captures an image of the test plate. The image is converted to a numerical fluorescence reading for each well, which is displayed on the computer screen. This reports the signal level for each well, and the minimum, maximum, and average readings from each plate (including standard deviation). This allows the operator to establish that cells have loaded with dye and that the loading is uniform across the plate. The sensitivity of the FLIPR can be adjusted by altering (1) laser output (2) camera aperture or, (3) camera exposure length. The authors find that for the majority of cell lines that they have used on FLIPR, camera aperture (f2) and camera exposure (0.4 s) can be kept constant and that varying laser output between 300 and 750 mW is sufficient to obtain good data. The FLIPR CCD camera reaches a saturated signal at approx 60,000 fluorescence units; therefore, sensitivity should be adjusted so that the peak response to agonist does not allow saturation of the camera. With most cell types the authors have used on FLIPR, an average reading of 10–15,000 fluorescence units/well has resulted in the generation of a good peak agonist response without the problem of camera saturation. Photobleaching of dye has not been an issue with laser output of up to 750 mW (*see* **Note 6**).

3.1.2. Suspension Cells

As previously described, the FLIPR is designed to collect fluorescence from the bottom of the well. To reduce the background fluorescence, the depth of field is limited, thereby allowing the optics to discriminate between the cell layer and bulk solution in the well. Therefore, to measure changes in fluorescence using suspension cells requires centrifugation of cells to the base of the well following dye loading, to effectively form a "monolayer" of cells on the base of the plate.

1. Cells used in experiments should be in exponential growth phase. The following protocol is one that the authors have adopted for use with Jurkat cells (*see* **Note 7**).
2. To 20 µL of 2 m*M* stock fluo-3/AM, add 20 µL of Pluronic F-127 solution ([20% w/v] solution in DMSO) and vortex. Transfer this mixture to 10 mL of complete culture medium (*see* **Subheading 2.**, **item 8**) so that final concentrations are as follows: 4 m*M* fluo-3/AM, 0.04% Pluronic F-127. Store in the dark until required. This will be sufficient for two 96-well plates.
3. For two 96-well plates seeded at 2.5×10^5 cells/well, resuspend 5×10^7 viable cells in 10 mL of loading medium (tissue culture medium) in a 50-mL polypropylene tube. Cap tube loosely and place in shaking water bath maintained at 37°C for 60 min, with shaking speed set to ~30 cycles/min.
4. At the end of the incubation period, add 25 mL of wash buffer (PBS) to the tube and centrifuge cells (800*g*, 5 min). Decant supernatant carefully and resuspend the cell pellet in 25 mL fresh wash buffer.
5. Allow to stand at room temperature for 5 min.
6. Repeat the centrifugation step and resuspend the cell pellet in 34 mL wash buffer (final cell density 1.6×10^6/mL).
7. Aliquot 150 µL of cell suspension into each well of the plate using a multichannel pipet or the Multidrop Pipettor system.
8. Sediment cells to the base of the plate by centrifugation for 5 min at 800*g*.
9. Transfer plate to FLIPR for assay (*see* **Subheading 3.1.1.**, **step 6**).

3.2. Example: $P2Y_2$ Response to UTP from ECV304 Adherent Cell Line in the Absence or Presence of the Receptor Antagonist Suramin

As described in **Subheading 1.**, the FLIPR system has a test chamber that holds up to three microtiter plates: one for the test plate containing the cells and two other positions for the addition of reagents.

1. Plate ECV304 cells, an adherent cell line expressing the P_2Y_2 receptor, at a density of 1×10^5 cells/well and incubate overnight.
2. Load cells using fluo-3/AM as previously described (**Subheading 3.1.1.**) and wash three times using the Denley Cellwash.
3. Leave a volume of 100 µL of wash buffer (HBSS) in each well and place the plate in the test chamber.
4. Use a "signal test" to establish that cells have loaded with dye and also to determine the laser output required for a mean fluorescent signal of approx 12,000 fluorescent counts/well.
5. Place addition plate 1 in the right-hand position of the FLIPR test chamber. This plate, a standard microtiter plate, contains varying concentrations of suramin, a $P2Y_2$ receptor antagonist.
6. Place addition plate 2 in the left-hand position of the FLIPR test chamber; it contains varying concentrations of receptor agonist UTP.
7. Set the system parameters as follows: laser power, 250 mW; camera aperture, f2; camera exposure time 0.4 s.

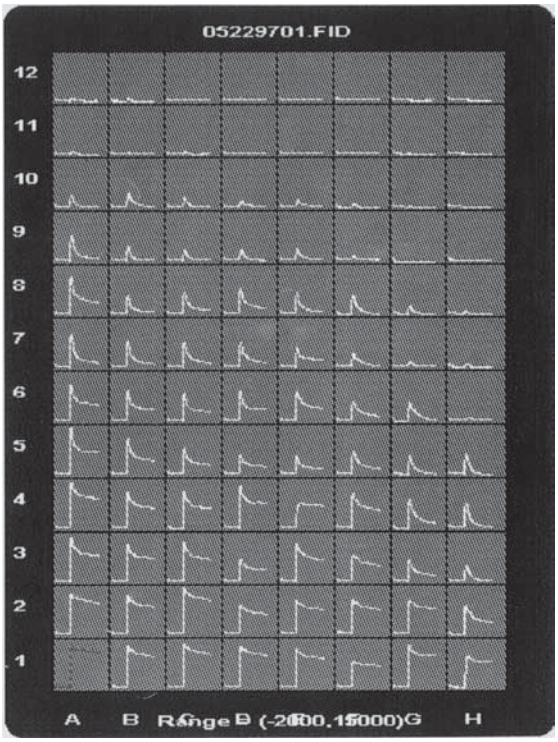

Fig. 3. P_2Y_2 response to UTP from ECV304 cell line in the absence or presence of the receptor antagonist suramin. UTP was added to the indicated wells at the following final assay concentrations: columns 1 and 2, 100 µ*M*; 3 and 4, 10 µ*M*; 5 and 6, 3 µ*M*; 7 and 8, 1 µ*M*; 9 and 10, 0.3 µ*M*; 11 and 12, 0.1 µ*M*. Additions of suramin were made to columns A–H as follows: A: control (no suramin), B: 0.3 µ*M*, C: 1 µ*M*, D: 3 µ*M*, E: 10 µ*M*, F: 30 µ*M*, G: 100 µ*M*, H: 300 µ*M* suramin.

8. Fifty microliter volumes of both suramin and UTP should be added to wells containing cells and 100 µL of buffer; stocks of both reagents are therefore made up as 4X stocks to give final concentrations in 200 µL volume. Add suramin solution to the target plate from addition plate 1 (50 µL) at a pipettor speed of 40 µL/s and at a pipettor height of 135 µL (*see* **Note 8**).
9. Take read updates every second for 60 s. Add UTP (50 µL) from addition plate 2 to the target plate at a pipettor speed of 40 µL/s and at a pipettor height of 185 µL. Make read updates every second for 60 s and thereafter every 5 s for a further 2 min. (Typical data obtained is illustrated in **Fig. 3**).

4. Notes

1. Cell lines utilized in this study were obtained from the American Type Culture Collection (Rockville, MD) and all cell culture reagents and materials were obtained from Gibco BRL, Paisley, UK.

2. Fura-2, which requires excitation at 340 nm, is not suitable for use in the FLIPR owing to (1) absorbance of light by the plastic of microplates at ultraviolet wavelengths, and (2) interference from fluorescent emission of test compounds at this wavelength.
3. Any appropriate physiological medium is acceptable, e.g., complete tissue culture medium or (HBSS) supplemented with 20 m*M* HEPES, pH 7.3. Loading medium should be stored in the dark until use and should only be prepared immediately prior to use. This is particularly important if a loading medium containing serum is employed, as esterases present in serum will hydrolyze ester groups from fluo-3/AM and result in impaired loading.
4. Preparation of 250 m*M* probenecid solution: Probenecid (0.71 g) is dissolved in 1 *N* NaOH (5 mL) prior to the addition of 5 mL of physiological buffer (e.g., HBSS + 20 m*M* HEPES, pH 7.3). Use at 1:100 dilution in all loading and wash solutions in order to minimize efflux of dye from cells. It is important to ensure that pH is readjusted to physiological values after addition of the strongly alkaline 250 m*M* probenecid stock to buffer; this is best achieved by the inclusion of 20 m*M* of HEPES in the buffer employed. This solution should only be made up on the day of use. Probenecid may be substituted by the anion transport inhibitor sulphinpyrazone (250 μ*M* final concentration), although the authors have found it to be less effective in preventing dye efflux than the former.
5. Optimization of the wash protocol for the Denley Cellwash is critical for adherent cell lines. Aspirate/dispense heights, dispense speeds, vacuum level, and number of washes can all be adjusted to ensure that the cell monolayer is not disrupted. The authors have found that some cell lines are more robust than others in their ability to withstand relatively vigorous washing.
6. Calcium Green-1/AM may be substituted in place of fluo-3/AM using the methodology described in **Subheading 3.1.1.**
7. The authors have successfully employed a number of suspension cell types on FLIPR, including Jurkat T-cell leukemic, U937 monocytic, and HL-60 promyelocytic leukemic cell lines, and also primary human neutrophils, eosinophils, and monocytes.
8. To ensure instantaneous mixing of reagents when added to the test plate, the authors add relatively large volumes of agonist/antagonist. For example, if two additions are to be made to the test plate containing cells in 100 μL of buffer, then 50 μL of 4X stocks of both added reagents should be used. Height and speed: Setting of the dispensation height of the pipettor is important in that a value should be selected ensuring that the tip of the pipet is below the meniscus level of fluid in the well following dispensation (to ensure no droplets remain on tips). However, disruption of the cell monolayer will result if the pipet tip is too close to the bottom of the well. The pipet height refers to the height the pipet tips are placed in the test plate and is measured as milliliters of fluid. The optimal dispense height should be determined by experiment. It is important to note that the depth of Polyfiltronics plates is greater than Costar plates: in general, one should therefore adjust the pipettor height ~25 μL downward if using a Costar plate in place of a Polyfiltronics plate (e.g., set height to 100 μL from 125 μL). For strongly adherent cell lines, the pipettor dispense speed of the instrument may be

set to 80 µL/s to ensure instantaneous mixing. However, if cells are weakly adherent or one is dispensing into a suspension culture, then the dispense speed must be reduced accordingly (e.g., to 30 µL/s) to avoid cell disruption. The optimal dispense speed is one that does not remove cells from the base of the well but is sufficiently rapid to ensure adequate mixing. The plate viewer is useful in visualizing the monolayer to identify whether there have been problems with cell detachment following reagent dispensing into wells.

Acknowledgments

The authors would like to thank Molecular Devices Corporation (MDC) for kindly allowing them to reproduce their figures. Thanks are also extended to Kirk Schroeder and Brad Neagle of MDC for help and advice in the development of the assays.

References

1. Clapham, D. (1995) Calcium signalling. *Cell* **80,** 259–268.
2. Thomas, A. P. and Delaville, F. (1991) The use of fluorescent indicators for measurements of cytosolic-free calcium concentration in cell populations and single cells, in *Cellular Calcium: A Practical Approach* (McCormack, J. G. and Cobbold, P. H., eds.), IRL, Oxford, England, pp. 1–54.
3. Epps, D., Wolfe, M., and Groppi, V. (1994) Characterisation of the steady-state and dynamic fluorescence properties of the potential sensitive dye bis-(1,3-dibutylbarbituric acid). *Chem. Phys. Lipids* **69,** 137–139.
4. Schroeder, K. S. and Neagle, B. D. (1996) FLIPR: A new instrument for accurate, high throughput optical screening. *J. Biomol. Screening* **1,** 75–80.

8

Measurement of Ca^{2+} Entry Using $^{45}Ca^{2+}$

Mercedes Villarroya, Manuela G. López, María F. Cano-Abad, and Antonio G. García

1. Introduction

For decades, the measurement of extracellular Ca^{2+} ($^{40}Ca_o^{2+}$) entry into cells, using $^{45}Ca^{2+}$ as carrier, has been a widely used technique. One of the first studies was performed by Hodgkin and Keynes ***(1)*** to measure the rate at which $^{40}Ca^{2+}$ labeled with $^{45}Ca^{2+}$ crosses the surface membrane of resting squid axons, or during nervous activity. In a few large excitable cells, it was also possible to measure Ca^{2+} entry indirectly through the measurement of inward currents through Ca^{2+} channels under voltage-clamp conditions ***(2)***; however, Ca_o^{2+} entry into small excitable cells could only be measured using $^{45}Ca^{2+}$. With the improvement of patch-clamp techniques ***(3)***, Ca_o^{2+} entry was measured via the analysis of single-channel or whole-cell inward currents through Ca^{2+} channels. The first detailed study of Ca^{2+} channel currents in small mammalian excitable cells was performed in 1982 ***(4)*** in bovine adrenal medullary chromaffin cells, in the laboratory of Erwin Neher, where patch-clamp methodologies were developed. As patch-clamp techniques evolved, it seemed that the measurement of Ca_o^{2+} entry using $^{45}Ca^{2+}$ would no longer be useful. Isotopes and scintillation fluids are expensive, administrative controls for good laboratory practices are always increasing, and the manipulation of isotopes becomes a growing nuisance. On the other hand, the time resolution of techniques using $^{45}Ca^{2+}$ entry are in the range of seconds, whereas the patch-clamp measurement of inward Ca^{2+} currents is in the range of milliseconds, three orders of magnitude lower.

Although patch-clamp techniques are available to measure whole-cell currents through Ca^{2+} channels, $^{45}Ca^{2+}$ entry is still used routinely as, on pharmacological grounds, a good correlation between data obtained with the two methodologies has been found. In addition, the use of $^{45}Ca^{2+}$ offers the

From: *Methods in Molecular Biology, Vol. 114: Calcium Signaling Protocols*
Edited by: D. G. Lambert

following advantages: (1) cells can be plated in multiwell plates (12–96 wells) at different densities, so that a screening of the effects of large numbers of drugs and toxins on $^{45}Ca^{2+}$ entry can be systematically performed; (2) direct chemical measurement of the actual Ca^{2+} entering the cells in mol/cell · s can be performed; (3) the time resolution for Ca^{2+} entry can be increased to 1 s; and (4) interference with intracellular Ca^{2+} buffering systems does not occur, since all $^{45}Ca^{2+}$ found in the cells at the end of a given experiment entered such cells from the extracellular space; this contrasts with the measurements of fura-2 Ca^{2+} transients ***(5)*** that do not distinguish between Ca^{2+} entry, intracellular Ca^{2+} sequestration, and/or intracellular Ca^{2+} mobilization.

2. Materials

1. Chromaffin cells isolated from the medulla of bovine adrenal glands.
2. Ca^{2+}-Mg^{2+}-free Locke buffer: 154 m*M* NaCl, 5.6 m*M* KCl, 3.5 m*M* $NaHCO_3$, 11 m*M* glucose, and 10 m*M* HEPES buffer, pH 7.2.
3. Krebs-HEPES solution: 140 m*M* NaCl, 5.9 m*M* KCl, 1.2 m*M* $MgCl_2$, 1 m*M* $CaCl_2$, 11 m*M* glucose, 10 m*M* HEPES, pH 7.2.
4. High K^+ solution: Krebs-HEPES containing 70 m*M* KCl with isosmotic reduction of NaCl.
5. DMPP solution: Krebs-HEPES with 100 μ*M* final concentration of the nicotinic receptor agonist dimethylphenylpiperazinium (DMPP).
6. Dulbecco's modified Eagle's medium (DMEM) (Gibco, UK).
7. Collagenase from *Clostridium histolyticum* (Boehringer-Mannheim, Germany).
8. Bovine serum albumin (BSA) fraction V.
9. Soybean trypsin inhibitor.
10. Cytosine arabinoside.
11. Fluorodeoxyuridine.
12. 1,1-dimethyl-4-phenyl-piperazinium (DMPP).
13. EGTA (Sigma, USA).
14. Percoll (Pharmacia, Sweden).
15. Fetal calf serum.
16. Penicillin and streptomycin (Gibco).
17. Scintillation fluid Ready micro (Beckman, USA).
18. ^{45}Ca (specific activity 10–40 mCi mg^{-1} calcium, Amersham, UK).
19. All other chemicals are reagent grade.

3. Methods

$^{45}Ca^{2+}$ entry has been measured in a large variety of organs, tissues, cells, organelles, and natural or artificial membranes. However, the authors will describe only the model that they most often use—the cultured bovine adrenal medullary chromaffin cell. Many of the issues raised for this model can be extrapolated to other biological models, although the conditions must be defined according to the questions formulated to each system. The authors

use this technique most often to study Ca^{2+} entry through voltage-dependent Ca^{2+} channels in chromaffin cells.

3.1. Isolation and Culture of Chromaffin Cells (see Note 1)

The bovine adrenal medullary chromaffin cells are widely used because large quantities of cells can be isolated from a few glands obtained from local abattoirs. In brief, the procedure is as follows (from **ref. *6***, with some modifications):

1. Obtain four adrenal glands from a local slaughtherhouse and bring to the laboratory in ice-cold Locke's buffer. Perform all further steps under sterile conditions.
2. Clean the adrenals of fat and cannulate the adrenal vein. Then, perform several fluid injections.
3. Through the adrenal vein, wash the glands three times with Ca^{2+}- and Mg^{2+}-free Locke's buffer at room temperature.
4. To carry out medullae digestion, inject, with a syringe, 5 mL of a solution containing 0.25% collagenase, 0.5% BSA fraction V, and 0.01% soybean trypsin inhibitor in Ca^{2+}-Mg^{2+}–free Locke's buffer, until the glands swell. Then incubate them at 37°C for 15 min; repeat this procedure three times.
5. Wash out the collagenase with a large volume of Ca^{2+}-Mg^{2+}–free Locke's buffer.
6. Filter the cells first with a 217-µm nylon mesh and thereafter with an 80-µm nylon mesh. Place them on a self-generated Percoll gradient containing 19 mL of Percoll (17.1 mL of Percoll plus 1.9 mL of 10-fold–concentrated Ca^{2+}-Mg^{2+}–free Locke's buffer at pH 5), plus 21 mL of cell suspension (approx 50–100 $\times$ 10^6 cells). Final pH of the mixture is 7.2.
7. Centrifuge the mixture at 13,000*g* for 20 min (rotor SS-34, Sorvall centrifuge Model RC-5, Dupont Instruments, USA) at 22°C. Take the lower band of the gradient (enriched in adrenaline-containing cells), wash it once with Ca^{2+}-Mg^{2+}–free Locke's buffer and a second time with DMEM.
8. Resuspend cells in DMEM supplemented with 10% FCS, 10 µ*M* cytosine arabinoside, 10 µ*M* fluorodeoxyuridine, 50 IU · mL^{-1} penicillin, and 50 µg · mL^{-1} streptomycin.
9. Plate cells on uncoated, 16-mm-diameter plastic culture wells (24 wells/plate), at a density of 5×10^5 cells/well, or in 5-mm-diameter plastic wells (96 wells/plate), at a density of 1.2×10^5 cells/well (in 0.2 mL of DMEM). Maintain cells at 37°C in a humidified incubator under an atmosphere of 95% air and 5% CO_2. Change the medium after 24 h, and replace with DMEM without FCS. Subsequently, change the medium every 3 d. Use cells 2–7 d after dissociation.

3.2. $^{45}Ca^{2+}$ Entry Studies in Chromaffin Cells Plated in Macrowells

Most of the studies available on $^{45}Ca^{2+}$ uptake into chromaffin cells have been performed in 24-well plates ***(7–17)***. The procedure comprises the following steps **(Fig. 1)**:

1. Wash the cells (2–7 d in culture) twice with 500 µL of Krebs-HEPES solution, over a 10-min period at 37°C (*see* **Note 2**).

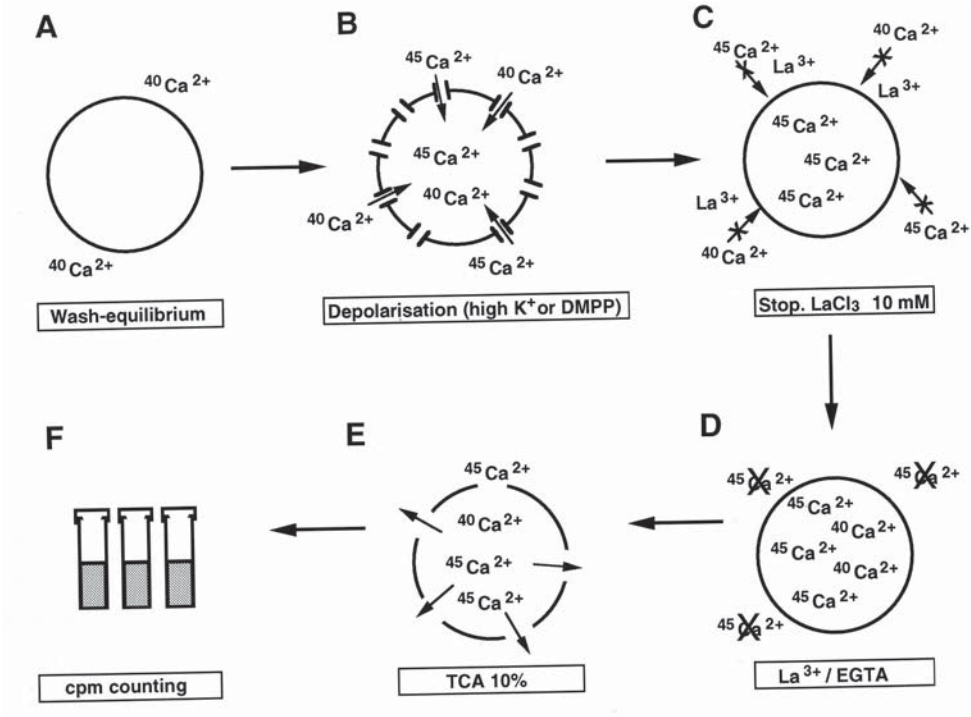

Fig. 1. Steps involved in the procedure used to measure $^{45}Ca^{2+}$ + $^{40}Ca^{2+}$ into chromaffin cells stimulated with high K^+ or with the nicotinic receptor agonist DMPP (*see* **Subheading 3.** for details).

2. Incubate the cells at 37°C (*see* **Note 3**) with $^{45}CaCl_2$, at a final concentration of 5 µCi · mL^{-1}, with Krebs-HEPES solution (basal uptake), high K^+ solution, or DMPP solution (*see* **Note 4**).
3. After a given stimulation time (1–60 s; *see* **Note 5**), rapidly aspirate and stop the reaction by adding 500 µL of cold Ca^{2+}-free Krebs-HEPES containing 10 m*M* $LaCl_3$ (*see* **Note 6**).
4. Wash the cells five times more with 500 µL of cold Ca^{2+}-free Krebs-HEPES containing 10 m*M* $LaCl_3$ and 2 m*M* EGTA, at 15-s intervals, to remove all extracellular $^{45}Ca^{2+}$ attached to the walls of the well and to the cell surface (*see* **Note 7**).
5. Add 500 µL of 10% trichloroacetic acid and scrape the cells with a plastic pipet tip.
6. Transfer the volume of each well to a polyethylene vial, add 3 mL of scintillation fluid, mix vigorously, and count in a scintillation beta counter (*see* **Note 8**).

3.3. $^{45}Ca^{2+}$ Entry Studies in Chromaffin Cells Plated in Microwells

$^{45}Ca^{2+}$ uptake can also be studied in cells plated in microwells. This is especially useful to save cells, when the compounds to be tested are expensive (i.e., ω-conotoxins to block Ca^{2+} channel subtypes, α-conotoxins to block neuronal

nicotinic acetylcholine receptor ion channels). In addition, when large numbers of compounds are to be tested for the blockade or activation of Ca^{2+} channels, or other ionic channels, indirectly responsible for an enhanced Ca^{2+} uptake (i.e., Na^+ channels, nicotinic receptor channels, Ca^{2+}-activated K^+ channels), this method in particular is useful.

Figure 2 shows the $^{45}Ca^{2+}$ taken up by cells in cpm, when plated at a density of 5×10^4 cells/well (white columns) or 10^5 cells/well. Note that doubling the number of cells does not lead to parallel increments of $^{45}Ca^{2+}$ uptake (**Figure 2A**). Hence, basal $^{45}Ca^{2+}$ entry increased by approx only 20%, whereas doubling of cells enhanced the DMPP response nearly threefold and the K^+ response nearly twofold. This indicates that cells cultured at higher densities express more nicotinic receptors and/or voltage-dependent $^{45}Ca^{2+}$ channels.

3.4. Calculation of Actual $^{40}Ca^{2+}$ Entry in Weight Units

Ca^{2+} channel current studies measure charge, and, thus, quantitations cannot be made at lower $[Ca^{2+}]_o$ (i.e., below 1–2 m*M*). On the other hand, fura-2 monitoring of Ca^{2+} entry only measures changes in cytosolic $[Ca^{2+}]$. Thus, the only method that directly determines the amount of Ca^{2+} entering the cell, measured chemically, involves use of $^{45}Ca^{2+}$ as a radiotracer and different concentrations of unlabeled $^{40}Ca^{2+}$ ***(18)***.

Table 1 summarizes the calculations required to determine various parameters of Ca^{2+} uptake, derived from the uptake (cpm) at the end of an experiment. The data were taken from one experiment similar to that shown in **Fig. 3**, performed in microwells containing 2×10^5 chromaffin cells. Cells were depolarized for 10 s with a solution containing 100 µ*M* DMPP, 5 µCi · mL^{-1} of $^{45}Ca^{2+}$ as tracer, and 1 mM of unlabeled $^{40}Ca^{2+}$. Basal $^{45}Ca^{2+}$ uptake was estimated in parallel wells by incubating the cells in a Krebs-HEPES solution lacking DMPP, and containing similar concentrations of $^{45}Ca^{2+}$ and $^{40}Ca^{2+}$.

Net cpm of $^{45}Ca^{2+}$ taken up by stimulated cells (2,310 cpm/2×10^5 cells) is obtained by subtracting the cpm in resting cells from the cpm in DMPP-stimulated cells. The specific activity of $^{45}Ca^{2+}$ + $^{40}Ca^{2+}$, estimated by counting an aliquot of 10 µL of Krebs-HEPES medium, is 7805 cpm/nmol. Hence, the 2310 net cpm of $^{45}Ca^{2+}$ found in 2×10^5 cells is equivalent to 0.296 nmol $^{40}Ca^{2+}$ or 296 pmol/(2×10^5 · cells) or 1.48 fmol/cell. Thus, each cell stimulated by DMPP over 10 s took up 1.48 fmol of unlabeled Ca^{2+}.

Now the rate of Ca^{2+} entry per unit time can be determined. A 20 µm diameter sphere has 1256 μm^2 of surface area, or 1.26×10^{-5} cm^2. Assuming that $^{45}Ca^{2+}$ uptake was linear during the first 10 s of DMPP stimulation, the 1.48 fmol/cell of Ca^{2+} taken up in 10 s becomes 0.15 fmol/(cell · s) or 0.15×10^{-15} mol/(cell · s), which, expressed by surface area becomes 11.7 pmol/(cm^2 · s).

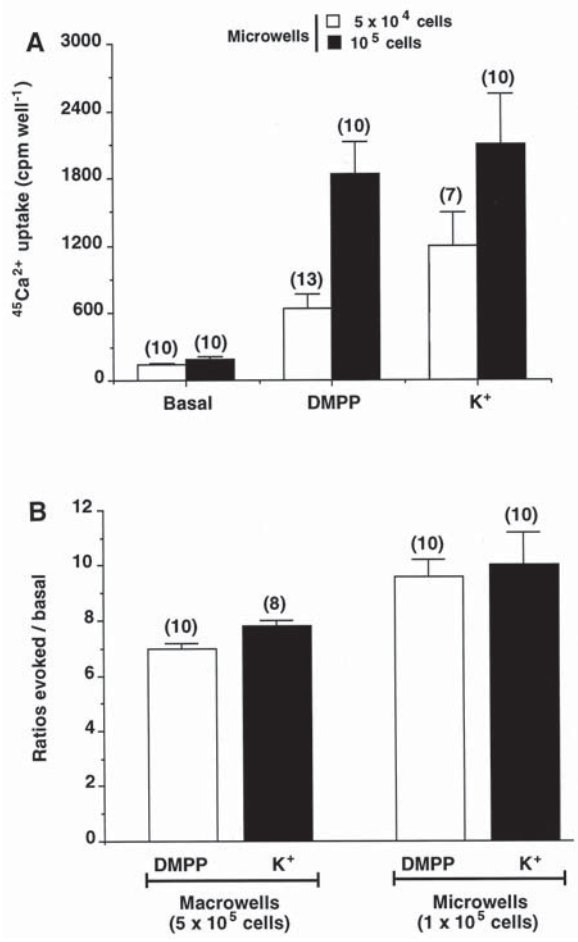

Fig. 2. Comparison of $^{45}Ca^{2+}$ uptake into bovine chromaffin cells cultured in 96-well plates (microwells) or 24-well plates (macrowells). **(A)** cpm of $^{45}Ca^{2+}$ taken up by cells plated in microwells, at a density of 5×10^4 cells/well (white columns) or at a density of 10^5 cells/well (black columns). In each case, cells were exposed to the $^{45}Ca^{2+}$ solution (4 μCi · mL^{-1} of $^{45}Ca^{2+}$ in 1 m*M* $^{40}Ca^{2+}$) either in Krebs-HEPES solution (basal), or in Krebs-HEPES containing 100 μ*M* DMPP or high K^+ (70 m*M* K^+, with isosmotic reduction of Na^+). **(B)** The ratios evoked:basal ($^{45}Ca^{2+}$ taken up by cells stimulated with DMPP or K^+, vs $^{45}Ca^{2+}$ taken up by resting cells). Data are means ± SEM of the number of wells shown in parentheses, from cells from at least two different cultures.

A third parameter that can be measured is the number of Ca^{2+} ions entering the cell through each individual Ca^{2+} channel in 1 s. Assuming that all Ca^{2+} channels are open during cell depolarization and that the bovine chromaffin

Table 1
Calculation of Rate and Amount of Ca^{2+} Entry into Single Chromaffin Cells, in Response to a Brief Depolarizing Stimulus (100 μ*M* DMPP for 10 s)[a]

Experimental conditions: microwells (96-well plate) containing 2×10^5 cells, 3 d in culture. 5 μCi · mL^{-1} of $^{45}Ca^{2+}$ plus 1 m*M* $^{40}Ca^{2+}$ were present in the extracellular solution.

$^{45}Ca^{2+}$ uptake (in cpm)

$^{45}Ca^{2+}$ taken up by resting cells: 571 ± 29 cpm 2×10^5 $cells^{-1}$

$^{45}Ca^{2+}$ taken up by cells stimulated with DMPP (100 μ*M*, 10 s): 2880 ± 225 cpm/2×10^5 cells.

Net $^{45}Ca^{2+}$ taken up by DMPP-stimulated cells (evoked/basal/evoked minus basal): 2310 ± 196 cpm/2×10^5 $cells^{-1}$

Conversion of cpm into mass units

$^{45}Ca^{2+}$ in 10 μL of DMPP-containing Krebs-HEPES (5 μCi · mL^{-1} of $^{45}Ca^{2+}$): 78,047 cpm

$^{40}Ca^{2+}$ present in DMPP-containing Krebs-HEPES medium: 1 m*M*

In 10 μL medium: 10 nmol of $^{40}Ca^{2+}$

In 10 μL of cell extract (cells stimulated with 100 μ*M* DMPP for 10 s): 2310 cpm

$^{40}Ca^{2+}$ in 2×10^5 cells: 296 pmol or 1.48 fmol of Ca^{2+}/cell in 10 s = 1.48×10^{-15} mol/cell 10 s

Rate of Ca^{2+} entry/unit surface area

Surface area of the cell: 1256 μm^2 = 1.26×10^{-5} cm^2

Rate of Ca^{2+} entry = 0.15×10^{-15} mol/cell · s/1.26×10^{-5} = 0.117×10^{-10} mol/cm^2 · s = 11.7 pmol/cm^2 · s

Rate of Ca^{2+}entry per single Ca^{2+} channel

Number of channels in a single chromaffin cell = 10/μm^2 = 12,560 channels/cell

Rate of Ca^{2+} entry = 0.15×10^{-15} mol/cell · s/12,560 channels = 1.19×10^{-20} mol/channel · s = 6740 ions/channel · s

Expected cytosolic Ca^{2+} concentration after 1-s depolarization

Volume of a single cell: 4×10^{-9} mL

Ca^{2+} in 1 mL of cytosol: (0.15×10^{-15} mol/cell · s) × (number of cells in 1 mL) = (0.15×10^{-15}) × (242×10^6) = 0.036×10^{-6} mol/mL = 0.036 mol/L = 36 μ*M*

[a]For these calculations, the chromaffin cell has been considered as a sphere of 20 μm diameter. Data are means ± SEM of nine wells from three different cultures.

cell plasmalemma contains 10 channels/μm^2 (***4,9,19,20***) 12,560 channels/cell, 6740 ions/(channel · s) enter the cell during DMPP stimulation.

The fourth parameter is the expected cytosolic [Ca^{2+}] reached after 1-s depolarization, considering a uniform intracellular distribution without Ca^{2+} buffering. The volume of a cell is 4×10^{-9} mL and the Ca^{2+} in 1 mL of cytosol (after 1-s depolarization) will be 0.036×10^{-6} mol/mL, which is equivalent to 36 μ*M*. If a cytosolic water space of 50% is considered, this figure is doubled: 72 μ*M*. This calculated [Ca^{2+}] is much higher than the few micromolar levels

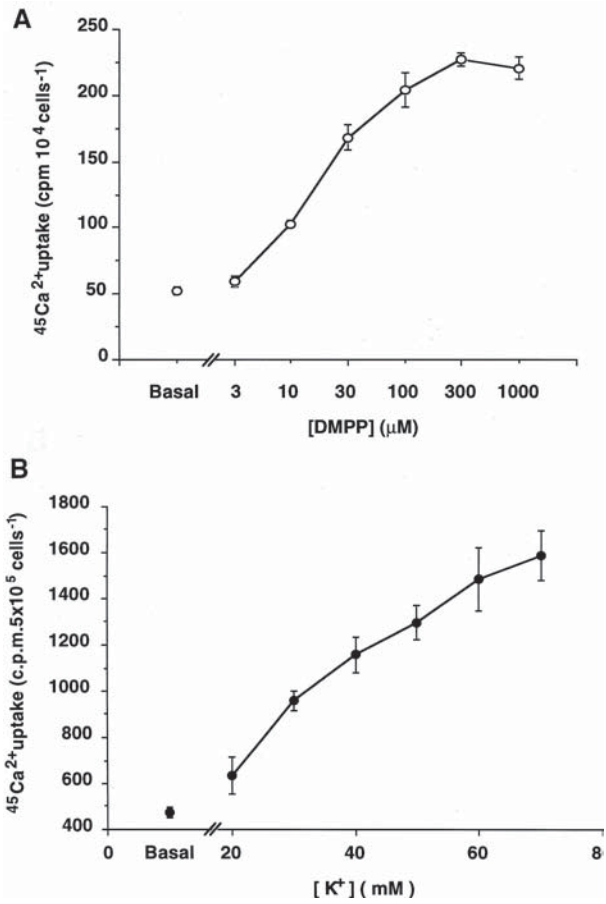

Fig. 3. $^{45}Ca^{2+}$ uptake into bovine chromaffin cells stimulated with increasing concentrations of the agonist for nicotinic acetylcholine receptors, DMPP **(A)** or with K^+ **(B)**. This experiment was performed following the procedure shown in **Subheading 3.** Cells (10^5), plated in microwells (A) were stimulated for 10 s with DMPP; cells (5×10^5) plated in macrowells (B) were also stimulated for 60 s with K^+. Data are expressed in cpm $^{45}Ca^{2+}$ retained by the cells (ordinate) and are means ± SEM of three to six wells from two different cell cultures.

of $[Ca^{2+}]_i$ increments obtained using Ca^{2+} fluorescent dyes. Of course, it is highly unlikely that this free cytosolic $[Ca^{2+}]_i$ is reached during cell depolarization (except at subplasmalemmal sites near the inner mouth of Ca^{2+} channels); powerful buffers will drastically and quickly reduce the $[Ca^{2+}]_i$. But the calculation using $^{45}Ca^{2+}$ measurements gives a more realistic idea of the huge

amounts of Ca^{2+} that circulate during cell activation; this cannot be estimated from any other technique measuring Ca^{2+} entry.

4. Notes

1. Separation and culture of viable adrenaline-containing and noradrenaline-containing cells in large amounts can also be achieved using combined Renografin and Percoll gradients ***(21,22)***. Because these cells have quite different physiological functions, and differ in their relative proportion of Ca^{2+} channel subtypes ***(23)***, this separation can be useful to study $^{45}Ca^{2+}$ uptake in each separate cell population.
2. Cells maintained in the incubator for several days in DMEM solution will need to be equilibrated with the Krebs-HEPES in which the $^{45}Ca^{2+}$ uptake measurement is going to take place. Usually a 10-min period is enough, but this can be extended up to 30 min.
3. Net $^{45}Ca^{2+}$ uptake stimulated by DMPP and K^+ is similar in the temperatures range of 24–37°C. However, a physiological temperature is preferable. To keep cells at 37°C the plate is placed on a temperature-controlled water bath, with the bottom submerged in the water 3–5 mm. The solutions to be added are kept at 37°C in assay tubes, also submerged in the water bath.
4. $^{45}Ca^{2+}$ is taken up by cells under resting conditions; thus, in every experiment, control unstimulated cells are always included. Usually, in a single 24-well plate every variable is measured in triplicate; hence eight variables are possible. For instance, if a concentration-response curve with a given toxin that blocks a given Ca^{2+} channel is desired, 3 wells are used to measure basal $^{45}Ca^{2+}$ uptake, another 3 to measure K^+-evoked $^{45}Ca^{2+}$ uptake through opened voltage-dependent Ca^{2+} channels, and the remaining 18 wells can be used to measure the effects of up to six concentrations of the toxin on K^+-evoked $^{45}Ca^{2+}$ (*see* **ref. *19***).
5. With 1–2-s depolarization times, there is no time to remove the depolarizing solution and replace it with La^{3+} solution. Therefore, it is better to stop the uptake reaction by adding 0.5 mL of a 20 m*M* $LaCl_3$-4 m*M* EGTA solution on top of the depolarizing solution, and then aspirate it slowly. Even in these conditions the process is unreliable at the 1–2-s time range.
6. Rapid aspiration does not mean uncontrolled aspiration of the fluid bathing the cells. If careful aspiration is not performed, cells will detach from the bottom of the well, and unreliable results will be obtained. The authors perform a gentle aspiration using a light vacuum pump connected with a tubing to a glass Pasteur pipet. The tip of the pipet is placed on the wall of the well, without touching the bottom, thus preventing cell aspiration. Triplicates are very important, and if they vary more than 10–20% they should be discarded.
7. More recently the authors have seen that **steps 3** and **4** (**Subheading 3.2.**) of the $^{45}Ca^{2+}$ uptake reaction can be performed as a single step, i.e., adding a washout solution containing 10 m*M* $LaCl_3$ and 2 m*M* EGTA.
8. **Figure 2** shows an example of experiments performed following this protocol. Note that a maximum $^{45}Ca^{2+}$ uptake (expressed as cpm 5×10^{-5} $cells^{-1}$ in the ordinates) was reached at DMPP concentrations of 20–50 μ*M*, and at 60–70 m*M* K^+.

References

1. Hodgkin, A. L. and Keynes, R. D. (1957) Movements of labelled calcium in squid giant axons. *J. Physiol.* **138,** 253–281.
2. Hagiwara, S. and Byerly, L. (1983) Calcium channel. *Annu. Rev. Neurosci.* **4,** 69–125.
3. Hamill, O. P., Marty, A., Neher, E., Sakmann, B., and Sigworth, F. J. (1981) Improved patch-clamp techniques for high-resolution current recording from cells and cell-free membranes patches. *Pflügers Arch.* **391,** 85–100.
4. Fenwick, E. M., Marty, A., and Neher, E. (1982) Sodium and calcium channels in bovine chromaffin cells. *J. Physiol.* **331,** 599–635.
5. Grynkiewicz, G. M., Poenie, M., and Tsien, R. Y. (1985) A new generation of Ca^{2+} indicators with greatly improved fluorescence properties. *J. Biol. Chem.* **260,** 3440–3450.
6. Livett, B. G. (1984) Adrenal medullary chromaffin cells in vitro. *Physiol. Rev.* **64,** 1103–1161.
7. Kilpatrick, D. L., Slepetis, R. J., Corcoran, J. J., and Kirshner, N. (1982) Calcium uptake and catecholamine secretion by cultured bovine adrenal medulla cells. *J. Neurochem.* **38,** 427–435.
8. Holz, R. W., Senter, R. A., and Frye, R. A. (1982) Relationship between Ca^{2+} uptake and catecholamine secretion in primary dissociated cultures of adrenal medulla. *J. Neurochem.* **39,** 635–646.
9. Ballesta, J. J., Palmero, M., Hidalgo, M. J., Gutiérrez, L. M., Reig, J. A., Viniegra, S., and García, A. G. (1989) Separate binding and functional sites for ω-conotoxin and nitrendipine suggest two types of calcium channels in bovine chromaffin cells. *J. Neurochem.* **53,** 1050–1056.
10. Gandía, L., Casado, L.-F., López, M. G., and García, A. G. (1991) Separation of two pathways for calcium entry into chromaffin cells. *Br. J. Pharmacol.* **103,** 1073–1078.
11. López, M. G., Fonteríz, R. I., Gandía, L., de la Fuente, M., Villarroya, M., García-Sancho, J., and García, A. G. (1993) The nicotinic acetylcholine receptor of the bovine chromaffin cell, a new target for dihydropyridines. *Eur. J. Pharmacol.* **247,** 199–207.
12. López, M. G., Abad, F., Sancho, C., de Pascual, R., Borges, R., Maroto, R., Dixon, W., and García, A. G. (1991) Membrane-mediated effects of the steroid 17-α-estradiol on adrenal catecholamine release. *J. Pharmacol. Exp. Ther.* **259,** 279–285.
13. Villarroya, M., Gandía, L., Lara, B., Albillos, A., López, M. G., and García, A. G. (1995) Dotarizine versus flunarizine as calcium antagonists in chromaffin cells. *Br. J. Pharmacol.* **114,** 369–376.
14. Gandía, L., Villarroya, M., Sala, F., Reig, J.-A., Viniegra, S., Quintanar, J.-L., García, A. G., and Gutiérrez, L.-M. (1996) Inhibition of nicotinic-receptor mediated responses in bovine chromaffin cells by diltiazem. *Br. J. Pharmacol.* **118,** 1301–1307.

15. Villarroya, M., Gandía, L., López, M. G., García, A. G., Cueto, S., García-Navio, J.-L., and Alvarez-Builla, J. (1996) Synthesis and pharmacology of alkanediguanidium compounds that block the neuronal nicotinic acetylcholine receptor. *Bioorg. Med. Chem.* **4,** 1177–1183.
16. Villarroya, M., de la Fuente, M.-T., López, M. G., Gandía, L., and García. A. G. (1997) Distinct effects of ω-toxins and various groups of Ca^{2+}-entry inhibitors on nicotinic acetylcholine receptor and Ca^{2+} channels of chromaffin cells. *Eur. J. Pharmacol.* **320,** 249–257.
17. Michelena, P., de la Fuente, M.-T., Lara, B., López, M. G., Gandía, L., and García, A. G. (1997) Drastic facilitation by α-latrotoxin of chromaffin cell exocytosis without measurable enhancement of Ca^{2+} entry or $[Ca^{2+}]_i$. *J. Physiol.* **502,** 481–496.
18. Artalejo, C. R., García, A. G., and Aunis, D. (1987) Chromaffin cell calcium channel kinetics measured isotopically through fast calcium, strontium, and barium fluxes. *J. Biol. Chem.* **262,** 915–926.
19. García, A. G., Sala, F., Reig, J. A., Viniegra, S., Frías, J., Fonteríz, R. I., and Gandía, L. (1984) Dihydropyridine Bay K 8644 activates chromaffin cell calcium channels. *Nature* **309,** 69–71.
20. Castillo, C. J. F., Fonteríz, R. I., López, M. G., Rosenheck, K., and García, A. G. (1989) (+)PN200-110 and ouabain binding sites in purified bovine adrenomedullary plasma membranes and chromaffin cells. *J. Neurochem.* **53,** 1442–1449.
21. Moro. M. A., López, M. G., Gandía, L., Michelena, P., and García, A. G. (1990) Separation and culture of living adrenaline- and noradrenaline-containing cells from bovine adrenal medullae. *Analytical Biochem.* **185,** 243–248.
22. Moro, M. A., García, A. G., and Langley, O. K. (1991) Characterization of two chromaffin cell populations isolated from bovine adrenal medulla. *J. Neurochem.* **57,** 363–369.
23. Lomax, R. B., Michelena, P., Núñez, L., García-Sancho, J., García, A. G., and Montiel, C. (1997) Different contributions of L- and Q-type Ca^{2+} channels to Ca^{2+} signals and secretion in chromaffin cell subtypes. *Am. J. Physiol.* **272,(Cell Physiol. 41),** C476–C484.

9

Measurement of [^{3}H]PN200-110 and [^{125}I]ω-Conotoxin MVIIA Binding

Kazuyoshi Hirota and David G. Lambert

1. Introduction

Intracellular Ca^{2+} ($[Ca^{2+}]_i$) can rise primarily via release from intracellular storage sites (e.g., the endoplasmic reticulum) or via entry across the membrane down the steep concentration gradient ***(1–3)***. Ca^{2+} can enter through two main classes of plasma membrane–located Ca^{2+} channels: receptor operated and voltage sensitive ***(4–7)***. Voltage-sensitive Ca^{2+} channels are involved in a wide and diverse array of physiological responses including neurotransmitter release ***(8)***. In addition, many guanine nucleotide protein (G) coupled receptors couple to voltage-sensitive Ca^{2+} channels to reduce Ca^{2+} influx ***(9,10)***.

1.1. Voltage-Sensitive Ca^{2+} Channels

Voltage-sensitive Ca^{2+} channels are classified into low voltage activated (T-channels) and high voltage activated (HVA, L-, N-, P/Q-, and R-channels). This further subclassification of LVA channels is based on the interaction of a range of inhibitors and toxins (**Table 1**) ***(4,8,11)***. LVA channels are comprised of four or five distinct subunits ($\alpha_{1/2}\beta\delta\gamma$) arranged in various combinations. The α_1-subunit arises from six distinct genes (**Table 1**) and is the pore-forming subunit of the channel. The α_1-subunit in the L-channel is also the site to which DHPs bind ***(4)***. In addition, ω-conotoxins bind to the α-subunit(s) ***(12,13)*** of the N-channel.

1.2. Radioligand Binding

Radioligand binding studies enable the properties of drug-receptor interaction to be studied. Two commonly estimated parameters are the total number of receptors/channels expressed in a particular tissue (B_{max}) and the affinity

From: *Methods in Molecular Biology, Vol. 114: Calcium Signaling Protocols*
Edited by: D. G. Lambert

Table 1
Classification of High-Voltage–Activated Ca^{2+} Channels

	L	N	P/Q	R
Specific inhibitor	DHPs[a]	ω-CgTx[b]	ω-Aga-IVA[c]	None
α_1-subunit gene	$\alpha_{1S,1C,1D}$	α_{1B}	α_{1A}	α_{1E}

[a]DHPs, dihydropyridines.
[b]ω-CgTx, ω-conotoxin GVIA/VIIA.
[c]P-channels blocked by low concentrations and Q-channels blocked by high concentrations.

(K_d) of a particular drug for a particular receptor/channel. Tissue samples are incubated with various concentrations of radiolabel until binding equilibrium is reached. The tissue and ligand are separated by either filtration or centrifugation and bound ligand is quantified. Receptor/channel binding is determined indirectly as the radiolabel will bind nonspecifically to nonreceptor protein. In practice, nonspecific binding (NSB) is defined by incubating an identical tube in the presence of a high concentration of an unlabeled drug that interacts with the receptor/channel. Specific binding is then the difference between total binding (in the absence of the unlabeled drug) and NSB (in the presence of the unlabeled drug) (**Fig. 1**).

Two types of experiments are commonly used:

1. Saturation in which the concentration of radiolabel increases until specific binding saturates (*see* **Fig. 1**). The saturation curve can be linearized to yield a straight line. Bmax and Kd can be estimated.
2. Displacement curves enable the affinity of unlabeled drugs to be estimated. A fixed concentration of receptors/channels is labeled with a fixed concentration of label, and increasing concentration of unlabeled drug is added to displace the label (**Fig. 1**). The concentration of unlabeled drug producing 50% displacement is related to its affinity (*see* **Subheading 3.5.**).

In this chapter, the authors will describe a radioligand binding protocol for [^{3}H]PN200-110 binding to L-type channels and [^{125}I]ω-conotoxin MVIIA binding to N-channels. This latter toxin is particularly useful because the binding is reversible. Using these protocols, it will be possible to determine channel density and interaction of unlabeled compounds with the radiolabel binding site. Indeed, the authors have recently reported an interaction of a range of iv general and local anaesthetic agents with the [^{3}H]PN200-110 binding site in a variety of tissue preparations ***(14–16)***. For functional studies of Ca^{2+} channel activity *see* Chapter 8.

2. Materials

2.1. Cell Culture

1. Undifferentiated SH-SY5Y human neuroblastoma cells (gift from Dr. J. L. Beidler, Sloane Kettering Institute, Rye, NJ).

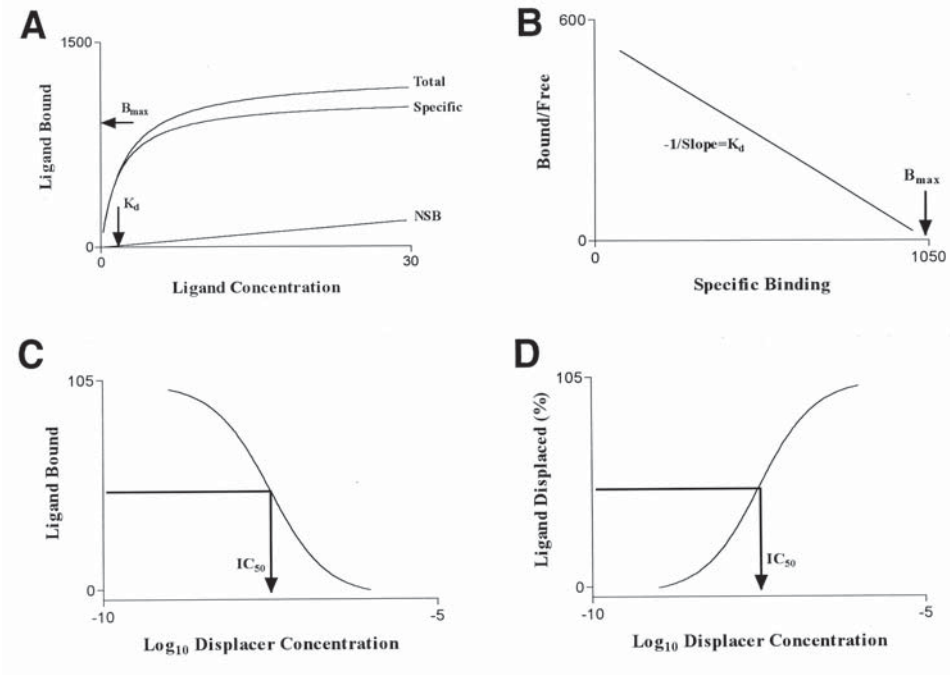

Fig. 1. Stylized saturation type assay used to determine B_{max} and K_d **(A)**. The specific binding curve is shown analyzed according to Scatchard [re] in **(B)**. In **(C)** and **(D)**, a stylized displacement type assay is depicted and used to estimate IC50 and calculate K_{50} for an unlabeled drug. Curves (C) and (D) are mirror images of each other indicating that as the amount bound decreases (C) the amount of displacement increases (D).

2. Culture medium for SH-SY5Y cells: minimum essential medium supplemented with 10% fetal calf serum (FCS), 2 m*M* glutamine, 100 IU/mL penicillin, 100 IU/mL streptomycin, and 2.5 µg/mL fungizone (*see* **Note 1**).
3. NG108-15 neuroblastoma X glioma hybrid cells (*see* **Note 2**).
4. Culture medium for NG108-15 cells: Dulbecco's minimum essential medium supplemented with 10% FCS, 2 m*M* glutamine, 100 IU/mL penicillin, 100 IU/mL streptomycin, 2.5 µg/mL fungizone, and HAT (hypoxanthine (0.1 m*M*), aminopterin [0.4 µM], thymidine [16 µM]) (*see* **Note 1**).
5. Cell harvest buffer: 10 m*M* HEPES-buffered 0.9% saline plus 0.05% EDTA, pH 7.4 (with 10 *M* NaOH).

2.2. Assay Buffers and Reagents

1. Assay buffer for L-channel binding: 50 m*M* Tris-HCl, pH 7.4.
2. Assay buffer for N-channel binding: 50 m*M* Tris-HCl, pH 7.4, with 0.1% bovine serum albumin (BSA) added.

3. Wash buffer for L- and N-channel binding: 50 m*M* Tris-HCl, pH 7.4.
4. Nifedipine, 50 m*M* stock in dimethyl sulfoxide (DMSO) stored frozen at –20°C in 50-µL aliquots in the dark.
5. [^{3}H]PN200-110 (Amersham International, Bucks, UK).
6. [^{125}I]ω-conotoxin MVIIA (NEN Du Pont, Brussels) at a specific activity of 2200 Ci/mmol and reconstituted in distilled water to 50 µCi/mL (*see* **Note 3**).
7. ω-Conotoxin MVIIA, 1-µ*M* stock stored frozen at –20°C in 10-µL aliquots (*see* **Note 4**).
8. Polyethylenimine, 0.1% solution made in distilled water.
9. Cell harvest buffer: 10 m*M* HEPES-buffered 0.9% saline plus 0.05% EDTA, pH 7.4 (with 10 *M* NaOH).

3. Methods

3.1. Preparation of Rat Brain Membranes

1. Stun and then decapitate female Wistar rats (250–300 g).
2. Rapidly remove the brain, detach the cerebrocortex from its internal structures, and place in 50 m*M* of Tris-HCl, pH 7.4, at 4°C.
3. Homogenize brain tissue using an Ultra Turrax T25 (6 × 5 s bursts on ice).
4. Centrifuge the resulting homogenate at 18,000*g* for 10 min and resuspend the pellet in Tris-HCl buffer.
5. Repeat this procedure three times.
6. Determine membrane protein according to Lowry et al. ***(17)*** and freeze the homogenate in aliquots at –40°C for [^{3}H]PN200-110 binding or use fresh for [^{125}I]ω-conotoxin MVIIA binding studies.

3.2. Preparation of SH-SY5Y and NG108-15 Cell Membranes

1. Maintain confluent monolayers (75 cm^2) of cells in the appropriate media.
2. Split one flask of confluent cells using trypsin (0.5g/L)-EDTA (0.2g/L, 5 mL) solution as supplied (*see* **Note 1**) into nine other flasks each containing 15 mL of supplemented media. After 2 d of incubation (37°C, 5% CO_2 incubator), remove the media and replace with 25 mL of fresh supplemented media.
3. Culture cells (feed 24 h before use with fresh medium) until confluent (use cells up to 3 d postconfluency).
4. On the day of the experiment, remove medium and add 5 mL of harvest buffer to the cell monolayer.
5. Remove 5 mL of harvest buffer immediately, and add a further 5 mL of fresh harvest buffer and incubate at room temperature for ~5 mins.
6. Gently tap the side of the flask to dislodge the adherent cell monolayer.
7. When all the cells are in suspension, transfer to a centrifuge tube. Rinse the cells out of the flask by adding approx 15 mL of harvest buffer. Transfer this to the centrifuge tube.
8. Sediment at 1000*g* in a low-speed centrifuge for 3 min.
9. Resuspend in 50 m*M* Tris-HCl, pH 7.4, at 4°C.

Table 2
[^{3}H]PN200-110 Saturation Binding Assay Addition Table to Determine K_d and B_{max}

Tube	Buffer	Nifedipine (50 μ*M*)	[^{3}H]PN200-110 (PN1–PN8)	Membranes
1. $Total_{PN1}$	700	—	200	100
2. $Total_{PN1}$	700	—	200	100
3. NSB_{PN1}	500	200	200	100
4. $Total_{PN2}$	700	—	200	100
5. $Total_{PN2}$	700	—	200	100
6. NSB_{PN2}	500	200	200	100
Continue in groups of 3 to total of 24 tubes using all 8 [^{3}H]PN dilutions.				

Eight concentrations of [^{3}H]PN200-110 are used with 3 tubes per concentration set up as duplicate totals and single NSB (8 × 3 = 24 tubes in total)

[a]Assay volume is 1000 μL. 50 μ*M* nifedipine stock is diluted 1:5 when added to the assay to yield a final concentration of 10 μ*M*.

10. Homogenize the suspension using an Ultra Turrax T25 (6 × 5 s bursts on ice).
11. Centrifuge the resulting homogenate at 18,000*g* for 10 min and resuspend the pellet in Tris-HCl buffer.
12. Repeat this procedure three times.
13. Determine the membrane protein according to Lowry et al. ***(17)*** and freeze the homogenate in aliquots at –40°C for [^{3}H]PN200-110 binding or use fresh for [^{125}I]ω-conotoxin MVIIA binding studies.

3.3. Measurement of [^{3}H]PN200-110 Binding

3.3.1. Saturation Binding Assays to Determine L-Channel Density (see **Note 5**)

1. Assay volume is 1 mL and one saturation assay uses 24 tubes in total.
2. Dilute nifedipine stock for determination of NSB to give 50 μ*M* in assay buffer (**Subheading 2.2.**, **item 1**). When 200 μL is added to the assay, the final "in the assay" concentration will be 10 μ*M* (200 μL/1000 μL = 1:5 dilution).
3. Make up a working stock of [^{3}H]PN200-110 of approx 2 n*M* in assay buffer (*see* **Note 6**).
4. Make seven serial dilutions of the 2 n*M* [^{3}H]PN200-110 stock by adding equal volumes of assay buffer. This will give eight concentrations as follows: 2, 1, 0.5, 0.25, 0.125, 0.0625, 0.0312, and 0.0156 n*M*.
5. Dilute prepared protein in assay buffer to give approx 200 μg/100 μL of brain membranes (but *see* **ref. *16***), or 800 μg/100 μL for SH-SY5Y and NG108-15 cells.
6. Add reagents to tubes as shown in **Table 2**.
7. Incubate at 20°C in the dark for 90 min.

8. During the incubation, soak Whatman GF/B harvester papers in 0.1% polyethylenimine to reduce NSB.
9. Separate bound and free radioligand by harvesting on a Brandell harvester (*see* **Note 6**).
10. Transfer the filters to scintillation insert vials and add 4.5 mL of scintillant. (The authors use OptiPhase "Safe" [LKB Wallac via Fisons, Loughborough, UK]).
11. Leave the filters for at least 8 h to extract, and then count on a scintillation counter for 3 min per sample.

3.3.2. Displacement Binding Assays to Determine Interaction of Unlabeled L-Channel Ligands (see **Note 8**)

1. Assay volume is 1 mL and uses 24 tubes in total.
2. Dilute nifedipine stock for determination of NSB to give 50 µ*M* in assay buffer (**Subheading 2.2.**, **item 1**). When 200 µL is added to the assay, the final "in the assay" concentration will be 10 µ*M* (200 µL/1000 µL = 1:5 dilution).
3. Make up a working stock of [^{3}H]PN200-110 of approx 0.2 n*M* in assay buffer. Try to keep this consistent between experiments (*see* **Note 6**).
4. Make up dilutions of displacing drugs ensuring that they are five times more concentrated so that when 200 µL is added to 1000 µL a fivefold dilution is made. For a 24-tube assay as shown in **Table 2**, up to 16 displacer concentrations can be included, e.g., in single points, 8 in duplicate, or combinations thereof (*see* **Note 9**).
5. Dilute prepared protein in assay buffer to give approx 200 µg/100 µL of brain membranes (but *see* **ref. *16***], or 800 µg/100 µL for SH-SY5Y and NG108-15 cells.
6. Add reagents to tubes as shown in **Table 3**.
7. Incubate at 20°C in the dark for 90 min.
8. During the incubation, soak Whatman GF/B harvester papers in 0.1% polyethylenimine to reduce NSB.
9. Separate bound and free radioligand by harvesting on a Brandell harvester (*see* **Note 7**).
10. Transfer the filters to scintillation insert vials and add 4.5 mL of scintillant. (The authors use OptiPhase "Safe" [LKB Wallac via Fisons, Loughborough, UK]).
11. Leave the filters for at least 8 h to extract, and then count on a scintillation counter for 3 min per sample.

3.4. Measurement of [^{125}I]ω-Conotoxin MVIIA Binding (see Note 10)

3.4.1 Saturation Binding Assays to Determine N-Channel Density

1. Assay volume is 0.5 mL and uses 24 tubes in total.
2. Dilute ω-conotoxin MVIIA stock for determination of NSB to give 50 n*M* in assay buffer (**Subheading 2.2.**, **item 2**). When 100 µL is added to the assay, the final "in the assay" concentration will be 10 n*M* (100 µL/500 µL = 1:5 dilution). Do not refreeze any unused stock.
3. Defrost [^{125}I]ω-conotoxin MVIIA aliquot. Make up a working stock of [^{125}I]ω-conotoxin MVIIA of approx 10 p*M* in assay buffer (*see* **Note 11**). Do not refreeze any unused stock.

Table 3
[³H]PN200-110 Displacement Binding Assay Addition Table to Determine Binding Properties of Unlabeled Drugs

Tube	Buffer	Nifedipine (50 μ*M*)	Displacer (various)	[³H]PN200-110 (0.2 n*M*)	Membranes
1. Total	700	—	—	200	100
2. Total	700	—	—	200	100
3. NSB	500	200	—	200	100
4. NSB	500	200	—	200	100
5. Displacer 1	500	—	200	200	100
6. Displacer 2	500	—	200	200	100
7. Displacer 3	500	—	200	200	100
↓					
20. Displacer 16	500	—	200	200	100
21. Total	700	—	—	200	100
22. Total	700	—	—	200	100
23. NSB	500	200	—	200	100
24. NSB	500	200	—	200	100

[a]Assay volume is 1000 μL. 50 μ*M* nifedipine stock and displacer dilutions are diluted 1:5 when added to the assay.

4. Make seven serial dilutions of the 10 n*M* [¹²⁵I]ω-conotoxin MVIIA stock by adding equal volumes of assay buffer. This will give eight concentrations as follows: 5, 2.5, 1.25, 0.625, 0.312, 0.156, 0.078, and 0.039 p*M*.
5. Dilute prepared protein in assay buffer to give approx 5 μg/100 μL of brain membranes, or 100 μg/100 μL for SH-SY5Y and NG108-15 cells.
6. Add reagents to tubes as shown in **Table 4**.
7. Incubate at 20°C in the dark for 30 min.
8. During the incubation, soak Whatman GF/B harvester papers in 0.1% polyethylenimine to reduce NSB.
9. Separate bound and free radioligand by harvesting on a Brandell harvester (*see* **Note 7**).
10. Transfer the dry filters directly to counting tubes suitable for one's γ-counter and count for 1 min/sample.

*3.4.2. Displacement Binding Assays to Determine Interaction of Unlabeled N-channel Ligands (*see **Note 8***)*

1. Assay volume is 0.5 mL and uses 24 tubes in total.
2. Dilute ω-conotoxin MVIIA stock for determination of NSB to give 50 n*M* in assay buffer (**Subheading 2.2.**, **item 2**). When 100 μL is added to the assay, the final "in the assay" concentration will be 10 n*M* (100 μL/500 μL = 1:5 dilution). Do not refreeze any unused stock.

Table 4
[^{125}I]ω-Conotoxin MVIIA Saturation Binding Assay Addition Table to Determine K_d and B_{max}[a]

Tube	Buffer	ω-conotoxin (10 n*M*)	[^{125}I]ω-conotoxin (C1–C8)	Membranes
1. $Total_{C1}$	300	—	100	100
2. $Total_{C1}$	300	—	100	100
3. NSB_{C1}	200	100	100	100
4. $Total_{C2}$	300	—	100	100
5. $Total_{C2}$	300	—	100	100
6. NSB_{C2}	200	100	100	100
Continue in groups of 3 to total of 24 tubes using all 8 [^{125}I]ω-conotoxin dilutions.				

Eight concentrations of [^{125}I]ω-conotoxin MVIIA are used with 3 tubes per concentration set up as duplicate totals and single NSB (8 × 3 = 24 tubes in total).

[a]Assay volume is 500 µL. 50 n*M* ω-conotoxin MVIIA stock is diluted 1:5 when added to the assay to yield a final concentration of 10 n*M*.

3. Defrost [^{125}I]ω-conotoxin MVIIA aliquot. Make up a working stock of [^{125}I]ω-conotoxin MVIIA of approx 1 p*M* in assay buffer (*see* **Note 11**). Do not refreeze any unused stock, and try to keep the concentration consistent between experiments.
4. Make up dilutions of displacing drugs ensuring that they are five times more concentrated so that when 100 µL is added to 500 µL a fivefold dilution is made. For a 24-tube assay as shown in **Table 4**, up to 16 displacer concentrations can be included, e.g., in single points, 8 in duplicate, or combinations thereof (*see* **Note 9**).
5. Dilute prepared protein in assay buffer to give approx 5 µg/100 µL of brain membranes, or 100 µg/100 µL for SH-SY5Y and NG108-15 cells.
6. Add reagents to tubes as shown in **Table 5**.
7. Incubate at 20°C in the dark for 30 min.
8. During the incubation, soak Whatman GF/B harvester papers in 0.1% polyethylenimine to reduce NSB.
9. Separate bound and free radioligand by harvesting on a Brandell harvester (*see* **Note 7**).
10. Transfer the dry filters directly to counting tubes suitable for one's γ-counter and count for 1 min per sample.

3.5. Data Analysis

Specific binding is calculated as the difference between total and NSB. B_{max} and K_d are obtained from Scatchard plots ***(18)***. In displacement studies (*see* **Note 12**), the concentrations of displacer producing 50% displacement of specific binding (IC_{50}) is obtained by computer-assisted curve fitting (GRAPHPAD-PRISM, *see* **Note 13**) and corrected for the competing mass of

Table 5
[^{125}I]ω-Conotoxin MVIIA Displacement Binding Assay Addition Table to Determine Binding Properties of Unlabeled Drugs[a]

Tube	Buffer	ω-conotoxin (50 p*M*)	Displacer (various)	[^{125}I]ω-conotoxin (1 p*M*)	Membranes
1. Total	300	—	—	100	100
2. Total	300	—	—	100	100
3. NSB	200	100	—	100	100
4. NSB	200	100	—	100	100
5. Displacer 1	200	—	100	100	100
6. Displacer 2	200	—	100	100	100
7. Displacer 3	200	—	100	100	100
↓					
20. Displacer 16	200	—	100	100	100
21. Total	300	—	—	100	100
22. Total	300	—	—	100	100
23. NSB	200	100	—	100	100
24. NSB	200	100	—	100	100

[a]Assay volume is 500 µL. 50 n*M* ω-conotoxin MVIIA stock and displacer dilutions are diluted 1:5 when added to the assay.

radioligand according to Cheng and Prusoff ***(19)*** to yield the affinity constant (K_{50}) (*see* **Note 14**).

4. Notes

1. All tissue culture media and reagents are supplied by Life Technologies.
2. From European Collection of Animal Cell Cultures (web site http://www.biotech.ist.unige.it/cldb/cname-dh.html).
3. Pack sizes of 10 and 50 µCi are available. These sizes refer to the stated activity reference date (normally one month after manufacture), which usually means that more is actually supplied if purchased close to the manufacture date. One should check this when ordering. The specific activity does not change because on decay [^{125}I]ω-conotoxin MVIIA undergoes decay catastrophe. The reconstituted stock should be frozen at –20°C in small aliquots in a dark lead-lined box. Typically the authors purchase 10 µCi close to the date of manufacture (~16 µCi), reconstitute in 320 µL, and store as 20 µL aliquots (1 µCi/aliquot = 2.22×10^6 cpm/aliquot).
4. This should be bought in the smallest pack size from Sigma (cat no. C1182) and made up fresh every 4 wk. Take care in preparation as the peptide content varies. Allow product as supplied to warm to room temperature before opening the pack. Avoid storage in a frost-free freezer to minimize freeze-thaw cycles.
5. A typical experiment using this protocol is shown in **Fig. 2** and should be examined in conjunction with **Subheading 3.5.**

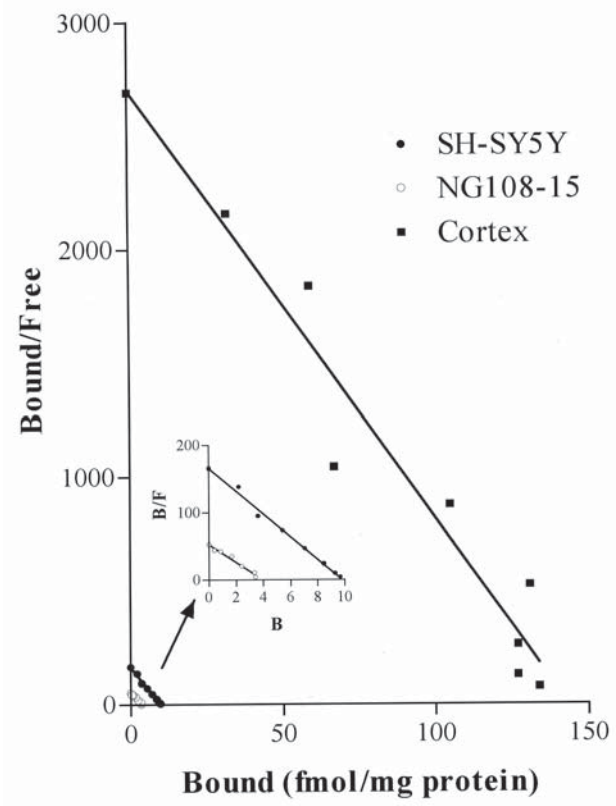

Fig. 2. Typical Scatchard analysis of [^{3}H]PN200-110 binding to rat cerebrocortical, SH-SY5Y, and NG 108-15 membranes. B_{max} and K_d values in each tissue were 143.5 fmol/mg protein and 53 p*M*, 9.9 fmol/mg protein and 60 p*M*, 4.0 fmol/mg protein and 75 p*M*.

6. To do this calculate from the specific activity the number of [^{3}H] DPM that would yield a 1-n*M* solution in an assay volume of 1 mL. This figure will vary for differing specific activities. The authors are currently using a batch that has a specific activity of 81 Ci/mmol. This is equivalent to 1/81 mmol/Ci or 0.01235 mmol/Ci. It is also equal to 0.01235 mmol $\times$ 10^{-6} mmol/μCi or 12.35 pmol/μCi. 12.35 pmol in a 1-mL assay is a 12.35-n*M* solution and 1 μCi = 2.22×10^6 dpm; therefore, a 1-n*M* solution is 2.22×10^6/12.35 or 179,757 dpm. Then add from [^{3}H]PN200-110 as sold sufficient to give approx 270,000 dpm (or 2 n*M*). The authors add approx 1 μL/mL to begin with and then count 200 μL to determine activity. Depending on the value obtained, either more [^{3}H] or buffer is added so that 200 μL will contain the desired 270,000 dpm. It is important to spend some time getting this right. Remember to make sufficient for the number of tubes set up in the assay and to make serial dilutions.

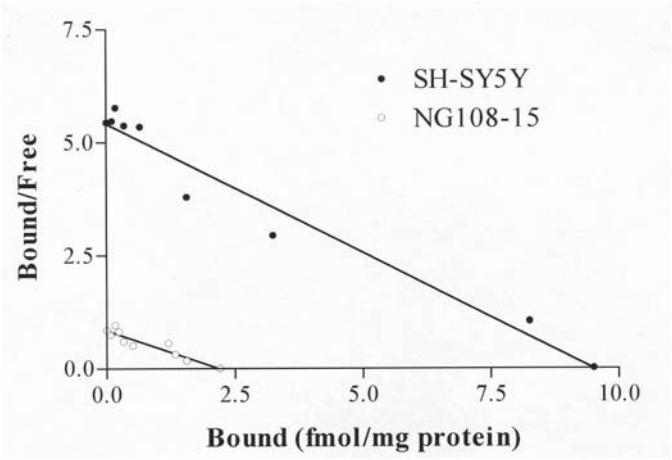

Fig. 3. Typical Scatchard analysis of [^{125}I]ω-conotoxin MVIIA binding to SH-SY5Y and NG108-15 membranes. B_{max} and K_d values in each tissue were 9.5 fmol/mg protein and 1.8 p*M*, and 2.2 fmol/mg protein and 2.6 p*M*.

7. All harvesting should be performed with cold (4°C) wash buffer. Initially dispense 4 mL of buffer and deposit the mixture onto the filter papers using the harvester according to the manufacturer's instructions. Wash the filters twice using the harvester. Harvest buffers do not contain BSA because this foams in the harvester waste trap.
8. A typical experiment using this protocol is shown in **Fig. 3** and should be examined in conjunction with **Subheading 3.5.**
9. When making up serial dilutions of displacing drugs, the authors make 10- and 3-fold dilutions. The choice of which concentration range to use depends on the displacer and its expected IC_{50}. When plotted on a log scale, this gives an even spread of data points ($\log_{10}$ 3 ~0.5). In addition, the solvent used to make up the displacer should be included to control for a solvent effect. The authors recommend that if a single solvent is used routinely, then a full displacement curve should be constructed. They have performed such an experiment with DMSO and have found that concentrations as high as 1% produce only 3% displacement of [^{3}H]PN200-110.
10. A typical experiment using this protocol is shown in **Fig. 4** and should be examined in conjunction with **Subheading 3.5.**
11. To do this calculate from the specific activity the number of [^{125}I] cpm that would yield a 1-p*M* solution in an assay volume of 0.5 mL. This figure will vary for differing specific activities. The batch that the authors are currently using has a specific activity of 2200 Ci/mmol. The calculations are as described in **Note 6**. When 1 p*M* [^{125}I]ω-conotoxin MVIIA in a 0.5-mL assay will give 2442 cpm, a 10-p*M* solution should contain 24,420 cpm. Then add from [^{125}I]ω-conotoxin MVIIA (as made in **Subheading 2.2.**, **item 6**) sufficient to give approx 24,420 cpm (or 10 p*M*). Count 100 µL to determine activity. Depending on the value obtained, either

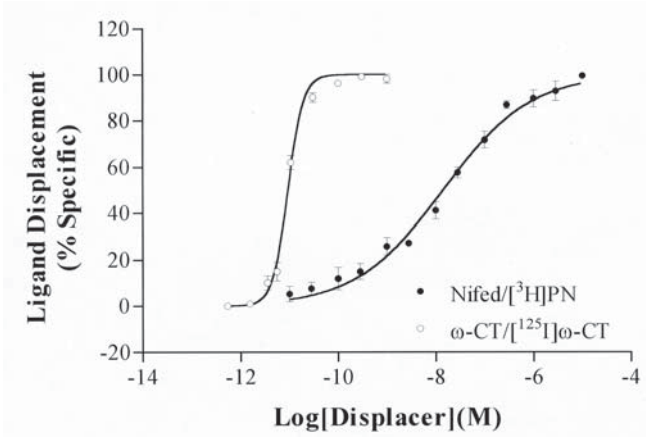

Fig. 4. Displacement of [^{3}H]PN200-110 by nifedipine and [^{125}I]ω-conotoxin MVIIA by unlabeled ω-conotoxin MVIIA in rat cerebrocortical membranes. K_{50} values were 3.2 n*M* and 9.2 p*M*. Data are mean ± SEM (n = 5-6). In [^{125}I]ω-conotoxin MVIIA binding study, the $IC_{50} = K_{50}$ (*see* **Note 11**) as the radiolabel and the displacer are the same drug (these "isotope dilution" data can also be used to calculate B_{max}). Note the steep nature of the ω-conotoxin MVIIA curve; this is consistent with **ref. *20***.

more [^{125}I] or buffer is added so that 100 µL will contain the desired 24,420 dpm. It is important to spend some time getting this right. Remember to make sufficient for the number of tubes set up in the assay and to make serial dilutions. Also, as the batch ages while the specific activity remains constant, the absolute activity declines; hence, more stock volume will be required to obtain a 10-p*M* solution.

12. Calculate specific binding by subtracting the average NSB (duplicates at the start and end of the assay). Displacement (%) is calculated as follows: $Total_{(specific\ counts)} - Displacer_{(specific\ counts)}/Total_{(specific\ counts)} \times 100$. Lowest concentration of displacer should give lowest percent displacement (highest counts) and approach total tubes. Highest concentration of displacer should give highest percent displacement (lowest counts).
13. The authors strongly recommend that the instructions manual and help menu are consulted in conjunction with a standard pharmacology text when interpreting data.
14. As the concentration of radiolabel increases, the amount of displacer required to produce 50% displacement increases (hence competitive binding assay). The Cheng and Prusoff ***(19)*** equation [$K_{50} = IC_{50}/(1 + (L/K_d)]$ (where IC_{50} is the concentration of displacer producing 50% displacement, L is the concentration of radiolabel, and K_d refers to the radiolabel) corrects the displacement curve to the position it would theoretically occupy in the absence of radiolabel.

References

1. Tsien, R. W. and Tsien, R. Y. (1990) Calcium channels, stores and oscillations. *Annu. Rev. Cell Biol.* **6,** 715–760.

2. Berridge, M. J. (1993) Inositol trisphosphate and Ca^{2+} signalling. *Nature* **361,** 315–325.
3. Clapham, D. (1995) Calcium signalling. *Cell* **80,** 259–268.
4. Spedding, M. and Paoletti, R. (1992) Classification of calcium channels and the sites of action of drugs modifying channel function. *Pharmacological Rev.* **44,** 363–376.
5. Miller, R. J. (1992) Voltage sensitive Ca^{2+} channels. *J. Biol. Chem.* **267,** 1403–1406.
6. Fasolato, C., Innocenti, B., and Pozzan, T. (1994) Receptor activated Ca^{2+} influx: how many mechanisms for how many channels. *Trends Pharmacol. Sci.* **15,** 77–83.
7. Berridge, M. J. (1995) Capacitative calcium entry. *Biochem. J.* **312,** 1–11.
8. Wu, L.-G. and Saggau, P. (1997) Presynaptic inhibition of elicited neurotransmitter release. *Trends Neurosci.* **20,** 204–212.
9. Miller R. J. (1990) Receptor mediated regulation of calcium channels and neurotransmitter release. *FASEB J.* **4,** 3291–3299.
10. Hille, B. (1994) Modulation of ion-channel function by G-protein coupled receptors. *Trends Neurosci.* **17,** 531–536.
11. Miller, R. J. (1997) Calcium channels prove to be a real headache. *Trends Neurosci.* **20,** 189–192.
12. Ellinor, P. T., Zhang, J.-F., Horne, W. A., and Tsien, R. Y. (1994) Structural determinants of the blockade of N-type calcium channels by a peptide neurotoxin. *Nature* **372,** 272–275.
13. Ichida, S., Wada, T., Akimoto, T., Kasamatsu, Y., Tahara, M., and Hasimoto, K. (1995) Characteristics of specific ^{125}I-ω-conotoxin GVIA binding and ^{125}I-ω-conotoxin GVIA labeling using bifunctional crosslinkers in crude membranes from chick whole brain. *Biochem. Biophys. Acta.* **1233,** 57–67.
14. Hirota, K. and Lambert, D. G. (1996) I.v. anaesthetic agents inhibit dihydropyridine binding to L-type voltage-sensitive Ca^{2+} channels in rat cerebrocortical membranes. *Br. J. Anaesth.* **77,** 248–253.
15. Hirota, K. and Lambert, D. G. (1997) Do local anaesthetics interact with dihydropyridine binding sites on neuronal L-type Ca^{2+} channels? *Br. J. Anaesth.* **78,** 185–188.
16. Hirota, K. and Lambert, D. G. (1997) A comparative study of L-type voltage sensitive Ca^{2+} channels in rat brain regions and cultured neuronal cells. *Neurosci. Lett.* **223,** 169–172.
17. Lowry, O. H., Rosebrough, N. J., Farr, A. C., and Randall, R. J. (1951) Protein measurement with Folin phenol reagent. *J. Biol. Chem.* **193,** 265–275.
18. Scatchard, G. (1949) The attraction of proteins for small molecules and ions. *Ann. NY Acad. Sci. USA* **52,** 660–672.
19. Cheng, Y. C. and Prusoff, W. M. (1973) Relationship between the inhibition constant (K_i) and the concentration of inhibitor which causes 50% inhibition (IC_{50}) of an enzymic reaction. *Biochem. Pharmacol.* **22,** 3099–3108.
20. Stoehr, S. J. and Dooley, D. J. (1993) Characteristics of ^{125}I-ω-conotoxin GVIIA binding to rat neocortical membranes. *Neurosci. Lett.* **161,** 113–116.

10

Measurement of Inositol (Poly)phosphate Formation Using [^{3}H]Inositol Labeling Protocols in Permeabilized Cells

Philip Swigart and Shamshad Cockcroft

1. Introduction

Hormones, neurotransmitters, chemoattractants, and growth factors all elicit intracellular responses, on binding to cell surface receptors, by activating inositol phospholipid-specific phospholipase C (PLC). Activated PLC catalyzes the hydrolysis of phosphatidylinositol bisphosphate (PIP_2), a minor membrane phospholipid, to form two second messengers, diacylglycerol (DAG) and inositol (1,4,5)trisphosphate [Ins(1,4,5,)P_3]. DAG is a direct activator of protein kinase C isozymes, Ins(1,4,5)P_3 mobilizes intracellular Ca^{2+}. G protein–coupled receptors couple to the PLC-β family via G proteins, and tyrosine kinase receptors activate PLCγ isozymes ***(1)***. Regardless of the PLC isozyme activated, the product is invariantly Ins(1,4,5)P_3.

To monitor the activation of PLC enzymes, the authors have established, in their laboratory, methods of using permeabilized cells. Permeabilized cells are useful for examining the regulatory components that are essential for Ins(1,4,5,)P_3 production. Calcium levels can be rigorously controlled as well as appropriate regulatory proteins such as phosphatidylinositol transfer protein (PITP) ***(2–4)***. Permeabilized cells can be used under conditions in which the cytosolic proteins are still present ("acutely permeabilized") and in which the cytosolic proteins have been allowed to leak out of cells. The loss of cytosolic proteins leads to the phenomenon of "rundown" in which the ability of GTPγS or a receptor agonist to stimulate PLC is diminished. The response can be "reconstituted" by addition of exogenously added cytosolic proteins ***(2)***. A major reconstituting factor in the cytosol is PITP ***(3–5)***.

From: *Methods in Molecular Biology, Vol. 114: Calcium Signaling Protocols*
Edited by: D. G. Lambert

Ins(1,4,5)P_3 is rapidly metabolized by phosphatases, and therefore the authors assay for the production of inositol (poly)phosphates. The stimulus for PLC activation can be a direct activator of G proteins, e.g., GTPγS or an agonist that interacts with an appropriate cell-surface receptor ***(3–5)***. The protocols can be applied to most cell lines. Commonly used cell lines in the authors' laboratory are HL60 cells (both undifferentiated and differentiated) and RBL-2H3, but other cell lines have also been used ***(3–5)***.

The basic principle is the labeling of the inositol lipids by growing the appropriate cell line in culture in the presence of [^{3}H]inositol for 2–3 d. This ensures that the inositol-containing lipids are prelabeled to near equilibrium prior to the experiment. Lithium at 10 m*M* inhibits the degradation of inositol phosphates to free inositol and is used to trap the inositol in the inositol polyphosphate forms. Inositol phosphates can be separated with ease from free inositol by using anion exchange chromatography. Approximately 40–60 samples can be easily processed in a single day.

2. Materials

1. Mammalian cells: HL60 available from American Type Culture Collection (ATCC), Rockville, MD.
2. [^{3}H]inositol is the *myo* [2-^{3}H]inositol and is obtained from Amersham Life Science (Little Chalfont, Buckinghamshire, UK) (product code TRK317).
3. Growth medium: RPMI-1640 available from Sigma (St. Louis, MO) as 10X solution (cat. no. R-1145).
   a. The growth medium at 1X can be stored at 4°C and supplemented with 12.5% heat-inactivated fetal calf serum (FCS) (*see* **Note 1**).
   b. Twelve milliliter penicillin/streptomycin (Sigma P-0906) and 25 mL glutamine solution (Sigma G-7513)/L when the medium is to be used (*see* **Note 2**).
   c. The supplemented medium can be stored at 4°C for 1–2 wk.
4. Labeling medium: Medium 199 (M199) available as a 10X solution from Sigma-Aldrich (Dorset, UK) (M-0650) (*see* **Notes 3** and **4**).
   a. Supplement the 1X M199 with 12 mL of penicillin/streptomycin and 25 mL of glutamine/L only when needed.
   b. Because FCS is excluded, supplement the labeling medium with insulin (Sigma I-5500) (5 µg/mL final) and transferrin (Sigma T-2252) (5 µg/mL final) as growth factors at the time of labeling.
5. PIPES buffer: 20 m*M* PIPES, 137 m*M* NaCl, and 3 m*M* KCl, pH 6.8.
   a. Made from stock solutions, 1 *M* PIPES:
      i. Dissolve 302.4 g of PIPES (Sigma P6757) in 600 mL of ddH_2O and adjust the pH to approx 6.0 with concentrated NaOH (*see* **Note 5**).
      ii. When the PIPES is fully dissolved, adjust to pH 6.8 and make up the volume to 1 L. The PIPES can be aliquoted and stored at –20°C for several months.

Table 1
Preparation of Ca2+ Buffer Stock Solutions

pCa	Vol. (mL) Ca · EGTA	Vol. (mL) EGTA
7 (100 n*M*)	0.996	7.004
6 (1 μ*M*)	4.698	3.302

6. 20X NaCl/KCl solution: Dissolve 159 g of NaCl and 4 g of KCl in 1 L of ddH_2O and store at 4°C, stable for months.
   a. For 100 mL PIPES buffer, take 5 mL of 20X NaCl/KCl stock plus 2 mL of 1 *M* PIPES stock to 100 mL with ddH_2O checking that the pH is still 6.8.
7. Permeabilization buffer: PIPES buffer supplemented with 1 mg/mL glucose and 1 mg/mL bovine serum albumin (BSA).
8. Streptolysin O (SLO) is obtained from Murex Diagnostics, Dartford, England (product no. MR16) (*see* **Note 6**).
   a. Each bottle contains 40 IU equivalents and is dissolved in 2 mL of ddH_2O to make a stock solution of 20 IU/mL.
   b. The stock solution is stored at 4°C for 1–2 wk and is used at 0.4–0.6 IU/mL in experiments (*see* **Note 7**).
9. 0.1 *M* MgATP stock solution: Dissolve 605 mg of disodium trihydrate ATP (Boehringer Mannheim, Lewes, East Sussex, UK) in a 10-mL solution containing 2 mL of 1 *M* Tris and 1 mL of 1 *M* MgCl (*see* **Note 8**). The solution is stable at –20°C for 1–2 yr at neutral pH.
10. Calcium buffers: required stock solutions are as follows:
    a. 100 m*M* EGTA prepared in 20 m*M* PIPES, 137 m*M* NaCl, 3 m*M* KCl, pH 6.8.
    b. 100 m*M* Ca · EGTA (100 m*M* EGTA, 100 m*M* $CaCl_2$ [*see* **Note 9**]) prepared in 20 m*M* PIPES, 137 m*M* NaCl, 3 m*M* KCl, pH 6.8. These stocks can be stored at –20°C for several months.
    c. To prepare Ca^{2+} buffers (pCa 7 and pCa 6) stock solutions, combine stock solutions of 100 m*M* Ca · EGTA and 100 m*M* EGTA to achieve the desired free Ca^{2+} (*see* **Table 1** and **Note 10**).
    These quantities are calculated for a final $[EGTA]_{total} = 3$ m*M*, $[MgCl_2] = 2$ m*M* and pH 6.8. Eight milliliters of each buffer stock solution are prepared by mixing the Ca · EGTA and EGTA solutions (100 m*M*) in the proportions indicated in **Table 1**. For use the buffer stocks (100 m*M*) (which do not contain Mg) are diluted to 3 m*M* $[EGTA]_{total}$.
11. Dimethyl sulfoxide (DMSO) from Sigma (D-5879).
12. 60 m*M* Dibutyryl cAMP (DbcAMP) (Sigma):
    a. Dissolve 100 mg of the powder in 3.08 mL of DMSO.
    b. The DbcAMP is used at a final concentration of 300 μ*M* (1 mL stock to 200 mL cells) to differentiate HL60 cells.
13. 1 *M* LiCl stored at –20°C for several months.

14. Preparation of Dowex 1-X8 anion exchange resin (*see* **Note 11**):
    a. Place 100 g of Dowex resin in a beaker.
    b. Add 400 mL of 1 *M* NaOH and stir with a glass rod.
    c. Allow the resin to settle (1–2 h).
    d. Carefully decant the NaOH solution, add 400 mL of 1 *M* formic acid, and stir with a glass rod.
    e. Allow the resin to settle and decant the formic acid.
    f. Wash the resin five times with 400 mL of ddH_2O. The resin can be left as a 50% slurry in ddH_2O at 4°C. One mL of the slurry is used per column and either Pasteur pipets or purchased columns (Bio-Rad, Hercules, CA) can be used (*see* **Note 12**).

3. Methods

3.1. Maintenance of HL60 Cell Cultures

1. Dilute HL60 cells to between 0.3 and 0.5×10^6 cells/mL. Generally, use 50 mL in 75-cm^2 tissue culture flasks with a 5% CO_2 atmosphere.
2. Grow the cells to confluence (usually takes 2 to 3 d) and dilute to between 0.3 and 0.5 × 106 cells again (*see* **Note 13**).
3. Use one flask to label, keeping one flask as a seed culture.

3.2. Differentiation of HL60 Cells (see Note 14)

1. Differentiate a confluent flask of cells in the presence of 300 µ*M* DbcAMP; the cells will be differentiated by 36–40 h.
2. Cells can be prelabeled with [^{3}H]inositol, by transferring them to M199 and labeling as described in **Subheading 3.3.** with the addition of the DbcAMP (1 mL of stock DbcAMP to 200 mL of cells).

3.3. Preparation of [^{3}H]Inositol-Labeled HL60 Cells (see Note 15)

1. Pellet 50 mL of confluent (2×10^6 cells/mL) cells by centrifugation at 1000*g* for 5 min at room temperature (Heraeus Megafuge 1.0, Brentwood, Essex, UK).
2. Resuspend the cells in 10 mL of M199 without FCS but with glutamine and penicillin/streptomycin.
3. Add the 10 mL of cells to 40 mL of M199 without FCS containing glutamine and penicillin/streptomycin, to which has been added 0.25 mL of a 1 mg/mL sterile solution of insulin and 0.25 mL of a 1 mg/mL sterile solution of transferrin (final concentrations of 5 µg/mL each).
4. Add 50 µCi (1 µCi/mL final) [^{3}H]inositol.
5. Grow cells for 48 h.
6. 50-mL cells are sufficient for 50 incubations.

3.4. PLC Activity in "Acutely Permeabilized" HL60 Cells

1. Centrifuge 50 mL of [^{3}H]inositol labeled cells at 1000*g* for 5 min at room temperature.

2. Discard the supernatant, which contains most of the radioactivity, and gently resuspend the cells in 40 mL of permeabilization buffer (PIPES buffer plus 1 mg/mL of glucose and 1 mg/mL of BSA).
3. Pellet the cells and wash once more with the permeabilization buffer.
4. After the final centrifugation, resuspend the cells in 2 to 3 mL of the permeabilization buffer.
5. Equilibrate the washed radiolabeled cells at 37°C for 10–25 min.
6. In a 1.5-mL Eppendorf tube (*see* **Note 16**), and 50 µL of labeled cells to the equivalent volume of permeabilization buffer supplemented with the following:
   a. SLO (0.4 IU/mL final).
   b. MgATP (1 m*M* final).
   c. $MgCl_2$ (2 m*M* final).
   d. Ca^{2+} buffered with 3 m*M* EGTA (pCa6).
   e. LiCl (10 m*M* final) (*see* **Note 17**).
   f. GTPγS (10 µ*M* final).
7. Incubate the mixture at 37°C for 20 min.
8. Place the reactions in an ice bath and terminate the reactions with one of two methods.
   a. Procedure 1
      i. Quench the assay with 500 µL of (chloroform:methanol [1:1 by vol/vol]) and vortexing.
      ii. Add 250 µL of ddH_2O and vortex.
      iii. Centrifuge the samples for 5 min at 1000*g* at 4°C (*see* **Note 18**).
      iv. Use 400 µL of the aqueous phase for inositol phosphate analysis.
   b. Alternative procedure:
      i. Quench the assay with 500 µL of ice-cold saline (0.9% NaCl).
      ii. Centrifuge at 2000*g* to sediment the permeabilized cells.
      iii. Use 400 µL of the supernatant for inositol phosphate analysis.

3.5. Separation of Inositol Phosphates

1. Load the 400-µL sample containing the radiolabeled inositol phosphates onto the prepared Dowex columns.
2. Allow the sample to gravity flow through the column.
3. Wash the columns with 6 mL of ddH_2O (*see* **Note 19**).
4. Wash the columns with 6 mL of 5 m*M* tetraborate/5 m*M* sodium formate (*see* **Note 20**).
5. Elute total inositol phosphate with 3 mL of 1 *M* ammonium formate/0.1 *M* formic acid directly into scintillation vials (*see* **Note 21**).
6. Add scintillant and measure radioactivity (*see* **Note 22**).
7. Regenerate the columns by washing with 6 mL of 2 *M* ammonium formate/0.1 *M* formic acid followed by extensive washing with ddH_2O (10–15 mL) (*see* **Note 23**).

3.6. Data Handling (see Note 24)

The dpm in inositol phosphates provides the level of PLC activity in individual experiments. The amount of dpm found in inositol phosphates is ulti-

mately dependent on the amount of label incorporated by the cells, which can vary from experiment to experiment. The increase in inositol phosphates can also be expressed as a function of the total radioactivity (dpm) incorporated into the inositol lipids. This allows results to be calculated as a percentage of the total lipids.

3.7. Determination of Radioactivity Incorporated into the Inositol Lipids

1. Carefully remove the total lipid chloroform extract obtained from the first procedure and transfer it to a clean scintillation vial.
2. Allow the chloroform to evaporate by leaving the vials open in a fume hood overnight.
3. Add 500 µL of methanol to the dried lipids followed by 2 mL of scintillation cocktail and measure dpm.

3.8. Establishing Conditions for Rundown of PLC Activity

1. Use 4.5 mL of washed [^{3}H]inositol labeled cells in the permeabilization buffer.
2. Add cocktail (0.5 mL) of SLO (0.4 IU/mL final), MgATP (1 m*M* final), and Ca^{2+}, pCa 7 (100 n*M* buffered with 100 m*M* EGTA final) to the cells.
3. At timed intervals, remove 4 × 50 µL-aliquots of cells and transfer to duplicate assay tubes containing 50 µL of a cocktail containing Ca^{2+}, pCa 6 (1 µ*M* buffered with 3 m*M* EGTA final), LiCl (10 m*M* final), $MgCl_2$ (2 m*M* final) ± GTPγS (10 µ*M* final).
4. Incubate the samples at 37°C for 20 min.
5. Quench the reaction using one of the two methods previously described in **Subheading 3.4.** and analyze [^{3}H]inositol phosphates as described in **Subheading 3.5.** (*see* **Note 25**).

3.9. Reconstitution of G Protein Stimulated PLC by Cytosolic Factors in Rundown Cells

1. Incubate 4.5 mL of washed [^{3}H]inositol-labeled HL60 cells in permeabilization buffer with 0.5 mL of cocktail containing SLO (0.4 IU/mL final), MgATP (1 m*M* final), and Ca^{2+}, pCa 7 (100 n*M* buffered with 3 m*M* EGTA final) for 10 min (*see* **Notes 26** and **27**).
2. After permeabilization, dilute the cells to 35 mL with ice-cold permeabilization buffer.
3. Centrifuge the cells at 2000*g* for 5 min to pellet the cells (*see* **Note 28**).
4. Resuspend the cell pellet in 2X assay buffer (permeabilization buffer supplemented with Ca^{2+}, pCa 6 with 6 m*M* EGTA final), LiCl (20 m*M* final), MgATP (4 m*M* final), and $MgCl_2$ (4 m*M* final) (*see* **Note 29**).
5. Prepare tubes in advance that contain 25 µL of cytosol, or other reconstituting factors (e.g., PITP) ± GTPγS at 20 µ*M*.
6. Transfer 25 µL of permeabilized cells to assay tubes on ice (*see* **Note 30**).

7. Transfer the assay tubes to a 37°C water bath and incubate the samples for 20 min.
8. Quench the assay as described in **Subheadings 3.4.8.** and **3.5.** and assay for inositol phosphates.

3.10. Assaying for PLC Activity Using a Receptor-Directed Agonist in Differentiated HL60 Cells that Express the FMetLeuPhe (FMLP) Receptor

1. Incubate 4 mL of washed differentiated [^{3}H]inositol-labeled HL60 cells in permeabilization buffer with 1 mL of cocktail containing SLO (0.4 IU/mL final), MgATP (1 m*M* final), and Ca^{2+}, pCa 7 (100 n*M* buffered with 3 m*M* EGTA final) for 10 min.
2. After permeabilization, dilute the cells to 35 mL with ice-cold permeabilization buffer.
3. Centrifuge the cells at 2000*g* for 5 min to pellet the cells.
4. Resuspend the cell pellet in 2X assay buffer (permeabilization buffer supplemented with pCa 6 [6 m*M* EGTA], LiCl [20 m*M*], MgATP [4 m*M*], and $MgCl_2$ [4 m*M*]).
5. Prepare tubes in advance that contain 25 µL of cytosol, or other reconstituting factors ± FMLP at 1 µ*M* final and GTP at 100 µ*M* final.
6. Transfer 25 µL of permeabilized cells per assay tube on ice.
7. Transfer the assay tubes to a 37°C water bath and incubate the samples for 20 min.
8. Quench the assay as described in **Subheadings 3.4.8.** and **3.5.** and assay for inositol phosphates (*see* **Note 31**).

4. Notes

1. FCS from Imperial (6-00014): heat inactivate before use by immersing a thawed bottle in a 56°C bath for 1 h.
2. Batches of RPMI-1640 can be stored with FCS added; however, the glutamine and penicillin/streptomycin must be added only as each bottle is needed.
3. Because RPMI-1640 medium contains relatively high levels of inositol, cells are labeled in M199. Concentration of inositol in different media are as follows: M199, 0.05 mg/mL, RPMI-1640, 35 mg/mL; DMEM, 7.2 mg/mL.
4. FCS is also excluded owing to high levels of inositol.
5. The solution will start out at approx pH 2.5–3.0 and will fluctuate as NaOH is added and the PIPES dissolves. Generally the PIPES is fully dissolved by pH 6.0–6.2.
6. SLO can also be obtained from Research Biochemicals, Natick, MA (product no. S-155) at 50 IU. Both forms are supplied in powder form.
7. The solution will become cloudy after a couple of days, but this will not affect permeabilization and can be partially cleared by warming to 37°C before use. Alternatively the SLO can be aliquoted and stored at –20°C for several weeks.
8. The use of 200 m*M* Tris (final) effectively gives a neutral final solution (pH 7.0). This should be checked and adjusted accordingly.
9. EGTA is from Fluka Chemika-Biochemica, Gillingham, Dorset, UK, and high quality is required. $CaCl_2$ is analytical grade from Sigma.

10. Values have been obtained using the program "Chelate" for a pH of 6.8 ***(6)***.
11. The resin is purchased from Sigma in the chloride form and must be converted to the formate form.
12. The Dowex is transferred to Pasteur pipets (0.5 mL bed volume) equipped with a glass wool plug (gloves should be worn when making the glass wool plugs).
13. HL60 cells are generally passed for 50–60 passages, and then fresh cells are thawed from liquid nitrogen. Always make sure that you have stocks from early passages saved for future use.
14. HL60 cells can be differentiated toward neutrophils by the addition of DbcAMP or DMSO. DMSO is flammable and must be kept from open flames.
15. Other cell lines can be used. The authors have successfully labeled and reconstituted RBL-2H3 cells. Cells are labeled with 1 μCi of [^{3}H]inositol/mL being added directly to the medium (Dulbecco's modified Eagle's medium + 5% FCS), and the cells are grown for 48 h. It is preferable to add the label when the cells have just been split.
16. Prepare the Eppendorf tubes with the appropriate reagents in an ice bath and transfer to a 37°C water bath 5 minutes prior to the addition of 50 μL cells.
17. LiCl inhibits the conversion of inositol phosphates back to free inositol. It can be kept as a 1 *M* stock at –20°C.
18. The lipids are present in the lower chloroform phase, and the upper aqueous phase contains the water-soluble components including the inositol phosphates.
19. This step washes out the [^{3}H]inositol.
20. This step elutes glycerophosphoinositol.
21. If inositol monophosphate (IP1), inositol bisphosphate (IP2), and inositol trisphosphate (IP3) are to be separated, elute stepwise:
    a. 3 mL of 0.2 *M* ammonium formate/0.1 *M* formic acid (IP1).
    b. 3 mL of 0.4 *M* ammonium formate/0.1 *M* formic acid (IP2).
    c. 3 mL of 1 *M* ammonium formate/0.1 *M* formic acid (IP3 and inositol tetraphosphate [IP4]).
22. The scintillation cocktail should be able to accommodate 1 *M* salt. (Use PCS [phase combining system] from Amersham or Ultima Flo from Canberra Packard, Pangbourne, Berkshire, UK).
23. The Dowex columns can be used and reused indefinitely if they are regenerated with 2 *M* ammonium formate/0.1 *M* formic acid after each use.
24. The increase in inositol phosphate can be expressed as a function of the total radioactivity (dpm) incorporated into the inositol lipids. This allows results to be calculated as a percentage of the total lipids.
25. Data can be plotted as the extent of GTPγS-stimulated PLC activity and a function of the permeabilization interval. Total rundown is typically 80–90% for GTPγS-stimulated PLC activity.
26. The permeabilization cocktail can be made up from stocks as follows: pCa7, 150 μL; SLO solution, 150 μL; MgATP, 50 μL; and permeabilization buffer (PIPES + glucose and BSA), 150 μL.

27. Longer permeabilization times (i.e., 40 min) allow many more cytosolic factors to leak out.
28. Care should be taken because the permeabilized cell pellet is quite loose and some cells may be lost when decanting the buffer.
29. 2X Assay buffer can be made up as follows: pCa6, 62.5 µL; MgATP (0.1 *M*), 40 µL; $MgCl_2$ (0.4 *M*), 10 µL; LiCl (1 *M*), 20 µL; permeabilization buffer, 865 µL.
30. The final concentrations during the incubation will be as follows: Ca^{2+}, pCa 6 (1 µ*M* final buffered with 3 m*M* EGTA final), LiCl (10 m*M* final), MgATP (2 m*M* final), $MgCl_2$ (2 m*M* final), and GTPγS (10 µ*M* final).
31. The FMLP receptor-driven response can be much weaker than the GTPγS response.

References

1. Rhee, S. G. and Bae, Y. S. (1997) Regulation of phosphoinositide-specific of phospholipase C isozymes. *J. Biol. Chem.* **272,** 15,045–15,048.
2. Thomas, G. M. H., Geny, B., and Cockcroft, S. (1991) Identification of a cytosolic polyphosphoinositide-specific phospholipase C (PLC-86) as the major G-protein-regulated enzyme. *EMBO J.* **10,** 2507–2512.
3. Thomas, G. M. H., Cunningham, E., Fensome, A., Ball, A., Totty, N. F., Troung, O., Hsuan, J. J., and Cockcroft, S. (1993) An essential role for phosphatidylinositol transfer protein in phospholipase C-mediated inositol lipid signalling. *Cell* **74,** 919–928.
4. Kauffmann-Zeh, A., Thomas, G. M. H., Ball, A., Prosser, S., Cunningham, E., Cockcroft, S., and Hsuan, J. J. (1995) Requirement for phosphatidylinositol transfer protein in epidermal growth factor signalling. *Science* **268,** 1188–1190.
5. Cunningham, E., Tan, S. W., Swigart, P., Hsuan, J., Bankaitis, V., and Cockcroft, S. (1996) The yeast and mammalian isoforms of phosphatidylinositol transfer protein can all restore phospholipase C-mediated inositol lipid signalling in cytosol-depleted RBL-2H3 and HL60 cells. *Proc. Natl. Acad. Sci. USA* **93,** 6589–6593.
6. Tatham, P. E. R. and Gomperts, B. D. (1990) Cell permeabilisation, in *Peptide Hormones—A Practical Approach* (Siddle, K. and Hutton, J. C., eds.), IRL, Oxford, England, pp. 257–269.

11

Measurement of Inositol(1,4,5)trisphosphate Using a Stereospecific Radioreceptor Mass Assay

Darren Smart

1. Introduction

Inositol(1,4,5)trisphosphate [Ins(1,4,5)P_3] is an intracellular second messenger that plays an important role in calcium homeostasis and, thus, many diverse cellular processes including neuronal signaling, smooth muscle contraction, fertilization, and sensory perception ***(1)***. Ins(1,4,5)P_3 formation is triggered by the activation of a wide variety of seven-transmembrane, G protein–linked receptors, e.g., muscarinic, glutamate, dopamine, and opioid receptors ***(1–3)***, as well as by the activation of the tyrosine kinase–linked growth factor receptors ***(1)***. Ins(1,4,5)P_3 is produced by the phospholipase C (PLC)–mediated hydrolysis of phosphatidylinositol 4,5-bisphosphate ***(1,4)***, and is metabolized by 3-kinase and 5-phosphatase ***(5)***, with the actual intracellular concentration of Ins(1,4,5)P_3 being dependent on the balance between formation and metabolism. Ins(1,4,5)P_3 in turn binds to the Ins(1,4,5)P_3 receptor on the smooth endoplasmic reticulum, causing a conformational change that opens the intrinsic calcium channel in the receptor, thus allowing the efflux of calcium ions from the intracellular stores ***(4)***. For further details, see the reviews by Berridge ***(1)*** and Furuichi and Mikoshiba ***(4)***.

Historically, Ins(1,4,5,)P_3 was measured in terms of total inositol polyphosphate turnover in the presence of lithium in cells that had been "loaded" with [^{3}H]inositol ***(6,7)***. This technique was subsequently refined by using separation columns or high-pressure liquid chromatography to separate the various inositol polyphosphates and, even to some degree, their isomers ***(7–9)***. However, there are several significant disadvantages associated with these [^{3}H]inositol loading techniques. First, the main assumption of these techniques

From: *Methods in Molecular Biology, Vol. 114: Calcium Signaling Protocols*
Edited by: D. G. Lambert

is that all pools of phosphoinositides are labeled to equilibrium under the assay conditions, yet there is very little experimental evidence for this ***(9)***. Second, it is almost inevitable that in [^{3}H]inositol-loaded cells, there would be some degree of agonist-induced changes in the specific radioactivity of the inositol trisphosphates ***(9)***. Third, these [^{3}H]inositol loading techniques do not take into account changes in the metabolism of Ins(1,4,5)P_3. For example, in rat acinar cells depolarization with K^+ stimulates polyphosphoinositide hydrolysis without affecting Ins(1,4,5)P_3 levels, because of a simultaneous enhancement of 3-kinase–mediated Ins(1,4,5)P_3 metabolism ***(10,11)***. Finally, the [^{3}H]inositol-loading techniques are less likely to detect small, transient changes in Ins(1,4,5)P_3 formation because they make only a minute contribution to total polyphosphate turnover, and this is masked by basal accumulation in the presence of lithium ***(2,3,11)***.

In 1988 a groundbreaking paper by Challiss et al. ***(9)*** was published that described a stereospecific radioreceptor assay for Ins(1,4,5)P_3 mass. This assay was superior to the [^{3}H]inositol-loading protocols because it made no assumptions about the establishment of equilibrium of label in various pools of polyphosphoinositides, nor was it susceptible to agonist-induced changes in specific radioactivity ***(9)***. Furthermore, subsequent studies have shown that the radioreceptor assay also takes into account changes in Ins(1,4,5)P_3 metabolism ***(10,11)***, and is able to detect small, transient changes in Ins(1,4,5)P_3 levels ***(2,3,11)***. This radioreceptor assay is based on the same simple principles as any other radioreceptor assay. The unlabeled Ins(1,4,5)P_3 in the sample competes with a fixed amount of [^{3}H]-labeled Ins(1,4,5)P_3 for a limited amount of a specific binding protein. The bound and free Ins(1,4,5)P_3 are separated by rapid vacuum filtration, and subsequent measurement of the radioactivity in the assay tube enables the amount of unlabeled Ins(1,4,5)P_3 in the sample to be determined by interpolation from a standard curve. The fundamental step in developing such an assay is the identification and purification of a suitable binding protein. Challiss et al. ***(9)*** used a relatively crude extract of the Ins(1,4,5)P_3 receptor prepared from bovine adrenal cortex. This was a suitable binding protein because the Ins(1,4,5)P_3 receptor displays the necessary high affinity and stereoselectivity for Ins(1,4,5)P_3, especially compared to Ins(1,3,4)P_3 ***(4,9)***, and it is both abundant in and easily extracted from bovine adrenal cortex ***(9)***. Rat cerebellum was also tested as a potential source of the binding protein, but was found to give smaller yields with lower affinity ***(9)***.

In the remainder of this chapter the author will describe how the binding protein is prepared, how the Ins(1,4,5)P_3 is extracted from the samples, how the radioreceptor assay is performed, and how the data are processed. Furthermore, the common pitfalls and how to avoid or deal with them will be described.

2. Materials

1. Ins(1,4,5)P_3 binding protein buffer (BP buffer): 20 m*M* $NaHCO_3$ and 1 m*M* dithiothreitol (DTT; *see* **Note 1**) in distilled water, pH 8.0 (*see* **Note 2**). Store at 4°C (*see* **Note 3**). Two L of this buffer is sufficient to prepare ~100 mL of binding protein from 10–12 adrenal glands.
2. 10–12 fresh bovine adrenal glands (*see* **Note 4**).
3. 1 *M* trichloroacetic acid (TCA). This should be stored in a glass-stoppered bottle at 4°C for no longer than 3 mo.
4. 10 m*M* EDTA in distilled water, pH 7.4. This should be stored at 4°C for no longer than 3 mo.
5. Freon/Octylamine (F/O): 1:1 (v/v) mixture of 1,1,2-trichlorofluroethane (Freon) and tri-*n*-octylamine, both of which are available from Aldrich, Poole, UK (*see* **Note 5**).
6. 25 m*M* sodium bicarbonate ($NaHCO_3$) in distilled water. This should be stored at 4°C for no longer than 3 mo.
7. Stock Ins(1,4,5)P_3 standard: 1 m*M* D-*myo*-inositol-1,4,5-triphosphate hexasodium monohydrate (Research Biochemicals International, MA) in distilled water. Store in 20-µL aliquots at –20°C (*see* **Note 6**).
8. Stock [^{3}H]Ins(1,4,5)P_3: This is obtained from Amersham (Braunschweig, Germany) at 10 µCi/mL. Store at –20°C for no longer than 4 wk past the activity date.
9. Tris-EDTA (TE) buffer: 100 m*M* Tris-HCl and 4 m*M* EDTA in distilled water at pH 8.0. Store at 4°C; keeps virtually indefinitely.
10. Diluent: Mix 3 mL of Krebs/HEPES buffer (*see* **Note 7**), 3 mL of TCA, 1.25 mL of EDTA, and 3 mL of F/O. Vortex well and then centrifuge at 500*g* for 2 min at 4°C. This mixture will now have separated into two distinct phases (layers). Take 5 mL of the upper phase and neutralize with 2.5 mL of $NaHCO_3$. The remainder of the upper phase as well as the lower phase should be discarded. The diluent should be made fresh on the day of use and then kept at 4°C.
11. Wash buffer: 25 m*M* Tris-HCl, 1 m*M* EDTA, 5 m*M* $NaHCO_3$ in distilled water, pH 7.8. This *must* be made fresh on the day of use and kept at 4°C. Two L is sufficient for a 72-tube assay.
12. A Brandell cell harvester and Whatman GF/B filters (Fisons, Loughborough, UK).

3. Methods

3.1. Preparation of the Ins(1,4,5)P_3 Binding Protein

1. Take the adrenal glands, halve longitudinally, remove the medulla (*see* **Note 8**), and then scrape the cortex from the capsule (*see* **Note 9**).
2. Pool the cortex tissue in a 500-mL glass beaker, dilute 1 in 6 with ice-cold BP buffer, and homogenize thoroughly, taking care that there are no lumps of cortex left intact.
3. Centrifuge the homogenate at 2000*g* for 10 min at 4°C (*see* **Note 10**).
4. Carefully decant (*see* **Note 11**) and keep the supernatant. Store the supernatant at 4°C.

5. Rehomogenize the pellet in a minimum volume of BP buffer (*see* **Note 12**) and then centrifuge at 2000*g* for 10 min at 4°C. Decant (*see* **Note 11**) the supernatant and pool it with the supernatant from **step 4**. Discard the pellet.
6. Centrifuge the pooled supernatant at 20,000*g* for 30 min at 4°C (*see* **Note 13**). A soft pellet will form at the bottom of the tube.
7. Carefully decant (*see* **Note 11**) the supernatant into fresh centrifugation tubes and store the pellet at 4°C. Recentrifuge the supernatant at 20,000*g* for 30 min at 4°C (*see* **Note 13**). A smaller soft pellet will form at the bottom of the tube.
8. Repeat **step 7**.
9. Pool all the pellets and resuspend in BP buffer at ~30 mg/mL (*see* **Note 14**).
10. Then dispense the binding protein into 1-mL aliquots and store at –20°C until needed (*see* **Note 15**).

3.2. Sample Preparation

1. Incubate the relevant cells with the appropriate agonist for the required time (e.g., *see* **ref. *3***), in a final volume of 0.3 mL in polypropylene tubes (12 × 75 mm; Sarstedt, UK). Terminate reactions by the addition of an equal volume (0.3 mL) of ice-cold 1 *M* TCA (*see* **Note 16**).
2. Next vortex the samples and centrifuge at 500*g* for 10 min at 4°C.
3. Carefully decant the uppermost 500 µL of the supernatant (*see* **Note 17**) into fresh polypropylene tubes. Discard the remaining supernatant and "pellet."
4. Add 125 µL of EDTA and 500 µL of F/O to the supernatant, cap the tubes, vortex, and then centrifuge at 500*g* for 2 min at 4°C. At the end of this process, the samples will have separated into two clearly delineated phases (layers).
5. Take 200 µL of the upper phase, which contains the Ins(1,4,5)P_3, and place into fresh tubes. Neutralize this with 100 µL of 25 m*M* $NaHCO_3$, cap, and vortex the tubes. Discard the remaining upper, as well as the lower, phase. The samples should be stored at 4°C for no longer than 1 wk, and must not be frozen.

3.3. Radioreceptor Ins(1,4,5)P_3 Mass Assay

1. It is essential that the entire assay is carried out on ice. At the start of the assay, make up fresh wash buffer (*see* **Subheading 2.**, **item 11**) and place in a refrigerator to cool.
2. Label the appropriate number of polypropylene tubes (12 × 75 mm; Sarstedt), i.e., the relevant number of samples (single or in duplicate) and the standard curve, consisting of total counts (TOT), nonspecific binding (NSB), and six standards (std. 0.036, 0.12, 0.36, 1.2, 3.6, and 12 pmol tube) in duplicate. These labeled tubes should be placed in a Brandell harvester rack on ice at the start of the assay.
3. Thaw out the correct amount (1 mL/30 tubes) of binding protein (*see* **Note 18**).
4. Make up fresh diluent (*see* **Subheading 2.**, **item 10**) and store on ice.
5. Dilute the stock Ins(1,4,5)P_3 standard with diluent in the following manner (*see* **Note 19**):
   a. NSB: 20 µL of stock + 480 µL of diluent.
   b. 12 pmol std: 10 µL of NSB + 990 µL of diluent.

c. 3.6 pmol std: 100 µL of 12 pmol std. + 200 µL of diluent.
d. 1.2 pmol std: 20 µL of 12 pmol std. + 180 µL of diluent.
e. 0.36 pmol std: 20 µL of 3.6 pmol std. + 180 µL of diluent.
f. 0.12 pmol std: 20 µL of 1.2 pmol std. + 180 µL of diluent.
g. 0.036 pmol std: 20 µL of 0.36 pmol std. + 180 µL of diluent.
These standards should be stored on ice until pipetted into the relevant tubes, as described in **step 9**.

6. Prepare the working concentration of the tracer {[^{3}H]Ins(1,4,5)P_3} by adding stock [^{3}H]Ins(1,4,5)P_3 to TE buffer at 15 µL/mL (*see* **Note 20**). Allow 1 mL of tracer/30 tubes. Store on ice until used.
7. Pipet 30 µL of TE buffer into each of the labeled tubes in the Brandell harvester rack (*see* **Note 21**).
8. Pipet 30 µL of diluent into the two TOT tubes (*see* **Note 21**).
9. Pipet 30 µL of standard/sample into the appropriate tubes (*see* **Notes 21** and **22**).
10. Pipet 30 µL of the working concentration of [^{3}H]Ins(1,4,5)P_3 into each tube (*see* **Notes 21** and **23**).
11. Gently vortex all the tubes for a few seconds (*see* **Note 24**).
12. Pipet 30 µL of the binding protein into each tube (*see* **Note 25**).
13. Gently vortex all the tubes for a few seconds, and allow to incubate on ice for 40 min (*see* **Note 26**). At this point the total assay volume is 120 µL.
14. Filter on a Brandell cell harvester (Whatman GF/B filters) with the ice-cold wash buffer (*see* **Note 27**), to separate the bound and free [^{3}H]Ins(1,4,5)P_3. Each tube should receive two washes of ~3 mL, each in quick succession (*see* **Note 28**). The bound material will be clearly visible as a brown deposit on the filter (*see* **Note 29**).
15. The filters should be extracted overnight in a suitable scintillant, e.g., Optiphase Safe (Wallac, UK), and then counted in a β-counter for 3 min/tube.

*3.4. Data Processing (*see Note 30*)*

1. Calculate the average cpm for each standard, and sample if assayed in duplicate (*see* **Note 31**).
2. Calculate the percent bound for each standard and sample as follows:

$$\% \text{ Bound} = \frac{(\text{Standard/sample dpm} - \text{NSB dpm})}{\text{TOT dpm} - \text{NSB dpm}} \times 100$$

3. The percent bound for the standards can then be plotted [against the relevant concentration of Ins(1,4,5)P_3] to generate a standard curve, using a suitable curve-fitting program (i.e., GraphPad Prism, CA) or by hand on semi-log graph paper. Then, using the relevant percent bound values, the concentrations of Ins(1,4,5)P_3 in the samples can be "read off" this curve.

4. Notes

1. DTT is harmful and should therefore be handled with all due care. However, its inclusion is essential or the binding protein will rapidly become degraded.
2. Although ideally this buffer should be at pH 8.0, any pH in the range 7.9–8.1 is acceptable.

3. This buffer should be prepared on the day of use, but can be used on the following day if stored at 4°C. Do not store for longer than 24 h prior to use.
4. These are obtained from an abattoir and can come from cattle of any age or either sex. Most abattoirs will allow direct dissection of the adrenal gland, and many will cut out the glands for a small fee. However, it should be borne in mind that the vast majority of abattoir workers do not know what the adrenal gland looks like or where it is located and, therefore, are likely to provide the wrong material. It is preferable to collect intact glands, but "bits" of gland, when the gland has been damaged during the butchery of the cattle, can still be used. The glands must be "fresh," i.e., collected as soon as possible after the cattle have been slaughtered, and must not be frozen. It is best to minimize the delay between the removal of the glands and the preparation of the binding protein, but if this delay is likely to exceed 2 h, the glands (wrapped in a plastic bag) need to be transported on ice.
5. Care should be taken when handling these chemicals and their mixture, as they are potent irritants. The F/O mixture should be made up just prior to use and, being somewhat unstable, cannot be stored for more than a couple of hours. Furthermore, exposure to the F/O mixture does cause some plastics to become extremely brittle, hence the reason that sample preparation and the assay are conducted in polypropylene tubes.
6. The stock Ins(1,4,5)P_3 standard must not be thawed and then refrozen, as this causes significant breakdown of the standard, leading to high NSB values and a poor quality standard curve. The stock standard still degenerates slowly even when frozen and thus should be discarded after 2 mo.
7. Or, whatever physiological buffer the cell incubations were performed in can be used.
8. The medulla is the "off white" material in the center of the adrenal gland, and is best removed by pulling it gently upward with a pair of forceps while cutting it away from the underlying cortex using a pair of fine-dissecting scissors. It is essential to remove as much of the medulla as possible, to minimize NSB.
9. The cortex is the reddish-brown material that surrounds the medulla, and is easily scrapped from the semitransparent, tough outer membrane or capsule, using a small metal spatula.
10. It is essential from this moment on that the crude binding protein is kept at 4°C. If all the material in a given step cannot be handled at once, then store any excess on ice or in the refrigerator, until the material can be dealt with.
11. This is best done using a long, fine-pointed, disposable glass pipet, and care must be taken not to suck up any of the pellet. If any of the pellet is decanted, then the pipet and its contents should be discarded, rather than risk contaminating the rest of the supernatant.
12. If there is still material from **step 2** waiting to be rehomogenized, then use this, rather than the BP buffer, to resuspend the pellet. However, note that if this is done then the subsequent pellet will still need to undergo **step 5**, as part of this pellet has not been washed twice.
13. Alternatively, centrifuge at 40,000*g* for 20 min at 4°C.

14. The protein content of the combined pellets resuspended in a minimum volume of BP buffer should be measured using a suitable assay (e.g., Follins-Lowry) prior to the full resuspension. In general, 10–12 adrenal glands should yield ~80 mL of binding protein.
15. The binding protein can be thawed and refrozen once, but repeated freeze/thaw cycles should be avoided. The binding protein will keep for ~6 mo at –20°C, although it should be noted that the binding protein will gradually degrade over this period, causing the total binding to fall and the NSB values to rise.
16. Once the TCA has been added, the sample can be stored at 4°C for up to 1 h prior to undergoing the rest of the extraction procedure. This allows "batching" of the samples and thus more effective time management.
17. If using a Gilson pipet to decant the supernatant, it is advisable to first remove the waste tip dispeller.
18. Allow the binding protein to thaw slowly. Do not heat the frozen binding protein in a water bath or by other means, as this causes considerable degradation of the binding protein, leading to high NSB values.
19. The standards and NSB are made at these concentrations to obtain the correct final concentrations in the assay, in which there is a 1 in 4 dilution factor.
20. The appropriate procedures for handling radioactivity should be used at all times. The dilution of 15 µL of stock/mL of TE buffer is based on the assumption that the specific activity of the stock [^{3}H]Ins(1,4,5)P_3 is ~40 Ci/mmol. If the specific activity is significantly higher, add proportionally less stock/mL; if the specific activity is significantly lower, then add proportionally more stock/mL.
21. Remember to do all pipetting into the tubes while the tubes are still on ice. Furthermore, care must be taken when pipetting as the volumes involved are very small. The most common problem is drops of the assay components sticking to the sides of the tube. These can be brought down by gently tapping the base of the tube, or by using a fine disposable pipet to blow the drops down.
22. NSB tubes receive 30 µL of the NSB "standard" made in **step 5** of **Subheading 3.3.**
23. All due care should be maintained when pipetting radioactive material.
24. This step is essential for obtaining a smooth standard curve (*see* **Note 31**). If there are any drops on the sides of the tubes, then these must be brought down prior to vortexing (*see* **Note 21**).
25. Particular care must be taken when pipetting out the binding protein. The aliquot of binding protein being used must be vortexed frequently (approximately every minute), to keep the binding protein uniform. Furthermore, as the binding protein is very viscose, it is particularly prone to sticking to the sides of the assay tubes (*see* **Note 21**).
26. Timing of this step is crucial. If the incubation is too short, equilibrium will not have been achieved and there will be a far greater degree of intra-assay variability. On the other hand, if the incubation is too long, there is a tendency toward increased NSB values. Fourty min is optimal, but anywhere between 38 and 50 min is acceptable.

Table 1
Common Assay Problems and Their Causes

Problem	Possible cause
High NSB (>10%)	• The stock [^{3}H]Ins(1,4,5)P_3 may have degraded. This is usually associated with a low TOT cpm. • The stock standard may have degraded. This is usually associated with a distorted standard curve. • Binding protein may have degraded. This is usually associated with all tubes having low cpm.
All tubes have low cpm	• The binding protein has degraded (associated with high NSB) or is too dilute (*see* **Note 29**). • The tracer is too dilute (*see* **Note 20**) or has degraded (usually associated with high NSB)
Standard curve is distorted	• Stock standard has degraded (associated with high NSB) or has been diluted incorrectly. • **Step 11** of **Subheading 3.3.** has not been performed.
Standards have low cpm, but samples are normal	• Standards were incorrectly diluted, or have degraded (associated with high NSB).
TOT > 2500 dpm	• This is often associated with a shallow standard curve. • Tracer has been incorrectly diluted (*see* **Note 20**).

27. It is advisable to wash the first filter with the wash buffer prior to harvesting the samples. Care must be taken to ensure that the filters are fitted properly to avoid leaking.
28. Do not overfill (more than 3/4) the tubes, or there will be a risk of overflow and the associated loss of material. Be aware that not all tubes will fill at the same rate.
29. If the deposit is somewhat "faded" (i.e., sandy rather than brown) in color, this indicates that the binding protein is not concentrated enough. This is inevitably associated with low total counts (*see* **Note 31**). If this occurs, concentrate the remaining binding protein prior to its use by centrifuging the thawed binding protein at 5000*g* for 15 min at 4°C and then pipetting off 250 µL of the "clear" supernatant. Vortex vigorously to resuspend the binding protein.
30. Most modern counters have packages on them that will automatically plot the standard curve and calculate the sample values.
31. Ideally TOT should lie in the range of 1000–2500 dpm and the NSB should be 5–10%. This is the stage at which most assay problems will become apparent. **Table 1** describes the most common problems and their usual causes. However, it should be borne in mind that other factors will also affect assay performance, most notably temperature and pH. Therefore, at all times it is essential to ensure that the assay is performed on ice, that dilutions are made correctly, and that all the buffers are at the optimal pH.

References

1. Berridge, M. J. (1993) Inositol trisphosphate and calcium signalling. *Nature* **361,** 315–325.
2. Smart, D., Smith, G., and Lambert, D. G. (1994) Halothane and isoflurane enhance basal and carbachol-stimulated inositol(1,4,5)triphosphate formation in SH-SY5Y human neuroblastoma cells. *Biochem. Pharmacol.* **47,** 939–945.
3. Smart, D., Smith, G., and Lambert, D. G. (1994) μ-Opioid receptor stimulation of inositol(1,4,5)trisphosphate formation via a pertussis toxin-sensitive G protein. *J. Neurochem.* **62,** 1009–1014.
4. Furuichi, T. and Mikoshiba, K. (1995) Inositol 1,4,5-trisphosphate receptor-mediated Ca^{2+} signaling in the brain. *J. Neurochem.* **64,** 953–960.
5. Shears, S. B. (1989) Metabolism of the inositol phosphates upon receptor activation. *Biochem. J.* **260,** 313–324.
6. Kendall, D. A. and Nahorski, S. R. (1984) Inositol phospholipid hydrolysis in rat cerebral cortical slices: II. Calcium requirement. *J. Neurochem.* **42,** 1388–1394.
7. Wojcikiewicz, R. J. H., Lambert, D. G., and Nahorski, S. R. (1990) Regulation of muscarinic agonist-induced activation of phosphoinositidase C in electrically permeabilized SH-SY5Y human neuroblastoma cells by guanine nucleotides. *J. Neurochem.* **54,** 676–685.
8. Yu, V. C. and Sadee, W. (1986) Phosphatidylinositol turnover in neuroblastoma cells: Regulation by bradykinin, acetylcholine, but not μ and δ opioid receptors. *Neurosci. Lett.* **71,** 219–223.
9. Challiss, R. A. J., Batty, I. H., and Nahorski, S. R. (1988) Mass measurements of inositol(1,4,5)trisphosphate in rat cerebral cortex slices using a radioreceptor assay: Effects of neurotransmitters and depolarization. *Biochem. Biophys. Res. Commun.* **157,** 684–691.
10. Zhang, G. H. and Melvin, J. E. (1993) Membrane potential regulates Ca^{2+} uptake and inositol phosphate generation in rat sublingual mucous acini. *Cell Calcium* **14,** 551–562.
11. Smart, D., Wandless, A., and Lambert, D. G. (1995) Activation of phospholipase C in SH-SY5Y neuroblastoma cells by potassium-induced calcium entry. *Br. J. Pharmacol.* **116,** 1797–1800.

12

Measurement of Calcium Fluxes in Permeabilized Cells Using a $^{45}Ca^{2+}$ Uptake and Release Assay

Robert A. Wilcox

1. Introduction

Many cell surface receptors activate phosphoinositidase(s) C, via G proteins that catalyze the hydrolysis of phosphatidylinositol 4,5-biphosphate to produce the second messengers, inositol(1,4,5)trisphosphate [Ins(1,4,5)P_3] and diacylglycerol ***(1)***. Ins(1,4,5)P_3 interacts with specific receptor populations of ligand-gated channels to mobilize nonmitochondrial intracellular calcium (Ca^{2+}) stores ***(1)***. Because Ins(1,4,5)P_3 is very hydrophilic, it cannot readily cross the intact plasma membrane. Consequently, Ins(1,4,5)P_3-induced Ca^{2+} release was initially demonstrated in permeabilized pancreatic acinar cells ***(2)***, and all subsequent studies in cells have involved the introduction of Ins(1,4,5)P_3 by rendering a cell population permeable ***(3)***, using microinjection techniques ***(4)*** or by the presentation of chemically modified membrane-permeable Ins(1,4,5)P_3 analogs, such as photolabile "caged Ins(1,4,5)P_3" ***(5)***. An alternative approach involves disruption of the plasma membrane and preparation of microsomes from the intracellular vesicular Ca^{2+} stores ***(6,7)***, however, these preparations exhibit a loss of Ins(1,4,5)P_3 responsiveness compared to cells. The author will describe a $^{45}Ca^{2+}$-release assay used to monitor Ins(1,4,5)P_3-induced Ca^{2+} mobilization from nonmitochondrial intracellular Ca^{2+} stores using "cytosol-like" buffer (CLB) and permeabilized SH-SY5Y neuroblastoma cell populations.

The $^{45}Ca^{2+}$-release assay is similar to those previously described ***(3,8)*** and involves preloading $^{45}Ca^{2+}$ into the intracellular Ca^{2+} stores of permeabilized cells and then monitoring the resultant release of $^{45}Ca^{2+}$ induced by concentrations

From: *Methods in Molecular Biology, Vol. 114: Calcium Signaling Protocols*
Edited by: D. G. Lambert

of Ins(1,4,5)P_3 and other agonists. The author has utilized this assay to assess the intrinsic activity of Ins(1,4,5)P_3, a wide range of Ins(1,4,5)P_3 analogs, and other Ca^{2+}-mobilizing agents. The assay can be undertaken at a low cell density to minimize cellular metabolism of the Ins(1,4,5)P_3 and other Ca^{2+}-mobilizing inositol polyphosphates (CM-IPs), or at high cell density to allow the metabolic sensitivity of the CM-IP to be estimated.

The method described here for monitoring Ca^{2+} fluxes induced by CM-IPs in permeabilized SH-SY5Y cells can be readily modified for other cell types and for testing a wide range of different Ca^{2+}-mobilizing agents.

2. Materials

1. Ultrapure H_2O derived from a specialist unit (Elgastat, High Wycomb, Bucks, UK, or Millipore, Watford, Herts, UK) (*see* **Note 1**).
2. Fura-2–free acid (Calbiochem-Novabiochem, Nottingham, Notts, UK; Molecular Probes, Eugene, OR) was prepared as a 1-m*M* stock solution.
3. $^{45}CaCl_2$ solution, 77 mBq/mL (CES3, Amersham, Amersham, Bucks, UK).
4. 200 m*M* CaCl2.
5. 200 m*M* EGTA/400 m*M* KOH solution (*see* **Note 2**).
6. HEPES-buffered saline (HBS)/EDTA solution: 0.02% (w/v) Na_2EDTA, 0.9% (w/v) NaCl, and 20 m*M* HEPES-free acid, corrected to pH 7.2–7.4 using 20% (w/v) NaOH.
7. Adenosine 5'-triphosphate disodium salt ($Na_2 \cdot ATP$; grade 1, Sigma A-2383, Poole, Dorset, UK).
8. CLB stock should be prepared as a fivefold stock solution in ultrapure H_2O, to yield final concentrations of 120 m*M* KCl, 2 m*M* KH_2PO_4, 5 m*M* $(CH_2COONa)_2 \cdot 6H_2O$, 2 m*M* $MgCl_2 \cdot 6H_2O$, and 20 m*M* HEPES-free acid. Since the ATP required is relatively unstable in alkaline solutions, the working CLB solution should be prepared just prior to use.
9. EGTA (10 m*M*/20 m*M* KOH).
10. Saponin or β-escin (Sigma) 1 mg/mL solution prepared fresh in working stock CLB.
11. Ionomycin from *Streptomyces conglobatus*; calcium salt (Sigma I-0634, formula wt 747.1) or free acid (Calbiochem-Novabiochem) and antibiotic A23187 (Calbiochem-Novabiochem) are prepared as 2 m*M* (*see* **Note 3**).
12. Silicon oil mixture for separation of the aqueous phase and cell pellet: Dow Corning (British Drug House [BDH], Toronto, Ontario, Canada) silicone fluids 556 (0.98 g/mL; 60%) and 550 (1.07 g/mL; 40%) shaken thoroughly (*see* **Note 4**).
13. 0.4% Azur A (Fluka, Buchs, Switzerland) stock in ATP-free CLB, pH 7.2.
14. Oligomycin (Sigma) 5 mg/mL solution made up in EtOH (*see* **Note 5**).
15. Ins(1,4,5)P_3 (CellSignals, Lexington, Semat Technical St. Albans, Herts, UK [UK agents for Research Biochemicals]) 1–2 m*M* 20-μL stock solution (*see* **Note 6**).
16. Lumasolve (Lumac, Landgraaf, The Netherlands) and Emulsifier-safe scintillation cocktail (Packard, Meriden, CT).

17. Fluorescence spectrophotometer (fluorimeter) with variable excitation and emission optics, ideally with a chart recorder or computer interface for fura 2 experiments (*see* **Note 7**).
18. Benchtop microcentrifuge, with a capacity for 24 standard 1.5-mL microcentrifuge tubes (Heraeus, Dusseldorf, Germany, and Desaga, Sarstedt-Gruppe, Wiesloch, Germany).
19. Electroporator (Gene-Pulser, Bio-Rad, Hemel Hampstead, Herts, UK).
20. IBM Pentium PC or compatible with Prism version 2.01 (Graph-Pad Software, San Diego, CA) for computer-assisted curve-fitting calculations (*see* **Note 8**).

3. Methods

3.1. Preparation of CLB Working Solution and Buffering of Ca^{2+}

1. Add the fivefold CLB stock (1 vol) to a container with preweighed $Na_2 \cdot ATP$ (2 m*M* final) and dilute this to 5 vol with H_2O and the correct pH (~5.3) 7.2 using 20% (w/v) KOH and 1 m*M* of HCl.
2. Buffer the contaminating-free Ca^{2+} ($[Ca^{2+}]_{free}$) to a final concentration of between 60 and 120 n*M*, by addition of an appropriate aliquot of EGTA (10 m*M*/20 m*M* KOH) (*see* **Note 9**).
3. Confirm the $[Ca^{2+}]_{free}$ of the CLB using a tracer concentration of fura-2 (100 n*M*). Briefly place a sample of EGTA-buffered CLB (2 mL) in a fluorimeter cuvet with 4 µL of 50 µ*M* fura-2. Determine the fluorescent intensity (F_{CLB}) of the buffer at excitation and emission wavelengths of 340 and 510 nm, respectively. Recording the resultant *F* values, add 2 µL of the 200 m*M* $CaCl_2$ solution (200 µ*M* final; F_{max} value), followed by 40 µL of 200 m*M* EGTA (2 m*M* final; F_{min} value), and then calculate $[Ca^{2+}]$ from the Grynkiewicz equation ***(9)*** in which the K_d for fura-2 is approx 139 n*M* at 25°C and 224 n*M* at 37°C (*see* **Note 10**):

$$[Ca^{2+}]_{free}\ (nM) = (F_{CLB} - F_{min}/F_{max} - F_{CLB}) \times K_d$$

3.2. Permeabilization of Cells

1. Electropermeabilization ***(10)*** or the cholesterol-specific detergents saponin ***(3)*** and β-escin ***(11)*** are routinely utilized to produce Ins(1,4,5)P_3-responsive permeabilized cells. Both of these methods require empirical determination of optimal conditions for each cell type used. The DNA dye Azur A (0.025% [w/v] CLB) can be used to quantify permeabilization, since it is excluded from intact cells but specifically stains the nucleus of permeabilized cells blue. When permeabilized with 20–100 µg/mL of saponin or β-escin or via optimized electropermeabilization, >99% Azur A–stained SH-SY5Y neuroblastoma cells are obtained.
2. Electropermeabilization is rapid and efficiently generates plasma membrane pores, which allow free passage of inositol polyphosphates. Electropermeabilization of SH-SY5Y cells in 0.8 mL volume is accomplished in a Gene-Pulser using 3–12 discharges of a 3-µF capacitor with a field strength of 1.5 kV/cm and a time constant of 0.1 ms (*see* **Note 11**).

3.3. $^{45}Ca^{2+}$-Release Assay

1. Produce an inositol polyphosphate dilution series in CLB that is twofold the final required concentration (*see* **Note 12**).
2. Use ionomycin (10 µ*M* final, free acid or calcium salt) and Ins(1,4,5)P_3 (20–30 µ*M*) prepared as twofold stocks in CLB as internal controls to define, respectively, the total mobilizable and Ins (1,4,5)P_3-sensitive cellular Ca^{2+} pools in permeabilized SH-SY5Y cells.
3. All agents were added as duplicate 50 µL-aliquots to decapped 1.5-mL microcentrifuge tubes, and two duplicate blanks (CLB alone) defined the baseline calcium release (*see* **Note 13**).
4. Wash a postconfluent SH-SY5Y monolayer (175-cm^2 flask) once and then harvest using the HBS/EDTA solution (*see* **Note 14**).
5. Resuspend and centrifuge to wash the cell suspension twice in 5 mL of CLB (500*g*, 1 min).
6. Discard the supernatant and add 1.8 mL of CLB to resuspend the cells. Add 200 µL of saponin stock solution (1 mg/mL, ~100 µg/mL final) to the cells, mix gently and leave for 40–60 s, and then centrifuge (500*g*, 2 min).
7. Resuspend the pellet in approx 5 to 6 mL of CLB; for SH-SY5Y cells, this corresponds to a cell density of approx 2–4 × 10^6 cells/mL, 0.5–0.8 mg/mL protein ***(12)***, or a cellular DNA content of 100–200 µg/mL ***(18)***.
8. Add 1 µL of oligomycin and 1 µL of $^{45}Ca^{2+}$ per 2 mL of permeabilized cells.
9. Quickly and gently vortex the cells and $^{45}Ca^{2+}$ and leave for 15–20 min at 18–20°C, with periodic vortexing (*see* **Note 15**).
10. Using a repeating pipet (Eppendorf-Netleter-Hinz GmbH, Hamburg, Germany), titurate the cell suspension, and then add 50 µL of the cell suspension to 50 µL of the agonist in the decapped 1.5-mL microcentrifuge tubes.
11. Immediately add 300–400 µL of silicon oil mixture, and after 30–90 s, load the tubes into a microcentrifuge and centrifuge the cells through the oil (16,000*g*, 3 min) (*see* **Note 16**).
12. Remove the aqueous phase and most of the silicon oil, but avoid disturbing the cell pellet or "smear" on the opposite side of the tube.
13. Invert the tubes on paper underlayered with foil for 30 min to remove the oil.
14. Add 1 mL of scintillant, and when the pellets are solubilized, vortex the tube and count the retained $^{45}Ca^{2+}$ (*see* **Note 17**).
15. Calculate the percentage release of $^{45}Ca^{2+}$ using the average value of the four CLB blanks, these define the zero $^{45}Ca^{2+}$ release value (or 100% loaded $^{45}Ca^{2+}$ retained in the pellet) (*see* **Note 18**).

3.4. Optimizing the $^{45}Ca^{2+}$-Release Assay for Different Cell Lines

$^{45}Ca^{2+}$ assays have been successfully performed using many adherent and nonadherent cell lines, such as L15, L vec, Rat-1, Swiss 3T3 and NIH-3T3 mouse fibroblasts, J774.2 mouse macrophages cell, SaOS-2 human osteoblasts, Yac-1 mouse cells, 1321N1 human astrocytomas, and also primary cultured

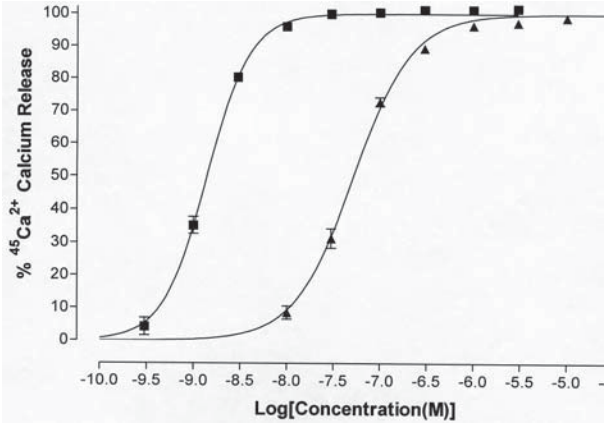

Fig. 1. The percentage $^{45}Ca^{2+}$ released at 20–22°C from the Ins(1,4,5)P_3-sensitive intracellular stores of saponin-permeabilized SH-SY5Y cells ($n \geq 4$) by IP_3 (▲), and adenophostin A (Ada) (■). AdA is a highly potent metabolically resistant Ins(1,4,5)P_3 receptor agonist ***(19)***. It released $^{45}Ca^{2+}$ from SH-SY5Y cells with a $\log_{10}[EC_{50}\ (M)]$ of -8.857 ± 0.021 ($EC_{50} = 1.4$ n*M*) and thus was ~40-fold more potent than Ins(1,4,5)P_3 {$\log_{10}[EC_{50}\ (M)] = -7.288 \pm 0.019$ ($EC_{50} = 52.1$ n*M*)}. (Ada was a gift from Prof. Van Boom's laboratory, Leiden, The Netherlands.)

bovine adrenal chromaffin cells. However, it is crucial that the conditions used for each cell type be optimized empirically:

1. Use Azur A staining; confirm that >95% of cells are effectively permeabilized and choose the minimal insult to the cells that effectively produces permeabilization.
2. Select an appropriate cell density, in which $^{45}Ca^{2+}$ release is readily detected, but in which cellular metabolism of inositol polyphosphate is minimal over 2 to 3 min (*see* **Note 19**).
3. Produce a time course for $^{45}Ca^{2+}$ loading and identify the plateau at which an equilibrium loading state is obtained and maintained; for most cells this occurs between 10 and 40 min.

4. Notes

1. The most critical consideration is the reduction of Ca^{2+} contamination during the preparation of all solutions, especially CLB. Reagents used must be the highest purity available, especially divalent metal salts such as $MgCl_2 \cdot 6H_2O$. Ultrapure water is essential and all solutions must be prepared and stored in plastic containers—never glass, which leaches significant quantities of metal cations.
2. The solution may require sonication for solubilization.
3. Store as 10-µL stock aliquots in ethanol or dry dimethyl sulfoxide.
4. The efficiency of the silicon oil mix is batch dependent and must be empirically tested as alternative mixing ratios can be more effective. Alternatively, if the

cells are pelleted first, then a 1/1 (v/v) mixture will effectively separate the pellet and aqueous phase during the second spin.

5. This acts to exclude Ca^{2+} uptake into the mitochondrial pool. However, the addition of oligomycin is not critical since at $[Ca^{2+}] < 1$ μ*M*, mitochondrial Ca^{2+} uptake (Km ~10 μ*M*) is minimal ***(14)***.
6. Stock solutions of stimulating agonists such as inositol polyphosphates must be checked for calcium contamination, since Ca^{2+} levels exceeding 200–400 n*M* can inhibit IP_3-induced Ca^{2+} release ***(15–17)***. Stock solutions can be readily pretreated to remove Ca^{2+} contamination with solid phase Ca^{2+} chelating agents such as chelex-100 (Bio-Rad) or immobilized-BAPTA–based "Ca^{2+}-sponges" (Molecular Probes). The author has treated a wide range of inositol polyphosphates with these chelators and have detected no loss owing to adsorption.
7. The author utilizes the model LS5β and LS50β fluorimeters (Perkin Elmer, UK).
8. Prism is an excellent and easy to use program, but many similar curve-fitting programs are also available.
9. Usually 10–20 μL/100 mL of CLB (1 to 2 μ*M* EGTA final) is sufficient.
10. Ideally the $[Ca^{2+}]_{free}$ should be 60–120 n*M*, certainly <200 n*M*, to avoid significant mitochondrial uptake ***(14)*** and Ca^{2+} inhibition of Ins(1,4,5)P_3 receptor responses ***(15–17)*** . If it exceeds this, then add more 10-m *M* EGTA stock to the CLB, mix well, take a fresh 2-mL sample, and repeat the procedure. Once determined, the $[Ca^{2+}]_{free}$ value should remain relatively stable for a given batch of fivefold CLB stock, and a stable supply of high-purity water.
11. However, under some conditions the process can generate significant concentrations of aluminium ions (Al^{3+}) from the disposable cuvets used, and this may affect cellular metabolism of inositol polyphosphates ***(18)***. Consequently, the author has favored saponin and β-escin permeabilization, which generate large plasma membrane pores and offer the flexibility of initiating an experiment with the permeabilization event.
12. For example, Ins(1,4,5)P_3 concentrations of 30, 10, 3, 1, 0.3, 0.1, 0.03, and 0.01 μ*M* fully cover the Ca^{2+}-release dose response range in most cell types the author has tested.
13. Thus, a typical experiment consisted of 22 to 24 tubes; these were stored on ice and then allowed to come to room temperature for 15 min prior to addition of the permeabilized cells.
14. Cell clumping occurs particularly with fibroblasts and can cause reduced precision; gently titurating the cells 2 to 3 times through a 19 G needle generally produces a single cell suspension. Alternatively, trypsinized cells can be used in the assay following deactivation of the trypsin via centrifugation through underlayered fetal calf serum.
15. In SH-SY5Y cells, $^{45}Ca^{2+}$ loading into intracellular Ca^{2+} stores proceeds rapidly and reached equilibrium within 10 min.
16. Alternatively the cells can be pelleted after 1–15 s (16,000*g*, 2 min). The silicon oil is then added and a second centrifugation performed (16,000*g*, 1 min). This procedure was not ideal for time course studies; however, once optimal stimulation times are determined, this procedure yields identical data and the solid and reproducible pellets produce more consistent data values.

17. Large cell pellets may require solubilization in 100 µL of Lumasolve, prior to the addition of scintillation cocktail.
18. Typically in most cells ionomycin (10 µ*M*) mobilizes 90% of the total loaded $^{45}Ca^{2+}$, whereas in SH-SY5Y cells a maximal dose of Ins(1,4,5)P_3 mobilizes 70% of the total loaded $^{45}Ca^{2+}$.
19. For SH-SY5Y cells, the author selected a cell density in which 30–50% of the $^{45}Ca^{2+}$ spike (~2 to 3 µ*M*) is incorporated into the intracellular stores. Utilizing fura-2, it was confirmed that the ~2.4 µ*M* of $^{45}Ca^{2+}$ added to CLB supplemented with 2 µ*M* EGTA produces an initial increase in total $[Ca^{2+}]_{free}$ from approx 60–350 n*M*.

References

1. Berridge, M. J. (1993) Inositol trisphosphate and calcium signalling. *Nature* **361,** 315–325.
2. Streb, H., Irvine, R. F., Berridge, M. J., and Schulz, I. (1983) Release of Ca2+ from a nonmitochondrial intracellular store in pancreatic acinar cells by inositol-1,4,5-triphosphate. *Nature* **306,** 67–69.
3. Strupish, J., Cooke, A. M., Potter, B. V. L., Gigg, R., and Nahorski, S. R. (1988) Stereospecific mobilization of intracellular Ca^{2+} by inositol 1,4,5-triphosphate. *Biochem. J.* **253,** 901–905.
4. Berridge, M. J., and Taylor, C. W. (1988) Inositol triphosphate and calcium signalling, in *Cold Spring Harbor Symposia on Quantitative Biology*. **53**, pp. 927–933.
5. Walker, J. W., Somlyo, A. V., Goldman, Y. E., Somlyo, A. V., and Trentham, D. R. (1987) Kinetics of smooth and skeletal muscle activation by laser pulse photolysis of caged inositol 1,4,5-triphosphate. *Nature* **327,** 249–252.
6. Ely, J. A., Hunyady, L., Baukal, A. J., and Catt, K. J. (1990) Inositol 1,3,4,5-tetrakisphosphate stimulates Ca^{2+} release from bovine adrenal microsomes by a mechanism independent of the inositol 1,4,5-trisphosphate receptor. *Biochem. J.* **268,** 333–338.
7. Joseph, S. K., Hansen, C. A., and Williamson, J. R. (1989) Inositol tetrakisphosphate mobilizes calcium from cerebellum microsomes. *Mol. Pharmacol.* **36,** 391–397.
8. Gershengorn, M. C., Geras, E., Purrello, V. S., and Rebeccchi, M. J. (1984) Inositol trisphosphate mediates thyrotrophin-releasing hormone mobilization of nonmitochondrial calcium in rat mammotrophic pituitary cells. *J. Biol. Chem.* **259,** 10,675–10,681.
9. Grynkiewicz, G., Poenie, M., and Tsien, R. Y. (1985) A new generation of Ca^{2+} indicators with greatly improved fluorescent properties. *J. Biol. Chem.* **260,** 3440–3449.
10. Knight, D. E. and Scrutton, M. C. (1986) Gaining access to the cytosol: the technique and some applications of electropermeabilization. *Biochem. J.* **234,** 497–506.
11. Kobayashi, S., Kitazawa, T., Somlyo, A. V., and Somlyo, A. P. (1989) Cytosolic heparin inhibits muscarinic and α-adrenergic Ca^{2+} release in smooth muscle: Physiological role of inositol 1,4,5-trisphosphate in pharmacomechanical coupling. *J. Biol. Chem.* **264,** 17,997–18,004.

12. Bradford, M. M. (1976) A rapid and sensitive method for the quantitation of microgram quantities of protein utilising the principle of protein-dye binding. *Anal. Biochem.* **72,** 248–254.
13. Labarca, C. and Paigen, K. (1980) A simple, rapid and sensitive DNA assay procedure. *Anal. Biochem.* **102,** 344–352.
14. Carafoli, E. (1987) Intracellular calcium homeostasis. *Annu. Rev. Biochem.* **56,** 395–433.
15. Bezprozvanny, I., Watras, J., and Ehrlich, B. E. (1991) Bell-shaped calcium-response curves of Ins(1,4,5)P_3- and calcium-gated channels from endoplasmic reticulum of cerebellum. *Nature* **351,** 751–754.
16. Danoff, S. K., Suppattapone, S., and Snyder, S. H. (1988) Characterization of a membrane protein from brain mediating the inhibition of inositol 1,4,5-trisphosphate receptor binding by calcium. *Biochem. J.* **254,** 701–705.
17. Finch, E. A., Turner, T. J., and Goldin, S. M. (1991) Calcium as a coagonist of inositol 1,4,5-trisphosphate-induced calcium release. *Science* **252,** 443–446.
18. Loomis-Husselbee, J. W., Cullen, P. J., Irvine, R. F., and Dawson, A. P. (1991) Electroporation can cause artifacts due to solubilization of cations from electrode plates. Aluminium ions enhance conversion of inositol 1,3,4,5-tetrakisphosphate into inositol 1,4,5-trisphosphate in electroporated L1210 cells. *Biochem. J.* **277,** 883–885.
19. Takahashi, M., Tanzawa, K., and Takahashi, S. (1994) Adenophostins, newly discovered metabolites of Penicillium brevicompactum, act as potent agonists of the inositol 1,4,5-trisphosphate receptor. *J. Biol. Chem.* **269,** 369–372.

13

Microinjection of *myo*-Inositol(1,4,5)trisphosphate and Other Calcium-Mobilizing Agents into Intact Adherent Cells

Robert A. Wilcox, Ian D. Forsythe, and Terence J. McCann

1. Introduction

Many receptor tyrosine kinases and seven-transmembrane receptors are directly coupled or coupled via G proteins, respectively, to the activation of phosphoinositidase Cs ***(1)***. These enzymes catalyze the hydrolysis of phosphatidylinositol 4,5-bisphosphate to produce the second messengers, *myo*-inositol(1,4,5)trisphosphate [Ins(1,4,5)P_3] and diacylglycerol ***(1)***. Ins(1,4,5)P_3 interacts with a specific receptor that is a ligand-gated channel that allows mobilization of non-mitochondrial intracellular calcium (Ca^{2+}) stores ***(1)***. Because Ins(1,4,5)P_3 is plasma membrane impermeant, this phenomenon was first demonstrated in permeabilized pancreatic acinar cells ***(2)***, and all subsequent studies in cells have involved introduction of Ins(1,4,5)P_3 by rendering a cell population permeable ***(3)***, using microinjection techniques ***(4)***, or by the presentation of chemically modified membrane-permeable Ins(1,4,5)P_3 analogs, such as photolabile "caged Ins(1,4,5)P_3" ***(5)***. An alternative approach involves disruption of the plasma membrane and preparation of microsomes from the intracellular vesicular Ca^{2+} stores ***(6,7)***; however, microsomal preparations exhibit a loss of Ins(1,4,5)P_3 responsiveness compared to permeabilized and intact cells.

This chapter will outline a semiautomated method for the microinjection of Ins(1,4,5)P_3 and other hydrophilic Ca^{2+} mobilizing inositol polyphosphates (CM-IPs) and pharmacological agents. Dynamic Ca^{2+} imaging using fura-2–loaded cells was used to measure Ca^{2+} fluxes at the single cell level. Because microinjected Ins(1,4,5)P_3 and CM-Ins(1,4,5)P_3 rapidly mobilize intracellular Ca^{2+} stores, the use of fully automated, multiple microinjection was considered

From: *Methods in Molecular Biology, Vol. 114: Calcium Signaling Protocols*
Edited by: D. G. Lambert

redundant. However, this is a powerful technique for the injection of more latent agents such as DNA, peptides, and antibodies and has been extensively described elsewhere ***(8–11)***. Ca^{2+} fluxes are acutely examined just prior to the moment of microinjection to obtain a baseline, then followed for several minutes after the microinjection. The authors have utilized a number of different cell types, but have conducted the majority of their experiments with mouse L-fibroblasts overexpressing the type I Ins(1,4,5)P_3 receptor (L15 cells) ***(12,13)*** and SaOS-2 human osteoblasts ***(14)***.

2. Materials

2.1. Reagents and Buffers

1. Ultrapure H_2O derived from a specialist unit (e.g., Elgastat, Elga, High Wycomb, Bucks, UK, or Millipore, Watford, Herts, UK). All solutions are prepared in plasticware and using ultrapure water unless otherwise stated. Glass leaches significant concentrations of ions, including Ca^{2+}, into aqueous solutions. Consequently, glassware should be avoided when making nominally Ca^{2+}-free buffers, especially for storage of solutions.
2. The fluorescent calcium chelating dye fura-2–free acid (Calbiochem-Novabiochem, Nottingham, Notts, UK, and Molecular Probes, Eugene, OR) is prepared as 0.5 or 1 m*M* stock solutions in H_2O, distributed into 10-, 20-, and 50-µL aliquots, and stored at ≤–20°C protected from light in an aluminum foil–covered container. Fura-2/AM, the cell-permeant derivative of fura-2 (Calbiochem and Molecular Probes), is relatively insoluble in H_2O and, thus, should be prepared in dry dimethyl sulfoxide (DMSO) as a 1 to 2 m*M* stock solution and stored at ≤–70°C protected from light. The use of dry DMSO solution is crucial; thus, DMSO (Sigma, Poole, Dorset, UK) should be purchased in small sealed ampules and opened just prior to solubilization of the fura-2/AM.
3. Ca^{2+} calibration top stocks are used for the determination of the F_{max} (fluorescence at saturating [Ca^{2+}]) and F_{min} (fluorescence at zero [Ca^{2+}]) values of fura-2 and fluo-3, in solution. For F_{max} a 1/400 dilution of 200 m*M* $CaCl_2$ (0.5 m*M* final) fully Ca^{2+} saturates both fluorescent dyes. For F_{min} a 1/100 dilution of 400 m*M* EGTA/400 m*M* KOH, pH 7.2 (4 m*M* final) essentially chelates all available Ca^{2+}. The 400 m*M* EGTA/400 m*M* KOH, pH 7.2, solution will require sonication for solubilization of the EGTA. Alternatively a 1/50 dilution of 400 m*M* BAPTA (Molecular Probes and Calbiochem), pH 7.2, will more efficiently and rapidly chelate Ca^{2+}. BAPTA readily solubilizes in H_2O, but fresh stock must be made every 7 d. All solutions are stored at 4°C between use.
4. Ca^{2+}-buffering stocks: EGTA (10 m*M*/20 m*M* KOH, pH 7.2) or BAPTA (10 m*M* aqueous solution, pH 7.2) prepared via aqueous dilution from the Ca^{2+} calibration top stocks.
5. HEPES-buffered saline (HBS)-EDTA solution for removal of adherent cells: 0.02% (w/v) Na_2EDTA, 0.9% (w/v) NaCl, and 20 m*M* HEPES-free acid, corrected to pH 7.2–7.4 using 20% (w/v) NaOH.

6. Ins(1,4,5)P_3 (CellSignals, Lexington, KY, Semat Technical [UK agent for Research Biochemicals], St. Albans, Herts, UK), L-*myo*-inositol(1,4,5)trisphosphate [L-Ins(1,4,5)P_3] (Sigma), and adenophostin A (AdA) (a kind gift from Sankyo, Tokyo, Japan) are prepared as 1–5 m*M*, 20-µL aqueous stock solutions. Aqueous stocks of all CM-IPs are pretreated with Chelex-100 (Bio-Rad, Hemel Hampstead, Herts, UK) to chelate divalent cations and then with BAPTA-based polystyrene-immobilized "Ca^{2+}-sponge" (Molecular Probes) to specifically remove contaminating Ca^{2+} (*see* **Note 1**).
7. Glass cover slips (no. 1. thickness, Chance-Propper, Smethwick, Warley, UK) are used. Tissue culture grade plastic slides cannot be used because they exhibit autofluorescence and thus interfere with fura-2 measurements.
8. HEPES-buffered Krebs-Henseleit (K/H buffer): 118 m*M* NaCl, 4.64 m*M* KCl, 1.18 m*M* KH_2PO_4, 1.18 m*M* $MgSO_4 \cdot 7H_2O$, 11.7 m*M* glucose, 4.2 m*M* $NaHCO_3$, 10 m*M* HEPES-free acid, and 1–1.3 m*M* $CaCl_2 \cdot 2H_2O$ (pH 7.4). Use of HEPES-buffered solutions is crucial in order to ensure that the pH remains stable during the microinjection procedure; bicarbonate-buffered solutions are not used since when open to the air, they rapidly develop a basic pH. $CaCl_2$ is omitted from nominally calcium-free HEPES-buffered Krebs-Henseleit (Ca^{2+}-free K/H buffer). The Ca^{2+} contamination present in nominally Ca^{2+}-free K/H buffer generally 1–3 µ*M* as assessed using 50 n*M* fluo-3 (*see* **Note 2**).
9. Cells are grown in a variety of growth media, supplemented with 10% fetal calf serum (FCS) and 100 IU/mL penicillin, 100 µg/mL streptomycin, and 2.5 µg/mL fungizone (Gibco, Paisley, Renfrewshire, UK). Mouse L-fibroblasts and transfects overexpressing the type 1 Ins(1,4,5)P_3 receptor derived from L-fibroblasts are initially a kind gift from Prof. Mikoshiba (Tokyo, Japan). These are subcultured 1/10–1/20 weekly and grown in HEPES-buffered Dulbecco's modified Eagle's medium (DMEM). SaOS-2 cells from American Type Culture Collection, Rockville, MD (ATCC) are subcultured 1/10 weekly and maintained in a DMEM/Nutrient Mix F12 (1:1)–based growth medium ***(14)***.
10. Confluent adherent cell monolayers (25-cm^2 flask) are washed once, then harvested using the HBS/EDTA solution. The cells are washed twice in tissue culture media (5 mL), and sometimes the cells are centrifuged through a layer of 0.5 mL of FCS to remove cell debris.
11. Before cells are plated, the glass cover slips are treated in two steps to clean and then sterilize the surface. All procedures are carried out under sterile conditions in a cell culture class II flow cabinet. First, using fine tip forceps, 22-mm-diameter glass cover slips are dip washed in analytical grade ethanol or methanol to clean the cover slip surface. This removes most of the dust and any organic material (*see* **Note 3**). Second, the cover slips are dipped twice in a 70% ethanol (or methanol)/30% H_2O solution, blotted onto a sterile tissue, flamed briefly using a Bunsen burner, gently air cooled, and then placed into 35-mm-diameter plastic culture dishes (Nunc, Roskilde, Denmark). The prepared cells are diluted and plated in 2 mL volumes, onto the glass cover slips in the culture dishes. Cells are plated to give approx 5% confluence on the glass cover slip and used for microinjection when they have reached 10–15% confluence; usually this takes 1–3 d in culture.

2.2. Equipment

1. The most important piece of equipment for successful microinjection is a good quality microscope with some kind of contrast enhancement optics (phase or differential interference). The better the image obtained, the easier it will be to inject the target cells. For adherent cells flattened onto a glass cover slip, a good optical image is especially important. The authors use a Nikon Diaphot (Nikon, Kingston Upon Thames, UK) with phase contrast optics, including a high numerical aperture quartz objective for compatibility with the ultraviolet (UV) wavelengths used to excite the fluorescent dyes. An inverted microscope is essential for injecting adherent cells grown on glass cover slips.
2. Fluorescence spectrophotometer (fluorimeter) with variable excitation and emission optics ideally with a chart recorder or computer interface is used to determine the free Ca^{2+} concentration of solutions including the K/H buffer. The authors utilize the model LS50β fluorimeter (Perkin-Elmer, Beaconsfield, Bucks, UK), which allows large variations in the selection of wavelengths and excitation and emission slit widths, thus permitting fluorescent measurements to be made over a large dynamic range.
3. IBM 486/586 PC or compatible computer. The Perkin-Elmer fluorescence data manager (FLDM) software is used to run the fluorimeter.
4. For single cell fluorimetric analysis of Ca^{2+} fluxes, the authors utilized a Nikon Diaphot 200 fluorescent microscope (Nikon) coupled to a Ca^{2+}-imaging system. For the data collection, they used the MiraCal PRO (Life Science Resources, Cambridge, UK), which included an 8-bit digital, cooled charge-coupled device camera, filter wheel and Windows95™-based image acquisition and analysis software. A myriad of other inverted fluorescent microscope and imaging systems are available, but the MiraCal PRO system is flexible and easy to use. New Ca^{2+}-imaging systems are continuously being introduced, offering better technological features and generally at decreasing prices. When purchasing a Ca^{2+} imaging system, the authors recommend an extensive and current assessment of several systems, to determine one's personal requirements.
5. Benchtop microcentrifuge, with a capacity for 24 standard 1.5-mL microcentrifuge tubes (Heraeus, Dusseldorf, Germany and Desaga, Sarstedt-Gruppe, Wiesloch, Germany). Prior to loading into the microinjection needles, all stimulants are centrifuged at top speed for 5 min, at 4°C, to pellet any microparticles in the solution. This is a crucial step as microparticles derived from the solution or the air can readily block the narrow tip of the microinjection needle and prevent successful microinjection. The solution should be recentrifuged after the tube has been opened to the atmosphere.
6. Microinjections are accomplished using an integrated system consisting of Eppendorf Micromanipulator 5170 and Microinjector 5242 (Eppendorf-Netheler-Hinz GmbH, Hamburg, Germany), but several other popular microinjection systems are available, e.g., the Picospritzer II (General Valve, East Hanover, NJ). Generally prepulled "femtotip" micropipets with internal filaments and a 0.3–1-µm tip opening diameter are utilized (Eppendorf-Netheler-Hinz, cat. no. 5242-

956.008). Femtotips are favored since they are individually sealed free of microparticles and are sterile, have a standardized length, and can be directly screwed onto the injector capillary holder. Alternatively, it is possible to prepare one's own micropipets, if one has access to a suitable microelectrode puller (e.g., Sutter Instrument, San Rafael, CA; model P-87). Pulling microinjection pipets is an art form in itself ***(15)***, and entire books have been written about this subject ***(16)***. The author's have successfully used thin-walled borosilicate glass capillaries, with an internal filament to aid filling (GC120TF-10, Clark Electromedical Instruments, Reading, Berkshire, UK), to inject cultured mammalian cells. The advantages of making one's own micropipets are primarily cost and flexibility. The cost per micropipet is significantly lower than for femtotips, although the initial investment in a puller is high. In addition, it is possible to prepare micropipets for a variety of applications (e.g., injection, impalement, patch-clamp) from one machine.

7. The micropipets are backloaded with Eppendorf microloader pipet tips (Eppendorf-Netheler-Hinz, cat. no. 5242-956.003). A yellow tip (Anachem, Luton, Beds, UK) is used as a guide to assist threading the thin microloader tip into the rear of the femtotip. Generally, approx 0.5–3 µL of stimulant is loaded. The internal filament in the micropipet increases the capillary flow of the solution, and hence the tip fills easily; gentle tapping or shaking can be used to encourage the solution to flow directly into the tip or to remove bubbles if necessary. Care should be taken to reduce exposure of the microloader to air particles; between loading they are stored in their sealed box in an airtight plastic container (*see* **Note 4**).
8. Magnetic stirrer and control unit for cuvets (Rank Brothers, Bottisham, Cambridge, UK), magnetic stirrer bars for cuvets (Perkin-Elmer), and disposable fluorimetry cuvets (Sarstedt, Leicester, Leicestershire, UK).
9. A temperature-controlled cell perfusion chamber incorporating a cell cover slip holder is constructed in-house (*see* **Fig. 1**). Although normal body temperature is from 36 to 37°C, most imaging and electrophysiological experiments are conducted at room temperature (20–25°C). Even though this has the advantage of slowing rapidly occurring events and increasing temporal resolution, many cellular processes have differing temperature dependence (Q10). In addition, many laboratories have temperatures that vary over the time course of hours and are subject to seasonal fluctuations. When collating results over a period of time, such fluctuations will add further variance to the data. To avoid this source of error, in the authors' experiments, the experimental temperature is precisely controlled by bipolar feedback through Peltier devices. These solid-state heat pumps induce a temperature difference between their two surfaces that is proportional to the magnitude of the electrical current flow through the device. By reversing the current flow, one can change from heating to cooling. By assembling such devices into the stage of the experimental microscope and incorporating some feedback control, one can precisely control the experimental temperature over a range of approx 0°C–50°C. Hence, experiments are performed at any set temperature, independent of the ambient temperature, and including physiologically relevant

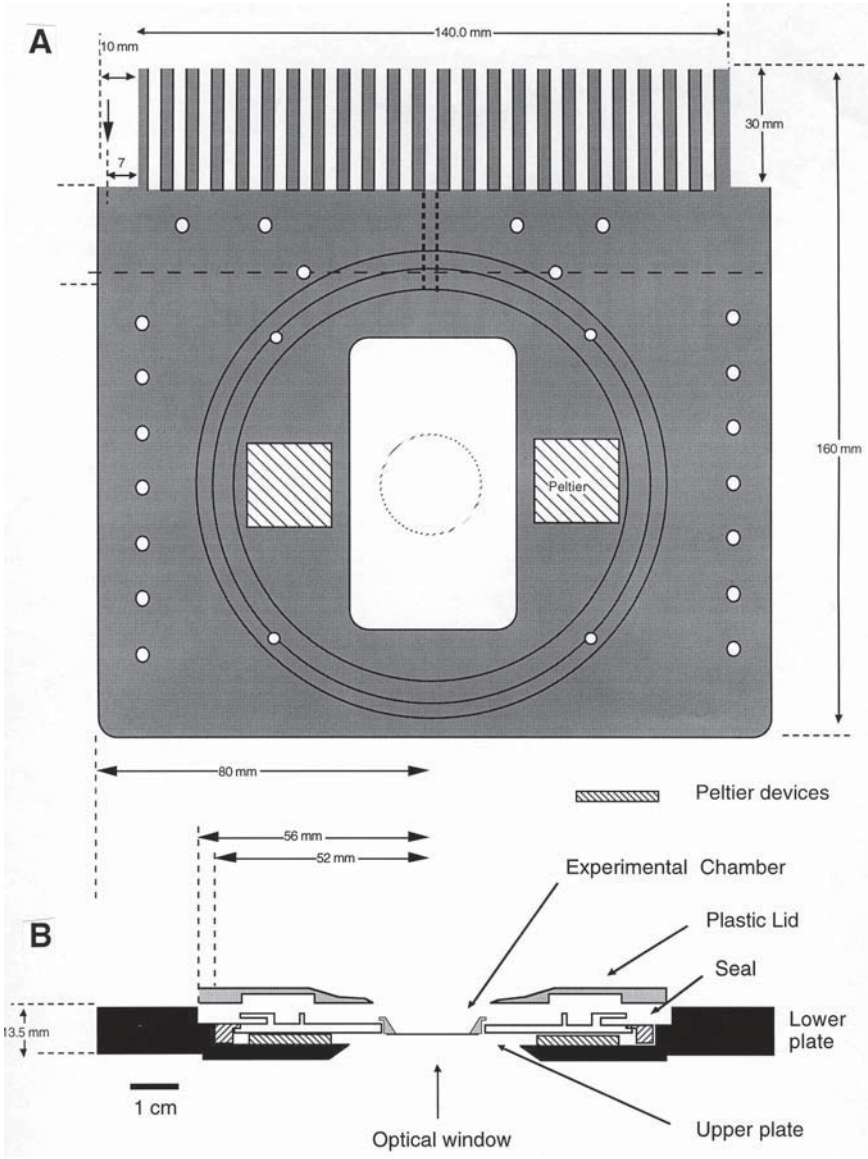

Fig. 1. *(continued on opposite page)* Construction and design plan of the heated perfusion chamber **(A)** Lower plate (material: anodized aluminum). This plate forms the base and is fixed to the microscope stage. It also acts as a heat source or sink for the Peltier devices. **(B)** An exploded side view is shown with all the components in their relative positions. The Peltier devices are effectively sandwiched between the upper and lower plate, with a heat-sink compound used to improve thermal conductivity. An aluminum ring drops into the central hole to form the experimental chamber. **(C)** Upper plate (mate-

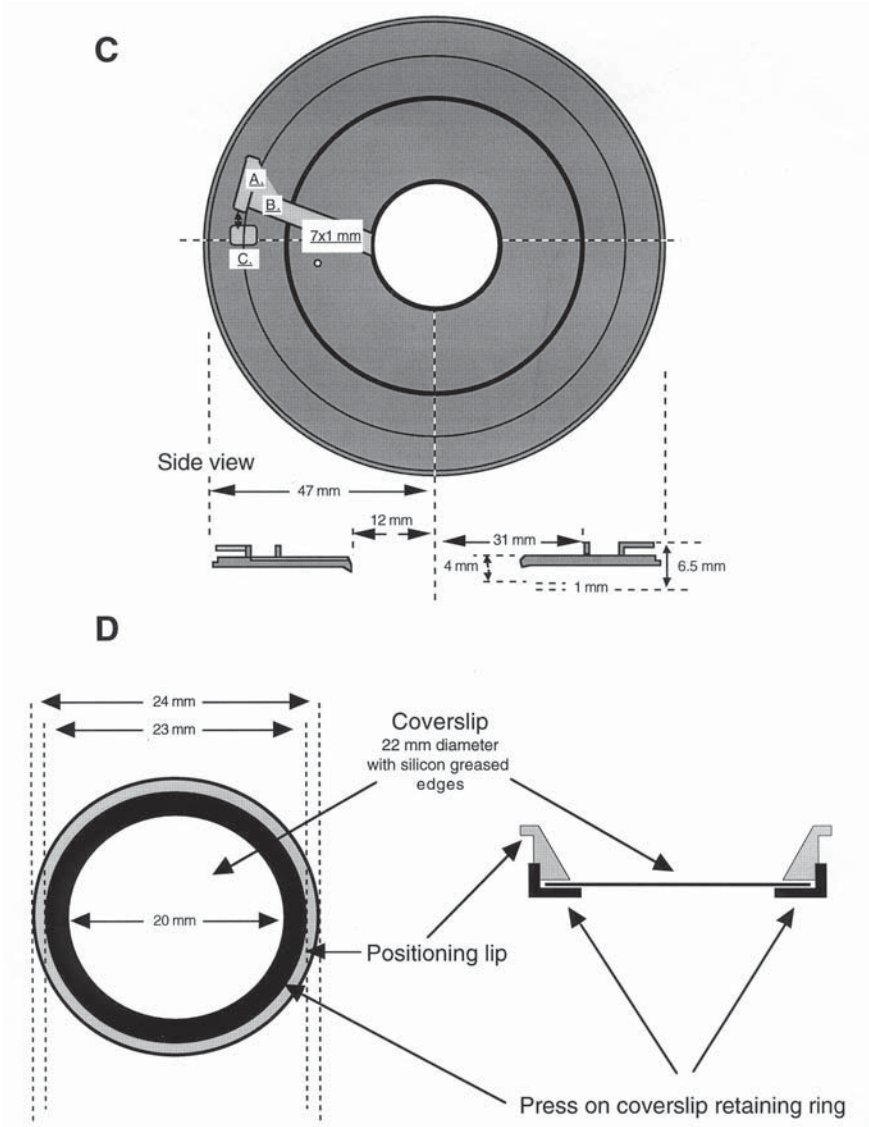

rial: anodized aluminum). The outer lip forms a slot through which plastic tubes carrying saline are coiled forming a heat exchange. The tubes enter at the slot marked "x," pass around 350°, and then pass along a shallow groove (indicated by the gray area) to reach the central hole in the middle of the plate (which receives the experimental chamber; *see* [B]). Gas mixture can also be passed over this heat exchange. The top plate is covered by a plastic lid (not shown). The solution delivery tubes can be readily connected to a peristaltic pump, and with the addition of a waste suction tube placed at the opposite side of the bath, a continuous flow of warm fresh solution at variable rates is possible. **(D)** Experimental chamber and cover slip holder (material: aluminum or polypropylene).

temperatures. The design used is based on a previous version ***(17)*** that has been modified for use on either inverted or conventional microscopes. It is suitable for both tissue culture and brain-slice preparations ***(18,19)***. The experimental chamber is formed by an aluminum ring with a glass cover slip forming the optical window. This chamber is secured into an aluminum plate, which forms the heat exchange surface (controlled by the Peltier device). The stage incorporates three elements of temperature control: (1) the experimental chamber is in thermal contact with the heat exchange; (2) the saline passes across the same heat exchange surface; and (3) an air or gas mixture can also be passed over the heat exchange (**Fig. 1**). This latter element is useful for reducing the thermal losses from the saline to the atmosphere because the experimental chamber is open on the upper surface to permit access. Similar temperature-controlled cell perfusion chambers are commercially available (IntraCel, Royston, Herts, UK; Applied Imaging, Sunderland, Tyne and Wear, UK; Medical Systems, NY).

9. The microscope and integrated micromanipulator and microinjection system are mounted on a large antivibration table ("Micro-g" series, Technical Manufacturing, Peabody, MA).

3. Methods

3.1. Preparation of Cells for Injection

1. Cells are plated at low density onto 22-mm-diameter cover slips in 2 mL of tissue culture medium in 40-mm-diameter tissue culture Petri dishes and grown for 1–3 d prior to loading with fura-2/AM and microinjection (*see* **Subheading 2.1., item 11**). Fura-2/AM loading is conducted within the culture dishes, and the cover slips are washed twice with 2 mL of K/H buffer (pH 7.4) to remove debris and all traces of serum and culture medium. The cover slip cells are then loaded with fura-2/AM (3.3 μ*M*) for 20–40 min at room temperature in 2 mL of K/H buffer. A small magnetic flea is placed in the Petri dish adjacent to the cover slip, and this is used to mix gently the fura-2/AM during the loading (*see* **Subheading 2.2., item 8**).
2. The cover slip is then washed twice with 2 mL of K/H buffer and left for >15 min, to allow for de-esterification of the dye. The cover slip is removed from the culture dish and quickly mounted into the coverslip holder, which was sealed with silicone grease (silicone compound MS4, Dow Corning GmbH, Munich, Germany) to prevent leaks. K/H buffer (37°C, 0.5 mL) is placed in the small chamber to cover the cells, and then the whole chamber is mounted into the heated cell perfusion chamber (37°C). Just prior to setting up the microinjection, the cell chamber should be washed twice with 0.5 mL of 37°C Ca^{2+}-free K/H buffer (pH 7.4).

3.2. Setting Microinjection Needle Pressures

3.2.1. Compensation Pressure (Pc)

The microinjection needle is subject to capillary suction forces as soon as it is submerged into the buffer bathing the cells. Thus a Pc is applied that pre-

vents that particular buffer from flowing into the needle and diluting the injection solution. Practically a Pc value is set empirically that ensures a permanent slight discharge from the femtotip when in Ca^{2+}-free K/H buffer. Eppendorf suggests a Pc range of 30–100 hPa for femtotips depending on the surface tension and viscosity of both the injection and buffer solution. The authors determine their working Pc value by loading 0.5–1 m*M* fura-2–free acid into a femtotip; the femtotip is then immersed in Ca^{2+}-free K/H buffer supplemented with 1.3 m*M* $CaCl_2 \cdot 6H_2O$. Using the appropriate oscillating light source and fluorescent microscope system to visualize the tip opening of the femtotip, the Pc value is gradually increased from 30 hPa until fura-2 can be directly observed very slowly discharging into the buffer. In the authors' buffer, a Pc value of 30–40 hPa is appropriate.

3.2.2. Injection Pressure (Pi)

Pi is generally significantly higher than Pc (but *see* **Note 5**). Eppendorf suggests a Pi of 50–500 hPa for femtotips; however, for small mammalian cells the lower end of this range is more appropriate. Obviously Pi must be higher than the internal pressure of the microinjected cell, but extensive inflation of the cell or nucleus indicates that the set Pi needs to be reduced. The injection time *(t_i)* defines the period for which Pi will be maintained inside the cell; it is generally set empirically between 0.4 and 1.5 s. For an injection time of 0.5 s, the authors use Pi values between 70 and 160 hPa, at which a barely noticeable cellular inflation accompanies the injections and cellular integrity is maintained.

3.2.3. The Cleaning or Rinsing Pressure (Pr)

Should the pipet become blocked by solution particles or the tip occluded with cellular debris, a rinsing pressure (Pr ~3000 hPa) can be applied in an attempt to blow the contamination away. Never use the Pr close to a cell monolayer as the high pressure will invariably damage or wash cells away. If several applications of Pr fail to dislodge cell debris, replace the femtotip as subsequent microinjections are usually compromised.

3.3. Estimating Microinjection Volume

Typically microinjected volumes range from 0.01 to 0.05 pL for nuclear injections and 0.1–0.5 pL for cytoplasmic injections into mammalian cells ***(11,20)***. Several methods have been used to quite accurately measure the microinjection volume using fluorescence ***(21)*** or radioactivity ***(22)***. The authors have used a relatively crude method to estimate injected volume because most of their experiments involved a single microinjection of a stimulant at supramaximally effective concentrations. An estimate of the cell volume is made by calculating the volume of freshly harvested "rounded up" cells. A

microscope micrometer is used to measure the average diameter of 100 cells, the average radii *(R)* determined, and the spherical volume *(V)* estimated, using $V = 4\pi R^3/3$. The estimated injection volume is calculated by delivering tens of injections of fura-2 into a cuvet containing 2 mL of K/H buffer. Since the fura-2 added will be completely saturated by the 1.3 m*M* in the K/H buffer, the resulting fluorescence can be directly calibrated against known volumes of fura-2 (10 n*M*) added to K/H buffer. This is a relatively inaccurate calculation owing to population variance in the size of the microinjected adherent cells, but corresponds well with the estimated microinjection volume of 5–10% of cell volume suggested by others ***(11,20)***. Thus microinjected stimulants are loaded into the microinjection needles at 10–20-fold the desired final concentration.

3.4. Finding the Cell and Aligning Cells for Microinjection

1. For the initial microinjection, locate a single cell or small group of cells for microinjection, using contrast enhancement optics, and then tilt back the microscope condenser head.
2. Load the micropipet, mount it onto the injection apparatus, and, using the micromanipulator on the high-speed mode, roughly center the tip over the objective and carefully lower it below the buffer surface. Watch out for a meniscus forming around the tip of the micropipet; this indicates that it has entered the solution (shining a beam from a penlight on the solution will make it easier to see the meniscus).
3. As soon as the micropipet tip has been submerged, switch the manipulator to the slow-speed mode and check the centering of the tip over the objective. If possible, carefully tilt the condenser head back to its normal position without hitting the micropipet; again, a penlight will help one to see what is happening (but *see* **Note 6**).
4. Finding the micropipet tip and aligning it above the cells can be frustratingly difficult, but switching to bright field illumination (rather than contrast enhancement) greatly increases the depth of field, making it much easier to locate the micropipet. To do this on a Diaphot with phase contrast optics, rotate the condenser phase annular ring out of the light path and replace it with the aperture diaphragm; one should still see an image of the cells (albeit with little contrast). Reducing the aperture size will further increase the depth of field. Focus initially on the cells and then raise the focal plane a "large" distance above the cells (i.e., focus "up").
5. Now it is necessary to locate the "shadow" of the out-of-focus micropipet. It is easier to detect a moving shadow than a stationary one, so begin by moving the micropipet gently backward and forward in the Y-plane only. When the shaft of the micropipet has been located, move it in the X-plane, in the direction that will bring the tip into the field of view (i.e., "backward"). The shadow of the end of the micropipet should now be visible through the microscope. Initially lower the tip slowly until the focus improves significantly as it enters the focal plane (*see* **Note 6**).

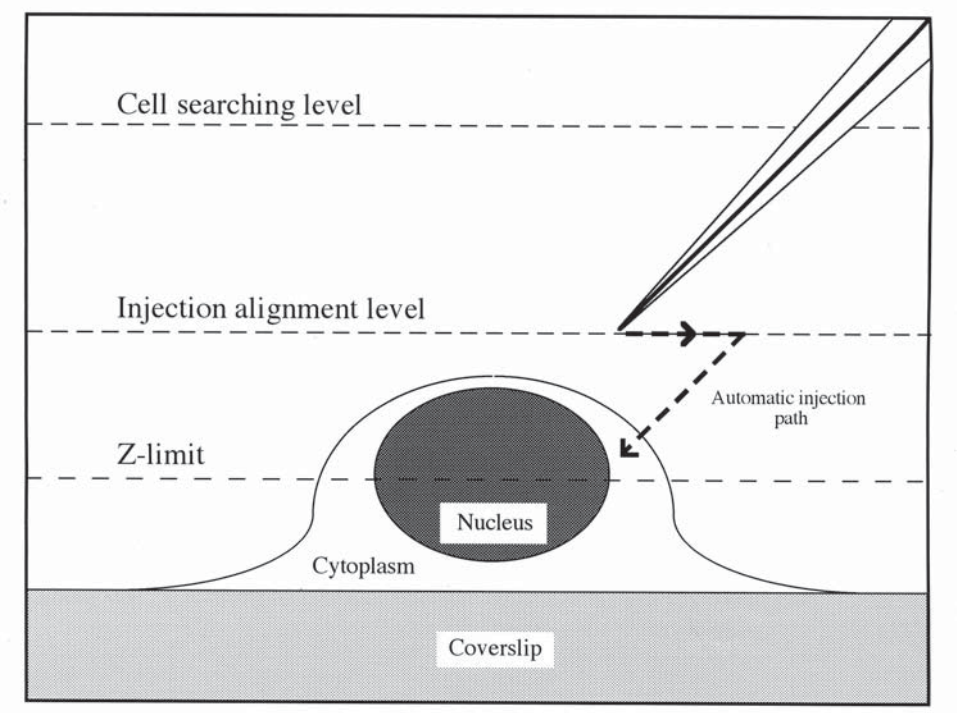

Fig. 2. Microinjection of adherent cells. Note microinjections are preferentially delivered into the thick cytoplasm of the perinuclear region.

6. Switch back to contrast enhancement microscopy and focus "down" toward the cells. Then bring the micropipet slowly down until it comes into focus again. This process is repeated several times until the tip of the micropipet lies above the cell monolayer a distance of about two to three times the maximum cell height of the monolayer. This cell searching level (**Fig. 2**) allows alignment of the tip above cells without the danger of stripping off the cell monolayer (*see* **Note 7**).

3.5. Microinjection

1. Adherent cells usually resemble a fried egg, with the perinuclear region raised above rest of the cell (**Fig. 2**); aim to inject just outside the nucleus where the cell is thickest. The Eppendorf microinjection system permits an axial 45° angle automatic injection process. The tip of the micropipet is aligned immediately above the desired injection point, and when the injection is activated the tip is driven first backward and then axially downward at 45° to the preset "Z-limit," impaling the cell and delivering a microinjection for time (t_i).
2. The micropipet is then axially withdrawn and retraces its path to return to the starting position (*see* **Fig. 2**). Consequently, before a microinjection is possible, a

Z-limit (which restricts the downward movement of the tip) must be preset. For this a cell is sacrificed by lowering the tip of the micropipet into the target cell, or by gently "stroking" the plasma membrane of the cell near the nucleus. The Z-limit function is then activated, and the micropipet is returned to the cell-searching level (*see* **Note 8**).

3. Cells chosen for injection can then be aligned and automatically microinjected as described above (*see* **Subheading 3.5., item 1** and **Note 9**). When imaging Ca^{2+} levels in conjunction with microinjection, work quickly to start recording the experiment, taking care not to disturb the microscope as the light output to the camera port is redirected.

3.6. Did the Microinjection Kill the Cell?

Following microinjection damage, a dead cell will appear refractory under phase contrast. Additionally fura-2 will leak out of the cell cytoplasm. But injection of high concentrations of Ca^{2+}-releasing agents is often cytotoxic. Consequently, one often takes advantage of the fact that Ins(1,4,5)P_3 and many Ins(1,4,5)P_3 analogs will pass through gap junctions into adjacent cells. Therefore, Ca^{2+} mobilization in several adjacent cells can be followed, even when the viability of the initially microinjected cell is compromised.

4. Notes

1. To effectively measure cellular Ca^{2+} release induced by microinjection, it is crucial that the introduced stimulant is free of contaminating Ca^{2+}, which would cause artifacts. Aqueous stocks of all stimulating inositol polyphosphates and AdA are pretreated with Chelex-100 (Bio-Rad) to chelate divalent cations and then with BAPTA-based polystyrene-immobilized "Ca^{2+}-sponge" to specifically remove contaminating Ca^{2+}. Treatment is repeated until final concentration of contaminated [Ca^{2+}] is <10 n*M* at the highest final inositol polyphosphate concentration (10 µ*M*) solubilized in control cytosol-like buffer (CLB). Small columns containing 10–20 mg of Chelex-100 or BAPTA "sponge" are utilized to remove divalent cation contamination. These are made from disposable 250-µL yellow tips or 1000-µL blue tips (Anachem, Luton, Bedfordshire, UK) with a retaining filter in their base made from 40-µm nylon mesh (Plastok Associates, Birkenhead, Merseyside, UK). Alternatively, small volumes of known aqueous stock concentrations of inositol polyphosphates (<40 µL) can be "cleaned" by treatment with 5–10 mg of Chelex-100 or BAPTA "sponge" in microcentrifuge tubes. The tubes are then vortexed for 60 s, centrifuged (13,000*g*, 1 min at 4°C), and the supernatant is harvested and transferred to a fresh tube. Centrifugation of the harvested supernatant is repeated until no chelating beads pellet. Although 5–10% of the volume of the aqueous stock solution is lost using this treatment, the authors have treated a wide range of inositol polyphosphates with these chelators and have detected no loss of compound owing to adsorption.
2. The concentration of contaminating-free Ca^{2+} ($[Ca^{2+}]_{free}$) in the nominally Ca^{2+}-free K/H buffer is determined using a tracer concentration of fluo-3 (100 n*M*).

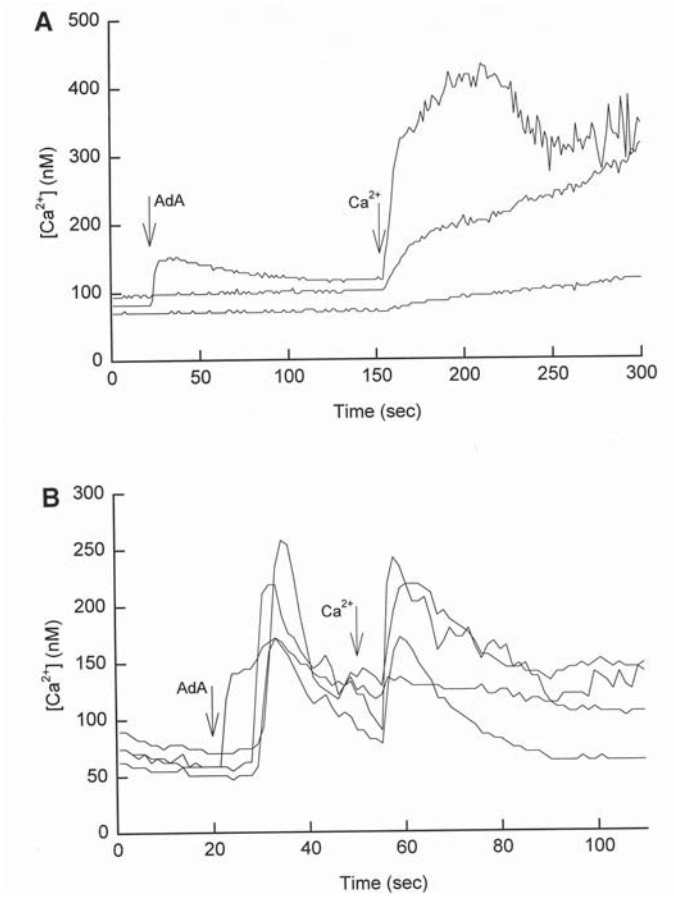

Fig. 3. The effect of microinjecting SaOS-2 cells **(A)** and m3-L15.20 cells **(B)** with a maximally effective concentration of the metabolically resistant Ins(1,4,5)P_3 analog, AdA. Cells are initially microinjected with AdA (~2 μ*M*) in Ca^{2+}-free KHB and Ca^{2+} is then added to a final concentration of 1 m*M*, where indicated. In SaOS-2 cells, AdA only produced detectable mobilization of intracellular Ca^{2+} stores in 1/3 cells, but some degree of capacitative Ca^{2+} entry was observed on Ca^{2+} add back in all three injected cells. By contrast, L15.20 cells exhibited both Ca^{2+} release from internal stores and significant capacitative Ca^{2+} entry on Ca^{2+} add back in 4/4 injected cells. Significantly, L15.20 cells are derived from L15 cells that were transfected with and stably overexpress the type 1 Ins(1,4,5)P_3 receptor ***(12,13)***.

Briefly a sample of Ca^{2+}-free K/H buffer (2 mL) is placed in a fluorimeter cuvet with 4 μL of 50 μ*M* fluo-3. The fluorescent intensity (F_{CLB}) of the buffer is determined at excitation and emission wavelengths of 505 and 530 nm, respectively. After recording the resultant *F* values, 5 μL of the 200 m*M* $CaCl_2$ solution (F_{max}),

is added followed by 25 µL of 200 m*M* EGTA (F_{min}). $[Ca^{2+}]$ is then calculated from the equation of Grynkiewicz ***(23)*** in which the K_d for fluo-3 is approx 400 n*M* at 25°C and 864 n*M* at 37°C ***(24)***:

$$[Ca^{2+}]_{free}\ (nM) = (F_{CLB} - F_{min}/F_{max} - F_{CLB}) \times K_d$$

Ideally the $[Ca^{2+}]_{free}$ at 37°C should be 1–3 µ*M*—certainly <5 µ*M*, to avoid significant Ca^{2+} inflow following microinjection and subsequent Ca^{2+} inhibition of $Ins(1,4,5)P_3$ receptor responses ***(25)***. $[Ca^{2+}]_{free}$ can be reduced by adding an appropriate aliquot of EGTA (10 m*M*/20 m*M* KOH) or BAPTA (10 m*M*); usually 2–10 µL/100 mL of CLB (0.2–1 µ*M* EGTA final) will effectively reduce the $[Ca^{2+}]_{free}$ to below 3 µ*M*.

High concentrations of EGTA and BAPTA are not used to completely chelate $[Ca^{2+}]_{free}$ from the nominally Ca^{2+}-free K/H buffer for several reasons. High concentrations of EGTA and BAPTA cause adherent cells to round up and detach from the cover slip, and they also tend to significantly deplete the intracellular Ca^{2+} stores. Additionally, recent evidence suggests that cell membrane resealing following microinjection requires the presence of some extracellular Ca^{2+} ***(26)***.

3. Never touch the surface of a cover slip with ungloved fingers; fingerprints leave smudges that both discourage cell attachment and also absorb light significantly in the UV wavelengths, the wavelength range used to stimulate fura-2.
4. The micropipets are filled just prior to use, rapidly screw mounted on the microinjector head, and the femtotip is quickly lowered into the buffer above the cells. Speed is critical here because exposure to air can rapidly dry out the sample in the end of the femtotip, causing clogging.
5. Pc can be set slightly higher and then utilized for relatively gentle manual microinjection. Essentially the cell can be manually impaled and the injection solution allowed to discharge slowly inside the cell.
6. The focus on the femtotip will never be perfect because it is oriented at 45° to the cell monolayer. Consequently, aim to get a reasonable focus on the very end of the femtotip. Remember it should not be in exactly the same plane of focus prior to injection, or it would be in contact with the cells or cover slip.
7. The cover slip surface is not completely even. Consequently when searching for cells to inject utilizing relatively long X-Y movements, use the slow speed to avoid breaking the tip or stripping off the cell monolayer.
8. Appropriate setting of the Z-limit is crucial: if it is set too high, the cell will not be effectively microinjected; if set too low, the tip can be broken on the coverslip or the injection can be delivered underneath the cell monolayer.
9. The whole microinjection procedure requires practice; while learning expect to break a lot of tips. These tips are quite expensive, so even after breaking a tip it is best to continue practicing with the broken tip until the procedure is mastered.

Acknowledgments

The authors are most grateful for the expert technical assistance provided by David Jones in the Biological Sciences workshop at the University of Leicester, especially for the construction of the heated perfusion chamber.

References

1. Berridge, M. J. (1993) Inositol trisphosphate and calcium signalling. *Nature* **361,** 315–325.
2. Streb, H., Irvine, R. F., Berridge, M. J., and Schulz, I. (1983) Release of Ca^{2+} from a nonmitochondrial intracellular store in pancreatic acinar cells by inositol-1,4,5-triphosphate. *Nature* **306,** 67–69.
3. Strupish, J., Cooke, A. M., Potter, B. V. L., Gigg, R., and Nahorski, S. R. (1988) Stereospecific mobilization of intracellular Ca^{2+} by inositol 1,4,5-triphosphate. *Biochem. J.* **253,** 901–905.
4. Berridge, M. J. and Taylor, C. W. (1988) Inositol triphosphate and calcium signalling, in *Cold Spring Harbor Symposia on Quantitative Biology*. **53**, pp. 927–933.
5. Walker, J. W., Somlyo, A. V., Goldman, Y. E., Somlyo, A. V., and Trentham, D. R. (1987) Kinetics of smooth and skeletal muscle activation by laser pulse photolysis of caged inositol 1,4,5-triphosphate. *Nature* **327,** 249–252.
6. Ely, J. A., Hunyady, L., Baukal, A. J., and Catt, K. J. (1990) Inositol 1,3,4,5-tetrakisphosphate stimulates Ca^{2+} release from bovine adrenal microsomes by a mechanism independent of the inositol 1,4,5-trisphosphate receptor. *Biochem. J.* **268,** 333–338.
7. Joseph, S. K., Hansen, C. A., and Williamson, J. R. (1989) Inositol tetrakisphosphate mobilizes calcium from cerebellum microsomes. *Mol. Pharmacol.* **36,** 391–397.
8. Proctor, G. N. (1992) Microinjection of DNA into mammalian cells in culture: theory and practise. *Meth. Mol. Cell. Biol.* **3,** 209–213.
9. Pepperkok, R., Scheel, J., Horstman, H., Hauri, H. P., Griffiths, G., and Kreis, T. E. (1993) β-COP is essential for biosynthetic membrane transport from the endoplasmic reticulum to the Golgi complex in vivo. *Cell.* **74,** 71–82.
10. Pepperkok, R., Herr, S., Lorenz, P., Pyerin, W., and Ansorge, W. (1993) System for quantitation of gene expression in single cells by computerized micro-imaging application to c-fos expression after microinjection of anti-casein kinase II (CKII) antibody. *Exp. Cell. Res.* **204,** 278–285.
11. Pepperkok, R. (1995) Microinjection and electroporation of macromolecules into live cells, in *Cell Cycle—Materials and Methods* (Pagano, M., eds.), Springer, London, pp. 75–86.
12. Miyawaki, A., Furuichi, T., Maeda, N., and Mikoshiba, K. (1990) Expressed cerebellar-type inositol 1,4,5-trisphosphate receptor (P_{400}) has calcium release activity in a fibroblast L cell line. *Neuron.* **5,** 11–18.
13. Mackrill, J. J., Wilcox, R. A., Miyawaki, A., Mikoshoba, K., and Nahorski, S. R. (1996) Stable overexpression of the type-1 inositol 1,4,5-trisphosphate receptor in L fibroblasts: Subcellular distribution and functional consequences. *Biochem. J.* **318,** 871–878.
14. Rifas, L., Fausto, A., Scott, M. J., Avioli, L. V., and Welgus, H. G. (1994) Expression of metalloproteinases and tissue inhibitors of metalloproteinases in human osteoblast-like cells—differentiation is associated with repression of metalloproteinase biosynthesis. *Endocrinology.* **134,** 213–221.
15. Ogden, D. (1994) *Microelectrode Techniques: The Plymouth Workshop Handbook.* Company of Biologists, Cambridge, England.

16. Brown, K. T. and Flaming, D. G. (1986) Advanced micropipette techniques for cell physiology. *Methods in the Neurosciences Vol. 9,* John Wiley & Sons, Chichester, UK.
17. Forsythe, I. D. (1991) Microincubator for regulating temperature and superfusion of tissue-cultured neurons during electrophysiological or optical studies, in *Methods in Neurosciences, Vol. 4, Ion Channels and Electrophysiology* (Conn, P. M., eds.), Academic Press, London, UK, pp. 301–320.
18. Forsythe, I. D. (1994) Direct patch recording from identified presynaptic terminals medicating glutamatergic EPSCs in the rat CNS, in vitro. *J. Physiol.* **479,** 381–387.
19. Barnes-Davies, M. and Forsythe, I. D. (1995) Pre- and post-synaptic glutamate receptors at a giant excitatory synapse in rat auditory brain stem slices. *J. Physiol.* **488,** 387–406.
20. Pepperkok, R., Zanetti, M., King, R., Delia, D., Ansorge, W., Philipson, L., and Schneider, C. (1988) Automatic microinjection system facilitates detection of growth inhibitory mRNA. *Proc. Natl. Acad. Sci. USA* **85,** 6748–6752.
21. Lee, G. M. (1989) Measurement of volume injected into individual cells by quantitative fluorescence microscopy. *J. Cell. Sci.* **94,** 443–447.
22. Zavortink, et al. (1983) The distribution of calmodulin in living mitotic cells. *Exp. Cell. Res.* **149,** 367–385.
23. Grynkiewicz, G., Poenie, M., and Tsien, R. Y. (1985) A new generation of Ca^{2+} indicators with greatly improved fluorescent properties. *J. Biol. Chem.* **260,** 3440–3449.
24. Merritt, J. E., McCarthy, S. A., Davies, M. P. A., and Moores, K. E. (1990) Use of fluo-3 to measure cytosolic Ca^{2+} in platelets and neutrophils. *Biochem. J.* **269,** 513–519.
25. Danoff, S. K., Suppattapone, S., and Snyder, S. H. (1988) Characterization of a membrane protein from brain mediating the inhibition of inositol 1,4,5-trisphosphate receptor binding by calcium. *Biochem. J.* **254,** 701–705.
26. Steinhart, R. A., Bi, G., and Alderton, J. M. (1994) Cell membrane resealing by a vesicular mechanism similar to neurotransmitter release. *Science* **263,** 390–393.

14

Photolysis of Caged Calcium Using a Low-Cost Flash Unit

Gommert A. van Koeveringe and Ron van Mastrigt

1. Introduction

Photolabile calcium chelators have been designed to study intracellular calcium-dependent processes ***(1,2)***. These "caged" calcium compounds are useful tools to bypass rate limiting steps, i.e., in muscular excitation-contraction coupling ***(3–5)***. When using chelators intracellularly ***(6–8)***, it is possible to evoke a stepwise increase in the intracellular calcium concentration [Ca^{2+}], by exposing the cells to high-intensity ultraviolet (UV) light. The minimum energy density required for photolysis of the caged calcium compound Nitr5 is approx 250 mJ/cm^2 in a wavelength band from 320 to 370 nm ***(9,10)***. The commonly used frequency-doubled ruby laser ***(6,7)*** meets these specifications during a flash of 25 ns, but is quite expensive. When a longer flash duration, ±4 ms, is acceptable, the commercially available xenon flashlamp developed by Rapp and Güth ***(11)*** can be used. At one-fourth of the price of the laser, it is still not a very economical alternative. We decided to develop a UV light source for the release of caged Ca^{2+} based on a standard photo flashlamp, costing one-tenth of the price of the commercially available xenon flash unit. An additional advantage of this system is that it is battery powered, thus avoiding interference on the power lines. A modified Metz® 60 CT 4 flash unit, which is widely used in professional photography, was used. When the unit is used for photographic applications, the UV light from the flashtube is absorbed by a filter in the front window, and a long flashtube is used to illuminate a large area evenly. For photolysis experiments, however, the UV light has to be transmitted and concentrated. Therefore, the front window was removed and the original flashtube replaced with a short-arc xenon flashlamp, to produce a more concentrated

From: *Methods in Molecular Biology, Vol. 114: Calcium Signaling Protocols*
Edited by: D. G. Lambert

light source. The UV light emitted by the flashlamp was concentrated even more using a dual elliptical mirror arrangement, which provided a high efficacy and an even illumination of a small preparation. The driver and trigger circuit of the unit was slightly modified. The external trigger system of the photo flash unit could easily be used for synchronization.

The efficacy of the developed UV light source was quantified by measuring the increase in free calcium on exposure of a 20-µL sample of caged calcium with a calcium-selective electrode. To illuminate a small piece of tissue evenly from multiple sides in the elliptical mirror configuration, a special organ bath was also developed. Air, glass, and fluid transients had to be avoided to reflect as little UV light as possible.

2. Materials

2.1. UV Light Source

1. Photo flash unit: A Metz Mecablitz 60 CT 4 flash unit (METZ-Werke GmbH, Fürth/Bay, Germany).
2. Flashtube: Type DG 8907 ST II Xenon flashtube 300 J/flash, 120 W (EG&G-Heimann®, Wiesbaden, Germany).
3. Electronic parts: 22 µH choking coil: 49 windings of 0.8-mm copper wire on a 21-mm diameter plastic tube.
4. Heavy duty diode: BYX 21/200 R or alternative.
5. Capacitor: 0.22 µF, 1000 V, type MKS.
6. Elliptical mirror: Type 02 REM 001 (Melles and Griot®, St. Irvine, CA); focal distance: 155 mm; front diameter: 74 mm; back diameter: 12.7 mm; distance from back opening to first focus: 12.8 mm.
7. Complementary elliptical mirror: A second 02 REM 001 can be used. If a good glassworks facility is available, the complementary mirror can be manufactured there.
8. A custom-made construction on the basis of an optical bench to position the short arc flashlamp in the focus of the elliptical mirror and a filter in the front of the mirror.
9. A 70-mm diameter UG11 glass filter, 3 mm thick, 74 mm in diameter, 80% transmission peak between 320 and 370 nm wavelength (Schott Glass, Germany).

2.2. Fluid Sample Illumination Setup

1. Test tube: Quartz glass tubular container; 1.8-mm inner diameter, 7 mm in length, 200-µm wall thickness.

2.3. Ion-Selective Calcium Electrode Setup

1. Calcium-selective electrode: Type 93-20 (Orion Research, Boston, MA). Double-barrel reference electrode type 900200 (Orion), inner compartment filled with saturated AgCl solution; type 900011 (Orion) outer compartment filled with 4*M* KCl.
2. A custom-made (punched) Teflon spacer ring: 0.3 mm thickness, 6-mm inner diameter, 12-mm outer diameter.
3. A pH/mV meter and a chart recorder.

4. Calibration solutions: Mix solutions containing saturated Ca^{2+}-EGTA and containing EGTA alone in proportions calculated so that free [Ca^{2+}] of 10^{-8}, 10^{-7}, 10^{-6}, and 10^{-5}*M* are established at pH 6.8; keep total EGTA concentration at 3 m*M*. Make standards with 10^{-4} and 10^{-3}*M* free [Ca^{2+}] by diluting a 2×10^{-3}*M* $CaCl_2$ (Merck®, Amsterdam, Netherlands) standard solution with deionized water ([Ca^{2+}] 2×10^{-6}).
5. Make solutions containing 1.00 m*M* Nitr5 (Calbiochem®, La Jolla, CA); add 10 m*M* KCl to adjust the ionic strength (according to Orion® Ca^{2+} selective electrode manual). Add $CaCl_2$ to obtain solutions with 11 different added concentrations of [Ca^{2+}]: 10^{-7}, 10^{-6}, 10^{-5}, 5×10^{-5}, 1×10^{-4}, 1.5×10^{-4}, 2×10^{-4}, 2.5×10^{-4}, 3×10^{-4}, 5×10^{-4}, 10^{-3}*M*.

2.4. Tissue Illumination Setup

1. Modified Krebs fluid: 118 m*M* NaCl, 4.7 m*M* KCl, 25 m*M* $NaHCO_3$, 1.2 m*M* KH_2PO_4, 1.8 m*M* $CaCl_2$, 1.2 m*M* $MgSO_4$, 11 m*M* glucose, pH 7.4; aerate with 95% O_2/5% CO_2 (being blown over the surface).
2. Small Perspex block: 10 mm long, 4 mm high; width is not important.
3. Two syringe pumps (HOSPAL® Dasco S.p.A. 41036, Medolla, Italy)
4. Two platinum ring electrodes made of 0.3-mm diameter platinum wire, with 4-mm ring diameter.
5. A 0.3-mm diameter glass rod (micropipet tip).
6. Halogen lamp (Philips®, 12 V, 20 W, 6°, type 6483).
7. Two hundred micrometer diameter thermocouple (Omega®, Stamford, CT), with measurement and optional control device.
8. Two 400-µm diameter tweezers (Scientific Instruments®, Heidelberg, Germany).
9. KG3 force transducer connected to a BAM3 amplifier (Scientific Instruments).

3. Methods

3.1. UV Light Source

The following procedure should be carried out using extreme caution. Touching parts in the interior of a photo flash unit can be very dangerous. High voltages persist, even when the unit is switched off.

1. Remove the front window of the Metz 60 CT 4 flash unit and replace the 70-mm long flashtube with a 300J, type DG 8907 ST II Xenon short arc flashtube (*see* **Note 1**).
2. Position the short arc lamp (arc length 7 mm) in the focus of a Melles and Griot type 02 REM 001 elliptical mirror (*see* **Notes 2** and **3**). Lengthen the leads to the anode and cathode with Teflon insulated 0.8-mm diameter twisted copper wire. Lengthen the cathode pole at the lamp with a 5-cm long piece of copper pipe. Fix the copper pipe to a nylon insulator that can be moved back and forth on a small optical rail (*see* **Fig. 1**) to position the lamp in the focus. At the front of the mirror, add a holder to carry a glass filter; in our case the Schott UG11 filter was used (*see* **Note 4**).

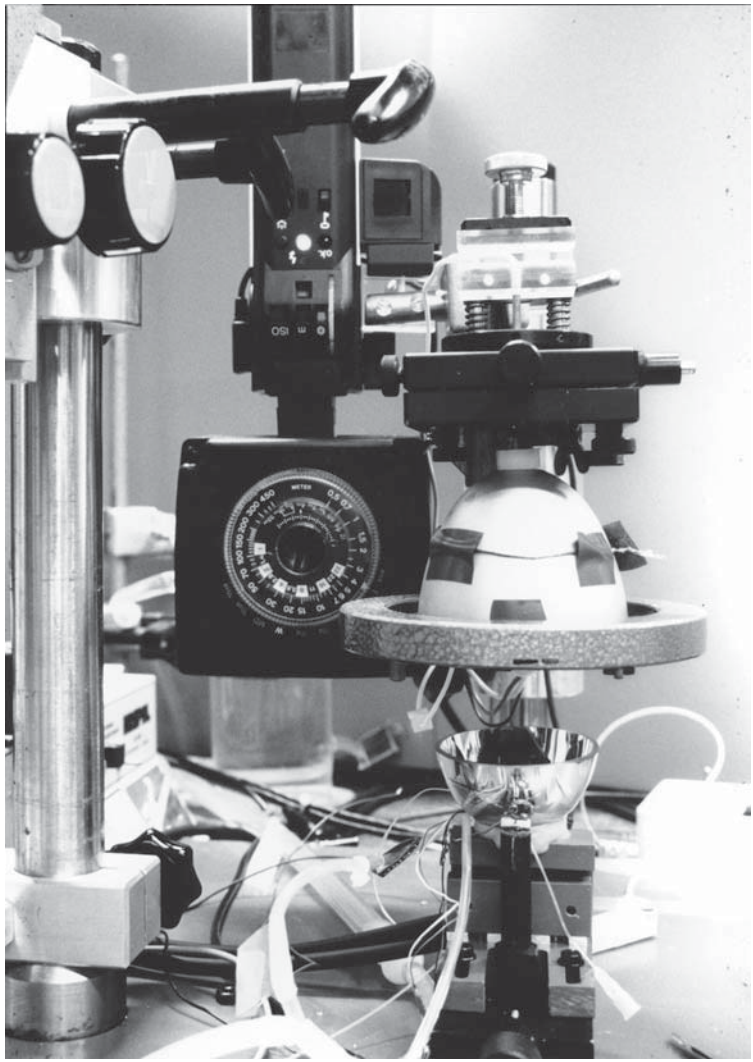

Fig. 1. Flash unit based on a photoflash unit with two complementary elliptical mirrors, the lower containing a tissue incubation and illumination setup as shown in **Fig. 4**.

3. To compensate for the lower impedance of the short arc lamp (20 Ω as opposed to 1.5 Ω of the original 70-mm tube), place an extra choking coil of 22 μH in series with the short arc lamp at the anode side. Place a heavy-duty diode parallel to the coil with reversed polarity (cathode at the anode side) in order to damp reversing currents.
4. Alterations in the trigger circuit: Move the trigger transformer as close to the lamp as possible to keep the (well-insulated) wire on top of the transformer, that

connects to the trigger ring around the lamp, as short as possible. Lengthen the three other connections to the transformer. Replace the 0.1-µF capacitor in series with the primary coil of the trigger transformer with a 0.22-µF/1000-V MKS4 capacitor to facilitate triggering (*see* **Note 5**).

5. Position a custom-made second elliptical reflector complementary to the 02 REM 001 around the sample or piece of tissue to gain a more intense and even exposure. Determine the shape of this reflector by drawing two elliptical shapes in perpendicular directions manually: Place two poles on a drawing board at a distance of 155 mm, the distance between the two focal points. Sweep a rope around both of the poles and a pencil. Adapt the length of the rope so that the 02 REM 001, with its known specifications, can be drawn on one end. Trace the complement by drawing the entire ellipse. If the size of the focal points is not the same in the perpendicular direction, repeat the described procedure in the other direction. Make a cedar wooden mold for this reflector using a computerized milling machine. Ask an experienced glassblower to blow the glass for the reflector inside this mold to a wall thickness of 2 mm. Coat the inside surface of the elliptically shaped glass with aluminum.

3.2. Fluid Sample Illumination Setup

1. To expose a fluid sample, place it in a 20-µL quartz tubular container in the second focus of the elliptical reflector, as shown in **Fig. 2**.

3.3. Ion-Selective Calcium Electrode Setup

1. Position the Ca^{2+} electrode (*see* **Notes 6** and **7**) upside down, according to the setup shown in **Fig. 3**, and place a Teflon spacer ring around the 6-mm diameter Ca^{2+}-sensitive membrane. Apply a 20-µL fluid sample centrally in the ring on the membrane. Lower the reference electrode gently onto the membrane and load it with a mass of 1.5 kg, so that a fluid film covering the Teflon ring can make contact with the peripheral junction of the reference electrode. Measure the potential between both electrodes with a pH-mV meter, and record it on a chart recorder.
2. Read the values after allowing 20 s for stabilization. Rinse the calcium-sensitive membrane, the ring, and the reference electrode extensively with deionized water and dry with a clean tissue between measurements (*see* **Notes 8** to **14**).
3. An efficacy study ***(12)*** with the calcium-selective electrode has indicated that it is possible using one flash from a low-cost UV flash unit ($1500) to evoke a physiological [Ca^{2+}] increase, from 10^{-7} to 1.1×10^{-5}*M*, in a 20-µL sample containing 1.00 m*M* Nitr5 (*see* **Notes 8** and **9**).

3.4. Tissue Illumination Setup

1. Make a perspex block (as shown in **Fig. 4**) with at least two small bore holes for in- and outflow by two syringe pumps to refresh the solution continuously at a rate of 40 µL/min.

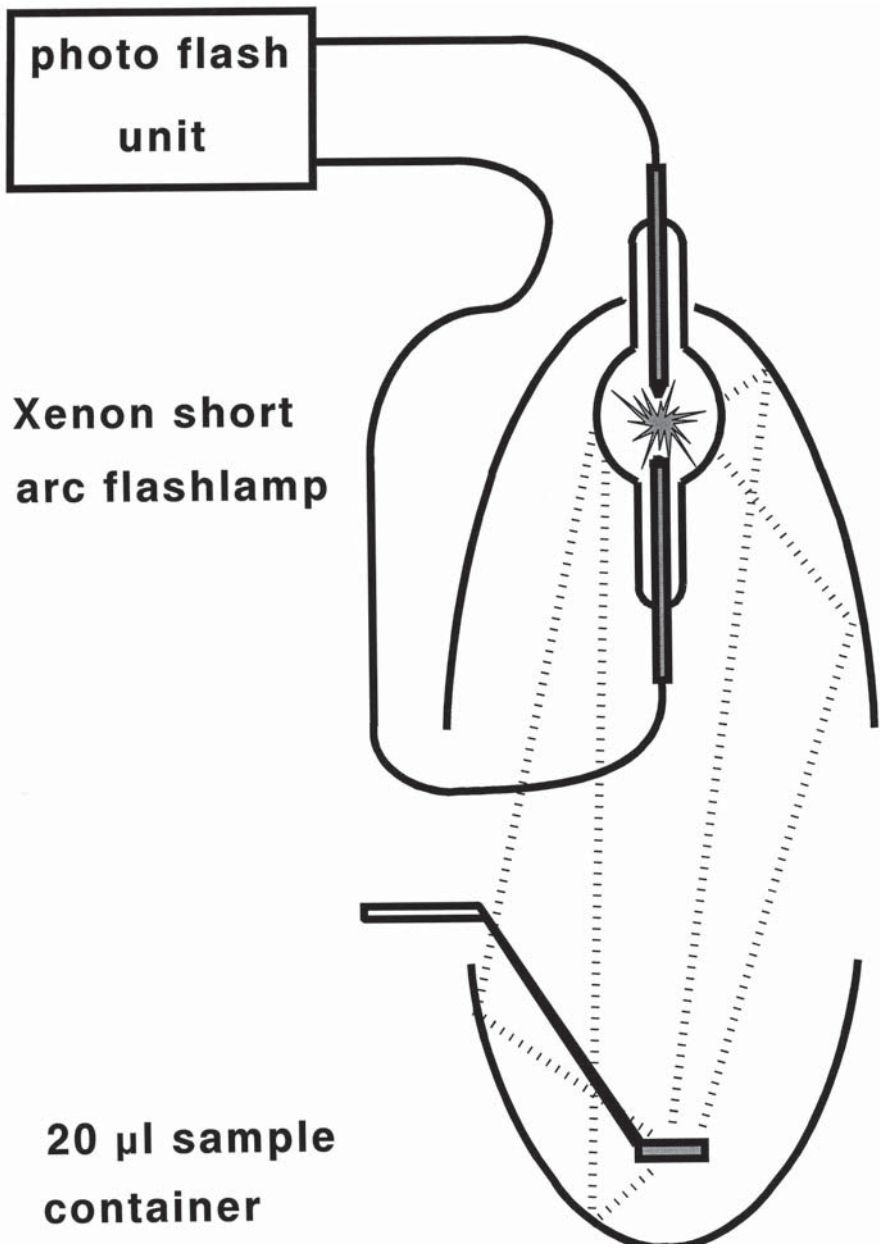

Fig. 2. A schematic representation of the fluid sample illumination setup. A short arc xenon flash lamp is mounted in an elliptical reflector and driven by a modified Metz 60 CT 4 photo flash unit. A 20-µL cuvet is placed in a complementary second elliptical reflector.

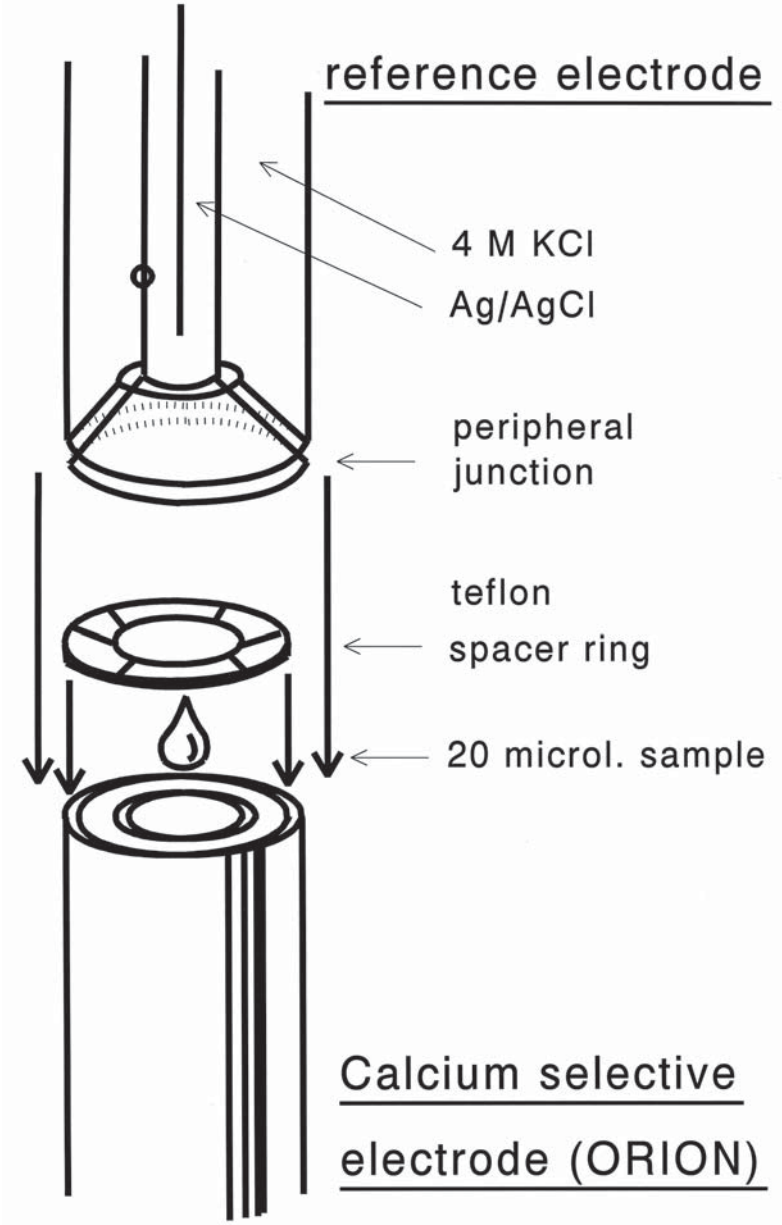

Fig. 3. A schematic representation of the ion-selective calcium electrode setup. The calcium selective electrode is positioned upside down, the 20-µL sample is applied centrally on the membrane, and the reference electrode is lowered so that a fluid film covering the ring makes contact with the peripheral junction of the reference electrode.

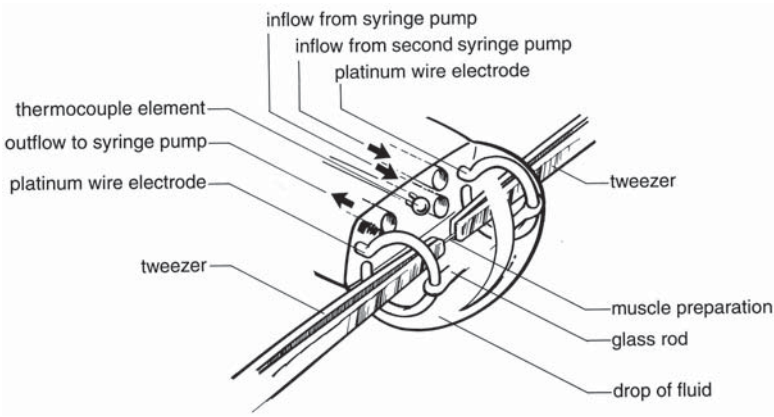

Fig. 4. Tissue incubation setup. A drop of 20 µL of Krebs fluid is supported by two platinum wire electrodes attached to a small Perspex block. The drop remains in position through surface tension and is stabilized by a glass rod connecting the two electrodes. The Krebs solution is continuously refreshed using an inflow and an outflow syringe pump. The muscle preparation is positioned in the centre of the drop between two micro tweezers.

2. Place two platinum ring electrodes at either end of the strip for electrical stimulation and support of a 20-µL drop of modified Krebs fluid by surface tension. Glue a glass rod to the other side of the electrodes as in **Fig. 4**.
3. Keep the temperature at 37°C using infrared radiation from a halogen lamp, which shines into the complementary mirror from the side. Control the temperature using a 200-µm diameter thermocouple in the drop.
4. Mount strips (i.e., muscle), inside the drop of Krebs fluid, between two tweezers, 400 µm diameter (**Fig. 4**). Attach one to a KG3 force transducer connected to a BAM3 amplifier.
5. As an application of the developed technique, small strips of urinary bladder smooth muscle (*see* **Notes 8**, **10**, and **14**) can be illuminated while measuring force development. The described tissue illumination setup (**Fig. 4**) combined with the complementary elliptical mirror (*see* **Notes 2** and **3**; **Fig. 1**) enables exposure of a tissue sample from multiple sides.

4. Notes

1. The light spot in the focus of the low-cost flash unit is larger in diameter than one would expect from a lamp with 7-mm arc length. This effect is most likely due to the fact that the discharge is not only limited to the arc between the anode and cathode but more or less extends through the entire 15-mm diameter bulb of the Xenon lamp.
2. A frame-by-frame analysis of images recorded on videotape of the flash on a graduated gray screen in the focus reveals that an intense spot in the focus with a

diameter of 5 mm is surrounded by a larger, less intense spot, with a total diameter of 30 mm. This halo is reflected back to the preparation with the complementary elliptical reflector.

3. The photolysis response is twofold enhanced by a complementary second elliptical mirror, which can be explained by the illumination of the preparation from both sides.
4. A 3-mm thick Schott® UG11 filter decreases the increase in free [Ca^{2+}] by 3%, which indicates that the effect measured is mainly evoked by UV light with a wavelength between 320 and 370 nm.
5. The flash duration of 4 ms can be measured by means of a photodetector with amplifier connected to a storage oscilloscope and the input energy calculated to be 240 J ***(13,14)***.
6. An efficacy measurement of the light source using a Ca^{2+} selective electrode has the advantage of multidirectional sensitivity as opposed to most electronic detectors, which are sensitive in only one direction.
7. Using a calcium-selective electrode in combination with a peripheral junction reference electrode and a spacer ring (**Fig. 3**) enables the analysis of a very small sample while preventing the efflux of the reference solution from directly influencing the contents of a sample. Both flashed and unflashed Nitr5 solutions can be incubated in a 20-µL container in front of the flash lamp for the same period of time and transferred to the Ca^{2+} measurement site with a 20-µL Hamilton® syringe (Reno, NV) approx 1 min after the flashes.
8. **Figure 5** shows that five flashes (we flashed five times in order to obtain a better readability of the responses) increase the free [Ca^{2+}] markedly in the range between 0.92 and 1.07 m*M* total [Ca^{2+}]. The amplitude of the calcium increase, which can be read from the *y*-axis, is variable along this range. By interpolation one can estimate that, at a free [Ca^{2+}] of $10^{-7}M$, which corresponds approximately to the intracellular [Ca^{2+}] of a muscle cell in the relaxed state, five UV flashes would evoke an increase in free [Ca^{2+}] to $1.7 \times 10^{-5}M$. Such an increase in free [Ca^{2+}] in the 20-µL sample is similar to or greater than the physiological calcium increase that has been measured intracellularly on activation of a muscle cell ***(12,15)***.
9. We have shown that the effect of five flashes measured in 1.00 m*M* Nitr5 with a $2.3 \times 10^{-4}M$ added [Ca^{2+}] was not 5 times but only 1.5 times higher than the effect of 1 flash. Thus, as opposed to a $1.7 \times 10^{-5}M$ Ca^{2+} increase in response to five flashes, a $1.1 \times 10^{-5}M$ Ca^{2+} increase would be attainable in response to one flash.
10. In solutions containing 1.00 m*M* Nitr5 and added [Ca^{2+}]'s below $10^{-4}M$, the free [Ca^{2+}] reduces dramatically. The differences between the potentials measured in standard Ca^{2+} solutions and those obtained in solutions with a low added [Ca^{2+}] can be explained by the strong Ca^{2+} buffering capacity of Nitr5. This implies that in tissue experiments, cells should be loaded slowly with Nitr5 in order to prevent the intracellular [Ca^{2+}] from falling too low. The buffering effect also explains why at lower added [Ca^{2+}]'s the response to a flash is decreased: all released Ca^{2+} is directly reabsorbed by empty "cages." The steep rise in free [Ca^{2+}] shown in the

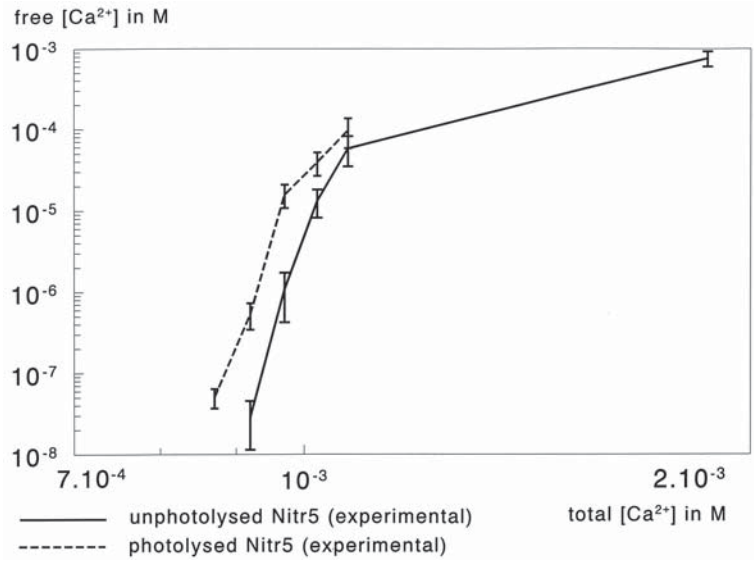

Fig. 5. Free [Ca^{2+}] as a function of total [Ca^{2+}], i.e., added [Ca^{2+}] plus the calcium bound initially to the 10^{-3}*M* Nitr5. The solid line represents average values ±SEM for a solution containing 1.00 m*M* Nitr5. The thick dashed line shows the values for 1.00 m*M* Nitr5 after exposure to five UV light flashes.

unphotolysed Nitr5 curve in **Fig. 5** between 0.87 and 1.07 m*M* total [Ca^{2+}] can be explained by Ca^{2+} saturation of the empty cages of 1.00 m*M* Nitr5 in this region. Therefore, a flash evokes the largest increase in free [Ca^{2+}] in this region. A consequence of this strong buffering capacity of Nitr5 is that, when it is loaded intracellularly as the Nitr5-acetoxymethyl ester, it makes high demands on the calcium homeostasis mechanism of the cell, and might even interfere to a large extent with these mechanisms.

11. We have found that the performance of the electrode depends on the order in which measurements are made if free [Ca^{2+}]'s are far apart. Therefore, the low free [Ca^{2+}] range, the high free [Ca^{2+}] range, and the steep part in the curve (**Fig. 5**) at which saturation of Nitr5 occurred should be measured in separate sessions to allow for intermediate Ca^{2+} reloading and stabilization of the electrode.
12. According to the Orion Ca^{2+} selective electrode manual, the experiments should be performed at a low-ionic strength (10 m*M*) in order to be able to measure lower [Ca^{2+}]'s. For EGTA ***(16)*** it has been shown that the K_d value decreases with decreasing ionic strength. By using the formula described by Thomas ***(16)***, it is possible to calculate that the K_d for Nitr5 will decrease twofold with a 10-fold decrease in ionic strength. Earlier, we described how K_d decreases even more at very low ionic strengths, necessary to measure very low calcium concentrations ***(12)***.

13. When interpreting data from measurements performed with the described Ca^{2+} selective electrode setup, one must be aware of a possible reduction of overall buffer capacity other than by an altered K_d of the same buffer. This might be the case when the UV light destructs the cages rather than changes the buffering properties. In light of these uncertainties, it is not possible to calculate a precise ratio of photolysed to unphotolysed Nitr5 in this manner.
14. A disadvantage of the Ca^{2+} selective electrode arrangement can be a gradient in Ca^{2+} release from the surface toward the middle of the container, which was earlier described by Lando and Zucker ***(9)***. However, this implies that the measured calcium release is a conservative estimate because the diameter of a muscle or other tissue preparation will be at least a factor of 10 or less.

Acknowledgments

We are grateful to J. B. F. Ekas, H. J. Wong-Loi-Sing, P. Strzelczyk, and R. Zartner for their technical advice and assistance. We also thank Dr. H. R. de Jonge and Dr. B. C. Tilly for biochemical advice, and C. Canion for his support. This work was funded by Grant C90.1061 from the Dutch Kidney Foundation.

References

1. Gurney, A. M., Tsien, R. Y., and Lester, H. A. (1987) Activation of a potassium current by rapid photochemically generated step increases of intracellular calcium in rat sympathetic neurons. *Proc. Natl. Acad. Sci. USA* **84,** 3496–3500.
2. Malenka, R. C., Kauer, J. A., Zucker, R. S., and Nicoll, R. A. (1988) Postsynaptic calcium is sufficient for potentiation of hippocampal synaptic transmission. *Science* **242,** 81–84.
3. Lea, T. J. and Ashley, C. C. (1990) Ca^{2+} release from the sarcoplasmatic reticulum of Barnacle myofibrillar bundles initiated by photolysis of caged Ca^{2+}. *J. Physiol. Lond.* **427,** 435–453.
4. Lea, T. J., Fenton, M. J., Potter, J. D., and Ashley, C. C. (1990) Rapid activation by photolysis of nitr-5 in skinned fibres of striated adductor muscle from the scallop. *Biochim. Biophys. Acta.* **1034,** 186–194.
5. van Koeveringe, G. A., and van Mastrigt, R. (1991) Excitatory pathways in smooth muscle investigated by phase-plot analysis of isometric force development. *Am. J. Physiol.* **261,** R138–R144.
6. Näbauer, M. and Morad, M. (1990) Ca^{2+} induced Ca^{2+} release as examined by photolysis of caged Ca^{2+} in single ventricular myocytes. *Am. J. Physiol.* **258,** C189–C193.
7. Niggli, E. and Lederer, W. J. (1990) Voltage-independent calcium release in heart muscle. *Science* **250,** 565–568.
8. Valdeolmillos, M., O'Neill, S. C., Smith, G. L., and Eisner, D. A. (1989) Calcium-induced calcium release activates contraction in intact cardiac cells. *Pflügers Arch.* **413,** 676–678.

9. Lando, L. and Zucker, R. S. (1989) "Caged Calcium" in Aplasia pacemaker neurons. Characterization of calcium-activated potassium and nonspecific cation currents. *J. Gen. Physiol.* **93,** 1017–1060.
10. Tsien, R. Y. and Zucker, R. S. (1986) Control of cytoplasmic calcium with photolabile tetracarboxilate 2-nitrobenzhydrol chelators. *Biophys. J.* **50,** 843–853.
11. Rapp, G. and Güth, K. (1988) A low cost high intensity flash device for photolysis experiments. *Pflügers Arch.* **411,** 200–203.
12. van Koeveringe, G. A. and van Mastrigt, R. (1994) Photolysis of caged calcium using a low cost flash unit and efficacy analysis with a calcium selective electrode. *Cell Calcium* **15,** 423–430.
13. Edgerton, H. E. (1979) *Electronic Flash, Strobe.* M. I. T. Press, Cambridge, MA, pp. 6–47.
14. Phillips, R. (1983) *Sources and Applications of Ultraviolet Radiation.* Academic, London, pp. 303–331.
15. Yagi, S., Becker, P. L., and Fay, F. S. (1988) Relationship between force and Ca^{2+} concentration in smooth muscle as revealed by measurements on single cells. *Proc. Natl. Acad. Sci. USA* **85,** 4109–4113.
16. Thomas, M. V. (1982) *Techniques in Calcium Research.* Academic, London, pp. 40–45.

15

Measurement of Ca^{2+} Flux Through Ins(1,4,5)P_3 Receptor–Ca^{2+} Channels in Lipid Bilayers ("Dip-Tip" and "Schindler" Methodology)

Edwin C. Thrower

1. Introduction

The inositol (1,4,5)trisphosphate [Ins(1,4,5)P_3] receptor [Ins(1,4,5)P_3-sensitive–Ca^{2+} channel] is an intracellular Ca^{2+} release channel located within the membrane of the smooth endoplasmic reticulum (ER). The study of kinetics and regulation of the Ins(1,4,5)P_3 receptor is greatly complicated by problems of the heterogeneity of its environment (such as vesicle size or the number of receptors per unit area of membrane), and difficulties arise in achieving tight control of the ionic composition on the luminal side of the channel. These problems can be overcome, to a certain extent, by monitoring single-channel characteristics of the Ins(1,4,5)P_3 receptor (such as channel unit conductance and open and closed times) in artificial planar lipid bilayers and relating this information to that obtained from various other studies.

Two different techniques have been used for bilayer formation and reconstitution of the Ins(1,4,5) P_3 receptor: (1) The dip-tip method ***(1)***, and (2) folded bilayers from vesicle suspensions ***(2,3)***.

1.1. Dip-tip Method

The dip-tip procedure (as described in **ref.** ***1***) is based on the patch-clamp technique ***(4,5)***, which relies on the formation of a seal between a membrane patch and a clean glass pipet, good enough to result in a greater than giga-ohm electrical resistance. Major advantages include low noise electrical measurements and minimal pretreatment of the pipet tip (*see* **Notes 1** and **2**).

The method has been developed for preparation of artificial planar lipid bilayers ***(6–10)*** known as dip-tip bilayers.

From: *Methods in Molecular Biology, Vol. 114: Calcium Signaling Protocols*
Edited by: D. G. Lambert

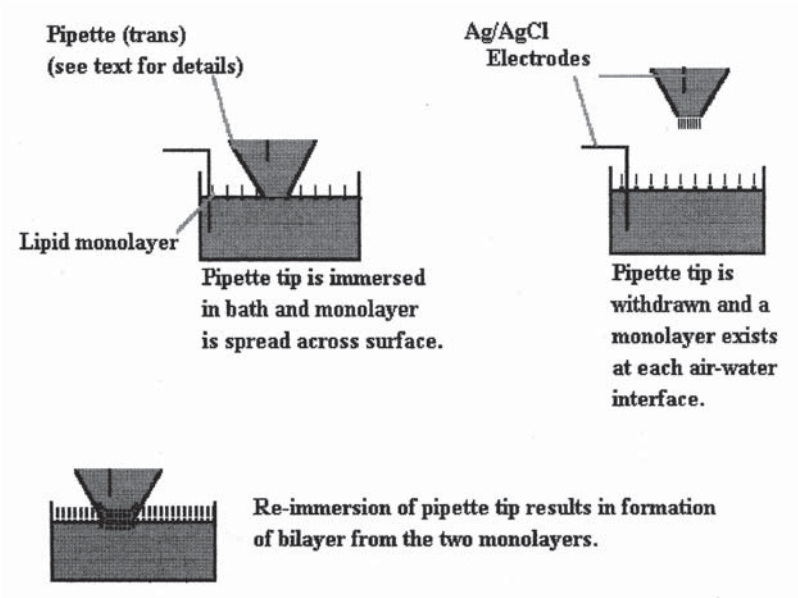

Fig. 1. A representation of the dip-tip technique (*see* text for details).

The basic procedure for forming a dip-tip bilayer is given in **Fig. 1**. Primarily, a monolayer needs to be formed at the air-water interface by allowing 10 µL (minimum) of a lipid solution in a highly volatile solvent (i.e., hexane) to spread across the surface of an aqueous solution in a bath. A glass pipet is then moved through the surface by use of a micromanipulator and a monolayer forms at the tip of the pipet. The pipet is then removed and reimmersed whereupon the monolayers at the pipet tip and air-water interface meet to form a bilayer. The pipet can be moved a few micrometers below the surface, although it is ideally kept at the interface to prevent bilayer instability (*see* **Notes 3** and **4**). The electrical connection to the measuring equipment is achieved by using reversible electrodes (Ag/AgCl), either directly or via agar bridges (*see* **Notes 5** and **6**).

Bilayers formed in this way are relatively solvent free and have small areas (the diameter of the tip being between 1 and 5 µm), thereby giving low signal-to-noise ratios in electrical current recording. Although this type of bilayer is relatively stable even at high membrane potentials, there are disadvantages. The small area reduces the rate of protein incorporation, and any slight mechanical movement of the aqueous solution can readily break the bilayer (**Note 7**).

Purified Ins(1,4,5)P_3 channel protein (1 µg), solubilized in 0.1% 1-O-*n*-octyl-β-D glucopyranoside (*n*-octylglucoside) or 0.1% 3-[(3-Cholamidopropyl) dimethylammonio]-1-propane-sulfonate (CHAPS) (Sigma-Aldrich Company Ltd., Poole, Dorset, UK) can then be added to the bath (*cis* or "cytosolic" compartment) (*see* **Note 8**).

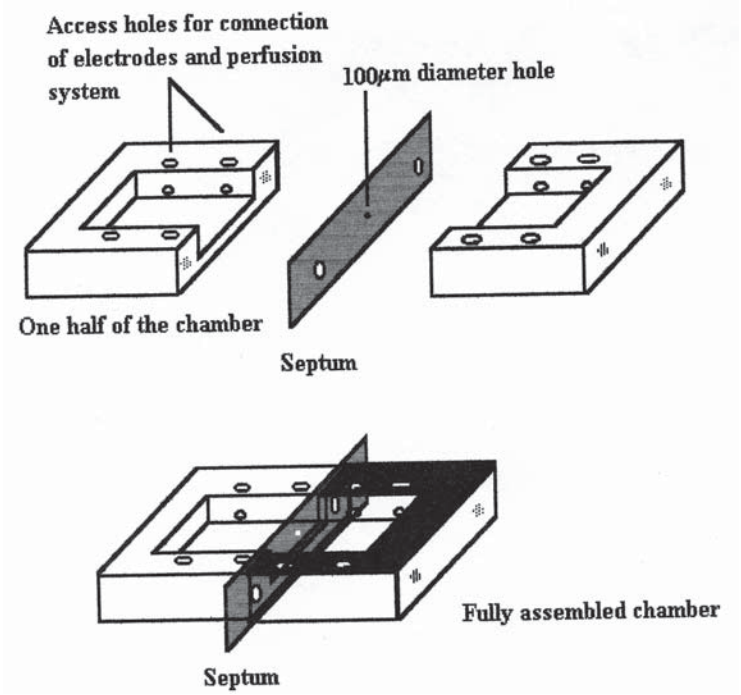

Fig. 2. A typical chamber as used in the Schindler technique.

Following its subsequent incorporation into the bilayer, 50 μ*M* ATP and 150 μ*M* $CaCl_2$ (giving a $[Ca^{2+}]_{free}$ of 200 n*M*) (*see* **Note 9**) are added to the *cis* compartment, and no channel events should be observed. However, after addition of 10 μ*M* Ins(1,4,5)P_3, single channel events are recorded. Since Ins(1,4,5)P_3 is only present on the *cis* side of the bilayer, it is logical to assume that channel activity will only be seen from channel molecules incorporated with the Ins(1,4,5)P_3-binding domain oriented on that side of the bilayer. Channel activity is abolished by the addition to the *cis* side of heparin (15 μg/mL), an Ins(1,4,5)P_3 receptor–specific antagonist.

1.2. Folded Bilayers from Vesicle Suspensions (Schindler Method)

The monolayers from which folded bilayers are formed may be spread directly at the air-water interface ***(11–13)*** or spontaneously by equilibration with a liposome suspension ***(2,3)***. In both cases, after formation of the monolayer, the bilayer may be formed across a hole in the partition separating the two compartments, by raising the monolayers on each side in turn from just below the hole to just above. The type of chamber used in these experiments can be seen in **Fig. 2**.

Two rectangular cavities (8 mm × 8 mm × 8 mm) are machined in a Teflon block (30 mm × 25 mm × 11 mm) and a thin Teflon film (100-μm thickness)

affixed between the two, using high vacuum silicone grease for electrical insulation. A 100-μm hole is burned in the film with an electric spark prior to mounting it in the chamber.

Soybean lecithin, 0.5 mL of a solution, in hexane (Sigma; 0.5 g/10 mL), is deposited as a thin film onto the surface of a round-bottomed flask using a stream of nitrogen. An electrolyte solution (10 mL) (which can vary according to the experiment) containing glass beads is added to the flask and thoroughly shaken until a lipid vesicle suspension is formed. The hole in the Teflon film is pretreated on either side with a coating solution (10 μL of hexadecane dissolved in *n*-pentane, 1:100). This pretreatment wets the PTFE surface, thus providing a suitable support for the lipid bilayer. A small amount of the lipid vesicle solution is placed in each compartment (denoted *cis* and *trans*) of the chamber and left for 30 min to enable a stable monolayer to form spontaneously at the air-water interface. The levels on either side are then raised to form a bilayer across the hole. Electrical connection of the membrane to the measuring equipment can be achieved using reversible electrodes (Ag/AgCl)—again, directly or indirectly via agar bridges (*see* **Note 6**).

Once the membrane is formed, channel incorporation can then take place. Receptor is added either as a solubilized preparation or incorporated into liposomes (*see* **Note 10**). On fusion of the receptor and addition of 4 μ*M* $Ins(1,4,5)P_3$, channel activity is recorded.

1.3. Electrical Setup of Bilayer Systems

The equipment described here is primarily intended for the Schindler technique, although there are some modifications required for the dip-tip method. These modifications are better addressed in **Subheading 3.3**. Each piece of apparatus will now be considered in turn, and the setup as a whole is shown in **Fig. 3**.

1.3.1. I/V Converter

The I/V converter measures the current across the bilayer at a given membrane potential. As currents measured in bilayer experiments can be in the picoampere range, I/V converters of sufficient sensitivity must be used. The most simple I/V converter consists of an operational amplifier, a feedback resistor, and a power supply. The input resistance of the operational amplifier must be as high as possible ($>10^{12}$ Ω). The feedback resistor employed is usually 10^9 Ω to give an output signal of at least 1 mV/pA. The output signal can be calculated according to the following equation:

$$V_{out} = I_{in} \times R$$

in which V is the output voltage, I is the input current, and R is the feedback resistance.

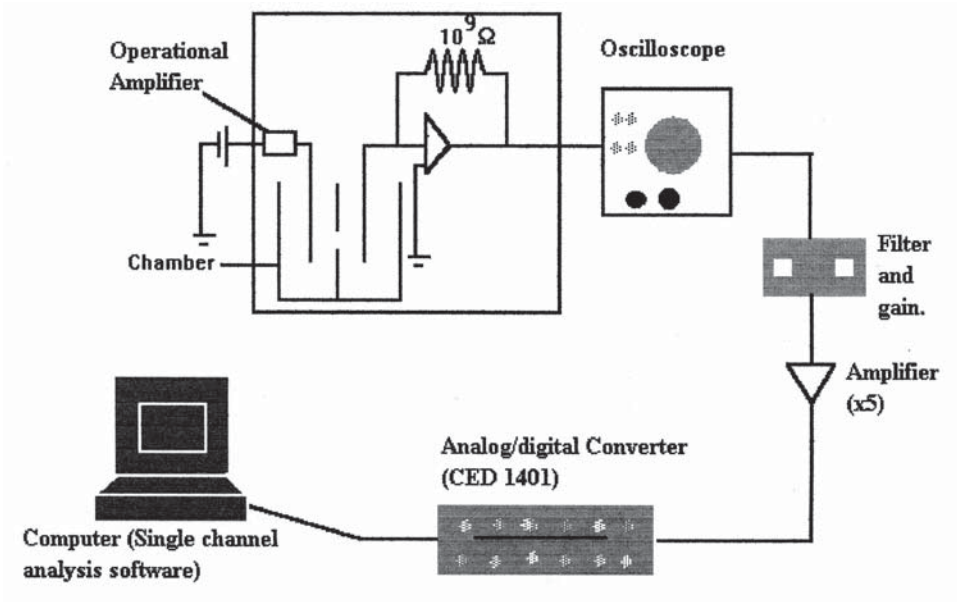

Fig. 3. Electrical setup of bilayer systems (*see* **Subheading 1.3.** for details).

A typical amplifier used in this kind of study is HAMK2TC (supplied by R.A.P. Montgomery, London, England). Besides attention to low noise characteristics, this device includes frequency compensation.

1.3.2. Command-Voltage Supply

A command voltage must be supplied to the bilayer in order to measure a current across it and is supplied to the I-V card either from a battery source or by the CED interface.

1.3.3. Capacity Measuring Devices

A continuous voltage pulse, in the form of a triangular wave, can be applied to the bilayer. From the equation

$$I = C \times dV/dt$$

in which I is current (pA), C is capacitance, and dV/dt is the change in voltage as a function of time, the capacity can be calculated from the resulting square wave.

1.3.4. Recording Devices

An oscilloscope is used for monitoring the capacitance and current traces of the bilayer. The current signal from the setup (which has already been amplified by 10^9) is passed through variable low-pass filters (Kemo Ltd., Beckenham, Kent, UK), and the overall gain usually employed is 5×10^{11}. This signal

is digitized using a CED 1401 interface (Cambridge Electronic Design, Cambridge, UK) and recorded on a microcomputer (PC), using software supplied by J. Dempster, University of Strathclyde. The degree of sensitivity described proves necessary to allow measurement of small current fluctuations generated by Ins(1,4,5)P_3 receptor activity.

2. Materials

2.1. Purification of the Ins(1,4,5)P_3-Sensitive Calcium Channel

1. Buffer A: 50 m*M* Tris-HCl, pH 7.7, 1 m*M* EDTA, 1 m*M* 2-mercaptoethanol containing protease inhibitors: 1 µL/mL pepstatin, 4 µL/mL aprotinin, and 4 µL/mL leupeptin (add 2-mercaptoethanol and protease inhibitors fresh; store at 4°C).
2. Solubilization buffer: Buffer A plus 1% Triton X-100 (v/v; will need to warm the buffer initially for Triton X-100 to dissolve). Keep at 4°C.
3. Equilibration buffer for heparin column: Buffer A plus 0.25 *M* NaCl and 0.1% Triton X-100 (v/v). Keep at 4°C.
4. Wash buffer: Buffer A plus 0.25 *M* NaCl and 0.1% CHAPS (w/v; add fresh). Keep at 4°C.
5. Elution buffer: 50 m*M* Tris-HCl, pH 7.7, 0.5 *M* NaCl, 0.1% CHAPS (w/v; add fresh), 1 m*M* 2-mercaptoethanol (add fresh).
6. Hi-Trap Heparin column (1 mL) (Pharmacia, Bellefonte, PA). Equilibrate with appropriate buffer (*see* **item 3**). For storage: 50% ethanol at 4°C.

2.2. [^{3}H]Ins (1,4,5)P_3 Binding Assay

1. Binding buffer: 50 m*M* Tris-HCl, 1 m*M* EDTA, pH 8.3 (at 4°C).
2. [^{3}H]Ins(1,4,5)P_3, potassium salt, ethanol:water (1:1 v/v) solution (Amersham Life Sciences, Amersham, UK). Specific activity 1.4 TBq/mmol, 38.0 Ci/mmol. Store at –20°C.
3. 0.5% γ-globulin (w/v) (Sigma). Dissolve 0.05 g in 10 mL to give sufficient quantities for large assay numbers. Always make up fresh. γ-globulin will not always dissolve, it forms a cloudy suspension, this is normal.
4. 30% Polyethylene glycol (w/v) (PEG) M_r 8000. Dissolve 30 g of PEG in 100 mL of binding buffer. PEG is difficult to dissolve and it will take several minutes, with constant stirring. Store at 4°C.
5. *Eco-scint A* scintillation fluid (National Diagnostics, Atlanta, GA). Use approx 4–6 mL of scintillation fluid/sample.

2.3. The Dip-Tip Technique

1. The micropipets used are made from borosilicate glass capillaries (Clark Electromedical Instruments, Pangbourne, Reading, UK, GC150-15; 1.5-mm outer diameter, 0.86-mm inner diameter) using either a KOPF vertical pipet puller, or a Flaming/Brown micropipet puller, Model P-87 (Sutter Instrument Intracel, Shepreth, Royston, Hertfordshire, UK). The filament type is from Clark Electromedical Instruments, code no. FT 330B for the P-87, and required settings are as follows: heat = 480; pull = 0; velocity = 40; time = 110 (*see* **Notes 1** and **2**).

2. Buffer for the *trans* compartment (i.e., the pipet): 25 m*M* KCl, 53 m*M* Ba $(OH)_2$/HEPES, pH 7.35 (*see* **Note 11**).
3. The buffer in the *cis* compartment (i.e., the bath): 25 m*M* KCl, 250 m*M* HEPES-KOH, 1 m*M* *N*-hydroxyethylethylene-diaminetriacetic acid (HEDTA), pH 7.35.
4. Lipids: 1-palmitoyl-2-oleoyl-sn-glycero-3-phosphocholine (POPC) and 1,2-dioleoyl-sn-glycero-3-phosphoethanolamine (DOPE) in the ratio 7:3 (Avanti Polar Lipids, Alabaster, AL). Store in chloroform:methanol (1:1) at –70°C. For use, evaporate to dryness and redissolve in *n*-hexane.
5. Micromanipulator (Narishige, Willow Way, London, UK): Model no. VO-10, serial no. 94039.
6. Channel events are recorded using a PC together with an interface (CED 1401, Cambridge Electronic Design) for single-channel analysis (PAT V6.1, J. Dempster, University of Strathclyde), and Mathcad (Mathsoft).

2.4. Folded Bilayers from Vesicle Suspensions (Schindler Method)

1. Buffer 1: 500 m*M* KCl, 5 m*M* $CaCl_2$, 40 m*M* HEPES, pH 7.35. Addition of 30 m*M* HEDTA to chelate Ca^{2+} (*see* **Note 12**).
2. Lipid: Soybean lecithin (Sigma). Dissolve 0.5 g in 10 mL of hexane. Store at –20°C; should last up to 10 d.
3. Coating solution: 10 µL *n*-pentane in 1 mL hexadecane. Solution is supplied to hole using a micropipet; should be made up fresh.
4. Cleaning procedure for chambers: water, methanol; chloroform; and from time, to time water, sulfo-chromic acid; water, methanol; chloroform.
5. Agar bridges: 2% agar in 3 *M* KCl. Agar is heated until dissolved in 3 *M* KCl, then sucked through tubing via a syringe (1-mm diameter), and then allowed to cool and set. The 1 m or so of tubing is then sliced with a razor blade into 2- to 3-cm pieces for use in experiments. Care should be taken when inserting electrodes as the composition of the agar can be disrupted.

3. Methods

3.1. Purification of the Ins(1,4,5)P_3-Sensitive Calcium Channel

The Ins(1,4,5)P_3-sensitive calcium channel, or Ins(1,4,5)P_3 receptor as it is otherwise known, can be solubilized and purified from rat cerebellum, which is an abundant source of the receptor ***(14)***. Various modifications have been made to the procedure for economical and practical reasons (*see* **Notes 13–15**).

1. Remove cerebella from between 16 and 20 male rats and homogenize in 50 vol of ice-cold buffer A (*see* **Subheading 2.1., item 1**). Pellet by centrifugation (35,000 *g*, 15 min).
2. Decant the supernatant, resuspend the pellet in 50 vol of buffer A, and centrifuge as before. Repeat this step.
3. Resuspend the pellet in a final volume of buffer A plus 1% Triton X-100 to give 50 mg original wet wt/mL and incubate for 30 min at 4°C. Centrifuge the membranes for 1 h at 48,000 *g* and collect the supernatant.

4. Adjust the salt concentration of the solubilized fraction to 0.25 *M* in NaCl, and then pass over a heparin-sepharose column (1 mL) preequilibrated with buffer A plus 0.25 *M* NaCl and 0.1% Triton X-100 at a flowrate of approx 1 mL/min.
5. Wash the column with 20–40 mL of buffer A plus 0.25 *M* NaCl and 0.1% CHAPS or octylglucoside, and elute the Ins(1,4,5)P_3 receptor with buffer A plus 0.1% CHAPS and 0.5 *M* NaCl (collected as 6 × 0.5 mL fractions). Assay these fractions for protein concentration (standard Bradford assay) and ligand binding activity (*see* **Subheading 3.2.**). Sodium dodecyl sulfate-polyacrylamide gel electrophoresis can be performed using a 7.5% gel. The purified protein should appear as a doublet at approx 220 kDa following Coomassie staining.

3.2. [^{3}H]Ins(1,4,5)P_3 Binding Assay

There are several variations on the binding assay for both crude membranes and solubilized receptor. The assays rely on the competition between radioactive Ins(1,4,5)P_3 ("hot") and nonradioactive Ins(1,4,5)P_3 ("cold") for the specific Ins(1,4,5)P_3 binding site. The types of assay carried out include a standard assay whereby a saturating concentration of cold Ins(1,4,5)P_3 is used, and the difference in binding between a solely hot sample and a hot plus cold denotes the total specific binding. Another type of assay is the full binding or displacement curve whereby standard amounts of radioactive Ins(1,4,5)P_3 are present in each sample and varying concentrations of nonradioactive Ins(1,4,5)P_3 are present. The subsequent displacement of hot Ins(1,4,5)P_3 by the ever-increasing concentrations of cold Ins(1,4,5)P_3 yields information about the maximal concentration of Ins(1,4,5)P_3 bound, (B_{max}), and the dissociation constant, (K_d).

3.2.1. [^{3}H]Ins(1,4,5)P_3 Binding in Crude Membranes

1. Incubate tubes containing 0.2 mg of protein, 20,000 dpm [^{3}H]Ins(1,4,5)P_3, and various concentrations of cold Ins(1,4,5)P_3 (ranging from 0.1 n*M* to 20 μ*M*) in a final volume of 0.35 mL of buffer A (*see* **Subheading 2.2.**, **item 1**) for 10 min at 4°C.
2. Centrifuge the samples for 5 min at 10,000*g*, pelleting the protein and thus allowing separation of free from bound [^{3}H]Ins(1,4,5)P_3.
3. Remove the supernatant and rinse the surface of the pellet, resuspend, and add to 6 mL of *Eco-Scint* liquid scintillation mixture. The radioactivity is determined using the Rackbeta Excel liquid scintillation counter. Experiments should be performed in triplicate. Nonspecific binding (NSB) can be determined in the presence of 1 μ*M* cold Ins(1,4,5)P_3.

3.2.2. [^{3}H]Ins(1,4,5)P_3 Binding in Detergent-Solubilized and Purified Receptor

[^{3}H]Ins(1,4,5)P_3 binding to soluble fractions can be assayed by precipitation of solubilized proteins using γ-globulin as a protein carrier.

1. Incubate between 5 and 10 µg of Ins(1,4,5)P_3 receptor (0.05 mL) in 0.3 mL of buffer A (*see* **Subheading 2.1., item 1**) along with 20,000 dpm [^{3}H]Ins(1,4,5)P_3, and various concentrations of unlabeled Ins(1,4,5)P_3 for 15 min at 4°C.
2. Subsequently add 200 µL of 0.5% γ-globulin and 500 µL of 30% PEG (M_r 6000–8000) to each sample, mix, and leave for 5 min.
3. Centrifuge the samples at 10,000*g* for 5 min, aspirate the supernatant, and then rinse the pellet in buffer A (*see* **Subheading 2.1., item 1**). Resuspend in 0.1 mL of buffer A.
4. Add samples to 6 mL of *EcoScint* scintillation fluid and determine the radioactivity using the Rackbeta Excel liquid scintillation counter. Again, the assays should be carried out in triplicate. NSB is measured in the presence of 1 µ*M* unlabeled Ins(1,4,5)P_3.

3.3. The Dip-Tip Technique

1. The electrical setup for this method is slightly different from the general setup described in **Subheading 1.3.** The basic amplifier is similar to Montgomery's, but the initial I to V operational amplifier is mounted as a remote head amplifier to which a standard patch-clamp pipet carrier (Clark Electromedical Instruments) is fitted. The interior of the pipet acts as the *trans* (equivalent to the luminal space of the ER) compartment. The pipet must be pulled from a glass capillary (specifications in **Subheading 2.3.**; also *see* **Notes 1** and **2**) and filled with 25 m*M* KCl, 53 m*M* Ba $(OH)_2$/HEPES, pH 7.35. Filter all solutions using a 0.2-µm syringe filter to remove any contaminants, which could affect bilayer formation.
2. Fill pipet tips by suction followed by backfilling, and remove any bubbles by gentle tapping. Affix pipet to the appropriate electrode attachment, ensuring that the buffer solution within the pipet is in contact with the Ag/AgCl electrode (*see* **Note 5**).
3. Fill the *cis* compartment (bath) with 1 mL of buffer (25 m*M* KCl, 250 m*M* HEPES-KOH, 1 m*M* [HEDTA], pH 7.35), ensuring that the buffer is in contact with the electrode.
4. Using the micromanipulator, lower the pipet into the bath *(cis)*, and then carefully add 10 µL of lipid solution (POPC:DOPE, 7:3) to the surface of the *cis* buffer, allowing it to spread across, forming a monolayer at the air-water interface. After 5–10 min, raise the pipet and then lower it again, at which point the capacitance trace on the oscilloscope will change from rectangular to skewed-rectangular in shape. This signifies the formation of a bilayer (*see* **Notes 3** and **4**).
5. Add 1 µg of purified protein or proteoliposomes and allow for incorporation into the bilayer. This can be followed by gentle addition of 10 µ*M* Ins(1,4,5)P_3 and 150 µ*M* $CaCl_2$ (*see* **Notes 9** and **16**).
6. Channel events are recorded using a PC together with an interface, software PAT V6.1, for single-channel analysis, and Mathcad.

3.4. Schindler Technique

1. Remove lipid solution from refrigerator. Leave to stand for 30 min.
2. Rinse a round-bottomed flask initially with a half-volume of water followed by methanol, then chloroform, and then hexane.

3. Take 0.5 mL of the lipid solution and place in the flask, evaporating using a stream of nitrogen, while gently rotating the flask. Continue until a thin, even film is formed on the flask interior.
4. Filter 10 mL of buffer 1 (*see* **Subheading 2.4.**, **item 1**), mix with some glass beads, and then add the buffer and the beads to the lipid-coated flask. Shake vigorously until a cloudy liposomal suspension is formed.
5. Coat the hole in the Teflon film that bisects the chamber with 10 µL of coating solution (as described in **Subheading 2.4.**).
6. Cover the bottom surface of both the *cis* and *trans* compartments with a thin layer of liposomal solution.
7. Connect electrodes to the apparatus and to each compartment, and then allow 30 min for equilibration.
8. Raise the levels on either side of the chamber to just above the hole. There will be a distinct change in the capacitance trace on the oscilloscope. This depicts bilayer formation, and once this has occurred, it should then be viewed with the current trace on the oscilloscope.
9. Then add HEDTA to the *cis* side (final concentration of 30 m*M*) to chelate the Ca^{2+} present, thus giving a free Ca^{2+} concentration of 0.2–0.3 *M* (*see* **Notes 12** and **17**).
10. Add 1 µg of purified receptor, or proteoliposomes (*see* **Note 10**), to the *cis* compartment. On fusion of the receptor and addition of 4 µ*M* Ins(1,4,5)P_3, channel activity, when detected, can be recorded as previously described (**Subheading 3.3.**). A range of potential differences must be applied (e.g., +100 mV to –100 mV, with 25-mV intervals) when using K^+ as the current carrier.
11. To ensure efficient reuse of the chambers, utilize the following cleaning procedure:
    a. After an experiment, wash the chamber in distilled water to remove all salts and water-soluble compounds.
    b. Follow this by washing in methanol to remove water, then chloroform to remove lipids and other hydrophobic material, and subsequently methanol and water.
    c. Leave the chambers overnight to dry before using again. From time to time the chambers should be dismantled and the silicon grease carefully removed with a tissue. The septum and the two halves of the chamber can be immersed in sulfochromic acid for several hours and then rinsed thoroughly in distilled water followed by methanol and then chloroform. The chamber, once dry, is reassembled, using silicone grease carefully applied to the septum and surfaces to avoid any problems with leakage.

4. Notes

1. Many types of pipets used in patch clamping are coated with an insulating agent to reduce the capacitance between the pipet interior and the bath, and also the noise from the dielectric loss in the glass. In this case, precoating was not necessary as the borosilicate glass used readily forms an efficient seal.
2. Fire polishing the end of the pipet to smooth the edges of the tip improved the performance of the system. The pipet tip can be observed under a microscope at

a magnification of ×400–800 and the heat source is a platinum wire. A current is passed through the wire, and the pipet tip is moved into close proximity until it starts to melt and the desired tip size is obtained. A resistance of 500 kΩ was recorded on average for each pipet to give a final overall resistance of approx 10^9 Ω. A sufficient test for measuring the quality of the pipet is to immerse it in methanol and to pass air through the pipet tip using a 20-mL syringe. If small air bubbles are produced when the syringe reads at below 10 mL on the scale, then the pipet is deemed to be of standard quality. This is known as the "bubble test" and is commonly used in such systems.

3. Evaporation of the aqueous bath solution necessitates readjustment of the pipet position over a long time scale to maintain the interaction at the tip. Suction can be applied to the system during bilayer formation and can indeed be of assistance. Allowing a small quantity of pentane to run down the tip can aid bilayer formation, possibly by cleaning the tip and dissolving any excess lipid.
4. Occasionally the pipet tip can become blocked, and this can be detected quite easily by employing suction or blowing. If the capacitance trace remains unchanged despite the increased stresses, then the tip is invariably blocked. After formation of the bilayer, the seal and conductance can be tested by an additional voltage pulse.
5. The pipets are filled with just sufficient buffer solution to make contact with the electrode wire, leaving the holder dry, to avoid contamination effects inside it, which may otherwise lead to extraneous conductivity and noise effects.
6. In some experiments, agar bridges are necessary to prevent differences in chloride concentrations of the two bathing solutions from adding a junction potential to the bilayer.
7. Perfusion of these systems is incredibly difficult, whether of the bath or the interior of the pipet, and in the long term it is better to avoid perfusion, although this experimentally restricts the system somewhat.
8. Control experiments are necessary to determine whether detergents are detrimental to the stability and conductivity of the bilayers. Addition of an equivalent volume of buffer containing 0.1% of either detergent, but without protein, to the *cis* compartment is sufficient. In current studies, no significant effect on bilayer stability was detected with 0.1% octylglucoside or CHAPS.
9. Fifty μ*M* ATP has been shown to increase the frequency of channel opening ***(15)*** and 150 μ*M* $CaCl_2$ gives a $[Ca^{2+}]_{free}$ of 200 n*M*, i.e., within the range of free $[Ca^{2+}]$ found to maximize activity of the Ins(1,4,5)P_3-gated channel ***(16)***.
10. The method for forming proteoliposomes is by dilution in buffer A (1:1) (**Subheading 2.1.**). The detergent in which the receptor is solubilized is diluted sufficiently, thus causing the receptor to adopt an energetically favorable conformation by incorporating itself within the liposome. As there is no difference in channel activity, whether solubilized preparation or proteoliposomes are added, it is evident that initial exposure of the protein to 5 m*M* Ca^{2+} during the dilution method has no residual effect on channel activity after chelation.
11. Ba^{2+} was used as the current carrier because it is not thought to regulate the Ins(1,4,5)P_3 receptor, and single channel currents have been shown to be 60%

larger with a threefold increase in mean open time of the channels compared to experiments in which Ca^{2+} was the current carrier ***(15,16)***.

12. The presence of 40 m*M* HEPES is necessary to buffer the subsequent production of protons, which are a result of the chelation.
13. This purification procedure has been employed using CHAPS instead of Triton throughout each step ***(18)***, although, from an economic viewpoint, it is just as easy to carry out a detergent replacement at the final wash stage. It is necessary to replace Triton with CHAPS or octylglucoside because Triton detergent, irrespective of however low the concentration may be, disrupts bilayers and it cannot be readily dialyzed. CHAPS and octylglucoside, in sufficiently low concentrations, have been shown to have no apparent effect on bilayer stability. By monitoring the decrease in absorbance at 280 nm, the point at which all the Triton is displaced can be detected (*see* **Note 8**).
14. As yields of active protein and fold purification were low, the purification was not taken further in order to conserve protein for bilayer experiments. In the author's experience, the purity of the protein was sufficient for use in bilayer work because no other form of channel activity has ever been detected.
15. It is possible that some of the protein was denatured during the detergent exchange step, thus accounting for the low yields. Octylglucoside has a critical micellar concentration (CMC) (the minimum concentration at which detergents begin to form micelles) of 14.5×10^{-3} mol/L (25°C), which is significantly higher than that of Triton X-100 (0.2×10^{-3} mol/L [25°C]); thus, Triton may be washed off the column at a faster rate than octylglucoside can replace it, thereby causing some denaturation of the protein. Octylglucoside has also been reported as irreversibly inhibiting $Ins(1,4,5)P_3$ binding to the receptor ***(19)***, although in this particular instance (i.e., at a concentration of 0.1%) this is clearly not the case, as specific $Ins(1,4,5)P_3$ binding to the receptor preparation can be seen. Detergent exchange with 0.1% CHAPS does improve the yield of active protein, possibly because the CMC of CHAPS (4×10^{-3} mol/L [25°C]) is closer to Triton than that of octylglucoside.
16. The dose-response effects using the dip-tip technique are technically too difficult to achieve.
17. The presence of 5 m*M* Ca^{2+} on the *trans* side was assumed not to have an effect on the receptor ***(17)***. Indeed, having millimolar concentrations of Ca^{2+} present is a regular feature of this type of bilayer system. It is necessary for accelerating the spreading of the monolayer and can aid fusion of vesicles. Bilayers formed from negatively charged lipids can be highly unstable, and the presence of divalent cations such as Ca^{2+} or positively charged polypeptides can have a stabilizing effect.

References

1. Ehrlich, B. E. (1992) Planar lipid bilayers on patch pipettes: Bilayer formation and ion channel incorporation. *Methods Enzymol.* **207,** 463–471.
2. Schindler, H. and Feher, G. (1976) Branched molecular lipid membranes. *Biophys. J.* **16,** 109–111.
3. Schindler, H. (1980) Formation of planar lipid bilayers from artificial or native membrane vesicles. *FEBS Lett.* **122,** 77–79.

4. Hamill, O. P., Marty, A., Neher, E., Sakmann, B., and Sigworth, F. J. (1981) Improved patch-clamp technique for high resolution current recording from cells and cell-free membrane patches. *Pflügers Arch.* **391,** 85–100.
5. Sakmann, B. and Neher, E. (1983) *Single Channel Recording.* Plenum, New York.
6. Coronado, R. and Latorre, R. (1983) Formation of phospholipid bilayers on patch-clamp pipettes. *Biophys. J.* **43,** 231–236.
7. Schuerholz, T. and Schindler, H. (1983) Formation of lipid-protein bilayers by micropipette-guided contact of two monolayers. *FEBS Lett.* **152,** 187–190.
8. Suarez-Izla, B. A., Wan, K., Lindstrom, J., and Montal, M. (1983) Single channel recordings from purified acetylcholine receptors reconstituted in bilayers formed at the tip of patch pipettes. *Biochemistry* **22,** 2319–2323.
9. Wilmsen, U., Methfessel, C., Hanke, W., and Boheim, G. (1983) Channel current fluctuation studies with solvent free planar lipid bilayers using Neher-Sakmann pipettes, in *Physical Chemistry of Transmembrane Ion Motion* (Spach, G., ed.), Elsevier, Amsterdam, pp. 479–485.
10. Hanke, W., Methfessel, C., Wilmsen, U., and Boheim, G. (1984) Ion channel reconstitution into planar lipid bilayers on glass pipettes. *Biochem. Bioeng. J.* **12,** 329–339.
11. Langmuir, I. and Waugh, D. F. (1938) The adsorption of proteins at oil-water interfaces and artificial protein-lipid membranes. *J. Gen. Physiol.* **21,** 745–755.
12. Takagi, M., Azuma, K., and Kishimoto, U. (1965) A new method for the formation of bilayer membranes in aqueous solutions. *Annu. Rep. Biol. Fac. Sci. Osaka* **13,** 107–110.
13. Montal, M. and Mueller, P. (1972) Formation of bimolecular membranes from lipid monolayers and a study of their electrical properties. *Proc. Natl. Acad. Sci. USA* **69,** 3561–3566.
14. Danoff, S. K., Supattapone, S., and Snyder, S. H. (1988) Characterisation of a membrane protein from brain mediating the inhibition of inositol 1,4,5-trisphosphate receptor-binding by calcium. *Biochem. J.* **254,** 701–705.
15. Bezprozvanny, I. and Ehrlich, B. E. (1993) ATP modulates the function of inositol 1,4,5 trisphosphate-gated channels at two sites. *Neuron* **10,** 1175–1184.
16. Bezprozvanny, I., Watras, J., and Ehrlich, B. E. (1991) Bell-shaped calcium response curves for the Ins(1,4,5)P_3- and calcium-gated channels from endoplasmic reticulum. *Nature* **351,** 751–754.
17. Bezprozvanny, I. and Ehrlich, B. E. (1994) Inositol 1,4,5-trisphosphate ($InsP_3$)-gated Ca channels from cerebellum: Conduction properties for divalent cations and regulation by intraluminal calcium. *J. Gen. Physiol*. **104,** 821–856.
18. Ferris, C. D., Huganir, R. L., Supattapone, S., and Snyder, S. H. (1989) Purified inositol 1,4,5-trisphosphate receptor mediates calcium flux in reconstituted lipid vesicles. *Nature (Lond.)* **342,** 87–89.
19. Nakade, S., Rhee, S. K., Hamanaka, H., and Miksohiba, K. (1994) Cyclic AMP-dependent phosphorylation of an immunoaffinity-purified homotetrameric inositol 1,4,5-trisphosphate receptor (Type I) increases Ca^{2+} flux in reconstituted lipid vesicles. *J. Biol. Chem.* **269,** 6735–6742.

16

Continuous Fluorescent Monitoring of Cellular Calcium Fluxes

A Novel Perfusion System for the Investigation of Inositol(1,4,5)trisphosphate-Dependent Quantal Calcium Release Using Immobilized, Electropermeabilized Cells

Robert A. Wilcox and James Strupish

1. Introduction

Inositol(1,4,5)trisphosphate [Ins(1,4,5)P_3] is a well-characterized second messenger that interacts specifically with a family of Ins(1,4,5)P_3 receptor–operated Ca^{2+} channels to mobilize nonmitochondrial intracellular Ca^{2+} stores ***(1)***. Ins(1,4,5)P_3-induced Ca^{2+} mobilization (IICM) exhibits fascinating biphasic kinetics, whereby suboptimal concentrations of Ins(1,4,5)P_3 ***(2)*** induce a rapid release of only a fraction of the total Ins(1,4,5)P_3-sensitive Ca^{2+} pool, followed by a prolonged phase of slow Ca^{2+} efflux, with no significant further Ca^{2+} release until additional Ins(1,4,5)P_3 is added. This widespread phenomenon (reviewed in **refs. *3–5***) has been labeled "quantal Ca^{2+} release" (QCR) ***(2,6)*** or "incremental detection" ***(7)*** and directly contrasts with the behavior of other agents that mobilize intracellular Ca^{2+} stores. For example, suboptimal concentrations of ionophores such as ionomycin exhibit slower Ca^{2+} efflux, which nevertheless ultimately produces the same net release as maximally effective concentrations ***(8)***.

The authors have recently utilized a unique approach to investigate both incremental activation and inactivation of the Ins(1,4,5)P_3 receptor in SH-SY5Y human neuroblastoma cells during IICM ***(9)***. Continuous perfusion of immobilized electropermeabilized SH-SY5Y cells with Ins(1,4,5)P_3 and other Ca^{2+}-mobilizing inositol polyphosphates has allowed assessment of the effect of sustained stimulation, under conditions in which Ca^{2+} released from the intracellular stores

From: *Methods in Molecular Biology, Vol. 114: Calcium Signaling Protocols*
Edited by: D. G. Lambert

was perfused away from the cells and continuously monitored fluorometrically downstream. Using this system, the authors obtained experimental evidence in perfused SH-SY5Y cells supporting the hypothesis ***(10)*** that Ins(1,4,5)P_3 may intrinsically and directly activate and then inhibit the Ca^{2+} conductance of its receptor to produce QCR ***(9)***.

Continuous perfusion of immobilized, electropermeabilized cells with Ins(1,4,5)P_3 represents a unique approach for the assessment of incremental activation and inactivation events during Ins(1,4,5)P_3-induced QCR. The continuous perfusion of cells with Ins(1,4,5)P_3 offers several advantages over fixed volume cuvet-based fluorometric assays and $^{45}Ca^{2+}$ labeling and release assays. The continuous perfusion supplies fresh ATP, metabolic fuel, and Ins(1,4,5)P_3 (at a given concentration). Among the most pertinent features of this technique is that Ca^{2+} released from stores is perfused away from the immobilized cells. Consequently, a secondary steady-state Ins(1,4,5)P_3-dependent Ca^{2+} release can be observed in the absence of gross feedback by the initial peak of Ca^{2+} release, and without the use of high concentrations of Ca^{2+} chelators such as EGTA and BAPTA. Significantly, the assay described herein for monitoring inositol polyphosphates-induced Ca^{2+} fluxes in permeabilized SH-SY5Y cells can be readily modified for other cell types and for testing a wide range of different Ca^{2+}-mobilizing agents. Indeed, the basic concept of perfusion of immobilized and permeabilized cells may also be more generally applicable to the investigation of other cellular phenomena.

2. Materials

2.1. Reagents

1. Ultrapure H_2O is derived from a specialist unit (e.g., Millipore, Watford, Herts, UK). All solutions are prepared in plasticware and always using ultrapure water. Glass leaches significant concentrations of ions into aqueous solutions, particularly Ca^{2+}; consequently, the use of glassware should be avoided, especially for storage of solutions.
2. The fluorescent calcium chelating dyes fura-2–free acid and fluo-3–free acid (Calbiochem-Novabiochem, Nottingham, Notts, UK; Molecular Probes, Eugene, OR) are prepared as 0.5- or 1-m*M* stock solutions in H_2O, and are distributed into 10-, 20-, and 50-µL aliquots and stored at < –20°C protected from light in an aluminum foil–covered container. Fluo-3 exhibits a fluorescence at resting cellular [Ca^{2+}] (100–200 n*M*), and increases 5–10-fold (>1 µ*M*) following stimulation of Ca^{2+} release from intracellular stores ***(11)***. Indeed, fluo-3 has recently been used to successfully monitor Ca^{2+} release from many types of permeabilized cells ***(7,12–14)*** and cerebellar microsomes ***(15)*** (*see* **Notes 1** and **2**).
3. Ca^{2+} calibration top stocks are used for the determination of the F_{max} (fluorescence at saturating [Ca^{2+}]) and F_{min} (fluorescence at zero [Ca^{2+}]) values of fura-2 and fluo-3. F_{max} is determined with a 1/400 dilution of 200 m*M* $CaCl_2$ (0.5 m*M*

final), which will fully Ca^{2+} saturate both fluorescent dyes. For F_{min} a 1/100 dilution of 400 m*M* EGTA/400 m*M* KOH (pH 7.2) (4 m*M* final) essentially chelates all available Ca^{2+}. The 400 m*M* EGTA/400 m*M* KOH (pH 7.2) solution will require sonication for solubilization of the EGTA. Alternatively a 1/100 dilution of 400 m*M* BAPTA (pH 7.2) will more efficiently and rapidly chelate Ca^{2+}. BAPTA (Molecular Probes and Calbiochem) readily solubilizes in H_2O, but a fresh stock must be made every 7 d. All solutions are stored at 4°C, between use.

4. Ca^{2+} buffering stocks: EGTA (10 m*M*/20 m*M* KOH, pH 7.2) or BAPTA (10 m*M* aqueous solution, pH 7.2) are prepared via aqueous 1/40 dilution from the above 400-m*M* stocks (*see* **Subheading 2.1.3.**).
5. Nylon mesh, 40-µm pore size (Plastok Associates, Wirral, UK), is used to prevent passage of permeabilized cells and to filter BAPTA- and Chelex-100 beads from the treated inositol polyphosphate solution.
6. Glass wool (Fluka, Chemika-Bio-Chemika, Gillingham, Dorset, UK).
7. Concentrically luered 2-mL disposable polypropylene syringes (Scientific Industries, Loughborough, Leicestershire, UK).
8. HEPES-buffered saline (HBS)-EDTA solution for removal of adherent cells: 0.02% (w/v) Na_2EDTA, 0.9% (w/v) NaCl, and 20 m*M* HEPES-free acid, adjusted to pH 7.2–7.4 using 20% (w/v) NaOH. Repeated exposure to this solution is also utilized to extract divalent cations from the glass wool.
9. Adenosine 5'-trisphosphate disodium salt ($Na_2 \cdot$ ATP; Grade 1, Sigma A-2383, Poole, Dorset, UK).
10. Cytosol-like buffer (CLB) stock is prepared as a fivefold stock solution in ultrapure H_2O, to yield final concentrations of 120 m*M* KCl, 2 m*M* KH_2PO_4, 5 m*M* $(CH_2COONa)_2{\cdot}6H_2O$, 2 m*M* $MgCl_2{\cdot}6H_2O$ and 20 m*M* HEPES-free acid. Since the ATP required is relatively unstable in alkaline solutions, the working CLB solution is prepared just prior to use and adjusted to pH 7.2, at 22°C, with 20% (w/v) KOH (*see* **Note 3**).
11. Oligomycin (Sigma) 5 mg/mL solution is made in ultrapure ethanol; this acts to exclude Ca^{2+} uptake into the mitochondrial pool. However, the addition of oligomycin is not critical for experiments in which $[Ca^{2+}] < 1$ µ*M*, since mitochondrial Ca^{2+} uptake ($K_m \sim 2$–10 µ*M*) is minimal ***(16)***. Energized mitochondria have a critical physiological role in reversibly buffering high concentrations of released Ca^{2+}, and thus protect against Ca^{2+}-mediated cytotoxicity ***(17,18)***. In preliminary experiments, oligomycin and other mitochondrial inhibitors are found to accelerate the loss of cell viability. Thus, most of the authors' experiments are conducted without oligomycin, and owing to the presence of sodium succinate in the CLB, the energized mitochondrial ATP will endogenously regenerate ATP.
12. 0.4% Azur A (Fluka) stock in ATP-free CLB, pH 7.2.
13. $Ins(1,4,5)P_3$ (CellSignals, Lexington, KY; Semat Technical [RBI], St. Albans, Herts, UK), L-*myo*-inositol(1,4,5)trisphosphate [L-$Ins(1,4,5)P_3$] (Sigma) are prepared as 1–5-m*M*, 20-µL aqueous stock solutions. Aqueous stocks of all stimulating inositol polyphosphates are pretreated with Chelex-100 (Bio-Rad, Hemel Hampstead, Herts, UK) to chelate divalent cations and then with BAPTA-based

polystyrene-immobilized "Ca^{2+}-sponge" (Molecular Probes) to specifically remove contaminating Ca^{2+} (*see* **Notes 4** and **5**).

2.2. Equipment

1. Fluorescence spectrophotometer (fluorimeter) with variable excitation and emission optics, ideally with a chart recorder or computer interface for fluo-3 experiments. The authors utilize the model LS50β fluorimeters (Perkin-Elmer, Beaconsfield, Bucks, UK), which allow large variations in the selection of wavelengths and excitation and emission slit widths, thus allowing fluorescent measurements to be made over a large dynamic range.
2. Benchtop microcentrifuge with a capacity for 24 standard 1.5-mL microcentrifuge tubes (Heraeus, Germany, and Desaga, Sarstedt-Gruppe, Germany).
3. Electroporator (Gene-Pulser, Bio-Rad).
4. IBM 486/586 PC or compatible computer. The Perkin-Elmer FLDM (fluorescence data manager) software is used to run the fluorimeter. Raw fluorescence data is exported to the spreadsheet program Excel version 5 (Microsoft, Hanslow, Middlesex, UK), then subsequently to the scientific graphing program Origin version 3.5 (Microcal Software, Northampton, MA). Many other similar data manipulation and graphics programs are available.
5. Gilson Minipuls peristaltic pump and tubing (Anachem, Luton, Beds, UK).

3. Methods

3.1. Preparation of Ca^{2+}-Free Stock Solutions

1. The most critical consideration is the reduction of Ca^{2+} contamination during the preparation of all solutions, especially CLB. Reagents used must be of the highest purity available, especially divalent metal salts such as $MgCl_2 \cdot 6H_2O$, since low purity preparations contain significant calcium ion contamination. Ultrapure water is essential and all solutions must be prepared and stored in plastic containers—never glass (*see* **Subheading 2.1.**, **items 1** and **10**).
2. Ca^{2+}-mobilizing agents are prepared as 100- or 1000-fold stocks in H_2O, and checked for Ca^{2+} contamination in fluo-3 CLB or fura-2–supplemented CLB, since when conducting fluo-3 experiments, Ca^{2+} contamination can be misinterpreted as Ca^{2+} release. Stock solutions can be readily pretreated to remove Ca^{2+} contamination with solid phase Ca^{2+} chelating agents (**Subheading 2.1.**, **item 13**) (*see* **Note 4**).

3.2. Preparation of CLB Working Solutions and Buffering of Ca^{2+}

1. The fivefold CLB stock (1 vol) is added to a container with preweighed Na_2·ATP (2 m*M* final), and this is diluted to 5 vol with H_2O and the pH (~5.2) corrected to 7.2 using 20% (w/v) KOH and 1 m*M* HCl. Usually 50- and 100-mL volumes are used and made fresh every 3 to 4 h.
2. The contaminating-free [Ca^{2+}] in the CLB or CLB-R (*see* **Note 3**) is buffered to a final concentration of between 100 and 200 n*M*, by addition of an appropriate aliquot of 10 m*M* EGTA or 10 m*M* BAPTA. Usually 0–20 µL/100 mL of CLB is

utilized (0–2 μ*M* EGTA or BAPTA final). This is initially an iterative process (*see* **step 3**), adding 1 to 2 μL of chelator, assessing the buffer, and then repeating the process if necessary. However, once the approximate Ca^{2+} contamination and required buffering is determined, it should remain stable for a given batch of Na_2·ATP and fivefold CLB stock, assuming the quality of the ultrapure H_2O is maintained.

3. The $[Ca^{2+}]_{free}$ of the CLB is confirmed using a tracer concentration of fura-2 (100 n*M* final) (*see* **step 2**). Briefly a 2-mL sample of EGTA- or BAPTA-buffered CLB is placed in a disposable plastic fluorimeter cuvet (Sarstedt, Leicester, Leicestershire, UK) with 2 μL of 100 μ*M* fura-2. The fluorescent intensity (F_{CLB}) of the buffer is determined in a 2-mL sample of the buffer at excitation and emission wavelengths of 340 and 510 nm, respectively. Recording the resultant *F* values, add 5 μL of the 200 m*M* $CaCl_2$ solution (F_{max}, at $[Ca^2] = 0.5$ m*M* final), followed by 20 μL of 400 m*M* EGTA or BAPTA (F_{min}, at [EGTA] or [BAPTA] = 4 m*M* final) (*see* **Subheading 2.1.**, **item 3**). The $[Ca^{2+}]$ is then calculated from the equation of Grynkiewicz ***(19)***, in which the K_d for fura-2 is approx 139 n*M* at 25°C and 224 n*M* at 37°C:

$$[Ca^{2+}]_{free}\ (nM) = (F_{CLB} - F_{min}/F_{max} - F_{CLB}) \times K_d$$

Ideally the $[Ca^{2+}]_{free}$ should be 100–150 n*M*, certainly <300 n*M*, to avoid significant mitochondrial uptake ***(16)*** and Ca^{2+} inhibition of $Ins(1,4,5)P_3$ receptor responses ***(20)***. If it exceeds this, then add more 10 m*M* EGTA or BAPTA stock to the CLB and repeat the procedure.

4. A constant concentration of fluo-3 (0.5 or 1 μ*M*) is added to the CLB (fluo-3 CLB); fluo-3 has a K_d of approx 400 n*M* at 22°C and 864 n*M* at 37°C ***(21)***, and respective excitation and emission wavelengths of 505 and 530 nm. The addition of fluo-3 fails to significantly buffer the existing basal $[Ca^{2+}]$, since the $[Ca^{2+}]$ of fluo-3 CLB was <200 n*M* and fluo-3 has a relatively high K_d of fluo-3 even at room temperature (*see* **Note 6**).
5. Typically, $[Ca^{2+}]_{free}$ is 100–200 n*M* in fluo-3 CLB supplemented with 0.5–1 μ*M* fluo-3 at 22 °C as calculated via the Grynkiewicz equation ***(19)***. The calibration procedure involves preparation of 5-mL volumes of "F_{max}-fluo-3 CLB" and "F_{min}-fluo-3 CLB" solutions. These are produced by adding 12.5 μL of 200 m*M* Ca^{2+} and 50 μL of 400 m*M* EGTA or BAPTA to 5 mL of fluo-3 CLB, respectively. These two 5-mL solutions are passed through the flow cell in succession to obtain the calibrating F_{max} and F_{min} values for fluo-3 CLB (see **Subheading 3.6.**, **step 7**).

3.3. Preparation of the Cell Perfusion Holder and Fluorescence Flow Cell (Fig. 1)

1. The perfusion cell is constructed from a disposable plastic 2-mL syringe with a punched disk of 40-μm nylon mesh (Plastok Associates) placed in its base. Initially glass wool is very tightly packed down into a 0.1-mL volume, then it is loosely packed into a 400-μL volume.
2. These packed syringes are washed once with 5 mL of HBS-EDTA solution (*see* **Subheading 2.1.**, **item 8**), and submerged in plastic beakers for 30 min. The

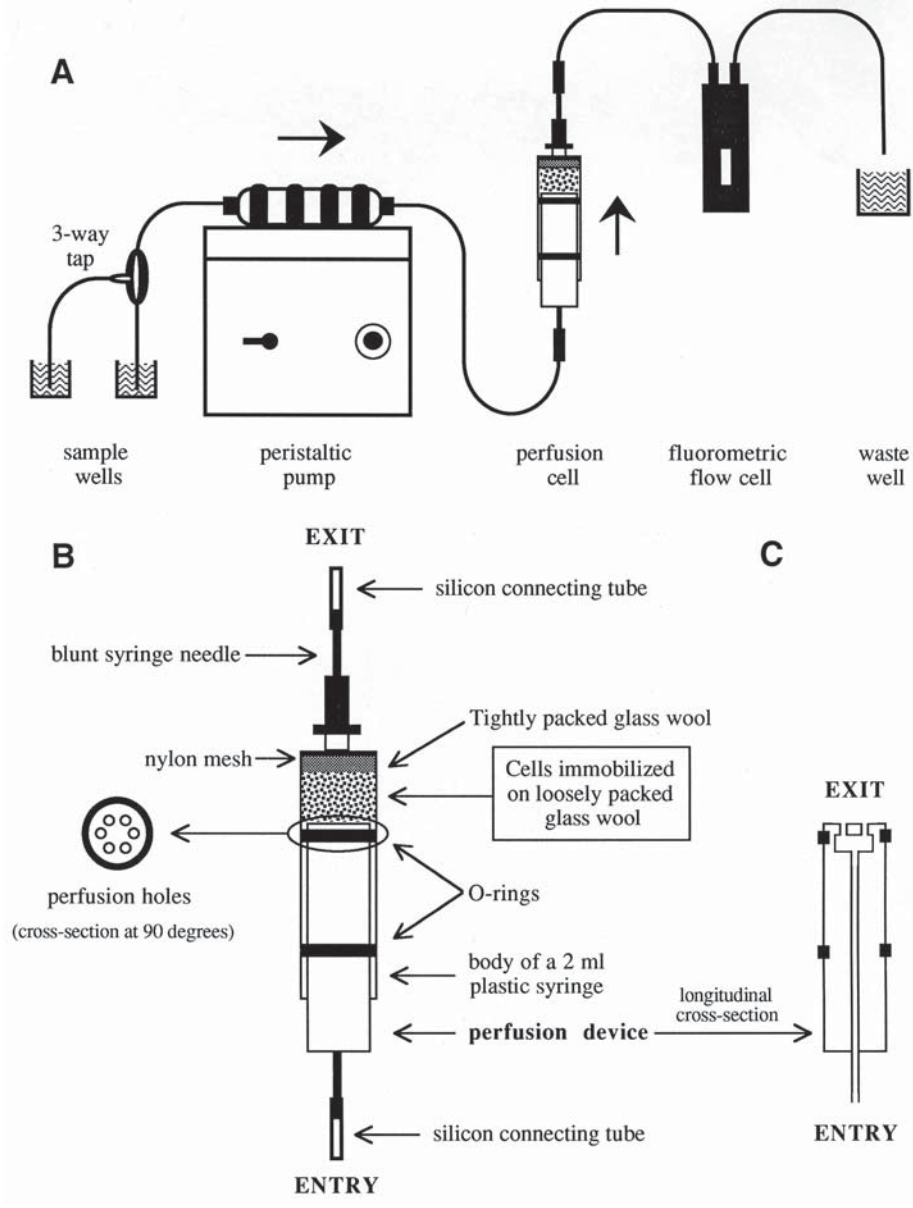

Fig. 1. The perfusion and fluo-3 fluorometric flow cells. (A) The experimental setup for fluo-3 monitoring of Ca^{2+} fluxes in perfused, electropermeabilized cells, showing the direction of perfusion. (B) The perfusion cell shown in detail. Note that the electropermeabilized SH-SY5Y neuroblastoma cells are immobilized on the loosely packed glass wool and trapped in the cell by the tightly packed glass wool and the nylon mesh. (C) Longitudinal cross-section of the perfusion device.

glass wool tends to trap air bubbles during this procedure. This trapped air is extracted from the glass wool by backfilling the syringe halfway with HBS-EDTA solution, inserting the syringe plunger, then placing a gloved fingertip over the luer opening, and rapidly pulling the syringe plunger backward. This in turn creates a negative pressure that extracts the air bubbles and allows the HBS-EDTA solution complete access to the surface area of the packed glass wool, ensuring that the EDTA solution can extract all the divalent cations from the glass wool. Once the perfusion process starts, first the fluo-3 CLB and then the cells become evenly distributed throughout the surface area of the wetted glass wool. After all the bubbles are extracted, the plunger is removed and the packed syringe is submerged and left to soak in 30 mL of EDTA solution overnight (*see* **Note 7**).

3. The perfusion cell is assembled as follows. With the syringe full of HBS-EDTA solution, insert the constructed perfusion device (*see* **Note 8**) avoiding trapped bubbles until it abuts the glass wool. The perfusion device is connected with orange/orange tubing to a Minipuls perfusion pump, the perfusate is evenly distributed over the glass wool via six ports, and after flowing through the glass wool is directed via a blunted 21 G needle into a compact 200 µL-fluorometric cell (3-mm path length, Suprasil I windows, Hellma, UK). The assembled cells are extensively perfused with ultrapure H_2O and then fluo-3 CLB until a stable fluorescent baseline equivalent to approx 100–200 n*M* $[Ca^{2+}]$ is obtained.

3.4. Electropermeabilization of Cells

1. The authors routinely utilize electropermeabilization (***22***) or the cholesterol-specific detergents saponin (***23***) and β-escin (***24***) to produce Ins(1,4,5)P_3-responsive permeabilized cells. Both of these methods require empirical determination of optimal conditions for each cell type used. The DNA dye Azur A (0.05% [w/v] in ATP-free CLB [pH 7.2] diluted 1/1 in CLB containing a sample of cells) is used to quantify permeabilization, since it is excluded from intact cells but specifically stains the nucleus of permeabilized cells blue. The authors obtain >99% Azur A–stained SH-SY5Y neuroblastoma cells when permeabilized with 20–100 µg/mL of saponin or β-escin, or via optimized electropermeabilization.
2. Electropermeabilization of SH-SY5Y cells in 0.8-mL vol is accomplished in a Gene-Pulser using 3–12 discharges of a 3-µF capacitor with a field strength of 1.5 kV/cm and time constant of 0.1 ms. The cells are electroporated in four 0.8-mL batches using ten 1.5-kV discharges of a 3-µF capacitor. Populations of SH-SY5Y cells electroporated in this manner are >99% permeable to vital dyes such as trypan blue and Azur A and do not reseal (*see* **Note 9**).

3.5. Use of Fluo-3 to Assess Ca^{2+} Uptake and Ins(1,4,5)P_3-Mediated Ca^{2+}-Release

1. SH-SY5Y human neuroblastoma cell monolayers (passage 70–90) (initially a gift from Dr. J. L. Biedler, Sloane-Kettering Institute, New York) are subcultured 1/5 to 1/10 weekly and grown in minimal essential media supplemented with 10% (v/v) newborn calf serum, 1% fetal calf serum, and 100 IU/mL penicil-

lin, 100 µg/mL of streptomycin and 2.5 µg/mL of fungizone (Gibco, Paisley, Renfrewshire, UK), as described ***(25)***. SH-SY5Y neuroblastoma cells are utilized since they are particularly responsive to Ins(1,4,5)P_3, have a large Ins(1,4,5)P_3-sensitive calcium pool, and the structure-function requirements of their IICM have been extensively characterized using an extensive range of Ins(1,4,5)P_3 analogues ***(13,26)***. Western blot analysis of SH-SY5Y membrane preparations, using Ins(1,4,5)P_3 receptor subtype-specific antibodies, has shown that they predominantly express the type 1 Ins(1,4,5)P_3 receptor ***(32)***, very low levels of type 2 Ins(1,4,5)P_3 receptor, and no detectable type 3 Ins(1,4,5)P_3 receptor ***(33)***. In addition, chronic carbachol pretreatment of SH-SY5Y cells can be used to efficiently downregulate the type 1 Ins(1,4,5)P_3 receptor while leaving (sarcoplasmic-endoplasmic reticulum Ca^{2+}-ATPase (SERCA) pump expression unaffected ***(32)***.

2. Two flasks of postconfluent SH-SY5Y human neuroblastoma monolayers (175-cm^2 flask) are washed once and then harvested using the HBS-EDTA solution. The cells are centrifuged (500*g*, 1 min), and the pellet is resuspended and centrifuge washed twice in 5-mL of fluo-3 CLB (500*g*, 1 min).
3. The supernatant is discarded, and the cells are resuspended in 4 mL of fluo-3 CLB at an approximate cell density of $4.5–9 \times 10^6$ cells/mL. For SH-SY5Y cells, this corresponds to 1.5–2.4 mg/mL of protein ***(34)***, or a cellular DNA content of approx 245–560 µg/mL ***(35)***.
4. Cells are then electroporated (*see* **Subheading 3.4.**, **step 2**) in five 0.8-mL volumes made up to a final volume of 5 mL and loaded into the perfusion cells as described below.

3.6. Loading Permeabilized Cells into the Perfusion Cell (Fig. 1)

1. The prepared flow cell is set up in two orientations the first for loading of the cells on the glass wool and the other for the long-term perfusion studies. Electropermeabilized SH-SY5Y cells (5 mL) are gently loaded directly via Minipuls gray/gray tubing through the perfusion device onto the glass wool of the flow cell using gentle negative pressure from the Minipuls peristaltic pump located at the syringe end of the cell. Throughout this procedure, the flow through the perfusion cell is vertically downward to assist the percolation of the cells into the loosely packed glass wool layer, and the cells are then retained by the tightly packed glass wool layer and the underlying 40-µm nylon mesh (**Fig. 1**).
2. Once the electropermeabilized cells are loaded, they are washed for 5 min with fluo-3 CLB. The peristaltic pump is then stopped and the flow cell reoriented for vertically upward perfusion driven by positive pressure from the peristaltic pump.
3. The experimental setup consists of two sample wells, the perfusion pump, the perfusion cell, the fluorescent flow cell, and the waste collection well, arranged in series (**Fig. 1**). The perfusion rate throughout is 0.5 mL/min, and the dead volume of the entire assembled system is 0.5 mL. Sample changes are accomplished without significant disruption of the perfusion process, using dual sample intakes and three-way taps. Thus, the electropermeabilized cells are continuously

exposed to fresh ATP and fluo-3 in the fluo-3 CLB, whereas the concentration of stimulating Ins(1,4,5)P_3 (or inositol polyphosphates) is seamlessly and reversibly increased or decreased in the incoming perfusate. Indeed, this reversible exposure to Ins(1,4,5)P_3 is virtually impossible to perform using standard experimental approaches in fixed volumes of buffer with permeabilized cells either attached to culture plates or in suspension (*see* **Note 10**).

4. Although SH-SY5Y cells exhibit quantal Ca^{2+} mobilization at 22°C and 37°C ***(13,30,31)***, experiments are conducted at 22°C rather than 37°C, because at 37°C buffer, ATP more rapidly decomposes, cells lose viability more rapidly, and the K_d of fluo-3 (864 n*M* at 37°C ***[21]***) makes the dye relatively insensitive to Ca^{2+} concentration changes below 500 n*M*. However, theoretically it should be possible to perform the entire assay at 37°C in a constant temperature room.
5. The Ca^{2+} content of the fluo-3 CLB perfusate is continually monitored in the 200-µL fluorescence flow cell that was placed in an LS-50β fluorimeter (Perkin-Elmer). Fluorescence intensity of the perfusing fluo-3 CLB is collected by both a chart recorder and an interfaced computer at 1-s intervals with excitation at 505 nm (5–7-nm slit width) and emission collected at 530 nm (5–7-nm slitwidth).
6. Once a stable baseline is obtained cells are exposed to stimulating concentrations of Ins(1,4,5)P_3 and other Ca^{2+}-mobilizing inositol polyphosphates. **Figure 2** is a typical example of the quality of data produced using this assay system. The experimental application of this technique to the investigation of Ins(1,4,5)P_3-dependent QCR is fully described elsewhere ***(9)***.
7. The fluorescence intensity values are calibrated (*see* **Subheading 3.2., step 5**) by assuming a K_d for fluo-3 of 400 n*M* at 22°C and F_{max} and F_{min} values by sequentialy passing the pre-prepared "F_{max}-fluo-3 CLB" (5 mL) and "F_{min}-fluo-3 CLB" (5 mL). The large data sets of collected fluorescent intensity values are then converted to estimated free Ca^{2+} values using Excel version 5 and then graphed using Origin version 4.1.

4. Notes

1. Recent batches of Molecular Probes fluo-3 have been found to give a significantly more intense signal than that supplied by Calbiochem.
2. Where practical, all fluorescent dye stocks, and solutions containing fluorescent dyes, are protected from light by covering storage containers with aluminum foil.
3. Alternatively ATP levels can be maintained with an ATP-regeneration system consisting of CLB (*see* **Subheading 2.1., item 10**) supplemented with a reduced $Na_2 \cdot$ ATP concentration (1 m*M*), creatine phosphokinase type 1 (10 µg/mL final, EC 2.7.3.2, Sigma C-3755), and phosphocreatine (10 m*M* final, Sigma P-6915); this is designated "CLB-R." Creatine phosphokinase and phosphocreatine are made up as 100-fold aqueous stocks, cleaned of Ca^{2+} contamination with Chelex-100, and added 1/100 to the CLB-R. The CLB-R is corrected to pH 7.2 before these additions and rechecked after. Since mitochondrial inhibitors are excluded from most of the authors' experiments (*see* **Subheading 2.1., item 11**), use of an exogenous ATP-regeneration system is generally considered redundant, because

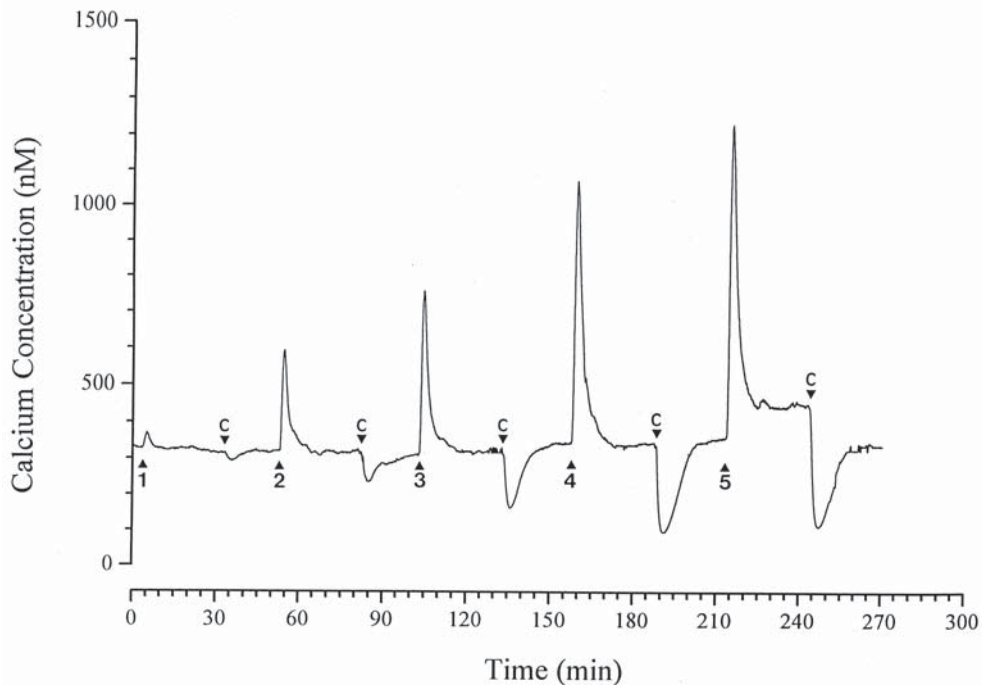

Fig. 2. The Ca^{2+} mobilization profile in immobilized, electropermeabilized SH-SY5Y human neuroblastoma cells to increasing concentrations of Ins(1,4,5)P_3, in which the intracellular Ca^{2+} stores are allowed to replete in Ins(1,4,5)P_3-free fluo-3 CLB between Ins(1,4,5)P_3 doses. Cells perfused with fluo-3 CLB are exposed to increasing concentrations of Ins(1,4,5)P_3 for 30 min (▲ 1 = 0.1 μ*M*; ▲ 2 = 0.3 μ*M*; ▲ 3 = 1 μ*M*; ▲ 4 = 3 μ*M*; ▲ 5 = 10 μ*M*). Following each dose of Ins(1,4,5)P_3, the cells are perfused with fluo-3-CLB for 20 min (▼ C), allowing them to replenish their Ca^{2+} stores. This is a representative trace of three qualitatively identical experiments.

the energized mitochondria are expected to endogenously regenerate ATP. Both CLB and CLB-R solutions can be stored at 4°C prior to use to reduce ATP degradation and to discourage the growth of microorganisms (*see* **Note 11**).

4. Treatment is repeated until the final concentration of contaminated [Ca^{2+}] is < 10 n*M* at the highest final inositol polyphosphate concentration (10 μ*M*) solubilized in control CLB. Small columns containing 10–20 mg of Chelex-100 or BAPTA "sponge" are utilized to remove divalent cation contamination. These are made from disposable 250-μL yellow tips or 1000-μL blue tips with a retaining filter in their base made from the 40-μm nylon mesh (Plastok Associates). Alternatively, small volumes of known aqueous stock concentrations of inositol polyphosphates (<40 μL) are "cleaned" by treatment with 5–10 mg of Chelex-100 or BAPTA "sponge" in microcentrifuge tubes. The tubes are then vortexed for 60 s, centrifuged (13,000*g*, 1 min at 4°C), and the supernatant harvested and transferred to a fresh tube. Centrifugation of the harvested supernatant is repeated until no chelat-

ing beads pellet. Although 5–10% of the volume of the aqueous stock solution is lost using this treatment, the authors have treated a wide range of inositol polyphosphates with these chelators and have detected no loss of compound owing to adsorption.

5. Synthetic Ins(1,4,5)P_3 from Cell Signals is of very high purity and is relatively inexpensive. Their E-mail address is CellSignal@.aol.com.
6. Because of its relatively high K_d for Ca^{2+} at 22°C (400 n*M*), fluo-3 measures [Ca^{2+}] below 200 n*M* relatively inaccurately; however, it has the advantage of not saturating until micromolar [Ca^{2+}] are attained. Unfortunately, the use of fluo-3 is not ideal for experiments involving caffeine, since this Ca^{2+}-mobilizing agent potently quenches fluo-3 fluorescence in a dose-dependent fashion. Indeed, it is crucial to pretest all experimental agents in fluo-3 CLB for both Ca^{2+} contamination and fluorescence quenching or enhancement, to avoid the production of artifactual fluorescence intensity data.
7. The overnight soak in HBS-EDTA is an essential step to remove all divalent cations. Generally the authors soak these for 48–72 h with 30 mL of fresh HBS-EDTA every 24 h.
8. The cylindrical perfusion device is machined from polycarbonate to fit just loosely inside a 2-mL syringe body. Two grooves are countersunk to house two silicon O-rings; these act to very tightly seal the perfusion device inside the syringe body. Plumber's tape (available from any hardware store) is also often used in front of the leading O-ring to improve the seal. Initially a 1-mm-diameter hole is concentrically drilled along the longitudinal axis of the machined cylinder. A second 5-mm deep × 5-mm diameter hole is countersunk at the leading edge with a square router bit, using the first hole as a guide. A stainless steel tube (1-mm outer diameter, 0.5-mm inner diameter) is then passed through the first hole until it reaches the lower base of the second countersunk hole and is glued into place. A disk (5-mm diameter × 3 mm depth) with six 0.4-mm-diameter holes drilled evenly over its surface is then glued into the top of the second countersunk hole. This creates a small 2-mm deep × 5-mm diameter well between the stainless steel delivery tube and the six holes through which the perfusate is distributed (*see* **Fig. 1B**,**C**). (The perfusion device is constructed by Mr. David Jones in the Biological Sciences workshop at the University of Leicester.)
9. Electropermeabilization is rapid and efficiently generates plasma membrane pores, which allow free passage of inositol polyphosphates and, unlike detergents, does not interfere with the Bradford protein assays ***(34)***. Under some conditions, the process can generate significant concentrations of Al^{3+} from the disposable cuvets used, and this may affect cellular metabolism of inositol polyphosphates ***(36)***. However, in these experiments any generated Al^{3+} should be removed in the perfusate, and because electropermeabilized SH-SY5Y neuroblastoma cells proved to be more robust in these studies, electropermeabilization is favored.
10. When interpreting the Ca^{2+} flux traces produced by the perfusion of electropermeabilized cells, it is crucial to recognize that the fluo-3 CLB perfusion buffer

can act as both a source of Ca^{2+} for uptake and a sink for Ca^{2+} released from the stores. This will depend largely on the activation state of the Ins(1,4,5)P_3 receptor and the filling state of the intracellular Ca^{2+} stores. That is, perfusion either can remove released Ca^{2+} or deliver Ca^{2+} to the intracellular stores; thus, the absolute amount of Ca^{2+} available to the cells can change. This contrasts with fixed volume cuvet and tube assay systems, in which the absolute amount of Ca^{2+} in the system remains constant at all times.

11. Experiments using the specific SERCA pump inhibitors, such as thapsigargin and cyclopiazonic acid, are possible, but the effects of these reagents are not completely reversible on washout. Thapsigargin, in particular, irreversibly inhibited the SERCA pumps and avidly adsorbed to the flow cells and pump tubing. In addition, this contamination could only be removed by extensive acid washing. The hexokinase-quench technique, which rapidly removes buffer ATP to inhibit SERCA pumps, has been used successfully with this assay system ***(9)***.

Acknowledgments

This chapter is dedicated to the staff of the Glenfield Hospital Orthopaedic Ward 23, especially the "red" nursing team, under whose excellent care R. A. W. found time to write this article.

References

1. Berridge, M. J. (1993) Inositol trisphosphate and calcium signaling. *Nature* **361,** 315–325.
2. Muallem, S., Pandol, S. J., and Beeker, T. G. (1989) Hormone-evoked release from intracellular stores is a quantal process. *J. Biol. Chem.* **264,** 205–212.
3. Taylor, C. W. and Richardson, A. (1991) Structure and function of inositol trisphosphate receptors. *Pharmacol. Ther.* **51,** 79–104.
4. Taylor, C. W. and Marshall, I. C. B. (1992) Calcium and inositol 1,4,5-trisphosphate receptors: a complex relationship. *Trends Biol. Chem. Sci.* **17,** 403–407.
5. Taylor, C. W. and Traynor, D. (1995) Calcium and inositol trisphosphate receptors. *Membr. Biol.* **145,** 109–118.
6. Irvine, R. F. (1990) 'Quantal' Ca^{2+} release and the control of Ca^{2+} entry by inositol phosphates—a possible mechanism. *FEBS Lett.* **263,** 5–9.
7. Meyer, T. and Stryer, L. (1990) Transient calcium release induced by successive increments of inositol 1,4,5-trisphosphate. *Proc. Natl. Acad. Sci. USA* **87,** 3841–3845.
8. Taylor, C. W. and Potter, B. V. L. (1990) The size of the inositol 1,4,5-trisphosphate sensitive Ca^{2+} stores depends on inositol 1,4,5-trisphosphate concentration. *Biochem. J.* **266,** 189–194.
9. Wilcox, R. A., Strupish, J., and Nahorski, S. R. (1996) Quantal calcium release in electropermeabilized SH-SY5Y neuroblastoma cells perfused with *myo*-inositol 1,4,5-trisphosphate. *Cell Calcium* **20,** 243–255.
10. Hajnóczky, G. and Thomas, A. P. (1994) The inositol trisphosphate calcium channel is inactivated by inositol trisphosphate. *Nature* **370,** 474–477.

11. Haugland, R. P. (ed.) (1992) *Molecular Probes: Handbook of Fluorescent Probes and Research Chemicals*, (Larison, K. D., ed.) Molecular Probes, Eugene, OR.
12. Missiaen, L., Taylor, C. W., and Berridge, M. J. (1991) Spontaneous calcium release from inositol trisphosphate-sensitive calcium stores. *Nature* **352,** 241–244.
13. Wilcox, R. A., Safrany, S. T., Lampe, D., Mills, S. J., Nahorski, S. R., and Potter, B. V. L. (1994) 2-position modification of *myo*-inositol 1,4,5-trisphosphate produces inositol tris- and inositol tetrakisphosphates with potent biological activities. *Eur. J. Biochem.* **223,** 115–124.
14. Wilcox, R. A., Strupish, J., and Nahorski, S. R. (ed.) (1995) Measurement of Ca^{2+} fluxes in permeabilized cells using $^{45}Ca^{2+}$ and fluo-3, in *Methods in Molecular Biology. Signal Transduction Protocols* (Kendall, D. A. and Hill, S. J., eds.), Humana Press, Totowa, NJ, pp. 215–227.
15. Michelangeli, F. (1991) Measuring calcium uptake and inositol 1,4,5-trisphosphate-induced calcium release in cerebellum microsomes using fluo-3. *J. Fluorescence* **1,** 203–206.
16. Carafoli, E. (1987) Intracellular calcium homeostasis. *Annu. Rev. Biochem.* **56,** 395–433.
17. Gunter, T. E., Gunter, K. K., Sheu, S.-S., and Gavin, C. E. (1994) Mitochondrial calcium transport: Physiological relevance. *Am. J. Physiol.* **267,** C313–C339.
18. Sparangna, G. C., Gunter, K. K., Sheu, S., and Gunter, T. E. (1995) Mitochondrial calcium uptake from physiological-type pulses of calcium. *J. Biol. Chem.* **270,** 27510–27515.
19. Grynkiewicz, G., Poenie, M., and Tsien, R. Y. (1985) A new generation of Ca^{2+} indicators with greatly improved fluorescent properties. *J. Biol. Chem.* **260,** 3440–3449.
20. Danoff, S. K., Suppattapone, S., and Snyder, S. H. (1988) Characterization of a membrane protein from brain mediating the inhibition of inositol 1,4,5-trisphosphate receptor binding by calcium. *Biochem. J.* **254,** 701–705.
21. Merritt, J. E., McCarthy, S. A., Davies, M. P. A., and Moores, K. E. (1990) Use of fluo-3 to measure cytosolic Ca^{2+} in platelets and neutrophils. *Biochem. J.* **269,** 513–519.
22. Knight, D. E. and Scrutton, M. C. (1986) Gaining access to the cytosol: The technique and some applications of electropermeabilization. *Biochem. J.* **234,** 497–506.
23. Strupish, J., Cooke, A. M., Potter, B. V. L., Gigg, R., and Nahorski, S. R. (1988) Stereospecific mobilization of intracellular Ca^{2+} by inositol 1,4,5-triphosphate. *Biochem. J.* **253,** 901–905.
24. Kobayashi, S., Kitazawa, T., Somlyo, A. V., and Somlyo, A. P. (1989) Cytosolic heparin inhibits muscarinic and α-adrenergic Ca^{2+} release in smooth muscle: Physiological role of inositol 1,4,5-trisphosphate in pharmacomechanical coupling. *J. Biol. Chem.* **264,** 17997–18004.
25. Lambert, D. G., Ghataorre, A. S., and Nahorski, S. R. (1989) Muscarinic receptor binding characteristics of a human neuroblastoma SK-N-SH and its clones SH-SY5Y and SH-EP1. *Eur. J. Pharmacol.* **165,** 71–77.
26. Nahorski, S. R. and Potter, B. V. L. (1989) Molecular recognition of inositol polyphosphates by intracellular receptors and metabolic enzymes. *Trends Pharmacol. Sci.* **10,** 139–143.

27. Safrany, S. T., Wojcikiewicz, R. J. H., Strupish, J., McBain, J., Cooke, A. M., Potter, B. V. L., and Nahorski, S. R. (1991) Synthetic phosphorothioate-containing analogues of inositol 1,4,5-trisphosphate mobilize intracellular Ca^{2+} stores and interact differentially with inositol 1,4,5-trisphosphate 5-phosphatase and 3-kinase. *Mol. Pharmacol.* **39,** 754–761.
28. Safrany, S. T., Wilcox, R. A., Liu, C., Potter, B. V. L., and Nahorski, S. R. (1992) 3-Position modification of *myo*-inositol 1,4,5-triphosphate: Consequences for intracellular Ca^{2+} mobilization and enzyme recognition. *Eur. J. Pharmacol.* **226,** 265–272.
29. Safrany, S. T., Wilcox, R. A., Liu, C., Dubreuil, D., Potter, B. V. L., and Nahorski, S. R. (1993) Identification of partial agonists with low intrinsic activity at the inositol 1,4,5-trisphosphate receptor. *Mol. Pharmacol.* **43,** 499–503.
30. Wilcox, R. A., Challiss, R. A. J., Traynor, J. R., Fauq, A. H., Ognayanov, V. I., Kozikowski, A. P., and Nahorski, S. R. (1994) Molecular recognition at the *myo*-Inositol 1,4,5-trisphosphate receptor: 3-position substituted *myo*-inositol 1,4,5-trisphosphate analogues reveal the binding and Ca^{2+} release requirements for high affinity interactions with the *myo*-inositol 1,4,5-trisphosphate receptor. *J. Biol. Chem.* **269,** 26815–26827.
31. Wilcox, R. A., Erneux, C., Primrose, W. U., Gigg, R., and Nahorski, S. R. (1995) 2-hydroxyethyl α-D-glucopyranoside 2,3',4'-trisphosphate, a novel metabolically resistant adenophostin A and *myo*-inositol 1,4,5-trisphosphate analogue potently interacts with the *myo*-inositol 1,4,5-trisphosphate receptor. *Mol. Pharmacol.* **47,** 1204–1211.
32. Wojcikiewicz, R. J. H. (1995) Type I, II and III inositol 1,4,5-trisphosphate receptors are unequally susceptible to down-regulation and are expressed in markedly different proportions in different cell types. *J. Biol. Chem.* **270,** 1–6.
33. Mackrill, J. J., Wilcox, R. A., Miyawaki, A., Mikoshiba, K., and Nahorski, S. R. (1996) Stable overexpression of the type 1 inositol 1,4,5-trisphosphate receptor in L-fibroblasts: subcellular distribution and functional consequences. *Biochem. J.* **318,** 871–878.
34. Bradford, M. M. (1976) A rapid and sensitive method for the quantitation of microgram quantities of protein utilising the principle of protein-dye binding. *Anal. Biochem.* **72,** 248–254.
35. Labarca, C. and Paigen, K. (1980) A simple, rapid and sensitive DNA assay procedure. *Anal. Biochem.* **102,** 344–352.
36. Loomis-Husselbee, J. W., Cullen, P. J., Irvine, R. F., and Dawson, A. P. (1991) Electroporation can cause artefacts due to solubilization of cations from electrode plates: Aluminium ions enhance conversion of inositol 1,3,4,5-tetrakisphosphate into inositol 1,4,5-trisphosphate in electroporated L1210 cells. *Biochem. J.* **277,** 883–885.

17

Measurement of Free [Ca^{2+}] Changes in Agonist-Sensitive Internal Stores Using Compartmentalized Fluorescent Indicators

Aldebaran M. Hofer

1. Introduction

The fact that acetoxymethyl (AM)-ester derivatives of fluorescent Ca^{2+} indicators accumulate not only in the cytoplasm but also in organelles was recognized long ago as a potential source of artifacts during measurements of cytoplasmic [Ca^{2+}] ***(1,2)***. Later it was observed that high-affinity dyes such as fluo-3 and fura-2, normally saturated in the high-[Ca^{2+}] environment of the agonist-sensitive Ca^{2+} store, could register [Ca^{2+}] changes in this compartment under special conditions (e.g., when pools were already partially empty) ***(3–6)***. The propensity of indicators to become compartmentalized was fully exploited, however, when investigators began to use lower affinity probes such as mag-fura-2 ***(7)***, to monitor [Ca^{2+}] changes in the inositol(1,4,5)trisphosphate [Ins(1,4,5)P_3]-sensitive store (a compartment largely accepted to be the endoplasmic reticulum [ER]). Thus, the release and reloading of this organelle with Ca^{2+}, as reported by ER-trapped dye, could be directly visualized in single permeabilized cells with high spatiotemporal resolution ***(8,9)***. This basic approach has been adopted by a number of laboratories to investigate phenomena ranging from Ca^{2+} oscillations ***(10–12)*** to quantal release ***(13–15)***, and the subcellular localization of Ca^{2+} storage sites ***(16–18)***.

This chapter provides a guide for the use of compartmentalized fluorescent dyes to measure free [Ca^{2+}] in the agonist-sensitive internal store of single cells. The basic steps involve incubating cells with the AM-ester derivative of the appropriate dye (resulting in partitioning of the probe in both the cytoplasm and organelles), and then permeabilizing the plasma membrane selectively to

From: *Methods in Molecular Biology, Vol. 114: Calcium Signaling Protocols*
Edited by: D. G. Lambert

Table 1
Indicators that Have Been Used to Measure [Ca^{2+}] in Agonist-Sensitive Internal Stores[a]

Indicator	K_d for Ca^{2+} (μ*M*)	Excitation (nm), emission (nm)	Comments
Mag-fura-2 ("furaptra")	53	345/375 ex., 510 em.	Ratiometric
Mag-fura-5	28	340/380 ex., 510 em.	Ratiometric
Fura-2-ff	35	340/380 ex., 510 em	Ratiometric; available from Teflabs
Mag-indo-1	32	351 ex., 405/485 em.	Ratiometric (emission)
Mag-fura-red	17	488 ex., 630 em.	Fluorescence decreases on Ca^{2+} binding
Fluo-3-ff	41	515 ex., 530 em.	Available from Teflabs; fluorescence increases on Ca^{2+} binding
Oregon Green BAPTA-5N	20	492 ex., 521 em.	Excited efficiently by 488-nm laser line; fluorescence increases on Ca^{2+} binding

Dyes are available from Molecular Probes unless otherwise noted.

release the fluorophore from the cytoplasm. Fluorescence of organelle-trapped indicator is then monitored as for the cytoplasm (*see* Chapters 2–4). On completion of the experiment, a calibration can be performed to convert fluorescence into approximate values of intraluminal [Ca^{2+}]. Other methods for eliminating cytosolic indicator (such as dialysis via a patch pipet) will also be described.

As is the case with the measurement of cytoplasmic [Ca^{2+}] using fluorescent indicators, the procedures involved are relatively straightforward. However, the interpretation of data can be confounded by many factors. Therefore, emphasis will be on the problems specific to this method that a beginner may encounter, and how to diagnose and circumvent artifacts.

2. Materials

1. Cells: A wide variety of mammalian cell types have been used previously, including hepatocytes, gonadotropes, smooth muscle cells, pancreatic acinar cells, gastric epithelial cells, RBL-1 cells, and BHK-21 fibroblasts (*see* **Note 1**).
2. Selection of dye: Spectral compatibility with the equipment is generally the main consideration when choosing a fluorescent indicator. **Table 1** lists dyes and their characteristics that have been used successfully to monitor [Ca^{2+}] changes in Ins(1,4,5)P_3-sensitive stores (*see* **Note 2**).
3. AM-esters of the chosen indicators (available from Molecular Probes, Eugene, OR, or Teflabs, Austin, TX; *see* **Note 3**) are prepared as 10-m*M* stock solutions

in anhydrous dimethyl sulfoxide (DMSO). It is advisable to make 10-µL aliquots of the dye and store in the freezer until use, as repeated freezing and thawing causes degradation of the probe.

4. *N,N,N′,N′*-tetrakis (2-pyridylmethyl)ethylene diamine (TPEN): 10 m*M* in ethanol (Molecular Probes, Eugene, OR).
5. Ionomycin (Calbiochem, La Jolla, CA): 10 m*M* in DMSO; store in freezer.
6. 4Br-A23187 (Molecular Probes): 10 m*M* in DMSO; store in freezer.
7. NTA (nitrilotriacetic acid): 1 *M* in H_2O (Sigma).
8. Digitonin: 5 mg/mL in water (Sigma).
9. EGTA: 0.5 *M* dissolved in KOH, pH 7.2 (Sigma).
10. $CaCl_2$: 1 *M* (Sigma).
11. Standard Ringer's solution: Use a composition appropriate for each cell type. For example: 145 m*M* NaCl, 2.5 m*M* K_2HPO_4, 1 m*M* $MgSO_4$, 10 m*M* HEPES, 10 m*M* glucose, 1.8 m*M* CaCl2, pH 7.4.
12. KCl rinse solution: 125 m*M* KCl, 25 m*M* NaCl, 10 m*M* HEPES, 0.2 m*M* $MgCl_2$, pH 7.25.
13. Intracellular buffer: 125 m*M* KCl, 25 m*M* NaCl, 10 m*M* HEPES, 0.5 m*M* Na_2ATP, 0.2 m*M* $MgCl_2$, 200 µ*M* $CaCl_2$, 500 µ*M* EGTA to give a final free [Ca^{2+}] of approx 100 n*M*. Pay careful attention to the pH of this solution (pH 7.25; *see* **Note 4**).
14. Permeabilization solution: Same as the intracellular buffer + 1 µL/mL of digitonin stock solution (final digitonin concentration 5 µg/mL).
15. Calibration solution: To KCl rinse solution add 10 µ*M* ionomycin or 4Br-A23187. For Ca^{2+}-free solution, supplement with 1 m*M* EGTA; for high-Ca^{2+} solution, add 10 m*M* $CaCl_2$ (*see* **Note 5**). Intermediate Ca^{2+} concentrations (100, 200, 300 µ*M*, and so on) can be prepared approximately (*see* **Note 6**) by simply adding $CaCl_2$, or if more accuracy is desired, NTA buffers can be used (*see* **Note 7**). Some sample compositions of NTA buffers (calculated from the excellent computer program described in **ref. *19***) are shown in **Table 2**.

3. Methods

3.1. Loading Cells with Indicators

Add dye directly to cells (in suspension or grown on cover slips) at a final concentration of 2–5 µ*M*, and mix gently. Cultured cells can be put back in the tissue culture incubator. The optimal loading time varies with cell type, but a good starting point is 30 min at 37°C (*see* **Note 8**).

3.2. Permeabilizing the Plasma Membrane with Digitonin

A variety of plasma membrane permeabilization techniques have been used previously with good results, e.g., using streptolysin-O (SLO) ***(20)*** or alpha-toxin ***(15)***. Here the use of digitonin is described for this purpose:

1. After loading with dye, rinse cells briefly with KCl rinse solution.
2. It is helpful to mount cells into the experimental chamber and follow the permeabilization process on the microscope stage during initial experiments in

Table 2
Free [Ca^{2+}] of NTA Buffers for In Situ Calibration as Calculated by the Computer Program Described in Ref. *19*

Free [Ca^{2+}] (μ*M*)	NTA (m*M*)	[$CaCl_2$]
100	1	489 μ*M*
200	1	760 μ*M*
300	1	956 μ*M*
400	1	1.12 m*M*
600	1	1.39 m*M*

order to establish optimal permeabilization conditions. Exchange KCl rinse solution with the permeabilization solution containing digitonin. After several minutes cells begin to lose the fluorophore from the cytoplasm resulting in a 70–90% drop in fluorescence intensity at 345 nm. The nucleus (which is devoid of organelles) will be readily apparent as a nonfluorescent central region whereas dye remaining in the periphery should have a reticular distribution (**Fig. 1**).

3. Switch to intracellular buffer without digitonin as soon as the majority of cells have become permeabilized (usually <5 min; *see* **Note 9**).

3.3. Measurement of Internal Store [Ca^{2+}]

Cells that have been properly permeabilized should have relatively high resting [Ca^{2+}] as reported by the fluorophore. Protocols for the measurement of intracellular fluorescence from individual cells (setting of appropriate wavelengths, capture speed, gain, background, and so on) are described in Chapters 2–4. Continuous superfusion with intracellular buffer during the experiment is useful to wash away dye that may have leaked from the cells (*see* **Note 10**).

3.4. Assessing the Presence of Multiple Ca^{2+} Stores

The AM-ester loading of dyes results in indiscriminate accumulation of indicator into a variety of organelles. When looking at a new cell type for the first time, it is helpful to determine in which functional compartments the dye reports [Ca^{2+}] changes. A typical measurement from a mag-fura-2–loaded, digitonin-permeabilized RBL-1 cell is shown in **Fig. 2**.

1. The cell was superfused continuously with intracellular buffer.
2. Addition of 10 μ*M* Ins(1,4,5)P_3 (a supramaximal dose) resulted in a large drop in the ratio owing to the release of Ca^{2+} from internal stores. The ratio recovered when Ins(1,4,5)P_3 was removed and the stores were refilled.
3. The cell was next treated with an inhibitor of the internal store Ca^{2+}-ATPase, thapsigargin (100 n*M*). In the absence of active uptake of the cation, a passive outward leak of Ca^{2+} was unmasked. A second stimulation with Ins(1,4,5)P_3

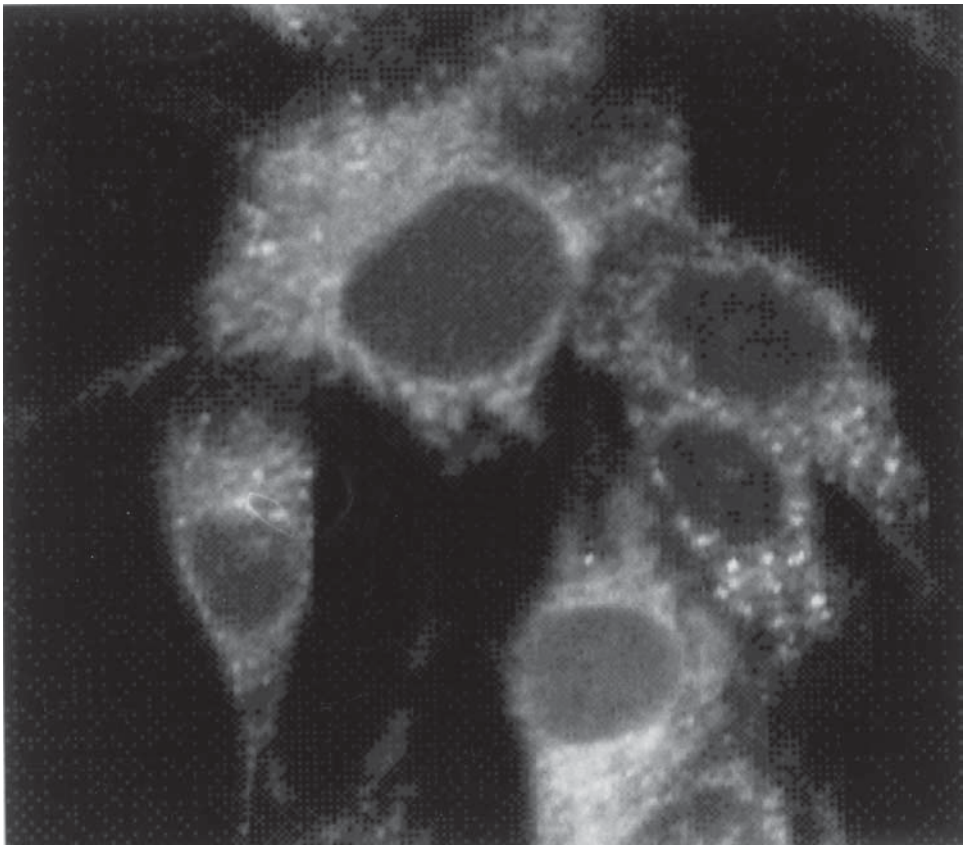

Fig. 1. Confocal image of mag-fura-2/AM–loaded BHK-21 cells permeabilized with digitonin. Excitation 351 nm, emission 510 nm.

released additional Ca^{2+} from the store, but there was no further decrease in the ratio for many minutes, indicating that the Ins(1,4,5)P_3 and thapsigargin-sensitive Ca^{2+} pool(s) were empty. At this time, ionomycin was given to release residual Ca^{2+}.

4. For this particular cell type, one can conclude that [Ca^{2+}] changes are measured mainly in an Ins(1,4,5)P_3- and thapsigargin-sensitive pool, but that a smaller store released only by ionophore is also present (*see* **Note 11**).
5. The contribution of mitochondria (*see* **Note 12**) and acidic Ca^{2+} compartments not accessible to ionomycin (*see* **Note 13**) can be assessed by treating with the appropriate agents. The presence of multiple compartments introduces a particular non-linearity in the measurement, and complicates the calibration of luminal [Ca^{2+}] ***(9)***.

3.5. Calibration

The most controversial aspect of the technique concerns the quantification of Ca^{2+} in internal stores ***(21)***. Many of the factors affecting the calibration are

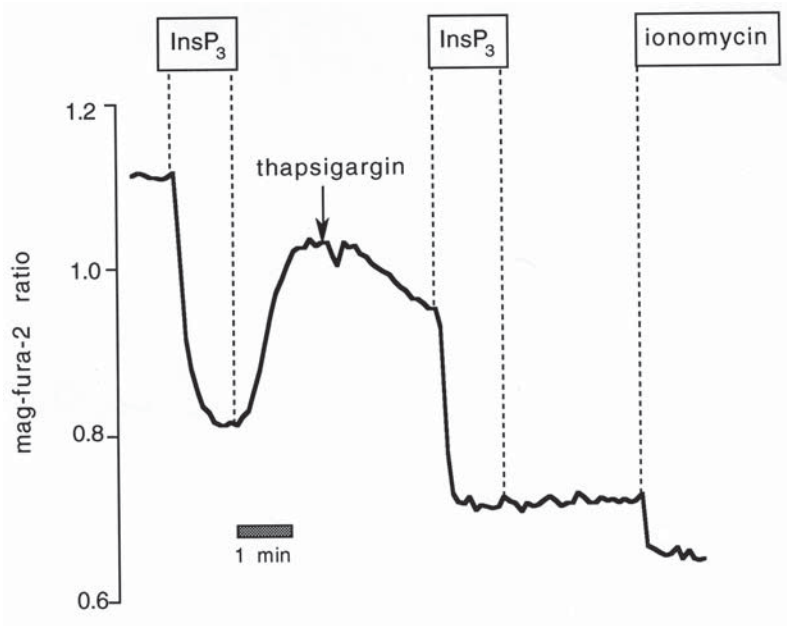

Fig. 2. Typical experimental protocol applied to mag-fura-2/AM–loaded RBL-1 cells to characterize intracellular Ca^{2+} pools (*see* text for details).

problems shared by all fluorescent Ca^{2+} indicators (*see* Chapters 2–4), e.g., vulnerability of dyes to pH, viscosity, ionic strength, bleaching, and so on. In addition, however, there are some special considerations for calibrating dyes in internal stores. Although the compartmentalized dye approach is an excellent way to monitor dynamic changes in Ca^{2+} stores [such as Ins(1,4,5)P_3-induced release], the many problems inherent in the calibration make it unfeasible to make precise quantitative comparisons, particularly among different cell preparations. When only qualitative information is desired, it is often sufficient to express $[Ca^{2+}]$ changes simply as the ratio (or fluorescence intensity changes for single wavelength indicators), keeping in mind that the ratio is not necessarily a linear measure of $[Ca^{2+}]$ (the distortions being more significant at higher $[Ca^{2+}]$). Here two basic calibration procedures are described for ratiometric indicators such as mag-fura-2.

3.5.1. Procedure 1

This method relies on the relationship originally described by Tsien and collaborators ***(22)*** for calibrating ratiometric probes such as fura-2:

$$[Ca^{2+}] = K_d \times (S_{f2}/S_{b2}) \times (R - R\text{min})/(R_{max} - R)$$

in which the K_d equals the dissociation constant of the probe, S_{f2} is the maximum fluorescence at 375 nm (in zero Ca^{2+}), S_{b2} is the minimum fluorescence

at 375 nm (in saturating Ca^{2+}), R is the measured ratio, and R_{min} and R_{max} are the minimum and maximum ratio in zero and saturating Ca^{2+}, respectively.

Figure 3A illustrates a typical calibration trace using mag-fura-2–loaded BHK-21 fibroblasts.

1. As in **Fig. 2**, the cells were initially bathed in intracellular buffer, and the $Ins(1,4,5)P_3$-stimulated release was monitored.
2. The minimum ratio (R_{min}) was next obtained by treating cells in Ca^{2+}-free calibration buffer with 10 μ*M* ionomycin.
3. Ca^{2+}-containing calibration buffer (10 m*M*) was then applied to estimate R_{max}.
4. From the raw fluorescence, S_{b2} and S_{f2} are collected.
5. These values are entered into the preceding equation (using a K_d of 53 μ*M*; *see* **Note 14**), to convert ratio data into free [Ca^{2+}] (**Fig. 3B**).
6. The apparent resting free [Ca^{2+}] of this cell using the standard calibration approach was 490 μ*M*; [Ca^{2+}] dropped to 60 μ*M* following $Ins(1,4,5)P_3$ stimulation.
7. A major problem with the preceding approach as applied to compartmentalized low-affinity dyes is that it is frequently quite difficult to obtain a reliable value for R_{max}. Ionophores have a limited capacity to equilibrate internal and external [Ca^{2+}] (the estimated K_d of ionomycin for Ca^{2+}, e.g., is approx 100 μ*M*), and large [Ca^{2+}] is required to truly saturate the indicator (10–20 m*M*).
8. An alternative for determination of R_{max} takes advantage of the fact that Mn^{2+} ions (also carried by ionophores) bind the dye with high affinity, and can be used as a surrogate for Ca^{2+} ions. Mn^{2+} quenches fluorescence at both wavelengths, but for mag-fura-2, Mn^{2+} and a saturating [Ca^{2+}] cause the same degree of quenching at the Ca^{2+}-sensitive wavelength of 375 nm (*see* **Note 15**). R_{max} can be approximated by taking the value of the fluorescence intensity at 345 nm immediately prior to Mn^{2+} addition ($F_{345\ nm}$), and dividing this by the Mn^{2+}-quenched intensity at 375 nm ($F_{375\ nm}$). It is assumed that the 345-nm intensity will not have changed dramatically over this time. Correspondingly, a more accurate value for S_{b2} (which is the same as $F_{375\ nm}$) can also be obtained. Using these new values for R_{max} and S_{b2}, a second calibrated trace is determined and is shown in **Fig. 3B**. Here the resting [Ca^{2+}] was 273 μ*M*, falling to 49 μ*M* after $Ins(1,4,5)P_3$ treatment.

3.5.2. Procedure 2

The second basic calibration approach is the more laborious *in situ* determination, which, in principle, should give more accurate results because the ratio changes are independent of the many factors that can influence the K_d of the dye (viscosity, ionic strength, and so on). One difficulty that remains is the equilibration of internal and external [Ca^{2+}], particularly at higher [Ca^{2+}] concentrations.

1. Cells were exposed to calibration buffer + ionomycin containing varying free [Ca^{2+}]. **Figure 4** shows a typical experiment.
2. In this case, there was modest agreement between the R_{min}/R_{max} approach and the values interpolated from the *in situ* data (223 μ*M* starting [Ca^{2+}] vs 147 μ*M*, respectively).

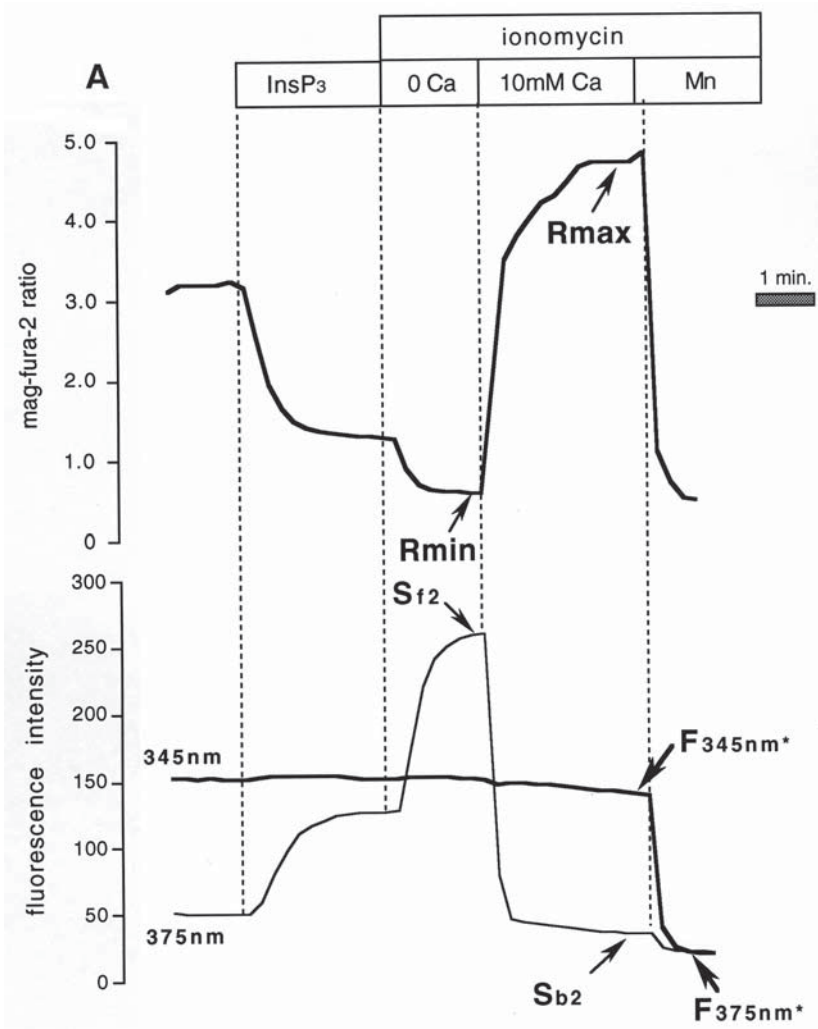

Fig. 3. **(A)** Calibration procedure for mag-fura-2–loaded BHK-21 cells permeabilized with SLO. Determination of R_{min}, R_{max}, S_{f2}, and S_{b2}, as well as an estimated R_{max} and S_{b2} based on Mn quenching at 375 nm. The 345-nm wavelength is insensitive to changes in $[Ca^{2+}]$ whereas the 375-nm excitation wavelength is inversely related to $[Ca^{2+}]$. Both wavelengths are quenched by Mn. An alternative way to estimate R_{max} using $F_{345\ nm}/F_{375\ nm}$ may circumvent difficulties in obtaining a true R_{max} with saturating $[Ca^{2+}]$. Note that $F_{375\ nm}$ replaces S_{b2} with this approach.

Both calibration procedures are subject to a serious problem: dye may also be present in compartments such as mitochondria in which $[Ca^{2+}]$ is low ("silent compartments"). Therefore, it is not possible to detect Ca^{2+} changes in these

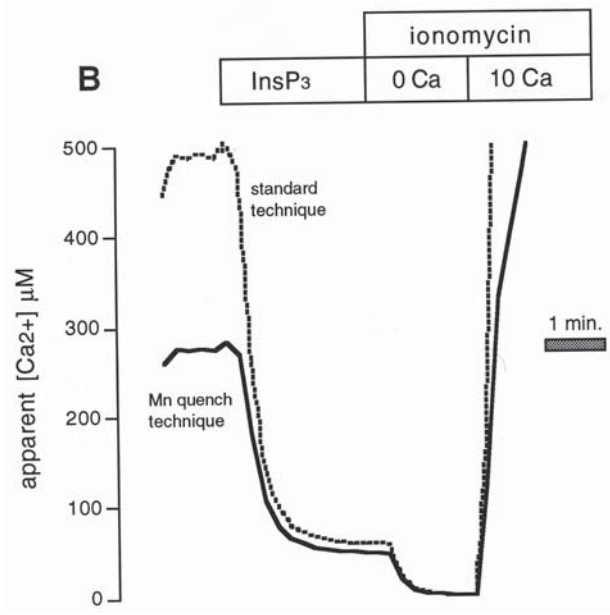

Fig. 3. *(continued)* **(B)** Comparison between calibrated Ins(1,4,5)P_3 response using R_{max} and S_{b2} obtained in saturating [Ca^{2+}] ("standard technique"; dotted line) and R_{max} and S_{b2} (the same as $F_{375\ nm}$) obtained with Mn^{2+} ("Mn^{2+} quench technique"; solid trace). Values for S_{b2}, S_{f2}, and $F_{375\ nm}$ were corrected for bleaching using the 345-nm wavelength prior to calculation of apparent [Ca^{2+}] (*see* **Note 14**).

organelles (and thereby assess whether they contain dye or not), yet this indicator nevertheless contributes to overall signal, potentially causing underestimation of ER [Ca^{2+}] (*see* **Note 16** and **ref. *21***).

3.6. Interference by Mg and Heavy Metals

1. Many of the popular indicators used for measuring [Ca^{2+}] in internal stores such as mag-fura-2, mag-fura-5, mag-indo-1, and mag-fura-red were, as the names would suggest, originally intended as Mg^{2+} indicators. Several studies have concluded that [Mg^{2+}] changes do not interfere significantly with the measurement of [Ca^{2+}] in Ins(1,4,5)P_3-sensitive internal stores ***(9,16,21,23)***, likely because the affinity of these probes for Ca^{2+} is so much higher than for Mg^{2+} (e.g., the K_d of mag-fura-2 for Mg in vitro is 1.5 m*M*; *see* **refs. *7*** and ***24***). Nevertheless, it should not be taken for granted that [Mg^{2+}] changes will not be reported by the dye under some conditions. The recent introduction of probes ***(25)*** with reduced sensitivity to Mg^{2+} (e.g., fura-2-ff, fluo-3-ff) provide the possibility to control for such potential artifacts.
2. Another concern is that of heavy metal contamination (**refs. *26*** and ***27***). As is the case with all fluorescent Ca^{2+} dyes, many heavy metals bind the dye molecule

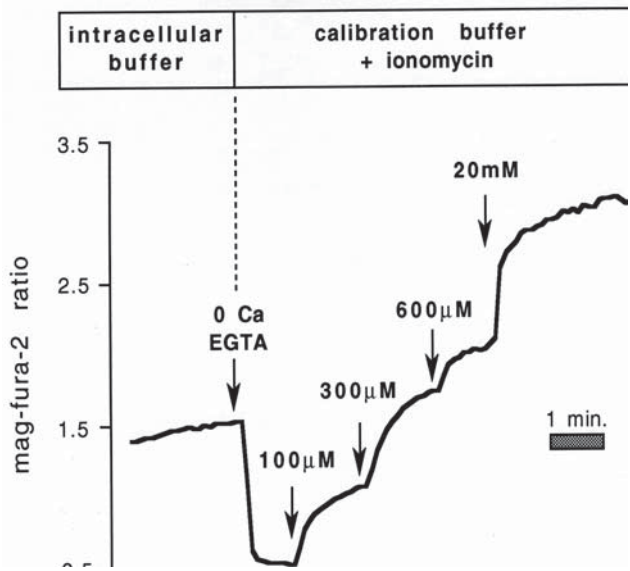

Fig. 4. *In situ* calibration using NTA buffers containing 100, 300, and 600 μ*M* free Ca^{2+}. Data from mag-fura-2/AM–loaded BHK-21 fibroblasts permeabilized with SLO (*see* text for details).

with far greater affinity than Ca^{2+} itself (*see* **Note 17**). In the author's experience, the extent to which heavy metals perturb the measurement depends a great deal on the cell type (*see* **Note 18**). Sometimes the spectral effect of these contaminating ions is to mimic Ca^{2+} ions, thus giving a false, high [Ca^{2+}] measurement. Alternatively, many heavy metals quench the fluorescence of indicators, causing a reduction in sensitivity toward Ca^{2+}.

3. To diagnose whether these ions are interfering with the measurement of internal store Ca^{2+}, supplement the intracellular buffer with a low dose (10 μ*M*) of the membrane-permeant heavy-metal chelator TPEN. In the case of mag-fura-2, the ratio may or may not drop whereas the individual fluorescence intensities will increase at both wavelengths as the TPEN competes for heavy metals bound to the dye. It may be necessary to perform control experiments in the presence of TPEN to test whether the biological phenomenon under study is influenced by contaminating ions.

3.7. Troubleshooting

Beginners of this technique may experience one or more of the following problems during the course of their experiments:

1. Cells and organelles appear not to load with dye. Check whether the nonpermeabilized cells also have a low fluorescence, which, assuming that the microscope optics and equipment are in proper order, may be improved by increasing dye concen-

tration, changing loading times, changing temperature, or trying a different indicator, if possible.
2. Cells are unresponsive to Ins(1,4,5)P_3. Are the cells really permeabilized or perhaps they are overpermeabilzed? Excessive loading can also yield poor results because of buffering of [Ca^{2+}] changes by the indicator (*see* also **Subheading 3.6.2.**). In the case of cultured cells, it is sometimes necessary simply to use a newer passage of cells, as some cell types seem to lose responsiveness to Ins(1,4,5)P_3 and agonists following many generations.
3. Starting Ca^{2+} concentrations are very low. Check that the background of the measuring system is set appropriately. Also be aware that some lipophilic Ca^{2+}-releasing agents such as thapsigargin and ionomycin can be extremely pernicious in sticking to plastic elements of the superfusion system (*see* **Note 19**); hence, stored Ca^{2+} may have been inadvertently released before the measurement even started.

3.8. Combined Patch-Clamp and Internal Store Ca^{2+} Measurements

In a whole-cell patch-clamp configuration, it is possible to dialyze the cytoplasmic indicator via the patch pipette, leaving behind organelle-trapped dye and an intact, functional plasma membrane. The combination of these techniques affords a number of exciting experimental possibilities. Tse et al. ***(10)*** used this approach to monitor hormone-induced Ca^{2+} oscillations in internal stores simultaneously with measurements of cytoplasmic Ca^{2+} (assessed indirectly as the activity of a Ca^{2+}-activated K^+ current). Alternatively, fluorescent indicators with compatible spectral properties can be loaded into the cytoplasm via the patch pipette, permitting simultaneous measurements of [Ca^{2+}] in both compartments ***(11)***. An example of another type of problem addressed by this approach is shown in **Fig. 5**.

1. A whole-cell current recording of I_{CRAC} (a Ca^{2+} current activated by depletion of internal stores) was monitored concurrently with internal store [Ca^{2+}] as measured by compartmentalized fura-2-ff ***(28)***. The time course for the dilution of the probe into the patch pipet is shown in **Fig. 5** (upper records).
2. Treatment with ionomycin resulted in a drop in the fura-2-ff ratio **Fig. 5** (middle record), and the activation of a Ca^{2+} current (bottom record).

3.9. Measurements in Intact Cells

While agonist-evoked changes of internal store [Ca^{2+}] were readily detectable in intact cells in the original mag-fura-2 measurements on gastric epithelial cells ***(8)***, releasing cytoplasmic indicator eliminated the large background fluorescence from this dye, and improved the resolution of the measurement enormously. Recently, however, the author and others have observed that in the absence of any special treatment, certain cell types seem to export cyto-

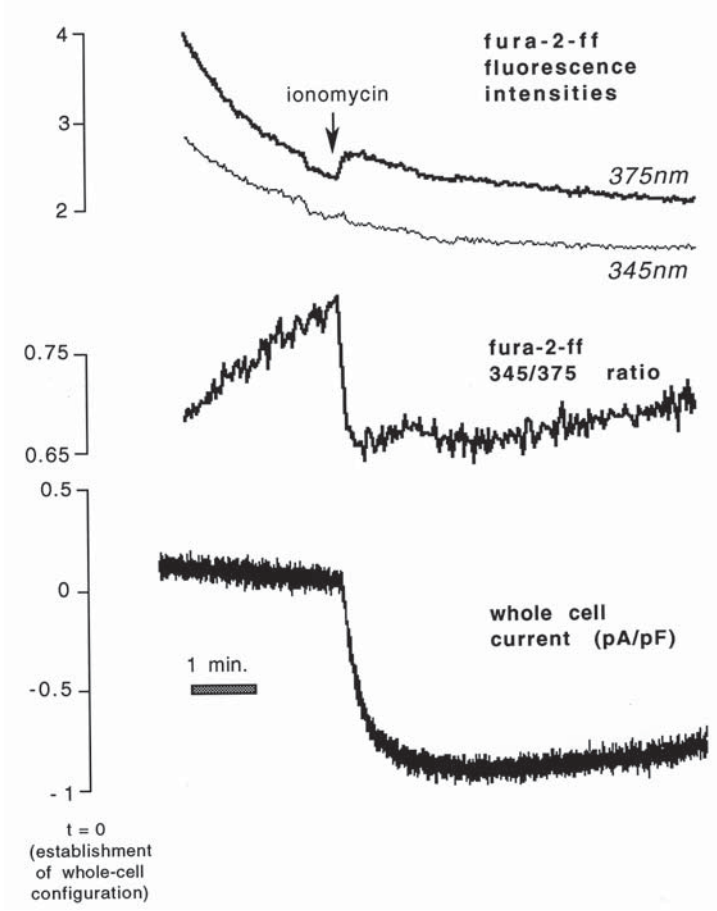

Fig. 5. Simultaneous whole-cell current measurement of I_{CRAC} and 345 nm/375 nm fluorescence ratio from compartmentalized fura-2-ff in RBL-1 cell. Top record shows individual fluorescence intensities, which declined as cytosolic dye was dialyzed into the patch pipette. Ionomycin caused a rapid drop in the ratio (middle record) and activated an inward current (bottom record).

plasmic dye, resulting in preferential accumulation of mag-fura-2 in organelles ***(17,29)***. In a large percentage of BHK-21 fibroblasts loaded with mag-fura-2 for 1 h, >85% (and often 100%) of the dye was localized in organelles. This has allowed high-resolution measurements of free [Ca^{2+}] changes in internal stores in response to native Ca^{2+}-mobilizing agonists in intact cells. Although the mechanisms responsible for this phenomenon are at present unclear, the further development of this approach offers many exciting possibilities for future studies.

3.10. Conclusions

Because many laboratories are already equipped for making cytoplasmic [Ca^{2+}] measurements with fluorescent probes such as indo-1 and fura-2, it is straightforward to combine existing equipment with the methodology described in this chapter toward the measurement of [Ca^{2+}] in agonist-sensitive Ca^{2+} stores. A major disadvantage of this approach is the nonspecific intracellular localization of dye. However, the unprecedented sensitivity afforded by this method makes it complementary to recently introduced approaches employing ER-targeted probes ***(30,31)***. In the future, one can expect the development of fluorescent indicators localized specifically to a wide variety of organelles and subcellular sites.

4. Notes

1. The success of the measurement relies to some extent on cell type, as cells differ greatly with respect to their cytological composition and their handling of dye (*see* **Subheading 3.4.**). For example, much better results have been obtained with BHK-21 fibroblasts than pancreatic acinar cells or RBL cells. RBL cells appear to have an ER that occupies a very small part of the cell volume, resulting in a poor signal-to-noise ratio.
2. Mag-fura-2 (also called "furaptra"), has been by far the most popular indicator for this purpose, to date. This probe is similar to fura-2 in its spectral properties: the 345 nm/375 nm excitation ratio (peak emission at 510 nm) is proportional to free [Ca^{2+}]. Mag-fura-2 is extremely bright and loads quite well into cells, generally giving very high levels of intracellular fluorescence.
3. New dyes suitable for this purpose continue to be developed. A good resource for information on new low-affinity Ca^{2+} indicators is the web site provided by Molecular Probes (www.probes.com), which sells most of the fluorescent dyes. Teflabs is also a good source of indicators, including some "unique" products available only through them.
4. One may have to experiment with different intracellular buffer compositions to find the recipe that works best for a given cell type. For example, [ATP] can be varied, or BAPTA may be used as the Ca^{2+} buffer instead of EGTA, the Ca^{2+} buffering properties of which are highly sensitive to pH. The author also observed that organelle morphology is better preserved when a portion of the Cl^- in the intracellular buffer is substituted with an impermeant anion such as gluconate (added, e.g., as K gluconate, leaving 25 m*M* of NaCl in the solution).
5. Be aware that when EGTA is added to a Ca^{2+}-containing solution (and vice versa), many protons are liberated in the process, resulting in dramatic acidification of the medium. Therefore, when making Ca^{2+}-free solutions it is best to add EGTA to a nominally Ca^{2+}-free buffer (otherwise, be sure to check the pH).
6. Remember that the activity coefficient for $CaCl_2$ in these solutions is roughly 0.88, meaning that the actual free [Ca^{2+}] (which is what is seen by the dye) is approx 88% of the total added Ca^{2+}.

7. A good computer program that can calculate free [Ca^{2+}] of multiple buffer systems, such as the MaxChelator program ***(19)***, is indispensable. By experimenting with these programs, one often learns many surprising things about the effects of pH, ionic strength, and interactions with other buffer constitutents, such as ATP, on the free [Ca^{2+}] in solution.
8. There is a lot of variability among the various cell types with respect to optimal loading times. For example, in the case of BHK-21 fibroblasts, loading for extended periods of time or with higher probe concentration does not necessarily yield better results (but *see* **Subheading 3.9.**). In some cells it appears that the probe is degraded or transported to other organelles (perhaps lysosomes), where it remains as a Ca^{2+}-insensitive form.
9. To maintain organelle integrity, incubate as briefly as possible with the minimum digitonin concentration. The permeabilization process is accelerated at 37°C. Digitonin appears to lose its membrane permeabilizing properties with excessive agitation.
10. Leaked dye can cause a suppression of mag-fura-2 ratio changes because this probe is bright in its Ca^{2+} unbound form. This means that extravesicular dye will contribute disproportionately to the background (*see* **ref. *21*** for details). Measurements in cuvets (in which released dye remains in the medium) may therefore be impractical with probes that share this spectral property.
11. Cell types vary greatly with respect to their organellar constitution, and their handling of dye. In contrast to RBL-1 cells, BHK-21 fibroblasts appear to measure [Ca^{2+}] changes only in a thapsigargin- and Ins(1,4,5)P_3-releasable pool, which greatly simplifies data analysis.
12. Mitochondrial inhibitors such as FCCP plus oligomycin block Ca^{2+} uptake by collapsing the electrochemical gradient across the inner mitochondrial membrane ***(32)***. Ruthenium red blocks the mitochondrial Ca^{2+} uniporter, the principal pathway for Ca^{2+} uptake. Although this organelle is notorious for compartmentalizing AM-esters, the high K_d of indicators such as mag-fura-2 may not permit detection of [Ca^{2+}] changes in this space because the [Ca^{2+}] is generally quite low (however, *see* **ref. *9***).
13. Because ionomycin functions as an electroneutral Ca^{2+}/H+ exchanger, it is inefficient at releasing Ca^{2+} from compartments with low pH, such as secretory granules. The combination of monensin (an Na^+/H^+ exchanging ionophore) plus ionomycin is more effective, and may reveal the presence of additional compartments ***(33)***.
14. As is the case with cytosolic indicators, the K_d *in situ* can vary considerably with respect to values determined in vitro ***(23)***. The ability to monitor the Ca^{2+}-insensitive wavelength is advantageous because corrections for the decline in intensity at both wavelengths over time (owing to bleaching, dye leakage) can be applied to values obtained for S_{b2} and S_{f2}.
15. This assumption should be checked when using indicators other than mag-fura-2.
16. The author has observed that the starting mag-fura-2 ratio values can be quite variable from cell to cell, but that these differences are reduced somewhat when

the indicator is calibrated. This variation may be, in part, the result of a form of dye trapped in compartments that is insensitive to Ca^{2+}, causing a large background that suppresses the ratio. Although it is quite possible that the actual free luminal [Ca^{2+}] may differ from cell to cell, the contribution of silent compartments may also vary, causing an apparent heterogeneity.

17. Mag-fura-2, e.g. is exquisitely sensitive to zinc ions (K_d = 20 n*M*; **ref. *34***), and in fact can potentially be used as an indicator for this cation, which is rather abundant in many cell types.
18. RBL-1 cells, e.g. have a considerable pool of heavy metals, whereas BHK-21 cells appear to have none as assessed by this technique.
19. Often the offending contaminants will not perturb measurements in intact cells (leading one to believe that their particular regimen of cleaning is adequate), but can pose problems in permeabilized cells, which tend to be much more sensitive to minute traces of these agents. Rinsing thoroughly with the appropriate solvent (e.g., ethanol) is advisable between experiments.

Acknowledgments

The author would like to thank the many colleagues who have given help and support over the years, including Drs. Paul Negulescu, Terry Machen, Irene Schulz, Silvana Curci, Barbara Landolfi, Wim Scheenen, and Tullio Pozzan.

References

1. Williams, D. A., Fogarty, K. E., Tsien, R. Y., and Fay, F. S. (1985) Calcium gradients in single smooth muscle cells revealed by the digital imaging microscope using Fura-2. *Nature* **318(6046),** 558–561.
2. Roe, M. W., Lemasters, J. J., and Herman, B. (1990) Assessment of fura-2 for measurements of free cytosolic calcium. *Cell Calcium* **11,** 63–73.
3. Terasaki, M. and Sardet, C. (1991) Demonstration of calcium uptake and release by sea urchin cortical endoplasmic reticulum. *J. Cell Biol.* **115,** 1031–1037.
4. Connor, J. A. (1993) Intracellular calcium mobilization by inositol 1,4,5-trisphosphate: intracellular movements and compartmentalization. *Cell Calcium* **14,** 185–200.
5. Glennon, M. C., Bird, G. St. J., Takemura, H., Thastrup, O., Leslie, B. A., and Putney, J. W., Jr. (1992) *In situ* imaging of agonist-sensitive calcium pools in Ar4-2J pancreatoma cells. *J. Biol. Chem.* **267(35),** 25,568–25,575.
6. Short, A. D., Klein, M. G., Schneider, M. F., and Gill, D. L. (1993) Inositol 1,4,5-trisphosphate-mediated quantal Ca^{2+} release measured by high resolution imaging of Ca^{2+} within organelles. *J. Biol. Chem.* **268(34),** 25,887–25,893.
7. Raju, B., Murphy E., Levy, L. A., Hall, R. D., and London, R. E. (1989) A fluorescent indicator for measuring cytosolic free magnesium. *Am. J. Physiol.* **256,** C540–C548.
8. Hofer, A. M., and Machen, T. E. (1993) Technique for *in situ* measurement of calcium in intracellular $InsP_3$-sensitive stores using the fluorescent indicator mag-fura-2. *Proc. Natl. Acad. Sci. USA* **90,** 2598–2602.

9. Hofer A. M. and Machen, T. E. (1994) Direct measurement of free Ca^{2+} in organelles of gastric epithelial cells. *Am. J. Physiol.* **267,** G442–G451.
10. Tse, F. W., Tse, A., and Hille, B. (1994) Cyclic Ca^{2+} changes in intracellular stores of gonadotropes during gonadotropin-releasing hormone-stimulated Ca^{2+} oscillations. *Proc. Natl. Acad. Sci. USA* **91,** 9750–9754.
11. Chatton, J.-Y., Liu, H., and Stucki, J. W. (1995) Simultaneous measurement of Ca^{2+} in the intracellular stores and cytosol of hepatocytes during hormone-induced Ca^{2+} oscillations. *FEBS Lett.* **368,** 165–168.
12. Hajnóczky, G. and Thomas, A. P. (1997) Minimal requirements for calcium oscillations driven by the IP3 receptor. *EMBO J.* **16(12),** 3533–3543.
13. Hirose, K. and Iino, M. (1994) Heterogeneity of channel density in inositol-1,4,5-trisphosphate-sensitive Ca^{2+} stores. *Nature* **372,** 791–794.
14. Sugiyama, T. and Goldman, W. F. (1995) Conversion between permeability states of IP3 receptors in cultured smooth muscle cells. *Am. J. Physiol.* **269,** C813–C818.
15. Steenberger, J. M. and Fay, F. S. (1996) The quantal nature of calcium release to caffeine in single smooth muscle cells results from activation of the sarcoplasmic reticulum Ca^{2+}-ATPase. *J. Biol. Chem.* **271(4),** 1821–1824.
16. Hofer, A. M., Schlue, W. R., Curci, S., and Machen, T. E. (1995) Spatial distribution and quantitation of free luminal [Ca^{2+}] within the $InsP_3$-sensitive internal store of individual BHK-21 cells: Ion dependence of $InsP_3$-induced Ca^{2+} release and reloading. *FASEB J.* **9,** 788–798.
17. Golovina, V. A. and Blaustein, M. P. (1997) Spatially and functionally distinct Ca^{2+} stores in sarcoplasmic and endoplasmic reticulum. *Science* **275(5306),** 1643–1648.
18. van de Put, F. H. and Elliott, A. C. (1996) Imaging of intracellular calcium stores in individual permeabilized pancreatic acinar cells: Apparent homogeneous cellular distribution of inositol 1,4,5-trisphosphate-sensitive stores in permeabilized pancreatic acinar cells. *J. Biol. Chem.* **271(9),** 4999–5006.
19. Nuccitelli, R. (ed.) (1994) A practical guide to the study of calcium in living cells, in *Methods in Cell Biology*, vol. 40. Academic, San Diego.
20. Hofer, A. M., Curci S., Machen T. E., and Schulz I. (1996) ATP regulates the passive leak from agonist-sensitive internal calcium stores. *FASEB J.* **10,** 302–303.
21. Hofer, A. M. and Schulz, I. (1996) Quantification of intraluminal free [Ca^{2+}] in the agonist-sensitive internal calcium store using compartmentalized fluorescent indicators: Some considerations. *Cell Calcium* **20(3),** 235–242.
22. Grynkiewicz, G., Poenie, M., and Tsien, R. Y. (1985) A new generation of Ca^{2+} indicators with greatly improved fluorescence properties. *J. Biol. Chem.* **260,** 3440–3450.
23. Sugiyama, T. and Goldman, W. F. (1995) Measurement of SR free Ca^{2+} and Mg in permeabilized smooth muscle cells with use of furaptra. *Am. J. Physiol.* **269,** C698–C705.
24. London, R. E. (1991) Methods for measurement of intracellular magnesium: NMR and fluorescence. *Annu. Rev. Physiol.* **53,** 241–258.
25. London, R. E., Rhee, C. K., Murphy, E., Gabel, S., and Levy, L. A. (1994) NMR-sensitive fluorinated and fluorescent intracellular calcium ion indicators with high dissociation constants. *Am. J. Physiol.* **266,** C1313–C1322.

26. Arslan, P., Di Virgilio, F., Betrame, M., Tsien, R. Y., and Pozzan, T. (1985) Cytosolic Ca^{2+} homeostasis in Ehrlich and Yoshida carcinomas: A new membrane-permeant chelator of heavy metals reveals that these ascites tumor cell lines have normal cytosolic free Ca^{2+}. *J. Biol. Chem.* **260,** 2719–2727.
27. Snitsarev, V. A., McNulty, T. J., and Taylor, C. W. (1996) Endogenous heavy metal ions perturb fura-2 measurements of basal and hormone-evoked Ca^{2+} signals. *Biophys. J.* **71,** 1048–1056.
28. Hofer, A. M., Fasolato, C., and Pozzan, T. (1998) Capacitative Ca^{2+} entry is closely linked to the filling state of internal Ca^{2+} stores: a study using simultaneous measurements of Icrac and intraluminal [Ca^{2+}]. *J. Cell Biol.* **140,** 325–334.
29. Hofer, A. M., Landolfi, B., Debellis, L., Pozzan, T., and Curci, S. (1998) Free [Ca^{2+}] dynamics measured in agonist-sensitive stores of single living intact cells: a new look at the refilling process. *EMBO J.* **17,** 1986–1995.
30. Montero, M., Brini, M., Marsault, R., Alvarez, J., Sitia, R., Pozzan, T., and Rizzuto, R. (1995) Monitoring dynamic changes in free Ca^{2+} concentration in the endoplasmic reticulum of intact cells. *EMBO J.* **14,** 5467–5475.
31. Kendall, J. M., Dormer, R. L., and Campbell, A. K. (1994) Changes in free calcium in the endoplasmic reticulum of living cells detected using targeted aequorin. *Anal. Chem.* **221,** 173–181.
32. Gunter, T. E. and Pfeiffer, D. R. (1990) Mechanisms by which mitochondria transport calcium. *Am. J. Physiol.* **258,** C755–C786.
33. Fasolato, C., Zottini, M., Clementi, E., Zacchetti, D., Meldolesi, J., and Pozzan, T. (1991) Intracellular Ca^{2+} pools in PC-12 cells: Three intracellular pools are distinguished by their turnover and mechanisms of Ca^{2+} accumulation, storage, and release. *J. Biol. Chem.* **266,** 20,159–20,167.
34. Simons, T. J. B. (1993) Measurement of free Zn^{2+} ion concentration with the fluorescent probe mag-fura-2 (furaptra). *J. Biochem. Biophys. Methods* **27,** 25–37.

18

Measurement of $[Ca^{2+}]_i$ in Smooth Muscle Strips Using Front-Surface Fluorimetry

Hideo Kanaide

1. Introduction

In regulating the contraction of smooth muscle cells, changes in the cytosolic concentrations of Ca^{2+} ($[Ca^{2+}]_i$) play a primary role as the initiation of contraction is associated with Ca^{2+} binding to calmodulin with the subsequent activation of myosin light chain kinase. During the contraction induced by receptor-mediated stimulation, however, there are temporal changes in the relationship between $[Ca^{2+}]_i$ and the developed tension. Furthermore, the receptor-mediated stimulation also produces a proportionately greater tension for a given change in $[Ca^{2+}]_i$ than does K^+ depolarization. Therefore, it is important to measure $[Ca^{2+}]_i$ and tension simultaneously in order to determine the molecular and cellular mechanisms in both the regulation of contraction and relaxation of smooth muscle. For this purpose, front-surface fluorimetry of fura-2, a $[Ca^{2+}]_i$ indicator dye ***(1)***, has been performed on small smooth muscle strips ***(2,3)***.

The technique of front-surface fluorimetry is commonly used for measuring tissue fluorescence. The first and, so far, the only successful technique known to monitor the naturally occurring fluorescence of intact tissue in surface fluorimetry was developed by Chance et al. ***(4)***. Using surface fluorimetry and a perfused rat heart, they reported the depth of penetration of excitation light (366 nm), and hence the detection of fluorescence (460 nm), to be 0.4 mm, and studied the kinetics of mitochondrial flavoprotein and the reduced form of pyridine nucleotide in the myocardium. They also developed a front-surface fluorometer utilizing a bifurcated fiber-optic light source to perform surface fluorimetry of the kidney ***(5)***. The underlying principle of front-surface fluorimetry is simple: the closer the distance between the excitation light source

From: *Methods in Molecular Biology, Vol. 114: Calcium Signaling Protocols*
Edited by: D. G. Lambert

(and also the detector) and the object, the easier and more accurate the detection of the emission light becomes.

In the author's front-surface fluorometer, concentric optic fibers are used: the excitation light is guided through quartz optic fibers arranged in an inner circle, and emission light is collected by glass optic fibers arranged in an outer circle. By preparing small-sized specimens of smooth muscle strips, the entire front surface of the sample can be illuminated, and almost the whole fluorescence signal from the front-surface can be detected by the use of concentric optic fibers placed close to the sample.

One of the advantages of using a fura-2 signal is the ratiometric measurement of two excitation wavelengths, which cancels the parallel changes in the intensities of the two emitted light signals induced by the moving artifact produced by the contraction, shortening, or torsion of the sample, and changing or bubbling of the solutions. In addition, since the emitted light from the entire front surface of the sample strip is detected by these confronted optical fibers, the amount of the observed fura-2 dye is thus kept constant, while any possible artifact owing to the movement or changing shape of the strips during contraction is eliminated as far as possible. Therefore, the signals obtained of front-surface fura-2 fluorescence simply indicate the changes in $[Ca^{2+}]_i$ of the smooth muscle cells and not the artifacts owing to either the contraction or movement of the smooth muscle strips.

2. Materials

1. $[Ca^{2+}]_i$ indicator dyes: These dyes are all directly purchased in special packaging from the manufacturers. Fura-2/AM (mol wt = 1002; an acetoxymethyl [AM] form of fura-2) is from Molecular Probes (Eugene, OR) and Dojindo Laboratory (Kumamoto, Japan), and fura-PE3/AM (mol wt = 1258) is from TEFLABS (Austin, TX). Small plastic tubes in special packaging contain either fura-2/AM or fura-PE3/AM dry powder, 50 μg each, and are stored at –20°C.
2. Fura-2 loading buffer: Oxygenated (bubbling with a mixture of 95% O_2 and 5% CO_2), Dulbecco's modified Eagle's medium (Gibco, Grand Island, NY) containing fura-2/AM (or fura-PE3/AM), 5% inactivated fetal bovine serum (FBS) (Gibco), and whenever necessary, pluronic F127 (TEFLABS), cremophor EL (Sigma, St. Louis, MO), and/or probenecid (Sigma), as shown in **Table 1**.
3. Normal physiological salt solution (PSS): 123 m*M* NaCl, 4.7 m*M* KCl, 15.5 m*M* $NaHCO_3$, 1.2 m*M* KH_2PO_4, 1.2 m*M* $MgCl_2$, 1.25 m*M* $CaCl_2$, and 11.5 m*M* D-glucose. Ca^{2+}-free PSS contains 2 m*M* EGTA instead of $CaC1_2$. High-K^+ PSS is of the same composition as normal PSS, except for the equimolar substitution of KCl for NaCl.
4. Quartz organ bath: A quartz cuvet (5 mL; $1 \times 1 \times 5$ cm) is used. Three faces of the cuvet are covered with a quartz water jacket to maintain the experimental temperature, whereas one free face of the cuvet is used for surface fluorimetry.

Table 1
Conditions for Fura-2 Loading on Smooth Muscle Cells[a]

Species	Smooth muscle	Concentrations of fura-2/AM (μ*M*)	Incubation time (h)	Other additions
Human	Umbilical artery	50	4	—
Bovine	Mid-cerebral artery	50	4	—
	Ophthalmic artery	50	4	—
	Coronary artery	50	4	—
	Pedal artery	50	4	—
Pig	Coronary artery	25	4	—
	Pulmonary artery	25	4	—
	Pulmonary vein	25	4	—
	Renal artery	50	4	—
	Trachea	50	4	—
	Urinary bladder	40[b]	6	0.1% Pluronic F127
Rabbit	Basilar artery	10	3	—
	Ear artery	40[b]	4	—
	Femoral artery	50	4	—
	Saphenous vein	40[b]	6	0.1% Pluronic F127
	Vein graft	40[b]	6	0.1% Pluronic F127
Rat	Basilar artery	25	3	—
	Aorta	25	3	0.08% Cremophor EL, 1 m*M* probenecid
	Myometrium	40[b]	6	0.1% Pluronic F127
	Cultured aortic cells	10	1	—

[a]FBS (5%) is added to all loading solutions and temperature is 37°C.
[b]Instead of fura-2/AM, fura-PE3 is utilized.

5. Force transducer: TB-612T (Nihon Koden, Japan).
6. Front-surface fluorometer (CAM-OF-1 or CAM-OF-3) ***(2,3,6)***:
   a. Fluorometer: In collaboration with the Japan Spectroscopic Co. (JASCO, Tokyo, Japan) dual wavelength excitation microscopic fluorometers on the market, a CAM-200 Ca^{2+}-Analyzer (JASCO) and a CAM-230 2-λ Microscopic Fluorometer (JASCO), are remodeled into the front- surface fluorometers, CAM-OF-1 and CAM-OF-3, respectively. The remodeling involves the conversion of the connection of dual wavelength excitation fluorometers to a fluorescence microscope to a configuration with a fiber-optic light guide.
   b. Optic fibers: In collaboration with FUJITOK Co. (Tokyo, Japan), the fiber-optic light guide Optical Assy 800 (FUJITOK) is specifically designed and made for front-surface fluorimetry. The light guide utilizes a bifurcated fiber-optic light source with quartz fibers (95 fibers [330–340-μm diameter × 500-mm length, ST200D-S]) in one branch and glass fibers (250 fibers [300–310-μm

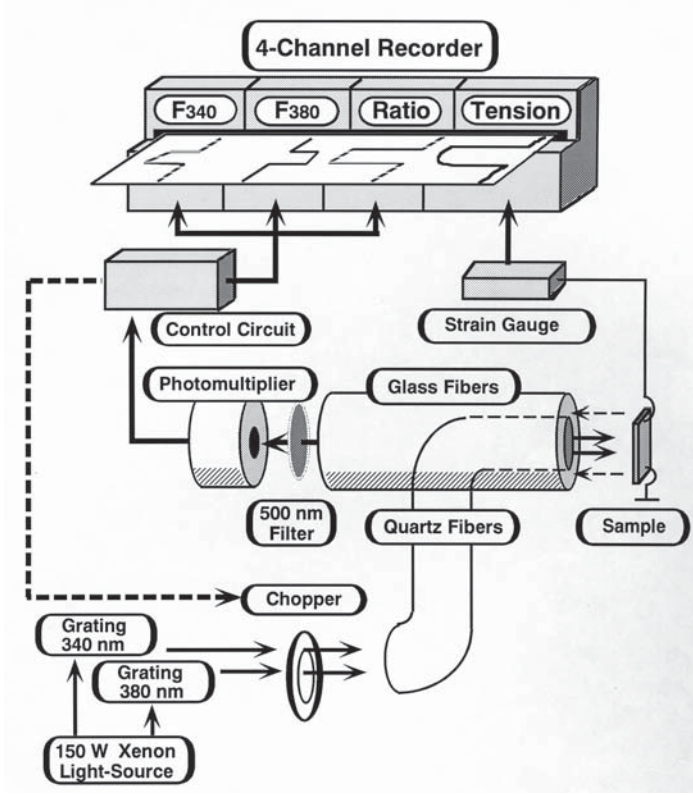

Fig. 1. A block diagram of the front-surface fluorimetry for fura-2 using CAM-OF-3.

diameter × 800-mm length, S0-230/250-50FE]) in the other branch. Fibers are concentrically arranged at the common end, which faces the samples. The quartz fibers are arranged in an inner circle (3 mm diameter) whereas the glass fibers are arranged in an outer circle (7 mm diameter) at the common end.

c. Photomultiplier, R-268 (Hamamatsu Photonics, Shizuoka, Japan) is utilized.

d. A block diagram of front-surface fluorimetry using CAM-OF 3 is shown in **Fig. 1**. Dual excitation light (340 nm, 380 nm) is obtained using two spectroscopes from a 150-W Xenon light source. Using a chopper wheel, the excitation light is then alternately (400 Hz) guided through quartz optic fibers and directly illuminates the sample strip (5-mm length × 1-mm width × 0.1-mm thickness). The fluorescence of the entire front surface is collected by glass fibers and introduced through a 500-nm band-pass filter into a photomultiplier. The ratio of the fluorescence intensities at 340 nm (F340) and 380 nm (F380) excitation, F340/F380, is monitored.

7. Recordings: All data (F340, F380, F340/F380, and tension) are recorded using a computerized data acquisition system (MacLab, Analog Digital Instruments, Castle Hill, Australia; Macintosh, Apple computer, Cupertino, CA), which

enables the $[Ca^{2+}]_i$-tension relationship of smooth muscle contraction and relaxation to be studied.

8. To take fluorescent microphotographs of the smooth muscle strips stained with fura-2, a fluorescence microscope (Axioskop, Zeiss, Germany), equipped with a water-immersion objective system (Plan-Neofluor 40, Zeiss) and appropriate combinations of filters (BP 340 for excitation light and BP 500-530 for fluorescence) is utilized.

3. Methods

3.1. Fura-2 Loading

1. Prior to each measurement, dissolve either 50 µg of fura-2/AM or fura-PE3/AM powder in 50 µL of dimethyl sulfoxide (DMSO), and then dilute with fura-2 loading solution (with the final concentration of DMSO ranging from 1 to 5%) and utilize only once.
2. Incubate smooth muscle strips in oxygenated fura-2 loading buffer using the conditions shown in **Table 1**. Fura-2 (or fura-PE3) loading for smooth muscle cells varies depending on the species and organ.
3. After loading with fura-2, incubate the smooth muscle strips in normal PSS for at least 1 h before starting the measurements, in order to remove the dye in the extracellular space and for the purpose of equilibration (*see* **Notes 1** and **2**).

3.2. Measurement of Isometric Tension Development

1. Perform the simultaneous determination of the tension and $[Ca^{2+}]_i$ of the smooth muscle strips at 37°C.
2. At the beginning of the fura-2 equilibration period, mount the strip vertically and connect to a force transducer in a quartz organ bath.
3. During this period, stimulate the strip with 118 m*M* K^+ PSS every 15 min and increase the resting tension in a stepwise manner until levels that will induce the maximal tension development are reached (*see* **Note 3**).
4. Record the responsiveness to 118 m*M* K^+ PSS before the start of each experimental protocol. The developed tension is expressed in percentages, assuming the values in normal PSS (5.9 m*M* K^+) to be 0%, and in 118 m*M* K^+ PSS to be 100%.

3.3. Front-Surface Fluorimetry

1. To minimize background fluorescence owing to any possible extraneous signals, fluorimetry must be performed in a darkroom (*see* **Notes 4** and **5**).
2. Using front-surface fluorimetry, simultaneously monitor changes in the fluorescence emission (F340, F380, and their ratio, F340/F380) from the entire front surface and tension development of fura-2–loaded smooth muscle strips (*see* **Note 6**).
3. The fluorescence ratio (F340/F380) is utilized as an index of $[Ca^{2+}]_i$, and is expressed as a percentage, assuming the values in normal (5.9 m*M* K^+) and 118 m*M* K^+ PSS to be 0% and 100%, respectively. The determination of the 100% levels of tension and fluorescence ratios are performed at the same time just prior to the start of the experimental protocol (*see* **Note 7**).

4. Estimate the absolute values of $[Ca^{2+}]_i$ for the 0% (5.9 m*M* K^+) and 100% levels (at the steady state of the contraction induced by 118 m*M* K^+-depolarization) of the fluorescence ratio (F340/F380) using separate measurements as follows: After recording the 100% levels of F340/F380 induced by the depolarization with 118 m*M* K^+ PSS, apply ionomycin (final concentration: 5 μ*M* for rat aorta, and 25 μ*M* for the porcine coronary artery). Thereafter, F340 further increases until reaching plateau levels ($F340_{max}$). The solution is then changed to Ca^{2+}-free PSS, and F340 gradually decreases until reaching a steady state ($F340_{min}$). $[Ca^{2+}]_i$ is calculated according to the following equation, which is the calibration equation for fura-2 using intensity values (F340) at only one wavelength:

$$[Ca^{2+}]_i = K_d\,(F - F_{min})/(F_{max} - F) \quad (1)$$

in which Kd is the apparent dissociation constant for Ca^{2+} at 37°C and is assumed to be 224 n*M* ***(1)***, F is the fluorescence signal of F340 expressed in percent, and F_{min} and F_{max} are $F340_{min}$ and $F340_{max}$, respectively. *F* at 5.9 m*M* K^+ and at 118 m*M* K^+ depolarization are assigned to be 0 and 100%, respectively. Thus, the $[Ca^{2+}]_i$ levels at *F* = 0% and F = 100% are assigned to be those at the fluorescence ratios (R; F340/F380) of 0 and 100%, respectively (*see* **Note 8**).

4. Notes

1. To show evidence that fura-2 is almost exclusively and homogeneously loaded in smooth muscle cells, it is recommended that fluorescence photomicrographs be taken of the sample using a fluorescence microscope (Axioskop).
2. The incubation time and the concentration of fura-2/AM for fura-2 loading appear to be long and excessive in comparison to those reported by other workers (**Table 1**). However, these are the most appropriate conditions to obtain reliable recordings. Under these conditions, the intracellular fura-2 concentration is expected to be approx 13 μ*M*, and the inhibition of tension development owing to Ca^{2+}-buffering action of fura,-2 is not recognized ***(6)***. The exclusive and homogeneous staining of smooth muscle cells with fura-2 can be confirmed by taking fluorescence photomicrographs. The insufficient loading of smooth muscles with fura-2/AM at its lower concentration or shorter incubation time frequently induces a smaller fluorescence signal with greater optical artifacts during measurements. For easier and homogeneous loading of fura-2, FBS, pluronic F127, cremophor EL, or probenecid ***(7)*** are used either alone, or in various combinations ***(8)*** (**Table 1**).
3. In proximal coronary arterial strips (5 × 1 × 0.1 mm) of the pig, an appropriate resting tension is approx 250 mg.
4. Background fluorescence: To avoid possible extraneous contamination of the signal the strip is suspended in a quartz organ bath and the measurements are performed in a darkroom. In addition, ratiometry continuously negates parallel changes in intensities of F340 and F380. Background fluorescence, if any, is always subtracted.
5. The nature of the autofluorescence of the tissue is pyridine nucleotide (reduced form), flavoproteins, or cytochromes, and is essentially related to energy metabolism.

The population of mitochondria is so small that the absorbance of excitation light or the fluorescence by these naturally occurring pigments is negligible in smooth muscle cells. In addition, the extinction coefficient and fluorescence quantum yield of fura-2 is so high that autofluorescence of the tissue is easily overcome.

6. With concentric optic fibers, which have a 3-mm quartz inner circle and a 7-mm glass outer circle at the common end, the most suitable distance between the optical fibers and the strip is approx 8 mm. The shorter the distance, the greater the excitation light and, hence, the emission signal. However, it must be noted that a greater intensity of excitation (ultraviolet) light may also cause a greater degree of tissue injury and photobleaching of the fluorescence dye, which will disturb the experiments over a long time course. Furthermore, if the distance is too close and the common end comes into contact with the strip, the emission from the area of the strip overridden by the inner circle cannot be detected by the outer circle. Thus, the distance and the angle between the common end of the optical fibers and the strip are adjusted to the most appropriate for each measurement. This is one of the most important principles regarding front-surface fluorimetry.
7. The absolute values of the fluorescence ratio, F340/F380, for the fura-2–Ca^{2+}-complex can not be obtained when CAM 230 is utilized, because this fluorometer is essentially designed for use in microscopic fluorimetry. The fluorescence intensities are not normalized by the intensity of the excitation light, which directly correlate with the intensities of the 340 or 380 nm signal of the xenon light source. The spectrum of the xenon light source indicates that the intensity of excitation light at 380 nm is much greater (approximately three times) than that at 340 nm. To perform ratiometry with a good balance of excitation between 340 and 380 nm, i.e., to make the F340/F380 reach approx 1 at rest (0%), a combination of appropriately sized metal-optical slits placed in both excitation light paths, in front of and after the grating spectroscopes are used. To estimate the changes in $[Ca^{2+}]_i$ in the experimental protocols, it is not essential to obtain the absolute values of F340/F380.
8. Estimation of the absolute values of $[Ca^{2+}]_i$:
   a. The absolute values of $[Ca^{2+}]_i$ are estimated in separate measurements: In prolonged experimental protocols, although the changes in fluorescence ratio to certain stimulations (such as to high K^+ depolarization) are well maintained, the responsiveness of the strips to ionomycin varies depending on the time course of the experimental protocols, and, thus, great variations in the calculated absolute values of $[Ca^{2+}]_i$ are observed. Therefore, it is not recommended to express the $[Ca^{2+}]_i$ levels with absolute $[Ca^{2+}]_i$ values calculated at the end of each experiment. Only for approximation purposes are the absolute values of $[Ca^{2+}]_i$ at the 0 and at 100% levels of the fluorescence ratio determined in separate measurements. In porcine coronary arterial smooth muscle cells, $[Ca^{2+}]_i$ at the 0 and 100% levels correspond to approx 100 and 900 n*M*, respectively.

b. Ionomycin induces an increase in the fluorescence signal in a concentration-dependent manner. The maximum response is obtained with 5 and 25 μ*M* ionomycin in rat aorta ***(9)*** and porcine coronary artery, respectively.
c. Grynkiewicz et al. ***(1)*** described the following equation to determine the absolute values of $[Ca^{2+}]_i$ in ratiometry:

$$[Ca^{2+}]_i = K_d\,(R - R_{min})/(R_{max} - R)(S_{f2}/S_{b2}) \quad (2)$$

where K_d is a dissociation constant and R is the fluorescence ratio (F340/F380). R_{max} is obtained by the addition of ionomycin in normal PSS (saturating Ca^{2+}), and R_{min} is obtained in Ca^{2+}-free PSS (zero Ca^{2+}). S_{f2}/S_{b2} is the ratio of proportionality coefficients of free fura-2 and Ca^{2+}-bound fura-2 at 380 nm, which is influenced by various optical factors, including excitation intensity, path length, and the instrumental efficiency. Therefore, in front-surface fluorimetry using optic fibers, the S_{f2}/S_{b2} values vary depending on the relation between the optic fibers and strips, even though they can be kept constant for each measurement. Since F380 is not stable at the time when F340 reaches $F340_{max}$ and $F340_{min}$, the recordings of R_{max} and/or R_{min} often appear to be difficult, and hence $[Ca^{2+}]_i$ cannot be determined. **Equation 1**, is thus considered to be the most appropriate for determining the absolute values of $[Ca^{2+}]_i$.
d. **Equation 2** is closely analogous to **Eq. 1**. From these two equations, the following form is obtained:

$$(F - F_{min})/(F_{max} - F) = (R - R_{min})/(R_{max} - R)(S_{f2}/S_{b2})$$

The S_{f2}/S_{b2} value can be adjusted to 1 by changing the optical slits in the light paths and/or by changing the relative positioning between the common end of the optic fibers and the strip. Empirically, in the range between $F = 0\%$ ($R = 0\%$) and $F = 100\%$ ($R = 100\%$), the following equation is obtained:

$$(F - F_{min})/(F_{max} - F) \approx (R - R_{min})/(R_{max} - R)$$

Thus, in the physiological range of changes in $[Ca^{2+}]_i$, one can employ the following equation to calculate the absolute values of $[Ca^{2+}]_i$:

$$[Ca^{2+}]_i \approx K_d\,(R - R_{min})/(R_{max} - R) \quad (3)$$

It has been noted, however, that the $[Ca^{2+}]_i$ values obtained are only an approximation of true $[Ca^{2+}]_i$ values.

References

1. Grynkiewicz, G., Poenie, M., and Tsien, R. Y. (1985) A new generation of Ca^{2+} indicators with greatly improved fluorescence properties. *J. Biol. Chem.* **269,** 3440–3450.
2. Hirano, K., Kanaide, H., Abe, S., and Nakamura, M. (1990) Effects of diltiazem on calcium concentrations in the cytosol and on force of contractions in porcine coronary arterial strips. *Br. J. Pharmacol.* **101,** 273–280.
3. Abe, S., Kanaide, H., and Nakamura, M. (1990) Front-surface fluorometry with fura-2 and effects of nitroglycerin on cytosolic calcium concentration and on tension in the coronary artery of the pig. *Br. J. Pharmacol.* **101,** 545–552.

4. Chance, B., Salkovitz, I. A., and Kovach, A. G. B. (1972) Kinetics of mitochondrial flavoprotein and pyridine nucleotide in perfused heart. *Am. J. Physiol.* **223,** 207–218.
5. Frank, H., Barlow, C. H., and Chance, B. (1976) Oxygen delivery in perfused rat kidney: NADH fluorescence and renal function state. *Am. J. Physiol.* **231,** 1082–1089.
6. Miyagi, Y., Kobayashi, S., Nishimura, J., Fukui, M., and Kanaide, H. (1995) Resting load regulates vascular sensitivity by a cytosolic Ca^{2+}-insensitive mechanism. *Am. J. Physiol.* **268,** C1332–C1341.
7. Di Virgilio, F., Steinberg, T. H., Swanson, J. A., and Silverstein, S. C. (1988) Fura-2 secretion and sequestration in macrophages: A blocker of organic anion transport reveals that these processes occur via a membrane transport system for organic anions. *J. Immunol.* **140,** 915–920.
8. Watanabe, C., Yamamoto, H., Hirano, K., Kobayashi, S., and Kanaide, H. (1992) Mechanisms of caffeine-induced contraction and relaxation of rat aortic smooth muscle. *J. Physiol.* **456,** 193–213.
9. Watanabe, C., Yamamoto, H., Kobayashi, S., and Kanaide, H. (1993) Extracellular Ca^{2+}-dependent potentiation by cocaine of serotonin- and norepinephrine-induced contractions in rat vascular smooth muscle. *Circ. Res.* **72,** 1191–1201.

19

Measurement of Calcium and Movement in Heart Cells

Leong L. Ng and Paulene A. Quinn

1. Introduction

Preparations of calcium-tolerant cardiac myocytes for studies on intracellular calcium ($[Ca^{2+}]_i$) signaling and contraction have been difficult owing to the susceptibility of these cells to the enzymatic digestion process. This often leads to the cells acquiring a bricklike contracted shape with a granular cytoplasm and membrane blebbing. A successful preparation results in single myocytes that do not show spontaneous contractions and that remain relaxed in Ca^{2+}-containing buffers, indicating that the sarcolemmal membrane was not damaged during enzymatic digestion and led to membrane depolarization.

A modification of the method of Eckel et al. ***(1)*** was used for isolation of cardiac myocytes ***(2)***. The perfusion with a low-Na^+ buffer reduces the influx of Na^+ during the digestion process, so that the operation of the cardiac Na^+-Ca^{2+} exchanger does not lead to $[Ca^{2+}]_i$ overload and death of the cardiac myocytes ***(3)***. Furthermore, the use of sucrose has a protective effect against the subsequent reintroduction of Ca^{2+} following the Ca^{2+}-free perfusion period that precedes introduction of the enzyme solution ***(1)***. This technique can be optimized to improve the yield of cells substantially, and following loading with the Ca^{2+} fluorophore fura-2 ***(4)***, it is possible to monitor changes in $[Ca^{2+}]_i$ and cell contractility using an epifluorescence microscope fitted with an edge detection device to measure movement ***(5)***.

2. Materials

1. Type V collagenase (EC 3.4.24.3, from *Clostridium histolyticum*, specific activity 435 U/mg) (*see* **Note 1**).
2. Hyaluronidase Type 1-S (EC 3.2.1.35, from bovine testes, specific activity 340 U/mg).

From: *Methods in Molecular Biology, Vol. 114: Calcium Signaling Protocols*
Edited by: D. G. Lambert

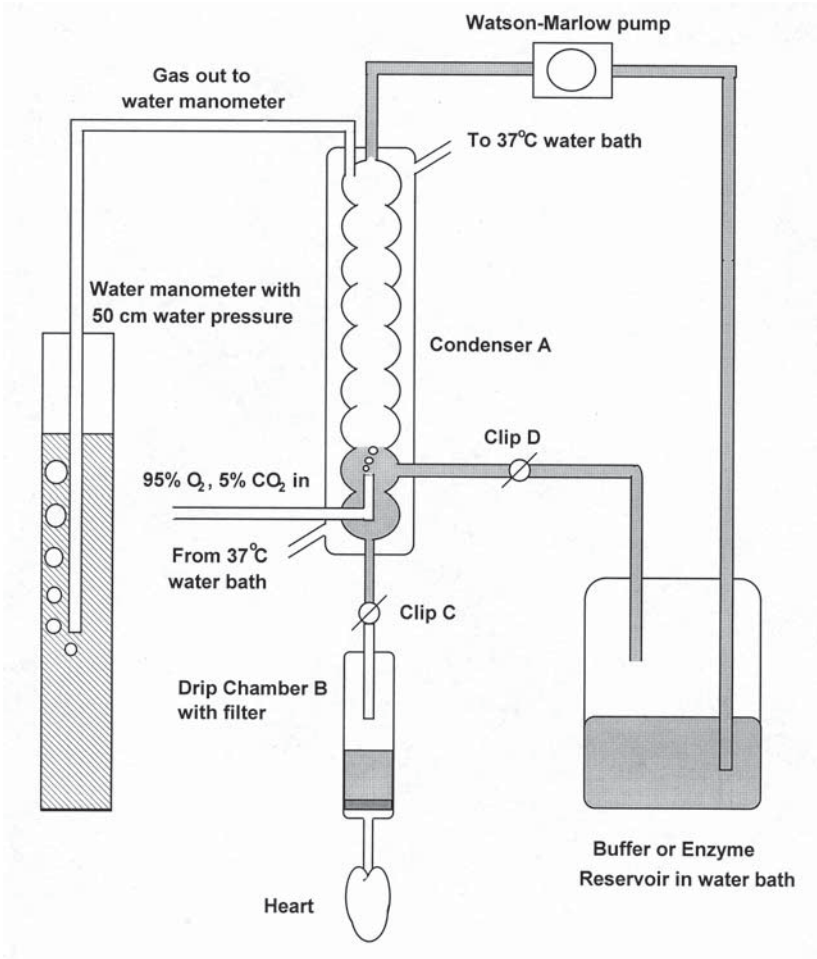

Fig. 1. Schematic representation of the "in-house" Langendorff apparatus.

3. Fatty acid–free bovine serum albumin (BSA).
4. Joklik's Minimal Essential Medium (MEM) were from Sigma, Poole, Dorset, UK.
5. Fura-2 acetoxyl methyl (AM) ester (fura-2/AM) is from Calbiochem, Nottingham, UK.
6. Ionomycin is from Calbiochem.
7. Cell-Tak is from Collaborative Research, Bedford, MA.
8. All other chemicals were of Analar grade and were from BDH, Poole, Dorset, UK.
9. The dual excitation Deltascan single-photon counting fluorometer is from Photon Technology International (PTI), South Brunswick, NJ.
10. The Video Edge Detection Device *(5)* is purchased from Crescent Electronics, Sandy, UT.
11. The Langendorff apparatus (**Fig. 1**) is made locally and consists of a glass condenser (A) for warming and oxygenating the buffer, which was pumped in by a

Watson-Marlow pump. The effluent from A can be recirculated to the buffer reservoir in a 37°C water bath or diverted into the drip chamber (B) cut from an intravenous set (Baxter Healthcare, Thetford, Norfolk, UK) (*see* **Note 2**).

a. 95% O_2, 5% CO_2 gas mixture is fed into the glass condenser at the bottom inlet and escapes via the top outlet into a manometer filled with water so that a pressure of approx 50 cm of water is maintained in the condenser and the drip chamber in order to perfuse the heart adequately.
b. Flow rate is regulated by a clip (C) just above the heart. Since the rate at which buffer is pumped in at the top of the condenser A will exceed the flow to the heart, any excess buffer that accumulates in the condenser has to be periodically released back into the buffer reservoir in the water bath through clip D.
c. Make a mark near the bottom on the side of the condenser A and the drip chamber B and measure the volume of fluid that is contained within the tubing, the condenser A, and the drip chamber B. This dead space will initially contain buffer A during the Ca^{2+}-free perfusion period and must be taken into account when the double-strength enzyme solution is introduced, so that the final enzyme solution that is recirculated during the digestion process becomes single strength enzyme buffer.

12. Buffer A is low-Na^+ buffer used for the enzymatic digestion of cardiac myocytes and is composed of 35 mmol/L NaCl, 4.75 mmol/L KCl, 1.19 mmol/L KH_2PO_4, 16 mmol/L Na_2HPO_4, 25 mmol/L $NaHCO_3$, 134 mmol/L sucrose, 1.2 mmol/L $MgSO_4$, 10 mmol/L HEPES, 10 mmol/L glucose, 5 mmol/L pyruvate, 20 mmol/L creatine, 2 mg/mL BSA (pH 7.4 when equilibrated with 95% O_2, 5% CO_2) (*see* **Note 3**).
13. Double-strength enzyme solution: buffer A with 1 mg/mL Type V collagenase, 2.5 mg/mL hyaluronidase Type 1-S and 100 µmol/L $CaCl_2$. A volume equal to the dead space of the Langendorff apparatus is measured into a reservoir and kept gassed and warmed at 37°C.
14. Buffer B is used for studying the $[Ca^{2+}]_i$ transients and consists of 134 mmol/L NaCl, 4 mmol/L KCl, 1.2 mmol/L $MgSO_4$, 10 mmol/L HEPES, 1.2 mmol/L NaH_2PO_4, 1.8 mmol/L $CaCl_2$, 11.1 mmol/L glucose, 2 mg/mL BSA 2 (pH 7.4 when bubbled with 100% O_2).

3. Methods

3.1. Cardiac Myocyte Isolation

1. Use Wistar rats weighing 250–300 g for isolation of Ca^{2+}-tolerant single ventricular myocytes.
2. Kill the animal with an ip injection of pentobarbital.
3. Open the chest and remove the heart quickly, ensuring that there is enough aortic stump to tie the heart onto the Langendorf apparatus without nipping the coronary arteries. Drop the heart immediately into ice-cold preoxygenated buffer A; it should stop beating after a few seconds.
4. Weigh the heart in this cold buffer A (*see* **Note 4**).

5. Start the Watson-Marlow pump running to fill the condenser A (**Fig. 1**) with the Ca^{2+}-free buffer A, and adjust the drip rate to approx 3 drops/s (1 mL = 20 drops). Return any buffer that builds up in the condenser to the buffer reservoir in the water bath by opening clip D.
6. Tie a cotton ligature loosely around the cannula and pick up the heart by the aortic stump and quickly tie onto the cannula, ensuring that the origins of the coronary arteries are not nipped in the process.
7. The retrograde perfusion of the heart with warm buffer A will lead to a few contractions that will empty blood from the ventricles, but these contractions rapidly stop owing to the lack of Ca^{2+} (*see* **Note 5**).
8. Adjust the rate of flow through the heart with clip C, so that the rate is maintained at 3 drops/s.
9. As the end of the Ca^{2+}-free period approaches, empty the level of the solutions down to the predetermined marks on the side of condenser A and drip chamber B by opening clip D (**Fig. 1**).
10. At 1 min, transfer the tubing from the buffer A reservoir in the water bath to the reservoir containing the premeasured volume of double-strength enzyme solution (the volume being equal to the dead space of the apparatus and the tubing, determined as detailed above).
11. Increase the pump rate to mix the dead space fluid with the double-strength enzyme solution rapidly, returning any excess accumulating in the condenser A to the reservoir by opening clip D (*see* **Note 6**).
12. Maintain the flow rate at 3 drops/min for a period of time (in minutes) equal to approx 1.5 multiplied by the weight of the heart (in grams) (*see* **Note 7**).
13. At the end of this time, the heart should feel soft and can be cut down from the cannula. Then coarsely cut it up on a McIlwain Tissue chopper (approx 1-mm cuts in two dimensions) and transfer the pieces into a plastic tube.
14. To achieve disaggregation, gently pipet (triturate) the pieces up and down in buffer A with a plastic Pasteur pipet with the tip cut off (without any added Ca^{2+}, other than the remains of the enzyme solution within the heart).
15. After allowing the large pieces of cardiac muscle to settle by gravity for 30 s, periodically inspect the turbid supernatant under the microscope; it initially contains many rounded granular dead cells or actively contracting rod-shaped cells, which are damaged cardiac myocytes. Following approx 5–10 min of periodic trituration, some rod-shaped cells that are not actively contracting will be released and these supernatants should be saved.
16. Carefully layer the supernatants containing quiescent rod-shaped cells onto buffer A containing 6 g/100 mL of BSA. Allow the cells to settle by gravity for 5 min, and remove the pellet at the bottom of the tube that contains the quiescent rod-shaped cells.
17. This can be performed two to three times to obtain a pellet consisting mostly of live undamaged cardiac myocytes.
18. Combine the pellets into Joklik's MEM (that does not contain Ca^{2+}) and recover the cells by centrifugation at 160*g* for 3 min on a benchtop centrifuge.

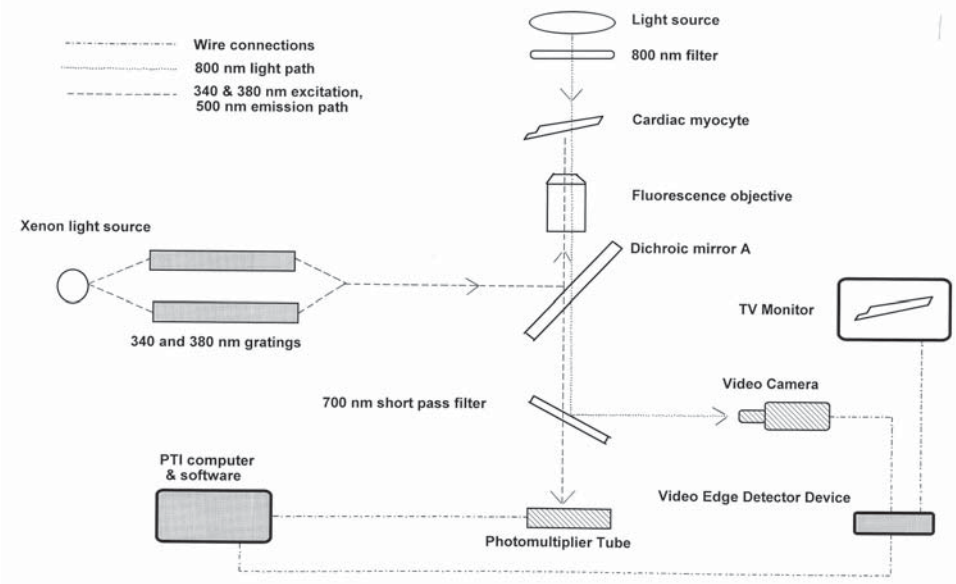

Fig. 2. System alignment for simultaneous measurements of Ca^{2+} and movement in isolated myocytes.

19. Resuspend the cells in Joklik's MEM at room temperature, add $CaCl_2$ to a final concentration of 0.25 mmol/L and allow the cardiac myocytes to adjust to this for 30 min before increasing the Ca^{2+} concentration to 1.8 mmol/L. The cells should be viable and Ca^{2+} tolerant for approx 24 h.

3.2. Measurement of $[Ca^{2+}]_i$ and Movement

1. The cardiac myocytes can then be loaded with fura-2/AM (5 µmol/L final concentration, premixed with Pluronic F127 100–200 mg/L before adding the Joklik's MEM containing 1.8 mmol/L of $CaCl_2$) for 30 min at 37°C.
2. Wash the cells twice to remove fluorophore, and they are left to de-esterify the fura-2/AM for 15–30 min at room temperature.
3. Then layer the cells onto quartz cover slips (Carl Zeiss, Welwyn, UK) that have been coated with Cell-Tak, a tissue adhesive approx 3.5 µg/cm^2, and leave to attach for 30 min (*see* **Note 8**).
4. Once cells are attached with the Cell-Tak, it is possible to change the solutions in the incubation chamber without washing off the cells. Buffer B can be used in most applications.
5. Cover slips with the attached cells are then inserted into a specially constructed cover slip holder that is held within a Peltier incubation platform, which maintains the cells at 37°C (*see* **Note 9**).
6. The instrumentation for measurement of epifluorescence emission and movement is detailed in **Fig. 2**.

7. Set dual excitation wavelengths at 340 and 380 nm with a data acquisition time of 50–100 ms (*see* **Note 10**).
8. To simultaneously measure movement, insert a near infrared filter (800 nm) beneath the microscope lamp (**Fig. 2**) so that long-wavelength light can be used to measure the movement of cells without interfering with the fluorescence measurements (*see* **Note 11**).
9. The PTI software allows both the 340/380 fluorescence ratios and the Reference Cell Quantum Counter (RCQC) outputs to be simultaneously displayed, and in this instance, the RCQC output represents myocyte length.
10. Recording of $[Ca^{2+}]_i$ and movement are made simultaneously, using platinum or silver wire electrodes to stimulate the cardiac myocytes to contract.

3.3. Calibration of Fura-2 Ratios and Video Edge Detector Outputs

1. Cells are superfused with glucose- and BSA-free buffer B, with the metabolic poisons carbonyl cyanide *m*-chlorophenylhydrazone (an inhibitor of oxidative phosphorylation) 5 µmol/L, amytal (an inhibitor of NADH dehydrogenase) 3.3 mmol/L ***(6)***. After 20 min, the intracellular ATP stores are sufficiently depleted so that manipulation of intracellular calcium does not cause contracture.
2. R_{max} for the fura-2 is determined by addition of the nonfluorescent ionophore ionomycin (10 µmol/L) in buffer B (which contains 1.8 mmol/L of Ca^{2+}).
3. R_{min} is obtained by addition of EGTA 10 mmol/L to chelate the Ca^{2+}. Intracellular free $[Ca^{2+}]_i$ can thus be calculated using the equation $[Ca^{2+}]_i = K_d \times (R - R_{min})/(R_{max} - R) \times S_f/S_b$, in which K_d is 225 nmol/L at 37°C, and S_f/S_b is the ratio of cellular fluorescence emission with excitation at 380 nm for Ca^{2+}-free and Ca^{2+}-saturated buffers ***(4)***.
4. To calibrate the output from the Video Edge Detector Device, a piece of glass capillary of known outer diameter is visualized at the same magnification as used for the cell measurements, and detection of the edges by changing the thresholds on the edge device would enable an output to the RCQC sockets of the PTI fluorometer to be measured and expressed as an absolute length measurement.

4. Notes

1. An alternative crude collagenase is the preparation from Boehringer Mannheim, Mannheim, Germany (collagenase A, cat. no. 103586). Each batch of these enzymes has to be tested for their activity on the preparation of cardiac myocytes and the time of digestion and concentration of the enzyme standardized. Some methods recommend protease (pronase E), which considerably speeds up the digestion, but it is difficult to control and kills the myocytes.
2. The drip chamber enables the flow rate to the heart to be controlled more accurately and also prevents air and particle embolization into the heart, resulting in infarction.
3. The free Ca^{2+} of this buffer is approx 1 µmol/L when Milli-Q water is used to make up the buffer. Ensure that the buffer A is fully oxygenated with 95% O_2, 5% CO_2 at 37°C for 15 min before the rat is killed.

4. The heart weight determines the duration of enzymatic digestion.
5. This Ca^{2+}-free perfusion period should be limited to 1 min to disrupt intercalated discs, but must not be continued for much longer since the heart could undergo a Ca^{2+} paradox when the enzyme solution with Ca^{2+} is subsequently introduced, leading to contracture and death of the cells.
6. The enzyme should start perfusing the heart, and it may commence beating for a few minutes.
7. This factor of 1.5 may need to be changed with different batches of collagenase, but is a good starting guide to the length of digestion.
8. The quartz cover slips are necessary since the excitation wavelengths for fura-2 are 340 and 380 nm, and ordinary glass would attenuate the 340-nm illumination.
9. It is also possible to gas the surface of the incubation buffers with air containing 5% CO_2 if bicarbonate buffers are used.
10. Dichroic mirror A (Fig. 2) had a half-pass wavelength of 400 nm and reflected the excitation light through the ×20 Nikon fluorescence objective lens onto the cardiac myocyte. The longer wavelength emitted by fura-2 was transmitted by dichroic mirror A. This light was transmitted through a short-pass filter B (half-pass wavelength of 700 nm) mounted at 45° in the side arm of the PTI fluorometer and impinged on the single-photon counting photomultiplier tube. Signals from this tube were collected by the computer, and the PTI software enabled the on-line computation of 340/380 fluorescence ratios. An estimate of the $[Ca^{2+}]_i$ could be read on-line if constants for the equation $[Ca^{2+}] = K_d \times (R - R_{min})/(R_{max} - R) \times S_f/S_b$ ***(4)*** are predetermined as detailed in **Subheading 3.3.** and fed into the software.
11. This long wavelength light was transmitted by dichroic mirror A and was reflected by the short-pass (700 nm) filter B into a video camera. The output from this camera is fed into the Video Edge Detection Device ***(5)***, and the video output from this is then connected to a TV monitor to visualize the cardiac myocyte (the original video input signal) together with the detection windows with the edge points marked. It may be necessary to change the thresholds of the device so that the contrast between the edge of the myocyte and the background can be successfully detected. The output from the Video Edge Detection Device can be fed into the PTI connector box, in the RCQC sockets.

References

1 Eckel, J., Pandalis, G., and Reinauer, H. (1983) Insulin action on the glucose transport system in isolated cardiocytes from adult rat. *Biochem. J.* **212,** 385–392.
2. Ng, L. L., Davies, J. E., and Quinn, P. (1993) Intracellular pH regulation in isolated myocytes from adult rat heart in HCO_3^-containing and HCO_3^--free media. *Clin. Sci.* **84,** 133–139.
3. Tani, M. and Neely, J. R. (1989) Role of intracellular Na^+ in Ca^{2+} overload and depressed recovery of ventricular function of reperfused ischemic rat hearts: Possible involvement of Na^+-H^+ and Na^+-Ca^{2+} exchange. *Circ. Res.* **65,** 1045–1056.

4. Grynkiewicz, G., Poenie, M., and Tsien, R. Y. (1985) A new generation of calcium indicators with greatly improved fluorescence properties. *J. Biol. Chem.* **260,** 3440–3450.
5. Steadman, B. W., Moore, K. B., Spitzer, K. W., and Bridge, J. H. (1988) A video system for measuring motion in contracting heart cells. *IEEE Trans. Biomed. Eng.* **35,** 264–272.
6. Li, Q., Altshuld, R. A., and Stokes, B. T. (1987) Quantitation of intracellular free calcium in single adult cardiomyocytes by fura-2 fluorescence microscopy: Calibration of fura-2 ratios. *Biochem. Biophys. Res. Commun.* **147,** 120–126.

20

Simultaneous Analysis of Intracellular pH and Ca^{2+} from Cell Populations

Raul Martinez-Zaguilan, Linda S. Tompkins, Robert J. Gillies, and Ronald M. Lynch

1. Introduction

Manipulation of cell function through stable transfection of agonist-specific receptors, components of second messenger cascades, or proteins with specific functional activities (enzymes, transporters, channels) has provided the tools to study intra- and intercellular signaling phenomena at a molecular level ***(1–4)***. In addition, cotransfection of cells with sequences coding for fluorescent markers such as green fluorescent protein has facilitated the selection and analysis of transfected cells ***(5)***. Techniques are also required to screen for and to monitor the functional changes associated with the genetic manipulation in order to investigate the physiological role of a component within a complex system such as a cell. Hormones and other agonists often elicit changes in intracellular pH (pH_{in}) ***(6,7)*** and/or calcium ($[Ca^{2+}]_i$) ***(8,9)*** that modulate cell responses. Thus, methods for comparing steady-state ion concentrations and the regulation of these ions between cell populations in which signaling pathways have been modified can provide an approach to screen for functional changes in signal transduction for selective agonists.

There are several fluorescent indicators for measuring pH and Ca^{2+} ***(10)***. These probes are commercially available in acetoxymethyl (AM) ester forms, which allow passive loading of cells with minimal effect on cell physiology ***(10)***. Optimally, these probes should be specific for the ion of interest and have a high quantum efficiency, and the affinity of the probe (K_d) for the ion of interest should be within the physiological range. To simultaneously monitor pH_{in} and $[Ca^{2+}]_i$, the probes need to have distinct excitation or emission

From: *Methods in Molecular Biology, Vol. 114: Calcium Signaling Protocols*
Edited by: D. G. Lambert

characteristics. An additional feature required for accurate analyses is that each probe exhibit at least two excitation or emission wavelengths reciprocally sensitive to the ion of interest. The ratio of ion-sensitive wavelengths provides a precise measure of ion levels that is relatively independent of dye concentration. An excitation or emission wavelength that is ion insensitive is also desirable, since analysis of signal intensity at this wavelength allows for simultaneous determination of the efficiency of dye loading, dye leakage from cells, as well as possible interactions between probes including quenching ***(11)***.

Two probes that meet the described criteria for simultaneous pH/Ca^{2+} measurements are snarf-1 and fura-2 ***(11,12)***. The ratio of fluorescence emission intensities at 644/584 nm for snarf-1, and the ratio of fura-2 fluorescence excited alternately at 340/380 nm can be used to generate calibration curves for pH and Ca^{2+}, respectively. The isoexcitation wavelength (ion insensitive) for fura-2 at 360 nm and the isoemission wavelength of snarf-1 at 600 nm are monitored to determine the stability of dye loading and to alert one to other potential artifacts.

Although changes in both pH_{in} and $[Ca^{2+}]_i$ have been observed in response to a variety of agonists, it is not clear whether these ionic events work independently or are coordinated to lead to a specific physiological response. One of the fundamental problems in studying these ionic events is that changes in pH_{in} modify Ca^{2+} regulatory mechanisms (e.g., Ca^{2+}-binding proteins, Ca^{2+} ATPase ***[13]*** Ca^{2+} channels ***[14]***) and changes in Ca^{2+} may modify pH regulation (e.g., Na^+/H^+ exchanger ***[15]***, H^+-ATPase ***[16]***). Therefore, it is desirable to use a technique that allows concomitant monitoring of these two ions in cell populations with high time resolution. Furthermore, like many Ca^{2+} binding proteins, all Ca^{2+}-sensitive fluoroprobes are inherently sensitive to pH owing to competition of H^+ for the Ca^{2+}-binding sites ***(17)***. Thus, changes in pH induced by an agonist can complicate analysis of the activated Ca^{2+} response when using Ca^{2+} fluoroprobes. Similarly, analysis of differences in steady-state Ca^{2+} between unique cell populations can be influenced by differences in resting cell pH. For example, resting pH in neoplastic cells is generally higher compared to normal controls ***(18)***. For most Ca^{2+} fluoroprobes, the sensitivity to H^+ is most prevalent at relatively acidic pH values ***(17,19)***. However, many cell lines do exhibit resting pH lower than 7.0, and some perturbations can lower pH into the sensitive range. Fortunately, the effect of pH on the Ca^{2+}-binding parameters can be predicted and used to correct the Ca^{2+} signal ***(12,19)***.

This chapter describes experimental paradigms that provide optimum conditions for simultaneous measurement of pH from the fluorescence emission of snarf-1, and Ca^{2+} using fura-2. The fluorescence spectra of these compounds are sufficiently different to allow simultaneous measurement of pH and Ca^{2+} both in vitro and in vivo. Moreover, the ratio of the H^+-sensitive wavelengths of

snarf-1 is unaffected by Ca^{2+}, or the concomitant presence of fura-2 in cells ***(19)***. Although the fluorescence ratio of fura-2 is insensitive to the presence of snarf-1, it is affected by pH, as indicated above. Therefore, the authors will describe procedures to correct for this effect and to obtain the calibration parameters (K_d or pK_a, R_{min} and R_{max}) for fura-2 and snarf-1 required to facilitate analysis of pH and Ca^{2+} concentrations within cell populations.

2. Materials

1. Three cell lines are used in the studies described:
   a. RIN-38 are an insulin-secreting transformed β cell line ***(20)***.
   b. Endothelial cells were isolated from human umbilical vein endothelium (HUVE) ***(21)***.
   c. RN1a cells are NIH-3T3 fibroblasts transfected with the sequence encoding for yeast p-type H^+-ATPase ***(3,18)***.
2. Cell culture media is Dulbecco's modified Eagle's medium supplemented with 5.6 m*M* glucose, 10% fetal bovine serum (FBS), 1U penicillin/mL, and 0.1 mg/mL streptomycin sulfate.
3. Cells are cultured for experiments on glass coverslips (9 × 22 mm) contained in 10-cm dishes at initial plating densities of approx 5×10^4 cells/dish. Cells are grown to near confluency for fluorescence experiments.
4. 0 Ca^{2+} buffer (KEGTA): 110 m*M* KCl, 20 m*M* MOPS, 20 m*M* NaCl, and 10 m*M* K_2H_2EGTA. The K_2H_2EGTA is obtained by mixing equimolar concentrations of EGTA and K_2CO_3. pH is adjusted using KOH.
5. Calcium-saturated buffer (CaEGTA): 110 m*M* KCl, 20 m*M* MOPS, 20 m*M* NaCl, and 10 m*M* $K_2CaEGTA$ obtained by mixing equimolar concentrations of EGTA and $CaCO_3$. The most critical requirement for this buffer is to contain equimolar concentrations of calcium and EGTA in order to achieve a stoichiometric balance. Because EGTA is rarely 100% pure, these buffers normally contain a 5% excess of EGTA by weight (*see* **Note 1**). This excess EGTA in K_2EGTA buffer is not likely to cause problems because the performance of calcium buffers is not very sensitive to total calcium concentration.
6. Standard experimental buffer (EB): 1.3 m*M* $CaCl_2$, 1 m*M* $MgSO_4$, 5.4 m*M* KCl, 0.44 m*M* KH_2PO_4, 110 m*M* NaCl, 0.35 m*M* NaH_2PO_4, 1 m*M* $NaHCO_3$, 5 m*M* glucose, 2 m*M* glutamine, and 25 m*M* HEPES, pH 7.15, at 37°C. Experiments can be performed under 5% CO_2/95% air if the EB contains HCO_3^- at a concentration set by its equilibrium with CO_2 at the desired pH value using **Eq. 1**

$$[HCO_3^-] = pK_a\ (1.52\ mM) \times 10\ (pH - 6.24) \qquad (1)$$

   in which 1.52 m*M* is the concentration of CO_2 in Hank's balanced salt solution at 37°C, and 5% ambient CO_2 (e.g., pCO_2 = 38 mmHg); and 6.24 is the pK for the process of CO_2 hydration ***(22)***.
7. In vitro pH values used for calibration are obtained with a Beckman (Fullerton, CA) model 71 pH meter, using a Beckman gel-filled combination electrode. The

electrode is calibrated at two known pH values using commercially prepared standards from VWR Scientific (San Francisco, CA).

8. Fluorescence measurements are performed in a temperature-controlled cuvet housed in an SLM 8000C fluorometer (SLM, Urbana, IL) using 4-nm band-pass slits and an external rhodamine standard as a reference. Sample temperature is maintained at 37°C by keeping both the water jacket and the buffer at 37°C using a circulating water bath. Spectral data for fura-2 are acquired by scanning the excitation monochrometer between 300 and 500 nm with the emission monochrometer set at 510 nm. Spectra from snarf-1 are acquired by setting the excitation monochrometer at 534 nm and scanning the emission monochrometer between 540 and 700 nm.
9. Cell holder for fluorometric measurements: Two cover slips containing cells are placed back to back (cells on the outside surface), and transferred to the quartz fluorometer cuvet using a holder/perfusion device as described previously ***(23)***. The holder maintains the cover slips upright in the fluorescence light path at an angle of 30° allowing for illumination of a spot at the same position on both cover slips. The use of quartz cuvets is essential when monitoring fluorescence in the ultraviolet region, as with fura-2. Tubing from a dual line peristaltic pump is used to introduce fresh media into the bottom of the chamber while removing an equal volume from the chamber top. Small bore tubing (Masterflex #13, Fluid Metering Inc., Syosset, NY) is used as the inlet and larger bore tubing (#14) for the outlet line. The cells are continuously perfused at a rate of 3.0 mL/min (*see* **Note 2**). Prototypes of this device with modifications have been published elsewhere ***(23,24)***. A commercially available cover slip holder for fluorescence measurements is also available (Spectronics Instruments, Rochester, NY).
10. Fluorometric data collection for simultaneous pH and Ca^{2+} measurements: Continuous data collection occurs while the emission and excitation modes are alternated as follows. Emission at 510 nm with sequential scanning to excitation wavelengths of 340, 360, and 380 nm (fura-2 conditions), followed by excitation at 534 nm with the emission monochrometer sequentially scanned to 584, 600, and 644 nm (snarf-1 conditions). An individual cycle requires 15 s. Temporal resolution is limited primarily by the slew rate of the monochrometer, and not integration time of the phototube. Data are translated to ASCII format for manipulation and analysis ***(19)***.
11. Data analysis: Conversions of ratio values to both pH_{in} and Ca^{2+} are performed using **Eqs. 2**, **3**, and **6** (**Subheading 3.1.**), and plotted using a commercial software (*see* **Note 3**; Sigmaplot, Statistical Product and Service Solutions, Chicago, IL). Analysis of both in vitro and *in situ* calibration curves, as well as estimation of the pK_as, R_{max}, and R_{min} values for snarf-1 and fura-2 are obtained from **Eqs. 1–5** using a simplex method and by least-squares regression analysis (MINSQ, MicroMath Scientific Software, Salt Lake UT, or Sigmaplot).
12. Fluoroprobes are obtained from Molecular Probes (Eugene, OR). For each day of experiments, a fresh batch of dye is used. AM dyes are prepared using anhydrous methylsulfoxide (MSO) as a solubilizing agent. The fluorescent probes can be obtained in 50-µg or 1-mg portions. MSO is removed from its container using a

syringe equipped with an appropriate gauge needle, or, for the small volumes required for the 50-µg containers, a Hamilton syringe can be used. If 1-mg quantities are prepared, the stock solution should be aliquoted into smaller portions (10 µL) and stored at –80°C until use. Freeze thawing of probes should be avoided. An alternate source for fluorescent ion indicators is Teflabs (Austin, TX).

13. Unless otherwise stated, all other chemicals were obtained from Sigma.

3. Methods

3.1. Calculation of pH and Ca^{2+} from the Ratio of Ion-Sensitive Wavelengths

Excitation or emission wavelengths that increase or decrease on cation binding are monitored. The ratio of fluorescence at the ion-sensitive wavelengths is used to determine the extent of ion-bound dye, and hence the free ion concentration by the following equations:

$$\mathrm{pH} = \mathrm{pK}_a + \log(S_{f2}/S_{b2}) + \log[(R - R_{min})/(R_{max} - R)] \quad (2)$$

$$[Ca^{2+}] = K_d(S_{f2}/S_{b2})[(R - R_{min})/(R_{max} - R)] \quad (3)$$

in which R, R_{min}, and R_{max} are the measured, minimum, and maximum ratios, respectively. For snarf-1, R increases with pH; hence R_{max} represents the ratio of fluorescence intensity of ion-sensitive wavelengths under fully deprotonated conditions, whereas R_{min} is the ratio for the dye when it is fully protonated. In the case of fura-2, R increases with increasing Ca^{2+}; hence R_{min} represents fura-2 in the absence of Ca^{2+} (Ca^{2+} <1 n*M*) whereas R_{max} represents the Ca^{2+}-fura-2 chelate. S_{f2} and S_{b2} are the fluorescence values at the denominator wavelengths for the free and bound forms of the dye, respectively. These values are used to correct the titration curve for the fact that denominator and numerator wavelengths are independently sensitive to ion binding. If an ion-insensitive wavelength is used as the denominator, S_{f2}/S_{b2} becomes 1 and the term is eliminated.

Since the ratio of fluorescence at the ion-sensitive wavelengths for fura-2 is affected by pH, corrections for changes in pH during an experiment, or when comparing steady-state values between populations is often warranted. The pH sensitivity of fura-2 can be described by the following equations which rely on data acquired from the calibrations described in **Subheading 3.2.** The effect of pH on the K_d is described by # (pH corrected):

$$K_d\# = (K_{d\,max} + \log10(\mathrm{pH}_{in} - \mathrm{pK}_a) \times K_{d\,min})/\log10(\mathrm{pH}_{in} - \mathrm{pK}_a) + 1 \quad (4)$$

whereas the effect of pH on the R_{min} and R_{max} of fura-2 is determined by

$$R\# = k1 \times (\mathrm{pH})^3 + k2 \times (\mathrm{pH})^2 + k3 \times (\mathrm{pH}) + k4 \quad (5)$$

Eq. 5 is empirically derived by fitting data acquired from the in vitro calibration curves generated for fura-2 as pH is varied. Thus, pH-corrected $[Ca^{2+}]$

($[Ca^{2+}]^{\#}$) can be estimated by using the following equation and fitting these parameters into the equation:

$$[Ca^{2+}]^{\#} = K_d\# \times (R - R_{min}{}^{\#})/R_{max}{}^{\#} - R) \quad (6)$$

The accuracy of the $[Ca^{2+}]$ estimate relies on the accuracy of *in situ* and in vitro titrations ***(19)***. It also relies heavily on appropriate estimations of pH. In many cases, the K_d of fura-2 for Ca^{2+} in vitro is similar to that measured *in situ*, so this parameter may not be cell-type dependent ***(12,19)***. However, other investigators have reported differences between the in vitro and *in situ* estimated K_d values ***(25,26)***. Moreover, the R_{max} and R_{min} values are likely to be cell-type dependent because the dynamic range of the dyes is determined by viscosity and interactions of dye with intracellular proteins. Thus, the authors emphasize the need for determining the calibration parameters in individual cell types if accurate quantification of $[Ca^{2+}]$ is required.

3.2. In Vitro Calibration of Snarf-1 and Fura-2

In vitro calibration of dyes allows estimation of pH and Ca^{2+} concentrations from the measured ratio values (**Fig. 1**). However, this calibration is also important to determine the dynamic range of the equipment and which R_{min} and R_{max} ratio values are reasonable. To calibrate the probes, Ca^{2+} concentration is varied at a set pH by combining fixed amounts of KEGTA and CaEGTA buffers that are held at constant and equal pH by strong buffers that do not bind Ca^{2+}, such as MOPS. A set of EGTA buffers are prepared between pH 5.5 and 8.0. Equal amounts of fura-2 and snarf-1 are added to each of the initial stock solutions. By serially diluting the KEGTA solution with CaEGTA at a given pH, calibration solutions are prepared with good precision. The magnitude of the increment in Ca^{2+} is determined by the effect of pH on the K_d EGTA; specifically, smaller (tenths of nanomolar increments) are obtained at alkaline pH, whereas larger increments (i.e., hundredths of nanomolar to micromolar) are obtained at acidic pH ***(27)*** (*see* **Note 4**).

1. Fura-2 and snarf-1 in their free acid forms are dissolved to final concentrations of 2 μ*M* and 1 μ*M*, respectively, into 30 mL of the KEGTA buffer held at 37°C and a specific pH between 5.5 and 8.0. pH is titrated using KOH.
2. A 3-mL aliquot is placed into a quartz cuvet, and the initial fura-2 excitation and snarf-1 emission data are acquired (zero Ca^{2+}).
3. Three mL of CaEGTA (at the same pH) containing 2 μ*M* fura-2– and 1 μ*M* snarf-1–free acids is added to the remaining 27 mL with stirring; e.g., 9 mmol KEGTA added to 1 mmol CaEGTA. Again, a 3-mL aliquot is taken to acquire fura-2 excitation and snarf-1 emission data.
4. Each 3-mL aliquot removed for fluorescence analysis is replaced with an equal volume of the CaEGTA to provide a continuous variation in Ca^{2+}. This procedure provides incremental changes in "cell" Ca^{2+}, as described previously ***(12,19)***.

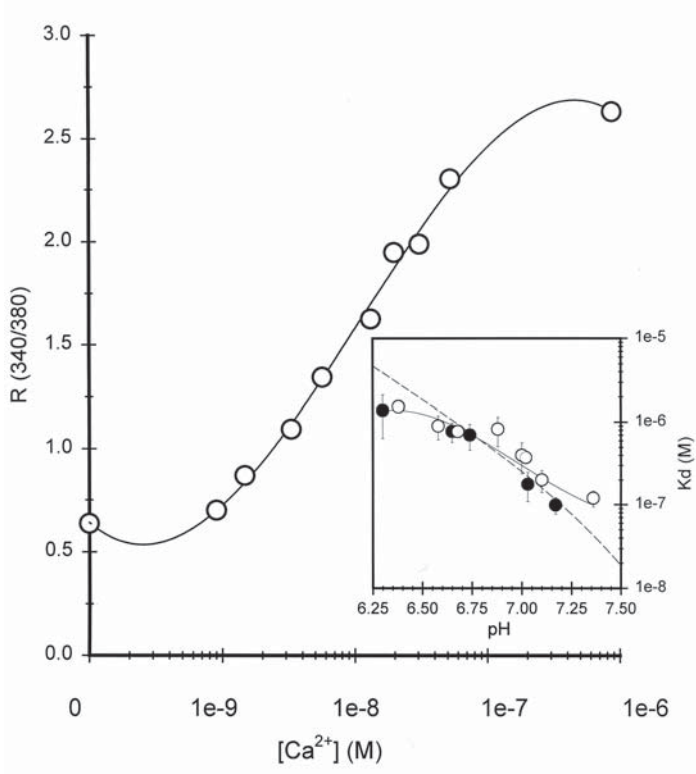

Fig. 1. *In situ* calibration of fura-2 in 3T3 Cells. The 340/380 ratio for fura-2 increases as Ca^{2+} is increased at fixed pH. Similar calibrations were repeated over a range of pH values indicated in the insert. The inset shows the effect of pH on the apparent affinity of fura-2 for Ca^{2+} estimated in vitro (i.e., dyes in solution; open circles) and in 3T3 cells (closed circles). Each point represents the mean ±SD of 9–11 different Ca^{2+} concentrations per pH value. H^+ and Ca^{2+} dissociation constants were calculated as described earlier. The dashed line indicates the effect of pH on the K_d of EGTA ***(19)***.

The estimated Ca^{2+} concentrations for each of 11 iterations at three distinct pH settings are provided in **Table 1** as an example.

5. Another set of 30-mL starting solutions of KEGTA and CaEGTA are titrated to a unique pH, and the procedure is repeated. Increments of 0.25 pH units are reasonable for the initial titration. However, subsequent calibrations can be performed using 0.5 pH unit increments.

3.3. Loading of Ion-Sensitive Indicators into Cells

The ion-sensitive probes in their AM forms are lipophilic and cell permeant. Cellular esterases cleave the ester groups to yield free acids that are relatively impermeant and, therefore, "trapped" within cells ***(10)***. *See* **Note 5** regarding

Table 1
Estimated Concentration of Ca^{2+} at Three Sequential Dilutions as Described in Subheading 3.2.

Dilution	1	2	3	4	5	6	7	8	9	10	11
pH 7.2	0	$1.0e^{-8}$	$2.11e^{-8}$	$3.35e^{-8}$	$4.73e^{-8}$	$6.25e^{-8}$	$7.94e^{-8}$	$9.83e^{-8}$	$1.19e^{-7}$	$1.42e^{-7}$	$1.68e^{-7}$
pH 7.0	0	$3.73e^{-8}$	$7.88e^{-8}$	$1.25e^{-7}$	$1.76e^{-7}$	$2.33e^{-7}$	$2.96e^{-7}$	$3.66e^{-7}$	$4.45e^{-7}$	$5.31e^{-7}$	$6.28e^{-7}$
pH 6.3	0	$4.69e^{-7}$	$9.9e^{-7}$	$1.57e^{-6}$	$2.22e^{-6}$	$2.93e^{-6}$	$3.72e^{-6}$	$4.6e^{-6}$	$5.58e^{-6}$	$6.67e^{-6}$	$7.88e^{-6}$

sequestration of probes into subcellular compartments, and **Note 6** regarding cell viability issues.

1. Two cover slips containing confluent or near confluent cell cultures are incubated for 30 min at 37°C in 3 mL of EB containing 7 μ*M* snarf-1/AM and 2 μ*M* fura-2/AM. This can be performed in a single well of a six-well cell culture dish, and all wash solutions can occupy other wells (*see* **Note 7**).
2. After the 30-min loading period, the cells are washed three times with EB containing 0.2% (v/v) FBS, followed by a second incubation in FBS containing EB for 30 min, to allow for the complete hydrolysis of the esters, and leakage of uncleaved dyes from the cells.
3. The two cover slips are placed back to back into the holder/perfusion device, which is subsequently inserted into the fluorometer cuvet for pH/Ca^{2+} measurements.

3.4. In Situ *Calibration of Snarf-1 and Fura-2*

In situ calibrations are important to compare absolute steady-state concentrations of the ions in different cell populations. This is particularly important when cells are transfected with vectors that influence growth rate, which often is associated with changes in steady-state pH ***(3,28)***. In addition, biological variability between cells must be recognized. By incubating cells in an "intracellular" buffer in the presence of selective ionophores for H^+, K^+, and Ca^{2+}, intracellular ion concentration can be manipulated by changing media concentrations, and therefore, the probes trapped within the cytosolic compartment can be adequately calibrated. 4Br-A23187, a nonfluorescent Ca^{2+} ionophore is used in combination with nigericin/valinomycin in high K^+/EGTA buffers to generate physiologically relevant calibration curves for intracellularly trapped fura-2 and snarf-1 (*see* **Note 8**). By varying pH_{ex} between pH 6.0 and 8.0 at 0.25 unit increments, one can obtain the pK_a of snarf-1 from the *in situ* calibration curves. Sequential incubation with media containing incrementally increasing Ca^{2+} concentration ranging from 0 to submicromolar or low micromolar to 250 μ*M* provides a full analysis of K_d, R_{min}, and R_{max} for fura-2 at each pH.

1. 300 mL of KEGTA containing 2 μ*M* 4Br-A23187, 2 μ*M* valinomycin, and 5 μ*M* nigericin is prepared.
2. Dye-loaded cells on cover slips are transferred to the fluorometer cuvet and perfused in KEGTA buffer at selected pH values. Fluorescence is then continuously recorded until equilibration of extracellular ions with the intracellular space is reached—typically 3–5 min.
3. Fura-2 excitation and snarf-1 emission spectra are acquired (*see* **Note 9**).
4. Sequential dilutions: **Steps 3–5** are identical to those carried out for in vitro calibrations (**Subheading 3.2.**). However, a minimum of 3 min is required for equilibration of ions between media and intracellular space at the new Ca^{2+}/pH setting (*see* **Note 10**).

3.5. Comparison of Steady-State Ion Concentrations Between Unique Cell Populations

To evaluate the validity of using *in situ* calibration parameters for estimating pH and Ca^{2+} in each specific experiment, the *in situ* R_{min} and R_{max} for both probes needs to be assessed. For simplicity and reliability, cells are perfused with KEGTA and CaEGTA buffers (containing ionophores) at three distinct pH values (i.e., 6.0, 7.0, and 7.5) to obtain the corresponding *R* values, thereby allowing comparison of the *in situ* titration parameters from a discrete number of points vs those generated from a complete *in situ* titration (*see* **Note 10**).

1. Dye-loaded cells on cover slips are transferred to the fluorometer cuvet and perfused in EB for 2 to 3 min prior to data acquisition. Full emission and excitation spectra are acquired to evaluate the quality of the spectra (*see* **Note 11**).
2. Fluorescence data at ion-sensitive wavelengths are then acquired, and ion-insensitive wavelengths are followed to determine if dye loading is stable or if dye is quenched (*see* **Notes 12** and **13**).
3. The resting ion concentrations are evaluated after a stable signal is obtained (*see* **Note 14**).
4. Full emission and excitation spectra of snarf-1 and fura-2 are acquired to confirm that the spectral characteristics are comparable to the calibration spectra.
5. The perfusion media are changed to KEGTA buffer containing ionophores at a selected pH value (e.g., 6.3; **Table 1**, *see* **Note 9**), and fluorescence is continuously recorded until equilibration of extracellular ions with the intracellular space is achieved—typically 3–5 min.
6. The perfusion media are changed to KEGTA diluted with CaEGTA held at equal pH to obtain a midrange Ca^{2+} concentration (e.g., approx 3 μ*M*, dilution 5; *see* **Note 9**, **Table 1**).
7. The perfusion media are changed to KEGTA diluted with CaEGTA held at equal pH to obtain the maximal Ca^{2+} concentration (dilution 11; *see* **Note 9**, **Table 1**).
8. Sequence 5–7 is repeated at two additional pH values (e.g., *see* **Note 4**).
9. Spectra obtained at each pH/Ca^{2+} value are compared to those obtained during the *in situ* calibrations at the same pH/Ca^{2+} values, to determine the validity of the limited calibration.

3.6. Experimental Protocols for Analyzing Ion Homeostasis

Alterations in expression of many specific proteins are translated into differences in cell function. Specific experimental protocols can be designed to test directly for the associated changes in handling of H^+ and Ca^{2+}. Analyses of these effects are simplified if each cell is used as its own control. However, as we will demonstrate, accurate *in situ* calibration can be crucial for determining the accuracy of a response under specific conditions. Provided in this section are examples that describe methods for testing some specific pathways impor-

tant for ion homeostasis. In addition, methods for standardizing responses between experiments are described.

3.6.1. Na^+/Ca^{2+} Exchanger

The effect of Na^+ removal on $[Ca^{2+}]_i$ can be used to evaluate the activity of the Na^+/Ca^{2+} exchanger ***(21,29,30)***. If the Na^+/Ca^{2+} exchanger is present, Na^+ removal results in a rapid increase in $[Ca^{2+}]_i$ owing to reversal of the exchanger. Na^+ removal can also result in a decrease in pH owing to inactivation of the Na^+/H^+ exchanger, although other pH regulatory mechanisms can compensate to maintain pH constant (i.e., activation of HCO_3^- transport or H^+-ATPases).

1. Dye-loaded cells are incubated in EB, and the ion-sensitive ratio for both probes is monitored to determine when a stabile signal is attained.
2. Perfusion media are changed to media in which NaCl has been replaced with 140 m*M* of *N*-methylglucamine-Cl, and the ion-sensitive ratios are monitored continuously.
3. At the end of the experiment, 25 m*M* NH_4Cl is added to the perfusion media to elicit a rapid alkalinization.
4. The perfusion media is replaced with NH_4Cl-free EB to allow recovery of pH (*see* **Note 15**).

Figure 2A shows the effect of Na^+ removal on pH and Ca^{2+} in HUVE, demonstrating the effect of pH on the Ca^{2+} signal response. Similar artifactual increases in the fura-2 ratio owing to decreasing pH following Na^+ replacement have been observed in ovarian luteal cells ***(30)***. This is contrasted by the authors' findings for cardiac myocytes, in which the magnitude of the Ca^{2+} change is large ***(29)***. The relevance of pH corrections on fura-2 data is difficult to evaluate *a priori*. However, the magnitude of these corrections is larger for acidic than for alkaline pH excursions ***(12,19)***.

3.6.2. Glucose Elicits Acidification and Ca^{2+} Removal from Cytosol in Cells Transfected with the Gene Encoding for H^+-ATPase ***(28)***

To study the relationship among tumorigenesis, glycolysis, and $[Ca^{2+}]_i$, NIH-3T3 cells were transfected with the yeast PMA1 gene that encodes for plasmalemmal H^+-ATPase ***(18)*** (**Fig. 2B**). These RN1a cells are not only tumorigenic, but also exhibit elevated rates of glucose usage and lactic acid production when compared to their nontumorigenic counterparts ***(28)***. Moreover, steady-state pH_{in} is at least 0.3 pH unit higher in RN1a cells, and the steady-state $[Ca^{2+}]_i$ is twofold higher ***(3)***.

1. Dye-loaded cells are incubated in EB containing 0.1 m*M* glucose, and the ion-sensitive ratio for both probes is monitored until a stabile signal is attained.
2. The perfusion media are changed to media containing 5 m*M* glucose, and the ion-sensitive ratios are monitored continuously.

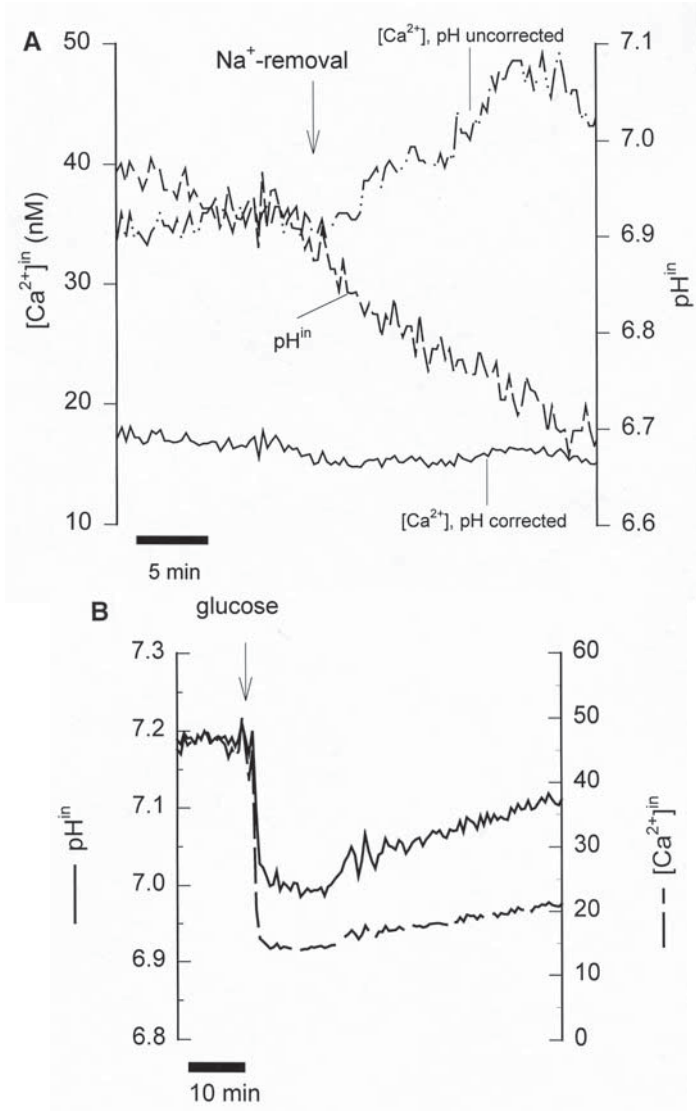

Fig. 2 **(A)** Effect of Na^+ removal on pH and Ca^{2+}. Effect of exchanging media Na^+ with *n*-methylglucamine on pH and Ca^{2+} in HUVEs. At the time indicated, perfusate was exchanged for an Na^+-free media isosmotically substituted with *N*-Me-Glucamine resulting in a decrease in pH associated with an increase in the fura-2 ratio and thereby in an apparent increase in Ca^{2+} (dashed lines, uncorrected Ca^{2+}). However, correction for the fura-2 signal response for the change in pH induced by Na^+ removal indicates that the sustained increase in fura-2 ratio is owing to altered pH rather than to a change in Ca^{2+}. As shown by the hatched line, correction for effects of pH on fura-2 parameters demonstrates that there are minimal Ca^{2+} changes ***(21)***. **(B)** Effect of glucose on

3.6.3. Normalization of Agonist-Stimulated Responses

Insulin secretion from pancreatic β-cells is primarily activated by increased metabolism of nutrients and, in particular, glucose with a K_m of approx 15 m*M*. Ca^{2+} is the second messenger that couples secretion to cell activation. Unlike normal β-cells, the RIN-38 cells are excited maximally at 1–5 m*M* glucose. Described is a protocol used to evaluate the effects of modulators of secretion on the glucose-activated response.

1. Dye-loaded cells are incubated in EB containing 0.1 m*M* glucose, and the ion-sensitive ratio for both probes is monitored to determine when a stabile signal is attained.
2. The perfusion media is changed to media containing 5 m*M* glucose, and the ion-sensitive ratios are monitored continuously (**Fig. 3**).
3. After the cell response has peaked, the cells are perfused with low-glucose media to wash out the response.
4. After ion concentrations return to baseline, either a second response is initiated (control), or a modulator is added.
5. In the case for testing the effect of a modulator on a subsequent response, the second agonist (glucose) response is initiated by changing the perfusion media to one containing both glucose and the modulator.
6. At the termination of the experiment, 40–60 m*M* KCl is added to the perfusion media to elicit a maximal signal response.

The second response to elevated glucose is compared to the initial response (% initial) to analyze the effect of modulator. This approach normalizes the effect of a modulator among different experiments independent for differences in absolute signal responses. Comparison among repetitive glucose responses without modulator evaluates the variability of the control response. The KCl pulse provides a measure of the maximal signal response for a given experiment; however, use of this maximal response to normalize between experiments may not be optimal since the sensitivity of the Ca^{2+} dye is sigmoidal.

3.6.4. Knockout of the Sulfonylurea Receptor (Isoform 1 [SUR1]) in RIN-38 Cells

In response to increasing glucose from 0.05 to 5 m*M*, the initial decrease in Ca^{2+} observed in the parental line is maintained, but the secondary elevation in Ca^{2+} that activates the secretory response is absent. Addition of KCl demon-

---

pH and Ca^{2+} in 3T3 cells transfected with the yeast gene encoding for plasmalemmal H^+-ATPase. RN1a cells were perfused with 0.1 m*M* glucose, and at the time indicated (glucose, arrows), perfusate was changed to one containing 25 m*M* glucose. The glucose-induced Ca^{2+} decrease is due to activation of ER-Ca^{2+}-ATPase and is blocked by inhibitors of this pump's activity, such as thapsigargin ***(28)***.

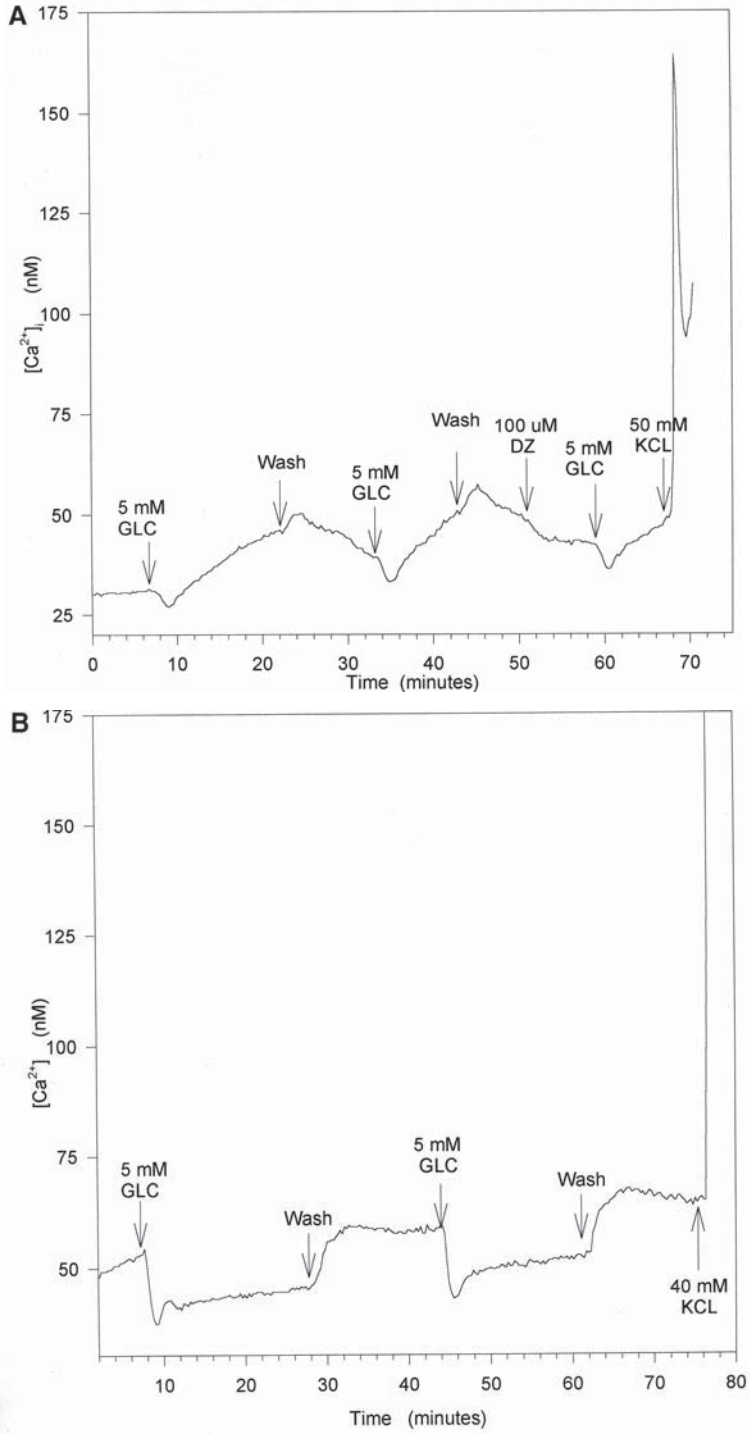
A
175
150
125
100
75
50
25
[Ca2+]i (nM)
5 mM GLC
Wash
5 mM GLC
Wash
100 uM DZ
5 mM GLC
50 mM KCL
0
10
20
30
40
50
60
70
Time (minutes)
B
175
150
125
100
75
50
[Ca2+] (nM)
5 mM GLC
Wash
5 mM GLC
Wash
40 mM KCL
10
20
30
40
50
60
70
80
Time (minutes)

strates that the dynamic range of fura-2 is not limiting the observation of the secondary rise in Ca^{2+} following glucose stimulation. Absence of a response to KCl would be indicative of a problem with dye loading or responsiveness, explaining a similar absence of response to the test agonist. Furthermore, the response after KCl may be used to normalize the original agonist response; i.e., data are analyzed as a percentage of the maximal (KCl) response (*see* **Note 16**).

4. Notes

1. Methods to assess the extent of EGTA impurity have been published ***(31)***. The impact of this lack of purity in estimating [Ca^{2+}] is larger at high buffer ratios. A simple empirical method for preparing solutions with stoichiometric balance is to assume that EGTA is approx 5% impure. Thus, a 5% excess EGTA is added to the buffer to compensate for the lack of purity ***(31)***.
2. All cells within the population will leak dye into the cuvet medium over time. Therefore, perfusion of the chamber to remove leaked dye is absolutely essential. Buildup of active probe in the medium will obviously lead to spurious results owing to profound differences in extracellular and intracellular ion levels and volumes.
3. Data obtained from simultaneous measurements are further analyzed using SigmaPlot. An advantage of using this system is that data obtained (from either SLM or PTI instruments) can be imported into the SigmaPlot spreadsheet. The equations needed to estimate pH and Ca^{2+} (i.e., **Eqs. 1–6**) can be written into this format and iteratively solved using built-in algorithms. Then, graph templates can be extracted and used to instantly plot the data. Thus, a plot can be generated in <1 min provided that there are only minor changes in the legends of the figure.
4. Because pH affects the K_d of EGTA for Ca^{2+}, i.e., K_d is larger at acidic than alkaline pH (*see* **Fig. 1**), it follows that the magnitude of the Ca^{2+} change for a given titration step is larger at acidic than at alkaline pH. The expected Ca^{2+}

Fig. 3. *(opposite page)* **(A)** Responses of insulin-secreting rat insulinoma cells (RIN-38) to repetitive challenges with glucose. Cells were incubated in media containing 0.1 m*M* glucose under resting conditions, and were returned to this media when the response was washed out. After Ca^{2+} returned to baseline, a second response was elicited. The magnitude and rate of response and recovery between the two responses are compared to determine the variability between repetitive activation by the agonist. The effect of a modulator between the two agonist-initiated responses on these parameters can be used to precisely determine modulator effect. Diazoxide ($10^{-7}M$) opens nucleotide-sensitive K^+ channels (K_{ATP}), leading to cell hyperpolarization and a decrease in Ca^{2+}. KCl is added at the end of each experiment to estimate the maximal (peak) signal response. **(B)** Effect of knockdown of the SUR1 in RIN-38 cells. The effect of glucose on eliciting Ca^{2+} increases is lost in RIN-38, which express limited SUR1. The absence of an elevation in Ca^{2+} could be due to loss of dye sensitivity or saturation, which can easily be tested by addition of KCl.

concentrations at three distinct pH values (using temperature- and pH-corrected K_d values for Ca^{2+} binding on EGTA) for typical calibration curves outlined in **Subheading 3.2.** (**steps 2** and **3**) are indicated in **Table 1**. The EGTA K_d values used for estimating free Ca^{2+} are 4.22 μ*M*, 336 n*M*, and 90 n*M* for pH values of 6.3, 7.0, and 7.2, respectively.

5. A general assumption related to dye loading is that the probes become localized within the compartment of interest, which, in this case, is the cell cytosol. Access to a fluorescence microscope facilitates the analysis of probe distribution. Unfortunately, depending on exact loading conditions, the ion-sensitive probes can become sequestrated into subcellular compartments. One relatively quick approach is to permeabilize the cell membrane with a detergent (saponin, 0.1%; 1 min), and to measure the level of fluorescence that remains in the cells. Normally >80% of the signal should be lost with this maneuver unless significant compartmentation or autofluorescence is present. Factors that can influence compartmentation of dye are concentration of AM dye in the loading media, the time of loading, and temperature at which loading is carried out. Approaches to specifically load probes into the cytosol have been described in detail ***(32)***, and should be consulted if unwanted compartmentalization of the probes occurs.
6. Dye toxicity: The effect of AM dyes on cell viability and proliferation should be evaluated. In the author's experience, when snarf-1 and fura-2/AM are used at concentrations of <15 μ*M*, there are only minimal effects on cell viability in the more than 40 different cell types they have used. Cell viability can easily be evaluated by trypan blue exclusion. If loss of viability occurs, the time required for cell loading, the temperature at which loading is carried out, or the dye concentration in the loading media can be decreased. On the other hand, even at concentrations as low as 1 μ*M* with incubation times of 5–10 min, followed by washout of the dye, cell proliferation is decreased without any apparent cytotoxic effect ***(19)***. The mechanisms underlying the inhibition in cell division are not apparent but may be related to ATP depletion or to aldehyde formation on cleavage of the AM form of these dyes ***(33)***.
7. To ensure homogeneous loading, the authors recommend the use of a rocker platform (Bellco, Vineland, NJ) or a belly dancer (Sorvall, Greenville, NC), which can be placed in the 5% CO_2 incubator, at 37°C. In addition, pluronic acid can be used to assist in dye loading, if problems with limited dye loading occur. Addition of 1 μL of a 20% stock solution of pluronic acid to 1 mL of loading media often facilitates enhanced levels and more uniform loading of AM dyes.
8. Use of nigericin plus valinomycin is essential to fully collapse the pH gradient and, therefore, to adequately calibrate fura-2 *in situ* because in many cells, varying Ca^{2+} levels can affect pH, which, in turn, affects fura-2 fluorescence ***(19)***.
9. If both signals are similar to those observed from in vitro experiments in terms of spectral shape, proceed with the experiment. If anomalous spectra are obtained, investigate whether the aberrant profiles are due to inherent properties of the cell (i.e., autofluorescence). This can be overcome by ensuring proper loading of the cells. Thus, load another set using higher fura-2 or snarf-1 concentrations. In

addition, it is critical that the relative fluorescence intensities of fura-2 and snarf-1 are equivalent (<50% difference in either dye is acceptable). Failure to ensure equivalent loading results in the intensity of one dye overwhelming the other due to inevitable spectral overlap, which will preclude correct measurement of both ions. Equal loading can be achieved by increasing/decreasing the concentration of the AM conjugates in the loading.

10. To obtain reliable *in situ* calibration parameters (i.e., K_d/pK, R_{max}, R_{min}) for estimating pH or Ca^{2+}, the authors recommend analyses from at least six different pH and Ca^{2+} concentrations (each in triplicate). For Ca^{2+}, titrations should be performed at a minimum of five different pH values because the goodness of the fit with **Eqs. 1–6** using nonlinear minimization routines is determined by the number of observations. In some cell types, it is problematic to perform complete *in situ* titrations for Ca^{2+}, because high Ca^{2+} levels can induce contractility and/or cell detachment. Similarly, it is often difficult to perform complete titrations at high pH, because most cells do not tolerate prolonged alkaline pH. Thus, it is difficult to obtain reliable ratio values at alkaline pH or high Ca^{2+}. Consequently, there is much error in estimates of *in situ* R_{max} values for both Ca^{2+} and pH indicators. One common solution to this problem is the use of the in vitro R_{max}, which can be generated to a high degree of accuracy. This phenomenon does not have a significant effect on characterizing the effect of pH on the K_d of Ca^{2+} indicators, because the pK of this effect is quite low, and thus the K_d is relatively insensitive at alkaline pH values. Although it is theoretically possible to partially overcome this problem by linearizing the data (requiring fewer points at high Ca^{2+} or high pH), in the authors' experience, both linear and nonlinear methods provide similar K_d/pK and R_{min} values, and more reproducible in situ R_{max} values are obtained from nonlinear methods.
11. If the calculated R_{min} or R_{max} values are distinct (>10%) from those obtained from the complete calibrations, it may indicate that the intracellular environment of the cell population has changed, and therefore new titrations are required. In the authors' experience with 3T3 cells, thawing of new cell cultures and complete *in situ* titrations are generally required every 12 passages. However, this must be tested for every batch and for each individual cell type.
12. On-line analyses of all useful wavelengths is important for correct interpretation of data. The behavior of these wavelengths, and not only ratios, should be continuously monitored during an experiment. Specifically, treatments that elicit increases in pH should elicit distinct increases and decreases in the signal at 644 and 584 without changes in the isoemissive wavelength. Similarly, increases in Ca^{2+} should be associated with increases and decreases in the fluorescence signals at 340 and 380 nm, respectively. This is particularly important when analyzing R_{min} and R_{max} for assessment of absolute ion concentrations.
13. Dye behavior at isoemissive/isoexcitation wavelengths should be assessed throughout an experiment. A drastic drift in the fluorescence signal may indicate that cells are detaching or exhibiting changes in cell volume. The ratio method partially corrects for this; however, if the changes are not symmetric, then the

ratio values also are modified. The signals at the isoexcitation and isoemissive point of fura-2 and snarf-1, respectively, are particularly useful for monitoring dye leakage. It is normal to observe a decrease in signal owing to dye leakage/extrusion or photobleaching of the probe. In the ratio mode, this will typically be corrected, and the resulting ratio should be stable.

14. Individual cells within a population of cultured cells can have very heterogeneous resting ion levels, which may be due to many factors, including their state of differentiation. A consideration when attempting to analyze "normal resting" levels is developing an approach to bring all cells to a similar level of activation. For example, RIN-38 cells are mildly activated by amino acids and other nutrient factors. The authors have found that treating these cells with alanine during the AM wash period stabilizes the subsequent responses of cells within the population to glucose, which results in a significant decrease in the variability of response to many agonists, and normalizes resting levels.
15. Addition of activators such as KCl or NH_4Cl at the end of an experiment provides general information regarding dye responsiveness. However, the signal response of the dye exhibits a nonlinear response at high ion concentrations, making such a maneuver difficult to interpret with respect to absolute ion concentration.
16. In cells that express voltage-activated Ca^{2+} channels, KCl can be used to elicit membrane depolarization at the end of an experiment to evaluate absolute maximal Ca^{2+} signal responses for an individual experiment. In the absence of voltage-activated Ca^{2+}-dependent channels, or lack of a response to KCl treatment, ionomycin or A23187 can be used to determine the maximal signal response.

References

1. Becker, T. C., Noel, R. J., Lynch, R. M., Johnson, J. H., Takeda, J., Bell, G. I, and Newgard, C. B. (1996) Adenovirus mediated overexpression of glucokinase isoforms in islets: Minimal secretory and metabolic effects relative to hexokinase overexpression. *J. Biol. Chem.* **271,** 390–394.
2. Hughes, S. D., Johnson, J. H., Quaade, C., and Newgard, C. (1992) Engineering of glucose-stimulated insulin secretion and biosynthesis in non-islet cells. *Proc. Natl. Acad. Sci. USA* **89,** 688–692.
3. Gillies, R. J., Martinez-Zaquilan, R., Martinez, G. M., Serano, R., and Perona, R. (1990) Tumorigenic 3T3 Cells maintain an alkaline intracellular pH under physiological conditions. *Proc. Natl. Acad. Sci. USA* **87,** 7414–7418.
4. Inagaki, N., Gonoi, T., Clement, J. P. IV, Namba, N., Inazawa, J., Gonzalez, G., Aguilar-Bryan, L., Seino, S., and Bryan, J. (1995) Reconstitution of IKATP: An inward rectifier subunit plus the sulphonylurea receptor. *Science* **270,** 1166–1169.
5. Pines, J. (1995) GFP in mammalian cells. *Trends Genetics* **11,** 326–327.
6. Busa, W. B. (1986) Mechanisms and consequences of pH-mediated cell regulation. *Annu. Rev. Physiol.* **48,** 389–402.
7. Moolenaar, W. H. (1986) Effects of growth factors on intracellular pH regulation. *Annu. Rev. Physiol.* **48,** 363–376.
8. Carafoli, E. (1987). Intracellular Ca^{2+} homeostasis. *Annu. Rev. Biochem.* **56,** 395–433.

9. Rozengurt, E. (1986) Early signals in the mitogenic response. *Science* **234,** 161–166.
10. Tsien, R. Y. (1989) Fluorescent indicators of ion concentration. *Methods Cell Biol.* **30,** 127–156.
11. Martinez-Zaguilan, R., Parnami, G., and Lynch, R. M. (1996) Selection of ion indicators for simultaneous measurement of pH and Ca^{2+}. *Cell Calcium* **19,** 337–349.
12. Martinez-Zaguilan, R., Gurule, M., and Lynch, R. M. (1996) Simultaneous measurement of pH and Ca^{2+} in single insulin secreting cells by microscopic spectral imaging. *Am. J. Physiol.* **270,** C1438–1446.
13. Dixon, D. A. and Haynes, D. H. (1990) The pH dependence of the cardiac sarcolemmal Ca^{2+}-transporting ATPase: Evidence that the Ca^{2+} translocator bears a doubly negative charge. *Biochem. Biophys. Acta* **1029,** 274–284.
14. Orchard, C. H. and Kentish J. C. (1990) Effects of changes of pH on the contractile function of cardiac muscle. *Am. J. Physiol.* **258,** C967–C981.
15. Sanchez-Armass, S., Martinez-Zaguilan, R., Martinez, G., and Gillies, R. J. (1994) Regulation of pH in rat synaptosomes. I. Role of sodium, bicarbonate, and potassium. *J. Neurophysiol.* **71,** 2236–2248.
16. Van Adelsberg, J. and Al-Awqati, Q. (1986) Regulation of cell pH by Ca^{2+}-mediated exocytotic insertion of H^+-ATPases. *J. Cell Biol.* **102,** 1638–1645.
17. Vorndran, C., Minta, A., and Poenie, M. (1995) New fluorescent calcium indicators designed for cytosolic retention or measuring calcium near membranes. *Biophys. J.* **69,** 2112–2124.
18. Perona, R. and Serrano, R. (1988) Increased pH and tumorigenicity of fibroblasts expressing a yeast H^+ pump. *Nature* **334,** 438–440.
19. Martinez-Zaguilan, R., Martinez, G. M., Lattanzio, F., and Gillies, R. J. (1991) Simultaneous measurements of intracellular pH and Ca^{2+} using the fluorescence of snarf-1 and fura-2. *Am. J. Physiol.* **260,** C297–C307.
20. Clark, S. A., Burnham, B. L., and Chick, W. L. (1990) Modulation of glucose-induced insulin secretion from a rat clonal B-cell line. *Endocrinology* **127,** 2779–2788.
21. Martinez-Zaguilan, R., Chinnock, B. F., Wald-Hopkins S., Bernas M., Way, D., Weinand, M., Witte, M. H., and Gillies, R. J. (1996). $[Ca^{2+}]_i$ and pH in homeostasis in Kaposi sarcoma cells. *Cell. Physiol. Biochem.* **6,** 169–184.
22. Gillies, R. J. and Martinez-Zaguilan, R. (1991) Regulation of intracellular pH in BALB/c-3T3 cells: Bicarbonate raises pH via $NaHCO_3$/HCl exchange and attenuates the activation of Na^+/H^+ exchange by serum. *J. Biol. Chem.* **266,** 1551.
23. Ohkuma, S. and Poole, B. (1978) Fluorescence probe measurement of the intralysosomal pH in living cells and the perturbation of pH by various agents. *Proc. Natl. Acad. Sci. USA* **75,** 3327–3331.
24. Iredale, P. A. and Dickenson, J. M. (1995) Measurement of intracellular free calcium ion concentration in cell populations using Fura-2. *Meth. Mol. Biol.* **41,** 203–213.
25. Konishi, M., Olson, A., Hollingworth, S., and Baylor, S. M. (1988) Myoplasmic binding of fura-2 investigated by steady-state fluorescence and absorbance measurements. *Biophys. J.* **54,** 1089–1104.

26. Bassani, J. W. M., Bassani, R. A., and Bers, D. M. (1995) Calibration on indo-1 and resting intracellular $[Ca^{2+}]_i$ in intact rabbit cardiac myocytes. *Biophys. J.* **68,** 1453–1460.
27. Harrison, S. M. and Bers, D. M. (1989) Correction of proton and Ca^{2+} association constants of EGTA for temperature and ionic strength. *Am. J. Physiol.* **256,** C1250–C1256.
28. Martinez, G. M., Martinez-Zaguilan, R., and Gillies, R. J. (1994) Effect of glucose on pH and Ca^{2+} in NIH-3T3 cells transfected with the yeast p-type H^+-ATPase. *J. Cell. Physiol.* **161,** 129–141.
29. Lax, D., Martinez-Zaguilan, R., and Gillies, R. J. (1994) Furazolidone increases thapsigargin-sensitive Ca^{2+}-ATPase in chick cardiac myocytes. *Am. J. Physiol.* **36,** H734–H741.
30. Martinez-Zaguilan, R., Wegner, J. A., Gillies, R. J., and Hoyer, P. B. (1994) Differential regulation of Ca^{2+} homeostasis in ovine large and small luteal cells. *Endocrinology* **135,** 2099–2108.
31. Klabusay M. and Blinks, J. R. (1996) Some commonly overlooked properties of calcium buffer systems: A simple method for detecting and correcting stoichiometric imbalance in Ca^{2+} EGTA solutions. *Cell Calcium* **20,** 227–234.
32. Roe, M. W., Lemasters, M. M., and Herman, B. (1990) Assessment of Fura-2 for measurements of cystolic free calcium. *Cell Calcium* **11,** 63–74.
33. Tiffert, T., Garcia-Sancho, J., and Lew, V. (1984) ATP depletion caused by low concentrations of formaldehyde and/or Ca^{2+}-chelator esters in human red cells. *Biochim. Biophys. Acta* **773,** 143–156.

21

Measurement of Cytosolic-Free Ca^{2+} in Plant Tissue

Martin R. McAinsh and Irina Staxén

1. Introduction

Several techniques have been used to measure the concentration of cytosolic-free Ca^{2+} ($[Ca^{2+}]_i$) in plants ***(1)***. These include Ca^{2+}-sensitive microelectrodes, luminescent photoproteins, and fluorescent Ca^{2+}-indicators. Ca^{2+}-sensitive microelectrodes ***(2)*** can be used only in cells that are able to withstand impalement with two electrodes or a double-barrelled electrode. In addition, microelectrodes suffer from slow response times and difficulties with calibration. These problems are particularly acute in plant cells in which the high turgor often results in partial displacement of the sensor, and the subsequent loss of sensitivity, following impalement. Consequently, the use of Ca^{2+}-sensitive electrodes has been limited to only a few studies in plants and algae ***(3,4)***.

Luminescent photoproteins, such as aequorin ***(5)***, emit light on binding Ca^{2+}. The luminescence is directly proportional to the concentration of free Ca^{2+} and can be measured by either photometry or imaging techniques. Because of its high molecular weight, aequorin has to be pressure injected into cells *(see below)*. Therefore, it has been used only to measure $[Ca^{2+}]_i$ in a limited number of plant cells ***(6,7)***. Recently transgenic plants have been produced with the aequorin protein targeted to the cytosol ***(8,9)*** or to specific organelles such as the chloroplasts ***(9)*** (aequorin has also been targeted to mitochondria in animal cells ***[10]***). This provides a noninvasive method for monitoring whole-plant $[Ca^{2+}]_i$ and organellar-free Ca^{2+}. However, at present this technique is limited to plant species such as tobacco and *Arabidopsis*.

Fluorescent Ca^{2+} indicators have been used extensively to measure plant $[Ca^{2+}]_i$ ***(1)***. These fall into two main categories: (1) nonratiometric indicators, which exhibit an increase in fluorescence across the whole of the emission

From: *Methods in Molecular Biology, Vol. 114: Calcium Signaling Protocols*
Edited by: D. G. Lambert

spectra on binding Ca^{2+}, and (2) ratiometric indicators, which exhibit a shift in either their excitation or emission spectra when they bind Ca^{2+}. For example, fura-2 exhibits a shift in its excitation maximum (510-nm emission) on binding Ca^{2+}, so that the fluorescence at 340 nm increases and the fluorescence at 380 nm decreases with increasing $[Ca^{2+}]_i$; the 340/380 nm fluorescence ratio is proportional to $[Ca^{2+}]_i$ ***(11)***. Quantification of $[Ca^{2+}]_i$ using nonratiometric indicators is complicated by cell-to-cell variation in the concentration and distribution of indicators within cells together with indicator loss during experiments ***(11)***. Therefore, ratiometric indicators are preferred for measurements of $[Ca^{2+}]_i$.

A number of techniques are available for loading fluorescent Ca^{2+}-sensitive indicators into plant cells, including low-pH loading, ester loading, electroporation, digitonin permeabilization, and microinjection ***(1)***. These have all met with varying degrees of success. Microinjection allows a wide range of compounds to be introduced directly into the cytosol of a cell and has been the most successful method in plants. There are two main techniques for microinjections: iontophoretic injection and pressure injection ***(12)***. Iontophoretic microinjection uses electrical current to carry charged molecules, such as the free acid forms of the Ca^{2+}-sensitive indicators, into cells ***(12)***. By contrast, pressure microinjection uses applied pressure to move solutions into a cell. This technique is complicated in plants by the presence of the cell wall and the high turgor of cells ***(13–15)***. Therefore, iontophoretic microinjection has been used widely to load Ca^{2+}-sensitive indicators into plant cells ***(1)***. In addition, patch-clamp techniques have also been used to introduce compounds into plant cell protoplasts in the whole-cell configuration ***(16)***.

The Ca^{2+}-dependent fluorescence signal of cells loaded with Ca^{2+}-sensitive indicators can be quantified using either photometric or imaging techniques such as conventional microscopy and confocal scanning laser microscopy (CSLM). The equipment required for each of these techniques differs markedly, although there are four common components. These are (1) an excitation light source that allows the selection of excitation wavelengths, (2) a specimen holder for the isolation and perfusion of cells, (3) a detector that enables the emission wavelengths to be specified, and (4) signal processing for amplification, recording, and analysis of data ***(1,12,17)***. Ratio photometry uses a photomultiplier tube to detect fluorescence emissions. This provides quantitative and temporal information about changes in whole-cell $[Ca^{2+}]_i$. Ratio imaging, employing conventional imaging techniques, uses a video camera to detect the fluorescence emissions, providing additional information about the spatial distribution of $[Ca^{2+}]_i$. Furthermore, three-dimensional spatial resolution can be achieved using CSLM and/or fluorescence resonance energy transfer techniques and two-photon microscopy ***(17)***.

There are two important factors that must be taken into account when using fluorescent Ca^{2+} indicators to measure $[Ca^{2+}]_i$ in plants: (1) cell autofluorescence, and (2) the signal-to-noise ratio (SNR). Plant cells are highly autofluorescent at the excitation wavelengths of many of the Ca^{2+}-sensitive indicators. Therefore, it is essential to correct for the contribution this makes to the total fluorescence signal at both excitation or emission wavelengths. Following autofluorescence correction, the signal from cells loaded with Ca^{2+}-sensitive indicators is often low, making measurements extremely noisy. The noise can be reduced by integrating successive fluorescence measurements, increasing the SNR ratio.

Many of the techniques required for the measurement of $[Ca^{2+}]_i$ in plant tissue, including specimen preparation, microinjection of fluorescent Ca^{2+}-sensitive indicators, quantification of the Ca^{2+}-dependent fluorescence, and calibration of the fluorescence signal, are illustrated clearly in studies of $[Ca^{2+}]_i$ in stomatal guard cells ***(16,18-27)***. These studies also highlight many of the problems, and their solutions, which are encountered during measurements of plant $[Ca^{2+}]_i$. In this chapter, the authors will describe a method for measuring $[Ca^{2+}]_i$ in guard cells of the model species *Commelina communis* using the ratiometric fluorescent Ca^{2+}-sensitive indicator fura-2.

2. Materials

1. Plant material: *C. communis* L. is grown from seed in John Innes No. 2 potting compost in a heated glasshouse (min. temperature 20°C, 16-h d, min. photon flux density of 100 µmol · m^{-2} · s^{-1}). Transfer the seedlings to a controlled environment chamber (temperature 25 ± 1°C, 16-h d, photon flux density of 100 µmol · m^{-2} · s^{-1}) several days before use. Maintain the plant free from H_2O stress at all stages of development ***(28)*** (*see* **Note 1**).
2. Isolation buffer: 10 m*M* 2-(*N*-morpholino)ethanesulfonic acid (MES) in distilled H_2O. Adjust to pH 6.15 with KOH. Store at 4°C (*see* **Notes 2** and **3**).
3. Perfusion buffer: 10 m*M* MES and 10 m*M* KCl in distilled H_2O. Adjust pH 6.15 with KOH. Store at 4°C (*see* **Notes 2** and **3**).
4. Opening buffer: 10 m*M* MES and 50 m*M* KCl in distilled H_2O. Adjust pH 6.15 with KOH. Store at 4°C (*see* **Notes 2** and **3**).
5. KCl stock solution: 3 *M* KCl in double-distilled H_2O.
6. Fura-2 stock solution: Prepare a 10 m*M* solution of fura-2 pentapotassium salt (Molecular Probes, Eugene, OR [*see* **Notes 4** and **5**]) in double-distilled H_2O. The stock solution of fura-2 should be made up in a 0.5-mL microfuge tube. Check that the pH is approx 7.0 by spotting a small aliquot of the solution onto pH paper. Adjust the pH using very small volumes of pH reagents (*see* **Note 6**). Store at –20°C. Thaw approx 30 min before use (*see* **Note 7**). Immediately prior to use, centrifuge the fura-2 stock solution at 13,000*g* for 10 min in a microfuge.
7. Coverslips: 18 × 18 and 22 × 64 mm (Chance Propper, Warley, UK).

8. Low melting point wax can be purchased from Agar Scientific, Essex, UK.
9. Petroleum jelly can be purchased from Chesbrough-Ponds, London, UK.
10. Low-power soldering iron can be purchased from RS Components, Northants, UK.
11. Perfusion system: Perfusion is provided under gravity from a temperature controlled reservoir mounted approx 50 cm above the specimen (*see* **Note 8**). The reservoir consists of a 6-L heated water bath (Grant, Cambridge, UK) and a purpose-built cooling coil. Perfusion media are delivered to the specimen along an insulated pipe. Excess media are removed from the specimen under vacuum ***(21)***. A schematic representation of the perfusion system used during measurements of guard cell $[Ca^{2+}]_i$ is shown in **Fig. 1** (*see* **Note 9**).
12. Microinjection of fura-2: Microelectrodes are fabricated from filamented borosilicate electrode glass (1.2-mm outside diameter [OD], 0.68-mm inside diameter [ID]) (Clark Electromedical, Reading, UK) using a vertical microelectrode puller (Kopf, Tujunga, CA) (*see* **Note 10**). Microelectrodes are positioned using a precision micromanipulator (Leitz-Leica, Milton Keynes, UK). Fura-2 is microinjected iontophoretically using a pulse generator/stimulator together with an intracellular amplifier (World Precision Instruments [WPI], Sarasota, FL). The reference electrode is positioned using a coarse micromanipulator (Prior, Leicestershire, UK). The injection current is monitored with a dual channel oscilloscope (RS Components, Northants, UK) ***(21)*** (*see* **Note 11**). A schematic representation of the system used to microinject guard cells is shown in **Fig. 1** (*see* **Note 12**).
13. Fluorescence microscopy: Specimens are viewed using an inverted epifluorescence microscope with ultra violet (UV) optics (*see* **Note 13**). Additional stage illumination is from a halogen cold light source (Schott, Cologne, Germany). Fluorescence excitation is from a xenon light source and is transmitted to the microscope via a liquid light guide (Cairn Research, Kent, UK). Excitation (340 and 380 nm, 10-nm bandwidth) and emission (510 nm, 20-nm bandwidth) wavelengths are specified using interference filters (Cairn Research, Surrey, UK) together with a 400 nm dichroic mirror (Nikon) (*see* **Note 14**). Excitation filters are selected using a spinning filter changer (Cairn Research). A ×40 oil immersion lens (1.30 numerical aperture) (e.g. a Nikon CF Fluor DL ×40, oil immersion lens) and nonfluorescent immersion oil are used for all measurements. A schematic representation of the epifluorescence microscope used in the measurement of guard cell $[Ca^{2+}]_i$ is shown in **Fig. 1**.
14. Measurement of $[Ca^{2+}]_i$: Fluorescence emissions (510 nm) are quantified using either ratio photometry or ratio imaging techniques. Photometric studies are performed using a Cairn Research spectrophotometer system ***(21-23,26,27)***. Imaging studies are performed using an ARGUS-50 image analysis system (Hamamatsu Photonics, Middlesex, UK) together with a Cairn spinning filter changer operating in a step mode ***(22)***. Fluorescence images are recorded using a cooled Extended ISIS-M intensified charge-coupled device camera (Photonic Science, Sussex, UK). A schematic representation of the photometric and imaging systems used to quantify the Ca^{2+}-dependent fluorescence of fura-2 in guard cells is shown in **Fig. 1** (*see* **Note 15**).

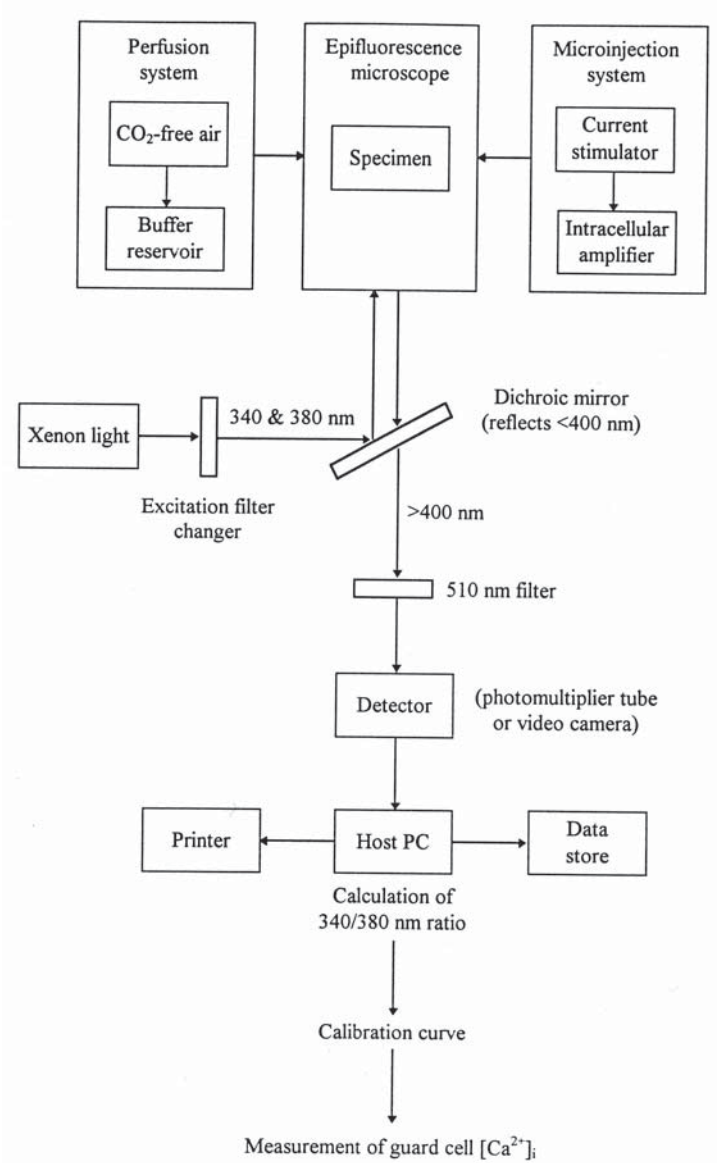

Fig. 1. A schematic representation of the essential components of the equipment required for measurements of $[Ca^{2+}]_i$ in stomatal guard cells using fura-2.

3. Methods

3.1. Preparation of Leaf Epidermis

1. Detach the leaf to be peeled immediately prior to each experiment ***(21)***.
2. Place the leaf on a glass plate and cut it into lamina strips of manageable widths (5–8 mm) with a razor blade or scalpel (*see* **Notes 16–19**).

3. Cut through the upper epidermis near one end, without damaging the lower epidermis, to form a tab in the lamina strip to obtain the abaxial epidermis (*see* **Notes 20** and **21**).
4. Turn the lamina strip over and pull the tab formed in **step 3** gently back with forceps for a few millimeters to separate the tissues.
5. Peel the remaining epidermis off by pulling the tab vertically away from the rest of the lamina, holding the latter in position with a mounted needle (*see* **Notes 22–24**).
6. Float the detached epidermis (cuticle up) on CO_2-free isolation buffer at 25°C. Remove the remaining leaf tissue from both ends of the epidermal strip using sharp scissors.

3.2. Perfusion System

1. Cut the freshly prepared epidermis in pieces 2 cm in length ***(21)*** (*see* **Notes 25** and **26**).
2. Mount the epidermal strip cuticle side down in the middle of a long no. 1.5 coverslip (*see* **Notes 27** and **28**).
3. Pipe a ring of petroleum jelly around the epidermal strip using a 1-mL syringe.
4. Secure the epidermal strip around the edge with four smaller cover slips. Press these down firmly on the petroleum jelly (*see* **Note 29**).
5. Attach the securing cover slips to the bottom cover slip using low melting point wax (*see* **Note 30**) creating a small open perfusion chamber, approx 0.5×1.0 cm and the one cover slip deep, over the center of the strip (*see* **Note 31**).
6. Place a drop of CO_2-free perfusion buffer at 25°C in the perfusion chamber to prevent the epidermis from drying out.
7. Mount the perfusion system on the microscope stage, with the exposed epidermis upward, as if it were a standard microscope slide.
8. Place the inlet and outlet of the perfusion system at the front and rear of the perfusion chamber, respectively.
9. Perfuse the specimen continuously (6 mL $\cdot$ min^{-1}) with CO_2-free perfusion buffer at 25°C in the dark (*see* **Note 32**).

3.3. Microinjection of Fura-2

1. Pull injection and reference microelectrodes (*see* **Notes 10**, **33**, and **34**).
2. Prepare the reference microelectrode by touching the tip of a microelectrode onto a piece of tissue. This will break off the tip to produce a microelectrode with a large tip diameter and a low tip resistance (*see* **Note 35**).
3. Fill the reference microelectrode with 3 *M* KCl using a syringe fitted with a WPI Microfil nonmetallic syringe needle (*see* **Note 36**).
4. Insert the microelectrode into an appropriate microelectrode holder of the correct dimensions (*see* **Note 37**).
5. Position the reference microelectrode toward the rear of the perfusion chamber close to the perfusion outlet (*see* **Note 38**).
6. Fill the tip of the injection microelectrode with fura-2 by capillary action; dip the nontapered end of the microelectrode into a solution of fura-2 (*see* **Notes 39** and **40**).

7. Back fill the injection microelectrode with 3 *M* KCl as described in **step 3** (*see* **Note 36**) and insert the microelectrode into an appropriate microelectrode holder of the correct dimensions as in **step 4** (*see* **Note 37**).
8. Position the injection microelectrode in the perfusion chamber close to the guard cell to be microinjected (*see* **Note 41**).
9. Determine the autofluorescence of each guard cell at 340 and 380 nm prior to microinjection as described below in **Subheadings 3.4.** and **3.5.**
10. Offset the output of the intracellular amplifier to zero (using the position control of the WPI Intra 767) to compensate for the microelectrode tip potential (*see* **Note 42**).
11. Impale the guard cell with the injection microelectrode (*see* **Notes 43** and **44**).
12. Load the fura-2 in the tip of the injection microelectrode into the cytosol of the guard cell using negative current pulses (1.0-nA negative current pulses, 2 Hz, 200-ms duration) for up to 1 min ***(20)***. Monitor the progress of injection at either 340 or 380 nm excitation (*see* **Notes 45–48**).
13. Remove the injection microelectrode from the cell following microinjection (*see* **Note 49**).
14. Perfuse the fura-2-loaded guard cells in opening buffer at 25°C under conditions of continuous illumination (photon flux density of 1000 $\mu mol \cdot m^{-2} \cdot s^{-1}$) from a halogen cold light source for 1 h to promote stomatal opening (*see* **Note 50**).
15. Select stomata that open to the same aperture as those on the rest of the epidermal strip (6–10 μm) and in which both the injected and noninjected cells of a single stoma exhibit the same increase in turgor for measurements of $[Ca^{2+}]_i$ (*see* **Notes 26**, **49**, **51**, and **52**).

3.4. Ratio Photometry

1. Use ratio photometry to monitor whole-cell $[Ca^{2+}]_i$ from a single guard cell (*see* **Note 53**).
2. Sample both the 340- and 380-nm Ca^{2+}-dependent fura-2 fluorescence (510-nm emission) at 64 Hz.
3. Average the signal over 1 s following autofluorescence subtraction on-line (**Subheading 3.3.**, **step 10**) (*see* **Note 54**).
4. Calculate the 340/380-nm ratio every second on-line ***(20–23,26,27)***.

3.5. Ratio Imaging

1. Use ratio imaging to monitor spatially localized changes in $[Ca^{2+}]_i$ (*see* **Note 53**).
2. Measure the camera dark signal prior to each experiment. Subtract this from images on-line.
3. Record alternate 340- and 380-nm excitation (510-nm emission) images at a resolution of 512 × 512 pixels and digitized to 256 gray levels.
4. Average both signals over eight individual frames (*see* **Note 54**).
5. Calculate the mean autofluorescence from the cytoplasmic region of an unloaded guard cell at both excitation wavelengths (*see* **Note 55**).
6. Subtract the mean autofluorescence values from each pair of averaged 340- and 380-nm images, pixel by pixel, at the end of the experiment.

7. Divide the autofluorescence-subtracted 340-nm image by the corresponding autofluorescence-subtracted 380-nm image, on a pixel-by-pixel basis, to produce a series of 340/380-nm ratio images.

3.6. Calibration

1. Perform an in vitro (external) calibration of the 340/380-nm fluorescence ratio vs $[Ca^{2+}]_i$ using Ca^{2+} calibration buffers (WPI) (10, 100, and 1000 n*M* of free Ca^{2+}) containing 0.5 µ*M* fura-2 (*see* **Notes 56** and **57**).
2. Determine the autofluorescence of a 20-µL drop of distilled H_2O on a glass cover slip (**Subheadings 3.4.** and **3.5.**).
3. Pipet 20-µL aliquots of each of the calibration buffers onto a glass cover slip.
4. Calculate the 340/380-nm fluorescence ratio for each of the calibration buffers using either ratio photometry (**Subheading 3.4.**) or ratio imaging (**Subheading 3.5.**).
5. Construct a standard curve of the 340/380-nm fluorescence ratio against the concentration of free Ca^{2+} ***(19,21,22)***.

4. Notes

1. Measurements of $[Ca^{2+}]_i$ have only been performed on stomatal guard cells of *C. communis* ***(18–23,26,27)***, *Vicia faba* ***(16,27)***, and the orchid *Paphiopedilum tonsum* ***(24)***. Growth conditions vary depending on the plant species.
2. Always use tissue culture grade MES. MES buffers should be aerated with CO_2-free air for 1 h before use and during experiments. CO_2-free air can be obtained by pumping air through a 15-cm column of soda lime (Sigma, Dorset, UK) ***(20)***.
3. MES buffers tend to become contaminated even when stored at 4°C. This can cause problems with perfusion systems and the microinjection of cells. Therefore, unused buffers should be discarded regularly.
4. The *Molecular Probes Handbook of Fluorescent Probes and Research Chemicals* ***(29)*** is an invaluable source of reference for researchers. The Molecular Probes web site provides up to date information on all Molecular Probes products (http://www.probes.com).
5. This is the maximum concentration to which fura-2 will dissolve in aqueous solution.
6. The pH of the stock solution seldom requires adjustment. If the pH differs markedly from pH 7.0, it should be adjusted using very small volumes of either 5 *M* KOH or HCl.
7. Refreeze the fura-2 stock solution after use. Fura-2 solutions can be subjected to repeated freeze-thaw cycles without any detrimental effects. However, the fura-2 stock solution should be aliquoted into smaller volumes if it is required for an extended series of experiments to minimize the number of times it is thawed and refrozen.
8. The perfusion rate can be adjusted by altering the height of the reservoir and/or the diameter of the perfusion tubing. Typically, a perfusion rate of 6 mL · min^{-1} is used ***(20–23,26)***. However, flow rates of up to 10 mL · min^{-1} have been used in studies of guard cell $[Ca^{2+}]_i$ ***(27)***. Alterations in the rate of delivery of plant hormones such as abscisic acid have been shown to affect stomatal responses ***(30)***.

9. Alternative perfusion systems used in studies of guard cell $[Ca^{2+}]_i$ include perfusion of guard cell protoplasts in the cell-attached configuration ***(23)*** and the exchange of perfusion media using low-noise peristaltic pumps ***(18,19)***.
10. Vertical and horizontal microelectrode pullers are commercially available. Microelectrodes can be fabricated from either filamented or nonfilamented aluminosilicate, borosilicate, and quartz glass capillaries. These can be obtained with an OD of 1.0, 1.2, or 1.5 mm, although larger sizes are available, and with a range of ID. The use of filamented glass capillaries helps with the filling of microelectrodes. Rigid, extremely sharp microelectrodes with a small tip diameter are required for the microinjection of plant cells. Microelectrodes with these characteristics are most frequently obtained from borosilicate and quartz glass capillaries with a larger OD and thicker walls (i.e., smaller ID). However, the harder quartz glass capillaries require a specialized laser-based microelectrode puller (Sutter Instruments, Novato, CA; Model P-2000 Micropipette Puller).
11. Iontophoretic microinjection is used to load cells with charged molecules such as the free acid form of fura-2. The pulse generator/stimulator is used to apply a variable command signal in the form of a train of pulses to the stimulus input of the intracellular amplifier. Using a constant current device such as the WPI Intra 767, the output from the intracellular amplifier is a constant current replica *(I)* of the command signal, the voltage *(V)* of which is determined by the resistance *(R)* in the circuit (owing mainly to the microelectrode) according to the relationship $V = I \times R$. The amount of fura-2 microinjected into a cell by iontophoresis is dependent largely on the size of the injection current. Therefore, under constant-current conditions the amount of fura-2 that is microinjected into the cell will be proportional to the time for which the current is passed.
12. Fura-2 has also been iontophoretically microinjected into guard cells using two barrels of a four-barrel electrode ***(27)*** and has been loaded into guard cell protoplasts via a patch-clamp pipet in the cell-attached configuration ***(23)***. In addition, pressure injection techniques have also been used to microinject plant cells with fura-2 ***(13–15)***.
13. The Nikon Diaphot TMD inverted epifluorescence microscope (and the new Eclipse from Nikon, Melville, NY) is often used in Ca^{2+} measuring systems ***(18–23,25,26)***. However, Olympus ***(24)*** and Zeiss ***(16)*** microscopes have both been used to measure guard cell $[Ca^{2+}]_i$.
14. Fura-2 suffers from photobleaching during prolonged exposure to high-intensity 340- and 380-nm light. This can be reduced by the inclusion of either metal gauze neutral density filters (Cairn Research, Oberkochen, Germany) or quartz neutral density filters (Ealing Electro-Optics, Watford, UK) in the light path. In addition, liquid light guides such as that supplied by Cairn Research attenuate the excitation light by up to 40%. Reducing the intensity of excitation to approx 3% of the original value allows extended measurements of guard cell $[Ca^{2+}]_i$ ***(20–23,26)***.
15. Guard cell $[Ca^{2+}]_i$ has been measured using commercial and purpose-built photometric ***(16,18–23,25–27)*** and imaging, both conventional ***(19,21,22)*** and CSLM ***(24)***, techniques.

16. In the case of *C. communis*, the epidermis is typically peeled from the youngest fully expanded leaf of 4-wk-old plants ***(18–23,25,26)***. This may vary among species ***(16,24,27)***.
17. Lamina strips are normally used immediately. If not, they are floated on CO_2-free isolation buffer at 25°C to avoid desiccation.
18. Turgid leaves are easier to peel than flaccid ones.
19. All experiments are conducted during the middle of the photoperiod, between 10 AM and 6 PM, to minimize the effects of diurnal changes in stomatal responses.
20. Great care should be taken to cut through the leaf only as far as the lower epidermis. This requires practice.
21. Adaxial epidermis can be obtained by cutting through the lower epidermis.
22. Leaving the final few millimeters of leaf tissue attached to the epidermis aids handling.
23. Maximum viability is achieved if the epidermis is peeled from the lamina strip at an even, slow speed, taking care to be consistent in the angle of peeling.
24. Peeling is best performed in a pool of CO_2-free isolation buffer at 25°C on a glass plate.
25. Guard cells with a low turgor are more easily microinjected than those with a high turgor. Therefore, it is important to use only epidermal strips in which stomata are open to <1 µm. This can be achieved by maintaining plants in the dark for 1 h before use. Stomatal apertures can be determined by mounting a small piece of epidermis from the epidermal strip in a drop of CO_2-free isolation buffer at 25°C on a glass slide. Cover the epidermis with a glass cover slip. Press the cover slip down gently with a mounted needle to expel all the air. The epidermis can then be viewed under the microscope and the stomatal apertures measured using an eyepiece graticule ***(28)***.
26. The use of epidermis in which stomata are open to <1 µm allows the stomata to be opened in CO_2-free opening buffer at 25°C following microinjection of fura-2. This provides an indicator of guard cell viability ***(21)***.
27. Transfer the epidermis to a long cover slip by holding one end with a pair of forceps while supporting the other with a mounted needle. If the strip rolls up, it is relatively simple to unroll it on the cover slip.
28. It is essential that the epidermal strip is completely flat on the cover slip. This can be achieved by carefully smoothing the strip with a mounted needle and then blotting it gently with a small piece of tissue.
29. The securing cover slips are fabricated from 18 × 18 mm cover slips. Cut into convenient sizes using a diamond-tipped knife (RS Components). Typically whole cover slips are used to secure the ends of the strip while the sides are secured with half cover slips.
30. The perfusion chamber is fabricated by using 2-mm strips of low melting point wax and a low power soldering iron to solder the cover slips together.
31. Large volume perfusion chambers introduce a lag period in the changeover of perfusion media during which mixing occurs. This can affect the kinetics of stimulus-induced changes in $[Ca^{2+}]_i$. The small volume of the perfusion chamber allows rapid, almost instantaneous changeover of the perfusion media.

32. Specimens should be perfused with CO_2-free perfusion buffer at 25°C in the dark for at least 10 min before use to determine whether they will retain focus.
33. Microelectrodes with tip diameters ranging from 0.1 to 1.0 µm have been used to microinject plant cells ***(1)***. Typically microelectrodes with a tip diameter of <0.25 µm fabricated from filamented borosilicate electrode glass (1.2-mm OD, 0.68-mm ID) are used for the microinjection of guard cells ***(20–23,26)***. The tip diameter of a representative sample of microelectrodes is measured by scanning electron microscopy ***(31)***.
34. Glass microelectrodes tend to go blunt overnight. Therefore, fresh microelectrodes should be pulled at the start of each experiment.
35. Reference electrodes can also be fabricated from an Ag/AgCl pellet microelectrode holder containing 3 *M* of KCl and connected to the perfusion bath via a 3% agar bridge made up in 3 *M* KCl ***(2)***.
36. Take care to exclude air bubbles by tapping the microelectrode with the tip pointed downward.
37. Microelectrode holders either contain an Ag/AgCl pellet half-cell or employ a silver wire as the electrical contact with fluid-filled microelectrodes. Ag/AgCl pellet half-cell holders require filling with 3 *M* KCl before the microelectrode is inserted. This is best achieved using a syringe fitted with a piece of thin tubing. Following insertion of the microelectrode, make sure there are no air bubbles present and carefully dry the outside of the holder with tissue. Silver wire holders should be chloridized before use. This is done by dipping the silver wire in 1 *M* HCl for a few minutes and then in a strong bleach solution for a similar period of time. It is safest to use a plain bleach and not one of the varieties that contain a mixture of detergents that could possibly affect cell membranes. To maximize the life of the microelectrode holder, it should be cleaned immediately after use with distilled H_2O and blown dry.
38. Positioning reference electrodes filled with 3 *M* KCl near the perfusion outlet reduces contamination of the perfusion chamber with high levels of KCl.
39. It is easier to fill microelectrodes if the fura-2 solution is kept in a cut down 0.5-mL microfuge tube (reduced in height by approx 0.5–1.0 cm).
40. Concentrations of Ca^{2+} indicators that have been used to fill microelectrodes range from 50 µ*M* to 10 m*M* ***(1)***. Increasing the concentration of fura-2 reduces the microinjection time required to achieve a given cytosolic concentration of fura-2. In turn, this reduces the potential damage caused by iontophoresis.
41. Positioning the injection microelectrode in the perfusion chamber is a highly exacting task and requires practice. It is often impractical to locate the microelectrode down the microscope using low magnifications because of the presence of immersion oil on the cover slip. However, by reducing the level of bright-field illumination using the field diaphragm, the microelectrode can normally be located by its shadow at high magnification. In addition, there is an open circuit until both the injection and reference microelectrodes are in the perfusion chamber. This can be monitored using the intracellular amplifier and provides a good indication of the position of the microelectrode.

42. Offsetting the output of the intracellular amplifier to zero allows changes in the potential difference across the injection circuit to be monitored. This is a valuable indicator of the position of the injection microelectrode.
43. Gentle tapping of the injection micromanipulator is often required to achieve penetration of guard cells.
44. Penetration of the guard cell will introduce a potential difference across the injection circuit owing to the membrane potential of the cell. The resting membrane potential of guard cells of *C. communis* has been reported to range from –70 to –90 mV in 50 m*M* KCl ***(21)***.
45. Fura-2 loaded into the cytosol of guard cells gives a discrete pattern of fluorescence around the edge of cells and in the region of the nucleus ***(19,20)***. However, Ca^{2+} indicators loaded into the guard cell vacuole give a uniform fluorescence over the entire cell ***(19)***. Cells should not be overloaded as this will buffer changes in $[Ca^{2+}]_i$.
46. The free acid of fura-2 carries a negative charge and is therefore injected using negative current. Positively charged compounds are injected by positive currents, whereas uncharged compounds can be coinjected into cells together with a high K^+ buffer.
47. Currents used for the iontophoretic microinjection of plant cells range from <0.1 to 10 nA passed for 10 s to 10 min ***(1)***. The use of high currents and/or fixed currents will tend to increase the potential damage caused by iontophoresis.
48. Limit the illumination of the specimen with 340- and 380-nm light to the center of the specimen, using the excitation diaphragm of the microscope, to reduce the potential damage to noninjected guard cells from high-intensity UV excitation.
49. The success rate for iontophoretic microinjection is <10%. Epidermal strips should be discarded after 30–60 min if microinjection is unsuccessful.
50. It is important to use a cold light source such as the Schott KL 1500 to provide continuous illumination of the perfusion chamber to prevent heating of the specimen.
51. Fura-2–loaded cells should meet all the criteria for estimating guard cell viability before use in measurements of $[Ca^{2+}]_i$ ***(19,21)***.
52. Occasionally microinjected guard cells lose some or all of the fura-2 from the cytosol during the opening protocol (**Subheading 3.3.**, **step 14**). These cells should be discarded.
53. Limit the area from which the fluorescence is recorded to a single guard cell using the emission diaphragm of the microscope.
54. The signal from fura-2–loaded cells is often quite low following autofluorescence correction, making measurements extremely noisy. The noise can be reduced by averaging both the 340- and 380-nm Ca^{2+}-dependent fura-2 fluorescence (510-nm emission) over a number of measurements, increasing the SNR.
55. In imaging studies of guard cell $[Ca^{2+}]_i$, autofluorescence subtraction is complicated by cell movements owing to stomatal closure making it impossible to subtract the initial image of the unloaded cell from all subsequent images. Ratio images calculated in the absence of autofluorescence correction typically underestimate $[Ca^{2+}]_i$ by 25% ***(19)***. Therefore, a mean autofluorescence calculated from

the cytoplasmic region of an unloaded guard cell at both excitation wavelengths is subtracted from images, pixel by pixel, at the end of each experiment ***(19,21,22)***.

56. Similar results are obtained for both in vitro and in vivo calibrations of the 340/380-nm fluorescence ratio in guard cells ***(19,21)***. Consequently, an in vitro calibration can be used routinely.
57. In vivo calibration is performed by perfusing fura-2–loaded guard cells with buffers containing different concentrations of free Ca^{2+} in the presence of a Ca^{2+} ionophore (10 n*M*–10 µ*M* Br-A23187). It is assumed that the $[Ca^{2+}]_i$ reaches equilibrium with the external concentration of free Ca^{2+} within 10 min. Calibrations can be performed by either (1) constructing a standard curve of the 340/380-nm fluorescence ratio against the concentration of free Ca^{2+} or (2) using the following equation:

$$[Ca^{2+}] = bK_d[(R - R_{min})/(R_{max} - R)]$$

where R = any cell ratio value, $b = Ca^{2+}_{free}/Ca^{2+}_{bound}$ fluorescence (380 nm), R_{min} = ratio in Ca^{2+}-free conditions, and R_{max} = ratio value in the presence of high (saturating) external Ca^{2+}. Practical difficulties are often encountered during in vivo calibration due to loss of fura-2 from cells following treatment with ionophore, inability to reach a steady R_{min} or R_{max}, or extremely slow or zero response to the ionophore.

Acknowledgments

The authors thank the Biotechnology and Biological Sciences Research Council (BBSRC), UK, for funding. They are also grateful to The Royal Society of the United Kingdom for the award of a University Research Fellowship.

References

1. Webb, A. A. R., McAinsh, M. R., Taylor, J. E., and Hetherington, A. M. (1996) Calcium ions as intracellular second messengers in higher plants. *Adv. Botanical Res.* **22,** 45–96.
2. Ogden, D. (1994) *Microelectrode Techniques: the Plymouth Workshop Handbook*, 2nd ed., Company of Biologists Ltd., Cambridge, UK.
3. Miller, A. J. and Sanders, D. (1987) Depletion of cytosolic free calcium induced by photosynthesis. *Nature* **326,** 397–400.
4. Felle, H. (1988) Auxin causes oscillations of cytosolic free calcium and pH in *Zea mays* coleoptiles. *Planta* **174,** 495–499.
5. Cobbold, P. H. and Lee, J. A. C. (1991) Aequorin measurements of cytoplasmic free calcium, in *Cellular Calcium: A Practical Approach* (McCormack, J. G. and Cobbold, P. H., eds.), Oxford University Press, New York, pp. 55–82.
6. Gilroy, S., Hughes, W. A., and Trewavas, A. J. (1989) A comparison between Quin-2 and Aequorin as indicators of cytoplasmic calcium levels in higher plant cell protoplasts. *Plant Physiol.* **90,** 482–491.
7. Williamson, R. E. and Ashley, C. C. (1982) Free Ca^{2+} and cytoplasmic streaming in the alga, *Chara*. *Nature* **296,** 647–651.

8. Knight, M. R., Campbell, A. K., Smith, S. M., and Trewavas, A. J. (1991) Transgenic plant aequorin reports the effects of touch and cold-shock and elicitors on cytoplasmic calcium. *Nature* **352,** 524–526.
9. Knight, H., Trewavas, A. J., and Knight, M. R. (1996) Cold calcium signalling in Arabidopsis involves two cellular pools and a change in calcium signature after acclimation. *Plant Cell* **8,** 489–503.
10. Rizzuto, R., Simpson, A. W. M., Brini, M., and Pozzan, T. (1992) Rapid changes of mitochondrial Ca^{2+} revealed by specifically targeted recombinant aequorin. *Nature* **358,** 325–327.
11. Grynkiewicz, G., Poenie, M., and Tsien, R. Y. (1985) A new generation of Ca^{2+} indicators with greatly improved fluorescence characteristics. *J. Biol. Chem.* **260,** 3440–3450.
12. Callaham, D. A. and Hepler, P. K. (1991) Measurement of free calcium in plant cells, in *Cellular Calcium: A Practical Approach* (McCormack, J. G. and Cobbold, P. H., eds.), Oxford University Press, New York, pp. 383–410.
13. Money, N. P. (1990) Measurement of hyphal turgor. *Exp. Mycology* **14,** 416–425.
14. Roberts, S. K., Gillot, I., and Brownlee, C. (1994) Cytoplasmic calcium and *Fucus* egg activation. *Development* **120,** 155–163.
15. Taylor, A. R., Manison, N. F. H., Fernandez, C., Wood, J., and Brownlee, C. (1996) Spatial organization of calcium signaling involved in cell volume control in the Fucus rhizoid. *Plant Cell* **8,** 2015–2031.
16. Schroeder, J. I. and Hagiwara, S. (1990) Repetitive increases in cytosolic Ca^{2+} of guard cells by abscisic acid activation of nonselective Ca^{2+} permeable channels. *Proc. Natl. Acad. Sci. USA* **87,** 9305–9309.
17. Gilroy, S. (1997) Fluorescence microscopy of living plant cells. *Annu. Rev. Plant Physiol. Plant Mol. Biol.* **48,** 165–190.
18. Gilroy, S., Read, N. D., and Trewavas, A. J. (1990) Elevation of cytoplasmic calcium by caged calcium or caged inositol trisphosphate initiates stomatal closure. *Nature* **346,** 769–771.
19. Gilroy, S., Fricker, M. D., Read, N. D., and Trewavas, A. J. (1991) Role of calcium in signal transduction of *Commelina* guard cells. *Plant Cell* **3,** 333–344.
20. McAinsh, M. R., Brownlee, C., and Hetherington, A. M. (1990) Abscisic acid-induced elevation of guard cell cytosolic Ca^{2+} precedes stomatal closure. *Nature* **343,** 186–188.
21. McAinsh, M. R., Brownlee, C., and Hetherington A. M. (1992) Visualizing changes in cytosolic-free Ca^{2+} during the response of stomatal guard cells to abscisic acid. *Plant Cell* **4,** 1113–1122.
22. McAinsh, M. R., Webb, A. A. R., Taylor, J. E., and Hetherington, A. M. (1995) Stimulus-induced oscillations in guard cell cytosolic free calcium. *Plant Cell* **7,** 1207–1219.
23. McAinsh, M. R., Clayton, H., Mansfield, T. A., and Hetherington, A. M. (1996) Changes in stomatal behaviour and guard cell cytosolic free calcium in response to oxidative stress. *Plant Physiol.* **111,** 1031–1042.
24. Irving, H. R., Gehring, C. A., and Parish, R. W. (1992) Changes in cytosolic pH and calcium of guard cells precede stomatal movements. *Proc. Natl. Acad. Sci. USA* **89,** 1790–1794.

25. Allan, A. C., Fricker, M. D., Ward, J. L., Beale, M. H., and Trewavas, A. J. (1994) Two transduction pathways mediate rapid effects of abscisic acid in *Commelina* guard cells. *Plant Cell* **6,** 1319–1328.
26. Webb, A. A. R., McAinsh, M. R., Mansfield, T. A., and Hetherington, A. M. (1996) Carbon dioxide induces increases in guard cell cytosolic free calcium. *Plant J.* **9,** 297–304.
27. Grabov, A. and Blatt, M. R. (1997) Parallel control of the inward-rectifier K^+ channel by cytosolic free Ca^{2+} and pH in *Vicia* guard cells. *Planta* **201,** 84–95.
28. McAinsh, M. R., Brownlee, C., and Hetherington, A. M. (1991) Partial inhibition of ABA-induced stomatal closure by calcium-channel blockers. *Proc. R. Soc. Lond.* B **243,** 195–201.
29. Haugland, R. R. (1996) *Molecular Probes Handbook of Fluorescent Probes and Research Chemicals.* Molecular Probes, Eugene, OR.
30. Trejo, C. L., Clephan, A. L., and Davies, W. J. (1995) How do stomata read abscisic acid-signals. *Plant Physiol.* **109,** 803–811.
31. Brown, K. T. and Flaming, D. G. (1986) *Advanced Micropipet Techniques for Cell Physiology.* John Wiley and Sons, Chichester, UK.

22

Assay and Purification of Calmodulin-Dependent Protein Kinase

Rakesh Kakkar and Rajendra K. Sharma

1. Introduction

Posttranslation covalent modification of proteins by phosphorylation represents an important mechanism in the control of many cellular functions ***(1,2)***. Protein kinases catalyze the transfer of the γ-phosphoryl group of ATP to an acceptor protein substrate. The activity of the enzyme is determined by the transfer of ^{32}P from [γ-^{32}P] ATP to protein substrate

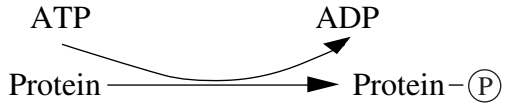

Ca^{2+} is an important intracellular second messenger that regulates cell function through Ca^{2+}-dependent phosphorylation of regulatory enzymes and proteins ***(3–5)***. Calmodulin (CaM) is a primary intracellular Ca^{2+} receptor that mediates Ca^{2+} stimulation of a variety of enzymes, most notably a family of Ca^{2+}/CaM-dependent protein kinases ***(6,7)***. Ca^{2+}/CaM-dependent protein kinase known as CaM kinase II constitutes one of a large family of enzymes known as multifunctional CaM-dependent protein kinases ***(8)***. They are capable of phosphorylating serine and threonine residues on multiple targets and coordinately modifying the activities of several regulatory enzymes and structural proteins ***(8,9)***. CaM kinases have received considerable attention in recent years because they play a pivotal role in various cellular processes, including responses to stimuli that are mediated by Ca^{2+} such as neurotransmitter release, muscle contraction, gene expression, and cell proliferation ***(7,8,10)***. To identify physiological functions of Ca^{2+} that are mediated by protein phosphorylation,

From: *Methods in Molecular Biology, Vol. 114: Calcium Signaling Protocols*
Edited by: D. G. Lambert

it is essential to purify and characterize each of these kinases and their protein substrates. A number of Ca^{2+}/CaM-dependent protein kinases have been characterized ***(7–9)***. The relative amount of CaM-dependent protein kinase II is low compared to other protein kinases; consequently, it is difficult to determine CaM-dependent protein kinase II activity by measuring the existence of the enzyme level in the presence or absence of Ca^{2+} or a CaM antagonist. In addition, like other protein kinases, the CaM-dependent protein kinase II is also autophosphorylated rapidly in the presence of Ca^{2+} and CaM, and it converts to a Ca^{2+}-independent form ***(11–14)***.

Several investigators have developed purification procedures for the preparation of homogeneous CaM-dependent protein kinase II from various tissues including brain, heart, skeletal muscle, liver, pancreas, and *Aspergillus nidulans* ***(12,15–19)***. All these methods involve the use of conventional purification approaches consisting of multiple column chromatographies. This chapter describes the assay method and rapid purification procedure of CaM kinase II that is suitable for large-scale preparation.

2. Materials

General laboratory chemicals are of analytical grade and are obtained either from Sigma, BDH, or Aldrich (Oakville, Ontario, Canada). All reagents are stable for several months at 0–4°C except [γ-^{32}P] ATP, cold ATP, and CaM, which should be stored at –20°C.

2.1. CaM-Kinase Assay

1. 1 *M* Tris-HCl: Dissolve 60.6 g of Tris-HCl in distilled water, adjust pH 7.0 with HCl, and make the final volume to 500 mL.
2. 1 *M* $MgCl_2$: Dissolve 20.3 g of $MgCl_2$ in 100 mL of distilled water.
3. 2-Mercaptoethanol.
4. Assay buffer: The standard assay buffer contains 950 µL of 1 *M* Tris-HCl, 50 µL of 1 *M* $MgCl_2$; and 5 µL of 2-mercaptoethanol; mix it thoroughly and it is ready for use.
5. 1 mCi [γ-^{32}P] ATP (ICN Radiochemicals, Irvine, CA).
6. 1.0 m*M* ATP: Dissolve 31 mg of ATP in distilled water, adjust to pH 7.0, and make the final volume to 50 mL. Calculate correct concentration by using the extinction coefficient for ATP, 15.4 m*M* cm^{-1} at 259 nm in 0.1 N HCl, and store at –20°C in small aliquots.
7. Working solution of ATP: 1 m*M* ATP, specific activity 100 cpm/pmol.
8. 1 m*M* $CaCl_2$: Dissolve 14.7 mg of $CaCl_2$ in 10 mL of distilled water.
9. 1 m*M* EGTA: Dissolve 38.0 mg of EGTA in distilled water, adjust pH 7.0 with 0.1 *N* NaOH; and make the final volume to 10 mL.
10. CaM: Available commercially or purify as described by Sharma ***(20)***. Make 1 mg/mL of CaM in 20 m*M* of Tris-HCl buffer, pH 7.0, containing 0.01 m*M* $CaCl_2$.

11. Substrate: Mixed histone, casein, or specific substrate. Make solution of 2 mg/mL; store in small aliquots.
12. 10% Trichloroacetic acid (TCA) and 2% phosphoric acid: Dissolve 100 g of TCA and 20 mL of phosphoric acid in 1 L of distilled water.
13. 5% TCA: Dissolve 50 g of TCA in 1 L of distilled water.
14. 95% Ethanol.
15. Whatman P81 phosphocellulose filter paper (3 mm) discs (Whatman Inc., NJ: Phosphocellulose filter paper is cut into 2-cm square discs, and the bottom edge is folded approx 0.5 cm and numbered with a pencil. Place filter paper square on cardboard so that the bottom folded edge is supporting the filter paper and the number is facing the front (*see* **Fig. 1A**).
16. Forceps (stainless steel) and flat cardboard.
17. Beckman ready safe scintillation cocktail.
18. Radioactive shield, Geiger-Müller counter, and liquid scintillation counter.

2.2. CaM–Sepharose-4B Affinity Gel

CaM-Sepharose column chromatography is an important step for purification of CaM-binding proteins. CaM is covalently linked to divinyl sulfone activated Sepharose-4B gel.

1. Sepharose-4B (Pharmacia Biotech, Quebec, Canada).
2. 0.2 *M* Sodium carbonate, pH 9.5: Dissolve 24.8 g of sodium carbonate in distilled water, adjust pH to 9.5, and make the final volume to 1 L.
3. 0.5 *M* Sodium carbonate, pH 11.0: Dissolve 62.0 g of sodium carbonate in distilled water, adjust pH to 11.0, and make the final volume to 1 L.
4. Divinyl sulfone (Aldrich).
5. Acetone.
6. Glycine.

2.3. Purification of CaM-Dependent Protein Kinase

1. DEAE-Sepharose CL-6B and Sephacryl S-300 (Pharmacia Biotech).
2. Homogenizing buffer: (20 m*M* Tris-HCl, 2 m*M* EDTA): Dissolve 2.42 g of Tris-HCl and 745 mg of EDTA in distilled water, adjust pH to 7.5 with 1*M* HCl, and make the final volume to 1 L. To the buffer add 100 mg of phenyl methyl sulfonyl fluoride (PMSF), 100 mg of partially purified soybean trypsin inhibitor, 700 µg of leupeptin, and 200 mg benzamidine (*see* **Note 1**).
3. Buffer A: This buffer will be required throughout the purification procedure. Make 40 times the concentrated stock. Dissolve 96.9 g of Tris-HCl, 2.73 g of imidazole, and 8.58 g of magnesium acetate in distilled water, adjust pH to 7.0 with HCl, and make the final volume to 1 L. Dilute 40 times before use to have final concentration of buffer A (20 m*M* Tris-HCl, 1 m*M* magnesium acetate, 1 mM imidazole, pH 7.0).
4. 100 m*M* $CaCl_2$: Dissolve 7.35 g of $CaCl_2$ in 500 mL of distilled water.
5. 100 m*M* EGTA: Dissolve 19.02 g of EGTA in distilled water, adjust pH to 7.0 with NaOH solution, and make the final volume to 500 mL.

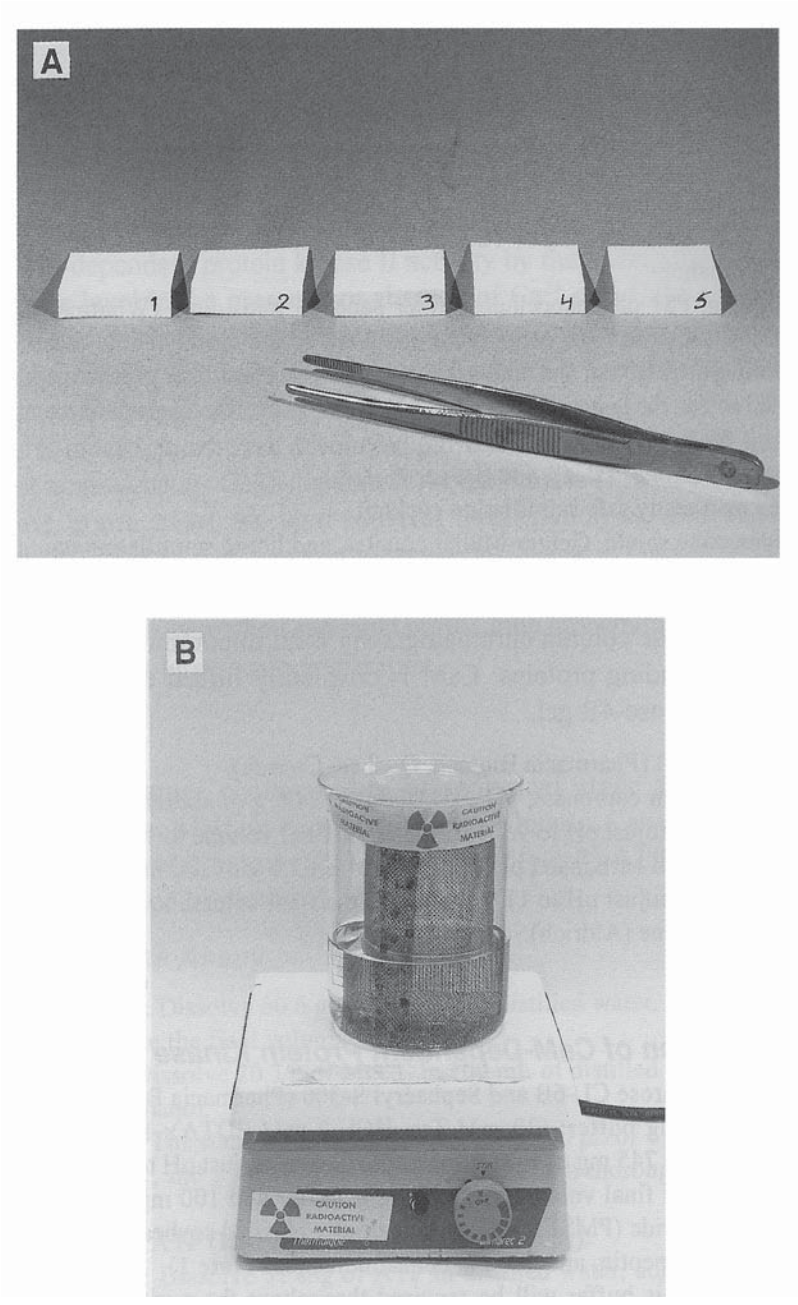

Fig. 1. Termination of CaM-kinase assay. **(A)** Arrangement of phosphocellulose P81 filter paper discs; **(B)** washing apparatus for radioactive phosphocellulose P81 filter paper discs.

3. Methods

3.1. Assay for CaM-Dependent Protein Kinase

CaM-dependent protein kinase activity is determined by a modification of the filter paper method described by Reimann et al. ***(21)*** (*see* **Note 2**). Units: One unit of protein kinase activity is defined as the amount of the enzyme that incorporates 1 µmol of phosphate/min at 30°C into substrate. The difference between the phosphorylation observed in the presence of Ca^{2+}/CaM and EGTA is used as CaM-dependent phosphorylation activity.

1. CaM-dependent protein kinase assay is carried out in a final volume of 50 µL.
2. Add 5 µL of assay buffer, 5 µL of either $CaCl_2$ or EGTA, 5 µL of CaM, 10 µL of substrate, and crude extract or purified protein kinase as an enzyme source at appropriate dilutions ensuring a linear rate of [γ-^{32}P] ATP incorporation into the protein substrate. (The final concentration of components in the reaction mixture is 100 m*M* Tris-HCl, pH 7.0, 5 m*M* $MgCl_2$, 5 m*M* 2-mercaptoethanol, 0.1 m*M* $CaCl_2$ or 0.1 m*M* EGTA, 100 µg/mL of CaM, and 400 µg/mL substrate.)
3. All the reagents and tubes are kept on ice during the additions. The final volume of the reaction is made up to 45 µL with distilled water. The added components are thoroughly mixed, and the tubes are transferred to a water bath at 30°C. Incubate the tubes for approx 1 min.
4. The reaction is initiated by the addition of 5 µL of [γ-^{32}P] ATP to a final concentration of 0.1–0.2 m*M* (specific activity, 100–200 cpm/pmol) (*see* **Note 3**).
5. The reaction is terminated after 10 min incubation or after an appropriate time period by spotting 25 µL onto Whatman P81 phosphocellulose filter paper (3 mm) discs (see **Note 4**). The discs are dropped by using forceps immediately into a wire basket lying in a beaker containing 10% TCA and 2% phosphoric acid (**Fig. 1B**). The basket provides an easy way of handling the discs during the washing and drying procedure. The beaker should contain washing solution above the level of the filter paper discs. To ensure efficient washing, stir the solution at slow speed and continue washing for 20 min.
6. The filter paper discs are further washed twice with 5% TCA for 20 min and then rinsed in 95% ethanol.
7. The discs are then dried for 5 min with a hair dryer and put into scintillation vials. Seven mL of Beckman ready safe liquid scintillation cocktail is added to each vial and the radioactivity is quantified in a Beckman liquid scintillation counter.
8. Since the phosphorylated protein binds to the filter paper discs, the discs can be removed carefully from the scintillation vials and vials can be reused after checking the background.

3.2. Calculation for Protein Kinase Activity

The activity of the enzyme is calculated as follows:

$$\textit{pmol phosphate/assay} = \frac{\text{Test-blank}}{\text{Specific activity of [}\gamma\text{-}^{32}\text{P] ATP (e.g., 100 cpm/pmol)}}$$

$$\times \frac{\text{Total assay volume (e.g., 50 µL)}}{\text{Volume spotted on P81 filter paper (e.g., 25 µL)}}$$

$$\textit{Activity (µmol phosphate} \cdot \textit{mL}^{-1} \cdot \textit{min}^{-1}) = \frac{1}{\text{pmol phosphate/assay volume (e.g., 50 µL)}} \times \frac{1}{10^6} \times \frac{1}{\text{Incubation time}}$$

$$\textit{Specific activity} = \frac{\text{Activity}}{\text{Protein concentration, mg/mL}}$$

3.3. Purification of CaM-Dependent Protein Kinase

3.3.1. Preparation of CaM-Affinity Gel—Activation of Sepharose-4B

1. Wash Sepharose-4B (400 g) in a glass sintered filter funnel with 4 to 5 L of deionized double-distilled water and then with 1 L of 0.5 *M* sodium carbonate, pH 11.0.
2. Transfer the washed gel to a 1-L beaker and mix with 400 mL of the same buffer.
3. Under a fume hood, add slowly 22 mL of divinyl sulfone to the gel suspension with gentle stirring. After 2.5 h, add 1-mL aliquots of divinyl sulfone eight times at 15-min intervals.
4. Transfer the gel to a glass filter funnel and wash with 10 L of deionized double-distilled water until the effluent is close to neutrality.
5. Wash the gel further with 1 L of acetone, and again with 4 L of double-distilled water. The activated Sepharose-4B gel can be stored for several months at 4°C as a water suspension in the presence of 0.02% sodium azide (*see* **Note 5**).

3.3.2. Conjugation of CaM to Activated Sepharose-4B

1. Wash activated Sepharose-4B (400 g) in a glass sintered filter funnel with 2L of 0.2 *M* sodium carbonate, pH 9.5, and then suspend in 400 mL of the same buffer in a 1-L beaker.
2. Mix pure CaM (400 mg/400 mL gel) that has been extensively dialyzed against 0.2 *M* sodium carbonate, pH 9.5, with the gel suspension. Stir the mixture gently at room temperature for 4 h and then in a cold room for 16 h.
3. Add glycine (1 g) to the gel suspension and stir at room temperature for 4 h.
4. The conjugate Sepharose-4B, after thorough washing with deionized double-distilled water, can be equilibrated and stored in any neutral buffer at 4°C until use.

3.4. Extraction

1. All steps are carried out at 4°C. Transfer the fresh bovine hearts obtained from a local slaughterhouse to the laboratory in packed ice.

2. Cut the heart (devoid of vascular tissue) into small pieces, grind (2 kg) in a meat grinder, and then homogenize in a Waring blender for 1 min in 2 vol of ice-cold homogenizing buffer containing protease inhibitors (*see* **Notes 1** and **6**).
3. Centrifuge the homogenate at 10,000*g* for 20 min, and filter the supernatant through glass wool. Add 2-mercaptoethanol (700 µL/L) and EGTA (from 100 m*M*, 1 mL/L) to the supernatant to make a final concentration of 10 and 0.1 m*M*, respectively.

3.4.1. DEAE-Sepharose CL-6B Column Chromatography

1. Apply the supernatant from the extraction step to a DEAE-Sepharose CL-6B (8.0 × 20.0 cm) column preequilibrated with buffer A, pH 7.0, containing 10 m*M* 2-mercaptoethanol (700 µL/L) and 0.1 m*M* EGTA (from 100 m*M*, 1 mL/L) (*see* **Note 7**).
2. Wash the column subsequently with two to three bed volumes of buffer A containing 10 m*M* 2-mercaptoethanol, 0.1 m*M* EGTA, and 0.05 *M* NaCl (1.17 g/L).
3. Elute the proteins with the same buffer containing 0.2 *M* NaCl (11.7 g/L), and pool the fractions containing high protein concentration.

3.4.2. CaM—Sepharose-4B Chromatography

The most efficient purification step in the procedure is the CaM–Sepharose-4B column chromatography, which is used to isolate proteins capable of undergoing Ca^{2+}-dependent association with CaM. The purification of the CaM-dependent protein kinase II is based on the manipulation of elution conditions from a CaM–Sepharose-4B column to resolve the CaM-dependent protein kinase II from other CaM-binding proteins. Endogenous CaM is removed from the heart supernatant by using DEAE-Sepharose CL-6B column chromatography.

1. Add $CaCl_2$ solution to the pooled sample of DEAE-Sepharose CL-6B column to a final concentration of 0.25 m*M* (from 100 m*M*, 2.5 mL/L), and stir the solution gently for 20 min (*see* **Note 8**).
2. Apply the sample to a CaM–Sepharose-4B affinity column (6.0 × 15.0 cm) that has been previously equilibrated with buffer A containing 10 m*M* 2-mercaptoethanol, and 0.25 m*M* $CaCl_2$ (*see* **Note 9**).
3. After sample application, wash the column with buffer A containing 0.1 m*M* $CaCl_2$ (from 100 m*M*, 1 mL/L) and 0.2 M NaCl (11.7 g/L), until no protein is detected in the eluate (approx 4 bed volumes). Then, further elute the column with one additional bed volume of the same buffer without NaCl.
4. First, elute the column with buffer A containing 1 m*M* EGTA. When the protein concentration in the column is returned to the basal level, elute the column further with buffer A containing 1 m*M* EGTA and 0.5 *M* NaCl (29.2 g/L). Two protein peaks (peaks A and B) are observed by this elution procedure (**Fig. 2**).
5. Pool both peaks A and B separately and concentrate by ultrafiltration through an Amicon PM-10 membrane (Amicon Division, MA). Peaks A and B represent 30–35% and 65–70% of total CaM-binding proteins, respectively. Peak A contains >85% activity of the CaM-dependent protein kinase II and 90% activity of CaM-

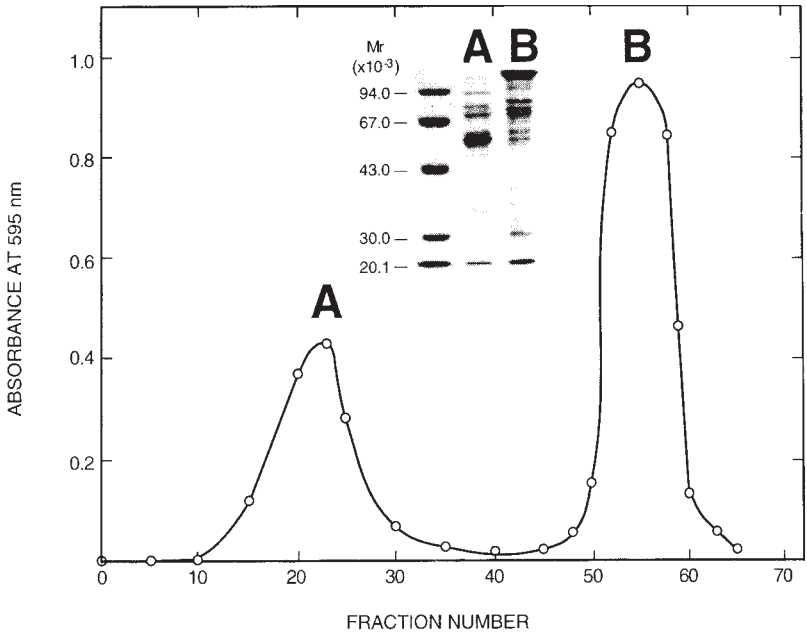

Fig. 2. Chromatography of CaM-binding proteins on a CaM–Sepharose-4B column. The pooled sample from a DEAE-Sepharose CL-6B column is applied on CaM-Sepharose 4B affinity column. After application, the column is washed with buffer A containing 0.1 m*M* Ca^{2+} and 0.2*M* NaCl (approx four bed volumes), and then one bed volume of the same buffer without NaCl. Proteins are eluted initially in buffer A containing 1.0 m*M* EGTA and subsequently in buffer A containing 1.0 m*M* EGTA and 0.5*M* NaCl. The fractions in the region of peak A and peak B are pooled separately. **(Inset)** Peaks A and B are analyzed by SDS-PAGE. Lane 1, molecular standards: phosphorylase *b*, BSA, ovalbumin, carbonic anhydrase, and soybean trypsin inhibitor. Lanes 2 and 3 are peak A and B, respectively. For details *see* **ref. *14***.

dependent cyclic nucleotide phosphodiesterase. Using sodium dodecyl sulfate-polyacrylamide gel electrophoresis (SDS-PAGE), it was shown that peak A is enriched with a 56,000-Dalton species whereas peak B is enriched with the high molecular weight CaM-binding protein ***(20)***.

3.4.3. Sephacryl S-300 Column Chromatography

1. Prepare a column of Sephacryl S-300 (1.5 × 95 cm), and equilibrate with buffer A containing 0.1 m*M* EGTA, 0.1 *M* NaCl (5.84 g/L), and 10% (w/v) sucrose (100 g/L).
2. Apply peak A from the CaM–Sepharose-4B column to the Sephacryl S-300 column.
3. Proteins are eluted with equilibration buffer at a flow rate of 6 mL/h. CaM-dependent protein kinase II activity is detected in a sharp peak that corresponds to the protein peak (**Fig. 3**). The CaM-dependent protein kinase II is separated from the CaM-dependent cyclic nucleotide phosphodiesterase and other CaM-binding proteins.

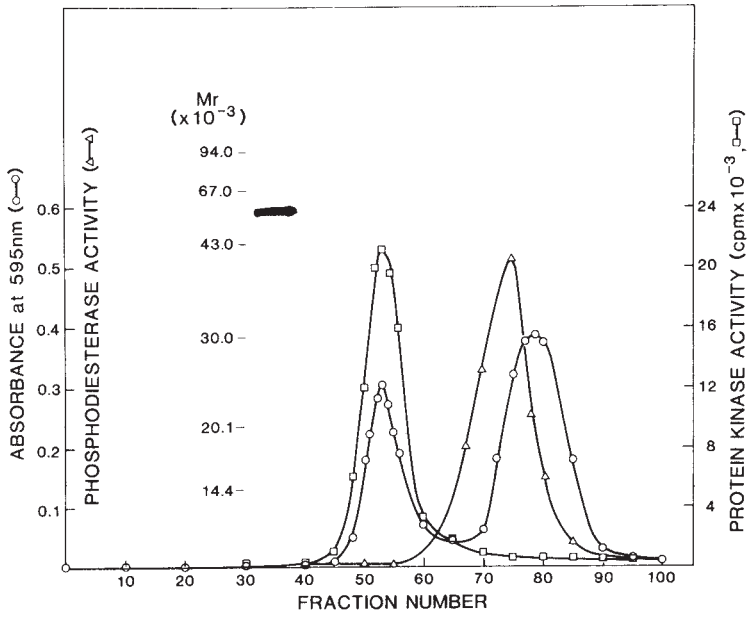

Fig. 3. Gel filtration column chromatography of CaM-dependent protein kinase II. Peak A is applied to a Sephacryl S-300 column. CaM-dependent protein kinase II (❑——❑) and CaM-dependent cyclic nucleotide phosphodiesterase (Δ——Δ) activity are monitored as described in **Subheading 3.** Protein concentrations are determined by the dye-binding method (○——○). **(Inset)** The purity of the pooled sample (fraction 50–57) is analyzed by SDS-PAGE. For details see ***(14)***.

4. Fractions under the peak region of CaM-dependent protein kinase activity are pooled and concentrated to 2 to 3 mL by ultrafiltration with an Amicon PM-10 membrane and stored in small aliquots at –70°C (*see* **Note 10**).

3.5. Other Methods

SDS-PAGE is carried out according to the method of Laemmli ***(22)***. Coomassie brilliant blue is used to visualize the protein bands on the gel. Protein assay is carried out as described by Bradford ***(23)*** using bovine serum albumin (BSA) as a standard.

3.6. Regeneration of DEAE and CaM–Sepharose 4B Columns

1. Regenerate the DEAE-Sepharose CL-6B column by washing with two bed volumes of 0.25 *M* NaCl (14.6 g/L) and 0.25 *M* NaOH (10 g/L) solution and then twice with double-distilled water. Wash the column further with one bed volume of 0.25 *M* HCl (9 mL/L) and then with two to three bed volumes of double-distilled water until chloride free.

2. Adjust the pH of the gel suspension to 7.0 by washing with buffer A containing 1 m*M* EGTA (1 mL from 100 m*M*/L) and 10 m*M* 2-mercaptoethanol (700 µL/L).
3. Regenerate the CaM–Sepharose-4B column by washing with one bed volume of 3 *M* urea (180 g/L) to remove tightly bound proteins, followed by three bed volumes of double-distilled water.
4. Equilibrate the column with buffer A containing 0.25 m*M* $CaCl_2$ (from 100 m*M*, 2.5 mL/L) and 10 m*M* 2-mercaptoethanol (700 µL/L) (*see* **Note 11**).

3.7. Purity, Molecular Weight, Subunit Structure and Stability of Cardiac CaM Kinase

The purity of the enzyme preparation is examined by SDS-PAGE. It exhibits essentially a single protein band with a mobility corresponding to a 56,000-Dalton polypeptide (**Fig. 3**, inset). The molecular weight of the CaM-dependent protein kinase II from cardiac muscle determined by the calibrated gel filtration column is 570,000 Dalton, which suggests that the CaM-dependent protein kinase II is composed of 10 identical subunits of 56,000 Dalton ***(14)***. The molecular and subunit weights of the bovine heart CaM-dependent protein kinase II reported here are similar to those reported previously for the bovine brain CaM-dependent protein kinase II ***(13)***. The size of the subunit in various tissues varies because that CaM-dependent protein kinase II may exist as distinct isozymes that possess tissue-specific functions. Like other members of the protein kinase family ***(7,8,13,18)***, the purified bovine heart CaM-dependent protein kinase II also has a relatively broad protein substrate specificity ***(14,16)***. The purified enzyme shows a specific enzyme activity of 2.4 µmol · min^{-1} · mg^{-1} protein in the presence of mixed histone. The recovery of the CaM-dependent protein kinase II from the gel filtration column is >75%. The purification scheme (**Fig. 4**) described here is simple, rapid, and suitable for large-scale preparation.

The authors have observed that storage for several months at –70°C results in the breakdown of the purified bovine cardiac muscle CaM-dependent protein kinase II into several apparent molecular species. The degraded preparation was less sensitive to Ca^{2+}/CaM. These results suggest that the enzyme either can be autophosphorylated or susceptible to protease degradation (*see* **Note 10**).

3.8. Properties of CaM-Dependent Protein Kinase II from Cardiac Muscle

3.8.1. Autophosphorylation

A common, but not universal, feature of protein kinases is that they undergo autophosphorylation. Autophosphorylation is the process in which the holozyme catalyzes the phosphorylation of one or more amino acids within its own structure through intramolecular reaction. It plays an important role in

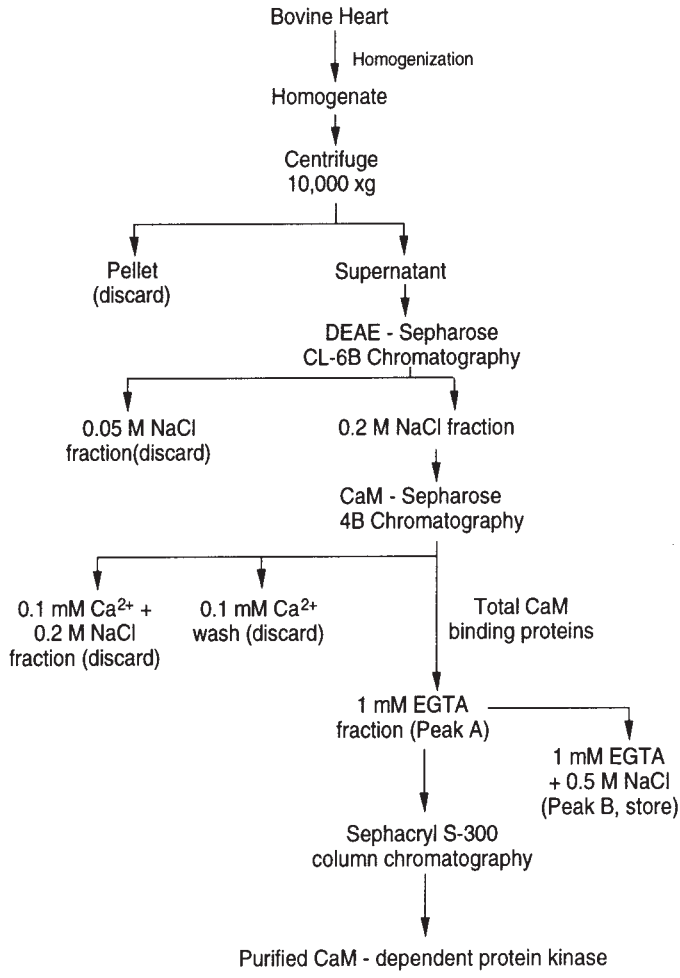

Fig. 4. Purification scheme of CaM-dependent protein kinase from bovine heart.

regulating various kinase functions in vivo. Like other members of the CaM-dependent protein kinase II family ***(11–13,24–27)***, bovine cardiac CaM-dependent protein kinase II also rapidly undergoes autophosphorylation ***(14)***. The autophosphorylation reaction is completely dependent on Ca^{2+} and CaM. The reaction is rapid and completed with a maximal incorporation of 1 mol phosphate/mol subunit of CaM-dependent protein kinase II. Autophosphorylated CaM-dependent protein kinase II becomes a completely Ca^{2+}-independent form for the phosphorylation of substrate (**Fig. 5**). The autophosphorylation of CaM-dependent protein kinase can be reversed through dephosphorylation by protein phosphatase I ***(27,28)***. Autophosphorylation of CaM-dependent protein

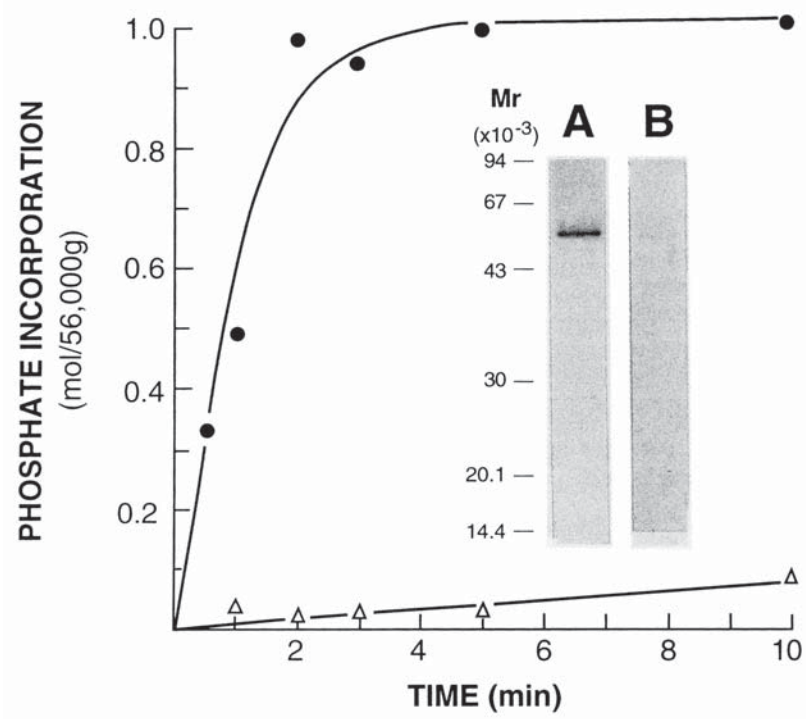

Fig. 5. Time course of stoichiometry of autophosphorylation of CaM-dependent protein kinase II. The purified CaM-dependent protein kinase II (50 µg/mL) is incubated in a standard reaction mixture containing 200 µg/mL of CaM and 500 µg/mL of BSA in the presence of 0.1 m*M* $CaCl_2$ (●——●) or 0.1 m*M* EGTA (Δ——Δ) as described in **Subheading 3.** Endogenous phosphorylation is allowed to proceed, and aliquots are taken at various time intervals indicated for γ-^{32}P incorporation into CaM-dependent protein kinase II. **(Inset)** After 10 min of reaction time, aliquots are subjected to electrophoresis followed by autoradiography. Lanes A and B: CaM-dependent protein kinase II in the presence of 0.1 m*M* $CaCl_2$ (●——●) and 0.1 m*M* EGTA (Δ——Δ), respectively, for details *see* **ref.** 14.

kinase II can be carried out using the same procedure as the protein kinase assay except a protein substrate is not added.

3.8.2. Phosphorylation as a Function of Ca^{2+} Concentration

The synergistic interaction between Ca^{2+} and CaM in the activation of various CaM-dependent enzymes has been reported repeatedly ***(12–14,29–32)***. The Ca^{2+}-dependence of the CaM-dependent protein kinase II was examined at saturating levels of CaM. **Figure 6** shows that Ca^{2+} and CaM interact synergistically in activation of CaM-dependent protein kinase II in the phosphorylation of casein. When the CaM concentration is increased, the Ca^{2+} concentration

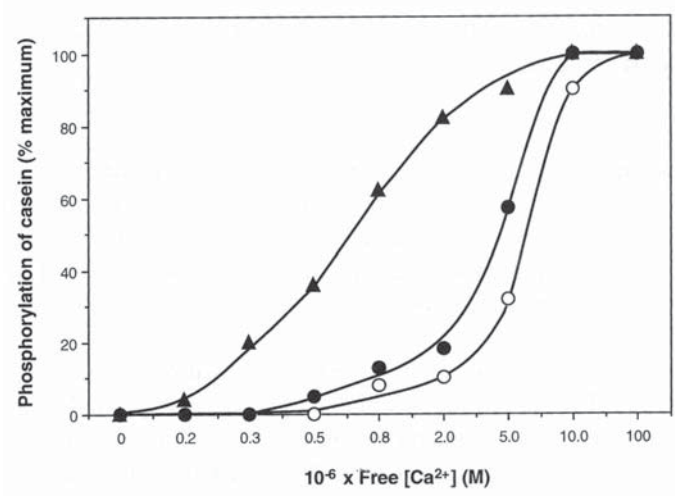

Fig. 6. Phosphorylation of casein by CaM-dependent protein kinase II as a function of Ca^{2+} concentration at different levels of CaM. The assay is carried out as described in **Subheading 3.** The casein is phosphorylated by CaM-dependent protein kinase II (6.4 µg/mL) for 40 min at 1 µ*M* (○——○), 5 µ*M* (●——●), and 20 µ*M* (▲——▲) of CaM. The free Ca^{2+} concentration in the EGTA-buffered solution is calculated as described previously ***(31)***. For details *see* **ref. *14***.

required for half-maximal activation is decreased. The half-maximal phosphorylation of casein is observed at 6.1, 4.4, and 0.67 µ*M* Ca^{2+} in the presence of 1, 5, and 20 µ*M* CaM, respectively. Although the physiological significance of the observed differential Ca^{2+} sensitivity of the CaM-dependent protein kinase in cardiac muscle is not known, it is noteworthy that the differential Ca^{2+} affinity of CaM-dependent protein kinase II is a mechanism by which the CaM regulatory reactions are adapted to the respective tissues.

3.8.3. Immunological Characterization

To examine whether the cardiac CaM-dependent protein kinase is similar to any other CaM-dependent protein kinase, immunoblotting is carried out by the method of Towbin et al. ***(33)***. A polyclonal antipeptide antibody raised against multifunctional CaM-dependent protein kinase II of rat brain is tested for immunoreactivity with the bovine cardiac muscle CaM-dependent protein kinase II ***(14)***. The antibody is raised against the synthetic peptides of the N- and C-terminal, CTRFTDEYQLFEEL and EETRVWHRRDGKWQNVHFHC corresponding to amino acids 7–20 and 514–533 of the multifunctional CaM-dependent protein kinase II β-isoform of rat brain (Upstate Biotechnology, New York; ***[34,35]***). Western blot of purified cardiac muscle CaM-dependent kinase II showed an immunoreactive band of 56,000 Dalton ***(14)***. This suggested that

cardiac muscle enzyme is immunologically similar to that of multifunctional CaM-dependent protein kinase II isozyme of rat brain.

4. Notes

1. Problems may arise by the presence of Ca^{2+}-dependent or -independent proteolytic enzymes. It is strongly recommended that the protease inhibitors are included in the buffers at the time of homogenization, up to the CaM–Sepharose-4B affinity chromatography step. (PMSF should be dissolved in isopropanol with vortex and then added in homogenizing buffer very slowly with continuous stirring.)
2. For protein kinase assay, wear gloves to avoid direct contact with skin from radioactive ATP. After finishing the assay, check working bench with Geiger muller counter for any spills, pipet tips, and so on. If anything is found contaminated, use safety procedures to handle the radioactive material.
3. The radioactive ATP has a half-life of 14.3 d, and calculating specific activity decay factor should be considered at each time.
4. The filter paper discs are numbered at the bottom with a pencil. The sample from the assay tubes should be spotted on the respective disc at the center.
5. The binding capacity of activated Sepharose-4B gel must be checked before adding CaM. Take 1–2 mL of gel in an Eppendorf tube and add approx 2–4 mg of ferritin; keep for occasional mixing for 4 h. Centrifuge the gel suspension at 320*g* for 2 min, and check the protein concentration of supernatant to see how much is bound to the gel. If protein is bound to the gel and no protein is detected in the supernatant, the gel is activated and ready for use.
6. Before centrifugation, the homogenate should be adjusted to pH 7.5 with 1*M* Tris and stirred for 15–20 min at 4°C.
7. The pH of the DEAE-Sepharose CL-6B column should be 7.0–7.5; if pH is <7.0, protein kinase will not bind to the column.
8. Before applying pooled DEAE-Sepharose CL-6B sample to the CaM–Sepharose-4B affinity column, $CaCl_2$ must be added to a final concentration of 0.25 m*M*.
9. The DEAE-Sepharose CL-6B column chromatography step is used mainly to remove an endogenous CaM from crude homogenate. If the total CaM-binding proteins do not bind to the CaM–Sepharose-4B column in the presence of $[Ca^{2+}]$, it suggests two possibilities: (1) the free Ca^{2+} is not high enough to overcome EGTA (*see* **Subheading 3.4.2.**), and/or (2) pooled sample from this step is contaminated with an endogenous CaM. Therefore, there will be competition between the solid phase (CaM–Sepharose-4B column) and the soluble phase, resulting in poor binding to the CaM–Sepharose 4B column.
10. The storage of CaM-dependent protein kinase II at –70°C for several months results in breakdown of the enzyme into several apparent molecular species. To increase the half–life of enzyme, store in small aliquots in either the presence of 10% glycerol or 10% sucrose. (Add 10% sucrose during elution from S-200 column.)
11. CaM–Sepharose-4B column can be stored for several years after regeneration by adding a small amount of sodium azide (0.02%) in equilibration buffer.

Acknowledgments

This work was supported by the Heart and Stroke Foundation of Saskatchewan, Canada. The authors are thankful to Dr. R. V. S. Raju, Department of Pathology, University of Saskatchewan for reading this chapter.

References

1. Cohen, P. (1992) Signal integration at the level of protein kinases, protein phosphatases and their substrates. *Trends Biochem. Sci.* **17,** 408–413.
2. Hunter, T. (1995) Protein kinases and phosphatases: The yin and yang of protein phosphorylation and signalling. *Cell* **80,** 225–236.
3. Berridge, M. J. (1975) The interaction of cyclic nucleotides and calcium in the control of cellular activity. *Adv. Cyclic Nucleotide Res.* **6,** 1–98.
4. Clapham, D. E. (1995) Calcium signalling. *Cell* **80,** 259–268.
5. Sharma, R. K. and Kalra, J. (1994) Molecular interaction between cAMP and calcium in calmodulin-dependent cyclic nucleotide phosphodiesterase isozyme system. *Clin. Invest. Med.* **17,** 374–382.
6. Klee, C. B. (1988) Interaction of calmodulin with Ca^{2+} and target proteins, in *Molecular Aspects of Cell Regulation*, vol. 5, (Cohen, P. and Klee, C., eds.), Elsevier Science, New York, pp. 35–56.
7. Nairn, A. C. and Picciotto, M. R. (1994) Calcium/calmodulin dependent protein kinase. *Semin. Cancer Biol.* **5,** 295–303.
8. Schulman, H. (1988) The multifunctional Ca^{2+}/calmodulin-dependent protein kinase. *Advances in Second Messenger and Phosphoprotein Research* **22,** 39–112.
9. Kemp, B. E. and Pearson, R. B. (1990) Protein kinase recognition sequence motifs. *Trends Biochem. Sci.* **15,** 342–346.
10. Soderling, T. R. (1995) Calcium-dependent protein kinases in learning and memory. *Advances in Second Messenger and Phosphoprotein Research* **30,** 175–189.
11. Hashimoto, Y., Schworer, C. M., Colbran, R. J., and Soderling, T. R. (1987) Autophosphorylation of Ca^{2+}/calmodulin-dependent protein kinase II: Effects on total and Ca^{2+}-independent activities and kinetic parameters. *J. Biol. Chem.* **262,** 8051–8055.
12. Zhang, G. Y., Wang, J. H., and Sharma, R. K. (1993) Bovine brain calmodulin-dependent protein kinase II: Molecular mechanisms of autophosphorylation. *Biochem. Biophys. Res. Commun.* **191,** 669–674.
13. Zhang, G. Y., Wang, J. H., and Sharma, R. K. (1993) Purification and characterization of bovine brain calmodulin-dependent protein kinase II. The significance of autophosphorylation in the regulation of 63 kDa calmodulin-dependent cyclic nucleotide phosphodiesterase isozyme. *Mol. Cell. Biochem.* **122,** 159–169.
14. Kakkar, R., Raju, R. V. S., and Sharma, R. K. (1996) Calmodulin-dependent protein kinase II from bovine cardiac muscle: purification and differential activation by calcium. *Cell Calcium* **20,** 347–353.
15. Bennett, M. K., Erondu, N. E., and Kennedy, M. B. (1983) Purification and characterization of a calmodulin-dependent protein kinase that is highly concentrated in brain. *J. Biol. Chem.* **258,** 12,735–12,744.

16. Iwasa, T., Inoue, N., Fukunaga, K., Isobe, T., Okuyama, T., and Miyamoto, E. (1986) Purification and characterization of a multifunctional calmodulin-dependent protein kinase from canine myocardial cytosol. *Arch. Biochem. Biophys.* **248,** 21–29.
17. Yang, S. D., Chang, S. Y., and Soderling, T. R. (1987) Characterization of an autophosphorylation-dependent multifunctional protein kinase from liver. *J. Biol. Chem.* **262,** 9421–9427.
18. Gorelick, F.S., Cohn, J. A., Freedman, S. D., Delahunt, N. G., Gershoni, J. M., and Jamisen, J. D. (1983) Calmodulin-stimulated protein kinase activity from rat pancreas. *J. Cell. Biol.* **89,** 440–448.
19. Bartelt, D. C., Fidel, S., Wolff, D. J., and Hammell, R. L. (1988) Calmodulin-dependent multifunctional protein kinase in *Aspergillus nidulans*. *Proc. Natl. Acad. Sci. USA* **85,** 3279–3283.
20. Sharma, R. K. (1990) Purification and characterization of novel calmodulin-binding protein from cardiac muscle. *J. Biol. Chem.* **265,** 1152–1157.
21. Reimann, E. M., Walsh, D. A., and Krebs, E. G. (1971) Purification and properties of rabbit skeletal muscle adenosine 3', 5'-monophosphate-dependent protein kinases. *J. Biol. Chem.* **246,** 1986–1995.
22. Laemmli, U. K. (1970) Cleavage of structural proteins during the assembly of the head of bacteriophage T4. *Nature* **227,** 680–685.
23. Bradford, M. M. (1976) A rapid and sensitive method for the quantitation of microgram quantities of protein utilizing the principle of protein-dye binding. *Anal. Biochem.* **72,** 248–254.
24. Schworer, C. M., Colbran, R. J., and Soderling, T. R. (1986) Reversible generation of a Ca^{2+} independent form of Ca^{2+}/calmodulin-dependent protein kinase II by an autophosphorylation mechanism. *J. Biol. Chem.* **261,** 8581–8584.
25. Lai, Y., Nairn, A. C., and Greengard, P. (1986) Autophosphorylation reversibly regulates the Ca^{2+}/calmodulin-dependence of Ca^{2+}/calmodulin-dependent protein kinase II. *Proc. Natl. Acad. Sci. USA* **83,** 4253–4257.
26. Miller, S. G. and Kennedy, M. B. (1986) Regulation of brain type II Ca^{2+}/calmodulin-dependent protein kinase by autophosphorylation: A calcium triggered molecular switch. *Cell* **44,** 861–870.
27. Saitoh, Y., Yamamato, H., Fukunaga, K., Matsukado, Y., and Miyamoto, E. (1987) Inactivation and reactivation of the multifunctional calmodulin-dependent protein kinase from brain by autophosphorylation and dephosphorylation: Involvement of protein phosphatases from brain. *J. Neurochem.* **99,** 1286–1292.
28. Bronstein, J. M., Farber, D. B., and Wasterlain, C. G. (1993) Regulation of type II calmodulin kinase: Functional implications. *Brain Res. Rev.* **18,** 135–147.
29. Sharma, R. K. and Wang, J. H. (1985) Differential regulation of bovine brain calmodulin-dependent cyclic nucleotide phosphodiesterase isozyme by cAMP-dependent protein kinase and calmodulin dependent phosphatase. *Proc. Natl. Acad. Sci. USA* **82,** 2603–2607.
30. Sharma, R. K. and Kalra, J. (1994) Characterization of calmodulin-dependent cyclic nucleotide phosphodiesterase isozymes. *Biochem. J.* **299,** 97–100.

31. Huang, C. Y., Chau, V., Chock, P. B., Wang, J. H., and Sharma, R. K. (1981) Mechanism of activation of cyclic nucleotide phosphodiesterase: Requirement of the binding of four Ca^{2+} to calmodulin for activation. *Proc. Natl. Acad. Sci. USA* **78,** 871–874.
32. Crouch, T. H. and Klee, C. B. (1980) Positive cooperative binding of calcium to bovine brain calmodulin. *Biochemistry* **19,** 3692–3698.
33. Towbin, H., Staehelin, T., and Gordon, J. (1979) Electrophoretic transfer of proteins from polyacrylamide gels to nitrocellulose sheets: Procedure and some applications. *Proc. Natl. Acad. Sci. USA* **76,** 4350–4354.
34. Means, A. R., Cruzalegui, F., Le Magueresse, B., Needleman, D. S., Slaughter, G. R., and Ono, T. (1991) A novel Ca^{2+}/calmodulin dependent protein kinase and a male germ cell specific calmodulin binding protein are derived from the same gene. *Mol. Cell. Biol.* **11,** 3960–3971.
35. Tobimatsu, T. and Fujisawa, H. (1989) Tissue-specific expression of four types of rat calmodulin-dependent protein kinase II mRNAs. *J. Biol. Chem.* **264,** 17,907–17,912.

23

Measurement of Ca^{2+}-ATPase Activity (in PMCA and SERCA1)

Danuta Kosk-Kosicka

1. Introduction

Ca^{2+}-ATP pumps play a vital role in intracellular calcium homeostasis and signaling. They remove excess Ca^{2+} from the cytoplasm, either into the lumen of the intracellular sarcoplasmic reticulum/endoplasmic reticulum (SR/ER) network or out of the cell, and fine-tune local calcium concentrations allowing for proper functioning of a variety of Ca^{2+}-dependent reactions. They are also integral components of Ca^{2+}-dependent cellular events and cascades that are regulated by precisely controlled Ca^{2+} concentrations.

Although Ca^{2+} transport is a physiological function of Ca^{2+} pumps, their Ca^{2+}-ATPase activity is so well characterized that it is used as an indicator of their function. In this chapter, three preparations—two membranes and a purified enzyme–best suited for studies of Ca^{2+}-ATPase activity are described. The two selected membranes are the human red blood cell (RBC) ghosts, a representative of plasma membranes (PM), and the rabbit skeletal muscle SR, an intracellular membrane. These contain the respective Ca^{2+}-ATPase forms: plasma membrane Ca^{2+}-ATPase (PMCA; PMCA 4 and 1) and SR Ca^{2+}-ATPase (SERCA; SERCA1). These preparations are the simplest, most commonly used, and well characterized in which Ca^{2+}-ATPases have been extensively studied. They are easy to prepare without contamination from other membrane types; thus, they contain a single specific Ca^{2+}-ATPase activity. In addition, these preparations are devoid of other Ca^{2+}-transporting systems, such as Na^+/Ca^{2+} exchanger. Moreover, the Na^+,K^+-ATPase activity in RBC membranes is very low, as compared to other plasma membranes. The only enzymatic activity that needs to be considered in the described P_i measurements is that of the Mg^{2+}-ATPase, which is also low and easily subtractable.

From: *Methods in Molecular Biology, Vol. 114: Calcium Signaling Protocols*
Edited by: D. G. Lambert

Ghost membranes are prepared in hypotonic solutions, and calmodulin (CaM) is removed by EDTA washing ***(1,2)***. Because the resulting ghosts are depleted of endogenous CaM, they are suitable for studies of the calcium-dependent CaM activation of PMCA. The strong interaction of CaM with PMCA has made possible its purification by affinity chromatography following detergent solubilization ***(1,2)***. Preparation of CaM–Sepharose-4B columns is included in the procedure (*see* **Note 1**). The author has extensively modified the originally published purification procedures, and the protocol allows for purification of PMCA soluble in $C_{12}E_8$, which is very stable on storage at –80°C in the presence of 20% glycerol and is easily activated by addition of phospholipids ***(3)***. The preparation is suitable for various studies, including spectroscopic measurements that cannot be conducted on the membranous enzyme owing to its low abundance (0.1% of membrane proteins) and the effects of various phospholipids ***(4)***. Slight modifications allow for application of this procedure to other plasma membranes, as has been recently described for the synaptosomal membranes of rat cerebellum ***(5)***. SERCA1 is conveniently studied in SR, in which it comprises up to 80% of SR membrane protein.

Biochemical characterization of the enzyme in the membrane and at different stages of purification from the membrane always includes determination of its steady-state Ca^{2+}-ATPase activity. The assay is especially useful for the purified, soluble PMCA as a rapid functional test to complement structural studies. Ca^{2+}-ATPase activity in combination with fluorescence resonance energy transfer, fluorescence polarization, and equilibrium centrifugation measurements performed on such preparations allowed the author to establish that enzyme concentration-dependent dimerization is a mechanism of PMCA activation ***(6–8)***. The enzymatic hydrolysis rate of ATP is determined by quantitation of the inorganic phosphate (P_i) resulting from ATP hydrolysis by the pump as a function of time. In the described protocol, P_i released during the ATPase reaction is subsequently measured colorimetrically as a complex of molybdovanadate ***(9,10)***. The method is simple (one-step), fast, sensitive, and reliable (*see* **Note 2**).

2. Materials

2.1. Reagents

1. Outdated packed human RBCs for preparation of ghost membranes are obtained from the local Red Cross or blood donation center.
2. Skeletal muscle SR is prepared from hind legs of the rabbit (New Zealand White).
3. Unless specified otherwise, the reagents, including egg yolk phosphatidylcholine (PC) (P5763), CNBr-activated Sepharose-4B, aprotinin, bovine brain CaM for affinity chromatography, and divalent cations ionophore A23187 were purchased from Sigma (St. Louis, MO).

4. CaM for Ca^{2+}-ATPase activity assays was from Calbiochem (San Diego, CA); standard solution was prepared by dissolving 1 mg of CaM in 1 mL of water and stored at –20°C.
5. 0.2-m*M* ionophore solution is made with ethanol.
6. Glycerol was from Serva (Boehringer Ingelheim Bioproducts Partnership, Heidelberg, Germany) (*see* **Note 3**).
7. Protein microassay and sodium dodecyl sulfate (SDS) were from Bio-Rad (Hercules, CA).
8. Octaethylene glycol mono-*n*-dodecyl ether, $C_{12}E_8$ (*see* **Note 4**), was from Nikkol (Tokyo, Japan). To prepare 0.1 *M* aqueous solution, pour the detergent (melted in a warm water bath) into warm deionized water (do not boil), and stir gently. Store at –4°C in a dark glass bottle.
9. Pellicon Cassette System used in preparation of RBC ghost membranes by molecular filtration is from Millipore (Bedford, MA) ***(2)***. The Cassette contains Millipore Pellicon HVLP filters (pore size 0.5 μm) in 20 sheets and it lasts for approx 15 preparations.
10. All solutions are prepared with deionized water.

2.2. Plasma Membranes: Human RBC Ghost Membranes

1. Washing solution: 130 m*M* KCl, 20 m*M* Tris-maleate, pH 7.4 (total volume 7 L).
2. Lysis solution: 5 m*M* Tris-maleate, 1 m*M* EDTA, pH 7.4 (23 L).
3. Ghost storage solution: 10 m*M* Tris-maleate, pH 7.4 (15 L).

2.3. Rabbit Skeletal Muscle SR Membranes

1. Solution 1: 10 m*M* MOPS, 10% sucrose, 0.1 m*M* EDTA, pH 7.0 (1 L).
2. Solution 2: 10 m*M* MOPS, 0.6 *M* KCl, pH 7.0 (0.5 L).
3. Solution 3: 10 m*M* MOPS, 30% sucrose, pH 7.0 (0.5 L).

2.4. Preparation of CaM–Sepharose-4B for Affinity Chromatography (11)

1. 1 m*M* HCl for swelling (200 mL).
2. Coupling solution: 100 m*M* sodium borate, 100 m*M* NaCl, 50 μ*M* $CaCl_2$, pH 8.2 (10 mL, freshly prepared).
3. Blocking solution: 500 m*M* ethanolamine/HCl (10 mL, freshly prepared).
4. Washing solution: 130 m*M* KCl, 10 m*M* Tris-HCl, pH 7.4 (150 mL).
5. Solution A for column regeneration: 0.1 *M* Trizma, 0.5 *M* NaCl, 0.755 m*M* $C_{12}E_8$, pH 8.5 (100 mL).
6. Solution B for column regeneration: 0.1 *M* CH_3COONa, 10-fold diluted acetic acid, 0.5 *M* NaCl, 0.755 m*M* $C_{12}E_8$, pH 4.5 (100 mL).

2.5. Purification of PMCA

1. Solubilization solution (2X): 40 m*M* Tris-maleate, pH 7.4, 1 m*M* $MgCl_2$, 260 m*M* KCl, 1.5 m*M* $C_{12}E_8$ (to be added separately), 0.1 m*M* $CaCl_2$, 40% glycerol, 4 m*M* dithiothreitol (DTT) (70 mL).

2. Equilibration solution: 10 m*M* Tris-maleate, pH 7.4, 0.5 m*M* $MgCl_2$, 130 m*M* KCl, 7.55 m*M* $C_{12}E_8$, 0.05 m*M* $CaCl_2$, 20% glycerol, 2 m*M* DTT (250 mL).
3. Washing solution: 10 m*M* Tris-maleate, pH 7.4, 0.5 m*M* $MgCl_2$, 130 m*M* KCl, 0.755 m*M* $C_{12}E_8$, 0.05 m*M* $CaCl_2$, 20% glycerol, 2 m*M* DTT (150 mL).
4. Elution solution: 10 m*M* Tris-maleate, pH 7.4, 0.5 m*M* $MgCl_2$, 130 m*M* KCl, 0.755 m*M* $C_{12}E_8$, 5 m*M* EGTA, 20% glycerol, 2 m*M* DTT (50 mL). PC suspension: Pipet 30 µL of PC solution (100 mg/mL) into a small glass tube and immediately place under a stream of nitrogen delivered slowly through a Pasteur pipet. Blow dry while turning the tube to achieve an even layer of PC on the bottom. Add 300 µL of elution solution and sonicate using a small probe, periodically placing the tube on ice to avoid overheating, until the solution clears (*see* **Note 5**).

2.6. Ca^{2+}-ATPase Activity Standard Assay Buffers

1. For ghost membranes: 50 m*M* Tris-maleate, pH 7.4, 8 m*M* $MgCl_2$, 120 m*M* KCl, 1 m*M* EGTA, 1.008 m*M* $CaCl_2$ to yield the required 17.5 µ*M* free calcium (*see* **Note 6**). $CaCl_2$ is omitted from the buffer used for Mg^{2+}-ATPase activity.
2. For SR membranes: 50 m*M* Tris-maleate, pH 7.4, 8 m*M* $MgCl_2$, 120 m*M* KCl, 1 m*M* EGTA, 10 µ*M* ionophore A23187, 1.008 m*M* $CaCl_2$ to yield the required 17.5 µ*M* free calcium (*see* **Note 7**). $CaCl_2$ is omitted from the buffer used for Mg^{2+}-ATPase activity.
3. For purified PMCA: 50 m*M* Tris-maleate, pH 7.4, 8 m*M* $MgCl_2$, 120 m*M* KCl, 1 m*M* EGTA, 0.150 m*M* $C_{12}E_8$, 1.008 m*M* $CaCl_2$ to yield the required 17.5 µ*M* free calcium. When preparing this assay buffer, take into account the composition of the elution solution in which PMCA is stored (*see* **Notes 8** and **9**).

2.7. P_i Measurement

1. Ammonium molybdate: Dissolve 5 g of $(NH_4)_6Mo_7O_{24} \cdot 4H_2O$ in water and add 0.5 mL of ammonia (sp gr 0.90) to make 50 mL.
2. Ammonium metavanadate: Dissolve 0.1175 g of NH_4VO_3 in 20 mL of boiling water, and cool under tap water immediately after vanadate dissolves; follow with addition of 0.305 mL of concentrated (sp gr 1.42) nitric acid that has been diluted with 0.7 mL of water. Add water up to 50 mL total volume.
3. 20% SDS solution: Dissolve 10 g of SDS in water to make 50 mL.
4. Mixed Lin-Morales reagent: Mix the solutions in **items 1–3** with 17.5 mL of concentrated nitric acid and make up to 0.5 L with water. Store in a dark glass bottle. This solution will keep for 1 to 2 mo; discard when a significant amount of precipitate forms on the bottom. For the assays described in **Subheading 3.3.**, use Lin-Morales solution diluted threefold with water.

3. Methods

3.1. Preparation of Membranes Containing Either PMCA (RBC Ghosts) or SERCA1 (SR)

All steps are carried out at 4°C either in the cold room or on ice. The solutions can be prepared up to 1 wk ahead of time and kept refrigerated. All glassware is chilled before use.

3.1.1. RBC Ghosts

The preparation takes 8–10 h.

1. Start with 3 U of packed erythrocytes (750 mL): Divide them among six 250-mL centrifuge bottles, fill with washing solution, and centrifuge at 4,000*g* for 10 min. Remove the supernatant and the fluffy coat of white blood cells. (Use a Pasteur pipet connected to an aspirator water pump.)
2. Wash two more times with 5 vol of washing solution using 12 centrifuge bottles.
3. Pour the washed cells into an Erlenmeyer flask containing 2 L of the lysis solution while continuously stirring gently by hand. Add lysis solution to a total volume of up to 4 L (the desired volume ratio of lysis solution to the washed erythrocytes is 8–10:1). Leave in a cold room for 15 min.
4. In the meantime, wash the Pellicon with 2 L of lysis solution and subsequently fill with lysate. Wash the RBCs by continuous application of fresh lysis solution (up to 12–15 L total volume), followed by 10–15 L of storage solution until the membranes are light pink (*see* **Note 10**).
5. Transfer the membranes to 40-mL centrifuge tubes (16 tubes). If necessary, fill up with washing solution. Centrifuge at 20,000*g* for 30 min. Aspirate supernatants.
6. Vortex the tubes and transfer the pellets with a Pasteur pipet into a beaker kept on ice. Wash the tubes with small aliquots of storage solution, and by transferring to consecutive tubes recover all material (*see* **Notes 11** and **12**).
7. Measure the total volume and set aside small aliquots for protein and preliminary Ca^{2+}-ATPase activity assays. Divide the ghosts into plastic tubes and place in a freezer at –80°C, where they can be stored for a prolonged time (*see* **Notes 13–15**).

3.1.2. Light SR Membranes **(12)**

The preparation takes approx 8 h.

1. Remove muscle from both hind legs of the rabbit and place in a large beaker of 0.1 m*M* EDTA.
2. Cut off the unwanted material and wash once in distilled water.
3. Weigh 170 g of muscle and add 510 mL of solution 1 (*see* **Note 16**). Blend 15 s every 5 min for 1 h. Check pH every 10–20 min; add 10% NaOH solution to maintain pH between 6.5 and 7.0.
4. Divide into four parts and centrifuge in 250-mL centrifuge bottles at 15,000*g* for 20 min.
5. Collect supernatant and filter through 1 to 2 in. of gauze. There should be about 320 mL of filtrate. Divide the filtrate into eight 40-mL tubes, and centrifuge at 40,000*g* for 90 min.
6. Discard supernatant and suspend sediments of alternate tubes in 10 mL of solution 2. Scrape off pellet with a glass rod and pour into next tube; scrape off second pellet and pour suspension into the homogenizer. Repeat with 5 mL of solution 2 again in alternate tubes. Use a total of 60–70 mL of solution 2.
7. Disperse aggregates with a glass homogenizer (40 mL Dounce). Homogenize in portions until uniform, avoiding foam. Incubate in a cold room for 40 min.

8. Divide the suspension into five to six 15-mL Corex tubes and centrifuge at 15,000*g* for 20 min.
9. Collect approx 10 mL of supernatant into each of five to six polycarbonate tubes. Do not take the very top layer or the very thick bottom layer. Centrifuge at 40,000*g* for 90 min.
10. Discard supernatant and dissolve pellet in 18 mL of solution 3 as described in **step 6**. Homogenize and divide into small polypropylene tubes. Quick freeze in liquid nitrogen or by placing in a –80°C freezer (*see* **Notes 17** and **18**).

3.2. Purification of PMCA from RBC Ghosts

3.2.1. Preparation of CaM–Sepharose-4B Affinity Chromatography Columns

For preparation of three affinity chromatography columns, use 2.8 g of dry Sepharose-4B (which will swell to 9.8 mL) and 8 mg of CaM.

1. Place 1.4 g of CNBr-activated Sepharose-4B in each of two 15-mL Corex tubes. Slowly add 14 mL of 1 m*M* HCl, stirring gently with a thin glass rod. Let this swell for 15 min at room temperature.
2. Spin down at low speed for 5–10 min. Aspirate HCl, taking care not to remove any Sepharose. Repeat five times more.
3. To each tube add 2 mL of coupling solution, hand mix end-to-end, and quickly follow with addition of 2 mL of coupling solution containing CaM at 2 mg/mL (*see* **Note 19**). Mix gently overnight in a cold room using a rotation apparatus (*see* **Note 20**).
4. Spin down at low speed for 10 min. To each tube add 4 mL of blocking solution and incubate for 2 h at room temperature. Determine the amount of unbound CaM (spectrophotometrically, with $E_{1\ mg/mL}$ at 276 nm) in the collected supernatant to calculate the coupling efficiency.
5. Wash the resin six times by alternating distilled water and washing solution. Suspend in washing solution with 0.02% merthiolate for storage at 4°C.
6. Prepare chromatography columns by slowly pouring the resin suspension into 10-mL plastic syringes fitted with plastic tubing and stoppers so that the flow rate can be easily controlled (*see* **Notes 21** and **22**).

3.2.2. Purification of PMCA

Two 3-mL columns are used in this 8- to 9-h long purification procedure. All steps are carried out at 4°C, either in a cold room or on ice. Use cold solutions. Include aprotinin in all solutions in **steps 1–4** (*see* **Note 23**).

1. Thaw 500 mg of ghosts by placing them in a water bath at room temperature. In the meantime, cool the centrifuge.
2. Vortex the thawed ghosts and divide into four 40-mL centrifuge tubes. Add the 2X solubilization solution without $C_{12}E_8$, vortex, and pipet $C_{12}E_8$ slowly in, while constantly vortexing the tube, to the final concentration of 0.755 m*M*. Add aprotinin. Keep protein concentration at 8–10 mg/mL (*see* **Note 24**).

3. After 10 min incubation on ice, centrifuge at 40,000*g* for 45 min. Collect the supernatant containing solubilized membrane proteins. Measure the volume, divide into two portions, and load onto two CaM-Sepharose columns at a flow rate of 0.25 mL/1 min. The loading step takes approx 2 h.
4. Wash each column with 30–40 mL of washing solution at a flow rate of 0.25 mL/min until no protein is coming out of the column (absorbance reading at 280 nm equals that of the washing solution).
5. Start adding elution solution and immediately change the flow rate to 0.5 mL/min. Collect 0.8–1-mL fractions, recording absorbance at 280 nm (*see* **Note 25**). Combine fractions with high protein concentration, these are usually fractions 3–5. Perform protein assay (*see* **Note 26**).
6. Supplement the eluted PMCA with PC suspension: 30 µL/1 mL eluent (*see* **Note 27**). Store the preparation in small aliquots (0.2–1 mL, *see* **Note 28**) at –80°C. At this point, 30–40 min have elapsed since initiation of PMCA elution from the column.
7. Run the rest of the elution solution through the column (total volume of 20 mL), and follow with 20 mL of equilibration solution with 0.02% merthiolate (*see* **Note 29**). To regenerate the columns, run 10 bed volumes (30 mL) of solutions A and B. Equilibrate with equilibration solution. Add 0.02% merthiolate if being stored.

3.3. Determination of Ca^{2+}-ATPase Activity

Ca^{2+}-ATPase activity is determined through measurements of P_i resulting from ATP hydrolysis by the Ca^{2+} pump.

1. Prepare 1.7-mL polypropylene tubes with appropriate assay buffer (*see* **Note 30**). Additionally, for determination of the CaM-dependent Ca^{2+}-ATPase activity, add 5 µL of CaM solution of appropriate concentration (*see* **Note 31**).
2. Add 2–10 µL membrane or purified enzyme preparation (*see* **Note 32**) to enough appropriate assay buffer and water to a total of 95 µL. Start the Ca^{2+}-ATPase reaction 15 s later by adding 5 µL of 60 m*M* ATP, cap the tube, vortex, and place in the rack in the water bath at 37°C (*see* **Note 33**). Start the stopwatch at the moment ATP is added. Repeat the procedure for each tube at 1-min intervals. Perform each data point in duplicates (*see* **Note 34**).
3. Stop the Ca^{2+}-ATPase reaction at 15 or 30 minutes (*see* **Note 35**) by adding 300 µL of the diluted Lin-Morales reagent to consecutive tubes at 1-min intervals. Vortex and transfer the whole aliquot to a cuvet, and read the absorbance at 350 nm at 30 s as timed from the addition of the Lin-Morales reagent (*see* **Notes 36** and **37**).
4. To quantify the amount of P_i present in the Ca^{2+}-ATPase assay, use a calibration curve obtained by this procedure (no incubation necessary) using K_2HPO_4 solutions of known concentrations as standards (*see* **Note 38**).
5. The Ca^{2+}-ATPase activity in the membranes is calculated as a difference between the activity determined in the appropriate standard assay buffer and the assay buffer in which calcium is omitted. By contrast, the purified PMCA has no Ca^{2+}-independent activity (*see* **Note 39**). The CaM-dependent activation is determined

as a difference in Ca^{2+}-ATPase activity in the presence and absence of CaM (*see* **Notes 40** and **41**).

4. Notes

1. Commercially available CaM–Sepharose-4B sometimes produces enzyme that is not CaM sensitive, suggesting CaM bleaching.
2. The only drawback to this method is that the solubility of SDS is sensitive to its ionic environment. SDS present in the Lin-Morales solution effectively denatures the assayed protein, thus stopping the reaction and dissolving the protein. Using a threefold-diluted Lin-Morales solution, we seldom encounter problems. Trace amounts of precipitation were observed only with some membranes, such as microvessels, and these could be removed by sedimentation in a countertop centrifuge without affecting the P_i measurement. On some occasions, such as studying the effects of solutes containing phosphate on Ca^{2+}-ATPase activity, instead of colorimetric measurement the released P_i may be determined by $^{32}P_i$ radioactivity measurement ***(13,14)***. In this procedure, ^{32}P-ATP is used to start the Ca^{2+}-ATPase reaction. Then, after the reaction is terminated with perchloric acid, $^{32}P_i$ is extracted with charcoal and, following a filtration through Millipore filters, extracted into a 2-methyl-1-propanol/benzene mixture. An aliquot of the organic phase is counted in a scintillation counter.
3. Enzyme purified in the presence of glycerol bought from other companies is often less active.
4. Substitution of $C_{12}E_8$ for Triton X-100 and addition of glycerol results in a stable PMCA preparation. Another advantage of $C_{12}E_8$ over Triton X-100 is lack of interference with protein absorbance at 280 nm, making it easy to monitor protein elution from the column.
5. PC suspension does not totally clarify. It takes some practice to reach exactly the desired point and not further. For future use write down your conditions.
6. Total calcium in solutions needs to be measured by atomic absorption for precise calculations of $CaCl_2$ to be added. This is especially important when Ca^{2+}-ATPase activity is measured as a function of free calcium concentration. Our experience shows that 16 μ*M* calcium contamination (from reagents, water, glassware, and so on) should be taken into account. Free Ca^{2+} concentrations are calculated based on the constants given by Schwartzenbach et al. ***(15)***, pH, and the competitive effects of Mg^{2+}, K^+, and nucleotide as described by Fabiato and Fabiato ***(16)***.
7. The composition of this assay buffer has been modified as compared to buffers used by other investigators. The author wanted it to be as close as possible to the assay buffer used for PMCA activity for the purpose of comparative studies on the two Ca^{2+} pumps. The specific activity of SERCA1 obtained using the author's conditions does not differ from the activity reported in other laboratories.
8. Depending on the volume of PMCA that is added, calculate how much $C_{12}E_8$ and EGTA will be delivered with the enzyme, and add appropriately less of each while preparing the assay buffer. For example, addition of 5 μL of PMCA per assay tube results in 0.0375 m*M* $C_{12}E_8$ and 0.25 m*M* EGTA, i.e., 25% of the

desired final concentrations of both components. To assure good reproducibility, the author prepares separate stock solutions of reaction mixture (RM) for experiments in which various amounts of PMCA are added (such as determination of Ca^{2+}-ATPase activity as a function of PMCA concentration, which reflects enzyme activation by self-association ***[6,7,16]***). Thus, for an experiment in which 5 µL of PMCA will be added to the assay tube, prepare 6.5 mL of RM (an amount adequate for 2 d of experiments) comprised of the following: 1 mL of 0.5*M* Tris-maleate, pH 7.4; 1.5 mL of 0.9*M* KCl; 0.8 mL of 0.1 *M* $MgCl_2$, 0.075 mL of 0.1 *M* EGTA, pH 7.4; 1.125 mL of 1 m*M* $C_{12}E_8$, 1.2595 mL of 8 m*M* $CaCl_2$, and 0.7405 mL water. Then to each tube, pipet in the following order: 65 µL of RM, 18–23 µL of water, 5 µL of CaM (if necessary), 2–7 µL of PMCA, and 5 µL of ATP. RM can be refrigerated for several days.

9. When Ca^{2+}-ATPase activity is measured as a function of free calcium concentration, prepare RM without calcium and pipet $CaCl_2$ separately to each tube. Since the commercially available standard $CaCl_2$ solutions have a low pH, dilute them with a Tris buffer to keep the pH reproducible in all assay tubes. Titrate calcium solution against EGTA solution.
10. An alternative way to remove hemoglobin after RBC lysis is repetitive centrifugation ***(1)***. This is performed at first in 250-mL centrifuge bottles at 11,000*g* for 20 min. When the pellet becomes fluffy, the material has to be transferred to 40-mL tubes for centrifugation at 20,000*g* for 20 min. A total of five washes with lysis solution is usually followed by four washes with storage solution until the supernatant is no longer red. Having compared the two methods, the author prefers to use the Pellicon because it is less tedious than repetitive centrifugation.
11. The pellet does not have to be white. Some reddish coloration does not interfere with the activity assays. Sometimes a red core is present in the pellets; make sure not to include it in the collected material.
12. At this stage, be very careful to recover all material; it is pure, concentrated ghost membranes.
13. The expected volume is 90–120 mL.
14. In the author's experience, preparations kept for 2 yr were still fully active without loss of Ca^{2+}-ATPase activity.
15. The preparation yields 600–800 µg of PMCA protein.
16. One 5–6-lb rabbit yields approx 150–200 g of muscle.
17. SR preparation stored at –80°C remains active for many years.
18. The preparation yields approx 100 mg SR protein.
19. Reactive groups hydrolyze at high pH at which coupling of CaM is performed; thus, perform this step quickly to ensure maximal coupling of CaM. Calculate the efficiency of coupling by comparing the absorbance at 276 nm for CaM solution in the coupling buffer before addition to the Sepharose, and in the supernatant after the coupling (*see* **step 4**). In the author's experience, the coupling efficiency is between 88 and 95%.
20. Alternatively, the coupling could be performed for 2 h at room temperature. We find the overnight incubation more convenient. Also, **step 4** (blocking) could be performed overnight in a cold room.

21. Place a small amount of glass wool on the bottom of the syringe. After packing the column, test different flow rates and make sure that the eluent is clear (if the resin is coming out, one will see it on the wall of the glass tube in which the eluent is collected).
22. The author has used a variety of chromatography columns, including commercially available ones, in different sizes; the described small-scale procedure using syringe columns provides consistently reproducible, active, and CaM-stimulated PMCA preparation. The columns last for 15–20 purifications.
23. Add 100 Kalikrein IU of aprotinin/mL of solution, right before using them. It is especially important at the beginning of the purification procedure when other proteins are still present. There is no need to add aprotinin to the elution solution.
24. For a final protein concentration of 10 mg/mL, the total volume is 12.5 mL. Add 6.25 mL of 2X solubilization solution and 0.95 mL of 10 m*M* $C_{12}E_8$. The volume of ghosts should be 5.3 mL. Ghost preparation is usually less concentrated than 23 mg/mL; thus, centrifuge the thawed ghosts in the four tubes (after filling them with the storage solution) at 20,000*g* for 20 min. Have the desired volume of 5.3 mL marked on the tube so that you will know when to stop aspirating the supernatant.
25. The UV_{280} absorbance of washing and elution solutions needs to be alike in order to observe the elution of the Ca^{2+}-ATPase protein. For this reason, we always prepare these solutions at the same time.
26. Before adding PC, determine protein concentration of the combined eluent, using Bio-Rad Protein Micro-assay, based on the Bradford dye-binding procedure. Add 10–20 µL to 790–780 µL of water (total volume 800 µL), and 200 µL of the reagent. The values (80–140 µg protein/mL) are usually close to the expected concentration based on UV readings. PC interferes with the assay. In the first preparation, before combining all fractions, collect small volumes of the eluted PMCA and perform the protein and Ca^{2+}-ATPase activity assay. This way the elution profile of the column will be known. One can also keep separately, if desired, the most active PMCA fractions.
27. It is recommended to initially divide the eluted enzyme into small aliquots and add to each of them different amounts of PC. Then, determine Ca^{2+}-ATPase activity in the presence and absence of CaM for each to establish optimal PC:enzyme molar ratio for activation of the preparation.
28. The author freezes PMCA in aliquots that can be used in 1-d experiments. It is not advisable to thaw a tube more than two to three times because significant loss of activity may occur.
29. It is safe to leave columns in elution solution until the next day. The columns are usually regenerated the next day, while performing the preliminary characterization of purified PMCA (Ca^{2+}-ATPase activity and purity by gel electrophoresis).
30. The reaction can be performed in small glass tubes of appropriate volume that would allow for good mixing of the reaction mixture and the Lin-Morales reagent. The author chose to perform the assay in sealed polypropylene tubes because they are suitable for studies on the effect of volatile anesthetics on the Ca^{2+}-ATPase activity.

31. In a typical assay, the author uses 2 μ*M* CaM (final concentration in the reaction is 100 n*M*).
32. The optimal amounts of protein in the assay at 37°C/25°C usually are 10–12/16–20 μg of ghost membranes, 0.20/0.36 μg of SR, and 0.2–0.3/0.4–0.65 μg (i.e., 30–50 n*M* final concentration in the assay) for the CaM-independent dimeric PMCA.
33. When the reaction is performed at a different temperature, the correct range of absorbance readings will be assured by either changing the amount of protein in the assay (an example is shown in **Note 32** for 25 vs 37°C) or the reaction time.
34. Reproducibility of the assay is very good. For some plasma membrane preparations, such as microvessels, there is significant scatter; in such cases, triplicates should be used.
35. The reaction is linear for at least 30–40 min. It is advisable to check first the linearity for your particular preparation before settling on performing the reaction for either 15 or 30 min. The author usually selects a 30-min reaction time, which allows for 30 tubes in one assay performed by one person.
36. Alternatively, the reading could be made at 30–60 min after the addition of the Lin-Morales reagent. In this case, the 1-min intervals between readings do not need to be made.
37. The absorbance of the samples is read against a blank prepared and treated the same way as the samples, with the exclusion of the studied protein. For membranous preparations, it is advisable to double-check that they are not contributing to the reading (at higher protein concentration some plasma membranes do—in such cases subtract the absorbance).
38. The calibration curve that expresses the sensitivity of the method shows linearity in the range of final P_i concentrations up to 1.75×10^{-4}*M*. 10 nmol of P_i in the tube gives an absorbance reading of 0.25. If desired, the sensitivity can be increased by using the nondiluted Lin-Morales reagent.
39. Specific activities for the Ca^{2+}-ATPase in the three preparations at 37°C are 0.8–1.4 μmol P_i/(mg protein · h) in ghost membranes, 300 μmol P_i/(mg protein · h) for SERCA1 in skeletal SR, and 180–300 μmol P_i/(mg protein · h) for the purified PMCA.
40. In a typical CaM-dependent Ca^{2+}-ATPase activity assay, CaM is added at 100 n*M* concentration to assure a molar ratio of CaM to PMCA of 2:1 ***(6,17,18)***.
41. By dividing the CaM-dependent by the CaM-independent activity, the CaM stimulation factor is derived. CaM stimulates the PM Ca^{2+}-ATPase activity up to five to sevenfold, depending on the particular membrane preparation and calcium as well as potassium concentrations. In the purified PMCA preparations, CaM stimulates only Ca^{2+}-ATPase activity of the monomeric enzyme whereas the dimers are fully activated through enzyme self-association ***(6–8,17)***.

References

1. Niggli, V., Penniston, J. T., and Carafoli, E. (1979) Purification of the (Ca^{2+} + Mg^{2+})-ATPase from human erythrocyte membranes using a calmodulin affinity column. *J. Biol. Chem.* **254,** 9955–9958.

2. Gietzen, K., Tejcka, M., and Wolf, H. V. (1980) Calmodulin affinity chromatography yields a functional purified erythrocyte (Ca^{2+} + Mg^{2+})-dependent adenosine triphosphatase. *Biochem. J.* **189,** 81–88.
3. Kosk-Kosicka, D., Scaillet, S., and Inesi, G. (1986) The partial reactions in the catalytic cycle of the calcium-dependent adenosine triphosphatase purified from erythrocyte membranes. *J. Biol. Chem.* **261,** 3333–3338.
4. Missiaen, L., Raeymaekers, L., Wuytack, F., Vrolix, M., DeSmedt, H., and Casteels, R. (1989) Phospholipid-protein interactions of the plasma-membrane Ca^{2+}-transporting ATPase. *Biochem. J.* **263,** 687–694.
5. Kosk-Kosicka, D. and Zylinska, L. (1997) Protein kinase and calmodulin effects on the plasma membrane Ca^{2+}-ATPase from excitable and nonexcitable cells. *Mol. Cell. Biochem.* **173,** 79–87.
6. Kosk-Kosicka, D. and Bzdega, T. (1988) Activation of the erythrocyte Ca^{2+}-ATPase by either self-association or interaction with calmodulin. *J. Biol. Chem.* **263,** 18,184–18,189.
7. Kosk-Kosicka, D., Bzdega, T., and Wawrzynow, A. (1989) Fluorescence energy transfer studies of purified erythrocyte Ca^{2+}-ATPase. *J. Biol. Chem.* **264,** 19,495–19,499.
8. Sackett, D. L. and Kosk-Kosicka, D. (1996) The active species of plasma membrane Ca^{2+}-ATPase are a dimer and a monomer-calmodulin complex. *J. Biol. Chem.* **271,** 9987–9991.
9. Lecocq, J. and Inesi, G. (1966) Determination of inorganic phosphate in the presence of adenosine triphosphate by the molybdo-vanadate method. *Anal. Biochem.* **15,** 160–163.
10. Lin, T.-I. and Morales, M. F. (1977) Application of a one-step procedure for measuring inorganic phosphate in the presence of proteins: The actomyosin ATPase system. *Anal. Biochem.* **77,** 10–17.
11. Pharmacia LKB Biotechnology. *Affinity Chromatography: Principles and Methods*. Amersham Pharmacia Biotech instruction booklet (Uppsala, Sweden).
12. Eletr, S. and Inesi, G. (1972) Phospholipid orientation in sarcoplasmic membranes: Spin-label ESR and proton NMR studies. *Biochim. Biophys. Acta* **282,** 174–179.
13. Carvalho, M. G. C., Souza, D. G., and deMeis, L. (1976) On a possible mechanism of energy conservation in sarcoplasmic reticulum membrane. *J. Biol. Chem.* **251,** 3629–3636.
14. Kosk-Kosicka, D., Kurzmack, M., and Inesi, G. (1983) Kinetic characterization of detergent-solubilized sarcoplasmic reticulum adenosinetriphosphatase. *Biochemistry* **22,** 2559–2567.
15. Schwartzenbach, G., Senn, H., and Andereff, G. (1957) *Helvetica Chimica Acta* **40,** 1886–1900.
16. Fabiato, A. and Fabiato, F. (1979) *J. Physiol. (Paris)* **75,** 463,464.
17. Kosk-Kosicka, D., Bzdega, T., and Johnson, J. D. (1990) Fluorescence studies on calmodulin binding to erythrocyte Ca^{2+}-ATPase in different oligomerization states. *Biochemistry* **29,** 1875–1879.
18. Kosk-Kosicka, D. (1990) Comparison of the red blood cell Ca^{2+}-ATPase in ghost membranes and after purification. *Mol. Cell. Biochem.* **99,** 75–81.